Author:
Alotaibi, Maha M S

Title:
Towards Aqueous Nanostructures Based on Oligo(aniline)s

Towards Aqueous Nanostructures Based on Oligo(aniline)s

Maha Moteb Alotaibi

School of Chemistry

University of Bristol

A thesis submitted to the University of Bristol in accordance with the requirements for award of the degree of Doctor of Philosophy in Chemistry in the Faculty of Science.

June 2019

Word count: 55.183

Abstract

Oligo(aniline)s are the ideal replacement of poly(aniline), as they exhibit the same optoelectronic properties and oxidation states, however, with excellent solubility, processability and switchability between different oxidation states. In addition, oligo(aniline)s provide a great platform to design and synthesize tunable and well-defined supramolecular structures and potentially even new functions.

In this thesis, a family of cationic amphiphiles based on oligo(aniline) was synthesised. The aim of this thesis is to provide tunable and switchable self-assembled structures of our oligo(aniline) based amphiphiles using an addressable packing parameter approach.

Two architectures, single-tailed and bola-type cationic **TANI**-based amphiphiles, were designed, allowing a comparison between the two. Moreover, the head groups were varied to include quaternary amines and quaternary phosphines. The prepared amphiphiles were characterised using NMR spectroscopy, MS spectrometry, and elemental analysis.

The self-assembled structures of the prepared oligo(aniline) amphiphiles in the EB state, **TANI** functionalised with pentyl trimethylphosphonium amphiphiles (**TANI-PTPB)**, **TANI** functionalised on both sides with pentyl trimethylammonium amphiphiles (**TANI-$(PTAB)_2$)**, and **TANI** functionalised on both sides with pentyl trimethylphosphonium amphiphiles (**TANI-$(PTPB)_2$)**, were investigated in detail and elucidated by atomic force microscopy, electron microscopy, small-angle x-ray scattering, and small-angle neutron scattering studies. The variations of head group sizes and structures were found to contribute to alterations in the self-assembling morphologies. These changes in morphology, from fibrous structures to vesicles, highlight the important role of packing parameter ($\boldsymbol{p = v / a_0 l_c}$). In other words, an increase of the headgroup's size results in a decrease in the packing parameter, causing the morphology to change.

A variety of dopants with different volumes and structures were found to increase the volume of the hydrophobic core, causing the packing parameter to increase as a consequence. The variations of the packing parameter promote various self-assembled structures, fibrous, chain-like structures, worm and spherical structures. These variations boost the role of the packing parameter to construct an avenue of well-defined and tunable structures for oligo(aniline)-based amphiphiles. Oligo(aniline) amphiphiles present an elegant and simple route to switchable and tunable functional materials. This work provides promising routes for applications in drug delivery.

Acknowledgements

First and foremost, praise and gratitude be to ALLAH almighty, without his gracious help, I would not have done this thesis.

I would like to express my gratitude to my supervisor Prof Dr Charl FJ Faul for his guidance, continuous support and encouragement throughout my PhD journey. His detailed insights and inputs during the years of my PhD were always helping me to bring out my best. I'm very grateful to Prof Dr Julian Eastoe for hosting me in his lab during my pregnancy and huge thanks go to his student Dr Chris Hill for his help and support with SANS measurements. I would like also to thank Dr Annela Seddon for helping me with SAXS and SANS measurements and fitting. Special thanks go to Dr George Whittell and Dr Wuge Briscoe for their advice and valuable input at my annual progress monitoring meetings.

I have been so lucky to be surrounded by such a wonderful and most helpful group members (Faul group) during my PhD. I would like to thank my current and past colleagues who were/are working in Faul group: Dr Alex Bell, Dr Ben Mills, Dr Carl Hu, Dr Piotr Wolanin, Dr Kazuyoshi Watanabe, Dr Charlie Jarret-Wilkins, Dr Liam MacFarlane, Dr Horatio He, Dr Wei Lyu, Dr Ozlem Erol, Dr James Thomas, Dr Long Pan, Dr Ben Baker, Dr Maciek Kopec, Dr Michael Dicker, D Jie Chen, Djen Kuhnel, Henry Symons, Nouf Zaghloul, Esther Townsend, Veronica del Angel, Christian Romero, Pongsathon (Nan) Boonrod, Robert Wilson-Kovacs, Marcos Villeda Hernandez, Maximilian Hagemann and Zihao Ren. From the Hall group, I would like to thank Dr Jason Potticary for helping me with ESR measurements. From the Briscoe group, I would like to thank Anna Slastanova for helping me with surface tension measurements.

I would like to extend my thanks to department staff and technicians in Chemistry school including Mass spectrometry, NMR spectroscopy, elemental analysis and Electron microscope unit. As an international student I was so lucky to have "Bristol International Student Centre", thank you for always being there to give a constant help and support, special thanks go to Jacqueline Conradie-Faul and Eric Green.

I would like also to thank my sponsors Royal Embassy of Saudi Cultural bureau and King Abdulaziz University for supporting me during my PhD journey, their helps to cover travel cost of some conferences over years of my PhD has been greatly appreciated. Thanks to the University of Bristol's Alumni Foundation for helping me to cover travel costs to Spring meeting ACS 2019 at Orlando, USA.

I owe a great debt of gratitude to my amazing parents for their support, motivation and being a solid support to encourage me. Literally they were/are behind all my life successes, without them this thesis wouldn't exist. I hope I have made them proud of me.

There are no words to express my gratitude to my husband, Nawaf, for his help, support, love and encouragement, and also to my lovely daughter, Nora, and my little son, Salman, who came to the world in the mid of this journey. Thank you from the bottom of my heart, without your patience I couldn't have done this.

Finally, my warmest thanks go to my sisters, my brothers and my friends who have given constant support, love and endless encouragement. I'm so lucky to have friends make my life in Bristol more enjoyable and fun. I have unforgettable memories with you my lovely friends. I'm so pleased to have you in my life.

Thank you all,

Maha

This thesis is dedicated to:

my inspiring parents

my lovely husband

Declaration

I declare that the work in this dissertation was carried out in accordance with the requirements of the University's Regulations and Code of Practice for Research Degree Programmes and that it has not been submitted for any other academic award. Except where indicated by specific reference in the text, the work is the candidate's own work. Work done in collaboration with, or with the assistance of, others, is indicated as such. Any views expressed in the dissertation are those of the author.

SIGNED: ..... DATE:.....

Publications

- Esther Townsend, Maha Alotaibi, Benjamin M. Mills, Kazuyoshi Watanabe, Annela M. Seddon and Charl F. J. Faul. Electroactive amphiphiles for addressable supramolecular nanostructures. *ChemNanoMat*, 4, 2018, 741-752. Part of **Chapter 1** has been reproduced from this review paper, M. Alotaibi contributed to research collection and wrote the introduction.

- Wei Lyu, Maha Alotaibi, O. Alexander Bell, Kazuyoshi Watanabe, Robert Harniman, Benjamin M. Mills, Annela M. Seddon, Sarah E. Rogers, Stephen M. King, Wei Yan and Charl F. J. Faul. An addressable packing parameter approach for reversibly tuning the assembly of oligo(aniline)-based supra-amphiphiles. ***Chem.Sci*. 9, 2018, 4392-4401.** Part of **Chapter 3** has been reproduced from this paper, M. Alotaibi contributed to the synthesis of **TANI-PTAB** and undertook self-assembly experiments to confirm the formed structures. Dr Sarah Rogers and Dr Annela Seddon are gratefully acknowledged for SAXS and SANS measurements and data analysis. Dr Ben Mills, Faul Research Group, is gratefully acknowledged for his help and advice regarding DFT modeling studies.

- Maha M. Alotaibi, O. Alexander Bell, Benjamin M. Mills, Annela M. Seddon, Christopher Hill, Robert L. Harniman, Jiang-Fei Xu, Xi Zhang and Charl F. J. Faul. Synthesis and tunable self-assembly of electroactive bolaamphiphiles based on oligo(aniline)s, ***submitted*.** Dr Annela Seddon and Dr Chris Hill are gratefully acknowledged for SAXS and SANS measurements and data analysis. Dr Ben Mills, Faul Research Group, is gratefully acknowledged for his help and advice regarding DFT modeling studies.

- Maha M. Alotaibi, Benjamin M. Mills, Annela M. Seddon, Robert L. Harniman, Jiang-Fei Xu, Xi Zhang and Charl F. J. Faul. Tunable self-assembled nanostructures from electroactive amphiphiles, ***in preparation.***

Table of Contents

List of Tables

List of Figures

List of Schemes

List of Abbreviations

AFM	Atomic force microscope
NH_2/NH_2	Amine/Amine capped
CSA	Camphorsulfonic acid
Xphos	2-Dicyclohexylphosphino-2',4',6'triisopropylbiphenyl
DMF	Dimethylformamide
DMSO	Dimethyl sulfoxide
DCM	Dichloromethane
ESR	Electron spin resonance
eSA	Electrotactic supra-amphiphiles
ES	Emeraldine salt
EB	Emeraldine base
FTIR	Fourier transformed infrared spectroscopy
HOMO	Highest occupied molecular orbital
HTAB	Heptyl trimethylammonium bromide
LUMO	Lowest unoccupied molecular orbital
MALDI-TOF	Matrix-assisted laser desorption/ionization-time-of-flight
MO	Molecular orbital
NMR	Nuclear magnetic resonance
OANI	Octa(aniline)
PANI	Poly(aniline)
PB	Pernigraniline base
Ph/NH_2	Phenyl/Amine capped
Ph/Ph	Phenyl/Phenyl capped
PTAB	Pentyl trimethylammonium bromide
PTPB	Pentyl trimethylphosphonium bromide
PXRD	Powder X-ray diffraction

SAXS	Small-angle x-ray scattering
SANS	Small-angle neutron scattering
THF	Tetrahydrofuran
TFA	Trifluoroacetic acid
TANI	Tetra(aniline)
UV/vis-NIR	Ultraviolet-visible-near Infrared

CHAPTER 1 INTRODUCTION

The scientific area of this thesis is materials science, in particular designing and exploring new electroactive materials based on olio(aniline)s. We are mainly focusing on tuning their self-assembled structures through doping and de-doping process. In order to introduce this topic, conjugated polymers and their redox switchable properties are discussed as oligomeric materials exhibit the same switchable properties and oxidation states of polymers.

1.1 Overview of conjugated and conducting polymers

Conducting polymers are attractive and promising candidates for a variety of applications such as organic photovoltaics[1], light-emitting diodes,[2,3] field-effect transistors,[4,5] gas sensors,[6,7] memory devices,[8,9] etc. There are several kinds of conducting polymers that have been prepared and their applications explored. Some of the most widely studied conducting organic polymers are poly(acetylene) (**PA**), poly(aniline) (**PANI**), poly(pyrrole) (**PPy**), poly(thiophene) (**PT**), and poly(phenylene vinylene) (**PPV**), as depicted in **Figure 1.1.**[10]

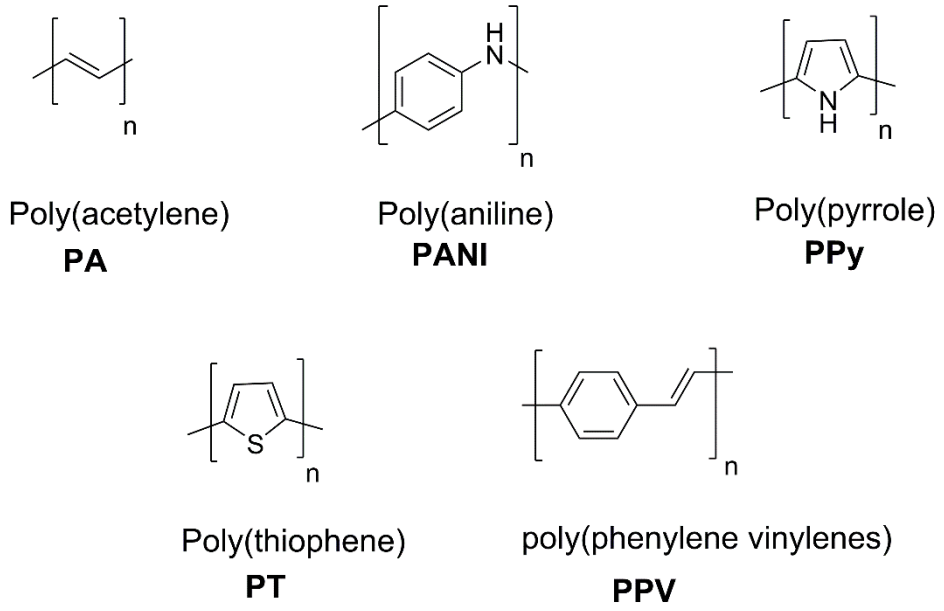

Figure 1.1 Structures of common conducting polymers.

PA is a conjugated linear polymer and the simplest example that can be used to understand the behaviour of conductive polymers.[11] The model of conductivity for **PA** can then be applied to other conductive polymers. **PA** comprises of a linear chain of sp^2-hybridized carbon atoms and the electronic structure of **PA**, is expected to form a uniform structure through the delocalisation of the σ-bond across the polymer backbone. This delocalisation should endow an equal C-C bond length (**Figure 1.2a**).[12] However, **PA** in fact does not present as a uniform structure due to the Peierl's instability effect, which assumes that "*a one-dimensional equally spaced chain with one electron per ion is unstable*".[13] Furthermore, PA shows semiconductor behaviour instead of metallic; this behaviour arises due to the presence of alternating single-double bonds in the **PA** chain (**Figure 1.2b**).[12] NMR measurements also confirm the alternation of bond lengths across the entire chain of **PA.** The effect of the previously described behaviour causes a partially-filled π-bond to split into a lower π valence band (filled) and an upper π* conduction band (empty), resulting in a semiconductor with bandgap of ~ 1.5eV (**Figure 1.3**).[14]

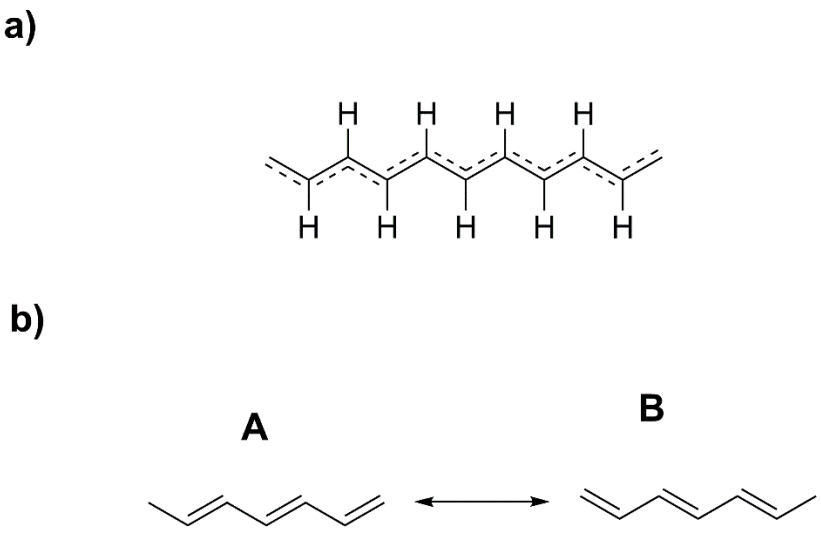

Figure 1.2 a) Structure of uniform **PA**, b) the alternation of unequal length single/double bond **PA** due to the deviation from the fully-delocalized structures.

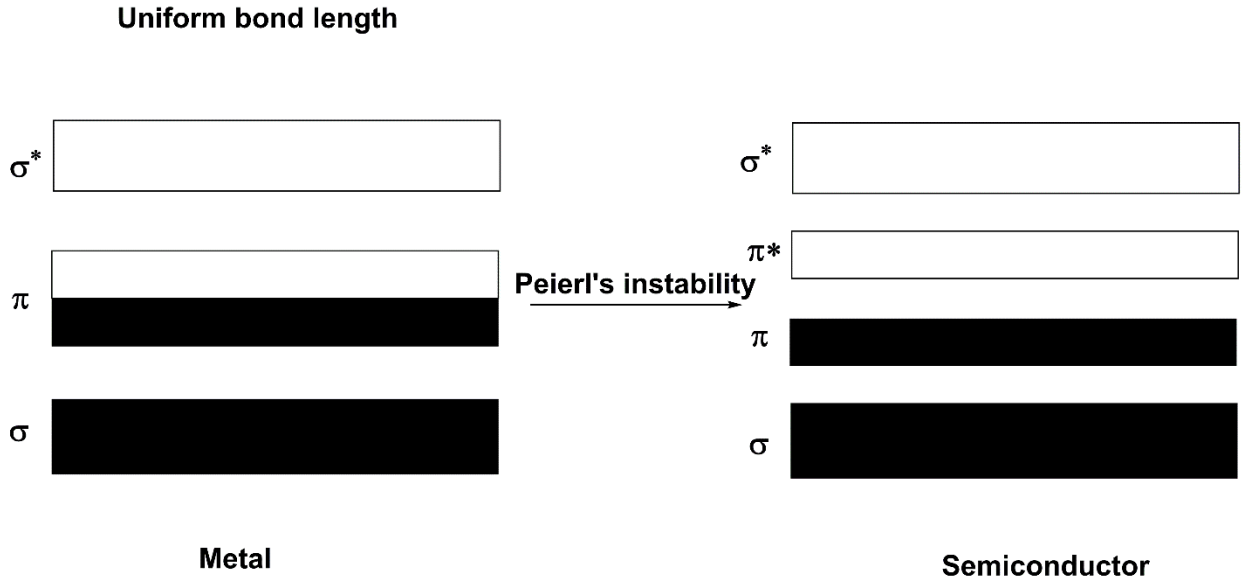

Figure 1.3 Schematic representation of a π band split into π and π* bands due to Peierl's instability, yielding a semiconductor material.

1.2 Basis of conductivity

The result of the alternation of single and double bonds across the **PA** chain backbone leads to the creation of two conformations: **A** and **B** structures. The first structure starts with a double bond and the latter starts with a single bond, which leads to defects on the polymer backbone, called solitons. These solitons are neutral, and are able to delocalise over a range of carbon atoms at the interface of the two structures (**A, B**) as presented in (**Figure 1.4**). However, solitons can also be positive when treated with an oxidant (charge +1, spin 0) as shown in (**Figure 1.5**). The polymer chain can also be treated with a reductant, resulting in negative solitons (charge –1, spin ½) [15,16]

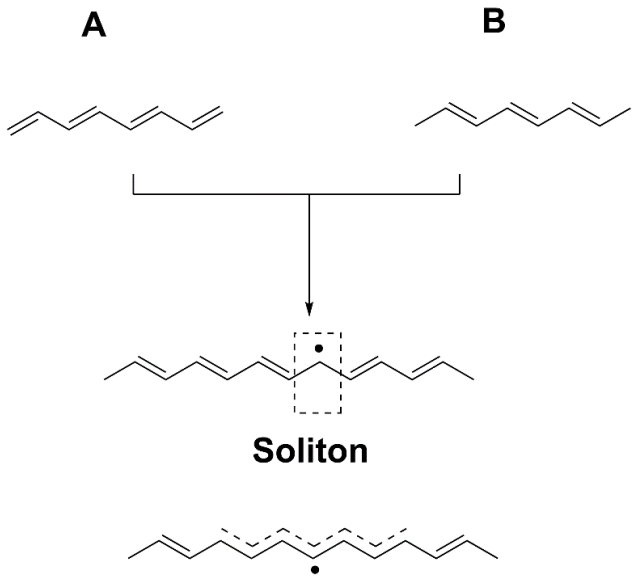

Figure 1.4 Different electronic structures of **PA** present in two conformations (A&B, top). Soliton defect exists at the boundary between two structures A&B (middle). Soliton delocalisation over carbon atoms (bottom).

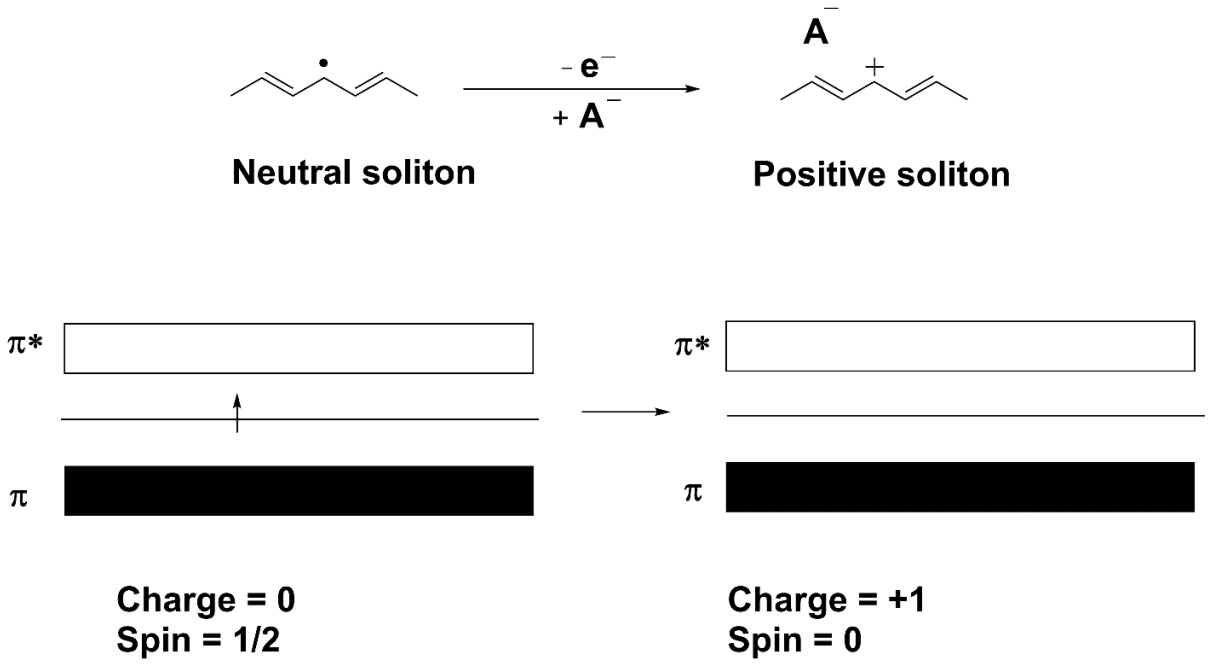

Figure 1.5 Neutral soliton presents in a separate band between the π and π* bands (left). The oxidation of the neutral soliton leads to the formation of a positive soliton with an empty band (right).[16]

PA can have multiple soliton defects on the polymer chain and these are not stable; therefore they tend to combine and form polarons and bipolarons. Polarons mean the charged solitons (either positive or negative) combine with neutral solitons as shown in (**Figure 1.6**). Bipolarons refer to a mixture of either two charged solitons or two polarons, in which state the two neutral solitons annihilate, as presented in (**Figure 1.7**). As a result of the presence of these defects, a new energy level is found between the lower π valence band and the upper π* conduction band.[16,17,18]

The new energy level facilitates charge movement. Upon doping, the number of charge carriers (polarons or bipolarons) will then introduce conductivity for such polymers.[11,17,19]

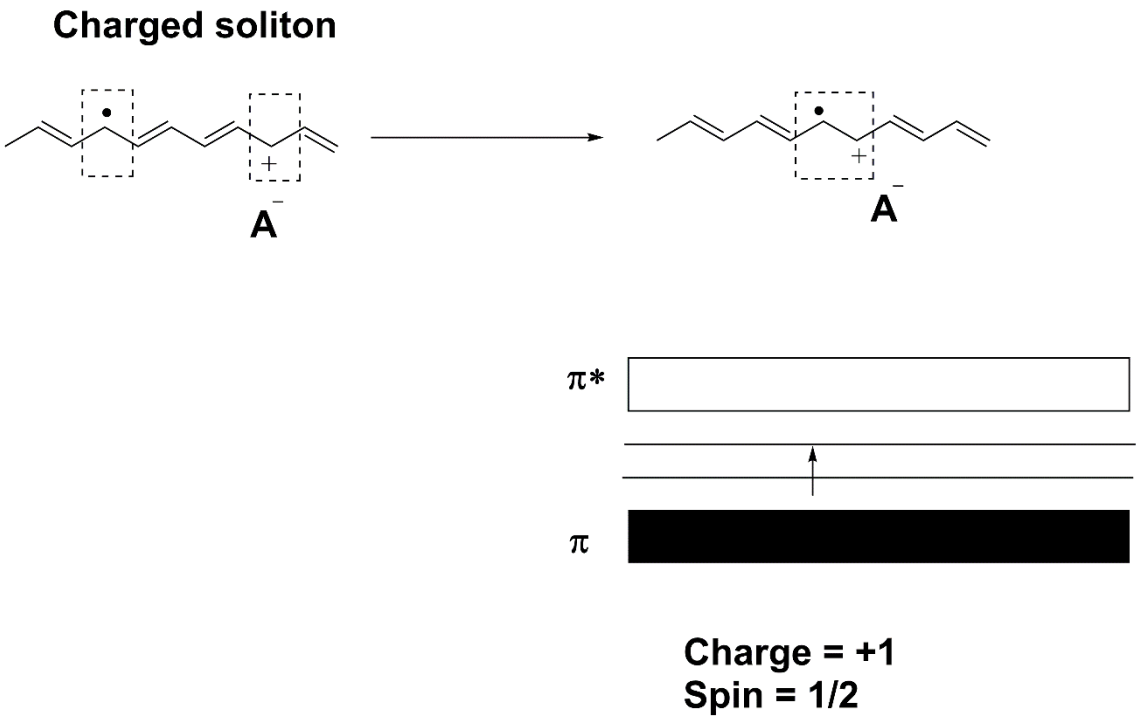

Figure 1.6 Formation of polaron species when neutral and positive solitons combine.[16]

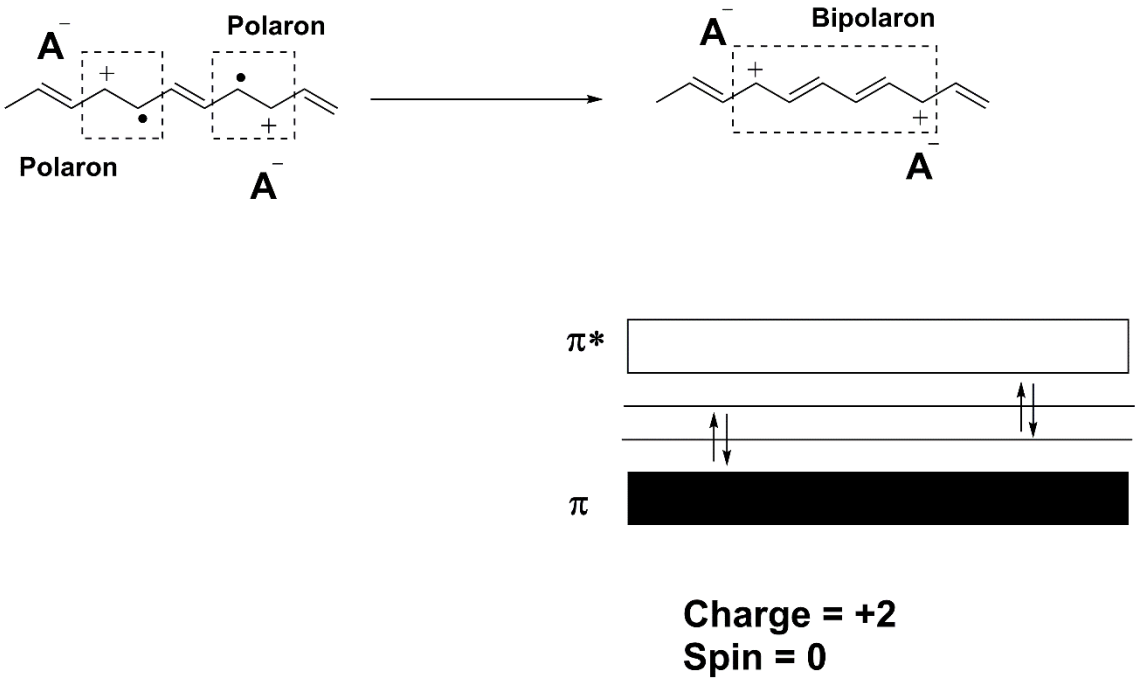

Figure 1.7 Formation of bipolaron species when two polarons combine.[16]

1.3 Poly(aniline)

1.3.1 Structure and synthesis

Amongst conjugated polymers, **PANI,** is considered as one of the most important and oldest, owing to its environmental stability, ease of synthesis, tunable properties, and fascinating redox properties.[20] **PANI** is made of connecting, repeating units of aniline and has the ability to exist in three different oxidation states. The oxidation state of **PANI** can be identified by the ratio of benzenoid rings to quinoid rings in the polymer structure. Each state has a different colour: the fully reduced form (leucoemeraldine), denoted as LEB (colourless), comprises just benzenoid rings linked by secondary amines. The half oxidized (emeraldine), denoted as EB (blue or violet), comprises of benzenoid and quinoid rings (with ratio 3:1) and the fully oxidized (pernigraniline) state, denoted as PB (orange or brown), comprises of alternating benzenoid and quinoid rings linked by imine groups.[21] All these forms of **PANI** are presented in **Figure 1.8**, and can be interconverted by redox processes.[21,22] These chromatic changes in PA have attracted much attention owing to the great potential for applications such as redox and pH indicators, display devices, etc.[1]

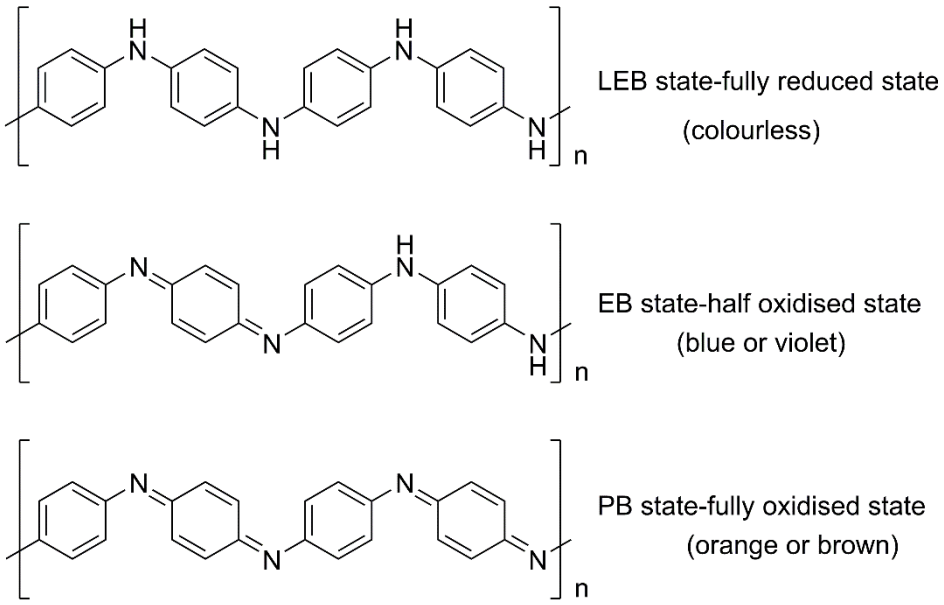

Figure 1.8 Oxidation states of **PANI**.

PANI is typically prepared through chemical or electrochemical methods.[23] and the oxidative [',polymerization is usually carried out in acidic media. The electrochemical polymerisation of aniline is normally used to prepare well-ordered films with a reasonable control over thickness.[24] For the chemical route, the oxidation reaction is performed in acidic aqueous media in the presence of an oxidizing agent such as ammonium peroxydisulfate[25] or ferric chloride hydrate.[26] The mechanism of the chemical oxidation polymerization of **PANI** was proposed by Wei et al[27] and is simply described in **Scheme 1.1**. This mechanism involves in general two steps: the first step is the oxidation reaction of the nitrogen atom of the monomer (aniline) to form a radical-cation species; the second is the addition of aniline in a radical-cation species form. Combining these two radical-cation species form a di(aniline), followed by the oxidation reaction of di(aniline) to form a di(aniline) radical-cation species. The successive addition of the monomer (aniline) in a similar fashion to that mentioned at the beginning of the polymerisation process results in a high molecular weight of **PANI.** This process is known as a step-growth polymerisation method.

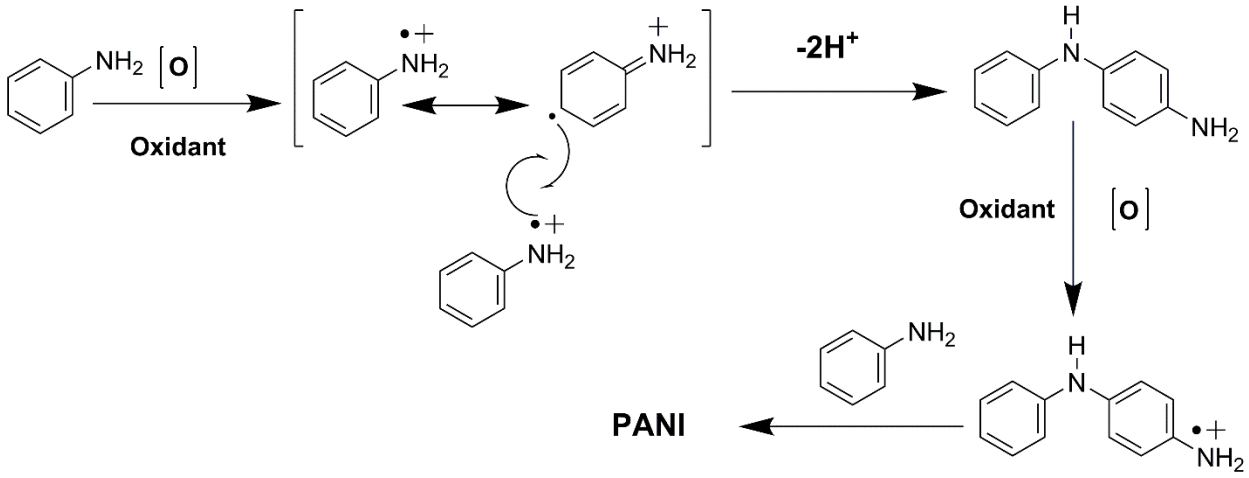

Scheme 1.1 Chemical oxidation polymerization of **PANI**.[27]

1.3.2 Doping and conductivity

It is important to note that none of these oxidation states are conductive without doping.[22] The doped state is also known as the protonated polymer. The LEB and EB oxidation states of **PANI** and their conversion to the ES state are shown in **Scheme 1.2**, The ES state can be accessed in two ways: either by oxidative doping of the LEB state or by acid doping of the EB state. Protonation and addition of anions is achieved through adding different acids, either inorganic or organic.[20] Simply, protonation of the EB state in an acidic medium gives a polaron structure which consists of two cationic radicals centered on nitrogen atoms that are delocalized over the π system. This polaron structure is responsible for electrical conduction.[3,28] HCl is commonly used as the dopant to increase the conductivity.[29] However, organic acids have a substantial impact on improving the conductivity of **PANI.**

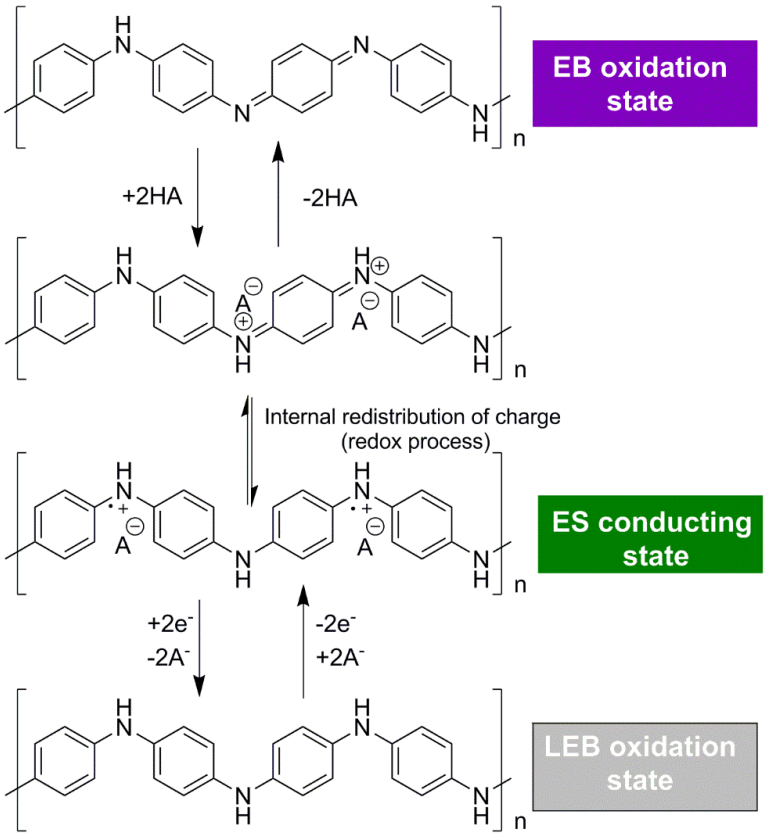

Scheme 1.2 Chemical and oxidative doping routes to the conducting ES state of **PANI**.

1.3.3 Self-assembly of PANI

An interesting feature of **PANI** is its ability to exhibit various morphologies over either nano- or micro- scales, which can be achieved by doping **PANI** with different acids, such as organic or non-organic acids or even acid surfactant.[30,31] **PANI** has been used as a platform to build various self-assembling architectures with controlled sizes and shapes.[32,33] The self-assembled structures can be tuned and controlled using a variety of factors such as pH, solvent, oxidant used for the preparation of **PANI**, temperature, ratio of reagent and types of dopants. Kaner and his group studied this self-assembly behaviour and have reported various **PANI** nanostructures. These structures are summarized in **Figure 1.9**.[31]

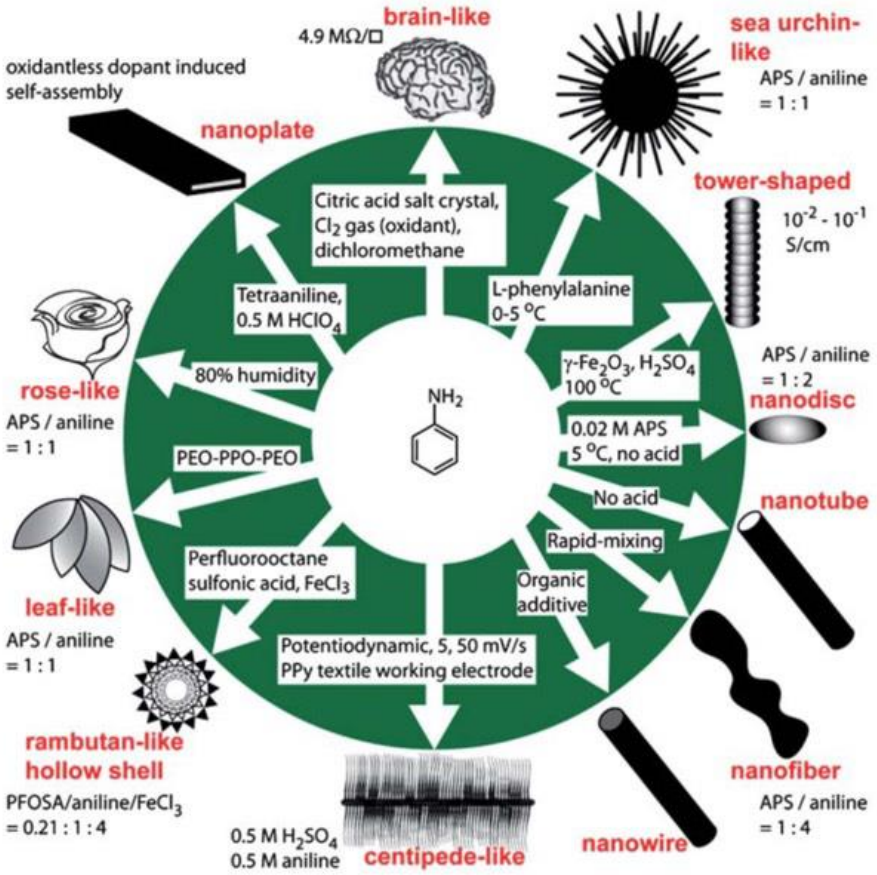

Figure 1.9 Various nanostructures of **PANI** resulting from the different synthetic routes.[31]

In general, one-dimensional (**1D**) nanostructures of **PANI,** such as nanofibers**,** show high surface area and high conductivity.[26,34] Hence, the unique combination of doping and electroactive tunable properties of **PANI** materials with high surface areas form a great platform for various applications such as chemical sensors, catalysis, energy devices and nanoelectronics.[10]

PANI doped by camphorsulfonic acid (CSA) has been used widely and extensively studied, owing to their ability to form a conductive nanofibrous material. The highest conductivity of **PANI** was recorded with values of 1000 $S \cdot cm^{-1}$.[35]

Furthermore, acid surfactants comprising of sulfonic groups and alkyl chains, in particular dodecylbenzene sulfonic acid (DBSA), have also been exploited to dope **PANI** in order to enhance the processability, the solubility and improve the self-organization of **PANI**.[30] Another interesting

example that showed good solubility for **PANI** in organic solvents is the combination of 4,4-bis(4-hydroxyphenyl)-valeric acid, benzene-1,2-dicarboxylic acid, 4-sulfo-1,2-di(2-ethylhexyl) ester (DEHEPSA) (**Figure 1.10**, for structures) together with either dichloroacetic acid (DCAA) or difluorochloroacetic acid (DFCAA) as solvents.[33,36,37]

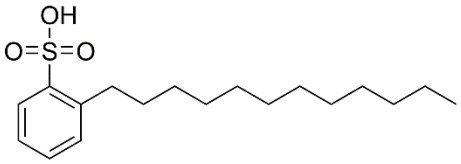

dodecylbenzene sulfonic acid (DBSA)

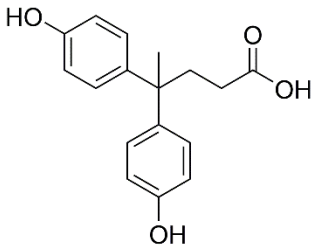

4,4-bis(4-hydroxyphenyl)-valeric acid

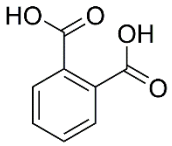

benzene-1,2-dicarboxylic acid

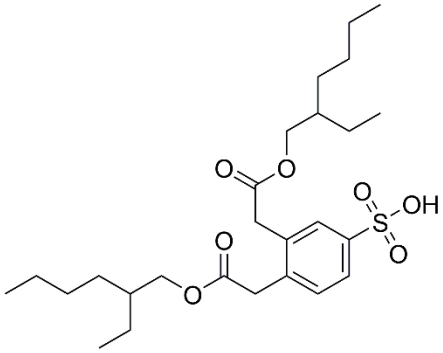

4-sulfo-1,2-di(2-ethylhexyl) ester (DEHEPSA)

Figure 1.10 Structures of PANI surfactant dopants.

1.4 Conjugated oligomers

There are several issues facing conducting polymers that make them difficult to work with and study in detail: they do not have well-defined chemical structures and are usually insoluble in most common solvents due to their high levels of conjugation, leading to planarity and rigidity, and ultimately to poor processability.[38] Oligomers have been explored to simplify the study of these polymers, and to avoid the difficulties and obstacles experienced when working with the polymers.[39] Furthermore, the oligomer approach provides a great platform to design and synthesize well-defined structures with well-defined function. Oligo(aniline)s have the same electronic properties as **PANI**, i.e., the LEB, EB and PB oxidation states are all accessible and doping can be performed by oxidation of the LEB state or acid treatment of the EB state.[38]

1.4.1 Tetra(aniline) synthesis and properties

Tetra(aniline) (**TANI**) is the shortest oligomer that can mimic the electronic properties of **PANI**, i.e., the LEB, EB and PB oxidation states are all accessible and doping can be achieved by an oxidation reaction either from the LEB state or acid treatment of the EB state as presented in **Figure 1.11**.[39] The formation of the EB state of **TANI** would require the ratio of quinoid to benzenoid rings (1:3) as shown in **Figure 1.11**. **TANI** in the EB state exhibits good solubility in common organic solvents, resulting in more processable materials and a versatile platform to produce various self-assembled structures as **PANI**.[38,40]

In terms of synthesis, oligo(aniline)s are easily synthesised via an oxidative route by treating di(aniline) with a strong oxidant such as $FeCl_3$ or H_2O_2 in different conditions. This results in a mixture of various length of oligomers (8- or 16-mers) as well as the tetramer.[39,] However, palladium-catalysed coupling of anilines and aryl halides provides a more accessible and controllable method to produce pure, monodisperse and controlled length oligomers. The powerful coupling approach was developed by Buchwald and Hartwig and applied to oligo(aniline)s materials since 1998.[41,42] The mechanism of Buchwald-Hartwig amination is simply explained in **Appendix A, Scheme A1**.[41,43,44,45] In general, oligo(aniline)s in the LEB state are not stable and oxidise in air, forming a mixture of EB and LEB states. To make the products of

the Buchwald-Hartwig coupling stable it is important to protect the amine groups after the coupling. Hence the reaction is followed by a Boc (di-tert-butyl decarbonate) protection to prevent the formation of the quinoid ring and hence oxidation to the EB state. The mechanism of Boc protection is provided in the **Appendix A, Scheme A2**.[46,47]

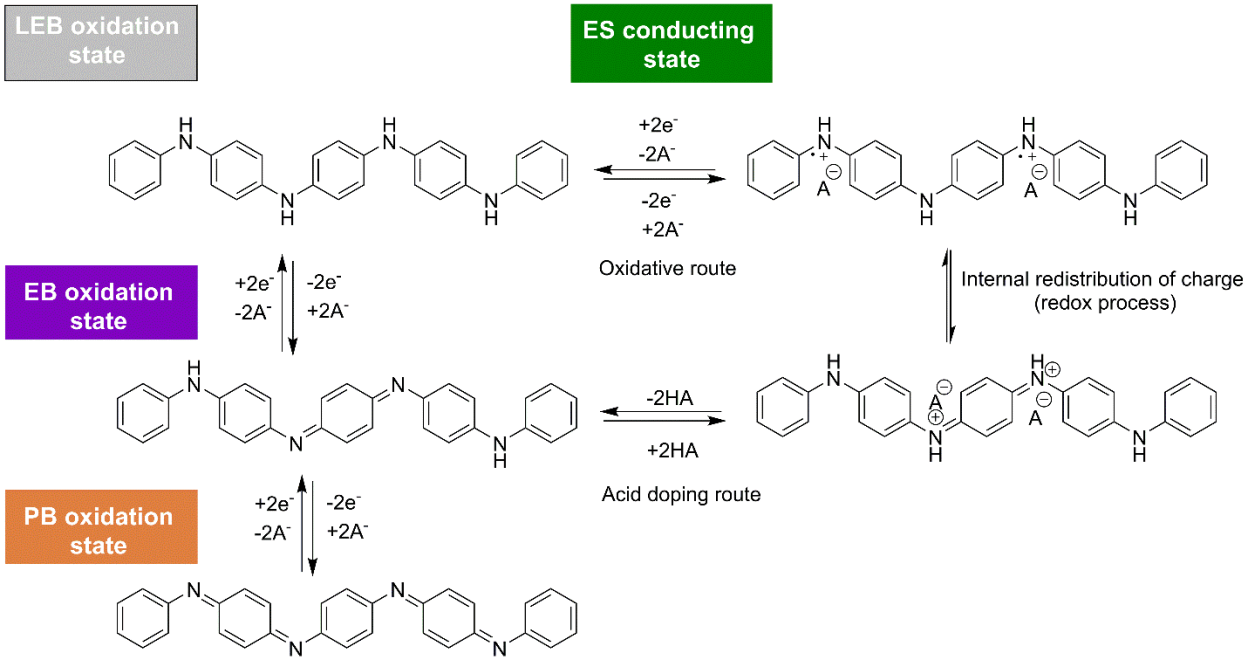

Figure 1.11 The oxidation states of **TANI**.

1.5 Amphiphiles and self-assembly

The term "molecular self-assembly" is defined as the spontaneous arrangement of molecules into stable and well-defined structures under equilibrium conditions, directed by noncovalent bonds.[48] Soft van der Waals interactions,[49] electrostatic,[50] π-π stacking,[51] hydrophobic and hydrophilic interactions,[52] and hydrogen bonds[53] can play a distinctive role in generating constructs with nanoscale dimensions.[54] The predominant noncovalent interactions that are observed for self-assembled systems and their strengths are presented in **Table 1.1**. The most

noteworthy examples of self-assembly are observed in biological systems, the most prominent being DNA, where two complementary helical strands become intertwined via hydrogen bonding and π-π stacking to form a highly organised and hierarchical structure.[55]

Researchers continue to be fascinated by self-assembly as a strategy to create (soft) nanostructures from various platforms, as discussed in various previous reviews.[56, 57, 58] As the field has developed and matured, recent advances have shown that it is now possible to use self-assembly to control structures over multiple length scales, and to prepare well-defined three-dimensional (3D) objects.[59]

Table 1.1 Table of some common interactions that are utilised in self-assembly and their strengths.[60]

Interaction	**Strength (kJ mol^{-1})**
Van der Waals	50
H-bonding	5-65
Coordination bonding	50-200
Amphiphilic	5-50
Ionic	50-250
Covalent	350

With this level of control over structure now possible, current challenges include exerting a similar level of control over both structure and function. Applications of such assembled functional constructs are emerging in a number of important areas: for example, our group showed recently that the ability to control the length of well-defined self-assembled fibre-like micelles can be utilized to control function in simple OFET devices.[61] Carefully designed peptide-based materials have shown potential to be applied as smart devices for biomedical applications.[62,63] Tuning the self-assembled structures in supramolecular materials has emerged as a new strategy to improve the performance in cancer diagnostics and therapy, finding application in the field of nanomedicine.[64,65] Further attractive properties that have been shown for nanostructured soft materials include self-healing,[66] self-regulation and emergent self-

replication[67] and artificial enzyme functionality,[68] of potential interest in, amongst others, bioelectronic applications.

Broadly speaking, one of the most widely studied self-assembled systems is that of surface-active agents, or surfactants. These species are amphiphilic and are composed of two distinct molecular regions, a hydrophilic (polar) head group and a hydrophobic (nonpolar) tail group. There are three main classes of amphiphiles, conventional amphiphiles, bolaamphiphiles and gemini amphiphiles. In a conventional amphiphile, there is one hydrophilic head group covalently linked to a hydrophobic tail. However, bolaamphiphiles comprise of two hydrophilic head groups, symmetric or asymmetric, covalently linked to a hydrophobic tail. In gemini amphiphiles, two hydrophilic head groups are connected by a spacer to two hydrophobic tails as shown in **Figure 1.12**. It can be noted that the concept of amphiphiles can be applied to polymers to form polymeric amphiphiles that have a hydrophobic tail and a hydrophilic head group linked covalently.[69] In addition, amphiphiles can also be classified depending on the charge on the head group: cationic, anionic, zwitterionic and non-ionic as shown in **Figure 1.13**.[70]

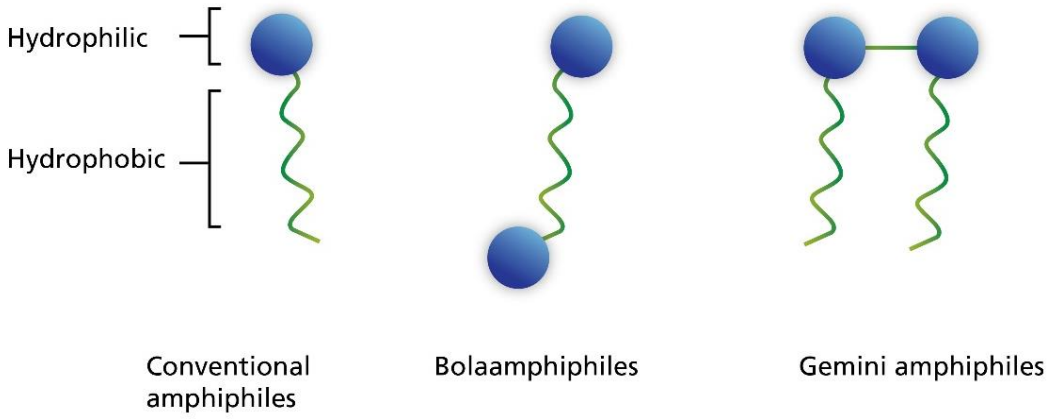

Figure 1.12 The three main types of amphiphiles, classified by hydrophobic and hydrophilic groups.

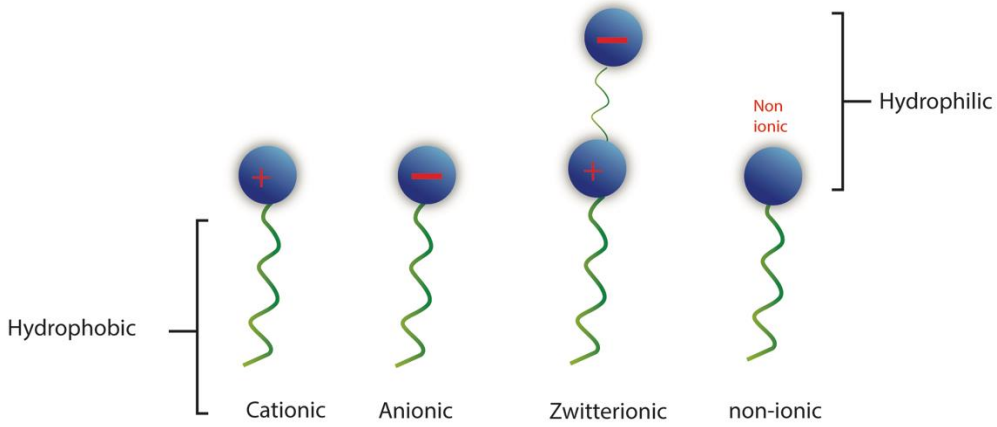

Figure 1.13 The common types of surfactants, classified by the headgroup charge: cationic, anionic, zwitterionic and non-ionic, respectively, from left to right.

The most striking feature is the ability of surfactants to change the interfacial energy of water. This is a consequence of unfavourable interactions between the hydrophobic sections and water. In aqueous solution, the surface tension and free energy of the system are decreased as a result of the surfactants adsorbed at the air-water interface, with polar headgroups exposed to the water and hydrophobic parts exposed to the less polar air. As concentrations increase surface tension decreases and once the interface is completely saturated, the additional surfactants will not cause any further decrease in surface tension. In order to segregate the hydrophobic part of the compound from the polar solvent, surfactants will be forced to aggregate in solutions and form self-assembled structures. In the aggregates, the hydrophilic part is in contact with the polar solvent, however the hydrophobic regions are sheltered.[52,71] The self-assembly of the amphiphile into micelles (spherical structures for the classical single-chained surfactant), and the process of formation of micelles is called micellisation. This occurs spontaneously above the critical micelle concentration (CMC). Above the CMC, the molecules aggregate and form micelles with a hydrophobic interior and hydrophilic exterior.[72] The CMC is affected by several factors, the most important of which is the length of the hydrocarbon chain.[18,19] In addition, the nature of the hydrophilic groups is also influential. These micelles can have different shapes and sizes depending upon several factors, including the type of surfactant, concentration and the solution

conditions.[73] These micelles can be spherical, globular, rod-like or vesicles, as seen in **Figure 1.14,** and are driven by decreasing unfavourable interactions of the hydrophobic part of surfactants with water (i.e. the hydrophobic effect). The hydrophobic effect arises when a surfactant nonpolar part appears in water, causing an interruption in the ordering of water molecules around the unassociated hydrophobic molecule. This interruption causes a decrease in entropy. Further, once these hydrophobic tails self-assemble into micelles. The "cage" of water molecules released of into the bulk, resulting in an increase in entropy. Some favourable enthalpic contributions are also anticipated as a result of the reformation of hydrogen bonds to bulk water. This reformation causes individually solvated hydrophobic groups to aggregate, resulting the high-energy interfacial water release.[52,69,71]

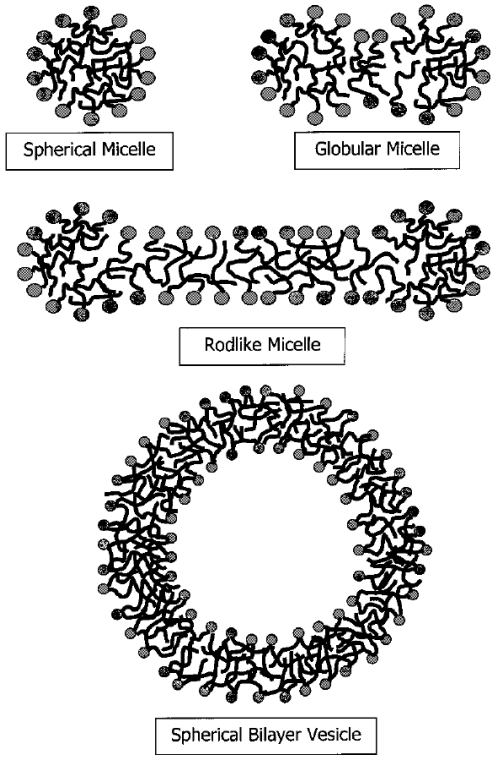

Figure 1.14 Micelles of various types.[21]

1.5.1 Packing parameter

The self-assembled structures depend on the chemical nature and architecture of the amphiphiles, the latter of which is defined by a geometric parameter, the packing parameter, p. The packing parameter can be used to predict the structure of the aggregate using the equation

$$p = v / a_0 l_c \qquad \text{Equation 1}$$

where v is the volume of the hydrophobic chain, l_c is the critical chain length, and a_0 is the surface area of the hydrophilic head group. With changes in these parameters, it is possible to predict the structures of aggregates: spherical ($p \leq \frac{1}{3}$), cylindrical ($\frac{1}{3} < p < \frac{1}{2}$), vesicles or flexible bilayer ($\frac{1}{2} \leq p < 1$), lamellar or planar bilayer ($p = 1$), and even inverted structures ($p > 1$).[70] The packing parameter has a strong influence on the morphology and size of the self-assembled structures as can be seen in **Figure 1.15**. The packing parameter shows the importance of the head group in identifying the geometry of the surfactant.[74] However, the tail group also has an impact on the equilibrium aggregate formation. Furthermore, the tail has a significant effect in the construction of rod-like micelles, spherical micelles and spherical bilayer micelles. The easiest way to demonstrate the packing parameter is by varying the tail length or changing the nature of the head group.

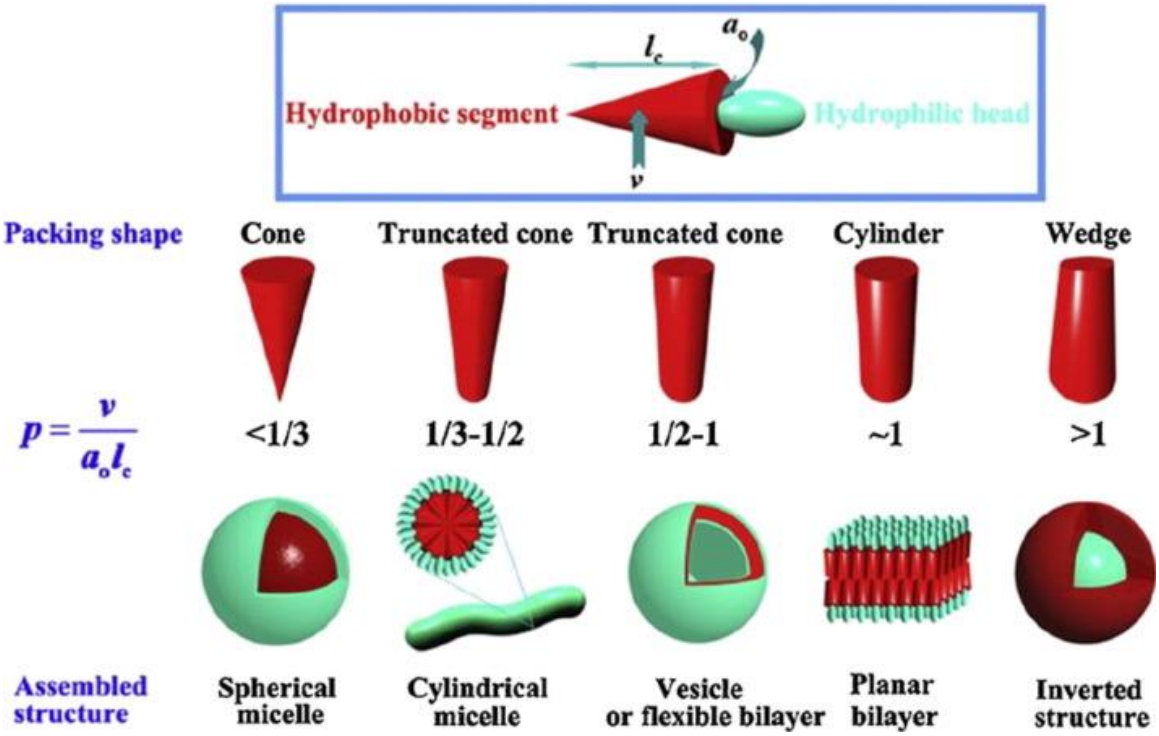

Figure 1.15 The variations of the self-assembled morphologies depending on the p (packing parameter).[75]

As an example of the influence of the packing parameter of the single-tailed amphiphiles on the self-assembled structures, Kunitake *et al*. [76] discussed in detail the factors that play an essential role in the formation of self-assembled structures and investigated the relationship between the amphiphile structures and the self-assembled morphology. The effect of the length and the structure of hydrophobic tail, either branched or linear chains, have been investigated. They found an amphiphile with an alkyl tail >7 C atoms could self-assemble into a stable bilayer vesicle or lamellar structures. The amphiphiles with a long alky tail possess stronger van der Waals interactions, which is essential to form a stable self-assembled structure. However, branching decrease packing and van der Waals interactions, weakening the self-assembled structure. Although van der Waals forces are the weakest of the noncovalent interactions, the accumulation of these forces over large length-scales have impact on the self-assembly. They furthermore investigated the influence of the rigidity of the various aromatic core of an amphiphile such as

diphenylazomethine, biphenyl, azobenzene and azoxybenzene units. The variations of the rigid core showed a profound effect on morphology as shown in Figure 1.16, with multiwalled vesicles formed when using diphenylazomethine unit as the rigid core. However, globular aggregates with an average diameter of 200-300 Å formed when biphenyl or azobenzene were used a rigid segment in the tail. In terms of the effect of head group, ammonium amphiphiles with an azobenzene core self-assembled into globular structures, while stacked disks are formed with a phosphocholine head group. Bilayer vesicles are formed when sulfonate is used as the head group.[76]

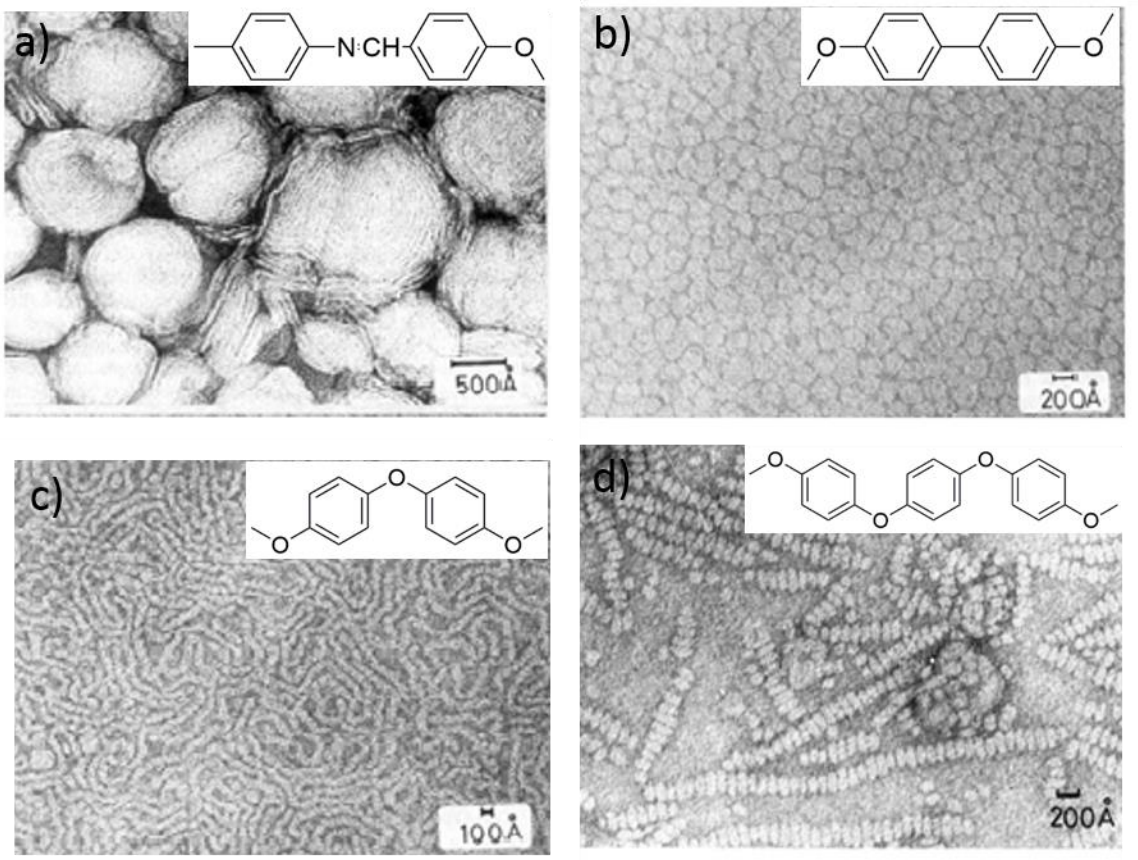

Figure 1.16 TEM images of the variations of the self-assembled morphologies a) multiwalled vesicles, b) globule structures, c) tubes, d) stacked disks, depending on the rigid core structures as depicted in the inset.

The modification of an amphiphilic structure could imply a tunable self-assembled structure from 0D to 1D structures such as micelles to fibers or from 1D to 2D structures such as from fibers to

sheet or planar structures.[77,78,79] To further illustrate this, Zhang and his group investigated the effect of packing parameter of cationic bolaamphiphiles bearing mesogenic cores (CBMs). They designed and synthesised a variety of CBMs based on bipyridine as mesogenic core with different head groups; various alkyl tails and the introduction of different counterions were also investigated.[77] A symmetric bolaamphiphile (5,5-B2NBr8) comprised of dipyridinium dibromide and functionalised with C8 alky tails, bearing bipyridine as a core, self-assembled into a long nanofibrous structure with a uniform width of 9 ± 1 nm. A fibrous structure with a smaller width of 7 ± 1 nm was observed when the head groups were changed from pyridinium to triethylammonium (TEA), suggesting that steric hindrance induced by the triethylammonium groups restricts the packing across the width. The length of alkyl tail was also investigated for 5,5-B2NBr with no fibrous structures observed in 5,5-B2NBr4 with a short alkyl tail (C4). However, 5,5-B2NBr12 with a long alkyl tail (C12) self-assembled into a helical fibrous structure with a width of 12 ± 2 nm. Furthermore, changing the position of the alkyl tails attached to the bipyridine could cause a profound effect on the self-assembled structures. 4,4-B2NBr8 self-assembled into sphere-like structures with an average diameter of 34 ± 4 nm rather than fibres. The introduction of larger counterions such as tosylate increased the packing parameter, resulting in 2D structures.[78] The self-assembled structures of cationic CBMs exhibit a transformation from fibrous to planar structures, resulting from the introduction of tosylate instead of bromide counterions as shown in **Figure 1.17**.

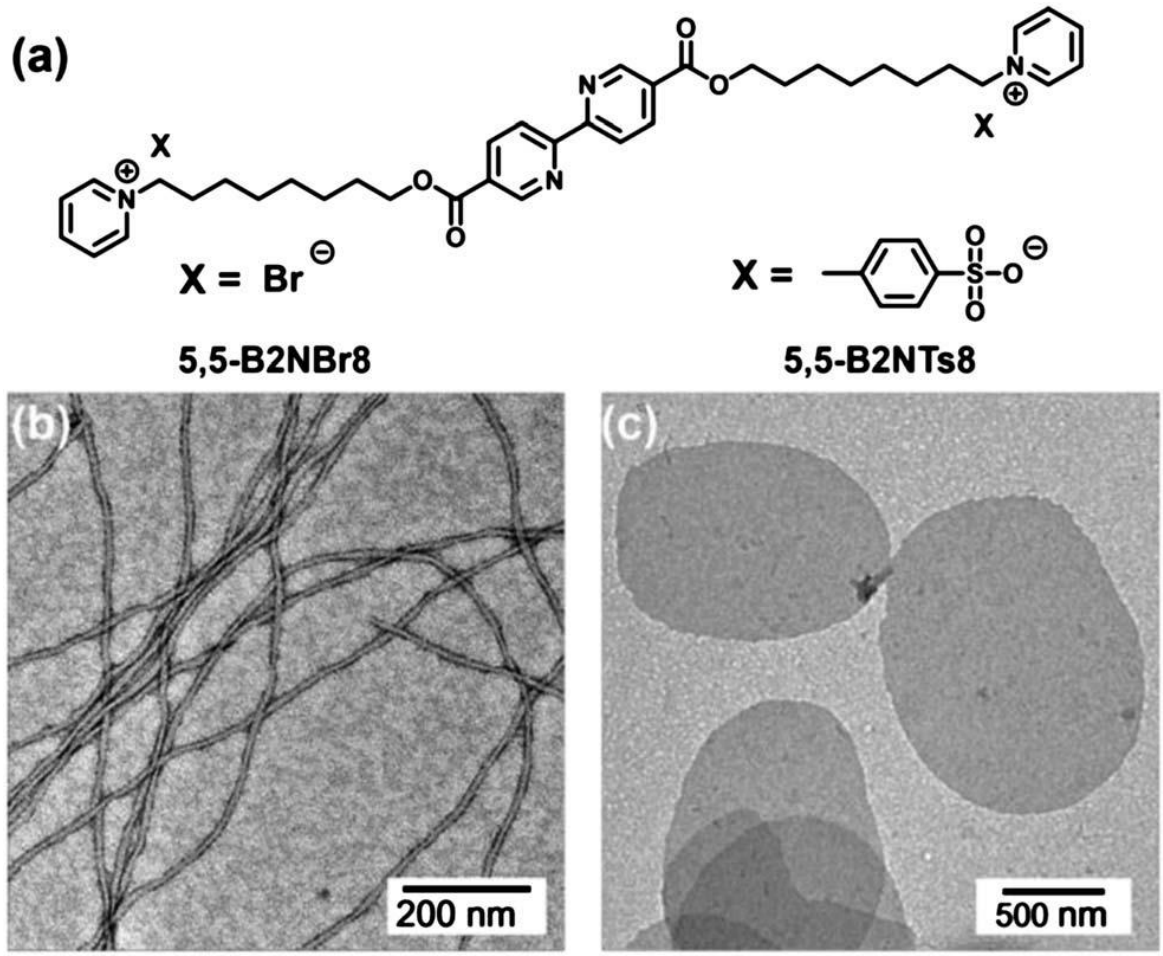

Figure 1.17 Different self-assembled structures of bolaamphiphiles 5,5-B2NX8 with different counterions, X= b) bromide ion and c) tosylate ion.[78]

The same group studied the effect of the counterion to different bolaamphiphile systems.[79] They synthesised cationic bolaamphiphiles based on diaryldiketopyrrolopyrrole (DPP) with different counterions (bromide and tosylate). The variation in the counterion caused a change in the self-assembled structures of DPP-11, 1D rod-like structures with an average width of 3.2± 0.1 nm and a length of ca. 70 nm were observed for DPP-11-Br as shown in **Figure 1.18a**. However, 2D planar structures with a width and length on the microscale were observed in case of DPP-11-Ts as shown in **Figure 1.18b.**

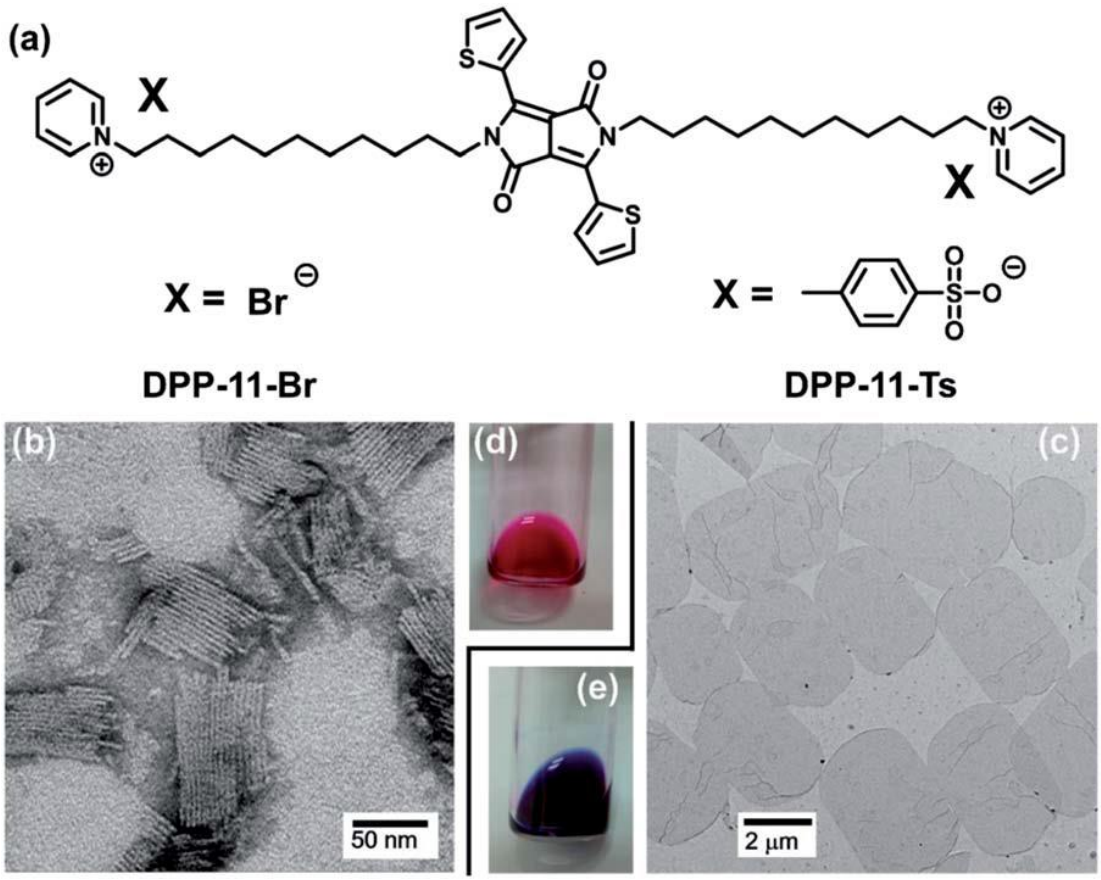

Figure 1.18 Different self-assembled structures of bolaamphiphiles DPP-11-X with different counterions, X= b) bromide ion and c) tosylate ion.[79]

1.5.2 Electroactive amphiphiles

Electroactive amphiphiles (EAAs) are a subclass of the family of amphiphiles, described as a class of amphiphiles functionalised with moieties that exhibit redox-switchable behaviour such as viologens, ferrocenes or oligo(aniline)s. In a recent review dedicated to this interesting class of materials classified according to their tunability in terms of structure and function, whilst highlighting possible applications as described in **Scheme 1.3**.[80]

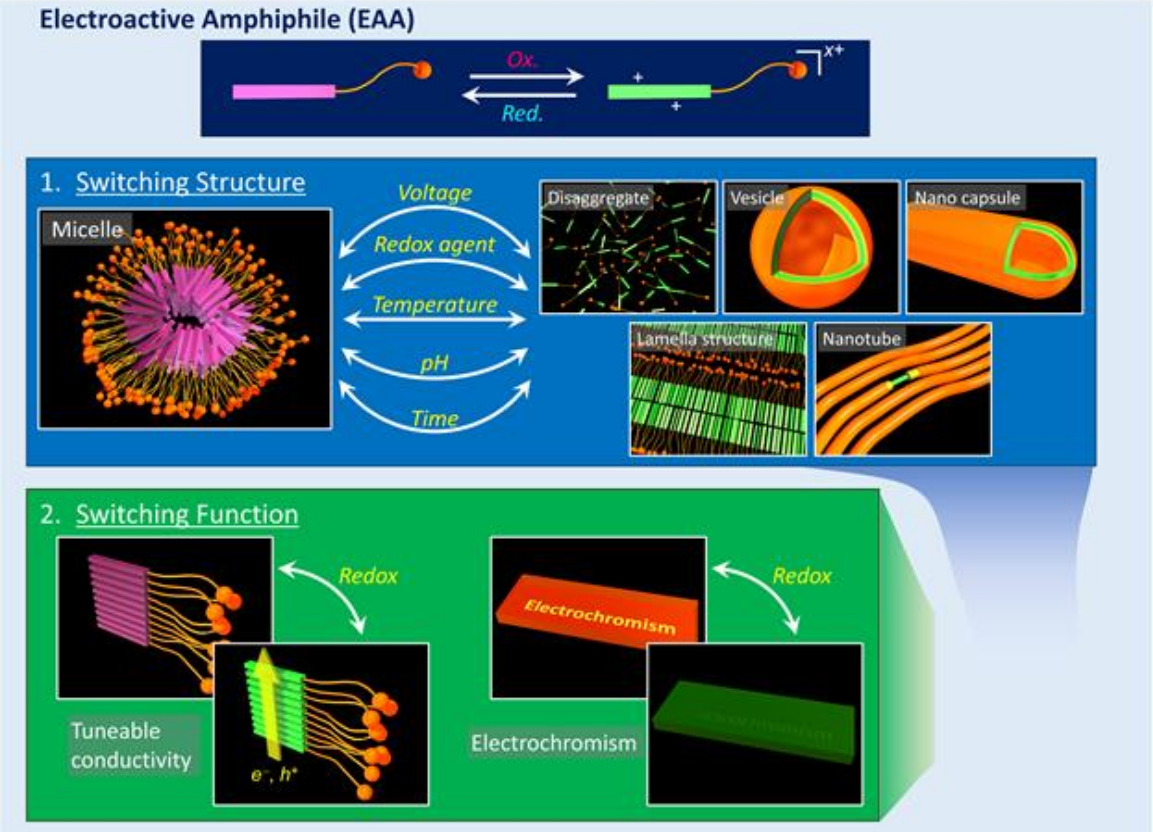

Scheme 1.3 EAAs and their switchable properties.[80]

1.5.2.1 Switching structure

The interesting aspect of EAAs is the ability to change their morphology by introducing an external stimulus, such as an oxidising/reducing agent or applied voltage. The structural change could either be a simple transition from an aggregated structure to non-aggregated monomer, or a more complicated one, i.e. transition from one aggregated structure to another aggregated structure such as from a spherical micelle to a nanorod. Some examples of structural switches are provided below with some proposed relevant applications.

Ferrocenyl-derived EAAs are the most studied example of EAA materials, and their self-assembling behaviour has been explored in detail. In general, ferrocene exhibits differences depending on whether these materials are reduced/ oxidised, existing as non-polar neutral Fe (2+) or as a polar ferrocenium cation (Fe (3+)), respectively. This change can lead to noticeable differences in the behaviour and solubility in water of any molecule containing this moiety. EAAs

based on ferrocene are synthesised in various architectures, either single- and double-tailed amphiphiles,[81,82] or amphiphiles functionalised with other molecules,[83,84] all showing pronounced changes in self-assembly with a change in oxidation state. Alkan and co-workers synthesised a ferrocene block co-polymer from ethylene glycol and glycidyl ether that aggregated into micelle-like structures in aqueous solutions; these structures were stable for months in the reduced form.[85] However, when oxidised, the micelles dissolved as ferrocenium cations formed, resulting in the conversion of the amphiphilic block copolymers to an amphiphile with two hydrophilic moieties. There are many possible uses to generate targeted structures, mainly focused on the controlled uptake and release of a hydrophobic substance that can be protected within and delivered by an EAA. Amphiphilic block copolymers based on ferrocene can be used to load and release a hydrophobic substance that could be used as a smart redox-responsive system.[85,86,87] The assembly and disassembly behaviour, induced by oxidation and reduction processes of a ferrocenyl EAA can be exploited also for purification purposes, providing microscale separation of hydrophobic compounds as reported by Rosslee and Abbott.[88]

Another interesting example of an electroactive material is tetrathiafulvalene (TTF). TTF is a π-electron donating molecule with multiple oxidation states that can be easily converted. Moreover, the presence of π–π and sulphur–sulphur interactions allows TTF and its derivatives to self-assemble into complex nanostructures.[89] TTF is a hydrophobic molecule and has been functionalised with a hydrophilic moiety to prepare a redox-responsive amphiphile that could be disrupted by introducing an oxidant such as $Fe(ClO_4)_3$.[90] The self-assembled structures of TTF-based materials could be interrupted when the TTF moiety was oxidised to the more hydrophilic radical cationic and dicationic states, as result of the introduction of electrostatic repulsion between amphiphiles. The aggregate morphologies (i.e., before disassembly) could assemble in various structures depending on the molecule shape; a dumb-bell-shaped amphiphile formed vesicles, while wedge-shaped amphiphiles formed smaller micelles.[91]

EAAs based on oligo(aniline)s are of interest and have been exploited for various application such as drug delivery applications owing to their biocompatibility and also for preparation of devices and sensor. An interesting feature of oligo(aniline)s is the ability to possess different oxidation

states as discussed previously. The states can be reversibly accessed with a chemical oxidant or oxidising voltage.

Wu *et al.* prepared amphiphilic diblock polymers based on TANI, where TANI was functionalised with poly(N-isopropylacrylamide), (TA-b-PNIPAM).[92] These amphiphilic structures self-assembled into large vesicles (~ 320 nm in diameter) and possess multiple bilayer structures that can be utilised for loading of the anti-cancer drug doxorubicin. When the amphiphiles were oxidised to the EB state the vesicle structures were damaged, resulting in the release of the drug. The amphiphiles showed multiple responsive properties with applied voltage as well as temperature and pH changes.[92]

An amphiphilic rod-coil molecule comprising TANI bearing a poly (ethylene glycol) group (denoted as TAPEG) was prepared.[93] Theses amphiphiles aggregated into vesicle-like structures in the LEB state (~ 8 nm in diameter, **Figure 1.19**). The oxidation state of the amphiphiles changes from LEB to EB by introducing an oxidising voltage, resulting in the split of vesicles into smaller puck-like micelles (~4 nm in diameter). The changes in morphology were explained by the difference in the packing densities between LEB and EB structures. In the EB state, there is an amine–imine hydrogen bonding formed that is not available in the LEB state. These vesicles can be re-formed by introducing a reducing voltage in a reversible fashion. The electrically switchable behavior of these amphiphiles can be useful for molecular delivery systems in biosensing and microfluidic devices.

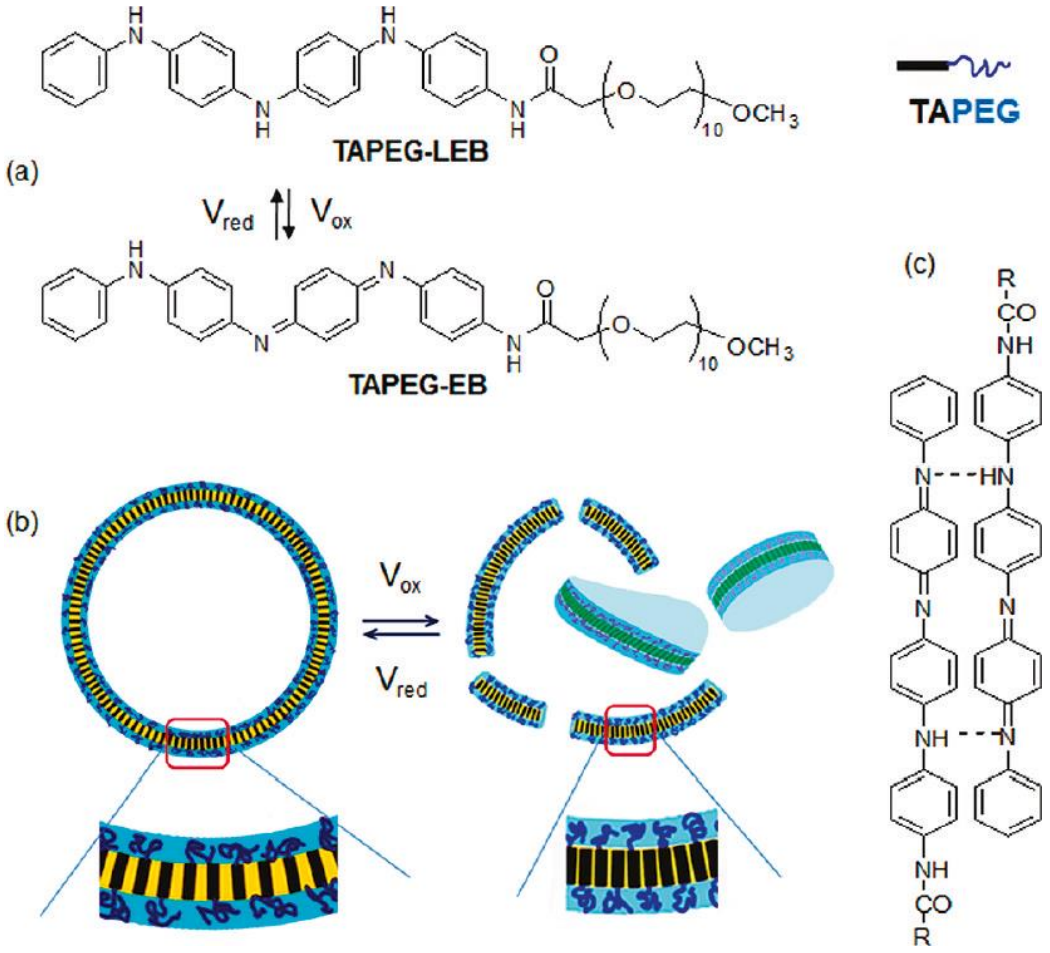

Figure 1.19 Voltage-responsive TAPEG rod-coil EAAs in aqueous solution, a) Chemical structures of TAPEG in the LEB and EB oxidation states, b) Schematic representation of redox switching between vesicles and puck-like micelles induced by the change in packing density in the membrane core, c) Amine-imine intermolecular hydrogen bonding in the EB form of TAPEG.[93]

The same group extended their studies to more complex structures (multiblock rod−coil polymer comprising hepta(aniline)s and oligoethylene glycol (OEG)).[94] Theses amphiphiles showed aggregation−disaggregation behaviour depending on the oxidation state. In the EB state, the polymers aggregated into networked puck-shaped micelles. However, reduction to the LEB state caused the micelles to be destroyed which can be an indicative of the disaggregation behaviour, resulting in water- soluble polymers as shown in **Figure 1.20**. The switchable behaviour of the assembly and disassembly of these amphiphiles could be useful for drug delivery.

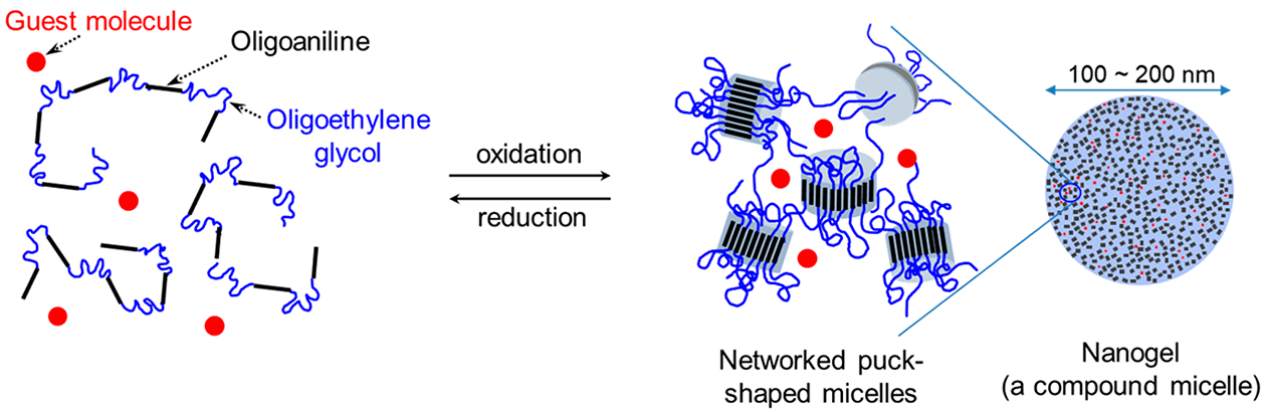

Figure 1.20 The amphiphilic multiblock rod–coil polymers aggregated into networked puck-shaped micelles and capture and release of guest molecules via the redox-responsive switching between LEB and EB state.[94]

EAAs based on oligo(aniline)s have attracted more attention owing to their redox-responsive self-assembling behaviour that can be used to tune and control the morphology in an elegant way. Here, Wu and co-workers synthesised a hybrid molecule based on tri(aniline) covalently linked with a polyoxometallate (POM).[95] It is worth mentioning that the structure here might not fit with that of a classical EAA, however the assembled system showed different morphologies depending on the oxidation state of the tri(aniline). When the oxidation reaction was performed to change the EB state to the PB state, the morphology changed from spherical vesicles to cylindrical vesicles (with 200 nm length and 100 nm diameter) as shown in **Figure 1.21.** However, reduction to the LEB state caused an increase in the size of spherical micelles from a diameter of 200 nm to 250 nm. This tunable self-assembling behaviour could be used for controlled surface wettability.

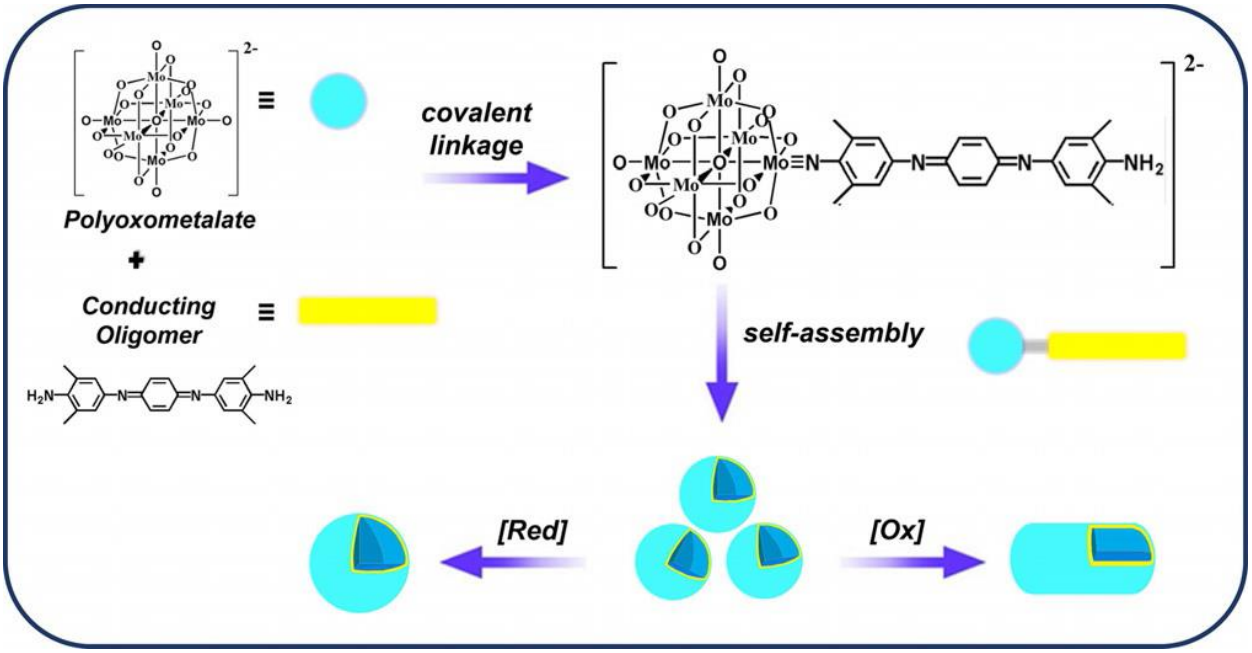

Figure 1.21 Schematic representation of POM-**TANI** and their self-assembled structure in different oxidations states.[95]

1.5.2.2 Switching function

Here we show some of the EAAs that respond to changes in oxidation state without corresponding in structural change. These EAAs could be exploited as a platform to build materials, in order to enhance the properties for conductivity, in electrochromic devices or in biomedicine. Some examples of functional switches are provided below with some proposed relevant applications.

Oligo(aniline)s are biocompatible molecules and have been functionalised with other bioactive moieties to enhance biochemical processes. Recently, Arioz and co-workers synthesised a peptide functionalised with an electroactive species, tetra(aniline).[96] The EAA-peptide self-assembled into fibrillar network structures and were utilised as scaffold for nerve regeneration. More interestingly, they found that the EAA-peptide improved neural cell differentiations compared to that of nonconductive materials.

Another interesting aspect of EAA-based materials is the ability to control the reaction rates of cells. Kaneko *et al.* designed an amphiphilic, cell-membrane permeable polymer which comprised

2-methacryloyloxyethyl phosphorylcholine and vinyl ferrocene as the redox-active unit (denoted as pMFc).[97] They found the EAA-based materials to be effective in permeating the cell membrane as an electron acceptor, resulting in cell growth improvement.

Some EAA materials exhibit electrochromic properties where these materials show reversible colour changes on application of a voltage. These materials could be desirable in various applications such as smart glass windows, sensors and electrochromic devices. Oligo(aniline)s are well-known for their electrochromic behaviour and rich redox properties with various oxidation states and each one exhibiting different colours. Hence, EAAs-based on oligo(aniline)s have attracted more attention in the preparation of electronic devices. Cao and co-workers synthesised a star-shaped block copolymer comprising a benzene core bearing three TANI-polyethylene glycol arms.[98] The EAA self-assembled into micelle-like structures in solution. Furthermore, micelles in solution formed a high-quality thin film when cast onto an indium tin oxide (ITO) substrate as presented in **Figure 1.22**, resulting in the improvement in electrochromic properties.

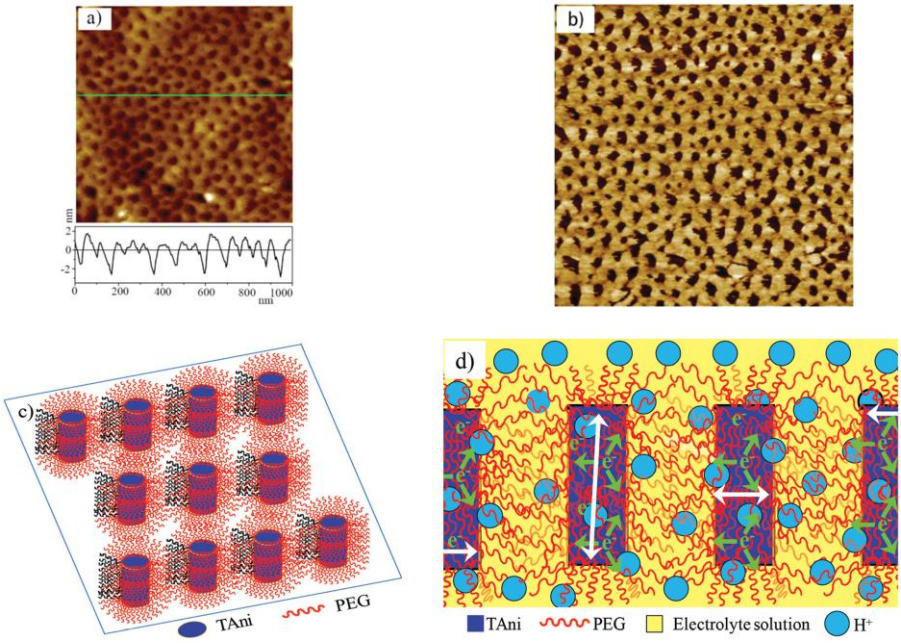

Figure 1.22 AFM images a) and phase contrast of (TANI-b-PEG)$_3$ copolymer thin film Schematic illustrations of c) the self-assembly of (TANI-b-PEG)$_3$ thin film, and d) ion and electron diffusion pattern in (TANI-b-PEG)$_3$ thin film in HCl electrolyte solution.[98]

The delocalised π-electron systems of EAA-based materials could be attractive and desirable for applications in the areas of organic electronics and photovoltaic.[99] The tunable self-assembled structures of these amphiphiles provide a feasible way to control the structures and minimise defect and domain boundaries in the π-conjugation chain.[12] As a result, charge carrier mobility could be increased.

The presence of charge carriers also provides conductivity for EAA-based materials. For instance, poly(aniline) and oligo(aniline)-based EAA are nonconductive materials in the LEB, EB and PB states, however when these EAAs are doped either with an acid or oxidative agent, this results in the conductive ES state. Our group is dedicated to exploit the properties of oligo(aniline)s to construct such interesting EAA based materials. **TANI**-based amphiphiles bearing a

trimethylammonium headgroup (**TANI-PTAB**, TANI-pentyl trimethylammonium bromide) were designed and their properties explored in detail.[100] In the EB state, **TANI-PTAB** self-assembled into wire-like structures with a 3 nm width. **TANI-PTAB** self-assembled into conducting nanowires with a 6 nm width when doped with camphorsulfonic acid as shown in **Figure 1.23**. These conducting nanowires could be interesting for organic electronics applications. More examples of this class of EAA-based materials will be discussed in terms of their design and properties, as explored in the following chapters.

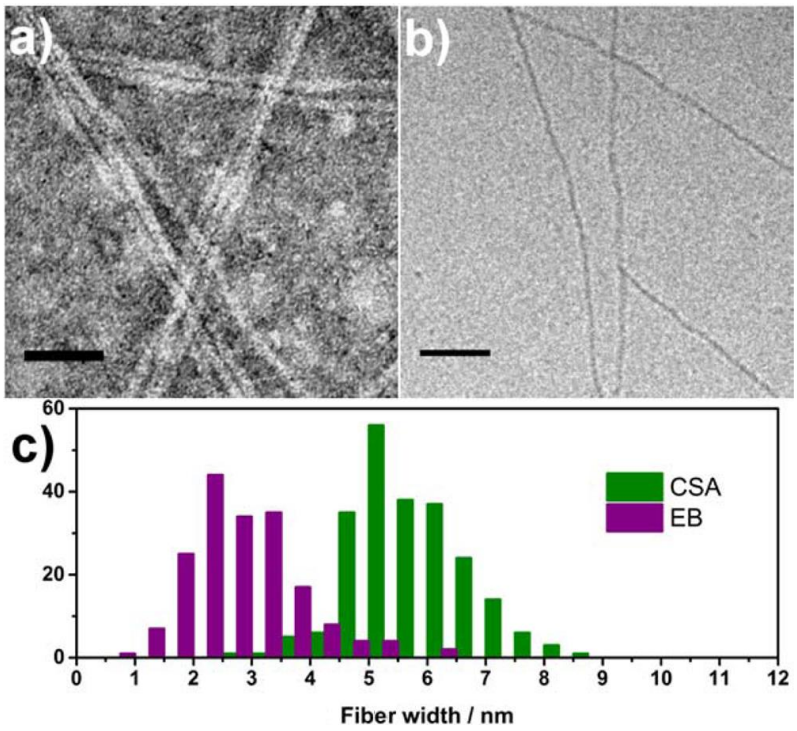

Figure 1.23 a) TEM (stained with 1% uranyl acetate), b) cryo-TEM (unstained) of **TANI(CSA)$_2$-PTAB** (4 × 10−3 M). c) Histogram showing comparison of measured nanowire widths for EB and CSA-doped **TANI-PTAB**. Scale bars: 50 nm.[100]

Overall, an interesting feature of **TANI**-based amphiphiles is the potential to tune the formation of self-assembled structures by changing the oxidation state or the structure of the amphiphiles. To the best of our knowledge, exploiting the role of the packing parameter of TANI-based amphiphiles has not been explored or studied before. Hence, our studies are focused on the role of packing to tune the morphology. As mentioned earlier, the packing parameter is reliant on the length and volume of hydrophobic species and the area of the head group. Hence, it is possible to alter the length of the hydrocarbon tail, which will lead to changes in the packing parameter and thus yield different self-assembled morphologies. Changing the volume of the tail would normally require further synthetic efforts (i.e., adding another chain, or adding branches to the existing chains). However, doping the EB state of **TANI** based amphiphiles with different types (with different volumes) of either inorganic or organic acids can lead to vast changes in the volume of the hydrophobic **TANI**-based tail structure. In other words, it is a novel strategy to tune the self-assembled supra-amphiphilic structures by adding different types of acids present in the ES state. Electrostatic interactions between the protonated imines and the counterions of the added acid form a so-called supra-amphiphile.[58] However, a **TANI**-based amphiphile can be de-doped by the addition of base, which leads to the transformation of the structure to the original morphology. Similarly, morphology can be altered by changing the size of the head group area; these possibilities are presented in **Figure 1.24**.

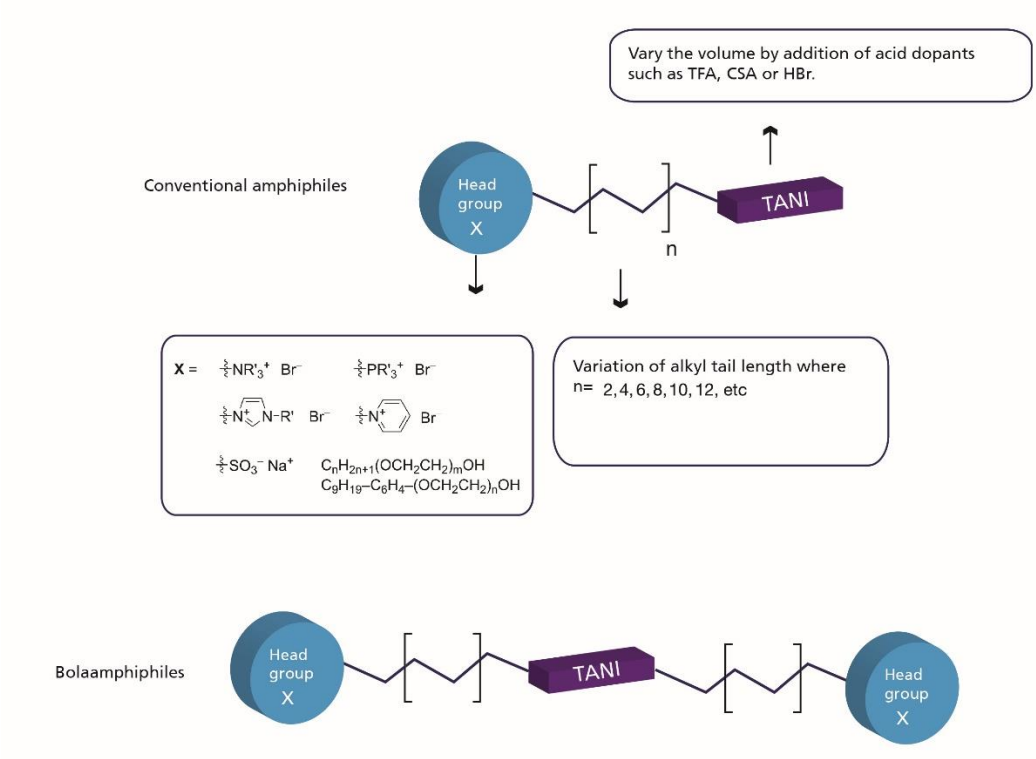

Figure 1.24 The possibility to tune the self-assembled structure of amphiphiles by tuning the packing parameter.

1.6 Aims and objectives

The overall aim of this project is the preparation of tunable water-soluble electroactive nanostructures based on oligo(aniline) amphiphiles.

To fulfil this aim, three objectives have been identified and the work towards achieving these goals is detailed below.

The first objective is to synthesise and characterise **TANI** block-like structures: a range of single-tailed amphiphiles and bolaamphiphiles consisting of Ph/NH_2 **TANI** and, NH_2/NH_2 **TANI** were functionalised with alkyl chains (C6 and C8). Ph/NH_2 **TANI**-C_6 will be quaternised with either trimethylamine to form ammonium cationic amphiphiles ($C_6Me_3N^+Br^-$) denoted as **TANI-PTAB** or trimethylphosphine to form phosphonium cationic amphiphiles ($C_6Me_3P^+Br^-$) denoted as **TANI-PTPB**. NH_2 /NH_2 **TANI**-C_6 will be quaternised with trimethylamine to form ammonium cationic bolaamphiphiles ($C_6Me_3N^+Br^-$) denoted as **TANI-(PTAB)$_2$** and ($C_8Me_3N^+Br^-$) denoted as **TANI-(HTAB)$_2$**. NH_2/NH_2 **TANI-**C6Br will be quaternised with trimethylphosphine to form phosphonium cationic bolaamphiphiles ($C_6Me_3P^+Br^-$) denoted as **TANI-(PTPB)$_2$.** All the structures of the synthesised materials are presented in **Figure 1.25**.

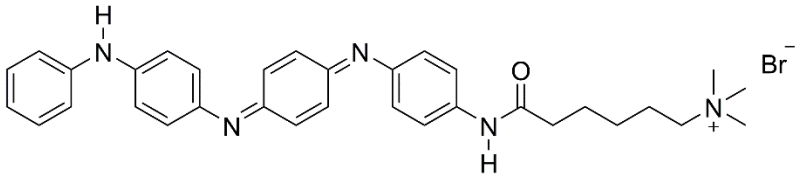

TANI-PTAB

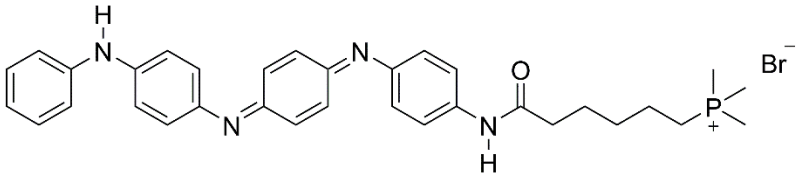

TANI-PTPB

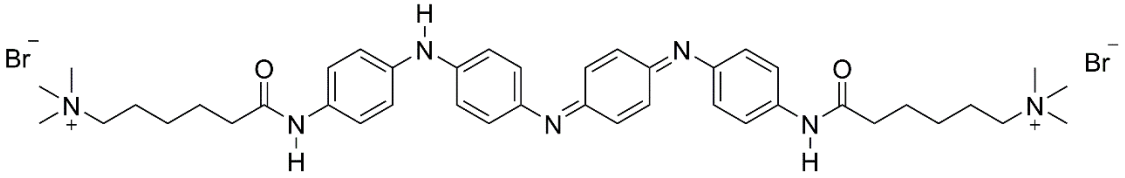

TANI-(PTAB)$_2$

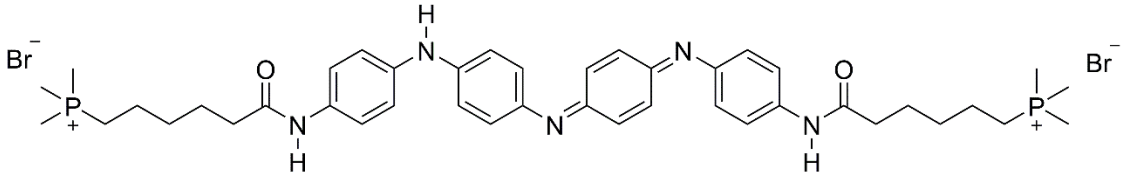

TANI-(PTPB)$_2$

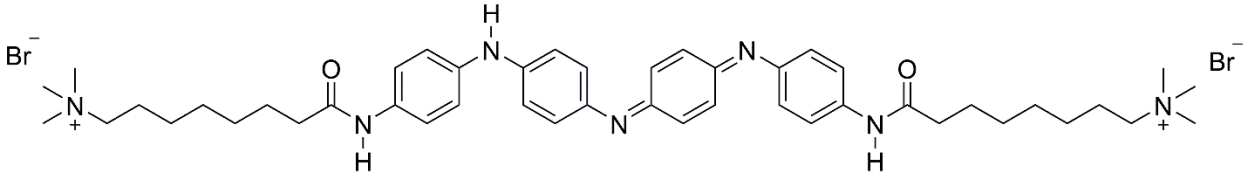

TANI-(HTAB)$_2$

Figure 1.25 The synthesised **TANI**-based amphiphiles investigated in this thesis.

<u>The second objective</u> is to prepare self-assembled nano or microstructures of all the synthesized amphiphiles in aqueous solution. Various spectroscopy, microscopy and scattering techniques were used to gain a full picture of the morphology of aggregates.

The third objective explores doping the diblock or triblock architectures of **TANI**-based amphiphiles with acids of varying volume to form tunable structures through addressing the packing parameter in a noncovalent fashion. Finally, the effect of type of dopants on the electroactivity of the synthesized oligomers will also be explored.

1.7 Outline of thesis

In order to fulfil the aim and objectives, the experimental work of this thesis is organised in the following chapters:

Chapter 2 describes the detailed synthesis of a number of cationic amphiphiles (i.e. TANI functionalised with an alkyl chain terminated with a cationic headgroup). TANI-based amphiphiles, either single-tailed or bola structures, were prepared in the EB state for further investigation of their self-assembling behaviour. The prepared materials are characterised by ^{1}H NMR, MS-MALDI/ESI, FT-IR, UV/Vis-NIR and elemental analysis.

Chapter 3 focuses on studying the self-assembling behaviour of the single-tailed amphiphiles (**TANI-PTAB**) and (**TANI-PTPB**) using various techniques including UV/Vis, fluorescence, TEM, AFM, temperature-dependent UV/Vis and ^{1}H NMR, SAXS, SANS and XRD. This chapter is comprised of two parts: the first part is focused on the self-assembling behaviour of **TANI-PTAB** in the ES state and it has been modified from W. Lyu, M. Alotaibi, O. A. Bell, K. Watanabe, R.Harniman, B.M. Mills, A. M. Seddon, S. E. Rogers, S. M. King, W. Yan and C. F. J. Faul An addressable packing parameter approach for reversibly tuning the assembly of oligo(aniline)-based supra-amphiphiles *Chem. Sci.*, 2018, 9, 4392–4401, is used to reflect M. Alotaibi's contributions. M. Alotaibi contributed to the synthesis of **TANI-PTAB** and undertook self-assembly experiments to confirm the formed structures. The second part of this chapter comprises of as yet unpublished results of tunable self-assembled nanostructures from electroactive amphiphiles. It mainly focuses on **TANI-PTPB** and its self-assembling behaviour in the EB and ES states. AFM images in this chapters were measured by Dr R. Harniman. SAXS and SANS samples. SAXS and SANS profiles in chapter were collected by Dr Sarah Rogers and Dr

Annela Seddon. The computational studies were carried out in collaboration with Dr Ben Mills**.** This chapter shows the switchable behaviour of **TANI**-based amphiphiles using the addressable packing parameter (APP) approach.

Chapter 4 focuses on studying the self-assembling behaviour of the bolaamphiphiles, **TANI-(PTAB)$_2$** and (**TANI-(PTPB)$_2$** using various techniques such as UV/Vis, fluorescence, TEM, AFM, temperature-dependent UV/Vis and ^{1}H NMR, SAXS, SANS and XRD. This chapter extends the comparison with the single-tailed amphiphiles (**Chapter 3**). It contains two parts: the first part presents the comprehensive studies of the self-assembling behaviour of **TANI-(PTAB)$_2$** in the EB and ES state and has been reproduced from the paper has just been submitted," Synthesis and tunable self-assembly of electroactive bolaamphiphiles based on oligo(aniline)s". The second part of this chapter comprises **TANI-(PTPB)$_2$** and their self-assembling behaviour in the EB and ES states. High resolution-TEM in this chapter was carried out by Dr Sean Davis and Dr Jean-Charles Eloi. AFM images in this chapters were measured by Dr R. Harniman. SAXS and SANS profiles in chapter were collected by Dr Chris hill and Dr Annela Seddon. The computational studies were carried out in collaboration with Dr Ben Mills**.** This chapter shows the switchable behaviour of **TANI**-based bolaamphiphiles using the concept of the addressable packing parameter.

In **Chapter 5** different architectures of non-ionic **TANI**-based amphiphiles functionalised with ethylene glycol are presented, and analysed with a range of measurements including NMR, mass spectrometery and elemental analysis. The challenges of removing the protecting groups of non-ionic amphiphiles are discussed.

Chapter 6 concludes the work of the previous chapters and provides suggestions for future projects and areas of exploration.

1.8 Refences

1 M. H. Petersen, S. A. Gevorgyan and F. C. Krebs, *Macromolecules*, 2008, **41**, 8986–8994.

2 A. P. Kulkarni, C. J. Tonzola, A. Babel and S. A. Jenekhe, *Chem. Mater*, 2004, **16**, 4556–4573.

3 S. Lo and P. L. Burn, *Chem. Rev.*, 2007, **107**, 1097–1116.

4 G. Horowitz, *J. Mater. Res*, 2004, **19**, 1946–1962.

5 C. R. Newman, C. D. Frisbie, A. Demetrio, S. Filho, J. Bredas, P. C. Ewbank and K. R. Mann, *Chem. Mater.*, 2004, **16**, 4436–4451.

6 H. Bai, C. Li, F. Chen and G. Shi, *Polymer*, 2007, **48**, 5259–5267.

7 X. B. Yan, Z. J. Han, Y. Yang and B. K. Tay, *Sensors Actuators B*, 2007, **123**, 107–113.

8 C. Meng, C. Liu and S. Fan, *Electrochem. commun.*, 2009, **11**, 186–189.

9 J. Sung, S. Kim and K. Lee, *J. Power Sources*, 2004, **126**, 258–267.

10 S. Bhadra, D. Khastgir, N. K. Singha and J. H. Lee, *Prog. Polym. Sci.*, 2009, **34**, 783–810.

11 N. Basescu, Z.-X. Liu, D. Moses, A. J. Heeger, H. Naarmann and N. Theophilou, *Nature*, 1987, **327**, 403–405.

12 H. Shirakawa, E. J. Louis, A. G. Macdiarmid, C. K. Chiang and A. J. Heeger, *J. Chem. Soc. Chem. Commun.*, 1977, **16**, 578–580.

13 A. J. Heeger, *Chem. Soc. Rev.*, 2010, **39**, 2354–2371.

14 C. S. Yannoni and T. C. Clarke, *Phys. Rev. Lett.*, 1983, **51**, 1191–1193.

15 A. J. Heeger, S. Kivelson, J. R. Schrieffer and W. -p. Su, *Rev. Mod. Phys.*, 1988, **60**, 781–580.

16 W. P. Su, J. R. Schrieffer and A. J. Heeger, *Phys. Rev. B*, 1980, **22**, 2099–2111.

17 C. K. Chiang, C. B. Fincher, Jr., Y. W. Park, A. J. Heeger, H. Shirakawa, E. J. Louis, S. C. Gau and A. G. Macdiarmid, *Phys. Rev. Lett.*, 1977, **39**, 1098–1101.

18 K. Fesser, A. R. Bishop and and D. K. Campbell, *Phys. Rev. B*, 1983, **27**, 4804–4825.

19 H. Shirakawa, *Angew. Chem. Int. Ed.*, 2001, **40**, 2574–2580.

20 A. Pron and P. Rannou, *Prog. Polym. Sci.*, 2002, **27**, 135–190.

21 J. G. Masters, Y. Sun, A. G. MacDiarmid and A. J. Epstein, *Synth. Met.*, 1991, 41, 715–718.

22 A. G. Macdiarmid, J. Chiang, W. Huang, B. D. Humphrey and N. L. D. Somasiri, *Mol. Crysf. Liq. Cryst.*, 1985, **125**, 309–318.

23 M. Yanılmaz and A. S. Sarac, *Text. Res. J.*, 2014, **84**, 1325–1342.

24 A. G. Macdiarmid, J. Chiang, M. Halpern, W. Huang, S. Mu, L. D. Nanaxakkara, S. W. Wu, S. I. Yaniger, A. G. Macdiarmid, J. Chiang, M. Halpern and W. Huang, *Mol. Crysr. Eq. Cryst*, 1985, **121**, 173–180.

25 J. Stejskal, I. Sapurina and M. Trchová, *Prog. Polym. Sci.*, 2010, **35**, 1420–1481.

26 L. Zhang, M. Wan and Y. Wei, *Macromol. Rapid Commun.*, 2006, **27**, 366–371.

27 Y. Wei, G. Jang, C. Chan, K. F. Hsueh, R. Hariharan, S. A. Patel and C. K. Whitecar, *J. Phys. Chem.*, 1990, **94**, 7716–7721.

28 G. Ciric-Marjanovic, *Synth. Met.*, 2013, **177**, 1–47.

29 E. Song and J.-W. Choi, *Nanomaterials*, 2013, **3**, 498–523.

30 X. Zhang and S. K. Manohar, *Chem. Commun.*, 2004, **20**, 2360–2361.

31 H. D. Tran, J. M. D. Arcy, Y. Wang, P. J. Beltramo, A. Strong and R. B. Kaner, *J. Mater. Chem.*, 2011, **21**, 3534–3550.

32 Q. Tang, J. Wu, X. Sun, Q. Li and J. Lin, *Langmuir*, 2009, **25**, 5253–5257.

33 T. E. Olinga, J. Fraysse, J. P. Travers, A. Dufresne and A. Pron, *Macromolecules*, 2000, **33**, 2107–2113.

34 W. Li and H. Wang, *J. Am. Chem. Soc.*, 2004, **126**, 2278–2279.

35 V. J. Babu, S. Vempati and S. Ramakrishna, *Mater. Sci. Appl.*, 2013, **4**, 1–10.

36 H. Xie, Y. Ma and D. Feng, *Eur. Polym. J.*, 2000, **36**, 2201–2206.

37 C. Anbalagan, S. Palaniappan, A. Puzari, P. Rannou and A. Pron, *Mater. Lett.*, 2007, **61**, 4204–4207.

38 Z. Wei and C. F. J. Faul, *Macromol. Rapid Commun.*, 2008, **29**, 280–292.

39 A. G. MacDiarmid, Y. Zhou and J. Feng, *Synth. Met.*, 1999, **100**, 131–140.

40 Y. Wang, H. D. Tran, L. Liao, X. Duan and R. B. Kaner, *J. Am. Chem. Soc.*, 2010, **132**, 10365–10373.

41 R. A. Singer, J. P. Sadighi and S. L. Buchwald, *J. Am. Chem. Soc.,* 1998, **120**, 213–214.

42 J. P. Sadighi, R. A. Singer and S. L. Buchwald, *J. Am. Chem. Soc.,* 1998, **120**, 4960–4976.

43 Z. Shao, P. Rannou, S. Sadki, N. Fey, D. M. Lindsay and C. F. J. Faul, *Chem. - A Eur. J.*, 2011, **17**, 12512–12521.

44 S. Shekhar, P. Ryberg, J. F. Hartwig, J. S. Mathew, D. G. Blackmond, E. R. Strieter and S. L. Buchwald, *J. Am. Chem. Soc.*, 2006, **128**, 3584–3591.

45 F. Paul, J. Patt and J. F. Hartwig, *J. Am. Chem. Soc.*, 1994, **116**, 5969–5970.

46 Z. Cheraiet, S. Hessainia, S. Ouarna, M. Berredjem and N.-E. Aouf, *Green Chem. Lett. Rev.*, 2013, **6**, 211–216.

47 S. Darnbrough, M. Mervic, S. M. Condon and C. J. Burns, *Synth. Commun.*, 2001, **31**, 3273–3280.

48 G. M. Whitesides, J. P. Mathias and C. T. Seto, *Science*, 1991, **254**, 1312–1319.

49 J. Hermann, R. A. D. Jr and A. Tkatchenko, *Chem. Rev.*, 2017, **117**, 4714–4758.

50 C. F.J. Faul, *Acc. Chem. Res.*, 2014, **47**, 3428–3438.

51 F. Würthner, C. R. Saha-Möller, B. Fimmel, S. Ogi, P. Leowanawat and D. Schmidt, *Chem.*

Rev., 2016, **116**, 962–1052.

52 D. Chandler, *Nature*, 2005, **437**, 640–647.

53 J. Ruokolainen, R. Makinen, M. Torkkeli, T. Makela, R. Serimaa, G. ten Brinke and O. Ikkala, *Science*, 1998, **280**, 557–560.

54 A. H. Gröschel and A. H. E. Mueller, *Nanoscale*, 2015, **7**, 11841–11876.

55 S. Neidle, L. H. Pearl and J. V Skelly, *Biochem J*, 1987, **243**, 1–13.

56 S. I. Stupp and L. C. Palmer, *Chem. Mater.*, 2014, **26**, 507–518.

57 S. S. Babu, S. Prasanthkumar and A. Ajayaghosh, *Angew. Chemie - Int. Ed.*, 2012, **51**, 1766–1776.

58 C. Wang, Z. Wang and X. Zhang, *Small*, 2011, **7**, 1379–1383.

59 H. Qiu, Y. Gao, C. E. Boott, O. E. C. Gould, R. L. Harniman, M. J. Miles, S. E. D. Webb, M. A. Winnik and I. Manners, *Science*, 2016, **352**, 697–702.

60 C. F. J. Faul and M. Antonietti, *Adv. Mater.*, 2003, **15**, 673–683.

61 X. Li, P. J.Wolanin, L. R. MacFarlane, R. L. Harniman, J. Qian, O. E. C. Gould, T. G. Dane, J. Rudin, M. J. Cryan, T. Schmaltz, H. Frauenrath, M. A. Winnik, C. F. J. Faul and I. Manners, *Nat. Commun.*, 2017, **8**, 15909–15917.

62 J. M. Fletcher, R. L. Harniman, F. R. H. Barnes, A. L. Boyle, A. Collins, J. Mantell, T. H. Sharp, M. Antognozzi, P. J. Booth, N. Linden, M. J. Miles, R. B. Sessions, P. Verkade and D. N. Woolfson, *Science*, 2013, **340**, 595–600.

63 V. Nguyen, R. Zhu, K. Jenkins and R. Yang, *Nat. Commun.*, 2016, **7**, 13566–13572.

64 B. Qin, S. Zhang, Q. Song, Z. Huang, J. Xu and X. Zhang, *Angew.Chem. Int.Ed.*, 2017, **56**, 7639–7643.

65 J. Zhan, Y. Cai, S. He, L. Wang and Z. Yang, *Angew. Chem. Int. Ed.*, 2018, **57**, 1813–1816.

66 P. Cordier, F. Tournilhac, C. Soulie-Ziakovic and L. Leibler, *Nature*, 2008, **451**, 977–980.

67 S. Ilday, G. Makey and G. B. Akguc, *Nat. Commun.*, 2017, **8**, 14942–14952.

68 R. Zhong, Q. Tang, S. Wang, H. Zhang, F. Zhang, M. Xiao, T. Man, X. Qu, L. Li, W. Zhang and H. Pei, *Adv. Mater.*, 2018, **30**, 1706887–1706895.

69 S. Bandyopadhyay, J. C. Shelley, M. Tarek, P. B. Moore and M. L. Klein, *J. Phys. Chem. B*, 1998, **102**, 6318–6322.

70 J. N. Israelachvili, D. J. Mitchell and B. W. Ninham, *J. Chem. Soc. Faraday Trans. 2*, 1976, **72**, 1525–1568.

71 F. Biedermann, W. M. Nau and H.-J. Schneider, *Angew. Chem. Int. Ed. Engl.*, 2014, **53**, 11158–11171.

72 R. Nagarajan and E. Ruckenstein, *Langmuir*, 1991, **7**, 2934–2969.

73 S. Svenson, *Curr. Opin. Colloid Interface Sci.*, 2004, **9**, 201–212.

74 R. Nagarajan, *Langmuir*, 2002, **18**, 31–38.

75 J. Zhang, X. Li and X. Li, *Prog. Polym. Sci.*, 2012, **37**, 1130–1176.

76 T. Kunitake, Y. Okahata, M. Shimomura, S. Yasunami and K. Takarabe, *J. Am. Chem. Soc.*, 1981, **103**, 5401–5413.

77 G. Wu, P. Verwilst, J. Xu, H. Xu, R. Wang, M. Smet, W. Dehaen, C. F. J. Faul, Z. Wang and X. Zhang, *Langmuir*, 2012, **28**, 5023–5030.

78 G. Wu, P. Verwilst, K. Liu, M. Smet, C. F. J. Faul and X. Zhang, *Chem. Sci.*, 2013, **4**, 4486–4493.

79 G. Wu, J. Thomas, M. Smet, Z. Wang and X. Zhang, *Chem. Sci.*, 2014, **5**, 3267–3274.

80 E. J. Townsend, M. Alotaibi, B. M. Mills, K. Watanabe, A. M. Seddon and C. F. J. Faul, *ChemNanoMat*, 2018, **4**, 741–752.

81 X. Liu and N. L. Abbott, *J. Colloid Interface Sci.*, 2009, **339**, 1–18.

82 K. Wang, S. Munoz, L. Zhang, R. Castro, A. E. Kaifer and G. W. Gokel, *J. Am. Chem. Soc.*, 1996, **118**, 6707–6715.

83 Q. Yan, J. Yuan, Z. Cai, Y. Xin, Y. Kang and Y. Yin, *J. Am. Chem. Soc.*, 2010, **132**, 9268–9270.

84 H. Zhang, W. An, Z. Liu, A. Hao, J. Hao, J. Shen, X. Zhao, H. Sun and L. Sun, *Carbohydr. Res.*, 2010, **345**, 87–96.

85 A. Alkan, S. Wald, B. Louage, B. G. De Geest, K. Landfester and F. R. Wurm, *Langmuir*, 2017, **33**, 272–279.

86 Y. Kakizawa, H. Sakai, A. Yamaguchi, Y. Kondo, N. Yoshino and M. Abe, *Langmuir*, 2001, **17**, 8044–8048.

87 Y. Kakizawa, H. Sakai, K. Nishiyama and M. Abe, *Langmuir*, 1996, **12**, 921–924.

88 C. A. Rosslee and N. L. Abbott, *Anal. Chem.*, 2001, **73**, 4808–4814.

89 D. Canevet, M. Sallé, G. Zhang, D. Zhang and D. Zhu, *Chem. Commun.*, 2009, **7345**, 2245.

90 X. J. Wang, L. B. Xing, F. Wang, G. X. Wang, B. Chen, C. H. Tung and L. Z. Wu, *Langmuir*, 2011, **27**, 8665–8671.

91 X. J. Wang, L. B. Xing, B. Chen, Y. Quan, C. H. Tung and L. Z. Wu, *Org. Biomol. Chem.*, 2016, **14**, 65–68.

92 Y. Wu, S. Liu, Y. Tao, Y. Zhang, J. Xu and Y. Wei, *ACS Appl. Mater. Interfaces*, 2014, **6**, 1470–1480.

93 H. Kim, S.-M. Jeong and J.-W. Park, *J. Am. Chem. Soc.*, 2011, **133**, 5206–5209.

94 T. Kim, C. Kim and J. Park, *Macromolecules*, 2017, **50**, 8185–8191.

95 S. She, Z. Huang, P. Yin, A. Bayaguud, H. Jia, Y. Huang, Y. Wei and Y. Wei, *Chem. - A Eur. J.*, 2017, **23**, 14860–14865.

96 I. Arioz, O. Erol, G. Bakan, F. B. Dikecoglu, A. E. Topal, M. Urel, A. Dana, A. B. Tekinay and M. O. Guler, *ACS Appl. Mater. Interfaces*, 2018, **10**, 308–317.

97 M. Kaneko, M. Ishikawa, K. Hashimoto and S. Nakanishi, *Bioelectrochemistry*, 2017, **114**, 8–12.

98 L. Cao, C. Gong and J. Yang, *Macromol. Rapid Commun.*, 2016, **37**, 343–350.

99 C. Edder and J. M. J. Frechet, *Org. Lett.*, 2003, **5**, 1879–1882.

100 O. A. Bell, G. Wu, J. S. Haataja, F. Broemmel, N. Fey, A. M. Seddon, R. L. Harniman, R. M. Richardson, O. Ikkala, X. Zhang and C. F. J. Faul, *J. Am. Chem. Soc.*, 2015, **137**, 14288–14294.

CHAPTER 2 SYNTHESIS OF OLIGO(ANILINE) AMPHIPHILES BASED ON TANI

2.1 Oligo(aniline)s

Oligo(aniline) is described as a linear chain of aniline molecules linked covalently by para C-N bonds between two molecules of aniline.[1,2] Furthermore, oligo(aniline)s have the same electronic properties as PANI, i.e., the LEB, EB and PB oxidation states are all accessible and doping can be performed by oxidation of the LEB state or acid treatment of the EB state.[3] Oligo(aniline)s such as tetra(aniline), **TANI**, and octa(aniline) are some of the conducting oligomers widely studied in the last few decades.[4] Oligo(aniline)s generally have superior properties to PANI in terms of function, structures and solubility.[5,6] However, providing environmentally friendly water-soluble materials based on oligo(aniline)s still presents an obstacle.[5] To overcome this issue, oligo(aniline)s were functionalised to provide the ability to be water-soluble materials. There are a number of reports regarding the variable functionalisation of oligo(aniline)s with hydrophilic moieties, allowing preparation of water-soluble block-like amphiphilic structures. Park and co-workers synthesised **TANI** functionalised with poly(ethylene glycol) to form anionic amphiphilic structures.[7,8] Anionic bolaamphiphiles based on penta(aniline) oligomers were also synthesised.[9] However, the first cationic amphiphiles based on **TANI** were synthesised by our group.[10,11]

TANI is the shortest oligomer with access to all oxidation states and is the main interest of this project. We use a naming convention developed for **TANI** by classifying oligomer structures according to their terminal groups, e.g., phenyl (Ph), amino (NH_2), and their arrangement. Thus, Ph/Ph **TANI** refers to a symmetrical tetra(aniline) capped with a phenyl ring at both ends, and the asymmetrical and symmetrical species Ph/NH_2 and NH_2/NH_2 **TANI**, respectively as shown in **Figure 2.1**, all these types of **TANI** have been prepared in our group.[5]

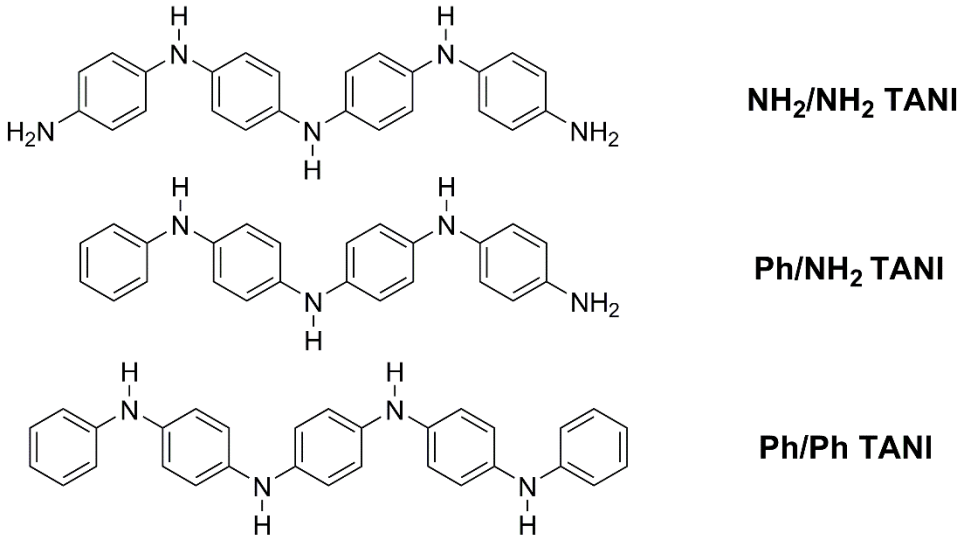

Figure 2.1 Three variants of **TANI**.

Ph/NH_2 **TANI** and NH_2/ NH_2 **TANI** are of the most interest due to their available primary amine which can be further functionalised with other moieties. Ph/NH_2 **TANI** and NH_2 /NH_2 **TANI** were used as the starting molecules to build different architectures of an amphiphilic molecule. Ph/NH_2 **TANI** functionalised with different hydrophilic moieties allows the preparation of AB diblock amphiphilic structures. However, NH_2/NH_2 **TANI** compound has two terminal amine groups that can be used to prepare triblock-like amphiphilic structures which are either symmetric or asymmetric.

Here we provide in detail the synthetic pathway of **TANI** precursors that were used to design **TANI**-based amphiphiles with different architectures: either single-tailed (AB diblock structures) or bolaamphiphiles (ABA triblock structures). Furthermore, amphiphiles were designed that have the same chemical structure with different head groups, **TANI-PTAB**, **TANI-PTPB, TANI-$(PTAB)_2$, TANI-$(PTPB)_2$**. These variations in structure and function enable extended comparisons to be made of the self-assembling behaviour of **TANI**-based materials.

2.2 Results and Discussion

2.2.1 Synthesis of TANI precursors

Boc Ph/NH_2 TANI synthesis

Ph/NH_2 **TANI** is generally made *via* an oxidative route,[12] but this method still presents issues in terms of purity and stability. Thus, a Boc-protected Buchwald Hartwig amination route was used, as shown in **Scheme 2.1**, based on that reported by Chen et al.[13] This method allows for a controlled, step-by-step preparation of fully Boc-protected Ph/NH_2 **TANI** in the **LEB** state in high purity and stability.

Boc-protected Ph/NH_2 **TANI** comprises two different groups at the termini; on one side an inert phenyl group and on the other side a reactive amino group. The inert phenyl group can work as a protecting group for further reactions. However, the reactive amino group gives an opportunity to react and attach several kinds of functional groups. Boc Ph/NH_2 **TANI** can be prepared using Pd-catalysed Buchwald-Hartwig amination reactions. The synthesis of **TANI** is based on adding Boc and CPh_2 groups, which are used as protecting groups for N-containing parts of the target compounds at different stages of the synthesis. This means that subsequent side reactions can be avoided. It well-known that **TANI** has low stability in the leucoemeraldine form, hence Boc protecting groups have emerged as a powerful method for the synthesis of stable **TANI**. *Tert*-butyloxycarbonyl protection was used to protect the non-terminal amines in **TANI**, in the presence of a base and catalyst. 4-Dimethylaminopyridine (DMAP) works as a catalyst for electrophilic activation of di-tert-butyl dicarbonate (Boc_2O). This reaction was carried out at a reasonable temperature of 62°C, but should be below the solvent boiling point. Boc-protection is conducted under anhydrous conditions. The synthetic pathway of Ph/NH_2 **TANI** has 6 steps in order to obtain the pure final product as shown in **Scheme 2.1**. All the products were confirmed by ^1H and ^{13}C NMR spectroscopy, mass spectrometry and elemental analysis.

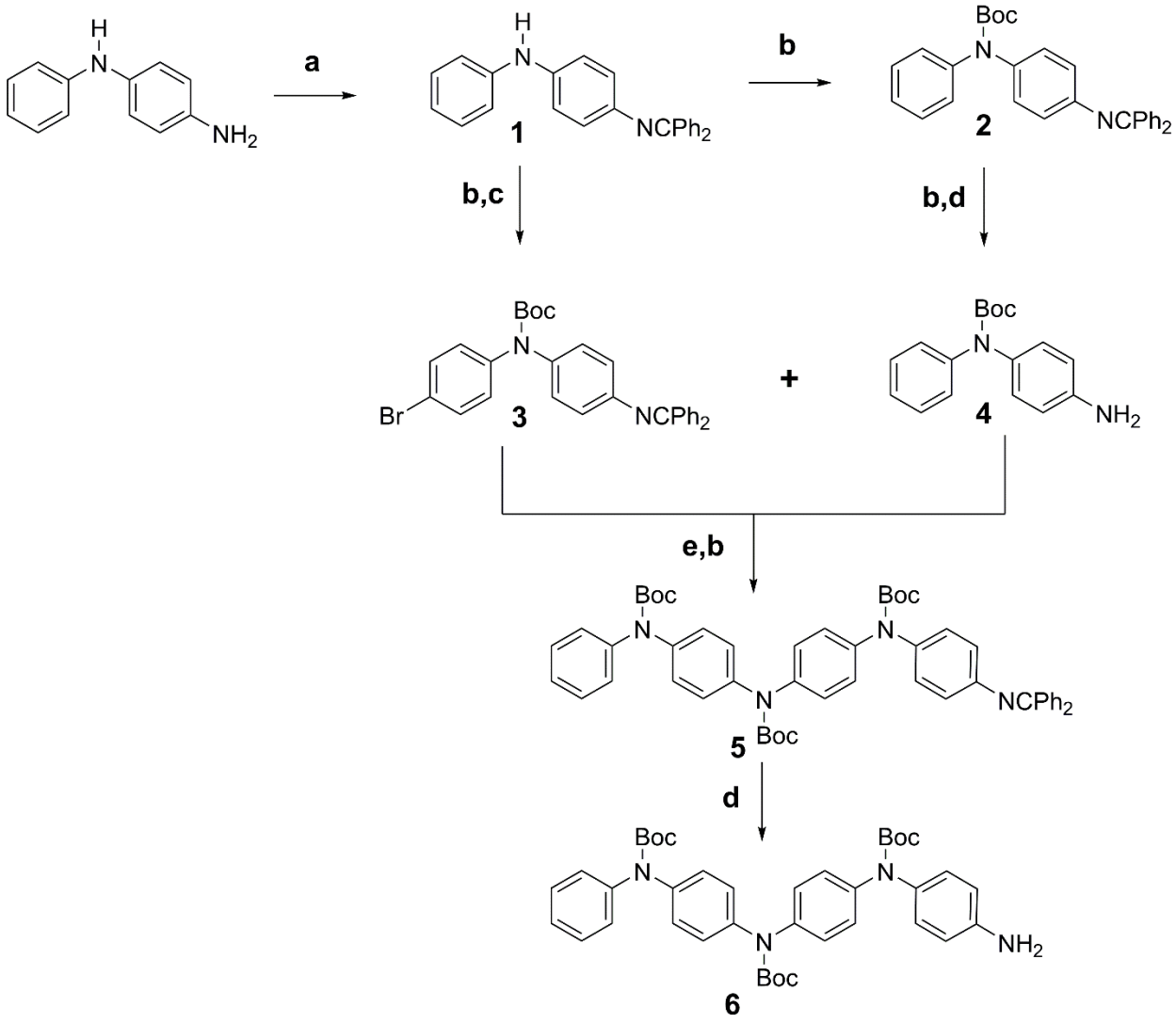

a: Ph_2CO, molecular sieves, toluene,110°C
b: Boc_2O, DMAP, THF, 65°C
c: $(n\text{-}Bu)_4NBr_3$, DCM, 1h
d: Pd/C, NH_4HCO_2, THF/MeOH, 6 h
e: $Pd(dba)_2$, Xphos, NaOtBu, toluene, 110°C

Scheme 2.1 Synthetic route to prepare Boc Ph/NH_2 **TANI**.

The fully Boc-protected **TANI** was successfully synthesised, as evidenced by ^{1}H NMR spectroscopy (**Figure 2.1**). The signals at chemical shift values 1.35-1.37 ppm were ascribed to the *t*-butyl in the Boc groups and the signal at 5.1 ppm was ascribed to terminal –NH_2 and ESI (electrospray ionisation) mass spectrum also confirming the purity of Boc Ph/NH_2 **TANI** with peak at m/z= 689.34 (Boc Ph/NH_2 **TANI** + Na^+).

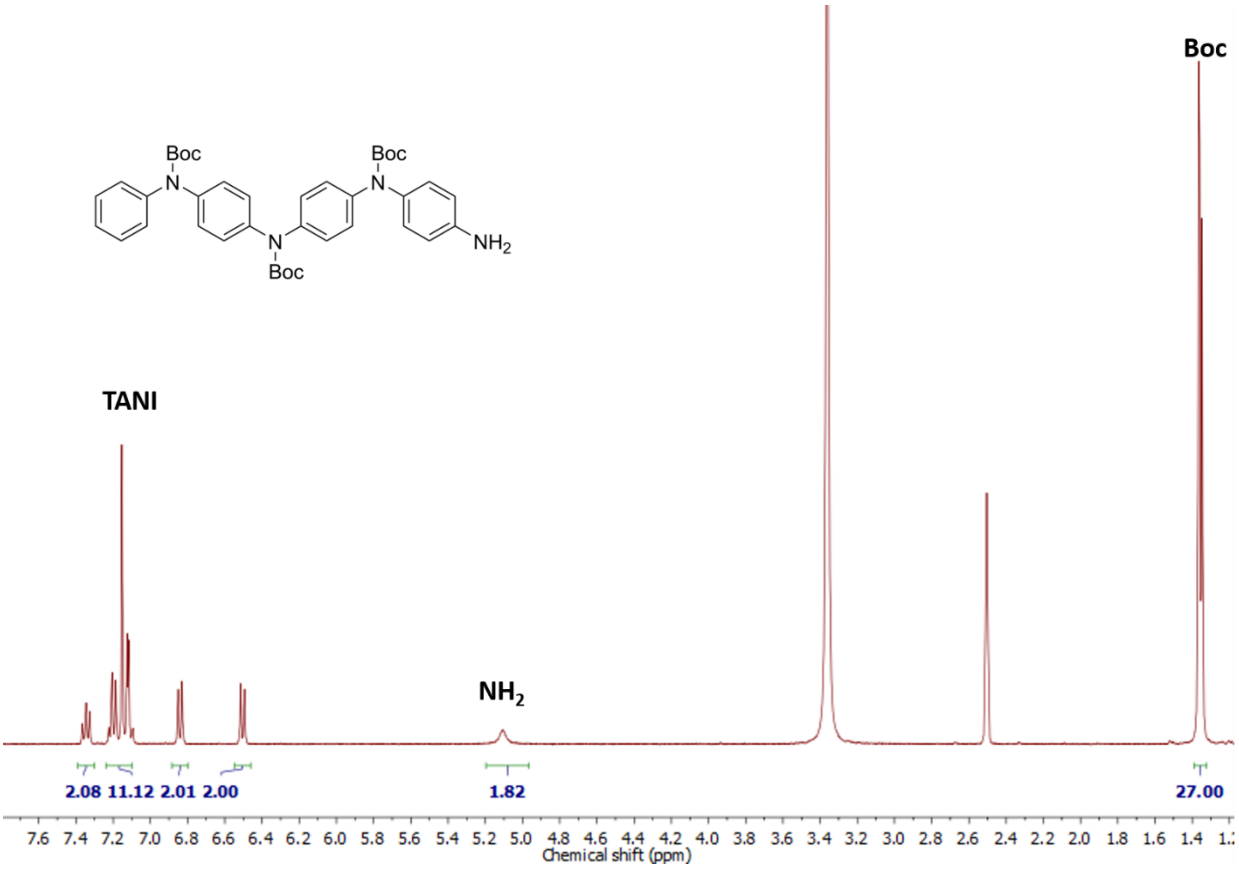

Figure 2.2 ^{1}H NMR of Boc Ph/NH_2 **TANI**.

Boc NH_2/NH_2 TANI synthesis

Boc NH_2/NH_2 **TANI** was prepared via a nucleophilic substitution reaction in a stepwise fashion (**Figure 2.2**). NH_2/NH_2 **TANI** was preliminarily prepared by Kulszewicz-Bajer and co-workers using dianiline to react with 1-fluoro-4-nitro benzene in presence of K_2CO_3 as base.[14] The resulting NO_2/NO_2 **TANI** was then reduced to form LEB NH_2/NH_2 **TANI**, followed by an oxidation reaction to form EB NH_2/NH_2 **TANI**. However, this procedure was performed without any protecting

groups, making it highly likely to form a mixture of oxidation states of **TANI**. Hence, some improvements for this reaction were required: addition of Boc groups after the coupling reaction were needed to prevent any oxidation of **TANI**. The reduction of the terminal -NO_2 to NH_2 groups was performed using palladium on carbon as a catalyst, in the presence of ammonium formate as a reducing agent rather than the harsh conditions (tin and concentrated HCl) that were used in the literature. The desired product was obtained in moderate yield (63%) and high purity.

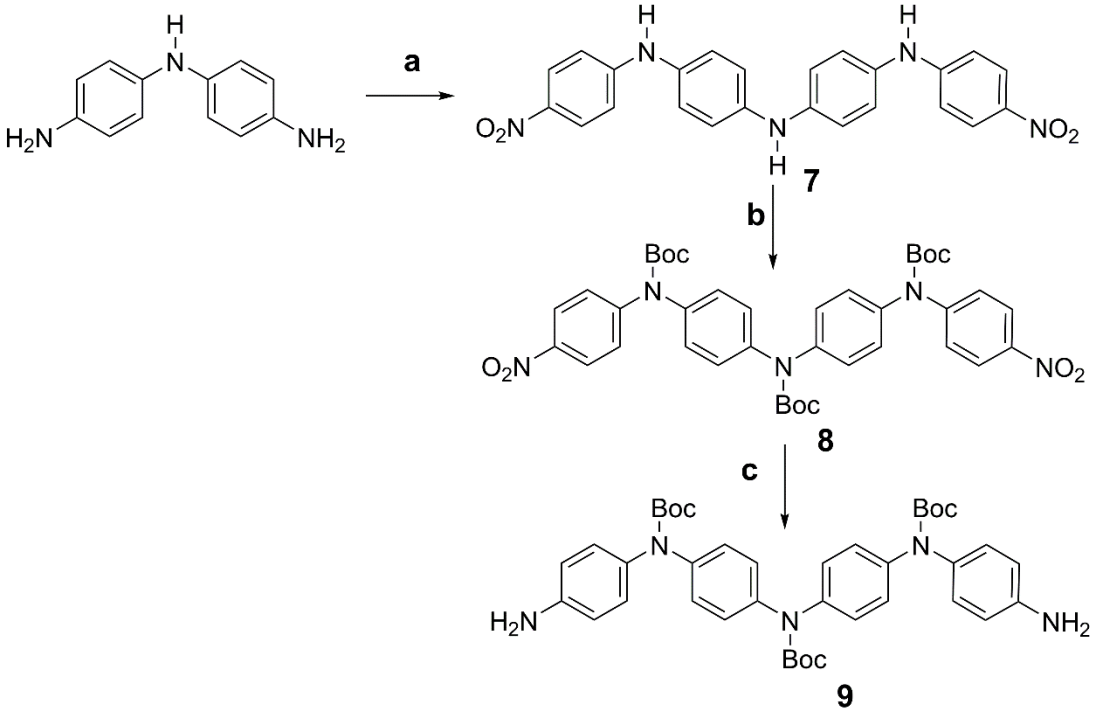

a: 4-fluoro-1-nitrobenzene, Et_3N, DMSO, 90°C, 24 h.
b: Boc_2O, DMAP, THF reflux, 24 h.
c: Pd/C, NH_4HCO_2 , THF/MeOH, reflux, 6 h.

Scheme 2.2 Synthetic route to prepare Boc NH2/NH2 **TANI**

The formation of pure Boc NH_2/NH_2 **TANI** was confirmed by ^{1}H NMR (**Figure 2.3**). The signals at 6.5 -7.4 ppm are ascribed to aromatic protons, whilst the signal at 1.35-1.37 ppm is attributed to Boc groups and the two terminal protons of NH_2 appear at 5.1 ppm.

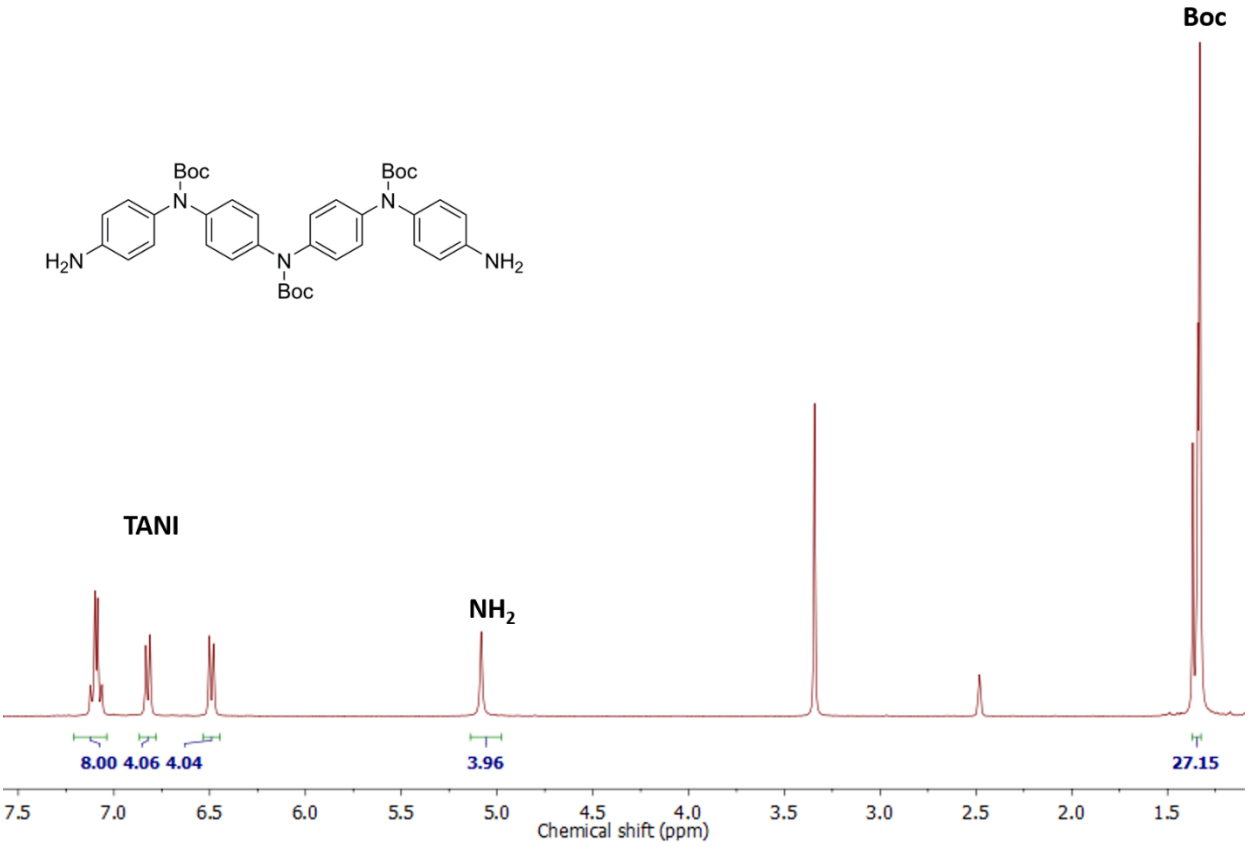

Figure 2.3 ^{1}H NMR of Boc NH_2/NH_2 **TANI**.

2.2.2 Synthesis of cationic single-tailed amphiphiles

Synthesis of Boc Ph/NH_2 TANI-C6Br

The first step in preparing AB diblock-like structures was the functionalization of **TANI** with an alkyl chain. This was carried out using the commercially available 6-bromohexanoyl chloride, as shown in **Figure 2.4a**. This proceeds via a nucleophilic substitution reaction S_N2 between the terminal amine of **TANI** and the acid chloride in the presence of triethylamine.

^{1}H NMR combined spectra (**Figure 2.4b**) of Boc Ph/NH_2 **TANI** and Boc Ph/NH_2 **TANI**-C6Br shows that the shift occurred due to the transformation of the amine group to an amide group and proton (**H_a** and **H_b**) peaks at 6.50 and 6.84 ppm shifted to 7.21 and 7.5 ppm, respectively. The signal at 5.10 ppm was ascribed to the terminal amine protons of Boc Ph/NH_2 **TANI**. However, this signal disappeared when the attachment of the alkyl chain occurred successfully to form a signal at 9.92 ppm, which is attributed to the proton in the amide group as well as the presence

of the protons of the alkyl chain of Boc Ph/NH_2 **TANI**-C6Br. The desired product was obtained in high yield (80%) and high purity.

a)

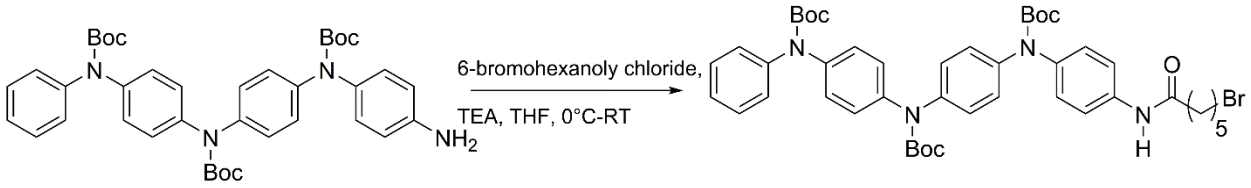

b)

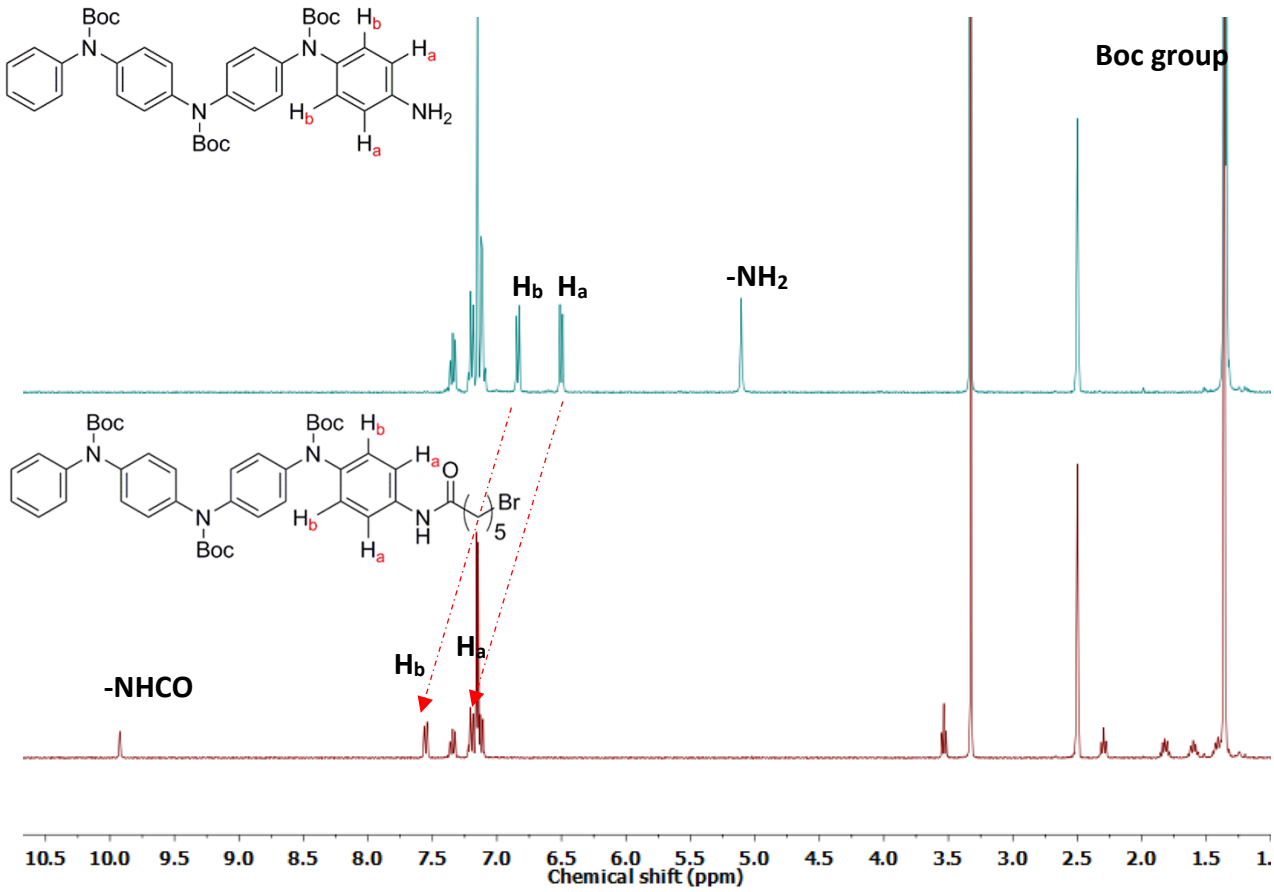

Figure 2.4 a) Synthesis of Boc **TANI**-C6Br, b) ^{1}H NMR spectra of the comparison of Boc-Ph/NH_2 **TANI** and Boc-Ph/NH_2 **TANI**-C6Br.

2.2.2.1 Synthesis of EB Ph/NH_2 TANI-($C_6NMe_3^+Br^-$), EB TANI-PTAB

Diblock-like structures containing oligo(aniline)s terminated with soluble moieties such as cationic head groups, to form cationic amphiphiles, are one of our interests as mentioned before. A single-tailed ammonium amphiphile EB Ph/NH_2**TANI**-C6$NMe_3^+Br^-$ (**EB TANI-PTAB**) was synthesised previously in our group as shown in **Scheme 2.3**.[10] The Boc protecting groups of Boc **TANI**-C6Br were cleaved using trimethylsilyl iodide (TMSI) and the formation of LEB **TANI**-C6Br was confirmed using ^1H and ^{13}C NMR and mass spectrometery. This step was followed by an oxidation reaction using ammonium persulfate as a strong oxidizing agent. Once oxidised, the water-insoluble EB **TANI**-C6Br was washed several times with water to remove any water-soluble impurities. Finally, EB **TANI**-C6Br was quaternised with trimethylamine (TMA) through an S_N2 reaction using DMF as solvent. Details of this reaction are provided in the experimental section.

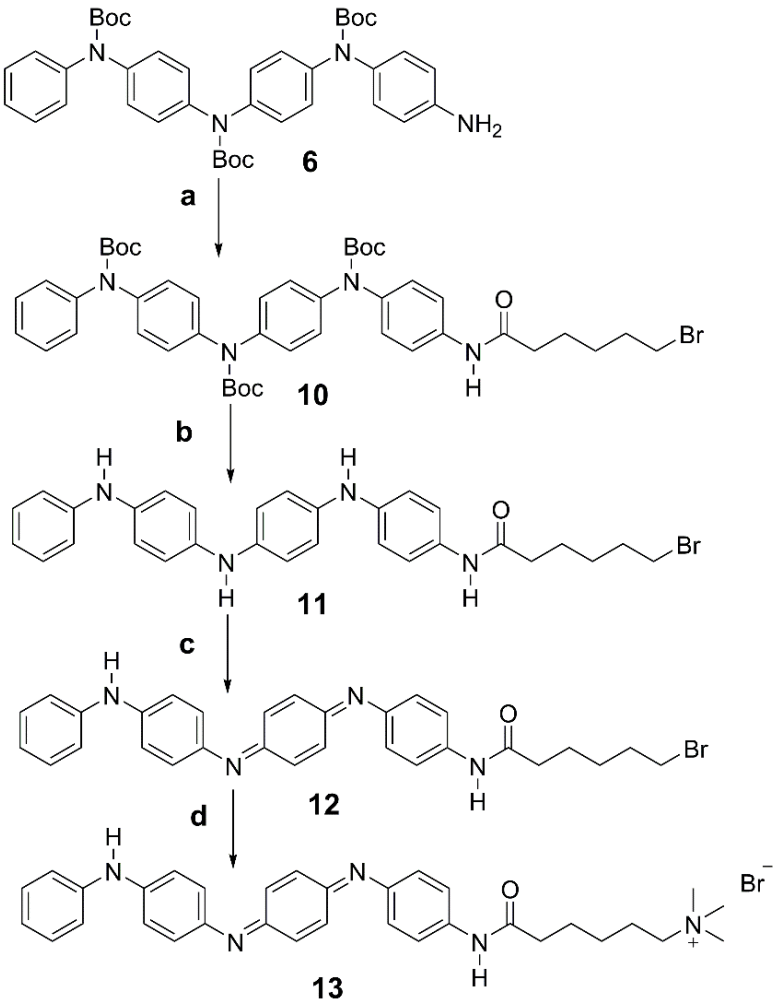

a: 6-bromohexanoly chloride, TEA, THF, 0°C-RT, overnight
b: i) Me_3SiI, DCM, 2h, RT
ii) MeOH, TEA, DCM, RT
c: i) $(NH_4)_2S_2O_8$, HCl (1M), DMF, RT
ii) NH_4OH, acetone, RT
d: NMe_3 (35 wt% in EtOH), DMF, RT

Scheme 2.3 Synthetic route to prepare **EB TANI-PTAB**.

2.2.2.2 Synthesis of EB Ph/NH_2TANI ($C_6PMe_3^+Br^-$), EB TANI-PTPB

A single-tailed phosphonium amphiphile EB Ph/NH_2**TANI**-C6$PMe_3^+Br^-$ (**EB TANI-PTPB**) was also synthesised for the first time and all details and challenges of this reaction are fully presented. First, the same procedure was followed as the single-tailed ammonium amphiphile, **EB TANI-PTAB**, where Boc protecting groups of Boc **TANI**-C6Br were removed using trimethylsilyl iodide (TMSI). A subsequent oxidation reaction was performed using ammonium persulfate to convert the oxidation state from LEB to EB. The water-insoluble EB **TANI**-C6Br was then washed several times with water to remove any water-soluble impurities. Finally, EB **TANI**-C6Br was quaternised with trimethylphosphine (TMP); this reaction was prepared carefully in a heavy walled flask. Furthermore, since quaternisation of **TANI**-C6Br via a S_N2 reaction with a tertiary phosphine was desired, it was important to choose an appropriate solvent as solvents play a significant role in the rate of S_N2 reactions. In the reported literature[15] the polar protic solvent isopropanol has been used for the quaternisation, however it was found to be ineffective for this reaction, resulting in a low purity and yield. DMF was tested and found to be a good solvent resulting in a pure product with good yield (70%), hence DMF was used for further reactions. This reaction was carried out under nitrogen for 48 hours to prevent oxidation of trimethylphosphine. The workup was performed carefully to remove excess trimethylphosphine. The solution mixture was then taken up into a large amount of cold diethyl ether followed by storage overnight in a freezer, which led to direct precipitation of the product. After washing several times with diethyl ether to remove DMF completely, once dried the amphiphile was dissolved in water and then centrifuged to get rid of water-insoluble impurities. Subsequently the aqueous solution was freeze-dried to give the desired product with a good yield of approximately 75%. It is noteworthy that the colour of the desired product was grey, which reflects the oxidation state of LEB **TANI**. In fact, TMP works as a reducing agent to convert **TANI** from the EB to LEB state. These issues could be avoided by using **TANI**-C6Br in the LEB state to be quaternised with trimethylphosphine (TMP) as shown in **Scheme 2.4**. Once quaternised, the workup was performed as mentioned earlier and crude product was obtained and the purity examined by different characterizations. This was followed by oxidation which took place using an excess amount of hydrogen peroxide

(30%) into acetonitrile and left stirring for 2 hours and the workup performed in a similar way as in the previous trial.

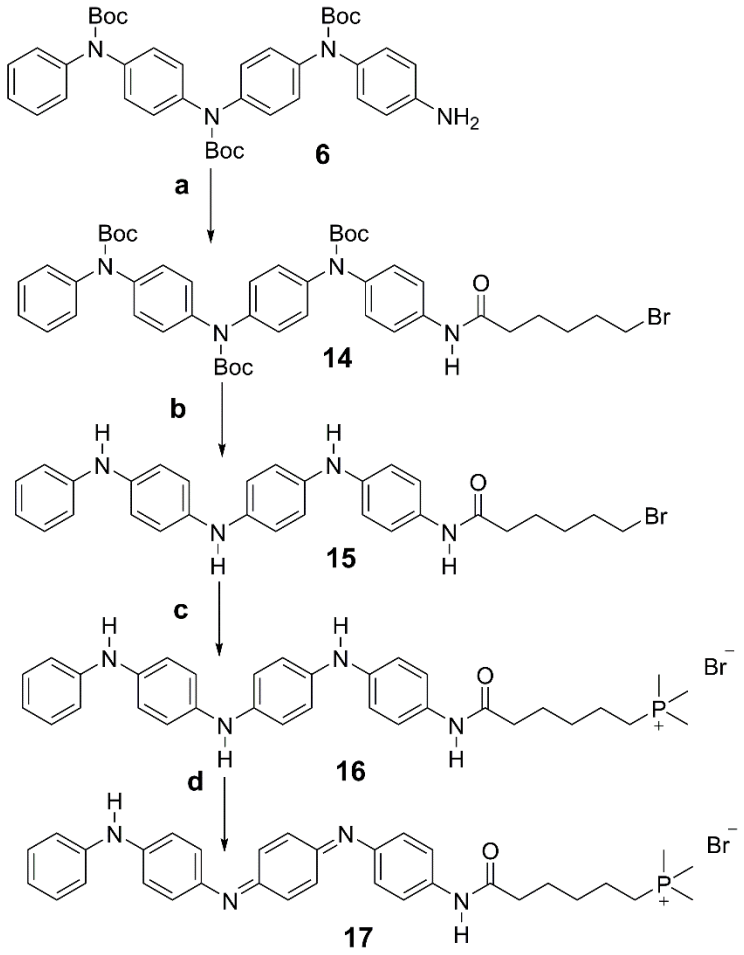

a: 6-bromohexanoly chloride, TEA, THF, 0°C-RT, overnight
b: i) Me_3SiI, DCM, 2h, RT
ii) MeOH, TEA, DCM, RT
c: PMe_3, DMF, 0-70°C, overnight
d: H_2O_2 (30 wt% in H_2O), CH_3CN, 2h, RT

Scheme 2. 4 Synthetic route to prepare **EB TANI-PTPB**.

Synthesis of functionalised EB **TANI**-C6Br with the phosphonium head group is confirmed by ^{1}H NMR. In **Scheme 2.5**, slight changes appeared in the chemical shift of the protons of the alkyl chain once LEB **TANI**-C6Br was functionalised with TMP due to the low electronegativity of phosphorus compared to the bromine and carbon groups. The signal of the two protons on the carbon adjacent to bromine shifted from 3.54 to 2.17 ppm, two signals of methylene groups of TMP in LEB state appeared at 1.82 ppm as well as the protons' signals of secondary amines of LEB state which were clearly observed at 7.58-7.71 ppm. However, signals of the Boc groups at 1.40 ppm disappeared in LEB **TANI**-C6Br indicating that the deprotection reaction was performed successfully. In addition, the NMR spectra show no changes of chemical shifts in the aromatic region, confirming that no decomposition happened during the reaction process.

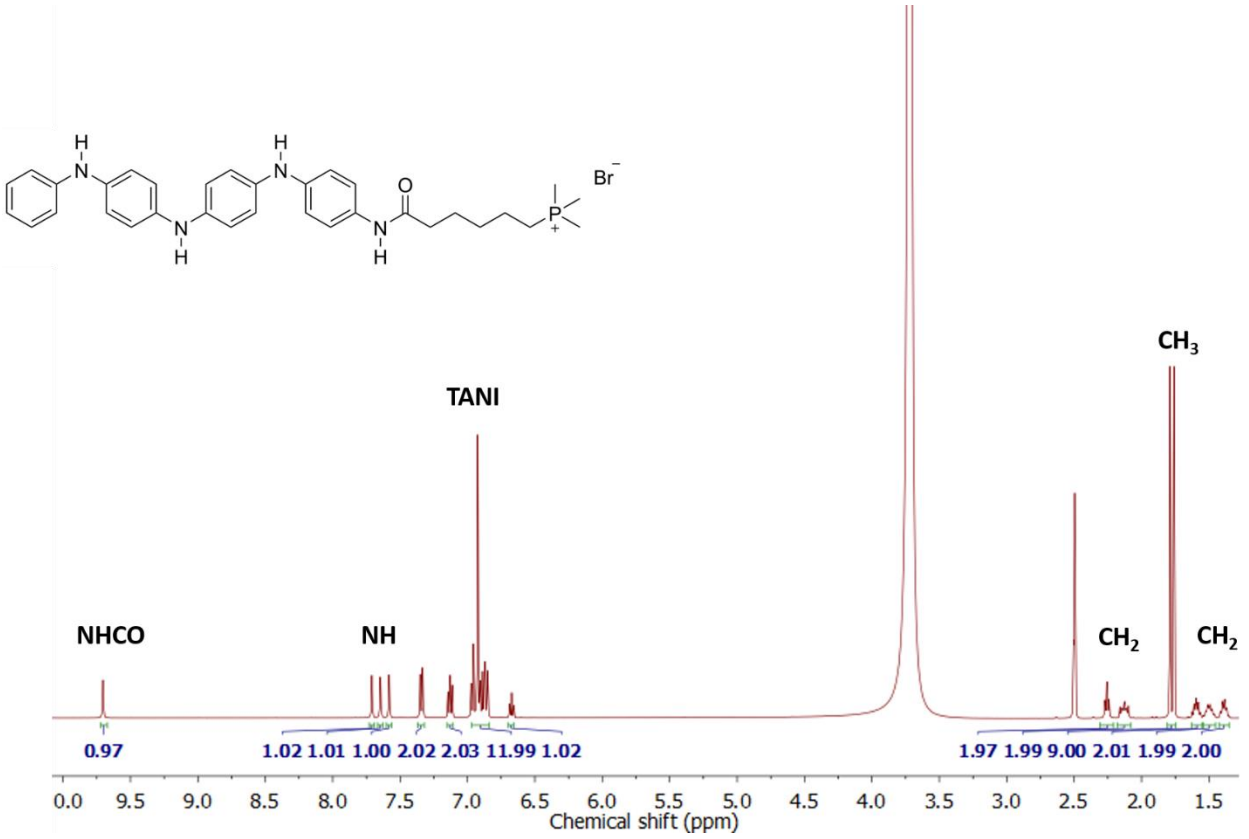

Figure 2.5 Cryo-^{1}H NMR spectrum of **LEB TANI-PTPB**.

2.2.3 Synthesis of cationic bolaamphiphiles based on TANI

Synthesis of Boc Ph/NH_2 TANI-$(C6Br)_2$

Boc NH_2/NH_2 **TANI** was reacted with 6-bromohexanoyl chloride via a nucleophilic substitution reaction to form Boc NH_2/NH_2 **TANI**-$(C6Br)_2$. The acetylation reaction was carried out with 2 equivalents of the acid chloride in the presence of triethylamine to yield the product of Boc NH_2/NH_2 **TANI** bearing two alkyl chains on both side (**Scheme 1.5**). Proton NMR spectra showed that the two amine groups converted to amide groups and the desired product was formed in high purity and a good yield (80%).

2.2.3.1 Synthesis of EB NH2/NH2 TANI $(C6NMe3^+Br^-)_2$, EB TANI-$(PTAB)_2$

Boc-deprotection of NH_2/NH_2 **TANI**-$(C6Br)_2$ was performed with the same procedure that was used for the single-tailed ammonium amphiphiles, **EB TANI-PTAB**. TMSI was used with 1. 2 equivalents per Boc group to ensure all Boc groups were cleaved. Once the intermediate compound (i.e. LEB Ph/NH_2 **TANI**-$(C6Br)_2$) formed, the oxidation reaction was carried out using ammonium persulfate in 1M HCl. The green colour of the solution mixture was indicative of the formation of the ES state. Hence, the solution mixture was centrifuged and the residues re-dispersed into acetone. This was followed by addition of 2 M ammonium persulfate to oxidise the compound and yield the desired product of Ph/NH_2 **TANI**-$(C6Br)_2$ in EB state as shown in **Scheme 2.5**, which was confirmed by NMR and mass spectrometry.

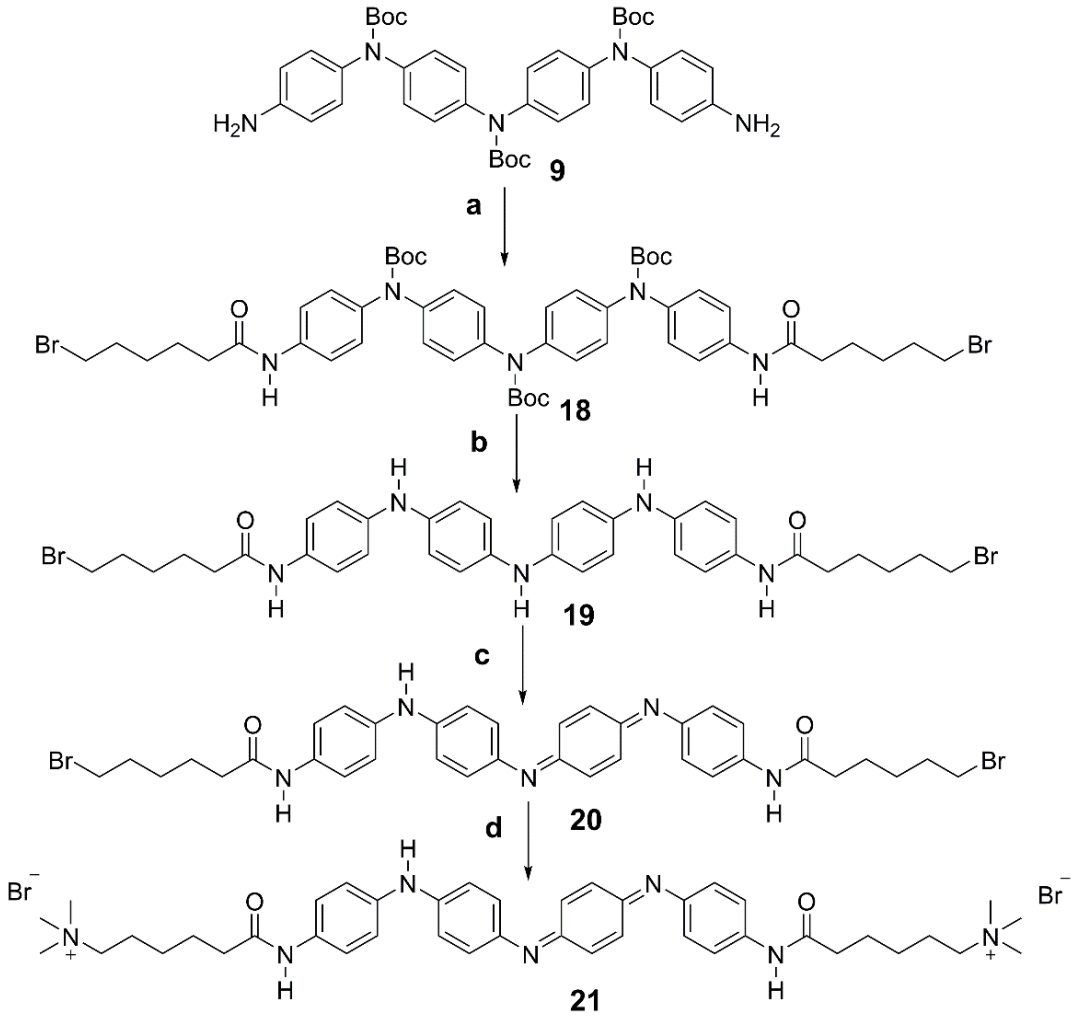

a: 6-bromohexanoly chloride, TEA, THF, 0°C-RT, overnight
b: i) Me_3SiI, DCM, 2h, RT
ii) MeOH, TEA, DCM, RT
c: i) $(NH_4)_2S_2O_8$, HCl (1M), DMF, RT
ii) NH_4OH, acetone, RT
d: NMe_3 (35 wt% in EtOH), DMF, RT

Scheme 2.5 Synthetic route to prepare **EB TANI-$(PTAB)_2$.**

2.2.3.2 Synthesis of EB NH_2/NH_2 TANI $(C_6PMe_3^+Br^-)_2$, EB TANI-$(PTPB)_2$

Following the same synthetic procedure as for **EB TANI-PTPB**, Boc NH_2/NH_2 **TANI** $(C_6\,Br)_2$ was dissolved in dry DCM and TMSI was added to remove the Boc groups, allowing formation of the deprotected intermediate LEB NH_2/NH_2 **TANI** $(C_6Br)_2$ compound. The LEB NH_2/NH_2 **TANI** $(C_6\,Br)_2$ compound was then functionalised with trimethylphosphine (TMP) and this reaction was performed carefully in a heavy-walled sealed flask. The excess TMP was removed under vacuum and the solution mixture was taken up into cold diethyl ether. The solution mixture was centrifuged, and residues were collected and dried in the vacuum oven. **LEB TANI-$(PTPB)_2$** was confirmed and characterised using NMR and high-resolution mass spectrometery. **LEB TANI-$(PTPB)_2$** was dissolved into acetonitrile and hydrogen peroxide (30%) was used to oxidise the sample to **EB TANI-$(PTPB)_2$** as shown in **Scheme 2.6**, which was confirmed by NMR and mass spectrometery.

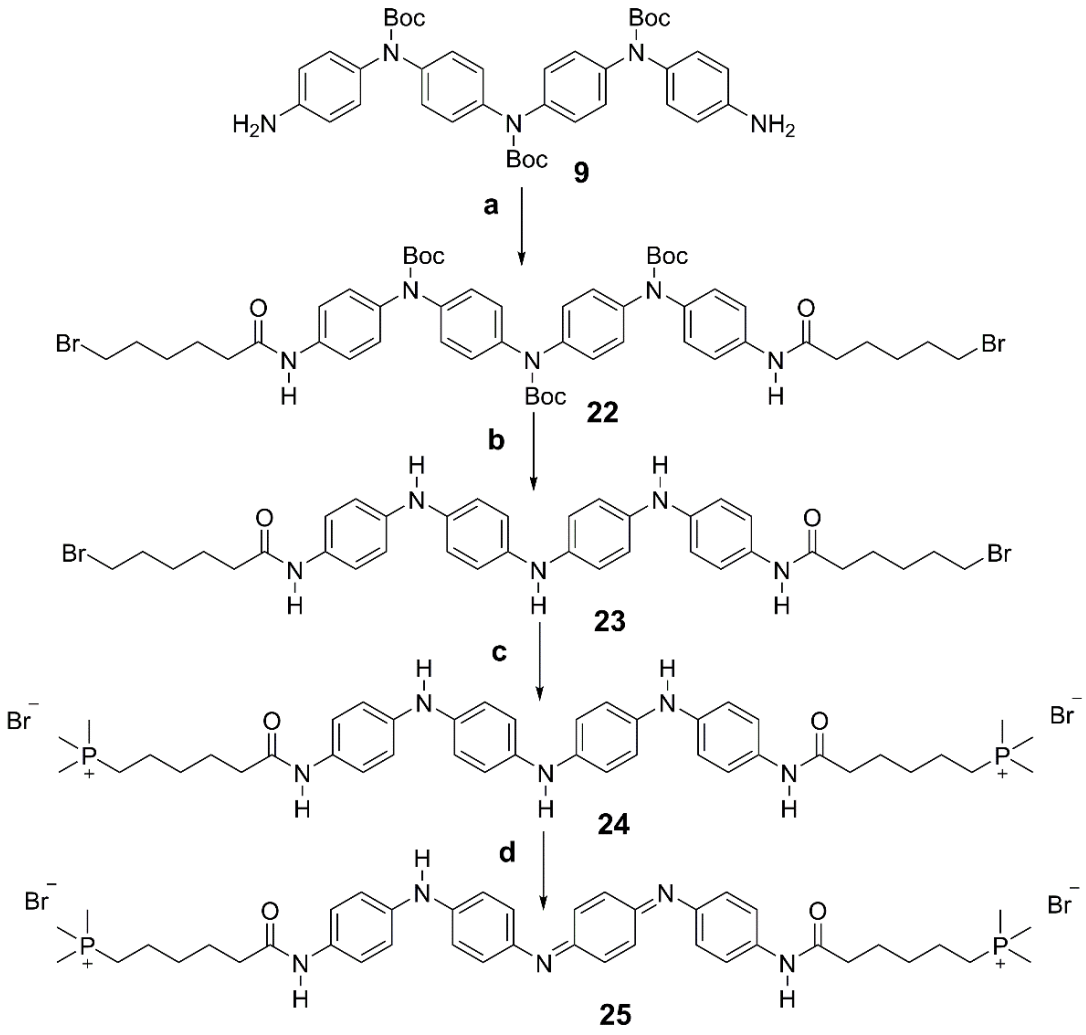

a: 6-bromohexanoly chloride, TEA, THF, 0°C-RT, overnight
b: i) Me_3SiI, DCM, 2h, RT
ii) MeOH, TEA, DCM, RT
c: PMe_3, DMF, 0-70°C, overnight
d: H_2O_2 (30 wt% in H_2O), CH_3CN, 2h, RT

Scheme 2.6 Synthetic route to prepare **EB TANI-(PTPB)$_2$**.

Synthesis of Boc Ph/NH$_2$ TANI-(C8Br)$_2$

Boc NH_2/NH_2 **TANI** bearing C8 alkyl chains were formed by reaction of 8-bromooctanoic acid with Boc NH_2/NH_2 **TANI** through EDC(1-Ethyl-3-(3-dimethylaminopropyl)carbodiimide) coupling, as shown in **Scheme 2.7**. Boc NH_2/NH_2 **TANI** bearing two alkyl chain on both sides was prepared

successfully and the reaction was monitored by TLC (1: 1 ethyl acetate: hexane) and using Bromocresol green as the staining agent (which is used to detect any excess of acidic compound, to ensure the consumption of starting materials). Once the completion of the reaction was confirmed by TLC and MALDI, the solvent was removed, and residues were washed with deionised water. Flash column chromatography (silica gel, 1:1 ethyl acetate: n-hexane) was used to purify the desired product resulting in a pure compound with a moderate yield (60 %).

2.2.3.3 Synthesis of EB Ph/NH_2 TANI ($C_8NMe_3^+Br^-)_2$, EB TANI-$(HTAB)_2$

Deprotection and oxidation reactions of the prepared materials were carried out following the procedure used for **EB TANI-$(PTAB)_2$**. Boc groups were cleaved using TMSI, resulting in LEB NH_2/NH_2 **TANI**-$(C8Br)_2$ in a good yield and purity. This was followed by oxidation using ammonium persulfate to yield EB NH_2/NH_2 **TANI**-$(C8Br)_2$. The latter was quaternised by TMA on both sides as shown in **Scheme 2.7**, and the completion of reaction was confirmed by MALDI. Once the reaction was completed, the solution mixture was centrifuged and residues were washed with deionised water to remove non-water soluble impurities. The desired product was characterised by NMR and mass spectrometery.

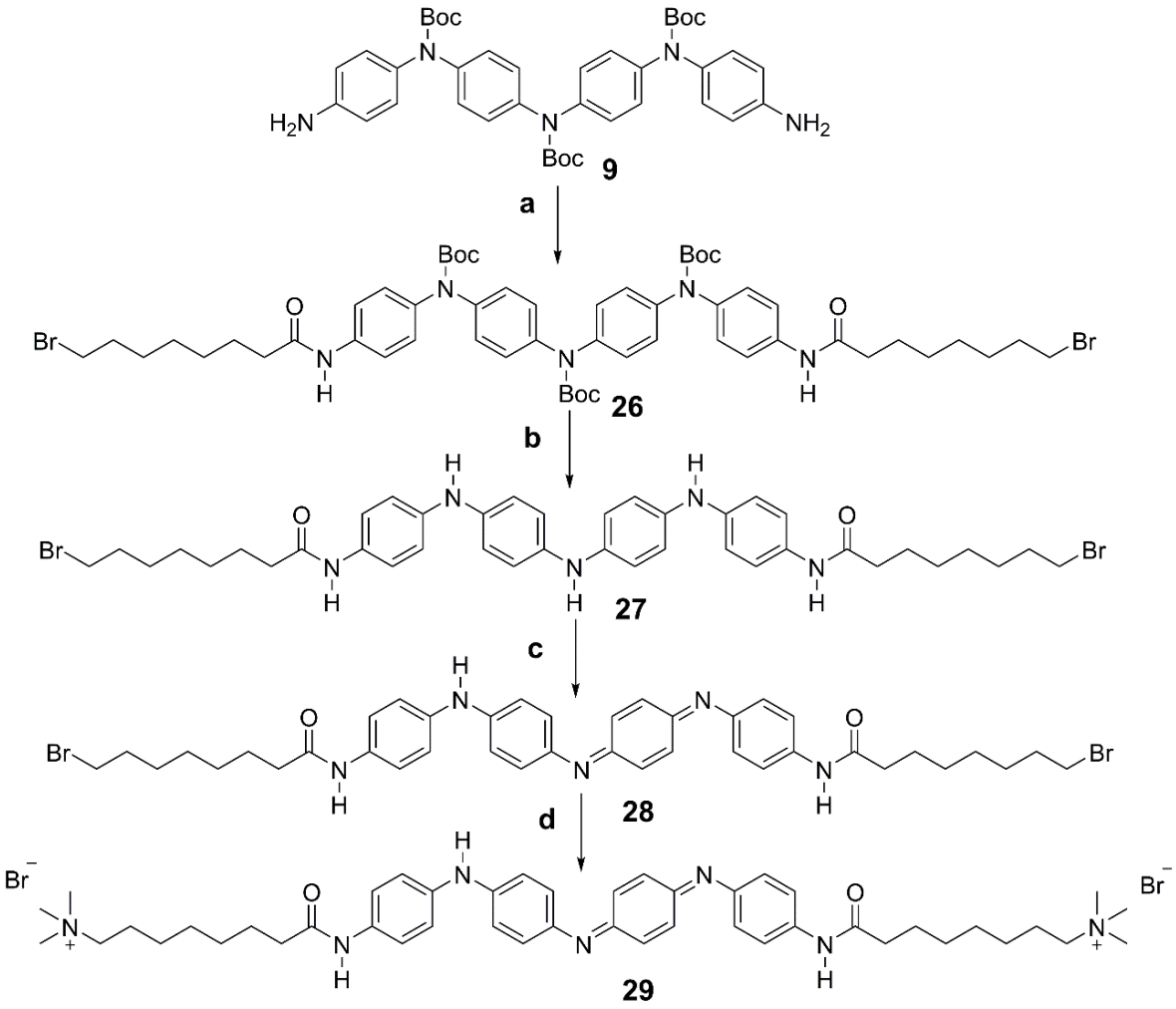

a: 8-bromooctanoic acid, EDC, DCM, 0°C-RT, overnight
b: i) Me_3SiI, DCM, 2h, RT
ii) MeOH, TEA, DCM, RT
c: i) $(NH_4)_2S_2O_8$, HCl (1M), DMF, RT
ii) NH_4OH, acetone, RT
d: NMe_3 (35 wt% in EtOH), DMF, RT

Scheme 2.7 Synthetic route to prepare **EB TANI-$(HTAB)_2$**

2.3 Conclusion

This chapter describes in detail the stepwise syntheses of tetra(aniline) cationic amphiphiles, starting with the synthesis of oligo(anilines)s (Ph/NH_2 **TANI**, NH_2/NH_2 **TANI**) as precursors. The methodology used to produce pure Ph/NH_2**TANI** was based on introducing the protecting groups tert-butyloxycarbonyl (Boc) and diphenylmethylene (CPh_2) on the secondary and primary amines, respectively. Protecting groups are not only required to produce pure materials, but they also prevent any side reaction that could take place. This stepwise route allows the reaction to be carried out on a large scale (> 10 g) and obtains a moderate overall yield (20% over 6 steps). Boc Ph/NH_2 **TANI** was functionalised with an alkyl bromide spacer to form an amide linker. After producing the AB diblock architecture structures, Boc Ph/NH_2 **TANI**-C6Br, Boc deprotection of the product was performed, followed by an oxidation reaction to form EB **TANI**-C6Br. To prepare single-tailed ammonium amphiphiles, the quaternisation reaction of EB **TANI**-C6Br with trimethylamine took place to form **EB TANI-PTAB**. Phosphonium amphiphiles were prepared by functionalising LEB Ph/NH_2 **TANI**-C6Br with trimethylphosphine to form **LEB TANI-PTPB.** In order to study the effect of doping on the synthesised materials, an oxidation reaction using hydrogen peroxide was performed to yield **TANI-PTPB** in the EB state

This methodology, including the synthesis of Boc protected precursors, was exploited to prepare a di-functional tetra(aniline) (NH_2/NH_2 **TANI)**. This material was synthesised with Boc groups protecting secondary amines and unprotected amine termini on both sides. NH_2/NH_2 **TANI** was used as the precursor to functionalise with two alkyltrimethylammonium and alkyltrimethylphosphonium head groups to form ABA triblock architecture structures. Bolaamphiphiles were designed for comparison with the corresponding single-tailed amphiphiles. **EB TANI-$(PTAB)_2$** and **EB TANI-$(PTPB)_2$** were synthesised in the same way as the single-tailed amphiphiles. Furthermore, Boc NH_2/NH_2 **TANI** $(C8Br)_2$ was formed by reaction of 8-bromooctanoic acid with Boc NH_2/NH_2 **TANI** via EDC coupling; Boc deprotection, oxidation and then quaternisation were carried out following the procedure mentioned before to yield ammonium bolaamphiphiles **EB TANI-$(HTAB)_2$.**

2.4 Experimental

2.4.1 Materials and instruments

Materials

All chemicals were purchased from Sigma-Aldrich UK and used as received without further purification. Molecular sieves were heated to 200°C overnight under vacuum to yield dried and activated molecular sieves. Unless specified, all solvents used were anhydrous. The dry solvents were obtained using a column of anhydrous alumina from Anhydrous Engineering (University of Bristol) and a drying system based on the Grubbs' design.

NMR spectrometry

^{1}H and ^{13}C NMR experiments were conducted using either a 400 MHz Varian VNMR 400 or a 500 MHz Bruker 500 NMR spectrometer and carried out in deuterated solvents. ^{31}P NMR spectra were carried out using 400 JEOL MHz spectrometers. All NMR spectra of the synthesised materials of this chapter are available in the **Appendix B**. Cryo-NMR experiments were conducted using a Bruker Avance III HD 500 Cryo.

Mass spectrometry

Mass spectrometry was conducted using either a Bruker Daltronics UltrafleXtreme or an Applied Biosystems 4700 Proteomic Analyser with *A*-Cyano-4-hydroxycinnamic acid matrix for matrix-assisted laser desorption/ionisation time-of-flight (MALDI-TOF), and either a Bruker Daltonics 7 Tesla Apex 4 or a MicrOTOF II for ESI-TOF. All mass spectra of the synthesised materials of this chapter are available in the **Appendix B.**

Elemental analysis

Elemental analysis was carried out on a Euro Vector Euro EA 3000 in the Microanalytical Laboratory of the University of Bristol.

2.4.2 Synthesis of TANI precursors

2.4.2.1 Boc Ph/NH_2 TANI synthesis

Synthesis of *N*-(diphenylmethylene)-*N'*-phenyl-*p*-phenylenediamine 1 (terminal amine CPh_2 protection) 1

Activated molecular sieves (100 g, 3Å), *N*-phenyl-*p*-phenylene diamine (1.05 eq., 27 g, 146 mmol) and benzophenone (1 eq., 25.33 mg, 139.04 mmol) were weighed out in that order into a three necked round-bottom flask with a stirrer bar and placed under N_2. The reactants were dissolved in dry toluene, and the mixture refluxed for 48 hours. Completion of the reaction was confirmed by TLC (4:1 petroleum ether: ethyl acetate). Once complete, the mixture was cooled to room temperature and decanted from the molecular sieves. THF was used to wash the sieves until colourless and the combined organic fractions were evaporated to give a brown oil which precipitated into a bright yellow solid when methanol (10 ml) was added. The suspension was filtered and the filtrate was concentrated and filtered again. The combined solids were recrystallized from methanol to yield yellow crystals of **1**; concentration of the filtrate yielded a second and a third crop of crystals. The yield is 75%. ^{1}H NMR (400 MHz, $CDCl_3$) δ 7.70 (d, J =7.2, 2H), 7.44 – 7.31 (m, 3H), 7.28 – 7.14 (m, 5H), 7.13 – 7.09 (m, 2H), 6.90 (d, J = 7.7 Hz, 2H), 6.86 – 6.78 (m, 3H), 6.63 (d, J = 8.7 Hz, 2H), 5.50 ppm (s, 1H). MS (ESI) m/z = 349.17 $[M+H]^+$. Anal. Calcd. for $C_{25}H_{20}N_2$: C 86.17, H 5.79, N 8.04 %; found C 86.22, H 5.72, N 8.06 %.

Synthesis of *N*-(diphenylmethylene)-*N'*-(*tert*-butoxycarbonyl)- *p*-phenylenediamine (Boc protection) 2

1 (1 eq., 10g, 28.69mmoles) was added to di-tert-butyl dicarbonate (1.2 eq., 7.33 g, 34.8 mmol) and dimethylaminopyridine (DMAP) (0.1 eq., 0.34 g, 22 mmol) and placed under a nitrogen atmosphere. The solids were dissolved in THF and the solution refluxed for 24 h. The reaction was monitored by TLC (4:1 petroleum ether: ethyl acetate) which was completed after 24 hrs. The mixture was cooled to room temperature and ethanol was added to precipitate the product. The mixture was cooled in the fridge overnight, filtered, and the resulting solid was recrystallized from ethyl acetate to yield fine yellow needles of **2** (80% yield). ^{1}H NMR (400 MHz, $CDCl_3$) δ7.74 (d, J=6.85, 2H), δ 7.42 (m, 3H) δ 7.27 (m, 6H), δ 7.13 (m ,5H), δ 6.97 (d, J=8.91 , 2H), δ 6.67 (d,8.3

J= ,2H) , 1.40 (s, 9H), MS (ESI) m/z = 449.2 $[M+H]^+$. Anal. Calcd. for $C_{30}H_{28}N_2O_2$: C 80.33, H 6.29, N 6.25 %; found C 80.75, H 6.21, N 6.17 %.

Synthesis of *N*-(Diphenylmethylene)-*N'*-(*tert*-butoxycarbonyl)-*N'*-(4-bromophenyl)-*p*-phenylenediamine (bromination and Boc protection) 3

Tetra-n-butylammonium tribromide (1.1 eq., 9.92 g, 30.8 mmol) was added to a mixture of **1** (1 eq., 10 g, 2.87 mmol) in dichloromethane (80 ml). The mixture was stirred at room temperature for 1 hour and a half before sodium sulfite (aq., 22%, 50 ml) was added. The mixture was stirred for a further 30 minutes at room temperature, then sodium hydroxide (2 M, 25 ml) was added with stirring. After 20 minutes the mixture was separated and the organic phase washed with pure water (3 x 40 ml), dried over anhydrous $MgSO_4$ then filtered. The solvent was removed under vacuum and to the residue was added di-tert-butyl dicarbonate (1.1 eq., 6.72 g, 30.8 mmol) and DMAP (0.1 eq., 0.35 g, 0.287 mmol) in dry THF (80 ml) and refluxed overnight at 66° C. Once the mixture cooled, ethanol (50 ml) was added and the mixture was kept in the fridge overnight. The mixture was filtered and then recrystallised from ethyl acetate to yield the product **3** as a fine pale-yellow powder. The yield is 60.42 %.^{1}H NMR (400 MHz, $CDCl_3$) δ 7.74 (d, J =7.6 Hz, 2H) 7.57 – 7.36 (m, 4H), 7.36 – 7.21 (m, 5H), 7.12 (d, J = 7.6 Hz, 2H), 7.02 (d, J = 8.3, 2.6 Hz, 2H), 6.94 (d, J =7.6 Hz, 2H), 6.68 (d, J = 8.7 Hz,2H), 1.39 ppm (s, 9H).MS (ESI) m/z = 527.1, 529.1 [M+H]. Anal. Calcd. for $C_{30}H_{27}BrN_2O_2$: C 68.31, H 5.16, N 5.13 %; found C 68.61, H 5.32, N 5.28 %.

Synthesis of *N*-(*tert*-butoxycarbonyl)-*N'*-phenyl-*p*-phenylenediamine (CPh2 deprotection) 4

To a flask containing ammonium formate (12 eq., 159.6 mmol, 10.064 g) was added **3** (1 eq., 13.278 mmol, 6 g) and palladium on carbon (10 % Pd by weight, 2.5 mol% Pd vs. 355,9 mg) and the mixture protected under nitrogen. THF and methanol were added (60 and 150 ml, respectively) and the mixture refluxed for 6 hours. After completion was confirmed by TLC (1:1 ethyl acetate: n-hexane), the reaction was cooled to room temperature and the solvent removed. The residue was taken up in dichloromethane (100 ml) and filtered through a plug of celite. The celite was washed with DCM and the filtrate evaporated. The residue was broken up and stirred into n-hexane (150 ml) followed by filtration and washing with hexane to yield the product as an off-white powder. The yield is 94.5% and the crude product was used in the next reaction without

further purification. ^{1}H NMR (400 MHz, $CDCl_3$) δ 7.34 – 7.07 (m, 5H), 6.81 – 6.84 (d, *J* = 8.4 Hz, 2H), 6.63 (d, *J* = 8.7 Hz, 2H), 3.62 (s, 2H), 1.45 (s, 9H). MS (ESI) m/z =229.02 $[M\text{-}tBu+2H]^+$, 285.16 $[M]^+$. Anal. Calcd. for $C_{17}H_{20}N_2O_2$: C 71.82, H 7.09, N 9.85 %; found C 72.04, H 6.94, N 9.73 %.

Synthesis of *N*-(diphenylmethylene)-*N'*-(*tert*-butoxycarbonyl)-*N'*{*N*-[4-(*N*-*tert*-butoxycarbonylanilino)]phenyl-*N*-(*tert*-butoxycarbonyl)}phenyl-*p*-phenylenediamine (Buchwald Hartwig/boc protection) 5

A dried three necked round-bottom flask was prepared containing **3** (5 g, 9.48 mmol, 1eq.), **4** (3.23 g, 11.4 mmol, 1.2 eq.), $Pd(dba)_2$ (108.90 mg, 2 mol%), XPhos (90.29 mg, 2 mol%) and sodium tert-butoxide (1.82 g, 2eq.). The reagents were placed under nitrogen and 50 ml of anhydrous toluene was added. The mixture was refluxed at 110 °C overnight for 24 hrs, until complete consumption of **3** was monitored by TLC (4:1 petroleum ether: ethyl acetate). The reaction was cooled to room temperature and filtered through celite, then the solvent was removed by vacuum. The residue was taken up in dichloromethane and washed with deionised water three times, followed by drying of the organic phase over anhydrous $MgSO_4$ and the solvent was removed by rotary evaporator. Di-tert-butyl dicarbonate (1.3 eq., 2.687 g) and DMAP (0.1 eq., 115, 69 mg) were added to the residue and dissolved in dry THF (100 ml), and the mixture was heated at 60^{o}C and placed under nitrogen for 24 hrs. Once complete, the solvent was evaporated and the residue washed with methanol and filtered to give the product as a beige powder. The yield is 54.8%. ^{1}H NMR (400 MHz, $CDCl_3$) δ 7.74 (d, *J* = 7.4 Hz, 2H), 7.49 – 7.38 (m, 3H), 7.30 (dd, *J* = 8.4, 7.1 Hz, 3H), 7.25 – 7.07 (m, 15H), 6.95 (d, *J* = 7.4 Hz, 2H), 6.66 (d, *J* = 8.3 Hz, 2H), 1.44 (s, 9H), 1.43 (s, 9H), 1.38 (s, 9H). MS (ESI) m/z =853.4 $[M+Na]^+$. Anal. Calcd. for $C_{52}H_{54}N_4O_6$: C 75.16, H 6.55, N 6.74 %; found C 74.67, H 6.44, N 6.71 %.

Synthesis of Boc-protected TANI (CPh_2 deprotection) 6

Ammonium formate (10 eq., 3.035 g, 48.13 mmol), **5** (1eq., 4.00 g, 4.81 mmol), and Pd/C (10% Pd content, 2 mol%, 0.102 g, 0.10 mmol) were added to a three necked round-bottom flask and placed under N_2. Dry THF and degassed methanol (1:2.5 respectively) were added to the flask. The mixture was refluxed at 65 °C until completion was observed by TLC (1:1 n-hexane: ethyl acetate) after 6 hours. The solvent was evaporated and the residue taken up in dichloromethane,

then filtered through celite. The filtrate was evaporated under vacuum and the residue stirred in hexane between 1 to 3 hours, then filtered to yield the product as an off-white powder. The yield is 96.4 %. ^{1}H NMR (400 MHz, $CDCl_3$) δ 7.33 – 7.27 (m, 2H), 7.21 – 7.06 (m, 11H), 6.97 (d, *J* = 7.8 Hz, 2H), 6.62 (d, *J* = 8.4 Hz, 2H), 5.10 (s, 2H), 1.51 – 1.33 (m, 27H). ^{13}C NMR (101 MHz, Chloroform-*d*) δ 168.64, 153.82, 149.04, 143.12, 139.51, 138.29, 136.11, 130.78, 129.52, 129.30, 129.24, 128.63, 128.48, 128.19, 128.14, 127.89, 127.43, 126.15, 125.08, 121.34, 116.82, 80.84, 28.20. MS (ESI) m/z =689.3 $[M+Na]^+$. Anal. Calcd. for $C_{39}H_{46}N_4O_6$: C 70.25, H 6.95, N 8.40 %; found C 70.04, H 7.17, N 8.49 %.

2.4.2.2 Boc NH_2/NH_2 TANI synthesis

NO_2/NO_2 TANI 7

A solution of diaminodiphenylamine sulphate (3 g, 10.1 mmol, 1 eq.), 4-fluoro-1-nitrobenzene (14.24 g, 100.9 mmol), triethylamine (21 ml) in dry DMSO (40 ml) was heated to 90°C overnight. The reaction mixture was cooled to room temperature and then poured into deionised water (500 ml) with vigorous stirring. The stirring was continued to ensure complete precipitation. The suspension was filtered and washed with water (100 ml), chloroform (100 ml) and hexane (50 ml). The residue was recrystallised with methanol and the precipitate was filtered yielding the product as a brown solid (60% yield). ^{1}H NMR (400 MHz, DMSO-d_6) δ 9.12 (s, 2H), 8.22 (s, 1H), 8.09 – 8.00 (m, 4H), 7.19 – 7.02 (m, 8H), 6.95 – 6.86 (m, 4H), 2.08 (s, 2H). MS (ESI) m/z = 464.2 $[M+Na]^+$. Anal. Calcd. for $C_{39}H_{43}N_5O_{10}$: C, 63.15; H, 5.84; N, 9.44%; found C 62.209, H 6.00, N 9.04%.

Boc NO_2/NO_2 TANI 8

NO_2/NO_2 **TANI** (7 g, 22.9 mmol, 1 eq.), di-tert-butyl dicarbonate (2.4 eq., 10 g) and dimethylaminopyridine (0.2 eq., 556 mg) were dissolved in dry THF (200 ml). The reaction mixture was refluxed overnight at 60°C and monitored by TLC in (1: 4 ethyl acetate: n-hexane) until completion of the reaction was observed, then the solvent was removed. The residue was taken up in DCM and washed with water, HCl (1M), NaOH (1M) and saturated brine, followed by drying over MgSO4. The solvent was evaporated to yield the product as a pink powder (85% yield). ^{1}H NMR (400 MHz, DMSO-d_6) δ 8.22 – 8.13 (m, 4H), 7.44 – 7.36 (m, 4H), 7.30 – 7.19 (m, 8H), 1.37 (d,

J = 4.3 Hz, 27H). MS (ESI) m/z = 764.3 $[M+Na]^+$. Anal. Calcd. for $C_{39}H_{43}N_5O_{10}$: C, 63.15; H, 5.84; N, 9.44%; found C 62.209, H 6.00, N 9.04%.

Boc NH_2/NH_2 TANI 9

A solution of Boc NO_2/NO_2 **TANI** (7 g, 9.43 mmol, 1 eq.), palladium on carbon (10% Pd content, 5 mol% Pd, 500 mg) and ammonium formate (20 eq., 11.9 g) in dry THF and methanol (1:2.5) was prepared under a nitrogen atmosphere then refluxed overnight. The reaction was monitored by TLC (1:1 ethyl acetate: n-hexane) to ensure consumption of starting materials. The reaction was cooled to room temperature and the solvent evaporated. The residue was taken up in DCM and filtered through celite. The filtrate was evaporated and the residue was recrystallized from methanol to yield a pale pink powder, with concentration of the mother liquor yielding a second crop (63% yield). ^{1}H NMR (400 MHz, DMSO-d_6) δ 7.21 – 7.04 (m, 8H), 6.87 – 6.78 (m, 4H), 6.53 – 6.45 (m, 4H), 5.08 (s, 4H), 1.37 – 1.33 (m, 27H). MS (ESI) m/z = 704.3 $[M+Na]^+$. Anal. Calcd. For $C_{39}H_{47}N_5O_6$: C, 68.70; H, 6.95; N, 10.27%; found C 68.275, H 7.02, N 10.29%.

2.4.3 Synthesis of single-tailed amphiphiles

2.4.3.1 EB TANI-PTAB synthesis

Boc Ph/NH_2 TANI-C_6Br

A solution of Boc Ph/NH_2 **TANI** (1 g, 1.499 mmol, 1 eq.) in anhydrous THF was placed under nitrogen in a flask equipped with a dropping funnel. The mixture was stirred and cooled in an ice bath before trimethylamine (3.14 ml, 22.5 mmol, 5 eq.) was added. A solution of 6-bromohexanoyl chloride (0.75 ml, 4.50 mmol, 1 eq.) in dry tetrahydrofuran (40 ml) was added dropwise into the mixture with continued stirring and ice cooling until the addition was complete. The reaction mixture was then allowed to warm to room temperature overnight. The reaction was monitored by TLC (1:1 n-hexane: ethyl acetate). Once the reaction was completed, the solvent was evaporated and the residue was taken up in ethyl acetate and filtered to remove impurities. The solution was then washed with HCl (1M, 25ml), NaOH (1M, 25 ml) and saturated brine, dried over dry $MgSO_4$ and the solvent removed under reduced pressure. The residue was purified by flash column chromatography (silica gel, 1:1 ethyl acetate: n-hexane). 150 ml of n-hexane was added to the purified residue, and the mixture was stirred overnight then filtered to

obtain the product as a white powder. Yield: 80%. 1H NMR (400 MHz, DMSO-d6) δ 9.92 (s, 1H), 7.58 – 7.51 (m, 2H), 7.34 (dd, J = 8.4, 7.2 Hz, 2H), 7.24 – 7.07 (m, 13H), 3.53 (t, J = 6.7 Hz, 2H), 2.29 (t, J = 7.3 Hz, 2H), 1.81 (p, J = 6.8 Hz, 2H), 1.59 (p, J = 7.4 Hz, 2H), 1.41 (d, J = 7.2 Hz, 2H), 1.35 (d, J = 1.2 Hz, 27H). MS (ESI) m/z =876.3 $[M+Na]^+$. Anal. Calcd. For $C_{45}H_{55}BrN_4O_7$: C 64.05, H 6.57, N 6.64, Br 9.47 %; found C 61.515, H 6.91, N 5.87, Br 9.52 %.

LEB Ph/NH_2 TANI-C_6Br

A solution of Boc Ph/NH_2 **TANI**-C_6Br (1 g, 1.19 mmol, 1 eq.) in anhydrous dichloromethane (30 ml) was placed in a flask under a nitrogen atmosphere. Trimethylsilyliodide (0.61 ml, 4.27 mmol, 3.6 eq.) was added slowly with stirring. The mixture was stirred for 2 hours, then anhydrous methanol (0.172 ml) was added dropwise until complete precipitation of the pale product was achieved. 0.5 ml of triethylamine (TEA) was added slowly and a colour change to pale purple was seen. The mixture was centrifuged, the supernatant removed and the residue was washed once with DCM and 3 times with diethyl ether (3 x 40 ml), then dried under reduced pressure to obtain the product (79% yield). ^{1}H NMR (400 MHz, DMSO-d_6) δ 9.61 (s, 1H), 7.75 (s, 1H), 7.64 (d, *J* = 19.3 Hz, 2H), 7.38 (d, *J* = 8.3 Hz, 2H), 7.14 (t, *J* = 7.7 Hz, 2H), 6.93 (dq, *J* = 18.6, 8.6 Hz, 13H), 6.67 (t, *J* = 7.3 Hz, 1H), 3.54 (s, 2H), 2.25 (d, *J* = 8.2 Hz, 2H), 1.87 – 1.78 (m, 2H), 1.60 (s, 2H), 1.42 (d, *J* = 9.9 Hz, 2H). MS (MALD) m/z = 542.27 $[M]^+$. Anal. Calcd. for $C_{30}H_{31}BrN_4O$: C 66.30, H 5.75, N 10.31, Br 14.70%; found C 65.607, H 5.687, N 10.151, Br 14.42%.

EB Ph/NH_2 TANI-C_6Br

LEB Ph/NH_2 **TANI**-C_6Br (400 mg, 0.735 mmol) was dissolved in DMF (12.5 ml). A solution of ammonium persulfate (1 eq., 167.94 mg) in HCl (1 M, 12.5 ml) was added and the reaction mixture stirred for 1 hour. The mixture turned dark green with a precipitate forming, which was collected by Centrifugation. The dark green precipitate was washed with water 3 times, then re-dispersed in acetone (300 ml), and NH_4OH (2 M, 12.5 ml) was added to the mixture before it was stirred for 30 minutes. The mixture turned dark purple and the acetone was removed under vacuum to leave a suspension of the product in water, which was centrifuged and washed with large amounts of water, before being dried overnight in a vacuum oven to give the desired product (80% yield). ^{1}H NMR (400 MHz, DMSO-d6) δ 9.94 (s, 1H), 8.41 (s, 1H), 7.92-6.42 (m, 17H),

3.52 (t, *J* = 6.8 Hz, 2H), 2.29(s, 2H), 1.81 (t, *J* = 7.5 Hz, 2H), 1.58 (d, *J* = 8.3 Hz, 2H), 1.40 (s, 2H). MS (MALD) m/z = 542.2 $[M]^+$. Anal. Calcd. for $C_{30}H_{29}Br\ N_4O$: C 66.54, H 5.40, N 10.35, Br 14.76%; found C 66.81, H 5.75, N 10.26, Br 14.21%.

EB Ph /NH_2 TANI-($C_6BrMe_3N^+Br^-$)

EB Ph/NH_2 **TANI**-C_6Br (200 mg, 0.370 mmol, 1 eq.) was dissolved in DMF (3 ml). A solution of trimethylamine (TMA) in ethanol (33 wt.%, 880 µL, 3.70 mmol, 10 eq.) was added and the solution mixture was stirred at room temperature for 3 days until completion was observed by TLC (100% ethyl acetate). Once completed, the reaction mixture was poured into ice-cold diethyl ether and left in a freezer overnight then centrifuged. The residue was dried overnight in a vacuum oven, followed by further aqueous washes, and the residue freeze dried to yield the desired product as a fluffy dark blue solid (69 % yield)..^{1}H NMR (400 MHz, Acetonitrile-d3) δ 9.21 (s, 1H), 8.71 (s, 1H), 7.73 (s, 1H), 7.42 (d, *J* =24.7 Hz, 1H), 7.27 (s, 1H), 7.18-6.87 (m, 14H), 3.28 (s, 2H), 3.04 (s, 9H), 2.41 (d, *J* =24.7 Hz, 2H), 1.79 (s, 2H), 1.73 (s, 2H), 1.41 (s, 2H). MS (ESI) m/z= 520.3 $[M-Br]^+$

2.4.3.2 EB TANI-PTPB synthesis

LEB Ph/NH_2 TANI-($C_6BrMe_3P^+Br^-$)

A solution of **LEB TANI-C6Br** (200 mg, 0.368 mmol, 1 eq.) in DMF (12 ml) was prepared in a flask under a nitrogen atmosphere at 0°C. Trimethylphosphine (0.552 ml, 0.552 mmol, 1.5 eq.) as a 1 M solution in toluene was added to the solution. The thick-walled flask was in an oil bath and tightly sealed then placed behind a blast shield. The temperature was then raised to 70°C for at least 16 h. After cooling to 0°C, the remaining trimethylphosphine was removed under vacuum then the mixture was poured into a large amount of cold diethyl ether and placed in freezer to precipitate the product. The solution mixture was centrifuged and residues were washed several times with diethyl ether (5 X 20 ml) to yield the desired (a) fluffy gray product (70 % yield). ^{1}H NMR (500 MHz, DMSO-d_6) δ 9.70 (s, 1H), 7.71 (s, 1H), 7.65 (s, 1H), 7.58 (s, 1H), 7.37 – 7.31 (m, 2H), 7.16 – 7.09 (m, 2H), 6.97 – 6.84 (m, 12H), 6.67 (t, *J* = 7.3 Hz, 1H), 2.26 (t, *J* = 7.3 Hz, 2H), 2.18 – 2.08 (m, 2H), 1.77 (d, *J* = 14.7 Hz, 9H), 1.59 (p, *J* = 7.4 Hz, 2H), 1.49 (dq, *J* = 11.2, 8.2, 7.4 Hz, 2H), 1.39 (td, *J* = 8.1, 4.9 Hz, 2H). ^{31}P NMR (162 MHz, DMSO-d_6) δ 28.17. ^{13}C NMR (126 MHz, DMSO-

d_6) δ 171.25, 145.72, 141.31, 138.99, 138.14, 136.42, 135.44, 130.96, 129.57, 121.28, 121.00, 119.85, 118.60, 118.57, 118.02, 115.90, 115.09, 36.27, 29.98, 29.85, 24.94, 22.73, 22.32, 20.84, 20.81, 7.76, 7.33. HRMS (ESI) m/z = 539.2930 $[M\text{-}Br]^+$.

EB Ph/NH_2 TANI-($C_6BrMe_3P^+Br^-$)

LEB TANI-PTPB (33 mg, 1 eq.) was dissolved in acetonitrile (5 ml) and H_2O_2 (30 wt.% in water, 0.5 ml, >12 eq.) was added. The solution mixture was stirred for 2-3 hours and then it was added dropwise to ice-cold diethyl ether (40 ml) and allowed to fully precipitate overnight in the freezer. The suspension was centrifuged and residues were collected and washed further with diethyl ether to remove residual acetonitrile. The residue was dried in a vacuum oven to remove ether, the dried residues was re-dissolved in deionised water (10 ml). These solutions were centrifuged to remove any water-insoluble impurities and freeze-dried to yield a fluffy blue solid product. ^{1}H NMR (400 MHz, DMSO-d_6) δ 10.15 – 9.77 (m, 1H), 8.43 (dd, *J* = 28.2, 4.2 Hz, 1H), 7.73 – 6.67 (m, 17H), 2.35 (ddd, *J* = 14.0, 9.1, 5.6 Hz, 2H), 2.20 (d, *J* = 16.0 Hz, 2H), 1.82 (dd, *J* = 14.8, 2.3 Hz, 9H), 1.64 (d, *J* = 9.7 Hz, 2H), 1.58 – 1.48 (m, 2H), 1.41 (d, *J* = 13.7 Hz, 2H). ^{31}P NMR (162 MHz, DMSO-d_6) δ 27.16. HRMS (ESI) m/z = 537.2776 $[M\text{-}Br]^+$.

2.4.4 Synthesis of bolaamphiphiles

2.4.4.1 EB TANI-$(PTAB)_2$ synthesis

Boc NH_2/NH_2 TANI-($C_6Br)_2$

A round bottom flask with a solution of Boc NH_2/NH_2 **TANI** (3.0 g, 4.50 mmol, 1 eq.) in dry THF was equipped with a dropping funnel and placed under nitrogen. The mixture was cooled in an ice bath before trimethylamine (3.14 ml, 22.5 mmol, 5 eq.) was added with stirring. A solution of 6-bromohexanoyl chloride (0.75 ml, 4.50 mmol, 1 eq.) in anhydrous tetrahydrofuran (40 ml) was added dropwise. The reaction mixture was then warmed to room temperature overnight. The reaction was monitored with TLC (1:1 n-hexane: ethyl acetate). Once the reaction was completed, the solvent was evaporated and the residue was taken up in ethyl acetate and filtered to remove precipitated impurities. The solution was then washed with HCl (1M), NaOH (1M) and (a) saturated brine and then dried over anhydrous $MgSO_4$ and the solvent evaporated. The

residue was purified by flash column chromatography (silica gel, 1:1 ethyl acetate: n-hexane). The residue was stirred in n-hexane (100 ml) overnight, then filtered to obtain the product as an off-white powder (88% yield). ^{1}H NMR (400 MHz, DMSO-d_6) δ 9.92 (s, 2H), 7.60 – 7.52 (m, 4H), 7.17 – 7.07 (m, 12H), 3.53 (t, *J* = 6.7 Hz, 4H), 2.30 (t, *J* = 7.3 Hz, 4H), 1.82 (p, *J* = 6.9 Hz, 4H), 1.60 (p, *J* = 7.5 Hz, 4H), 1.42 (q, *J* = 8.0 Hz, 4H), 1.36 (s, 27H). MS (ESI) m/z = 1058.3 $[M+Na]^+$. Anal. Calcd. for $C_{51}H_{65}Br_2N_5O_8$: C 59.13, H 6.32, N 6.76, Br 15.43 %; found C 59.21, H 6.23, N 6.60, Br 15.21 %.

LEB NH_2/NH_2 TANI-$(C_6Br)_2$

A solution of Boc NH_2/NH_2 **TANI**-$(C_6Br)_2$ (1.5 g, 1.44 mmol, 1 eq.) in anhydrous dichloromethane (50 ml) was placed in a flask under a nitrogen atmosphere. Trimethylsilyliodide (0.74 ml, 5.21 mmol, 3.6 eq.) was added gently with stirring. The mixture was stirred for 2 hours, then anhydrous methanol (0.21 ml) was added dropwise until no further precipitate appeared. Trimethylamine (TEA) was added slowly and a colour change to pale purple was observed. The mixture was centrifuged, the supernatant removed and the residue washed once with DCM and 3 times with diethyl ether then dried under vacuum to obtain the desired product (80% yield). ^{1}H NMR (400 MHz, DMSO-d_6) δ 9.59 (s, 2H), 7.63 (s, 2H), 7.54 (s, 1H), 7.35 (d, *J* = 8.4 Hz, 4H), 6.88 (d, *J* = 20.4 Hz, 12H), 3.52 (t, *J* = 6.7 Hz, 4H), 2.23 (t, *J* = 7.3 Hz, 4H), 1.80 (q, *J* = 7.1 Hz, 4H), 1.62 – 1.54 (m, 4H), 1.39 (t, *J* = 7.5 Hz, 4H). MS (MALDI) m/z = 735.32 $[M]^+$. Anal. Calcd. for $C_{36}H_{41}Br_2N_5O_2$: C 58.78, H 5.62, N 9.52, Br 21.73 %; found C 58.73, H 5.60, N 9.26 Br 21.39 %.

EB NH_2/NH_2 TANI-$(C_6Br)_2$

LEB NH_2/NH_2 **TANI**-$(C_6Br)_2$ (200mg, 0.27 mmol) was dissolved in DMF (5 ml). A solution of ammonium persulfate (1 eq., 62 mg) in HCl (1 M, 5 ml) was added and the mixture stirred for 1 hour. A colour change to pale green was observed, along with formation of a precipitate which was collected by centrifugation. After washing with water 3 times, the dark green precipitate was re-dispersed in acetone (250 ml), NH_4OH (2 M, 5 ml) was added and the reaction mixture was stirred for 30 minutes. A colour change to pale green was observed, and then the acetone was evaporated under vacuum to leave a suspension of the product in water, which was centrifuged and washed with large amounts of water, and dried overnight in a vacuum oven to get a dark

purple solid (70% yield). ^{1}H NMR (400 MHz, DMSO-d_6) δ 9.73 (d, *J* = 2.7 Hz, 1H), 8.33 (d, *J* = 3.1 Hz, 1H), 7.67 – 7.58 (m, 2H), 7.57 – 7.44 (m, 2H), 7.36 (d, *J* = 8.4 Hz, 1H), 7.14 – 6.78 (m, 13H), 3.51 (s, 4H), 2.34 – 2.20 (m, 4H), 1.80 (td, *J* = 9.0, 4.7 Hz, 4H), 1.59 (q, *J* = 7.6, 7.1 Hz, 4H), 1.43 – 1.35 (m, 4H). MS (MALDI) m/z = 735.2 $[M]^+$. Anal. Calcd. for $C_{36}H_{39}Br_2N_5O_2$: C 58.95, H 5.36, N 9.55, Br 21.79 %; found C 58.255, H 5.488, N 9.271, Br 21.39 %.

EB NH_2/NH_2 TANI-($C_6BrMe_3N^+Br^-$)$_2$

LEB **TANI**-(C6Br)$_2$ (200mg, 0.27 mmol) was dissolved in the minimum amount of DMF (2ml). Trimethylamine, TMA (33 wt.% solution in ethanol, 652.00 µl, 10 eq.) was added and the reaction was left to stir until completion was observed by TLC (100% ethyl acetate) and MALDI. Once completed, the reaction mixture was poured into ice-cold diethyl ether and left in the freezer overnight then centrifuged. The residue was dried under vacuum, followed by further aqueous washes (15 ml), and the residue freeze dried to yield the desired product as a fluffy dark blue solid (75% yield). ^{1}H NMR (500 MHz, DMSO-d_6) δ 10.07 (s, 1H), 9.84 (s, 1H), 8.39 (d, *J* = 3.7 Hz, 1H), 7.68 (td, *J* = 7.8, 6.3, 2.5 Hz, 2H), 7.53 (ddd, *J* = 8.9, 4.9, 2.6 Hz, 2H), 7.15 – 6.98 (m, 8H), 6.95 – 6.83 (m, 4H), 3.30 (d, *J* = 5.5 Hz, 4H), 3.06 (d, *J* = 1.9 Hz, 18H), 2.36 (dtd, *J* = 20.1, 7.3, 3.3 Hz, 4H), 1.76 – 1.63 (m, 8H), 1.37 – 1.29 (m, 4H). HRMS (ESI) m/z=345.7285 $[M]^+$.

2.4.4.2 EB TANI-(PTPB)$_2$ synthesis

LEB NH_2/NH_2 TANI-($C_6BrMe_3P^+Br^-$)$_2$

A solution of LEB **TANI**-(C6Br)$_2$ (340 mg, 0.462 mmol, 1 eq.) in DMF (12 ml) was prepared in a flask under a nitrogen atmosphere at 0^{o}C. Trimethylphosphine (2.31 ml, 2.311 mmol, 5 eq.), as a 1 M solution in toluene, was added to the solution. The thick-walled flask was placed in an oil bath and tightly sealed then placed behind a blast shield. The temperature was then raised to 70 °C for at least 16 h. After cooling to 0 °C, the remaining trimethylphosphine was removed under vacuum then the resulting mixture was poured into a large amount of cold diethyl ether to precipitate the product, then kept in the freezer overnight. The solution mixture was centrifuged and supernatant removed. Residues were washed several times with diethyl ether (5 X 20 ml) and dried in a vacuum oven overnight to yield the desired fluffy gray product (70% yield). ^{1}H NMR (400 MHz, DMSO-d_6) δ 9.62 (s, 2H), 7.75 (s, 2H), 7.66 (s, 1H), 7.61 (s, 1H), 7.37 (d, *J* = 8.8 Hz, 3H),

7.13 (s, 2H), 6.91 (d, *J* = 12.1 Hz, 13H), 6.66 (d, *J* = 7.4 Hz, 1H), 2.29 – 2.09 (m, 8H), 1.79 (d, *J* = 14.8 Hz, 18H), 1.65 – 1.57 (m, 4H), 1.52 (d, *J* = 8.1 Hz, 4H), 1.44 – 1.36 (m, 4H).^{31}P NMR (162 MHz, DMSO-d_6) δ 28.57. ^{13}C NMR (101 MHz, DMSO-d_6) δ 171.43, 170.93, 124.41, 121.90, 120.77, 118.97, 116.03, 65.58, 52.59, 40.53, 40.32, 40.11, 39.90, 39.69, 39.48, 39.27, 25.81, 25.12, 25.05, 22.36. MS (ESI) m/z = 363.7 $[M\text{-}2Br]^+$.

EB NH_2/NH_2 TANI-($C_6BrMe_3P^+Br^-$)$_2$

LEB TANI-(PTPB)$_2$ (170 mg, 1 eq.) was dissolved in acetonitrile (10 ml) and H_2O_2 (30 wt.% in water, 2.13 ml, >12 eq.) was added. The solution mixture was stirred for 1-2 hours and then it was added dropwise to ice-cold diethyl ether (40 ml) and allowed to fully precipitate overnight in the freezer. The suspension was centrifuged and residues were collected and washed further with diethyl ether to remove residual acetonitrile. The residues were dried in a vacuum oven to remove ether and the dried residues were re-dissolved in deionised water (80 ml). These solutions were centrifuged to remove any water-insoluble impurities and freeze-dried to yield a fluffy blue solid product. ^{1}H NMR (400 MHz, DMSO-d_6) δ 10.03 (s, 1H), 9.80 (s, 1H), 8.36 (d, *J* = 3.5 Hz, 1H), 7.64 (dd, *J* = 8.6, 5.3 Hz, 2H), 7.49 (dd, *J* = 8.8, 3.9 Hz, 2H), 7.21 – 6.65 (m, 11H), 2.38 – 2.25 (m, 4H), 2.14 (d, *J* = 15.5 Hz, 4H), 1.80 (dd, *J* = 14.8, 1.6 Hz, 18H), 1.60 (d, *J* = 16.0 Hz, 4H), 1.51 (s, 4H), 1.39 (d, *J* = 11.4 Hz, 4H). ^{31}P NMR (162 MHz, DMSO-d_6) δ 28.17. ^{13}C NMR (101 MHz, DMSO-d_6) δ 129.69, 121.92, 120.72, 119.97, 117.78, 40.59, 40.38, 40.17, 39.96, 39.75, 39.54, 39.34, 7.90, 7.36. HRMS (ESI) m/z = 362.6991 $[M\text{-}2Br]^+$.

2.4.4.3 EB TANI-(HTAB)$_2$ synthesis

Boc NH_2/NH_2 TANI-(C_8Br)$_2$

To a two-neck round bottom flask Boc NH_2/NH_2 **TANI** (2 g, 2.93 mmol, 1 eq.), 8-bromooctanoic acid (2.61 g, 11.7 mmol, 4 eq.) and EDC (2.25 g, 11.7 mmol, 4 eq.) were added and placed in an ice bath under nitrogen. DCM (anhydrous, 20 ml) was added and the mixture stirred for 10 min at 0^{o}C, the reaction mixture was then allowed to warm up to room temperature and stirred

overnight. Once TLC (1:1 ethyl acetate: n-hexane) confirmed consumption of the starting material, the solvent was evaporated and the residue washed 3 times with deionised water and centrifuged. The residue was taken up in ethyl acetate then washed twice with HCl (1 M), NaOH (1M) and saturated brine, and the organic phase dried over $MgSO_4$ with? (and) evaporation of the solvent to give the product. This was purified by flash column chromatography (silica gel, 1:1 ethyl acetate: n-hexane) to yield the product as a pale pink solid (60% yield). ^{1}H NMR (400 MHz, DMSO-d_6) δ 9.91 (s, 2H), 7.59 – 7.52 (m, 4H), 7.17 – 7.08 (m, 12H), 3.52 (t, *J* = 6.7 Hz, 4H), 2.28 (t, *J* = 7.4 Hz, 4H), 1.84 – 1.69 (m, 4H), 1.58 (s, 4H), 1.36 (s, 27H), 1.30 (q, *J* = 3.9 Hz, 8H). Anal. Calcd. for $C_{55}H_{73}Br_2N_5O_8$: C 60.49, H 6.74, N 6.41, Br 14.63 %; found C 60.416, H 6.71, N 6.58, Br 14.40 %. MS (ESI) m/z=1114.4 $[M+Na]^+$.

LEB NH_2/NH_2 TANI-$(C_8Br)_2$

A solution of Boc NH_2/NH_2 **TANI** $(C_8Br)_2$ (1 g, 0.916 mmol, 1 eq.) in anhydrous dichloromethane (30 ml) was placed in a flask under a nitrogen atmosphere. Trimethylsilyliodide (0.47 ml, 3.29 mmol, 3.6 eq.) was added gently with stirring. The mixture was stirred for 2 hours, then anhydrous methanol (0.13 ml) was placed under N_2 and added dropwise until complete precipitation was observed. Trimethylamine (TEA) (0.5 ml) was added slowly and a colour change to pale purple was observed. The mixture was centrifuged, the supernatant removed and the residue washed once with DCM and 3 times with diethyl ether then dried under vacuum to obtain the desired product (78% yield). ^{1}H NMR (400 MHz, DMSO-d_6) δ 9.57 (s, 2H), 7.62 (s, 2H), 7.37 – 7.33 (m, 4H), 6.94 – 6.83 (m, 13H), 3.51 (t, *J* = 6.7 Hz, 4H), 2.22 (t, *J* = 7.4 Hz, 4H), 1.77 (p, *J* = 6.9 Hz, 4H), 1.59 – 1.52 (m, 4H), 1.36 (d, *J* = 7.9 Hz, 4H), 1.30 – 1.24 (m, 8H). MS (MALDI) m/z= 791.4 $[M]^+$. Anal. Calcd. for $C_{40}H_{49}Br_2N_5O_2$: C 60.69, H 6.24, N 8.85, Br 20.19 %; found C 60.522, H 6.25, N 8.92, Br 19.91 %.

EB NH_2/NH_2 TANI-$(C_8Br)_2$

LEB NH_2/NH_2 **TANI** $(C_8Br)_2$ (170 mg, 0.21 mmol) was dissolved in DMF (5 ml). A solution of ammonium persulfate (1 eq., 49 mg) in HCl (1 M, 5 ml) was added and the mixture stirred for 1 hour. A colour change to pale green was observed with precipitation, which was collected by centrifugation. After washing with water 3 times, the dark green precipitate was re-dispersed in

acetone (250 ml), NH_4OH (2 M, 5 ml) was added and the reaction mixture was stirred for 30 minutes. A colour change to dark purple was observed with precipitation, and acetone was evaporated under vacuum to leave a suspension of the product in water, which was centrifuged and washed with large amounts of water, and dried overnight in a vacuum oven to get a dark purple solid (70% yield). ^{1}H NMR (400 MHz, DMSO-d_6) δ 9.87 (s, 2H), 8.40 (s, 1H), 7.30 (d, *J* = 232.0 Hz, 17H), 3.75 – 3.59 (m, 4H), 3.45 – 3.28 (m, 18H), 2.29 (d, *J* = 8.5 Hz, 4H), 1.91 – 1.73 (m, 4H), 1.60 (s, 4H), 1.35 (d, *J* = 29.3 Hz, 12H).MS (MALDI) m/z = 735.2 $[M]^+$.

EB NH_2/NH_2 TANI-($C_6BrMe_3N^+Br^-$)$_2$

EB TANI-(C8Br)$_2$ (200 mg, 0.27 mmol) was dissolved in DMF (2ml), followed by trimethylamine, TMA (33 wt.% solution in ethanol, 652.00 µl,10 eq.) and the reaction mixture was left to stir until completion was observed by TLC (100% ethyl acetate) and MALDI. The resulting solution was poured into ice-cold diethyl ether and left in freezer overnight then centrifuged. The residue was dried under vacuum, followed by further aqueous washes and freeze-dried to yield the desired product as a fluffy dark blue solid (75% yield). ^{1}H NMR (400 MHz, DMSO-d_6) δ 10.08 (s, 1H), 9.85 (s, 1H), 8.39 (d, *J* = 2.5 Hz, 1H), 7.67 (q, *J* = 4.9 Hz, 2H), 7.53 – 7.49 (m, 1H), 7.43 – 7.35 (m, 1H), 7.13 – 6.83 (m, 12H), 3.30 (d, *J* = 17.0 Hz, 10H), 3.05 (d, *J* = 2.0 Hz, 18H), 2.39 – 2.25 (m, 4H), 1.82 – 1.34 (m, 9H), 1.55 – 0.99 (m, 5H). MS (ESI) m/z= 373.76 $[M-2Br]^+$.

2.5 References

1 Y. Wang, H. D. Tran, L. Liao, X. Duan and R. B. Kaner, *J. Am. Chem. Soc.*, 2010, **132**, 10365–10373.

2 F. Lu, F. Wudl, M. Nowak and A. J. Heeger, *J. Am. Chem. Soc.*, 1986, **108**, 8311–8313.

3 J. Stejskal, I. Sapurina and M. Trchová, *Prog. Polym. Sci.*, 2010, **35**, 1420–1481.

4 Z. Wei and C. F. J. Faul, *Macromol. Rapid Commun.,* 2008, **29**, 280–292.

5 C. U. Udeh, N. Fey and C. F. J. Faul, *J. Mater. Chem.*, 2011, **21**, 18137-18153.

6 Z. Shao, Z. Yu, J. Hu, S. Chandrasekaran, D. M. Lindsay, Z. Wei and C. F. J. Faul, *J. Mater. Chem.*, 2012, **22**, 16230–16234.

7 H. Kim, T.-G. Kim and J.-W. Park, *Macromol. Res.*, 2013, **21**, 815–820.

8 H. Kim, S.-M. Jeong and J.-W. Park, *J. Am. Chem. Soc.*, 2011, **133**, 5206–5209.

9 J. Hu, X. Zhuang, L. Huang, L. Lang, X. Chen, Y. Wei and X. Jing, *Langmuir*, 2008, **24**, 13376–13382.

10 O. A. Bell, G. Wu, J. S. Haataja, F. Brömmel, N. Fey, A. M. Seddon, R. L. Harniman, R. M. Richardson, O. Ikkala, X. Zhang and C. F. J. Faul, *J. Am. Chem. Soc.*, 2015, **137**, 14288–14294.

11 W. Lyu, M. Alotaibi, O. A. Bell, K. Watanabe, R. Harniman, B.M. Mills, A. M. Seddon, S. E. Rogers, S. M. King, W. Yan and C. F. J. Faul, *Chem. Sci.*, 2018, **9**, 4392–4401.

12 S. P. Surwade, S. R. Agnihotra, V. Dua, N. Manohar, S. Jain, S. Ammu, and S. K. Manohar, *J. Am. Chem. Soc.,* 2009, **131**, 12528–12529.

13 R. Chen and B. C. Benicewicz, *Macromolecules*, 2003, **36**, 6333–6339.

14 I. Kulszewicz-Bajer, I. Rozalska and M. Kurylek, *New J. Chem.*, 2004, **28**, 669-675.

15 B. A. Pindzola and D. L. Gin, *Langmuir*, 2000, **16**, 6750–6753.

CHAPTER 3 SELF-ASSEMBLY OF TANI-BASED SINGLE-TAILED AMPHIPHILES IN AQUEOUS SOLUTIONS

3.1 Introduction

Amphiphiles comprise hydrophilic and hydrophobic groups and self-assemble into different architectures, such as micelles, vesicles, fibers, disks, tubes and lamellar structures.[1] These structures are formed owing to noncovalent interactions such as hydrogen bonding, electrostatic interactions, hydrophobic interactions, and van der Waals interactions. Tuning the self-assembled structures of a classical amphiphile, for example, from spherical micelles to disks, vesicles, sheets, fibres, is possible based on the packing parameter. The concept of the packing parameter was introduced by Israelachvili *et al* [2] and is defined as $\mathrm{p} = \mathrm{v} / \mathrm{a}_0 \mathrm{l}_\mathrm{c}$. The packing parameter, as described in detail in the **Chapter 1**, depends on the critical or stretched length, l_c, and volume, v, of the hydrophobic tail, and the optimal area of the head group, a_0. An initial prediction of self-assembled morphology can be made by calculating the packing parameter. The proposed structure of an aggregate depends on the packing parameter value. Hence, it can be spherical when $\mathrm{p} \leq \frac{1}{3}$, it forms cylindrical micelles when $\frac{1}{3} < \mathrm{p} < \frac{1}{2}$, and is lamellar when $\mathrm{p} = 1$. Vesicles or flexible bilayers can be obtained when $\frac{1}{2} \leq \mathrm{p} < 1$ and inverted micelles formed when $(\mathrm{p} > 1)$.

Conjugated oligomers have continued to receive much attention in the fields of chemistry and materials science because of their interesting and tunable optoelectronic properties[3,4] and applications. As discussed in **Chapter 1**, these oligomers have emerged as ideal models for their corresponding conjugated polymers owing to their solubility, processability, and formation of well-defined structures. Oligo(aniline)s are conjugated oligomers of aniline, related by structural and optoelectronic similarity to the well-known redox-active conducting polymer, poly(aniline) **(PANI)**.[5,6,7] Oligo(aniline)s have attracted attention as the conjugated structural unit for various

amphiphiles, including amphiphilic copolymers, and both conventional and bolaamphiphiles.[3,4] Among these oligomers, tetra(aniline) (**TANI**) is the smallest aniline oligomer that can display the same set of oxidation and doped states as PANI: the fully reduced leucoemeraldine state, denoted as **LEB** (colourless), the half-oxidized emeraldine base state, denoted as **EB** (blue or violet), the fully oxidized pernigraniline state, denoted as **PB** (black),[8,9] and the conducting emeraldine salt (**ES**) state.[10,11] It further retains similar chemical properties to those of **PANI,** but with improved solubility and processability.[5,6,7]

In general, π-conjugated oligomers such as **TANI** lack solubility in water. Interestingly, some studies have reported the functionalization of **TANI** with hydrophilic groups forming water-soluble amphiphiles. The most widely prepared and studied **TANI**-based amphiphiles are based on the addition of a poly(ethylene glycol) block.[12,13] Recently, our group designed and synthesised the cationic pentyltrimethylammonium bromide amphiphile based on **TANI, TANI-PTAB**, which self-assembled into high aspect-ratio nanowires.[14]

One aspect of the unique ability of oligo(aniline)-based materials to be doped that has not been exploited is the use of dopants to address not only the redox state, but also the volume of the electroactive component (induced volume changes in **PANI** have been exploited widely for the production of soft actuators).[15] Interestingly, acid dopants added to **TANI**-based amphiphiles would attach the TANI backbone and protonate the quinoid nitrogen atoms, resulting in the **ES** state.[3,16] The electrostatic interactions occurring between the protonated **TANI**-amphiphiles and the counterions of the added dopant results in materials classified as low molecular weight electrostatic supra-amphiphiles (eSA).[3] The addition of dopant would change the volume of the hydrophobic **TANI**-based tail structure,[17] in other words, increasing the packing parameter through changes in volume v. Hence, the intrinsic nature of the electroactive tail of **TANI**-based amphiphiles endow switchable pH-responsivity to such systems through protonic acid doping and de-doping, and thus form tunable supramolecular self-assembled structures in a reversible fashion. We have termed this approach the “addressable packing parameter approach”, APP.

Moreover, in terms of the role of the packing parameter, changing the amphiphilic head groups also has a strong impact on the self-assembled structures and has been reported before in

various amphiphilic systems.[18, 19] From this perspective, we are interested in exploring the effect the variation of the head groups of our **TANI**-based amphiphiles has on the self-assembling behaviour. Furthermore, phosphonium amphiphiles have not been extensively studied and explored when compared with ammonium amphiphiles due to the complexity of the phosphorus chemistry, which restricted synthesis and therefore self-assembly studies.[20] Phosphonium-based materials however offer many potential applications not observed with ammonium analogues such as antimicrobial activity and biomedical applications.[21,22,23,24,25] Nitrogen and phosphorus atoms showed a difference in terms of chemistry and size; the atomic radii of the N and P atoms are 0.56 and 0.98 Å, respectively. The length of a carbon–nitrogen bond is 1.48 Å, while a carbon–phosphorous bond length is 1.84 Å.[26] Furthermore, critical aggregation concentrations (CAC) for phosphonium-based amphiphiles are lower than their corresponding ammonium amphiphiles, suggesting that the electrostatic repulsion between head groups decreases as result of strong counterion binding.[25,27,28] These differences between ammonium and phosphonium amphiphiles could significantly affect their self-assembling behaviour.

To our knowledge, phosphonium amphiphiles based on **TANI** have not been synthesised or explored yet. We have dedicated several years in our group to explore and understand the behaviour of amphiphilic oligo(aniline)s with respect to the difference in the architectures of **TANI**-based amphiphiles. Herein, we designed and synthesised an ammonium single-tailed amphiphile based on **TANI, TANI-PTAB** and a new phosphonium single-tailed amphiphile, **TANI-PTPB.** The first part of this chapter focused on ammonium amphiphiles and the second part ‘focused on the phosphonium amphiphiles. In general, we explored novel ways to tune the self-assembly of **TANI**-based amphiphiles in an unprecedented way. We investigated the influence of noncovalent dopants with different size on the volume of the **TANI**-based surfactant tail and thus the packing parameter. Moreover, by changing the packing parameter by using different sized dopants we are able to generalize this approach to reversibly tune classical self-assembled amphiphile structures, e.g. from wires to worm-like micelles and bilayer structures. We demonstrate a feasible strategy for reversible switching structures based on tunable self-

assembly in response to changes in pH that control the reversible protonic doping of the **TANI**-based surfactant tail.

3.2 Result and discussion

3.2.1 Synthesis and self-assembly studies of electroactive single-tailed ammonium amphiphiles

3.2.1.1 Synthesis of tetra(aniline) single-tailed ammonium amphiphile, TANI-PTAB

We previously reported the preparation of a conventional amphiphile **EB** Ph/NH_2–**TANI**–($C_6NMe_3^+Br^-$) **TANI-PTAB**.[14] The synthesis of cationic amphiphiles comprising **TANI** functionalised with alkyltrimethylammonium head groups built on the successful synthesis of Ph/NH_2 **TANI** reported previously. Boc-protected Ph/NH_2 **TANI** was first synthesised via a nucleophilic substitution reaction (**Scheme 2.1**).[14] Subsequently, Ph/NH_2 **TANI** was used to prepare the electroactive amphiphile **TANI-PTAB** (**Scheme 2.3**). The formation of the desired water-soluble amphiphile was confirmed using different characterization techniques, including ^{1}H NMR spectroscopy and high-resolution mass spectrometry. All the synthetic details are presented in the **Experimental Chapter**.

3.2.1.2 Self-assembly studies of ES TANI(TFA)$_2$-PTAB

Amphiphiles based on **TANI** provide facile possibilities to tune their self-assembled structures by either changing the oxidation state (i.e. from the LEB state to EB state[12,29] or from the EB to ES state[14]) or by adding different size acid dopants to protonate the imine nitrogen atoms of **TANI**. The changes in the volume of the hydrophobic TANI-based tail structure lead to changes in the packing parameter and thus yield different self-assembled morphologies. This approach is referred to as the addressable packing parameter (APP). It is worth mentioning that exploiting the role of the packing parameter to alter the self-assembled structures of TANI-based amphiphiles has not been reported before. Our previous reported study focused on the synthesis and self-assembling behaviour of **TANI-PTAB**,[14] mainly on the undoped EB state of **TANI-PTAB**.

In aqueous solution, **TANI-PTAB** self-assembled into several micrometers long 3.19 nm wide π-stacked nanowires. Modelling of solution SAXS data suggested that these structures were flat and tape-like structures, with an average width of 3.19 nm. Camphorsulfonic acid **CSA,** a prototypical **PANI** acid dopant, was chosen for an initial doping study and showed the formation of thicker (6 nm wide) less well-defined conductive wire-like constructs.

The chemical structure of **EB TANI-PTAB** and **ES TANI(CSA)$_2$-PTAB** were modelled and optimised in Gaussian using the B3LYP functional, the 6-31G* basis set, and a polarisable continuum model (PCM) solvent environment.[30,31] The cross-sectional area of the polar group, a_0, was estimated to be 0.54 nm^2 by considering the bond lengths and bond angles, as in previous reports.[32] The parameters l_c, and v were obtained from QSAR in Spartan[33] and simple calculations were performed indicating that p changed from 0.37 (for **EB TANI-PTAB**) to 0.73 for **ES TANI(CSA)$_2$-PTAB** on the addition of 2 equivalents of **CSA** (see **Scheme 3.1** and **Table 3.1**). These changes and their potential influence on assembly were not explored or investigated in any way during the mentioned study.

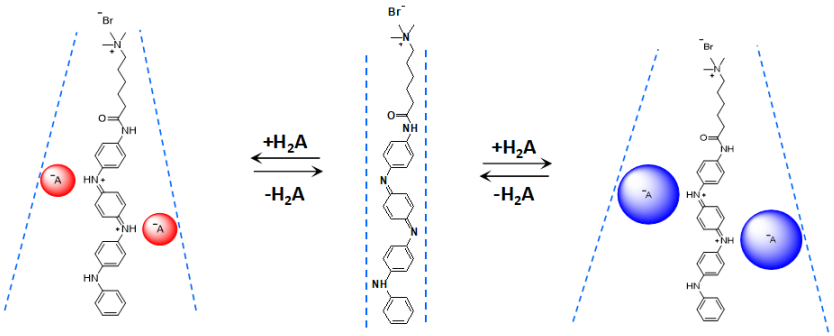

Scheme 3.1 Schematic showing the unique reversible doping/de-doping properties of **TANI**-based electroactive amphiphiles. Tail volume, and thus the packing parameter, can be changed through the use of dopants with different volumes.[17]

This proposed switchability was explored by investigating a range of acid dopants with varying volumes, leading us to choose **TFA** as the dopant of choice for the following reasons: a) **TFA** fully protonates TANI-based materials (pK_{aTFA} = 0.23), b) the calculated value of p for the doped **ES TANI(TFA)$_2$-PTAB** is = 0.49; and c) a series of further related acids with different volumes are available for additional investigations.

As expected, doping **EB TANI-PTAB** with **TFA** has a profound effect on the formed self-assembled structures: the addition of **TFA** converts **EB TANI-PTAB** with its well-defined 3.19 nm-wide nanowire morphology to doped **ES TANI(TFA)$_2$-PTAB**, with a very well-defined vesicular-like structure. UV/Vis-NIR absorption spectroscopy was used to confirm the ability of **TFA** to dope **EB TANI-PTAB** and form the ES state. As shown in **Figure 3.1a**, the three characteristics absorbance bands of the ES state of 1mM **TANI(TFA)$_2$-PTAB** were located at 302 nm, 420 nm, and 780 nm. These bands are attributed to π-electron transitions in the **TANI-PTAB** molecule that are comparable to the π-π*, polaron-π*, and π-polaron band transitions, respectively, in **PANI-ES**,[11,34] and are also characteristic of the **ES** state of doped oligo(aniline) species.[3,30] A recent publication from our group[31] regarding TD-DFT calculations on the core **TANI** electroactive unit have shown that absorption maxima in the range 780–800 nm correspond to the presence of the triplet **ES** state. The presence of these bands, as well as the absence of the absorption features typical for **EB**-state materials (especially the band at 600 nm) confirmed that the doping process was successfully completed as shown in **Figure 3.1a**. Circular objects with an average diameter of 27 ± 2 nm were clearly observed by TEM, (**Figure 3.1b**) and dynamic light scattering, DLS, was also used to confirm the existence of objects with similar size in solution. The average hydrodynamic diameter was determined to be 31 ± 7 nm (**Figure 3.1c**), in good agreement with the measurements from TEM, since the hydrodynamic diameter is expected to be larger than that of the dried sample.[35]

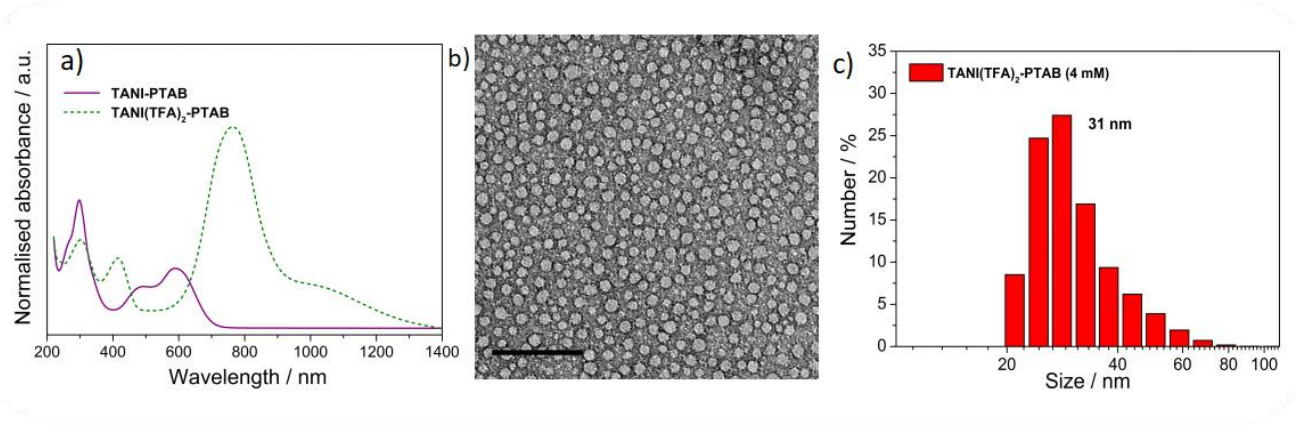

Figure 3.1 a) UV/Vis-NIR spectra of **EB TANI-PTAB** and TFA-doped **ES TANI(TFA)$_2$-PTAB** samples. b) TEM image of a 4 mM **TANI(TFA)$_2$-PTAB** sample (stained with 1% uranyl acetate). c) Number distribution of object sizes by DLS for a 4 mM **TANI(TFA)$_2$-PTAB** solution.

AFM was used to gain more information about the topology of these objects. AFM images of a 2 mM **TANI(TFA)$_2$-PTAB** solution, drop-cast on a mica surface, are shown in **Figure 3.2**. Highly monodisperse circular structures were clearly observed on the surface (**Figure 3.2a**), indicating that these objects were not droplets formed by drying. The average diameter and height of these objects, calculated from 317 counted objects, were 28.80 ± 3.33 nm and 5.01 ± 0.57 nm, respectively (**Figure 3.2b**). The value of average diameter was found to match very well with those measured by both DLS and TEM. Two representative structures were selected to show their structural detail in higher resolution and 3D images (**Figure 3.2c** and **d**, respectively). The measured heights of these two structures were found to be 5.5 nm and 5 nm, respectively (**Figure 3.2e**). With the theoretical length of the optimised **TANI(TFA)$_2$-PTAB** calculated to be 2.97 nm (a 2 nm contribution from the **TANI** core, and 0.97 nm from the alkyl chains), we deduce that the height is determined by the thickness of an interdigitated double layer of **TANI(TFA)$_2$-PTAB**. This layer is calculated to have a minimum height of ~4 nm (with fully interdigitated and overlapping π-conjugated surfaces and no tilt with respect to the surface) and maximum height of ~6.9 nm (an upright, non-interdigitated state), as depicted in the proposed molecular packing models in **Figure 3.2f**. Therefore, the measured average diameter was combined with the proposed

interdigitated double layer packing model, it was deduced that these structures are hollow double-layer vesicles. FT-IR spectra showed that the characteristic stretching vibrations of **TANI-PTAB** sample are located at 1596 cm^{-1}(γC=C for quinoid rings), 1508 cm^{-1}(γC=C for benzenoid rings), and 1167 cm^{-1}(γC-H out-of-plane of 1,4-aromatic substituted benzene rings), which are typical for **TANI** in the EB state. The three characteristic IR bands of **TANI$(TFA)_2$-PTAB** were found to be centered at 1581 cm^{-1}, 1504 cm^{-1}, and 1156cm^{-1} which correspond to (γC=C for quinoid rings), (γC=C for benzenoid rings), and (γ-NH^+=), respectively, which are typical for **TANI** in ES state. Moreover, the absence of the characteristic adsorption of strong asymmetric inter-chain NH+/N hydrogen bonds centered near 1100 cm^{-1} in the FT-IR spectrum of **TANI$(TFA)_2$-PTAB**, shown in **Figure 3.37** support the proposed packing model.

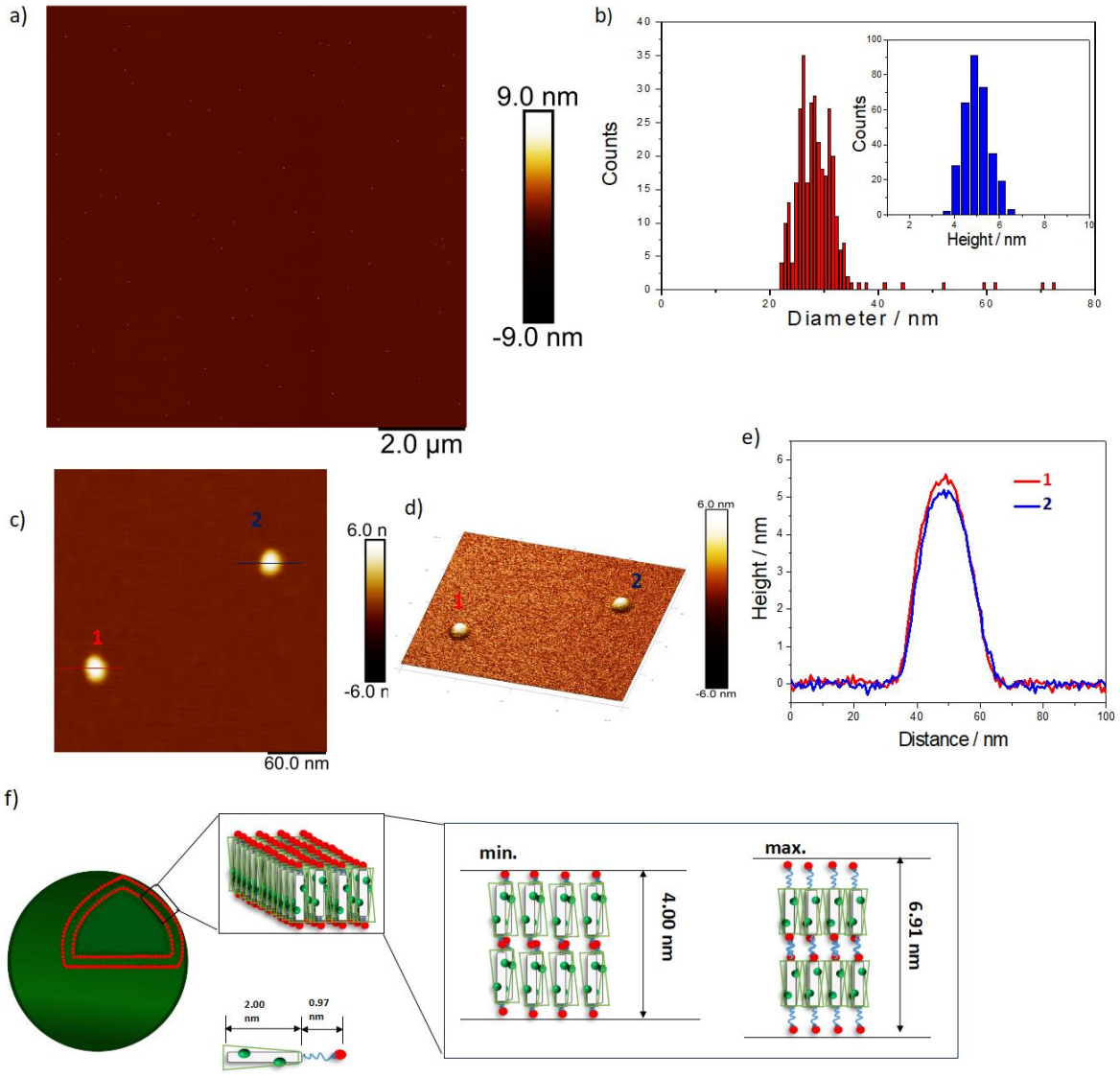

Figure 3.2 a) AFM image of 2 mM **TANI(TFA)$_2$-PTAB** sample on a mica surface. b) The corresponding diameter and height distributions counted from 317 particles. c) AFM image of two typical vesicles, d) the corresponding 3D image with Z-ratio increased by a factor of 3 for clarity and e) their cross-sectional height profile. f) A proposed scheme showing the possible molecular packing model for the self-assembled vesicles

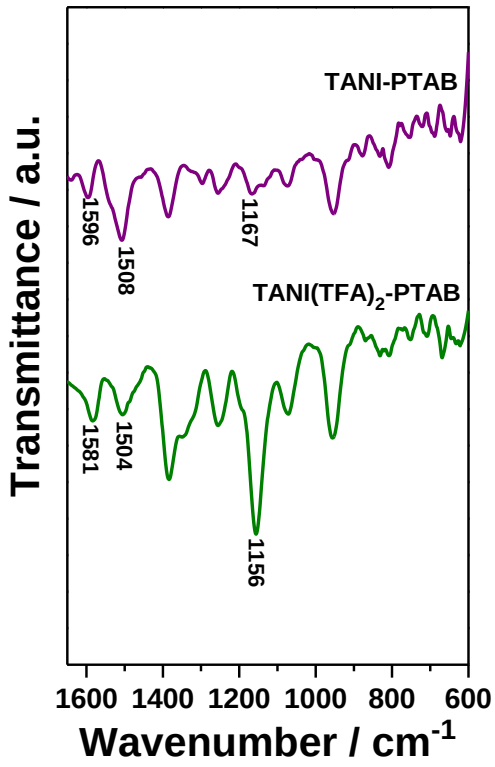

Figure 3.3 FTIR spectra of 2 mM solution of **TAN-PTAB** and 2 mM **TANI(TFA)$_2$-PTAB**.

Small-angle X-ray scattering, SAXS (in H_2O-based media)* and small-angle neutron scattering, SANS, (in D_2O-based media) investigations were also used to probe the shape and size of the objects formed in the 4 mM **TANI(TFA)$_2$-PTAB** system. See the **Appendix C** for representative data. The SANS data have the superior scattering contrast but both sets of measurements showed a pronounced Q^{-2} dependence. This behaviour is consistent with either the overall scattering from discoidal particles/platelets, or the sheet-like scattering from a unilamellar structure such as might surround a vesicle, but unfortunately there is no way to unambiguously differentiate between the two. However, if the TEM and DLS size data are to be believed, and the structures were discs/platelets, then one would expect to see a levelling off in the low-Q scattering in the measurement window of the SANS instruments, which is not observed. Instead the SANS data start to increase more steeply than Q^{-2} below Q~0.004 $Å^{-1}$, equivalent to a length scale of ~160 nm. The explanation for this observed increase is unclear. The absence of any oscillations in the SANS data at high Q is likely due to the significant polydispersity of the system

(**see Figure 3.1c**), but the absence of a pronounced diffraction peak at high Q also rules out any multilamellar structure.

3.2.1.3 Doping and de-doping of TANI-PTAB

The (optoelectronic) transition from the **EB** to the **ES** state of **TANI**-based materials can be achieved through the well-known doping/de-doping process. Tuning the morphology of **TANI**-based amphiphiles can be done in a reversible fashion through doping and de-doping processes, in other words, is pH-responsive. Furthermore, the morphology could be controlled through changes in packing parameter, and thus self-assembly behaviour is reversible and driven by an acid-dopant-induced packing parameter change of the addressable amphiphile, rather than a simple change in volume or concentration. Our starting point was thus to first prepare the **ES TANI(TFA)$_2$-PTAB** vesicular structures by doping an **EB TANI-PTAB** fibre-containing solution with **TFA**, as discussed above (**Figure 3.1b**). The small amount of concentrated NaOH solution (0.1 M, 0.03 ml) was required to de-dope **TANI(TFA)$_2$-PTAB** (1mM, 1.5 ml) and alter the pH with minimal change in volume. The full conversion of **ES TANI(TFA)$_2$-PTAB** to **EB TANI-PTAB** was clearly observed as shown in the UV/Vis spectra (**Figure 3.4a**), with the pH changing from 3.0 to 6.2.

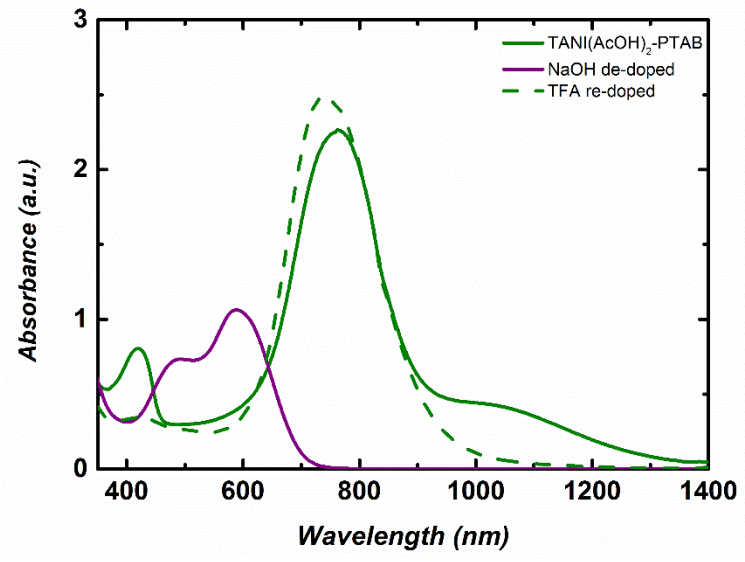

Figure 3.4 UV/Vis-NIR spectra of **TANI(TFA)$_2$-PTAB** sample, NaOH de-doped sample and TFA re-doped sample.

Investigation of the structures formed during the following series of doping/de-doping cycles (see **Figure 3.5**) showed the initial co-existence of vesicles and nanowires after addition of NaOH (**Figure 3.5b**). We propose that the found structures are indicative of a kinetically trapped state, rather than a thermodynamic minimum, as the UV/Vis-NIR data showed that all **TANI** moieties were fully de-doped. This suggestion was confirmed by leaving the sample undisturbed for 1 week, at which time a weak gel with a high concentration of bundles of nanowires, visible by TEM (**Figure 3.5c**), formed. To further explore the usefulness of the switchable nature of our oligo(aniline) functional unit for structural changes, we added TFA to the fibre-containing gelled samples. After leaving the samples to stand undisturbed for a further week, we obtained a low-viscosity solution containing vesicles again, as clearly shown in **Figure 3.5d** (and the inset photos below). The average diameter of the obtained vesicular structures was 42 ± 2 nm; larger than the sample aged 24 hours (which could possible attributed to the change in ionic strength in solution). Overall, a fully reversible doping/de-doping-induced morphology switching system was achieved.

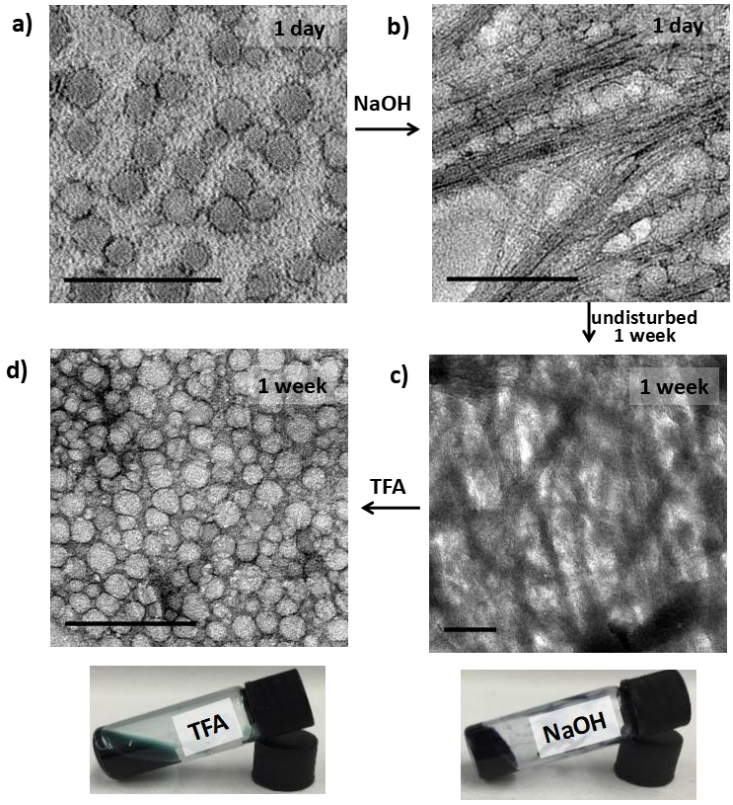

Figure 3.5 TEM images (stained with 1% uranyl acetate) of a) **TANI(TFA)$_2$-PTAB** (1 mM) after standing 1 day, b) NaOH-de-doped **TANI-PTAB** after 1 day, c) the same sample as (b) after 1 week, and d) **TANI(TFA)$_2$-PTAB** (0.92 mM) obtained by treating the same sample as (b, c) with **TFA**, after standing 1 week. Inset photographs (c and d) of the samples showing the gel-sol transition. Scale bars: 200 nm.

As shown in **Scheme 3.2**, the removal of the **TFA** counterions and protons (i.e., de-doping) modifies the packing parameter: through changing the volume of the **TANI**-containing amphiphile the vesicles formed by the ES state revert to nanowires.

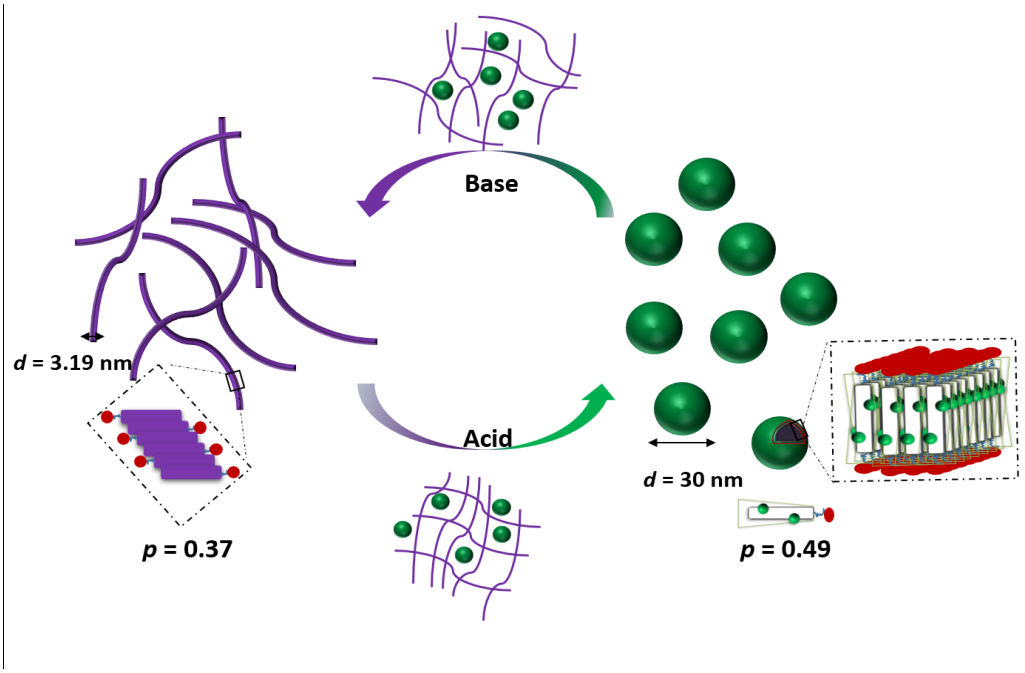

Scheme 3.2 Schematic showing the proposed doping/de-doping responsive self-assembly behaviour of **TANI(TFA)$_2$-PTAB** in aqueous solution.

3.2.1.4 Noncovalent packing parameter tuning: generalising the approach

Upon doping with acid, the volume of the hydrophobic section of **TANI** would normally increase, which was reflected in an increased surfactant packing parameter. However, a number of factors, such as the size, polarity and chemical nature of the conjugate base, could affect the range and type of noncovalent interactions between **TANI** molecules, making the doping-induced self-assembly of TANI-based **eSAs** a complicated process. In order to verify and generalise this exciting opportunity to reversibly vary p for our low molecular weight **eSA**, we doped **EB TANI-PTAB** with a range of either organic or inorganic acid dopants such as **HCl**, nitric acid **HNO$_3$**, acetic acid **AcOH** and dichloroacetic acid **DCA**. Hence, the dopants were chosen so that with different size and polarity the estimated packing parameter could be carefully varied from 0.37 (**EB TANI-PTAB**) through 0.89 (**ES TANI(HX)$_2$-PTAB**). Please see **Table 3.1** for an overview of the chosen acids, as well as a summary of the relevant molecular parameters.

Table 3.1 Estimated parameter and expected self-assembled structure for **TANI-PTAB** systems.

Molecule	**pK_a**	$V(Å^3)$	$l_c(Å)$	$a_0(Å^2)$	p	**Expected self-assembled structure**
TANI-PTAB	-	474.10	23.91	54.00	0.37	Cylindrical micelles
TANI(HCl)$_2$-PTAB	-7.00	535.31	24.28	54.00	0.41	Cylindrical micelles
TANI(HNO$_3$)$_2$-PTAB	-1.40	569.71	24.01	54.00	0.44	Cylindrical micelles
TANI(AcOH)$_2$-PTAB	4.76	607.62	24.04	54.00	0.47	Cylindrical micelles
TANI(TFA)$_2$-PTAB	0.23	634.87	24.03	54.00	0.49	Flexible bilayers, vesicles
TANI(DCA)$_2$-PTAB	1.35	663.39	23.94	54.00	0.51	Flexible bilayers, vesicles
TANI(CSA)$_2$-PTAB	1.20	933.91	23.78	54.00	0.73	Flexible bilayers, vesicles

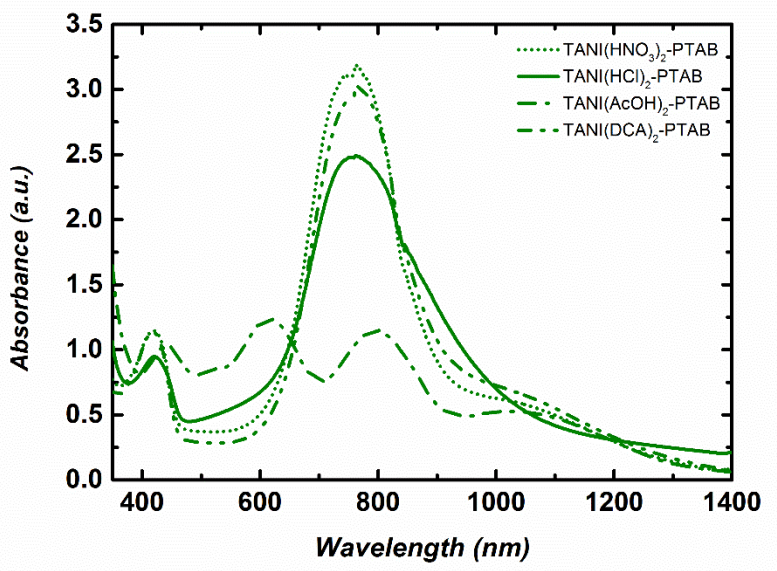

Figure 3.6. UV/Vis spectra showing **ES TANI-PTAB** doped by various acids in aqueous solution to form **ES TANI(HNO$_3$)$_2$-PTAB**, **ES TANI(HCl)$_2$-PTAB**, **ES TANI(AcOH)$_2$-PTAB**, and **ES TANI(DCA)$_2$-PTAB**.

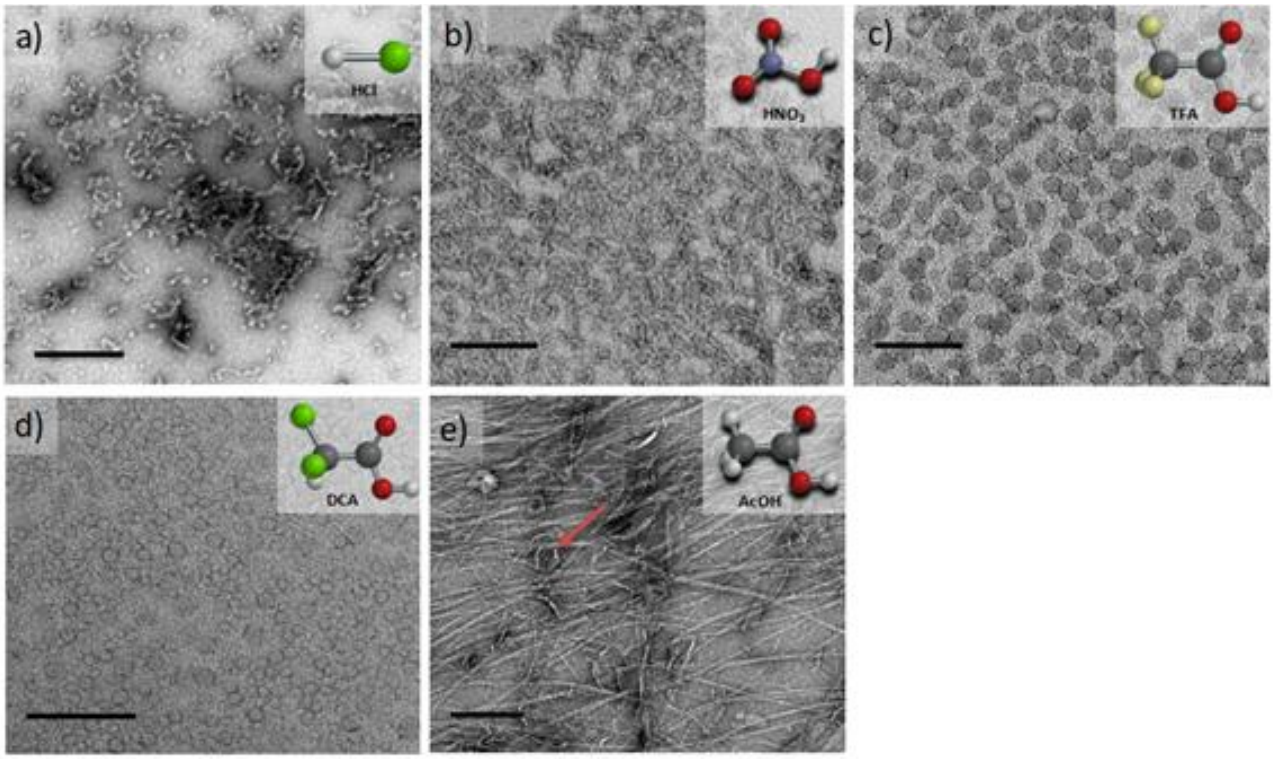

Figure 3.7 TEM images (1 mM solutions, stained with 1% uranyl acetate) of (a) **TANI(HCl)$_2$-PTAB**, (b) **TANI(HNO3)$_2$-PTAB**, (c) **TANI(TFA)$_2$-PTAB**, (d) **TANI(DCA)$_2$-PTAB** and (e) **TANI(AcOH)$_2$-PTAB**, with corresponding dopant molecular structures inset. Scale bars: 200 nm.

We started our packing parameter investigations with small inorganic acid dopants **HCl** and **HNO$_3$**, where p was calculated to be 0.41 and 0.44, respectively. Slightly elongated worm-like micelles were observed for both **TANI(HCl)$_2$-PTAB** (**Figure 3.6a**) and **TANI(HNO$_3$)$_2$-PTAB** (**Figure 3.6b**),which agreed with the morphology suggested by the packing parameter calculations.[36]

AcOH and **DCA** were chosen to dope **TANI-PTAB** and considered as analogous to **TFA,** where p was calculated to be 0.47 and 0.51, respectively. **TFA** doped **TANI-PTAB** is already discussed in the first part of our investigation and with packing parameters on either side of the value calculated for **TFA** (p = 0.49), as dopants, we found a significant difference in the formed self-assembled structures. **AcOH** was unable to fully dope the **TANI-PTAB** (with a molar ratio of 2:1) due to its high pK_a value (4.76), as shown by the presence of peaks (580 nm, and yy nm) attributed to both the EB and ES-state absorption bands in the UV/Vis-NIR spectra (**Figure 3.6**), indicating a

mixture of the two species co-existing. TEM investigations showed that **TANI(AcOH)$_2$-PTAB** formed a mixture of nanowires, vesicles and some intermediate states, as shown in **Figure 3.7c** (red arrow). It is clear that the low level of doping (a consequence of the high pKa) led to an undesired mixture of self-assembled structures, and therefore not a true reflection of the influence of dopant on the volume of the surfactant tail. Increasing the amount of **AcOH** to attempt to fully dope **TANI-PTAB** with mole ratio of 4:1 (**AcOH: TANI-PTAB**) induced the formation of more vesicles. However the increased excess of ions may make the system more complicated and some nanowires were still observed in the system (**Figure 3.8**). However, using the strong acid **DCA** (pKa = 1.35), the doped **TANI(DCA)$_2$-PTAB** amphiphile (**Figure 3.7**) formed well-defined vesicles with an average diameter of 34 nm (**Figure 3.7d**), very similar to those observed for **TANI(TFA)$_2$-PTAB**.

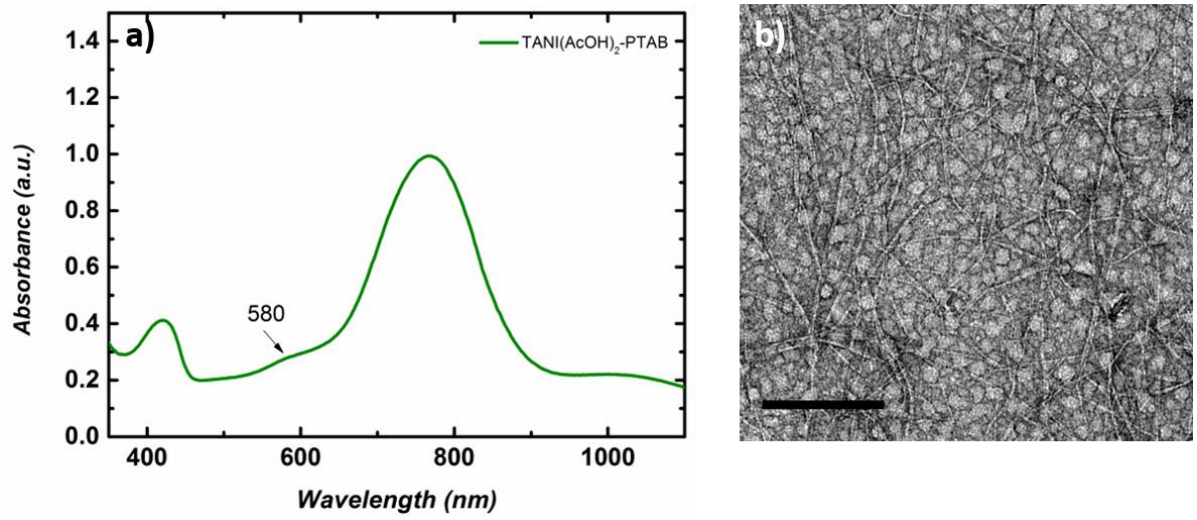

Figure 3.8 a) UV/Vis-NIR spectrum of AcOH-doped **TANI-PTAB** with a mole ratio of 4:1 (AcOH:TANI-PTAB) left to age for 24 h, and b) TEM image of this sample showing the co-existence of both fibers and vesicles. Scale bars: 200 nm.

Finally, we compared the structures of the oligo(aniline)-based **eSAs** (**HCl**, **HNO$_3$** and **DCA**) obtained here with those found for **TANI(CSA)$_2$-PTAB** (**CSA**, p = 0.73). For this system, we expected either lamellar or vesicular structures, however we found 6nm-thick wire-like

structures. One aspect of the molecular design and noncovalent interactions we have not considered in any of our discussions until now are additional secondary interactions between the dopant and the oligo(aniline) moiety. From previous discussions and investigations into the very successful doping of PANI with **CSA**,[37] molecular modelling suggested an exceptionally serendipitous fit of **CSA** into the molecular cavity formed between adjacent phenyl rings (Ph-N-Ph), with additional hydrogen-bonding interactions to the **PANI** backbone structure. These postulated fit-interactions, in combination with additional hydrogen-bonding capability, seem to play a significant role in the formation of stable wire-like structures (rather than the expected classical lamellar or vesicular structures). We are currently investigating the anomalous behaviour found for **CSA**-doped system in more detail.

In general, these initial investigations indicate that the strategy employed here, i.e., using a suitable dopant to regulate packing parameters and influence intermolecular assembly forces, is a feasible route produce controllable and tunable self-assembled structures of oligo(aniline)-based **eSAs** (**Scheme 3.3**).

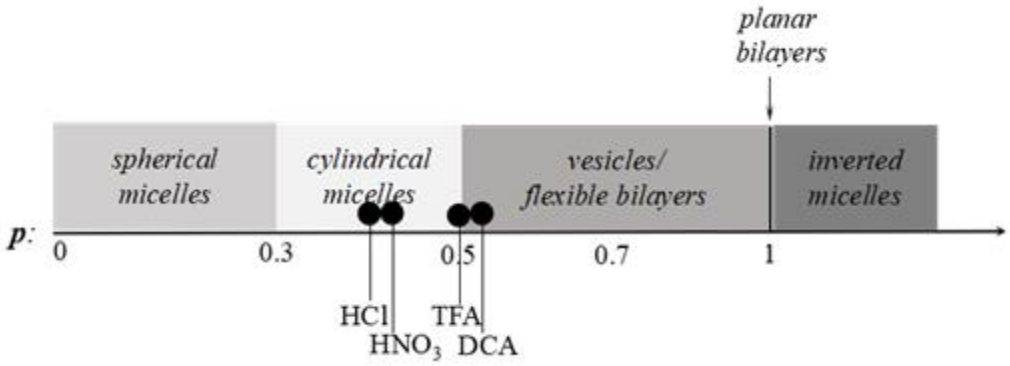

Scheme 3.3 Scheme showing the relationship between packing parameter and the obtained nanostructures using different dopants for **TANI-PTAB** system**.**

3.2.2 Synthesis and self-assembly of electroactive phosphonium amphiphiles

3.2.2.1 Synthesis of tetra(aniline) amphiphile TANI-PTPB

The synthesis of cationic amphiphiles comprising **TANI** functionalised with alkyltrimethylammonium head groups built on the successful synthesis of Ph/NH_2 **TANI** reported previously.[38] A single-tailed phosphonium amphiphile EB Ph/NH_2**TANI**-C6P$Me_3^+Br^-$ (**EB TANI-PTPB**) was synthesised for the first time. Boc Ph/NH_2**TANI**-C6Br was prepared previously in our group.[14] Boc protecting groups of **TANI**-C6Br were removed and the resulting product (LEB **TANI**-C6Br) was quaternised with trimethylphosphine (TMP). A subsequent oxidation reaction was performed using hydrogen peroxide to yield the desired water-soluble amphiphile, **EB TANI-PTPB**. The synthetic route to **TANI-PTPB** was not the same as the ammonium amphiphiles, all the difficulties and challenges encountered are presented in detail in the **Experimental Chapter.**

3.2.2.2 Self-assembly studies of EB TANI-PTPB

Concentration-dependent UV/Vis-NIR spectra of **EB TANI-PTPB** of aqueous solutions were performed to ascertain at which concentration aggregation starts. Solutions (0.1-1 mM) exhibit a shoulder peak at 485 nm as well as a 28 nm bathochromic shift in characteristic absorbance peak (λ_{max}= 590 nm at a concentration of 1 mM & λ_{max} = 562 nm for a 0.01 mM solution) as shown in **Figure 3.9a**. This concentration-dependent behaviour of UV/Vis-NIR spectra is consistent with previous reports.[14] Bathochromic shifts have been reported previously as a result of the changes in the environment and molecular packing, and provided insight into the mode of aggregation (i.e., J-aggregate formation).[39] To determine the self-assembling behaviour of the amphiphile, the critical aggregation concentration (CAC) was required and measured using pyrene as a fluorescent probe. The CAC was found to be 0.085 mM, with this value clearly pointed out by the sharp changes in I_1/I_3 ratio as depicted in **Figure 3.9b**.

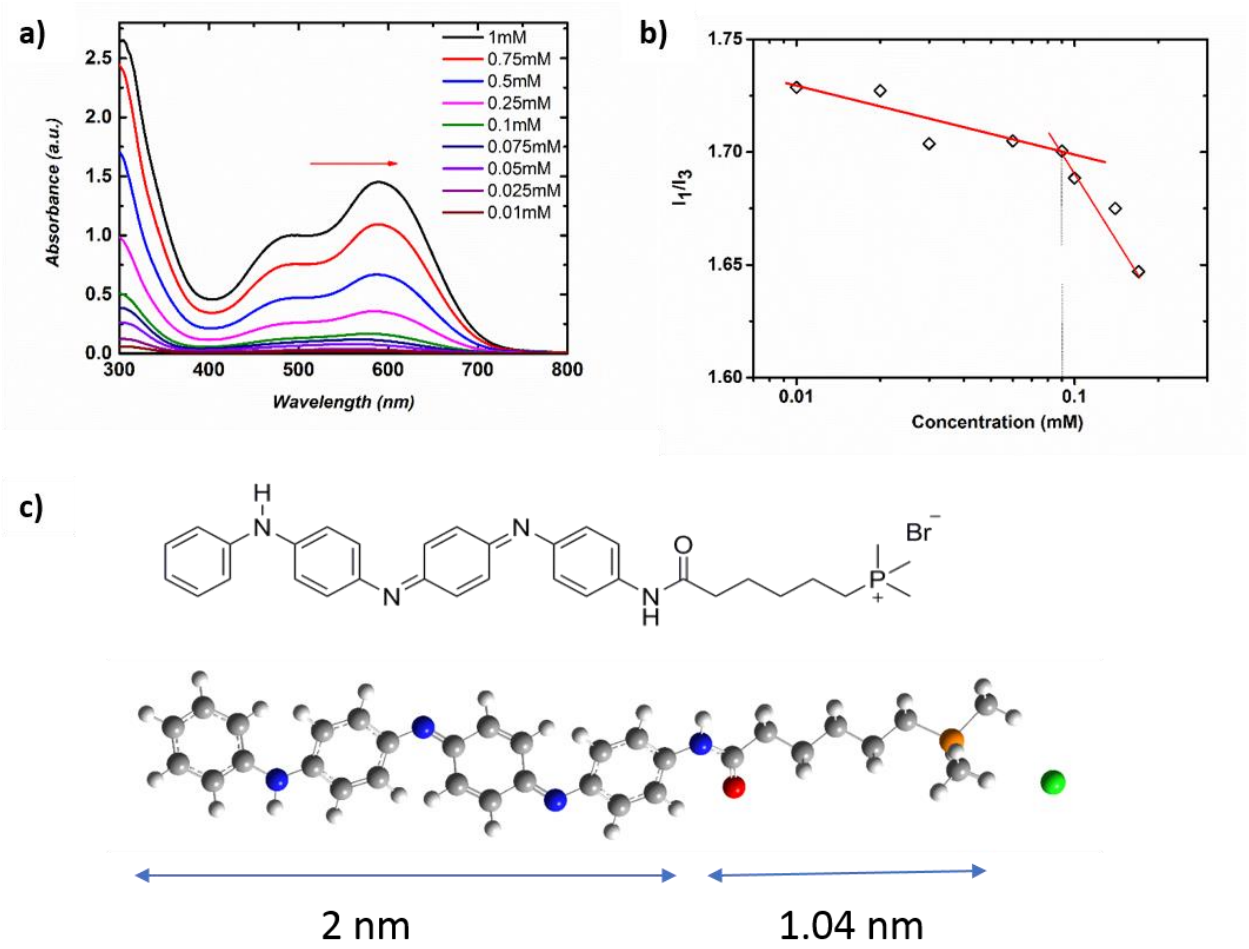

Figure 3.9 a) Change of λ_{max} of **EB TANI-PTPB** with concentration. Arrow indicates direction of change upon increasing concentration. b) Fluorescence of a pyrene probe to determine the CAC of **EB-TANI-PTPB**. CAC = 0.085 mM. c) Chemical structure of **TANI-PTPB**. DFT-modelling: comparison studies of simulated UV/Vis of **EB TANI-PTPB** and experimental spectra.

DFT-modelling: comparison of simulated UV/Vis of EB TANI-PTPB and experimental spectra

The geometric structure of **EB TANI-PTPB** was optimised in Gaussian using the B3LYP functional, the 6-31G* basis set, and a polarisable continuum model (PCM) solvent environment. However, CAM-B3LYP was teste d and found to be more accurate to yield simulated UV/Vis spectra for charge-transfer and π conjugated systems.[31] TD-DFT stimulations of **TANI-PTAB** showed a similar spectrum to experimental spectrum in acetonitrile (**Figure 3.10**). Acetonitrile was found to dissolve TANI-PTPB and was therefore used to exclude any effect of aggregation. The absorbance

maximum at 514 nm was attributed to the HOMO−LUMO transition of aqueous **TANI-(PTAB)$_2$**, where π-π* transitions are mainly involved (**Figure 4.3**). The absorbance peak of the first singlet excited state of **EB** state (2.41 eV, 514 nm) matched the transition observed experimentally in the UV/Vis spectrum (540 nm, see the **Appendix C** for further details).[30,38]

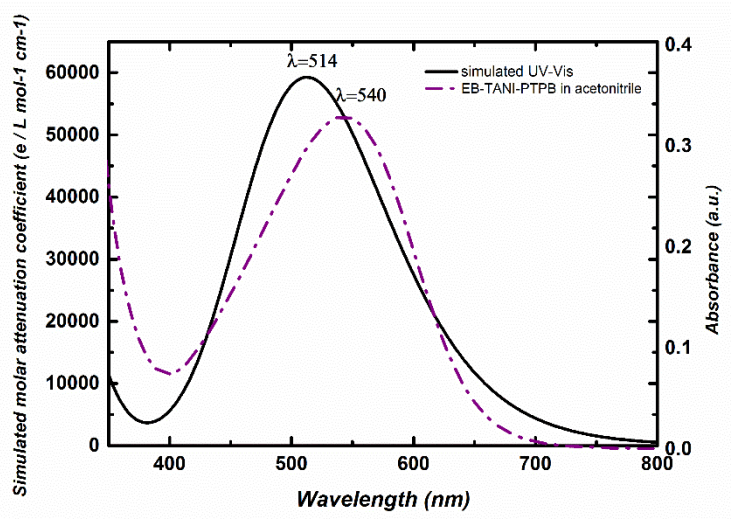

LUMO

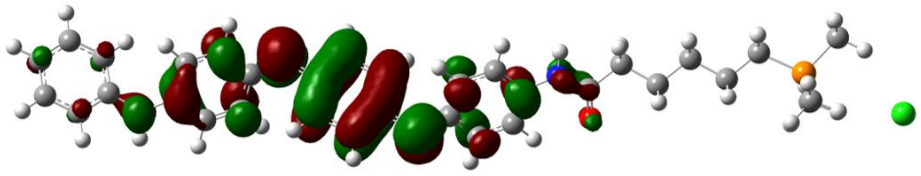

HOMO

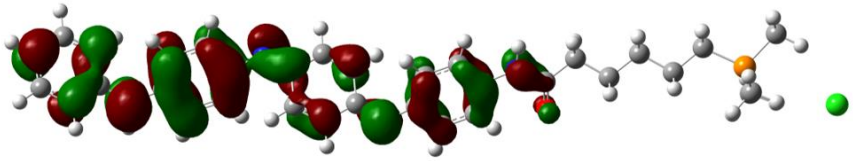

Figure 3.10 a) Comparison of simulated UV/Vis of **EB TANI-PTPB** and experimental spectra in acetonitrile, b) MOs of **EB TANI-(PTAB)$_2$** transition.

The self-assembled structure of **EB TANI-PTPB** was revealed using microscopy TEM and AFM. TEM showed that the predominant self-assembled structures of **EB TANI-PTPB** were nanofibre structures, however the spherical structures were also present at all the selected concentrations (0.4-8 mM).The increase of the concentration (from 1 mM to 8 mM) resulted in the spherical structures becoming more pronounced with increase of the width of the dominant fibre structures (**Figure 3.11h**) as shown in **Figure 3.11g-h.** These changes suggest that the increase of the concentration led to a decrease in the surface area of the head groups, and consequently the packing parameter increased leading to the formation of spherical structures.

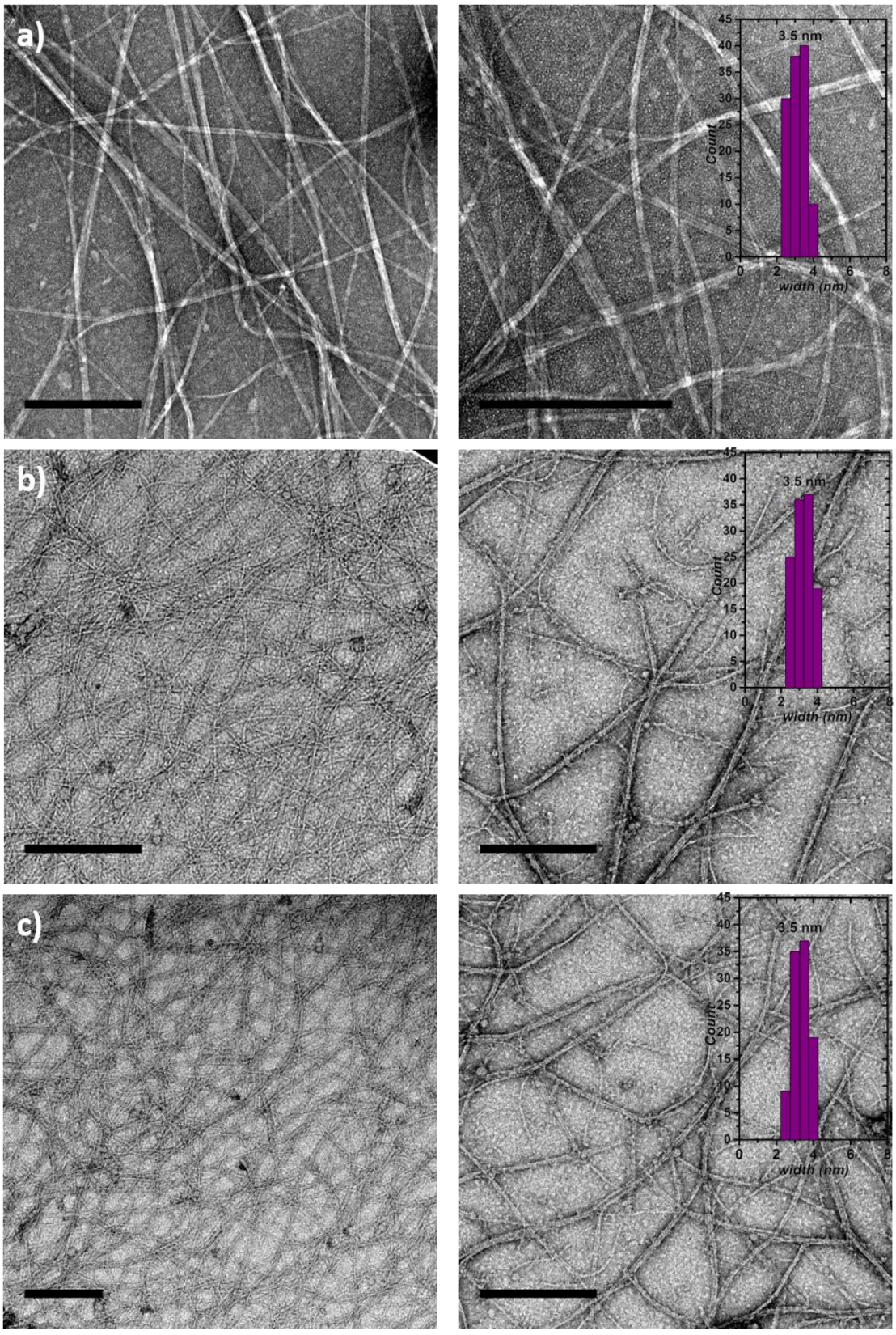
a)
b)
c)
3.5 nm
Count
width (nm)

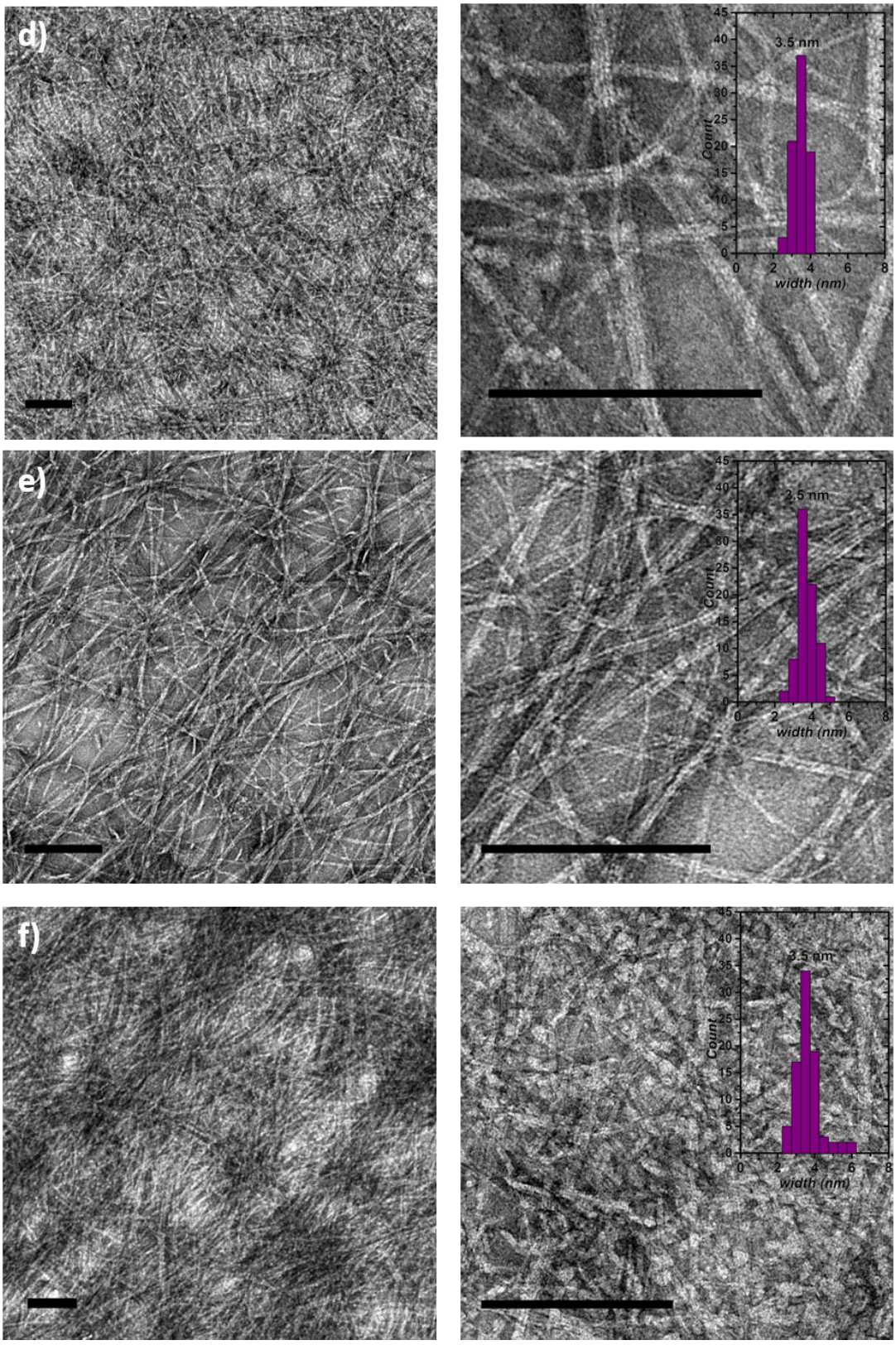
d)
3.5 nm
Count
width (nm)
e)
2.5 nm
Count
width (nm)
f)
3.5 nm
Count
width (nm)

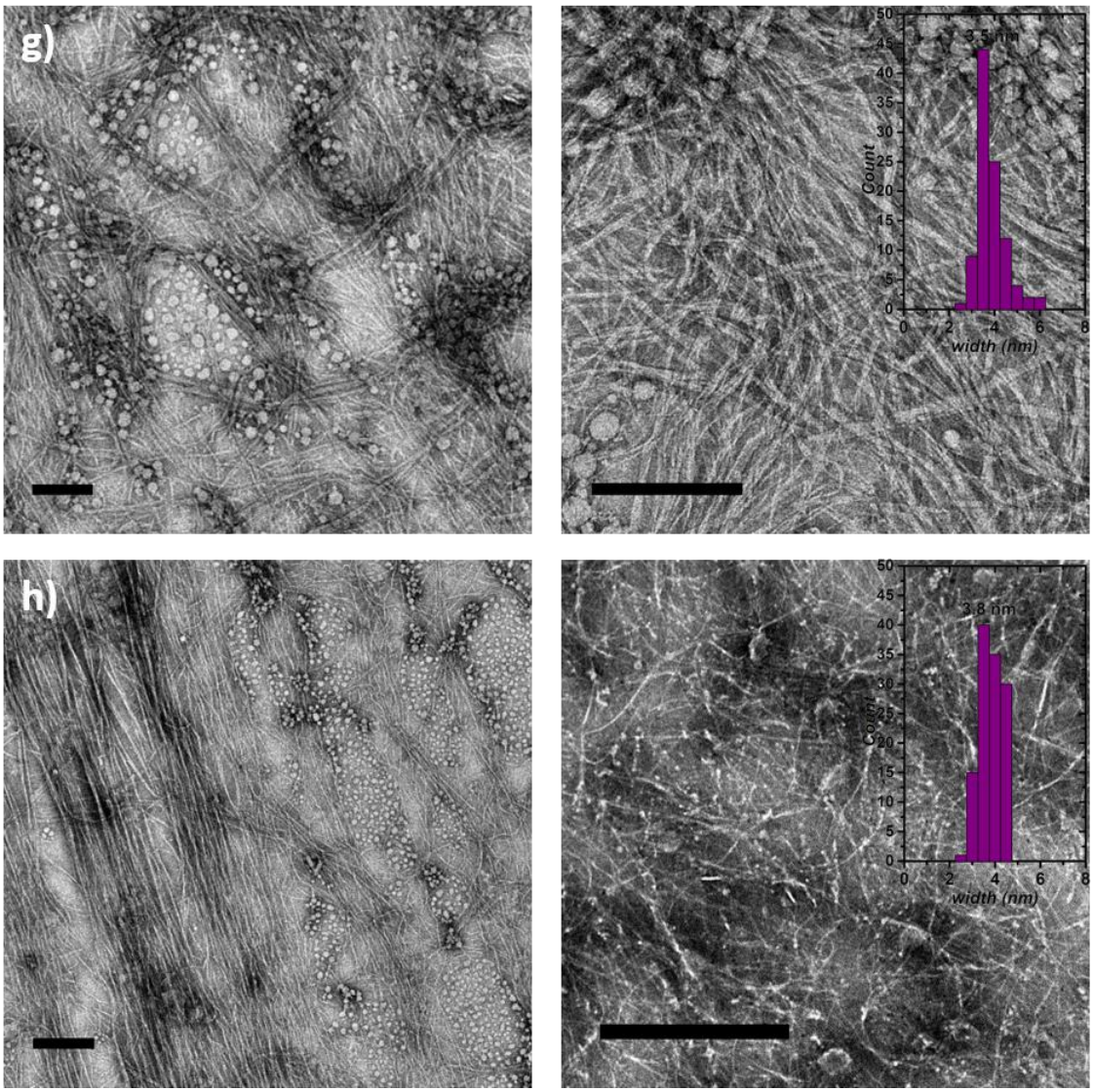

Figure 3.11 TEM images of **EB TANI-PTPB** (stained with 1% uranyl acetate) in solution at different concentrations: a) 0.4 mM, b) 0.6 mM, c) 0.8 mM, d) 1 mM, e) 2 mM, f) 4 mM, g) 6 mM and h) 8 mM (scale bar=200 nm). The images on the right and left side represent the same concentrations with different magnifications.

All TEM samples were prepared on a carbon-coated reference grid, allowing investigation of the same area by AFM as well. Hence, AFM measurements were performed on the same stained TEM sample to gain more information into the topology of the observed fibrous structures. As shown

in **Figure 3.12**, AFM images showed the same morphology as TEM images - dominant nanofibre structures with spherical objects also present.

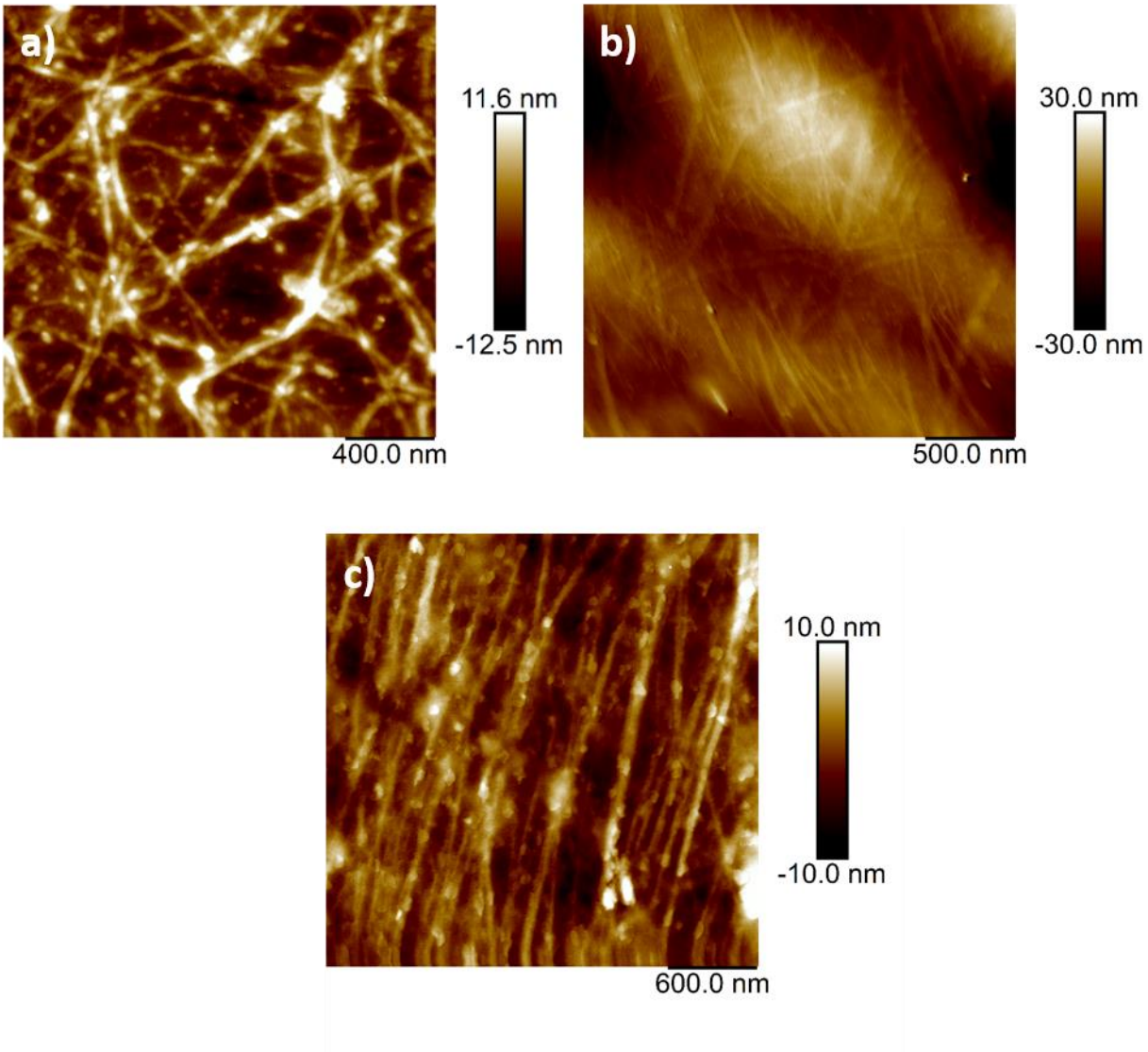

Figure 3.12 AFM images of **EB TANI-PTPB** (stained with 1% uranyl acetate) in solution drop-cast onto TEM grid at different concentrations: a) 1 mM, b) 2mM and c) 4mM.

We focused on 1mM AFM images of a **TANI-PTPB** solution and as shown in **Figure 3.13**, fibre-like structures with the average width of 2.4 to 4.8 nm were observed as depicted in **Figure 3.13a**, **c** and **d**. The found structures and dimensions remained consistent when measured on unstained samples as shown in **Figure 3.13b.**

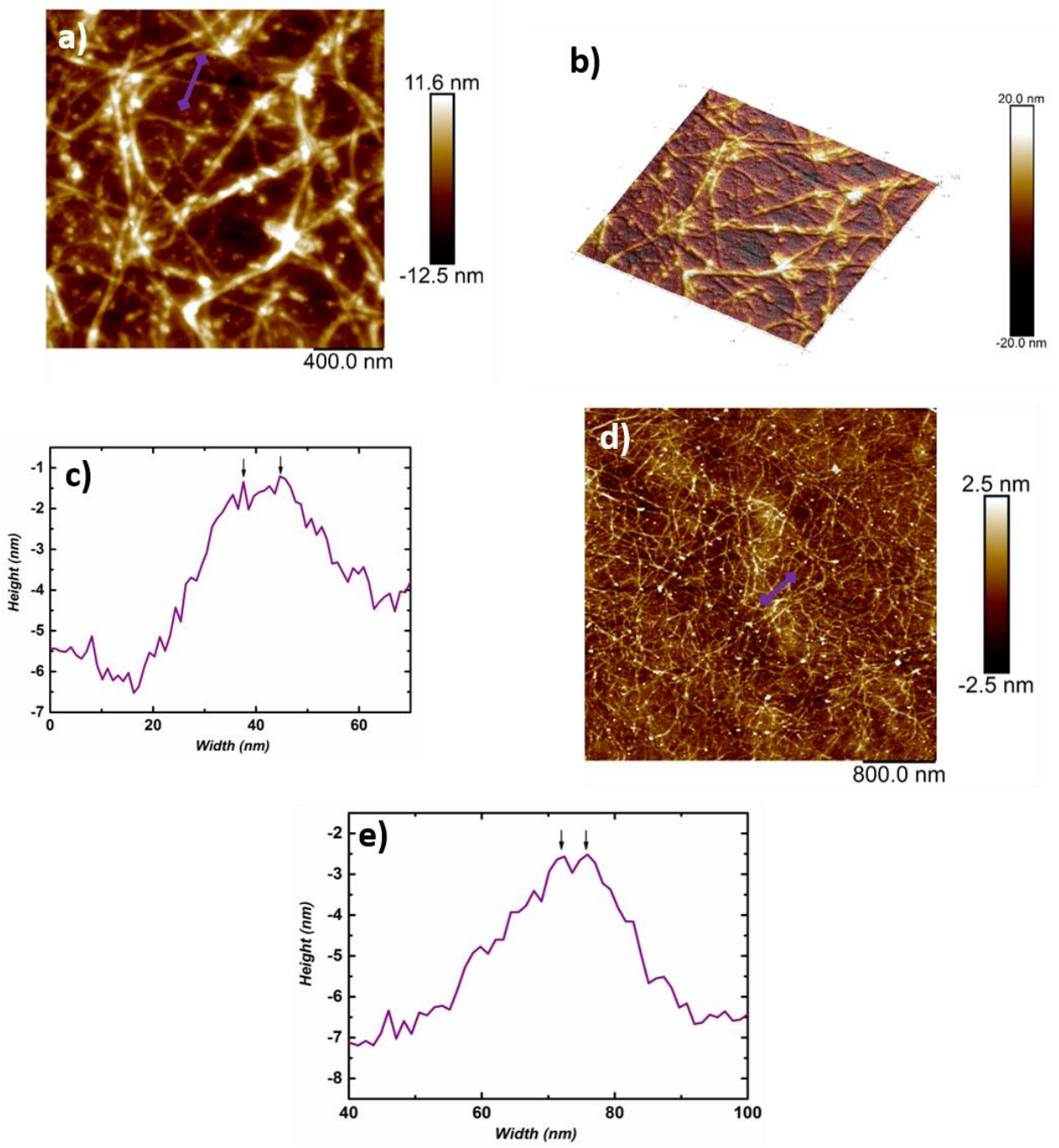

Figure 3.13 AFM images of 1 mM **EB TANI-PTPB** drop-cast onto TEM grid, a) stained with 1% uranyl acetate, b) 3D image of the stained sample (a), d) height profile of **EB TANI-PTPB** corresponding to the purple line shown in (a)**,** b) unstained sample and e) height profile of **EB TANI-PTPB** corresponding to the purple line shown in (d).

To gain more information about the shape and the size of the aggregated structures, small angle X-ray scattering (SAXS) of aqueous solutions of **EB TANI-PTPB** at different concentrations was performed. At the low concentrations (such as 1-4 mM), the data does not scatter sufficiently above the background once corrected for solvent to draw any firm conclusions. However, 6 mM **TANI-PTPB** solutions scatter sufficiently and fit to a flexible cylinder with an average diameter of 2.6 nm **Figure 3.14**; all the details of fitting are provided in **Appendix C (Table C.2)**. The value obtained for the average diameter agreed very well with the sizes obtained from TEM and AFM measurements, the obtained widths (**Figure 3.11d** and **Figure 3.13a**) were in the same range as the theoretical length of the optimised **TANI-PTPB**, which was 3.04 nm (a 2 nm contribution from the **TANI** core, and 1.04 nm from the alkyl chains, see **Figure 3.9c**).

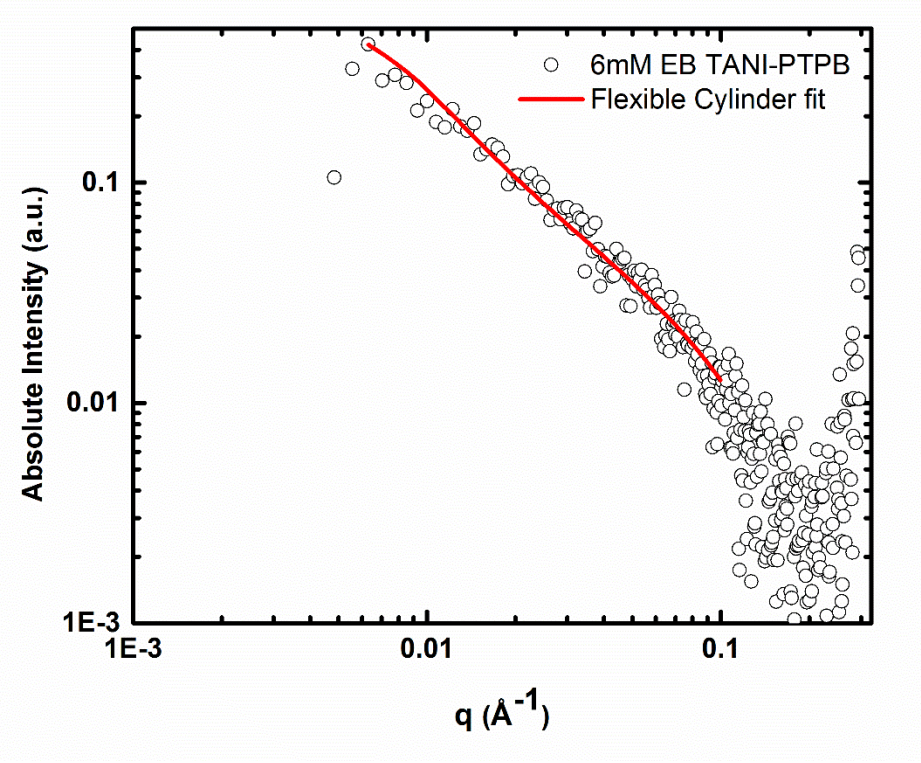

Figure 3.14 Small angle x-ray scattering data (black circles) collected for 6 mM **EB TANI-PTPB**. A simulated line (red) indicated the q=-2 dependence.

The formation of the nanofibrous structures of **TANI-PTPB** could be ascribed to the presence of strong π-π stacking between the **TANI**-based amphiphiles.[40] This effect can be identified by X-ray diffraction (XRD) patterns for a freeze-dried sample of 4mM **EB TANI-PTPB** solution. The most intense and pronounced peak in the X-ray diffraction pattern was assigned as shown in **Figure 3.15** at around 2θ = 21.8°, corresponding to a d-spacing of 0.41 nm. The d-spacing value can be an indication of the periodicity of a **TANI** chain in a parallel fashion and has been found previously in **PANI**. [41,42] The second observed peak was found at 2θ= 24° which corresponds to a d-spacing of 0.37 nm. This is a typical distance for π-stacking interactions, which acts as a driving force for the formation of the self-assembled structures of **TANI-PTPB.**

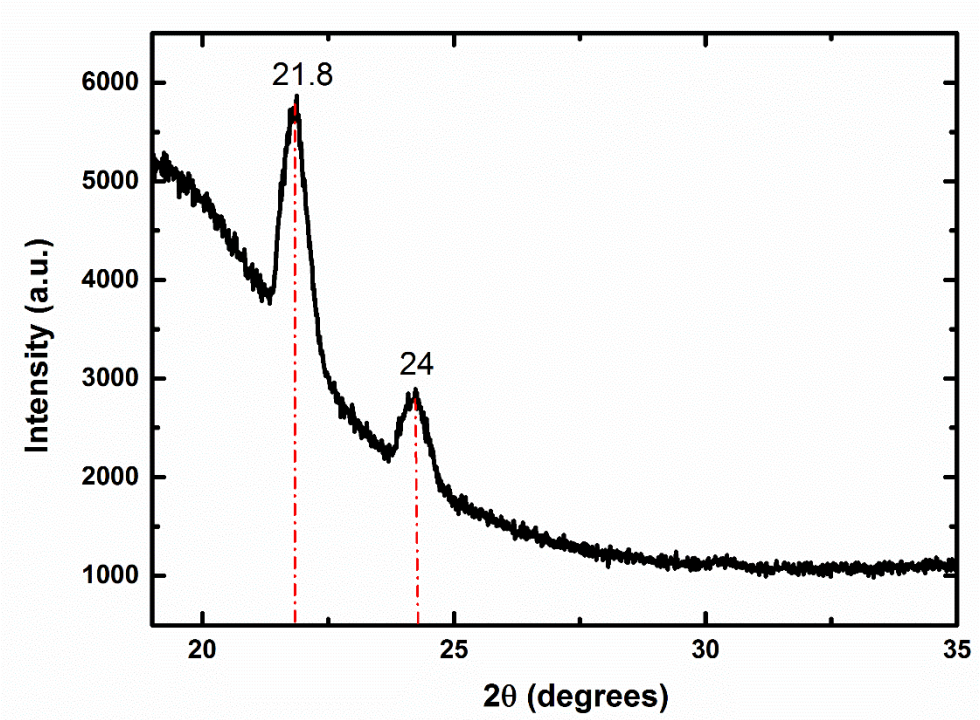

Figure 3.15 PXRD data of freeze-dried **EB TANI-PTPB** (concentration=8mM).

3.2.2.3 Temperature-dependent UV/Vis studies

The self-assembling behaviour of **TANI-PTPB** was investigated by temperature-dependent UV/Vis spectroscopy, which has been found to be the best method to identify the mechanism as either an isodesmic model (equal-K) or a cooperative (nucleation−elongation) model.[43] In order to study

the behaviour in detail, we investigated the effect of temperature on a 1 mM solution of **TANI-PTPB**. Heating of a 1 mM solution of **TANI-PTPB** to different temperatures showed a hypsochromic shift of 30 nm of the characteristics absorbance band from 590 nm to 560 nm as well as disappearance of the shoulder peak around 480 nm, as shown in **Figure 3.16**. This behaviour suggests that transition from an aggregated state to a monomeric state occurred in a similar manner to that observed previously for the ammonium amphiphile.[14]

Surprisingly, we found that the plotted curve of degree of aggregation as a function of temperature showed a combination of two modes of aggregation (sigmodal and non-sigmoidal, respectively) as depicted in **Figure 3.18a**.

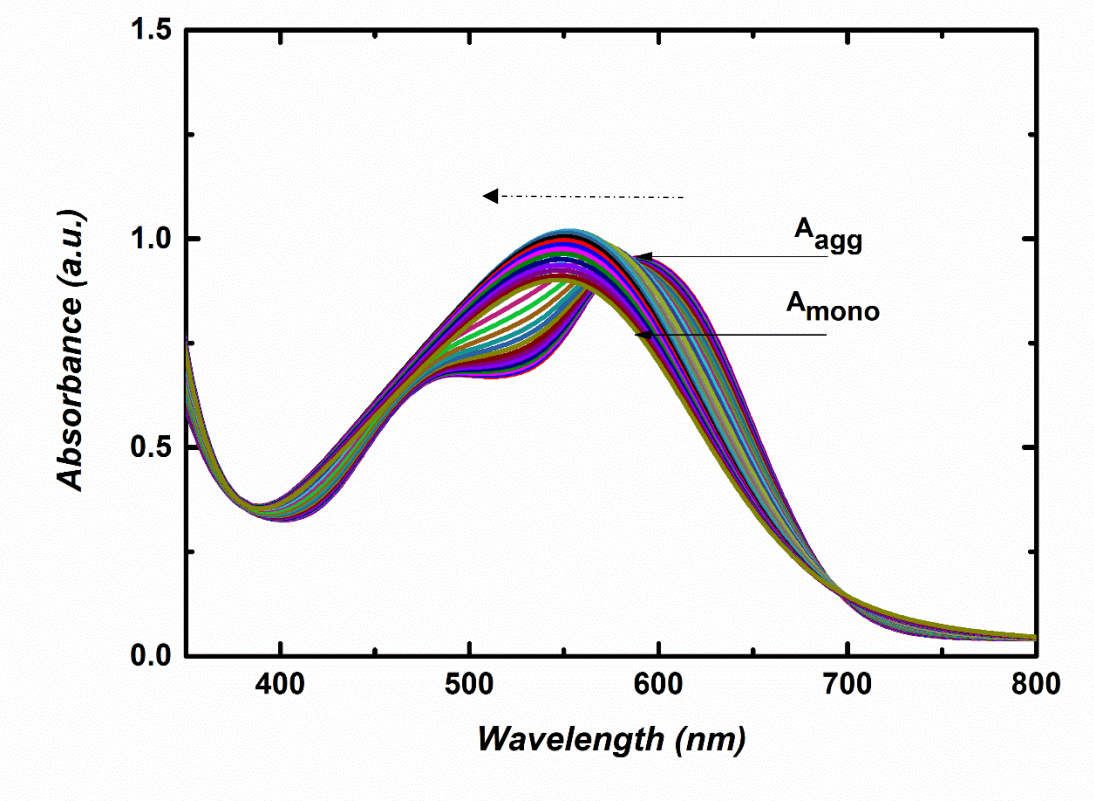

Figure 3.16 Effect of temperature on UV/Vis absorbance of 1mM of **EB TANI-PTPB**, the dashed arrow indicates change (at λ=590 nm) on heating solution (T=15-75°C).

The interesting shapes of cooling and heating curves of **TANI-PTPB** inspired us to investigate the morphology of a corresponding solution of 1 mM **TANI-PTPB** over time in order to help clarify

the proposed mechanism. Regarding the self-assembled structures found for 1mM **TANI-PTPB**, TEM imaging reveals the spherical morphology is more pronounced in the solutions aged a week and more as shown in **Figure 3.17**. This change suggests that the self-assembled structures of **TANI-PTPB** interconvert into a thermodynamically stable form of sphere-like structures over time whereas a kinetically trapped fibrous structure dominates after initially cooling to room temperature. The behaviour of cooling and heating curves for solutions aged 1 week and 3 weeks showed similar trends to the solution aged 24 hours. However, the heating curves showed less sharpness of nonsigmoidal curves potentially due to the increase of

the density of the aggregated structures as shown in **Figure 3.19a**. Upon cooling the aggregated structures reassemble again to form nanofibre structures as shown in TEM image **Figure 3.19b**. This behaviour suggests that the non-fibrous structures are kinetically favourable. The trend of cooling curves shown in **Figure 3.18** suggests that the fibrous structures self-assemble by an isodesmic mechanism. However, the presence of spherical structures increases the cooperativity as shown in the heating curves in **Figure 3.18**, suggesting these structures form by a cooperative mechanism. This interesting finding provides a potentially facile way to encapsulate and release a target molecule by increasing the temperature, while retaining its chemical structure.

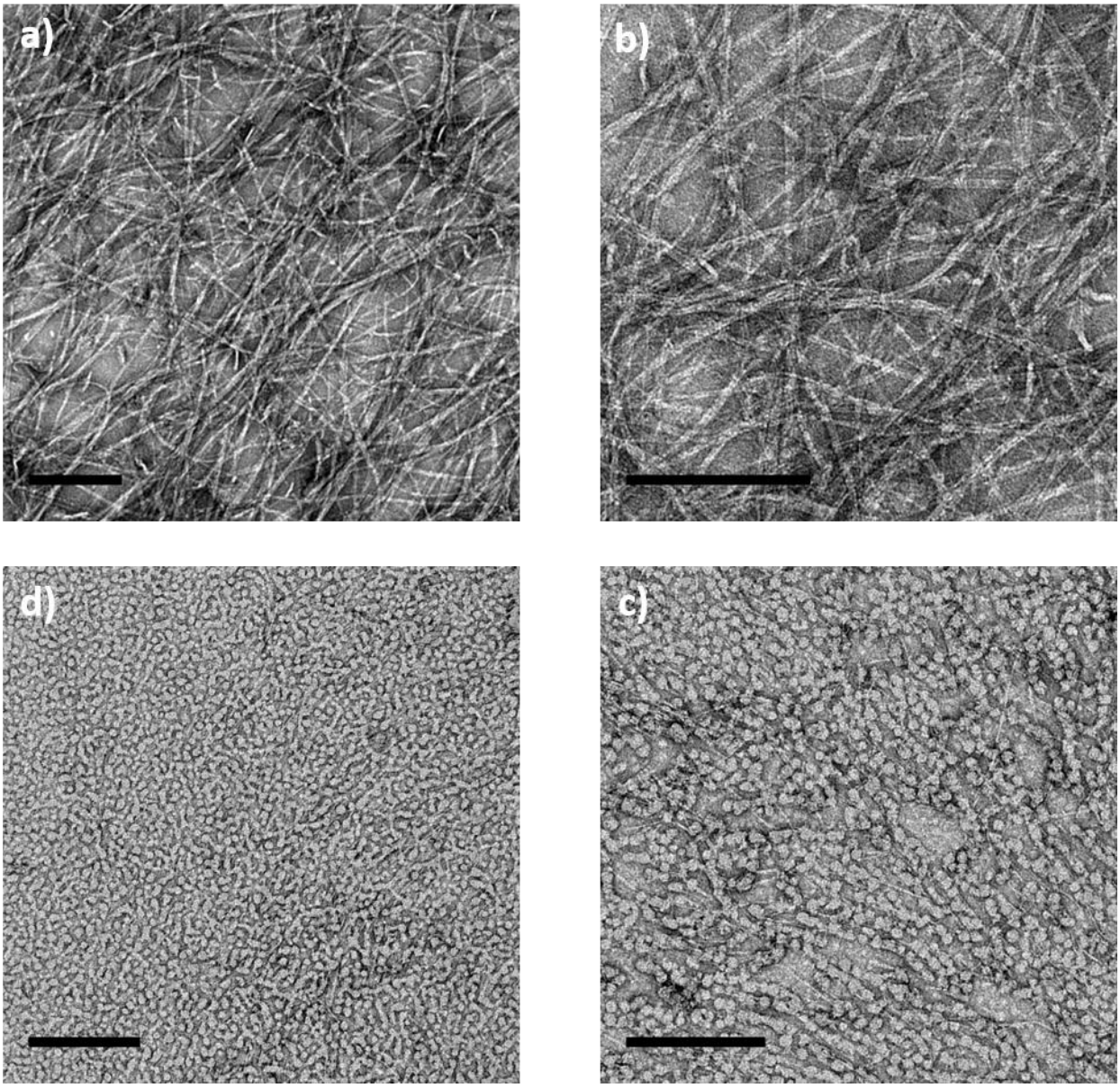

Figure 3.17 TEM images of 1mM **TANI-PTPB** over time a) 24h, b) 48h, c) one week and d) three weeks, respectively. Scale bar=200 nm.

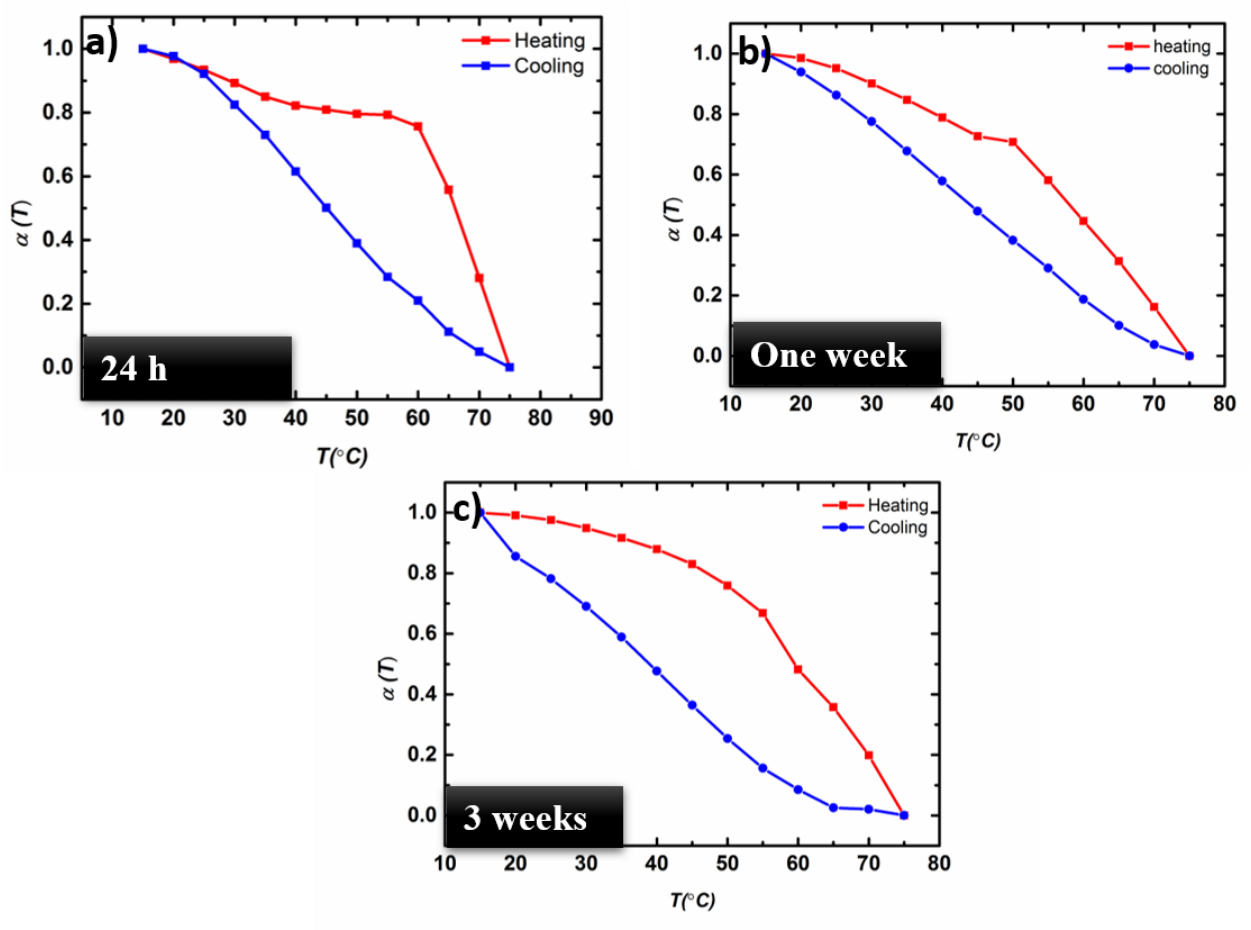

Figure 3.18 Change in degree of aggregation during the heating and cooling process of a 1mM **TANI-PTPB** solution over time, a) solution aged 24 h, b) solution aged one week and c) solution aged 3 weeks.

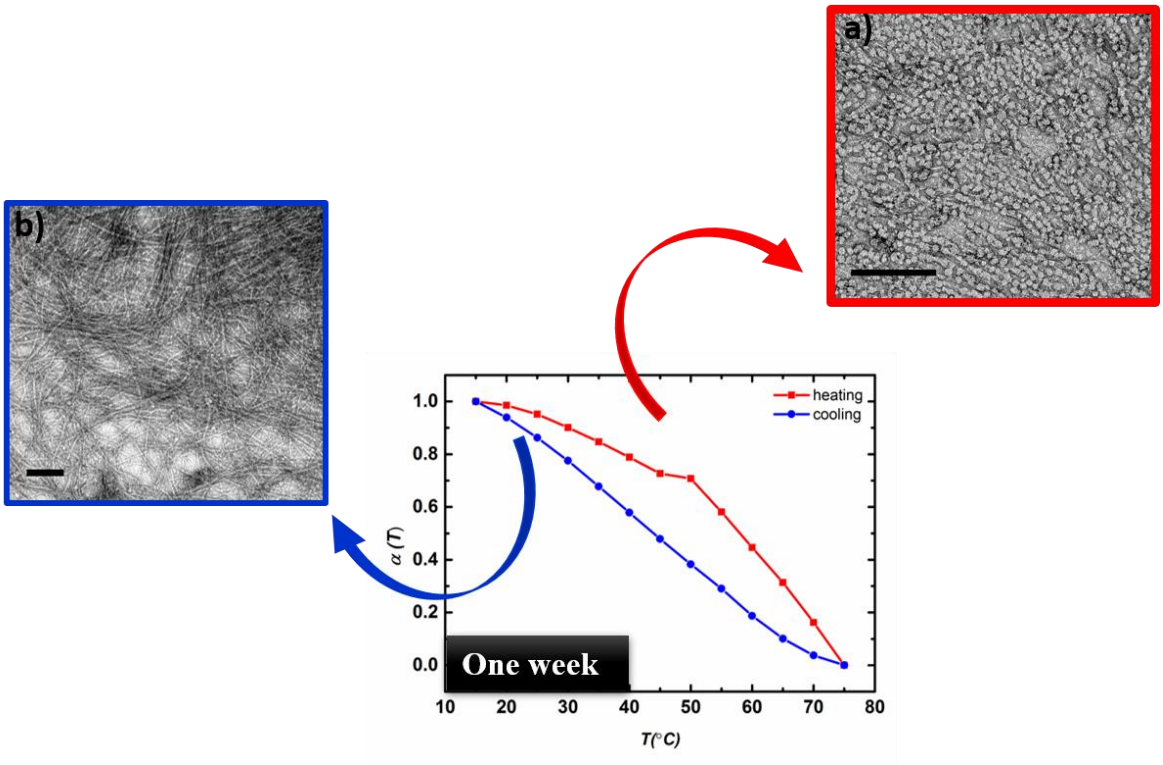

Figure 3.19 Change in degree of aggregation during the heating and cooling process of 1mM solution of **TANI-PTPB** after one week, a) TEM image of **TANI-PTPB** solution one week after preparation, b) TEM image of the same solution immediately after heating and cooling . Scale bar=200 nm.

3.2.2.4 Tuning the self-assembled structure of TANI-PTPB

According to our studies mentioned previously, the self-assembled structures of oligo(aniline)-based ammonium amphiphiles can be tuned successfully by applying the addressable packing parameter approach (**APP**). This approach can be achieved by addition of different size of dopants to **EB TANI-PTPB** that protonate the quoined nitrogen atoms in the backbone of TANI-amphiphile. As a result the volume of the hydrophobic tail would increase, subsequently the packing parameter would change leading to the formation of different morphologies. In terms of the packing parameter, the size of head groups may also play a role in the self-assembling behaviour, phosphonium groups have a larger volume and surface area compared to the corresponding ammonium groups. In this regard, we would expect to influence the self-assembled structures of phosphonium-based amphiphiles once the dopants are added. The

interesting morphologies observed for **CSA**-doped **TANI-PTAB** and **TFA**-doped **TANI-PTAB** inspire us to also investigate the effect of the two acids (**CSA**, **TFA**) on the phosphonium amphiphiles. To the best of our knowledge, polymerizable dopants have not been used to dope TANI-based amphiphiles, which makes this kind of dopants interesting to explore. 2-acrylamido-2-methylpropane sulfonic acid (**AMPS**) is a polymerisable dopant and used previously to prepare fibrous **PANI**,[44,45] Hence, **AMPS** was chosen. However, we also examined the efficiency of weak acids, such as acetic acid (**AcOH**), to dope our amphiphiles and **AcOH** also has the smallest volume of any dopant in this study.

As a result of the doping process, the solutions turned from intense blue to green, indicative of the formation of the ES state. In particular, the green solutions refer to the formation of a polaron species containing cationic radicals, and was confirmed also by UV-Vis/NIR absorption spectroscopy. The required molar ratio of dopants to **TANI-PTPB** was 2: 1, allowing the protonation of both imine nitrogen groups of **TANI**. The **ES** state of **TANI** in general exhibits three characteristic absorbance bands around 300, 400 and 800-1000 nm which correspond to π-π, polaron-π* and π-polaron transitions, respectively. However, the absence of the peaks around 600 nm (associated with the **EB** state) confirmed that the doping process was successfully completed as shown in **Figure 3.20**. However, AcOH was unable to dope **TANI-PTPB** owing to its high P_{Ka} value (4.76) as the characteristic peak of the EB state at 500 nm was clearly observed as shown in **Figure 3.20.**

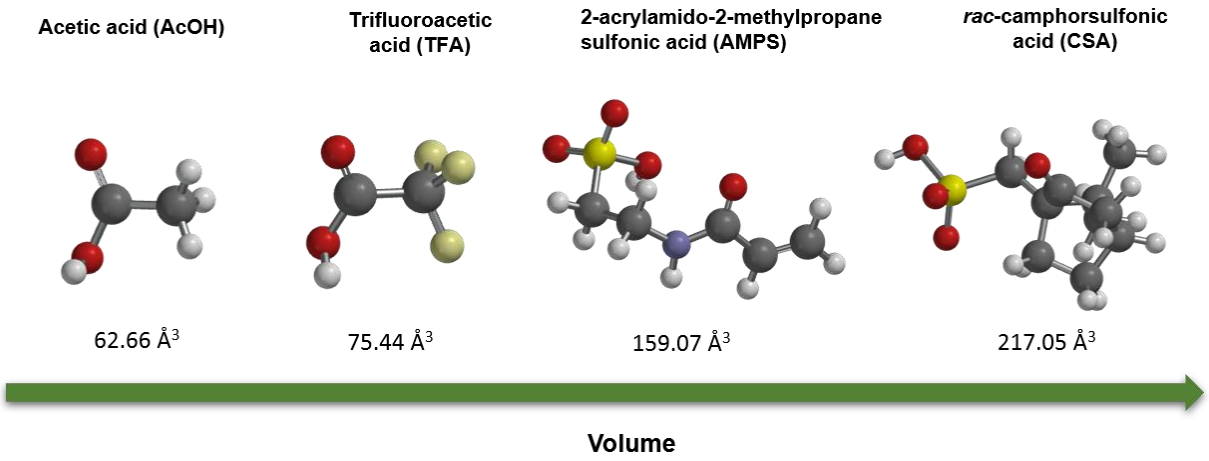

Scheme 3.4 Showing the chemical structures of the acid dopants with their volumes.

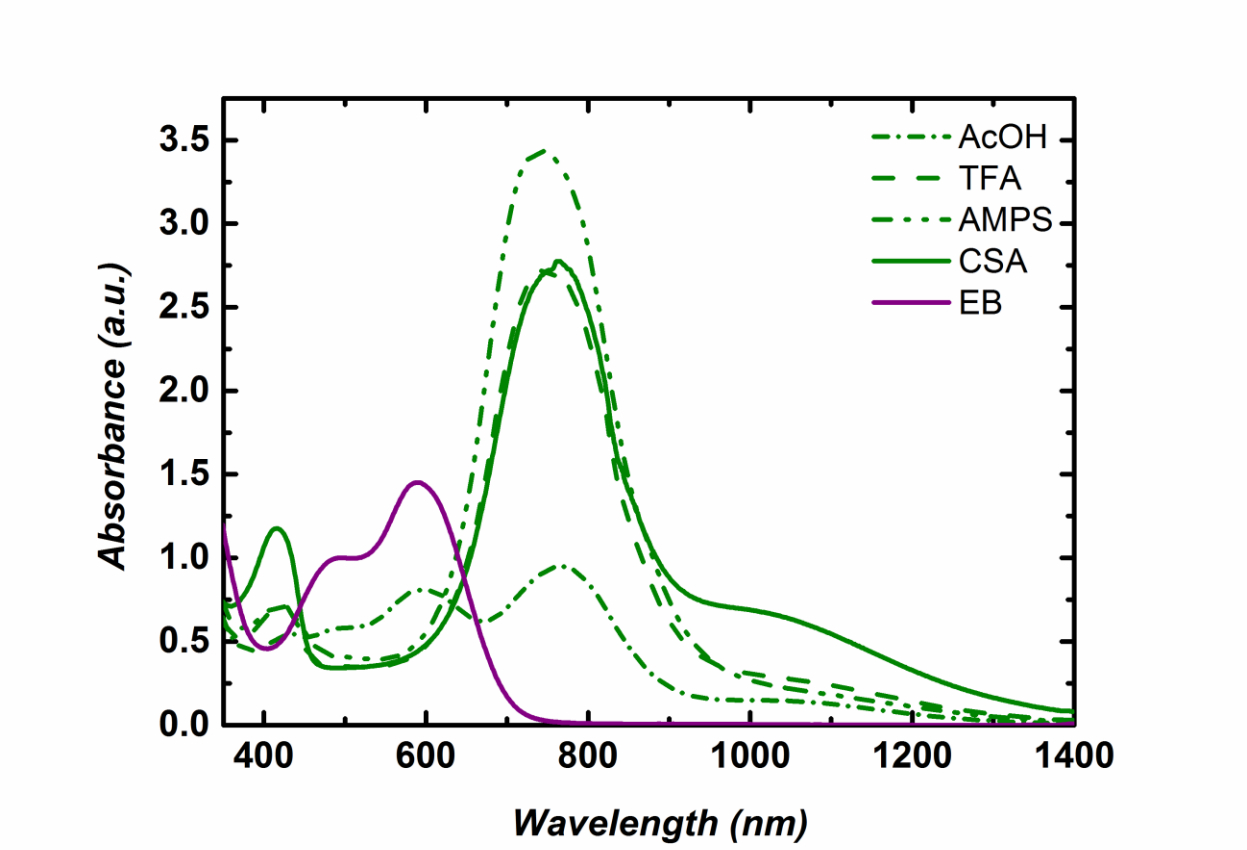

Figure 3.20 . UV/Vis spectra showing **EB TANI-PTPB** and doping with various organic acids in aqueous solution to form **ES TANI(AcOH)$_2$-PTPB, ES TANI(TFA)$_2$-PTPB, ES TANI(AMPS)$_2$-PTPB, ES TANI(CSA)$_2$-PTPB.**

As we showed in our earlier studies, the volume of the alkyl tail may be increased by the addition of a dopant through our APP approach. The estimated surface area of the phosphonium head group has not been reported before. In order to calculate the surface area, the surface tension of a solution of **TANI-PTPB** should be measured. Although two attempts were performed to measure the surface tension, the values were not feasible. These values could be an indication of the presence of some impurities but due to the limitation of time and materials we could not repeat the experiment. However, repeating this experiment should be considered for future work. The calculated volume, obtained from QSAR in Spartan,[33] of the trimethyl phosphonium (95.58 Å^3) is slightly larger than that of the trimethyl ammonium head group (83.16 Å^3). The difference in the volume of the head groups could be an indication of the larger surface area of

phosphonium compared to ammonium therefore resulting in a decrease of the packing parameter. However, the morphology of **TANI-PTPB** as observed in TEM is nanofibrous (**Figure 3.11**) indicating the formation of cylindrical micelles. This morphology suggests the packing parameter value between ($\frac{1}{3} < p < \frac{1}{2}$). Moreover, the formation of the fibres structures implied the presence of π-stacking between TANI molecules. We also investigated the possibility of tuning the self-assembled morphology of **TANI-PTPB** by varying the size of dopant acids (**AcOH, TFA, CSA, AMPS**, see **Scheme 3.4** for the structures and volumes). Starting with the smallest volume dopant, **AcOH**, TEM showed a mixture of nanofibres and vesicles as result of the presence of the two oxidation states **EB** and **ES**. The mixed oxidation states were also confirmed by UV/Vis-NIR (**Figure 3.20** and **3.21**).

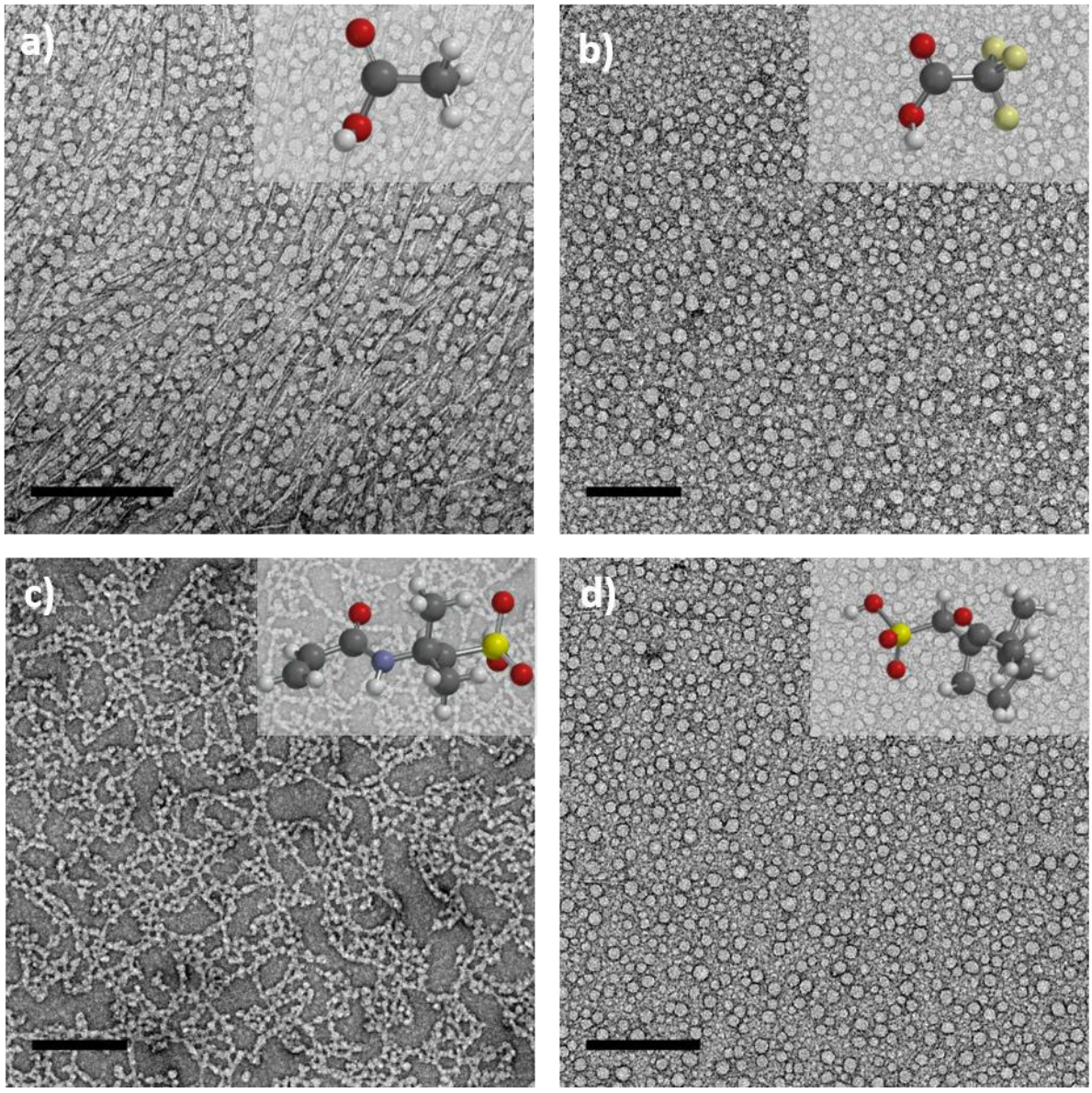

Figure 3.21 TEM images of 1mM **ES TANI-PTPB** doped by a) **AcOH**, b) **TFA**, c) **AMPS** and d) **rac-CSA**, respectively in solution (scale bar 200 nm).

TEM investigations showed that **TANI(TFA)$_2$-PTPB** formed a well-defined vesicle structure with an average diameter of 20 nm as shown in **Figure 3.21b**. Theses vesicles are smaller than vesicles observed previously in **TANI(TFA)$_2$-PTAB** (28 nm diameter). AFM investigations also confirmed the formation of vesicles with 22 nm diameter (Figure 3.22). The average diameter and height of these objects, calculated from 200 counted vesicles, were 22 ± 2 nm and 3.97 ± 2 nm,

respectively (**Figure 3.22c**). The average diameter was found to match very well with those measured by TEM.

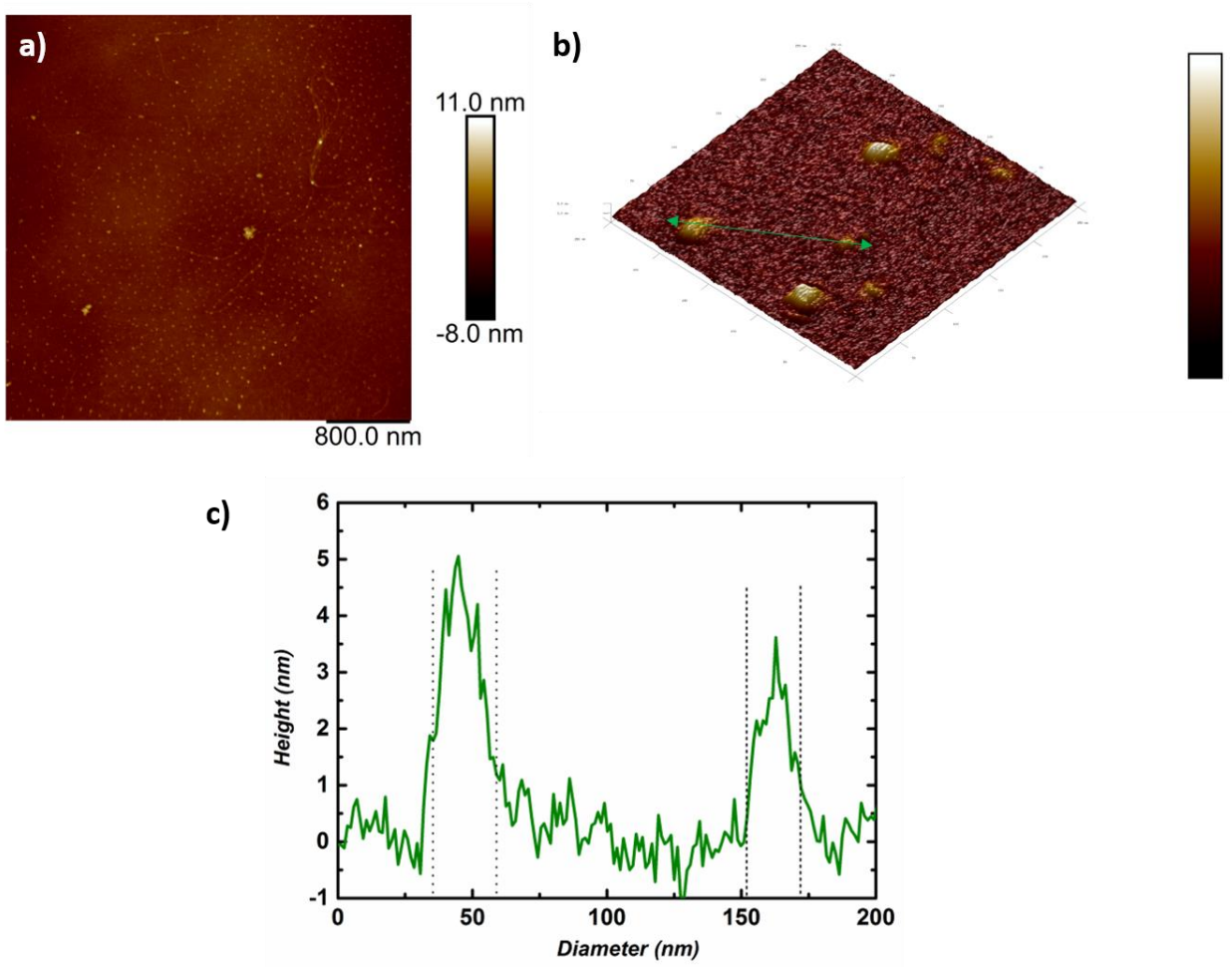

Figure 3.22 AFM images of 1m M **ES TANI(TFA)$_2$-PTPB** a) stained with 1% uranyl acetate, b) the corresponding 3D image of image (a), and c) height profile of **ES TANI(TFA)$_2$-PTPB** corresponding to the green line shown in (b).

TANI(AMPS)$_2$-PTPB formed an interesting structure that we called a chain-like linked structure, as shown in the TEM image in **Figure 3.21c.** In terms of the packing parameter, we would expect vesicles or lamellar structures formed as the volume of TANI-tail (**TANI-PTPB)** increased by adding **AMPS**. However we expect a strong hydrogen-bonding interaction to occur between **TANI-PTPB** and **AMPS** in a similar fashion to that reported in **AMPS** doped **PANI**.[46] **AMPS** molecules have

three functional groups (—NH—, —C=O, —S=O), **Figure 3.23**, which have the ability to form hydrogen-bonds as well as protonating **TANI-PTPB**.[46]

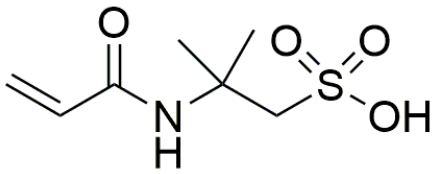

Figure 3.23 The chemical structure of **AMPS**.

Further investigation in regards with the topography of the self-assembled chain-like structures was obtained from AFM imaging. Initial measurements of AFM were conducted using stained TEM sample to compare with gathered TEM images. However, due to the presence of excess materials and the staining solution (as depicted in **Figure 3.24**), it was difficult to probe the details of the morphology. A further surface type was explored in order to identify the formed structure. Hence, 1 mM solution of **TANI(AMPS)$_2$-PTPB** was drop-cast onto mica and carbon-coated mica surfaces.

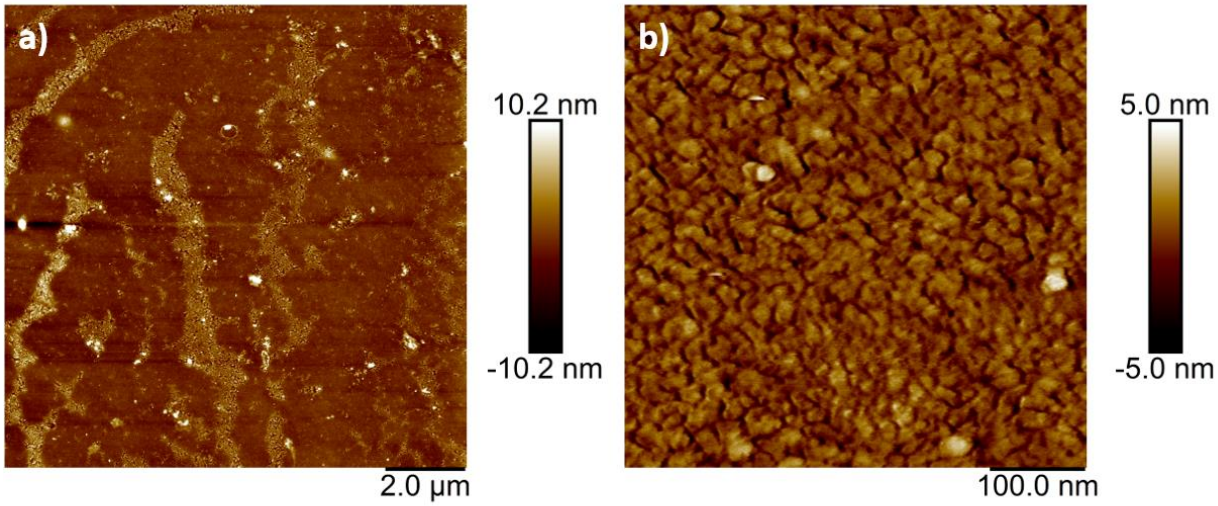

Figure 3.24 a), b) AFM image of 1mM **ES TANI(AMPS)$_2$-PTPB** (stained with 1% uranyl acetate).

Carbon-coated mica substrates mimic the carbon-coated TEM grids, allowing for comparison with TEM images. Close inspection of the AFM images (**Figure 3.25**) showed that a dense layer of material covered the surface forming a film, with unconnected chain structures formed on the surface during the drying process. This behaviour suggests that the height of the chain structures formed on the film was not consistent and showed as unconnected chain structures.

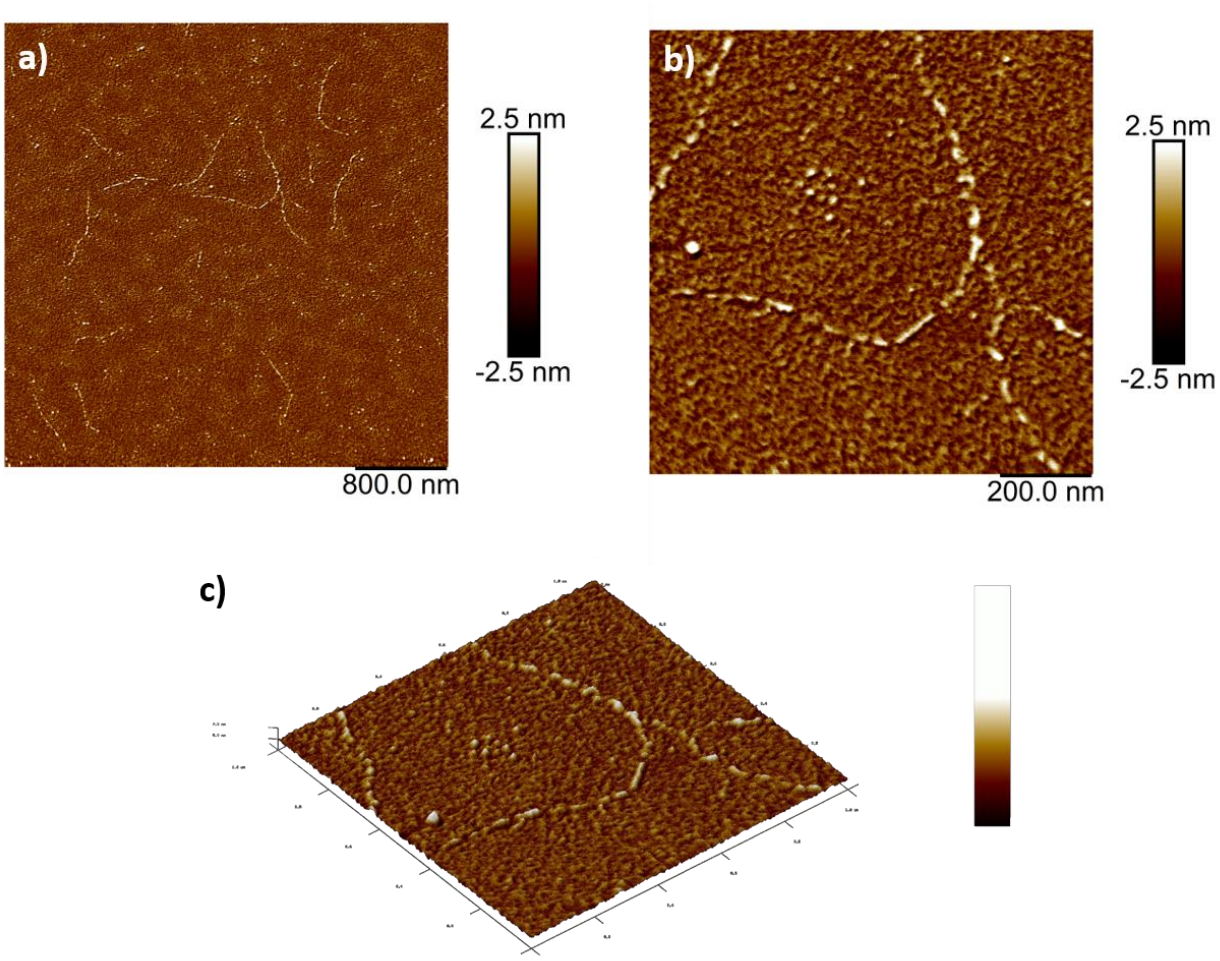

Figure 3.25 a), b) AFM images of 1mM **ES TANI(AMPS)$_2$-PTPB** drop-cast onto carbon-coated mica surface and c) the corresponding 3D image of image (b).

TANI(AMPS)$_2$-PTPB solution was drop-cast onto freshly cleaved mica (a polar surface and negatively charged) and after 10 seconds. the surface was purged with nitrogen to remove the excess material formed on the surface and then left 24 hours to dry before the measurement.

AFM images (**Figure 3.26**) showed that chain-like structures formed on mica closely resembled those seen by TEM.

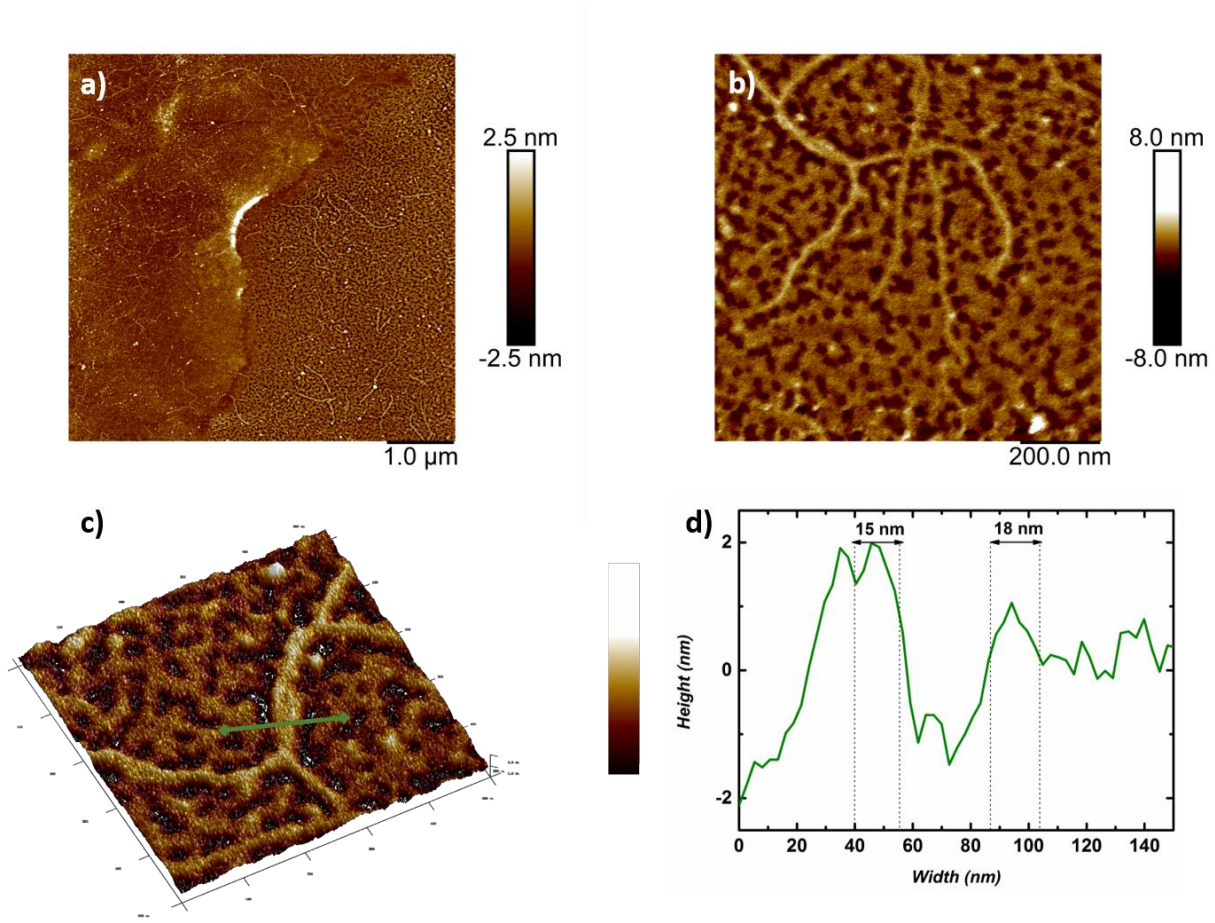

Figure 3.26 a), b) AFM images of 1mM **ES TANI(AMPS)$_2$-PTPB** drop-cast onto mica surface , c) 3D image of image (b), and d) height profile of **EB TANI-PTPB** corresponding to the green line shown in (c).

Rac-CSA was chosen to dope **TANI-PTPB** without inducing chirality. It also has the largest volume of the selected dopants. Interestingly, TEM showed **TANI(CSA)$_2$-PTPB** (**Figure 3.21d**) formed a well-defined vesicle-like structure with 20 nm diameter, but different from the morphology observed in the case of **CSA**-doped **TANI-PTAB**, which formed nanowires. In terms of packing parameter, we expect to tune the morphology from cylindrical micelles **(EB TANI-PTPB)** to vesicles **(ES TANI(CSA)$_2$-PTPB)** as the volume increases.

It is worth mentioning that CSA has been explored widely for its ability to induce chirality to self-assembled fibres of PANI once doped with CSA enantiomer.[47,48] However, there have been no reports regarding the effect of chirality on oligo(aniline)-based materials. We reported, for the first time, the effect of chirality of CSA on the fibrous structures formed in case of **TANI-PTAB**.[14] However, **TANI-PTPB** doped with CSA does not show a fibrous morphology, as discussed earlier and shown in **Figure 3.21d**.. We would not expect a vast change in the volume of CSA between enantiomers. However, there might be an effect on the self-assembled structures due to their interactions. To further elucidate, we prepared 1 mM solution of **TANI-PTPB** doped by *R*-CSA or *S*-CSA. TEM images indicated that when **TANI-PTPB is** doped by individual enantiomers *R*-CSA or *S*-CSA it exhibits ill-defined spherical assembled structures as shown in **Figure 3.27**.

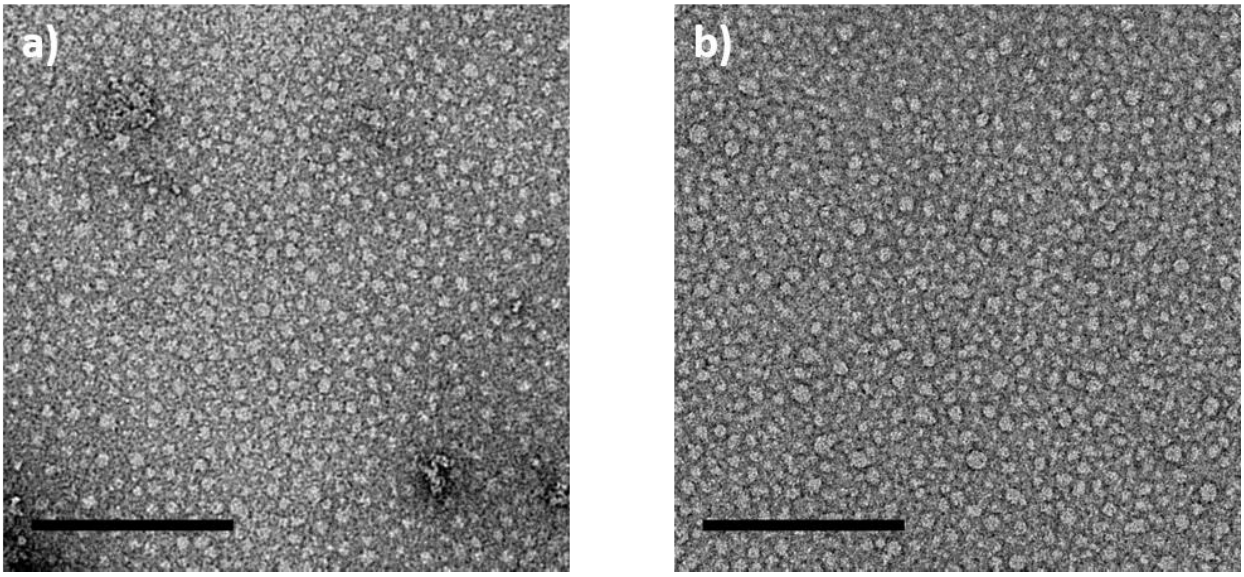

Figure 3.27 TEM images of 1m M **ES TANI-PTPB** doped by a) *R*-CSA and b) *S*-CSA, (scale bar 200 nm).

3.2.2.5 DFT-modelling: comparison studies of simulated UV/Vis-NIR of ES TANI-PTPB and experimental spectra

To gain a deeper understanding of UV/Vis-NIR spectra and spin properties of **ES TANI-**based amphiphiles, we should consider theoretical and experimental aspects. From this perspective, a comprehensive study of simulated UV/Vis-NIR spectra and spin properties of a series **TANI**-based

material in different oxidation states was recently reported by our group.[31] To extend this study with different systems, TD-DFT calculations were carried out using the CAM-B3LYP functional. **TANI-PTPB** in **ES** state exhibited peaks around λ= 811 nm, attributed to polaronic structures (triplet spin state, **TANI-^{3}ES**), and λ= 825 nm, attributed to bipolaronic structures (singlet spin state, **TANI-^{1}ES**). UV/Vis-NIR spectroscopy was carried out to compare between the experimental and theoretical studies. UV/Vis-NIR of **ES TANI(CSA)$_2$-PTPB** showed a peak at 767 nm with a slight shoulder at 1200 nm. The peak is matched to the simulated peak at 811 nm with 44 nm difference as shown in **Figure 3.27a**. However, the absorbance maxima of **ES TANI(CSA)$_2$-PTPB** solution aged one week showed a shift of 30 nm where λ= 797 with increase of the presence of shoulder peak at 1200 nm. This shift can be an indication of the transition from triplet state to singlet state and the absorbance maxima of the singlet state **TANI-^{1}ES** closely matched that of the simulation for the CSA-doped system (28 nm), as depicted in **Figure 3.27b**. For further confirmation of the transition from the triplet to the singlet state, time-dependent electron spin isomerism of **ES TANI(CSA)$_2$-PTPB** was recorded using electron spin resonance (ESR) spectroscopy. ESR spectra of 1mM **ES TANI(CSA)$_2$-PTPB** was investigated over different time after preparation (1 day, 4 days, 7 days). ESR spectra showed a signal confirming the triplet state and the signal decreased until was indistinguishable from background noise after one week. This change further confirms the observed changes in the UV/Vis-NIR spectra shown in **Figure 3.28**. These observations confirmed the spin state of the **ES TANI(CSA)$_2$-PTPB,** suggesting a facile route to switch the spin state of the **ES TANI**-based amphiphiles.

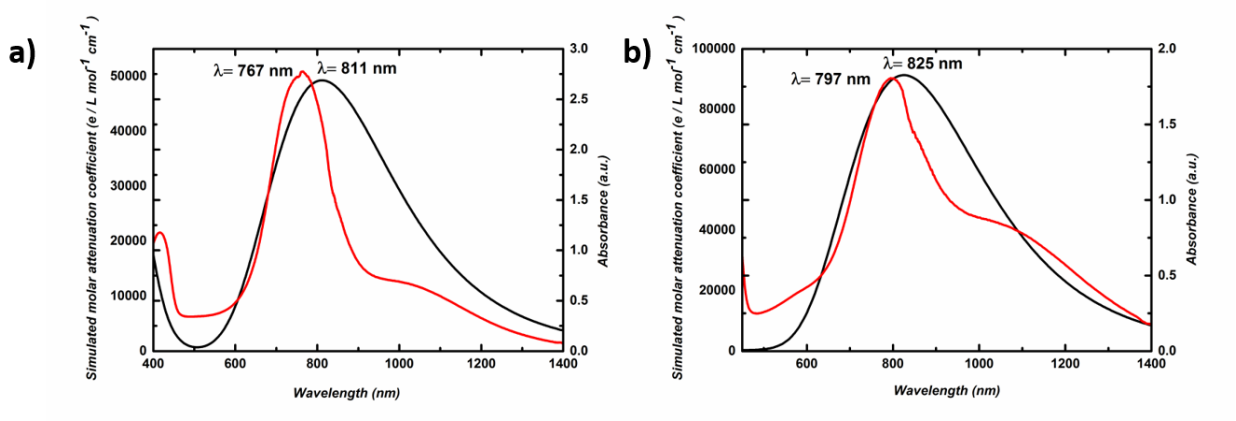

Figure 3.28 Comparison of simulated UV/Vis-NIR (black lines) and experimentally obtained spectra (red lines) of **ES TANI-PTPB**. a) Calculated high spin **(^{3}ES)** spectrum matched with the experimental spectrum obtained 24h after solution preparation; and b) calculated low spin **(^{1}ES)** matched with the experimental spectrum (red line) of **TANI(CSA)$_2$-PTPB** one week after solution preparation.

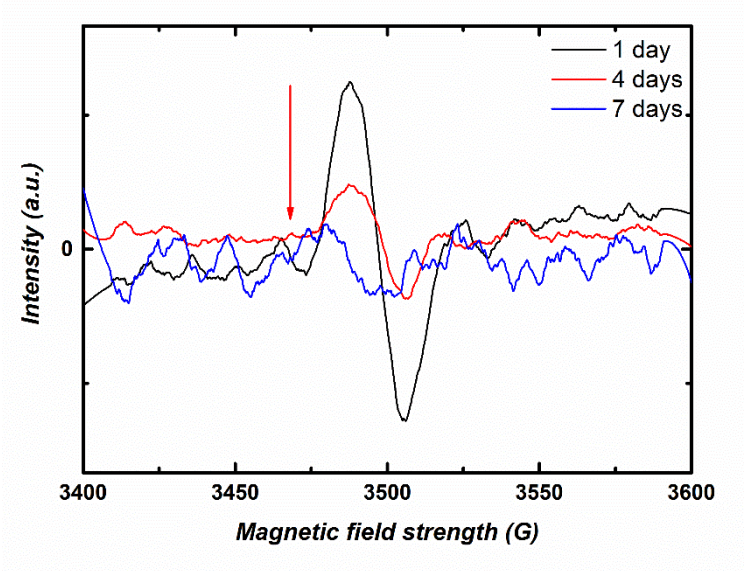

Figure 3.29 ESR spectra of solution of **TANI(CSA)$_2$-PTPB**.The arrow indicates the change on leaving the solution over time.

3.2.2.6 Doping and de-doping of TANI-PTPB

Tuning the morphology of **TANI-PTPB** can be done in a reversible fashion through the doping and de-doping processes, allowing control over the oxidation state from EB to ES and *vice versa* as discussed previously for **TANI-PTAB**. To investigate this in our new amphiphile, we prepared the blue **EB TANI-PTPB** fibre-containing solution mentioned above (shown in **Figure 3.31a**). Once doped by the addition of **CSA,** the solution turned green containing vesicular structures with an average diameter of 28 nm (**Figure 3.31b**). The EB state was easily regenerated through the addition of base (NaOH), with the **TANI-PTPB** solution once again containing fibre-like structures (**Figure 3.31c**). Two cycles of the transition from **EB** to **ES** state and *vice versa* were performed and confirmed by UV/Vis-NIR and TEM measurements as shown in **Figure 3.30**, **Figure 3.31** and **Scheme 3.5**. The second cycle of the doping process showed the initial co-existence of vesicles and nanofibers after addition of **CSA** (**Figure 3.31d**). We suggest that the found structures are indicative of a kinetically trapped state, rather than a thermodynamic minimum, as the UV/Vis-NIR data showed that all **TANI** moieties were fully doped. This behaviour has been observed previously in doping and de-doping cycles of **TANI(TFA)$_2$-PTAB**. After leaving the sample to stand undisturbed for 4 days, we obtained a solution exclusively containing vesicle structures again, as clearly observed in TEM (**Figure 3.31f)**. The efficiency of the switchability properties of these **TANI**-based amphiphiles makes them a promising platform for various applications.

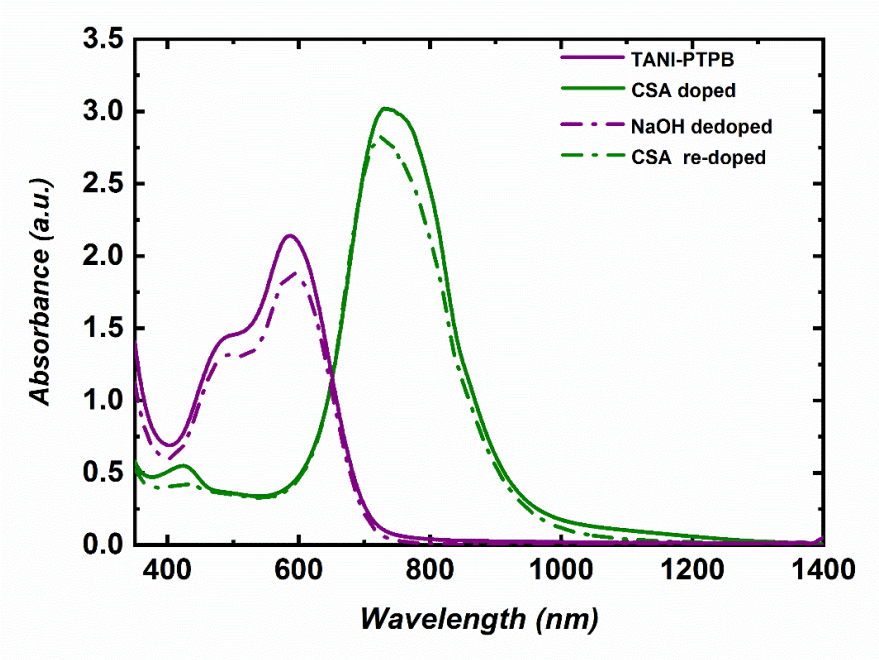

Figure 3.30. UV/Vis-NIR spectra of **EB TANI-PTPB**, **ES TANI(CSA)$_2$-PTPB** in solution (concentration = 1 mM), NaOH dedoped sample and CSA re-doped sample.

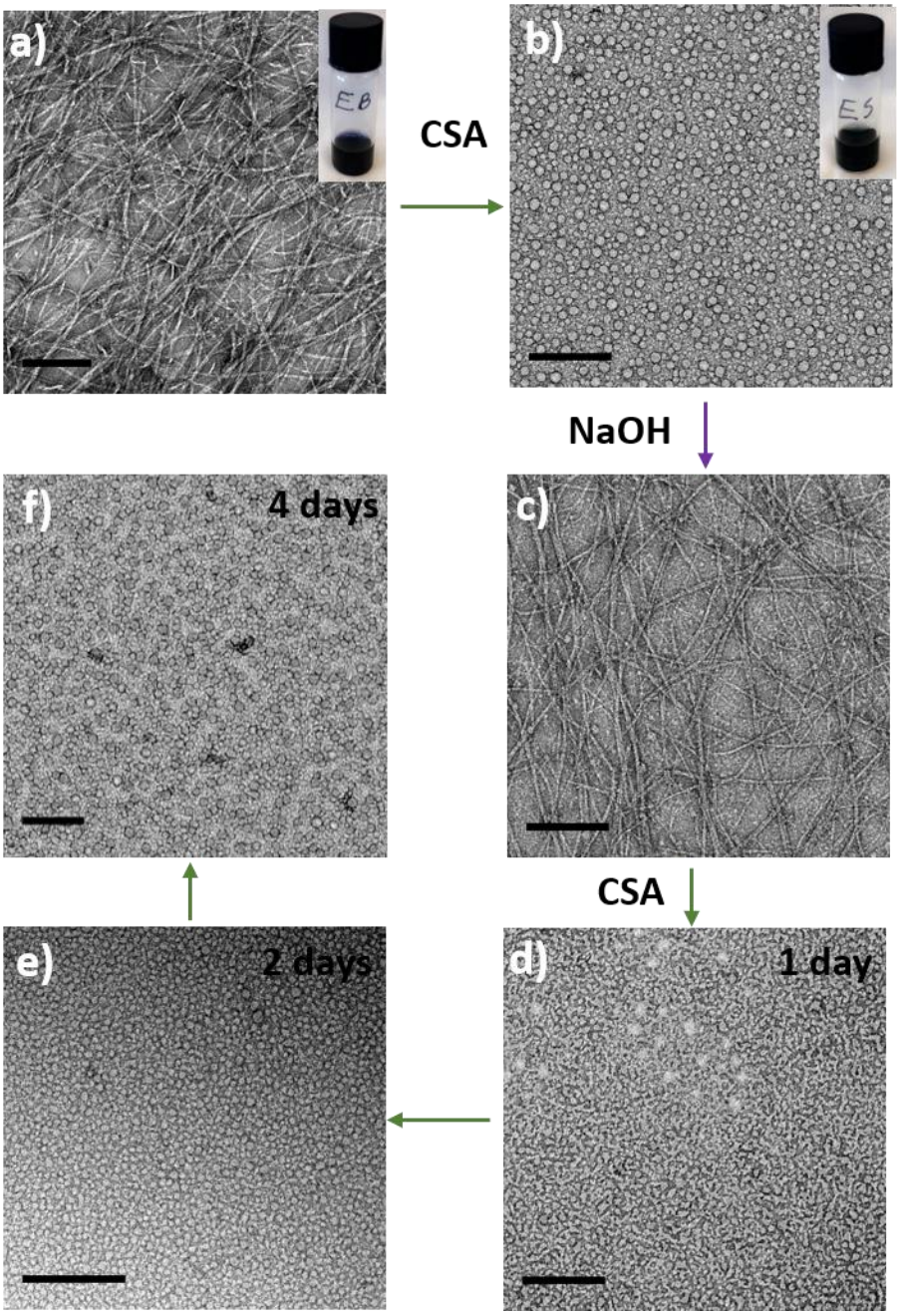

Figure 3.31 a) TEM images of **EB TANI-PTPB**, b) doped **ES TANI(CSA)$_2$-PTPB**, c) NaOH de-doped sample, d) re-doped **ES TANI(CSA)$_2$-PTPB** after 1 day, e) re-doped **ES TANI(CSA)$_2$-PTPB** after 2 days, f) re-doped **ES TANI(CSA)$_2$-PTPB** after 4 days (concentration=1mM). Scale bar=200 nm.

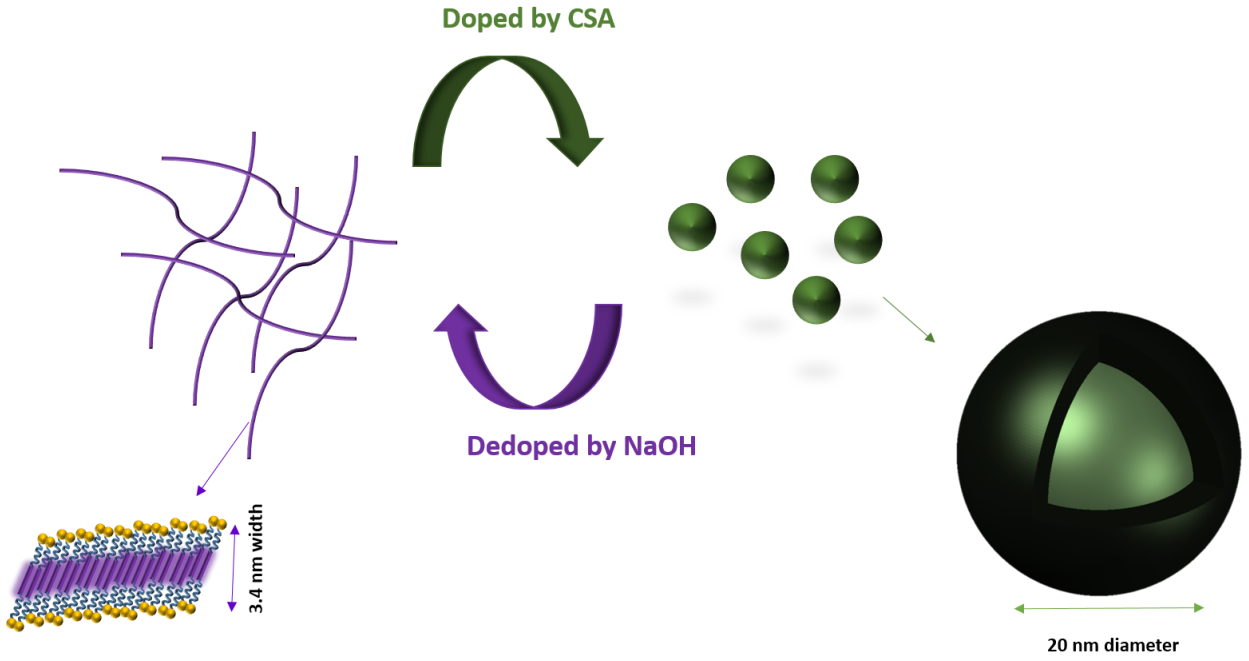

Scheme 3.5 Cartoon showing the reversible formation of fibers and spheres through doping and de-doping.

3.2.2.7 Tunable structure of ES TANI-PTPB with a polymerizable dopant

One of the selected dopants in this study was a polymerisable dopant (**AMPS**) that offers the ability to be polymerised to produce a polymerised ES **TANI(AMPS)$_2$-PTPB**. Polymerisable dopants have been used recently to enhance the conductivity and thermal stability of **PANI**.[49] Furthermore, AMPS was used to dope PANI and formed hollow fibres.[45] We were interested in exploring the effect of the polymerizable dopants after the polymerisation process occurred, and the ability to tune the self-assembled structures of **TANI(AMPS)$_2$-PTPB**. The polymerisation process was achieved in the presence of two different photoinitiators (2,2-dimethoxy-2-phenylacetophenone **(DMPA)** and phenyl bis(2,4,6-trimethylbenzoyl) phosphine oxide **(PBTBO)**) to polymerise AMPS. Once polymerised, TANI was added, with the synthetic route described in **Scheme 3.6**.

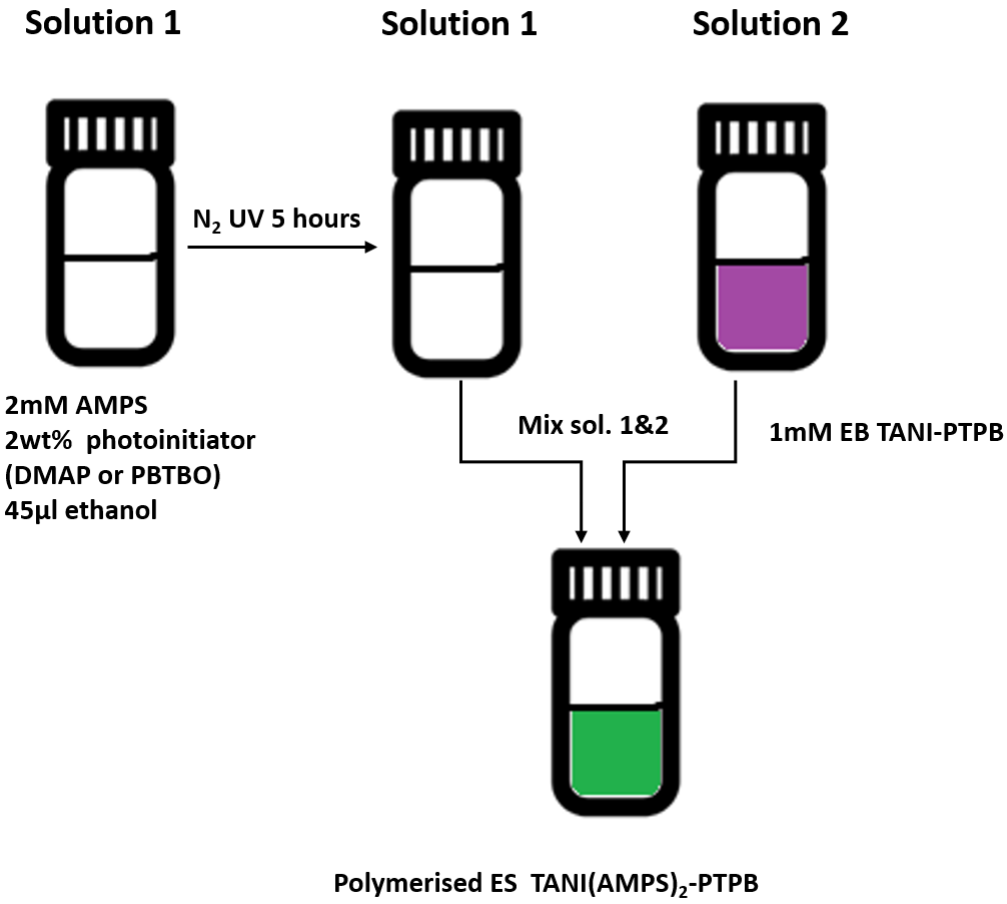

Scheme 3.6 Synthetic pathway to polymerise **TANI(AMPS)$_2$-PTPB**.

The addition of ethanol was used to increase the solubility of the photoinitiators in aqueous solutions. As expected, the addition of a small amount of ethanol (45µl) would not cause a large difference in the self-assembled structures of **TANI(AMPS)$_2$-PTPB** as clearly shown the formation of chain-like structures as depicted in **Figure 3.33a (Figure 3.21c for TEM images of TANI(AMPS)$_2$-PTPB without presence of ethanol)**. UV/Vis-NIR was used to confirm the oxidation state of the **TANI-PTPB** after the polymerisation process. UV/Vis-NIR spectra of all the ES solutions (**TANI(AMPS)$_2$-PTPB**, **TANI(AMPS)$_2$-PTPB** in the presence of ethanol, **TANI(AMPS)$_2$-PTPB-DMPA, TANI(AMPS)$_2$-PTPB-PBTBO**) showed the three characteristic absorbance bands around 300, 400 and 800 nm, respectively as shown in **Figure 3.32**. TEM was used to investigate the morphology

after the polymerisation occurred. An interesting structure was formed after polymerisation in the presence of either DMPA or PBTBO; in presence of DMPA **TANI(AMPS)$_2$-PTPB** self-assembled into a sphere-like structure with 15 nm diameter as shown in **Figure 3.33b**. However, in the presence of PBTBO **TANI(AMPS)$_2$-PTPB** self-assembled into a worm-like structure with an average width of 7 nm as depicted in **Figure 3.33c.** It is clear that the polymerisation process induced the formation of the altered self-assembled structures, suggesting that the polymerization process had taken place successfully.

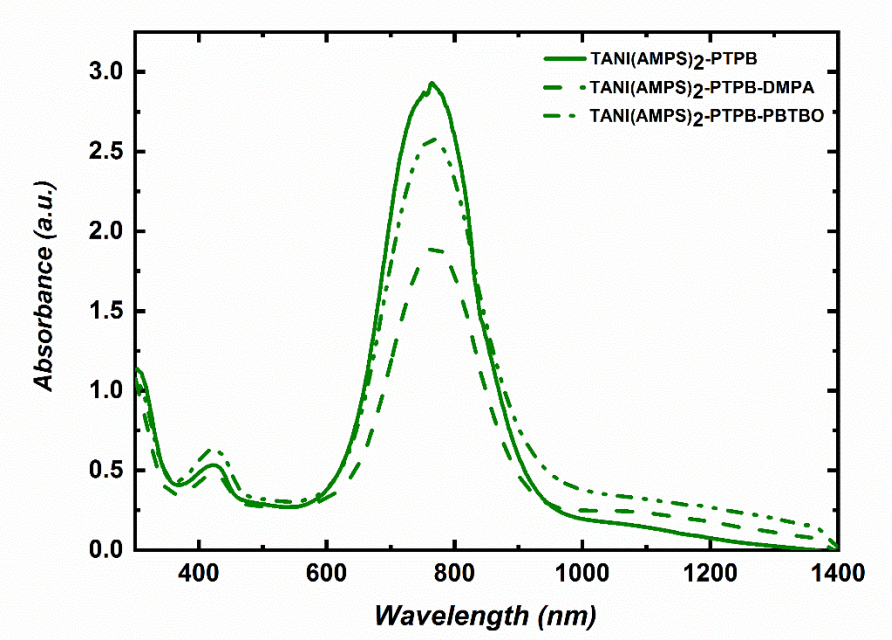

Figure 3.32 UV/Vis-NIR spectra of **ES TANI(AMPS)$_2$-PTPB** in solution (concentration = 1 mM).

FTIR spectroscopy was used to investigate any chemical bond changes which occurred during the polymerisation process. Both spectra of the polymerised and unpolymerised **ES TANI(AMPS)$_2$-PTPB** are very similar (**Figure 3.34a** and **b)**, and the presence of the C6 alky chain increases the difficulty of identifying and interpreting the spectra. However, ^{1}H NMR spectroscopy and MALDI might be a useful technique to confirm the completion of the polymerisation process.

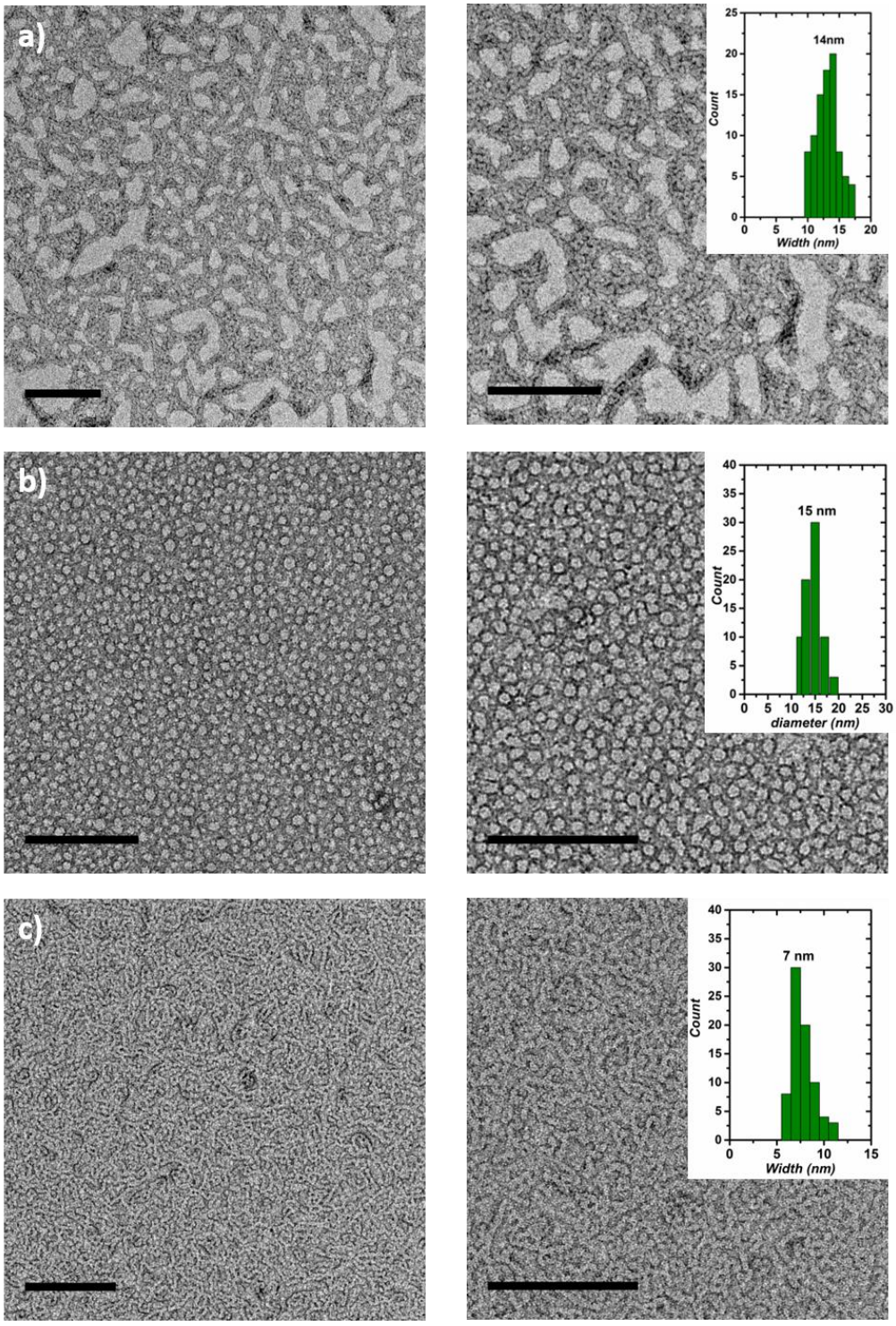

Figure 3.33 TEM images of 1mM **ES TANI(AMPS)$_2$-PTPB**, a) control experiment in presence of ethanol (45µl), b) in presence of DMPA as a photoinitiator, c) in presence of PBTBO as a photoinitiator (concentration=1mM). Scale bar=200 nm. The images on the right and left side represent the same concentrations with different magnifications.

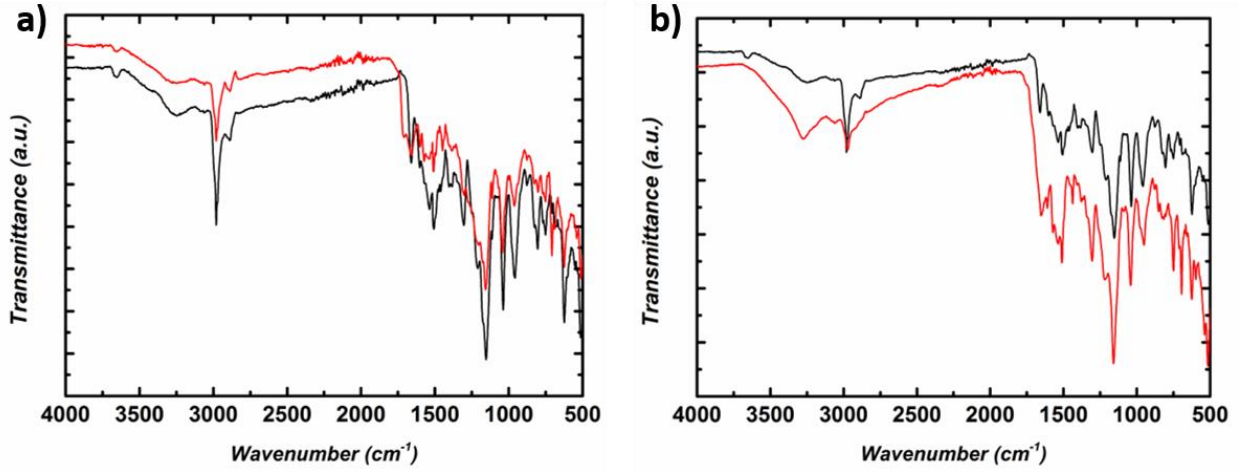

Figure 3.34 FTIR spectra of freeze-dried 1mM **ES TANI(AMPS)$_2$-PTPB**, black lines in (a), (b) are control experiment in the presence of ethanol (45µl), red line in (a) polymerised **ES TANI(AMPS)$_2$-PTPB** in the presence of DMPA as a photoinitiator, red line in (b) polymerised **ES TANI(AMPS)$_2$-PTPB** in the presence of PBTBO.

Dilution of **ES** state oligo(aniline)-based materials typically leads to de-doping and results in the **EB** state material. Interestingly, the polymerised **ES TANI(AMPS)$_2$-PTPB** diluted approximately 10 times still showed the same self-assembled structures observed in the 1 mM solution as depicted in **Figure 3.35**. This interesting observation could be an indication of the role of the polymerisation process to keep the same structure, in turn reflecting the oxidation state. To our knowledge, this fascinating aspect of the polymerisation effect on the self-assembled structures of oligo(aniline)s-based amphiphiles has not been reported before.

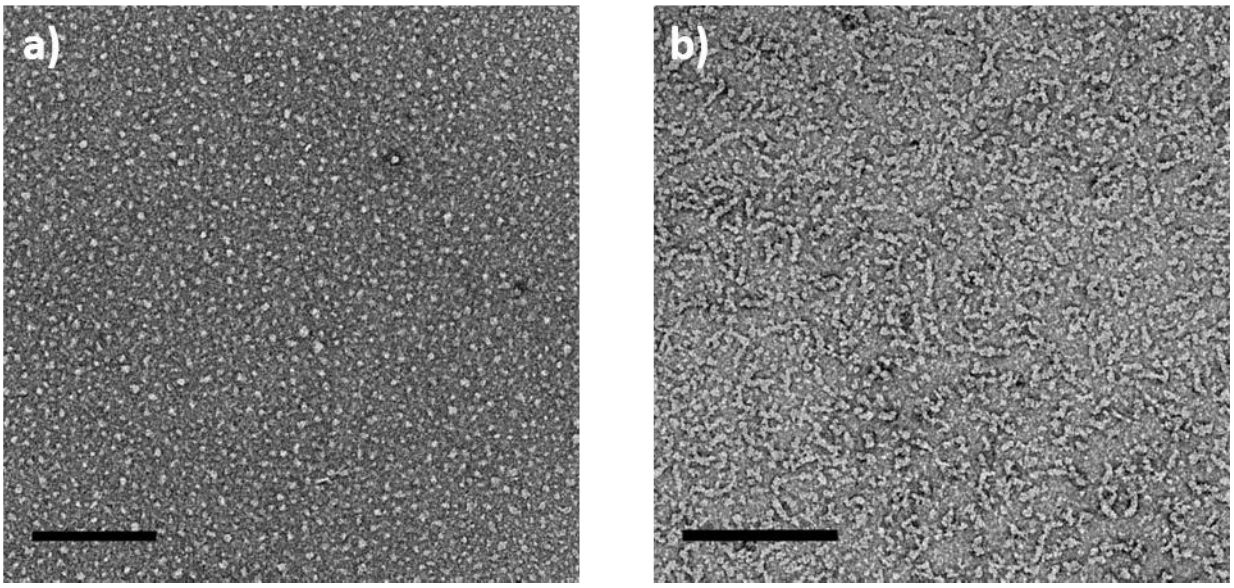

Figure 3.35 TEM images of the diluted samples (concentration=0.05mM) of **ES TANI(AMPS)$_2$-PTPB** , a) in presence of DMPA and b) in presence of PBTBO. Scale bar=200 nm.

3.3 Conclusions

This chapter describes two electroactive cationic amphiphiles, bearing either a single ammonium or phosphonium head group, that were successfully synthesized, and their self-assembled structures confirmed using a range of characterization techniques.

The first section is focused on the **ES TANI-PTAB** as we have developed a reversibly switchable self-assembling system using an oligo(aniline)-based **eSA**, **TANI-PTAB,** that showed dopant-dependent morphology transitions between vesicles and nanowires. This interesting behaviour arises from changes in the packing parameter of the protonated oligo(aniline) *vs*. the un-protonated form, caused by noncovalent association of the conjugate base as counter-ion to the protonated oligo(aniline). We therefore termed this an addressable packing parameter approach (APP). We also showed the facile and reversible switching of structures, exemplified by basic and acidic switching states from well-defined vesicles of 27 nm diameter, to infinitely long 3.19 nm wide nanowires.

In the second section we show the synthesis, for the first time, of a cationic phosphonium amphiphile based on **TANI**, **TANI-PTPB**. Detailed and comprehensive self-assembly studies of the half-oxidized **EB TANI-PTPB** using TEM, AFM, SAXS and temperature-dependent UV/Vis spectroscopy were performed, showing the formation of fibre-like assembled structures. We applied the addressable packing parameter approach, APP, to our TANI-based phosphonium amphiphiles. A range of dopants with different volumes and structures were also introduced to **TANI-PTPB** to investigate their effect on the formation of varied self-assembled structures. We also showed a feasible route to induce reversible alterations of the morphologies, from infinitely long 3.4 nm fiber-like structures to well-defined vesicles of 28 nm diameter.

We exploited the selected polymerisable dopant (AMPS) to explore the effect of the polymerisation process on the self-assembled structures of **EB TANI(AMPS)$_2$-PTPB.** As we reported there occurred the formation of interesting structures after the polymerisation (spherical structures with 15 nm diameter and worm-like structures with an average width of 7 nm in the presence of PBTBO and DMPA as a photoinitiator, respectively). Much of the work reported here about polymerisable **EB TANI(AMPS)$_2$-PTPB** represents a very promising start; however, more characterisation is required.

In this chapter, we showed the reversible switchable self-assembling behaviour of **TANI**-based amphiphiles in aqueous solution provides huge potential benefits for the development of novel switchable and addressable systems for use in encapsulation and delivery, as well as novel biomaterial applications.

3.4 Materials and instruments

High-resolution mass spectrometry measurements were carried out on a MicrOTOF II (ESITOF) mass spectrometer. ^{1}H NMR experiments were carried out on either a 400 MHz Varian VNMR 400 or a 500 MHz Bruker NMR spectrometer with CryoProbe, and deuterated solvents were used.

UV/Vis-NIR spectra were measured using a Shimadzu UV2600 spectrophotometer. Due to strong absorbance of the samples the spectra were analysed in a 1mm path length quartz cuvette. Temperature-dependent UV/Vis measurements were measured using a Perkin-Elmer Lambda 35 spectrophotometer with a Peltier temperature controller, preparing 1 mM aqueous solutions in a 1 mm quartz cuvette. Subtracting the baselines from the sample spectra to produce the final spectra. Fluorescence spectra were measured on a Hitachi F-7000 spectrofluorometer, using a cuvette with 10.0 mm path length, with the temperature controlled at 25 °C for all experiments. 10.0 µL of a 0.50 mg/ml pyrene solution in acetone was added to 1000 µL **EB TANI-PTPB** aqueous solutions with different concentrations. After sonicating for 10 min, the pyrene emission band (between 360 and 450 nm excited at 337 nm) was recorded for each solution. The CAC was chosen as the concentration where the pyrene showed an apparent decrease in the I_{373nm}/I_{383nm} ratio (denoted as I_1/I_3) with increasing concentration. Dynamic light scattering (DLS) was carried out on a Malvern Zetasize Nano-S apparatus with a 532 nm laser.

FTIR spectra were recorded using a Perkin Elmer Spectrum 100 FTIR spectrometer. Transmission electron microscopy (TEM) measurements were carried out using a JEOL 1400 TEM with a tungsten filament, performed at 120 kV and equipped with an Orius SC 200 (Gatan) camera using Digital Micrograph GMS 3 image software. All TEM samples were prepared by drop-casting of 5 µL of the samples onto carbon-coated copper grids, standing for a short time (30-90 seconds), then removing the excess using filter paper. The TEM samples were stained with aqueous uranyl acetate solution (1 wt. %) and the excess wicked away by filter paper after 20 seconds, allowing all the samples to dry at room temperature. Atomic force microscopy (AFM) measurements were carried out under ambient conditions using a Bruker Multimode VIII atomic force microscope equipped with a ScanAsyst-HR fast scanning module and a ScanAsyst-Air-HR probe (tip radius,

2 nm), utilizing peak force feedback control. Samples were drop-cast onto either carbon-coated copper grids or freshly cleaved mica.

X-ray scattering data were collected on a Ganesha SAXS/WAXS instrument (SAXSLAB) at room temperature over a Q-range of $0.001 < Q < 0.7$ Å^{-1} where

$$Q = \frac{4\pi \sin\frac{\theta}{2}}{\lambda} \qquad (1)$$

Q is the scattering vector, θ is the scattering angle and λ is the incident wavelength. Samples were loaded into borosilicate glass capillaries (Capillary Tube Supplies) and sealed with UV-curable adhesive (Norland Optical Adhesive). Data were collected over an exposure time of 3 hours and background-corrected with TFA, and intensity measurements were corrected for tube thickness. Data analysis was performed using SasView.[50] Small-angle neutron scattering (SANS) data were The L0Q small-angle diffractometer at the ISIS Pulsed Neutron Source (STFC Rutherford Appleton Laboratory, Didcot, U.K.).[51,52] This is a fixed-geometry "white beam" time-of-flight instrument which utilizes neutrons with wavelengths between 2.2 and 10 Å. Data are simultaneously recorded on two, two-dimensional, position-sensitive, neutron detectors, to provide a simultaneous Q range of 0.008−1.6 Å^{-1}. Each sample and background was placed in 2 mm path length quartz cuvettes and was measured for a total of 5 hours to gather data of high statistical precision. The beam diameter was 8 mm. Each raw scattering data set was then corrected for the detector efficiencies, sample transmission and background scattering and converted to scattering cross-section data ($\partial\Sigma/\partial\Omega$ vs Q) using the instrument-specific software.[53] These data were placed on an absolute scale (cm^{-1}) using the scattering from a standard sample (a solid blend of hydrogenous and perdeuterated polystyrene) in accordance with established procedures.[54] SANS data were subsequently collected, over the much lower Q-range of 0.0015 – 0.25 Å^{-1}, on the SANS2D small-angle diffractometer at ISIS, utilizing an incident wavelength range of 1.75 – 12.5 Å and employing an instrument configuration of L1 = L2 = 12 m (where L1 = source-sample distance, and L2 = sample-detector distance), with the 1 m^2 main detector offset vertically by 60 mm and sideways by 100 mm. The beam diameter was again 8 mm. These data were

processed in an analogous manner to that from LOQ. The SANS data were also analysed using SasView.

X-ray diffraction (XRD) data was collected with Cu-Kα radiation (λ = 1.5418 Å) on a Bruker D8 advance powder diffractometer fitted with a 0.6 mm fixed divergence slit, a LynxEye detector was used. Freeze-dried samples were placed onto a silicon wafer

For self-assembly experiments, solutions were prepared by dissolving the required mass of solid either **EB TANI-PTPB** in ultrapure deionised water and sonicated for 10 min in a bath sonicator to ensure homogeneity. The solutions should be allowed to sit, undisturbed, for 24 hours before analysis.

For doping experiments, acid-doped solutions were prepared by measuring the required mass of solid either **EB TANI-PTAB** or **EB TANI-PTPB**, followed by addition of the appropriate volume of an aqueous solution of the selected dopants to the solid. The appropriate volume of deionised water was added to reach the final concentrations where a doping ratio 2 acid: 1 **TANI**-amphiphiles. The prepared solutions were sonicated for 10 min to ensure homogeneity, and then allowed undisturbed for 24 hours before analysis. All the doped samples were kept in a fridge during the measurement.

3.5 References

1 E. W. Kaler, A. K. Murthy, B. E. Rodriguez and J. A. N. Zasadzinski, *Science*, 1989, **245**, 1371–1374.

2 J. N.Israelachvili, D. J. Mitchell and B. W. Ninham, *J. Chem. Soc. Faraday Trans. 2*, 1976, **72**, 1525–1568.

3 Z. Shao, P. Rannou, S. Sadki, N. Fey, D. M. Lindsay and C. F. J. Faul, *Chem. - A Eur. J.*, 2011, **17**, 12512–12521.

4 S. S. Zade, N. Zamoshchik and M. Bendikov, *Acc. Chem. Res.*, 2011, **44**, 14–24.

5 Z. Wei and C. F. J. Faul, *Macromol. Rapid Commun.*, 2008, **29**, 280–292.

6 Y. Wang, J. A. Torres, A. Z. Stieg, S. Jiang, M. T. Yeung, Y. Rubin, S. Chaudhuri, X. Duan and R. B. Kaner, *ACS Nano*, 2015, **9**, 9486–9496.

7 J. Stejskal, I. Sapurina and M. Trchová, *Prog. Polym. Sci.*, 2010, **35**, 1420–1481.

8 F. J. M. Hoeben, P. Jonkheijm, E. W. Meijer and A. P. H. J. Schenning, *Chem. Rev.*, 2005, **105**, 1491–1546.

9 S. Bhadra, D. Khastgir, N. K. Singha and J. H. Lee, *Prog. Polym. Sci.*, 2009, **34**, 783–810.

10 C. U. Udeh, N. Fey and C. F. J. Faul, *J. Mater. Chem.*, 2011, 21, 18137–18153.

11 Y. Wang, H. D. Tran, L. Liao, X. Duan and R. B. Kaner, *J. Am. Chem. Soc.*, 2010, **132**, 10365–10373.

12 H. Kim, S.-M. Jeong and J.-W. Park, *J. Am. Chem. Soc.*, 2011, **133**, 5206–5209.

13 Z. Yang, X. Wang, Y. Yang, Y. Liao, Y. Wei and X. Xie, *Langmuir*, 2010, **26**, 9386–9392.

14 O. A. Bell, G. Wu, J. S. Haataja, F. Broemmel, N. Fey, A. M. Seddon, R. L. Harniman, R. M. Richardson, O. Ikkala, X. Zhang and C. F. J. Faul, *J. Am. Chem. Soc.*, 2015, **137**, 14288–14294.

15 H. Gao, J. Zhang, W. Yu, Y. Li, S. Zhu, Y. Li, T. Wang and B. Yang, *Sensors Actuators B. Chem.*, 2010, **145**, 839–846.

16 E. J. Townsend, M. Alotaibi, B. M. Mills, K. Watanabe, A. M. Seddon and C. F. J. Faul, *ChemNanoMat*, 2018, **4**, 741–752.

17 W. Lyu, M. Alotaibi, O. A. Bell, K. Watanabe, R. Harniman, B. M. Mills, A. M. Seddon, S. E. Rogers, S. M. King, W. Yan and C. F. J. Faul, *Chem. Sci.*, 2018, **9**, 4392–4401.

18 M. Wang, D. Qiu, B. Zou, T. Wu and X. Zhang, *Chem. Eur. J.*, 2003, **9**, 1876–1880.

19 T. Kunitake, Y. Okahata, M. Shimomura, S. Yasunami and K. Takarabe, *J. Am. Chem. Soc.*, 1981, **103**, 5401–5413.

20 B. A. Pindzola, B. P. Hoag and D. L. Gin, *J. Am. Chem. Soc.,* 2001, **123**, 4617–4618.

21 Y. Xue, H. Xiao and Y. Zhang, *Int. J. Mol. Sci.*, 2015, **16**, 3626–3655.

22 A. Kanazawa, O. Tsutsumi, T. Ikeda and Y. Nagase, *J. Am. Chem. Soc.*, 1997, **119**, 7670–7675.

23 A. Gamarra, L. Urpí, A. Martínez De Ilarduya and S. Muñoz-Guerra, *Phys. Chem. Chem. Phys.*, 2017, **19**, 4370–4382.

24 E. S. Nigenda, T. M. Postma, M. Hezwani, A. Pirvan, S. Gannon, C. Smith and R. M. J. Liskamp, *Medchemcomm*, 2018, **9**, 982–987.

25 I. M. Herzog, R. Joseph, D. Kaizerman, M. Feldman, Y. Cohen, M. Hadar and M. Fridman, *Chem. Commun.*, 2016, **52**, 10656–10659.

26 V. P. Schnee and C. P. Palmer, *Electrophoresis*, 2008, **29**, 761–766.

27 G. A. Gainanova, G. I. Vagapova, V. V. Syakaev, A. R. Ibragimova, F. G. Valeeva, E. V. Tudriy, I. V. Galkina, O. N. Kataeva, L. Y. Zakharova, S. K. Latypov and A. I. Konovalov, *J. Colloid Interface Sci.*, 2012, **367**, 327–336.

28 M. Lukáč, F. Devínsky, M. Pisárčik, A. Papapetropoulou, M. Bukovský and B. Horváth, *J. Surfactants Deterg.*, 2017, **20**, 159–171.

29 T. Kim, C. Kim and J. Park, *Macromolecules*, 2017, **50**, 8185–8191.

30 B. M. Mills, N. Fey, T. Marszalek, W. Pisula, P. Rannou and C. F. J. Faul, *Chem. - A Eur. J.*, 2016, **22**, 16950–16956.

31 B. M. Mills, Z. Shao, S. R. Flynn, P. Rannou, D. M. Lindsay, F. Charl, J. Faul and N. Fey, *Mol. Syst. Des. Eng.*, 2019, **4**, 103 – 109.

32 R. Zana and E. W. Kaler, *Giant Micelles: properties and applications*, CRC Press, 2007, vol. 140.

33 R. A. Khalil and A. A. Zarari, *Appl. Surf. Sci.*, 2014, **318**, 85–89.

34 W. Lyu, J. Feng, W. Yan and C. F. J. Faul, *J. Mater. Chem. C*, 2015, **3**, 11945–11952.

35 W. Lv, J. Feng, W. Yan and C. F. J. Faul, *J. Mater. Chem. B*, 2014, **2**, 4720–4725.

36 D. F. Evans; and H. Wennerström, *The colloidal domain : where physics , chemistry , biology , and technology meet*, Wiley-VCH, 1999.

37 O. T. Ikkala, L. Ahjopalo, L. Pietilä, P. J. Passiniemi and H. Österholm, *J. Chem. Phys.*, 2002, **103**, 9855–9863.

38 O. A. Bell, G. Wu, J. S. Haataja, F. Brömmel, N. Fey, A. M. Seddon, R. L. Harniman, R. M. Richardson, O. Ikkala, X. Zhang and C. F. J. Faul, *J. Am. Chem. Soc.*, 2015, **137**, 14288–14294.

39 F. Würthner, T. E. Kaiser and C. R. Saha-möller, *Angew. Chem. Int. Ed.*, 2011, **50**, 3376–

3410.

40 F. Biedermann, W. M. Nau and H.-J. Schneider, *Angew. Chem. Int. Ed. Engl.*, 2014, **53**, 11158–11171.

41 Q. Tang, J. Wu, X. Sun, Q. Li and J. Lin, *Langmuir*, 2009, **25**, 5253–5257.

42 M. J. Winokur and B. R. Mattes, *Macromolecules*, 1998, **31**, 8183–8191.

43 M. M. J. Smulders, M. M. L. Nieuwenhuizen, T. F. A. de Greef, P. Van Der Schoot, A. P. H. J. Schenning and E. W. Meijer, *Chem. Eur. J.*, 2010, **16**, 362–367.

44 J. Zhou, G. Tzamalis, N. A. Zaidi, N. P. Comfort and A. P. Monkman, *J. Phys. Condens. matter*, 2001, **13**, 2503–2508.

45 J. Yang, S. M. Burkinshaw, J. Zhou, A. P. Monkman and P. J. Brown, *Adv. Mater.*, 2003, **15**, 1081–1084.

46 D. Yang, P. N. Adams, L. Brown and B. R. Mattes, *Synth. Met.*, 2006, **156**, 1225–1235.

47 W. Li and H. Wang, *J. Am. Chem. Soc.*, 2004, **126**, 2278–2279.

48 Y. Yan, Y. Zhang, W. Hu and Z. Wei, *Chem. - A Eur. J.*, 2010, **16**, 8626–8630.

49 Y. K. Choi, H. J. Kim, S. R. Kim, Y. M. Cho and D. J. Ahn, *Macromolecules*, 2017, **50**, 3164–3170.

50 Www.sasview.org.

51 Http://www.isis.stfc.ac.uk.

52 R. K. Heenan, S. E. Rogers, D. Turner, A. E. Terry, J. Treadgold and S. M. King, *Neutron News*, 2011, **22**, 19–21.

53 Http://www.mantidproject.org.

54 G. D. Wignall and F. S. Bates, *J.Appl. Crystallogr*, 1987, **20**, 28–40.

CHAPTER 4 SYNTHESIS AND TUNABLE SELF-ASSEMBLY OF ELECTROACTIVE BOLAAMPHIPHILES BASED ON OLIGO(ANILINE)S

4.1 Introduction

Amphiphilic molecules have been extensively studied because of their fascinating ability to self-assemble in an aqueous environments, thus generating a variety of either zero-dimensional **(0D),** one-dimensional **(1D)** or two-dimensional **(2D)** structures.[1] Special attention has been drawn to bolaamphiphiles, which are amphiphiles comprising two hydrophilic head groups, alike or dissimilar, bridged by a hydrophobic skeleton and linked by covalent bonds. This dipolar architecture[2] makes bolaamphiphiles a fascinating platform for generating a variety of complex supramolecular structures in a facile fashion.[2,3,4] The presence of the second polar head group in classical bolaamphiphiles generally leads to enhanced solubility of the amphiphile in aqueous environments and an increase in the critical aggregation concentration (CAC).[5] However, the addition of an additional hydrophobic group to the bolaamphiphile structure could lead to a decrease in the solubility of bolaamphiphiles and a decrease in the CAC when compared with corresponding conventional amphiphiles.[6,7] Significant research effort has been dedicated towards the use of bolaamphiphiles in diverse applications such as sensors,[8] electronic devices,[9] imaging,[10] and drug delivery.[11]

As mentioned in the previous chapter, the functionalization of **TANI** with hydrophilic groups led to the formation of water-soluble amphiphiles. To date, the most widely prepared and studied **TANI**-based amphiphiles are based on the addition of a poly(ethylene glycol) block, resulting in non-ionic amphiphiles.[12,13] We designed and synthesised the first cationic pentyltrimethylammonium bromide amphiphile based on **TANI, TANI-PTAB**, which self-assembled into high aspect-ratio nanowires.[14] Exploring further amphiphile architectures, it was noted that very few studies have exploited the **TANI** motif to prepare bolaamphiphilic molecules. Previously, anionic bolaamphiphiles containing penta(aniline) oligomers were examined for their ability to inhibit steel corrosion in acidic media.[15,16] Moreover, non-ionic bolaamphiphiles containing penta(aniline) oligomers showed a reversible transition between large spheres (1000

nm diameter) and microspheres (300 nm diameter) in response to changes in pH and applied potential.[17]

The shape and size of the aggregated structures formed by amphiphilic molecules can be controlled by packing parameter role[18] as discussed in the previous chapter. Again, the packing parameter p relies on the length and volume of hydrophobic species and the area of the head group. It is therefore possible to change the packing parameter and thereby tune the morphology of self-assembled aggregates. Changing the length or volume of the tail would normally require further synthetic efforts (i.e., adding another chain, or adding branches to the existing chains). However, doping of a **TANI**-based amphiphile with different inorganic or organic acids can lead to significant changes in the volume of the hydrophobic **TANI**-based tail structure as discussed in the previous chapter.[19] Thus, it is possible to tune the self-assembled supra-amphiphilic structure by addressing the packing parameter through protonating or doping the quinoid nitrogen atoms in **TANI** to reach the **ES** state. Such noncovalent dopant attachment in the **ES** state leads to a significantly greater molecular volume than for the **EB** state.[20,19,21] Constructs such as these that exploit the electrostatic interactions between the protonated imines and the counterions of the added acid are also classified as electrostatic supra-amphiphiles (eSA).[21] Increasing the pH to form the EB state, or reducing the **TANI** in such constructs to the **LEB** state will lead to removal of the electrostatic force binding the **TANI** moiety and the bulky acid molecules, allowing the structure to reversible return to its original morphology, as shown in **Chapter 3**.[19] It is worth mentioning that the packing parameter of bolaamphiphiles cannot be used in the same simple way as the single-tailed amphiphiles, owing to the presence of two head groups.[22] However, a comparable effect of packing parameter on the self-assembled structures of bolaamphiphiles can be observed as reported previously.[2,22,23] There are a few attempts in order to calculate the packing parameter have already been reported. Zichen and his group calculated the packing parameter of disodium phenyl-1,4-bis (oxyhexanoate) and found that the presence of two head groups led to a decrease in packing parameter. In addition, altering pH resulted in a change in morphology from tubes to vesicles and from vesicles to micelles. These alterations of morphology could be an indication of the packing parameter role.[22]

To date, there have been no reports regarding cationic bolaamphiphiles bearing addressable oligo(aniline)s nor has the effect of doping been studied on the formation of self-assembled architectures. Thus, to further explore the assembly behaviour of amphiphilic oligo(aniline)s, **TANI**-based bolaamphiphiles were designed for comparison with **TANI-PTAB** and **TANI-PTPB**. We synthesised a **TANI**-based bolaamphiphile bearing a cationic head group and explored their self-assembly. The first part of this chapter focused on ammonium bolaamphiphiles and the second part focused on phosphonium amphiphiles. We here report on this novel class of materials and propose a facile strategy for the reversible transition between vesicle-like structures and nanofibres based on the tunable self-assembly of these electroactive **TANI**-based bolaamphiphiles.

4.2 Result and discussion

4.2.1 Synthesis and self-assembly of electroactive ammonium bolaamphiphiles

4.2.1.1 Synthesis of tetra(aniline) bolaamphiphile TANI-$(PTAB)_2$

We previously reported the preparation of a conventional trimethylammonium amphiphile **EB TANI-PTAB**.[14] Using a similar approach, we synthesized the target bolaamphiphile comprising **TANI** functionalized with two alkyltrimethylammonium head groups based on the successful synthesis of the symmetrical NH_2/NH_2 **TANI** precursor reported previously.[24] Boc-protected NO_2/NO_2 **TANI** was first synthesised via a nucleophilic substitution reaction. The reaction followed a similar route to that used in the literature,[25] but with some improvements through addition of Boc groups to prevent any oxidation of **TANI** (**Scheme 2.2**). For the reduction of the NO_2 terminal moieties, we initially explored a route based on reduction using tin reported by Kulszewicz-Bajer *et al*.[25] However, as this route requires harsh acidic conditions that led to loss of the Boc groups and the undesired formation of multiple oxidation states, we employed palladium on carbon in the presence of ammonium formate as an alternative, milder reducing agent. Subsequently, NH_2/NH_2 **TANI** was used to prepare the electroactive bolaamphiphile **TANI-$(PTAB)_2$** (**Scheme 2.5**). The formation of the desired symmetrical water-soluble bolaamphiphile was confirmed using different characterization techniques, including ^{1}H NMR

spectroscopy and high-resolution mass spectrometry. All the synthetic details are presented in the **Experimental Chapter**.

4.2.1.2 Self-assembly studies of EB TANI-$(PTAB)_2$

In order to investigate the self-assembling behavior of **TANI-$(PTAB)_2$**, the critical aggregation concentration (CAC) was measured using pyrene as a fluorescent probe and determined to be 0.072 mM. This value was assigned by the sharp change in I_1/I_3 ratio as presented in (**Figure 4.1a**). The CAC of the bolaamphiphile is smaller than that of the conventional amphiphile (0.1 mM),[14] which shows that the bolaamphiphile has a stronger tendency to aggregate in solution, potentially as a result of the presence of the additional hydrophobic spacer group.[5,6]

Aqueous solutions of **EB TANI-$(PTAB)_2$** with different concentrations were prepared and analysed by UV/Vis spectroscopy to further elucidate the aggregation phenomena. A 44 nm bathochromic shift in the characteristic absorbance peak was observed as the concentration increased, with λ_{max} = 553 nm for 0.001 mM vs. 597 nm for 1 mM solutions, as shown in (**Figure 4.1b**). Bathochromic shifts have been reported previously as a result of the changes in the environment and molecular packing, and it also referred to the aggregation mode (i.e., J-aggregate).[26] When comparing the bolaamphiphilic **TANI-$(PTAB)_2$** with the simple amphiphile **TANI-PTAB** (λ_{max}= 580) at similar concentrations, a 17 nm bathochromic shift of the characteristic absorbance peak was observed. This shift could be attributed to a combination of the mode of packing as well as the presence of an additional electron-donating amide group in the bolaamphiphile.

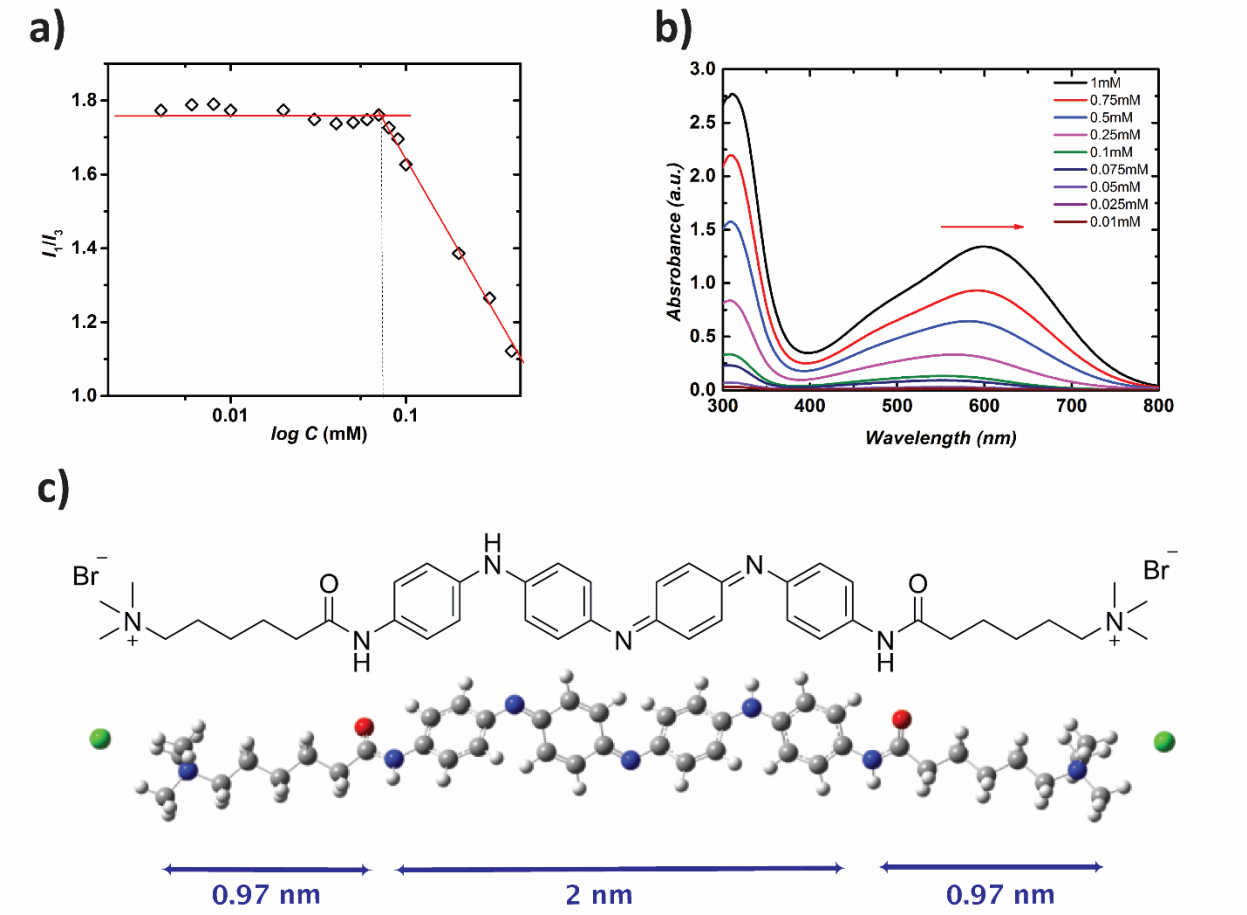

Figure 4.1 a) Fluorescence of a pyrene probe to determine the CAC of **EB TANI-(PTAB)$_2$**. CAC = 0.072 mM. b) Change of λmax of **EB TANI-(PTAB)$_2$** with concentration. The arrow indicates change on increasing concentration. c) Chemical structure and DFT-optimised structure.

4.2.1.3 DFT-modelling: comparison of simulated UV/Vis of EB TANI-(PTAB)2 and experimental spectra

The structure of **EB TANI-(PTAB)$_2$** was modelled and optimised in Gaussian using the B3LYP functional, the 6-31G* basis set, and a polarisable continuum model (PCM) solvent environment. In the case of simulated UV/Vis data, CAM-B3LYP was used and found suitable and yielded more accurate simulated spectra for charge-transfer and π conjugated systems in earlier studies.[27] TD-DFT simulations of **TANI-(PTAB)$_2$** yielded spectra similar to experimental spectra obtained in acetonitrile (**Figure 4.2**), which was chosen to avoid the observed bathochromic shift

corresponding to aggregated structures in water. The absorbance maximum at 521 nm was attributed to the HOMO−LUMO transition of aqueous **TANI-(PTAB)$_2$**, where π-π* transitions are mainly involved (**Figure 4.3**). The absorbance peak of the first singlet excited state of **EB** state (2.37 eV, 522 nm) matched the transition observed experimentally in the UV/Vis spectrum at 545 nm (see the **Appendix D** for further details).[14,27]

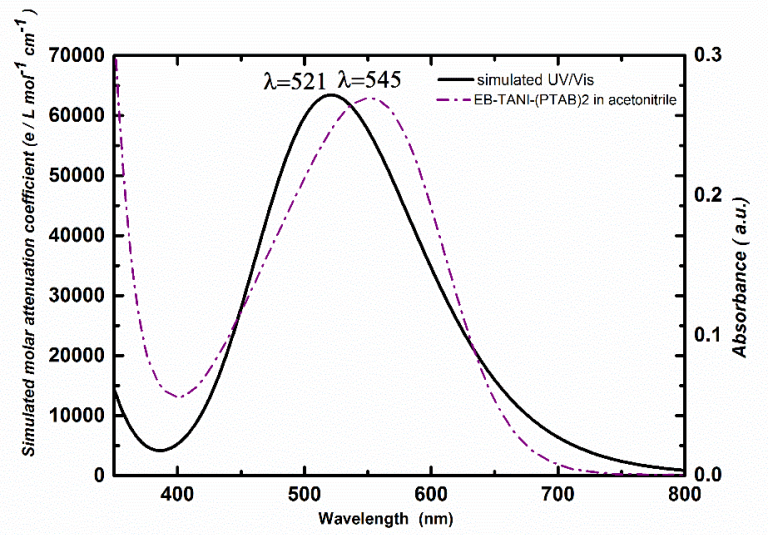

Figure 4.2 Comparison of the simulated UV/Vis of **EB TANI-(PTAB)$_2$** and experimental spectra in acetonitrile.

LUMO

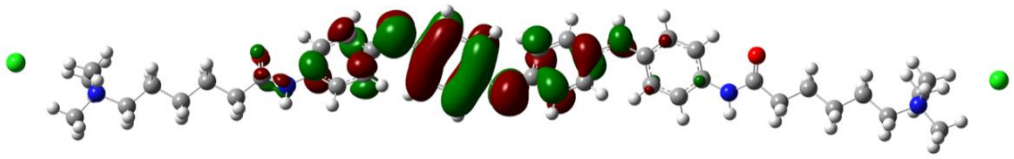

HOMO

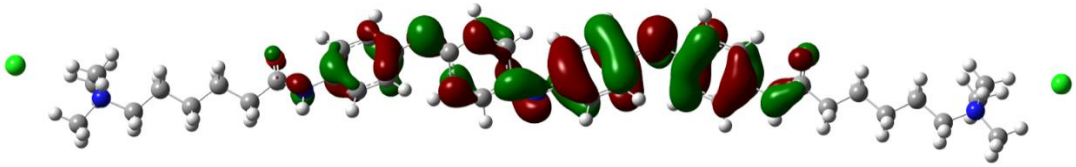

Figure 4.3 MOs of **EB TANI-(PTAB)$_2$** transition.

4.2.1.4 Structural investigations

The self-assembled structure of **EB TANI-(PTAB)$_2$** was investigated using transmission electron microscopy (TEM), Cryo- TEM and atomic force microscopy (AFM). Circular structures indicative of collapsed spheres were observed at 1 mM of **EB TANI-(PTAB)$_2$** as shown in **Figure 4.4** and **Figure 4.5**. For accurate characterization of the observed structures' dimensions by AFM, we focused on 1mM concentrations owing to the consistency of the discrete structures found (as judged by TEM). Diameters measured by both techniques were in good agreement for samples measured at 1mM: 22nm ± 1 from TEM (**Figure 4.4a**) and 22 ± 2nm for AFM. AFM images of a **TANI-(PTAB)$_2$** solution (1 mM), drop-cast on carbon-coated copper grids are shown in **Figure 4.4b**. Again, circular structures indicative of collapsed spheres were observed. The found structures and dimensions remained consistent when measured on mica surfaces (**Figure 4.6**). The average diameter and height of these structures were determined over 160 counted structures, and calculated to be 22 nm ±2 nm and 3.12 ± 0.3 nm, respectively (**Figure 4.4d, e**). While the value obtained for the average diameter agreed very well with the sizes obtained from TEM measurements, the obtained heights (**Figure 4.4e** and **f**) were in the same range as the theoretical length of the optimised **TANI-(PTAB)$_2$**, which was 3.96 nm (a 2 nm contribution from the **TANI** core, and 0.98 nm each from the alkyl chains, see **Figure 4.1c**).

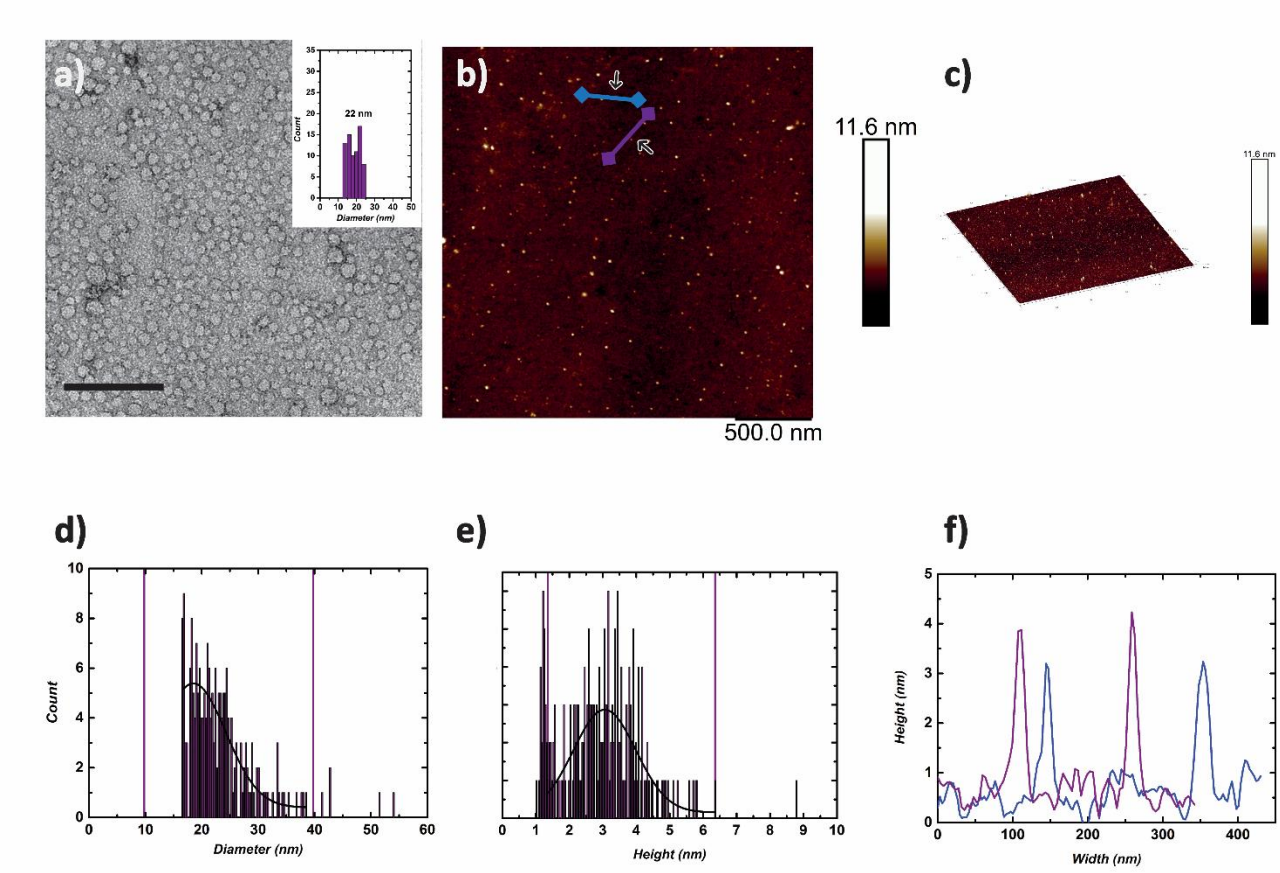

Figure 4.4 a) TEM images (stained with 1% uranyl acetate) of **EB TANI-(PTAB)$_2$** in solution (concentration=1mM), inset: histogram of particle size distribution by TEM for a 1 mM **TANI-(PTAB)$_2$** solution, scale bar=200 nm. b) AFM image of 1 mM **TANI-(PTAB)$_2$** sample on a carbon-coated grid. c) 3D AFM image with the Z-ratio increased by a factor of 3 for clarity. d), e) Histograms of particle diameter and height distributions respectively, each counted from 160 particles, f) height profile of formed **EB TANI-(PTAB)$_2$** structures, corresponding to the black and purple lines shown in (b).

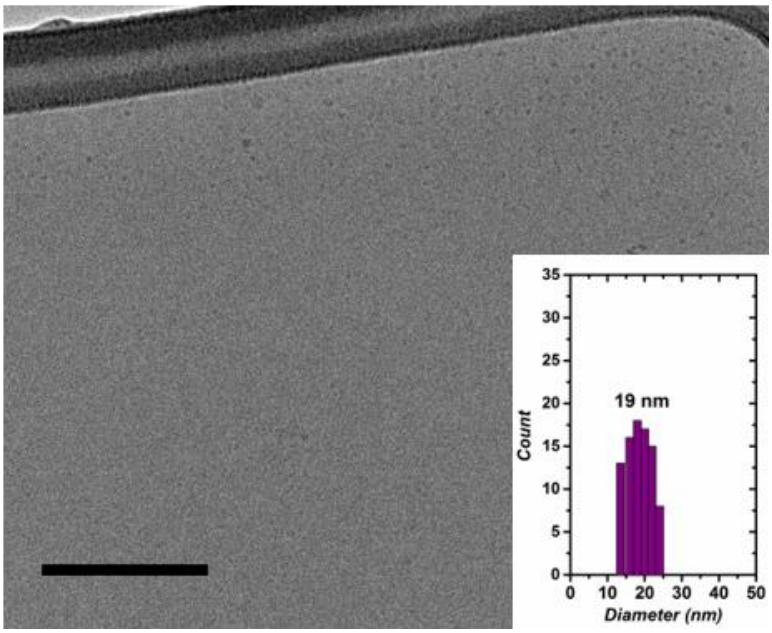

Figure 4.5 Cryo-TEM of 1 mM solution of **EB TANI-$(PTAB)_2$** (scale bar=200 nm).

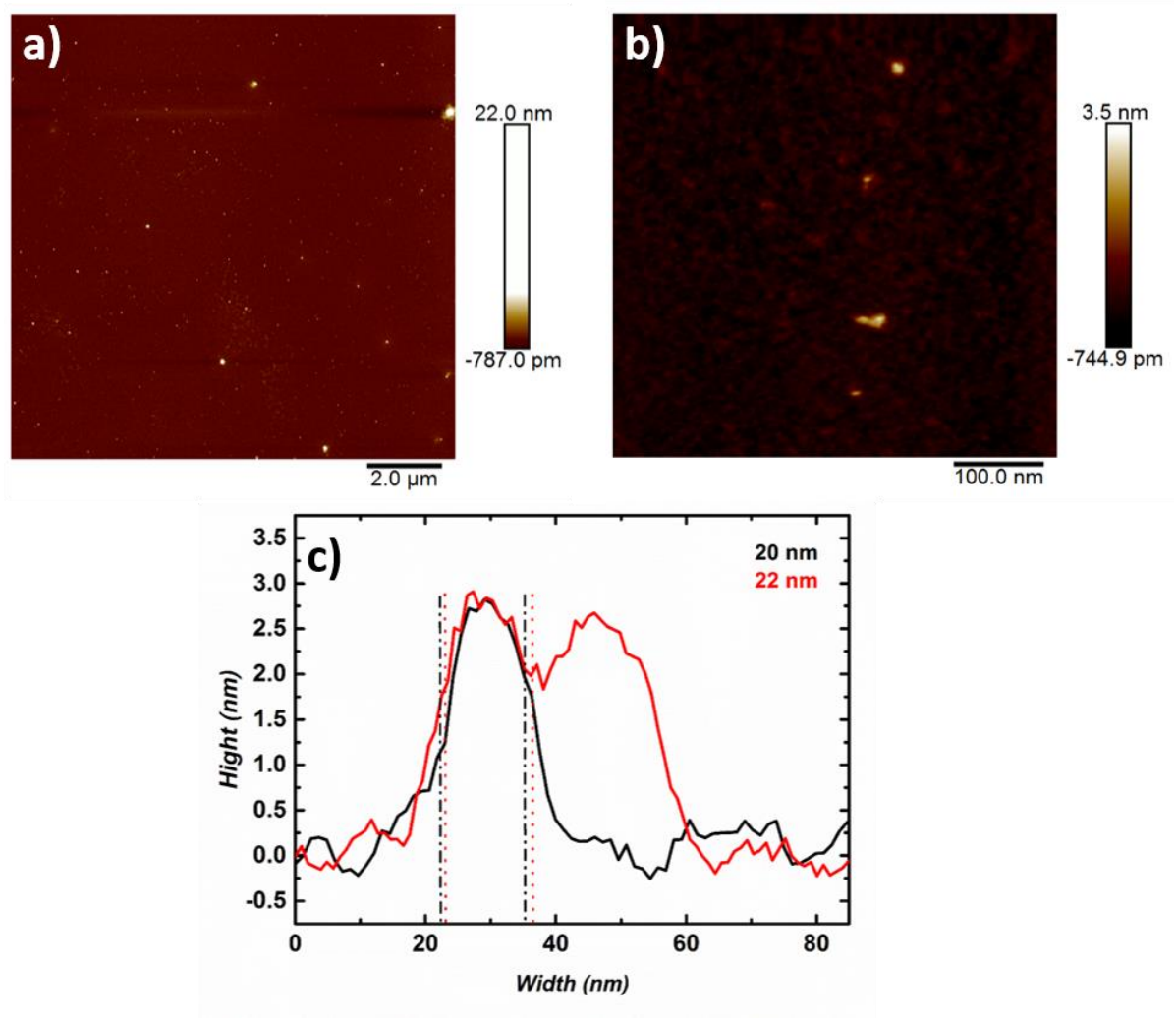

Figure 4.6 a), b) AFM images of 1mM solution of **EB TANI-(PTAB)$_2$** drop-cast onto mica surface, c) height profile of **EB TANI-(PTAB)$_2$** corresponding to the spherical structures shown in (b).

Furthermore, we explored the self-assembled structures of EB TANI-(PTAB)$_2$ at different concentrations in order the identify the effect of concentration on the self-assembling behaviour. As shown in **Figure 4.7**, TEM showed that the **EB TANI-(PTAB)$_2$** self-assembled into collapsed spheres structures at (2, 4, 8, 16 mM) with the same average diameter as 1 mM (~ 20 nm). AFM also showed spheres structure of 2 mM **EB TANI-(PTAB)$_2$** formed on carbon-coated TEM grid with the same dimeter and height as seen for 1mM (**Figure 4.8**).

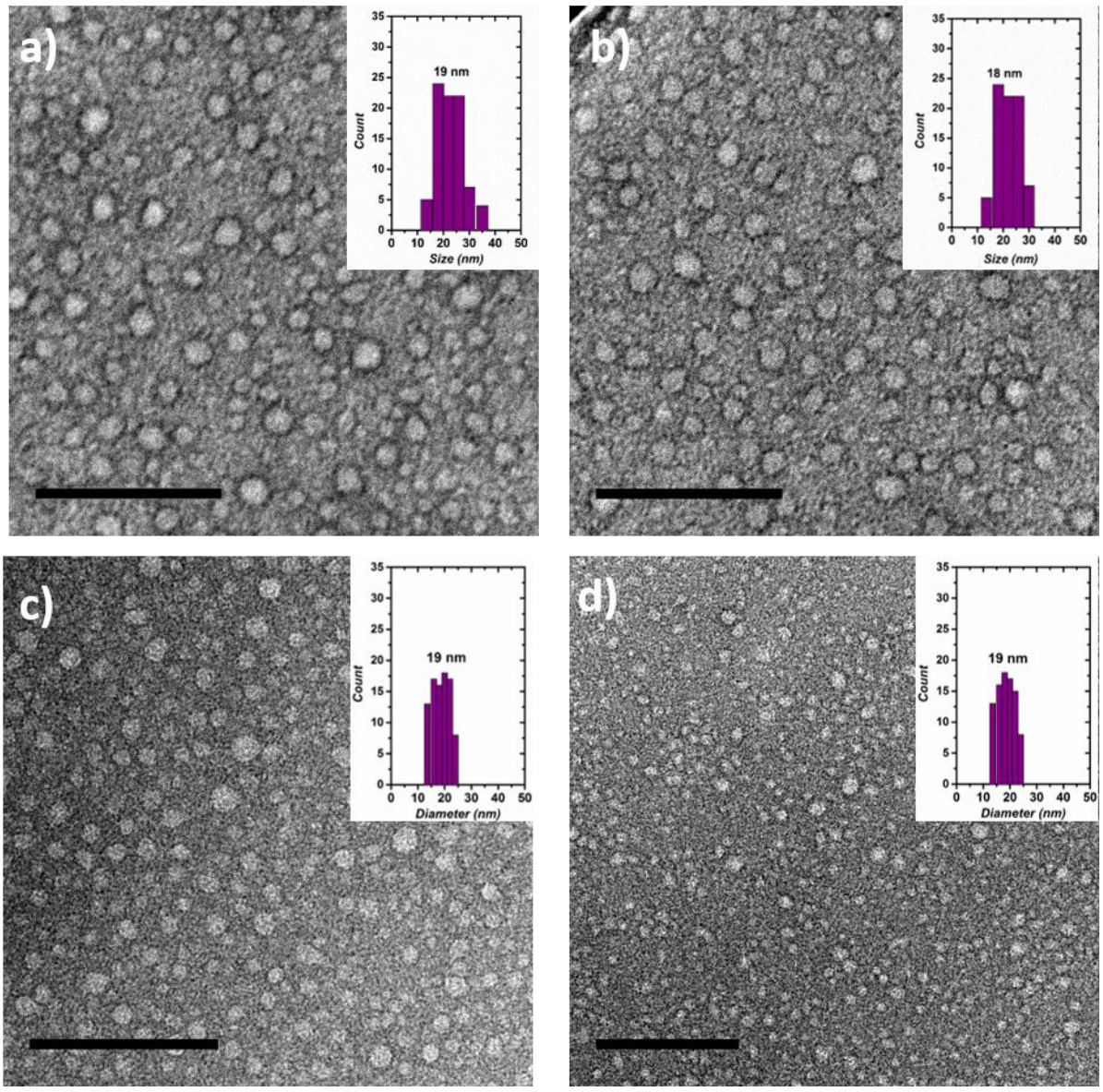

Figure 4.7 TEM images of **EB TANI-(PTAB)$_2$** in solution at different concentrations a) 2 mM, b) 4 mM, c) 8 mM, d) 16 mM, (scale bar=200 nm).

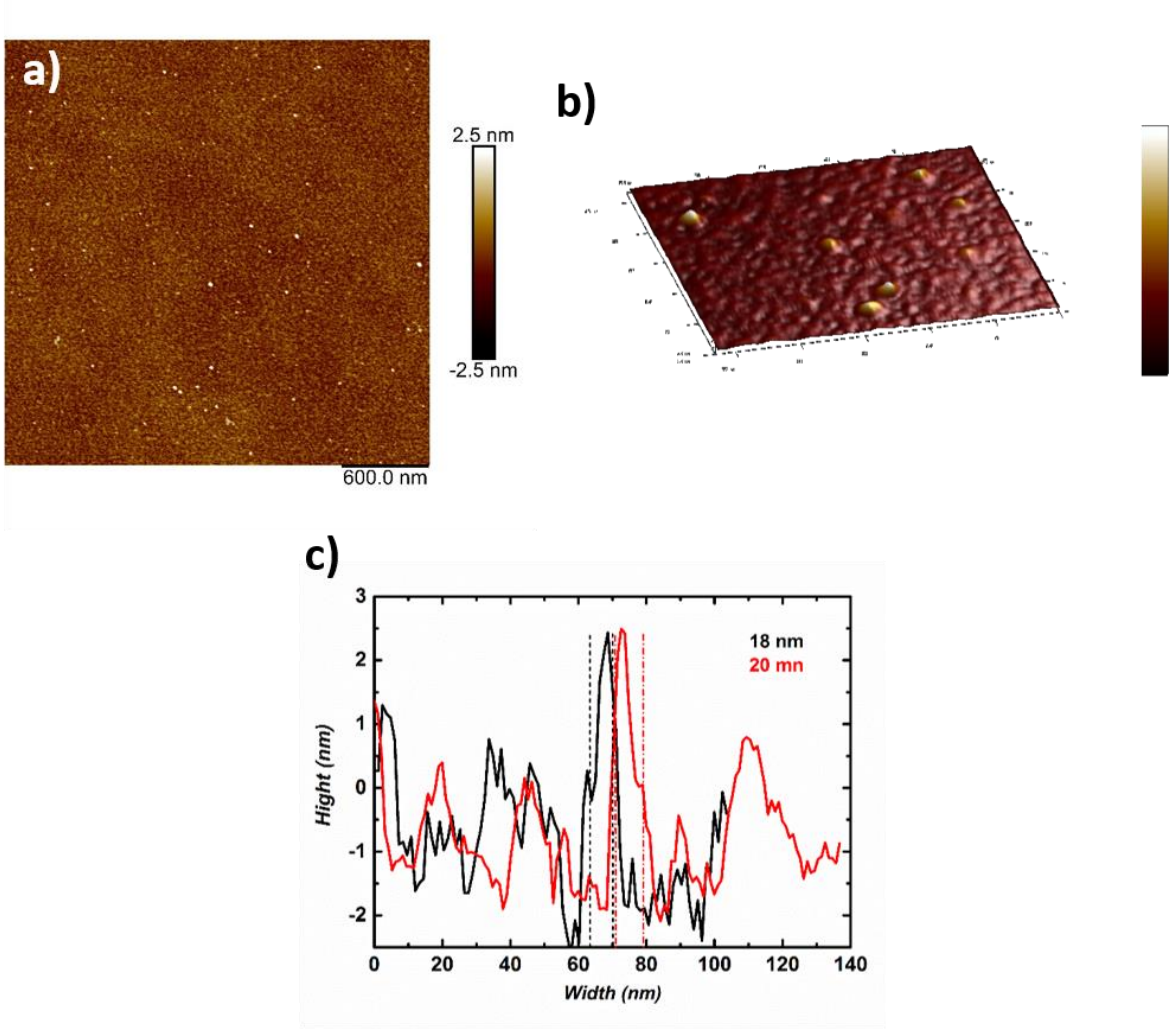

Figure 4.8 a) AFM images of 2 mM solution of **EB TANI-(PTAB)$_2$** drop-cast onto a carbon-coated grid, b) 3D image of the selected area with Z-ratio increased by a factor of 3 for clarity and, c) their cross-sectional height profile.

We also used small-angle X-ray and neutron scattering (SAXS and SANS, respectively) to identify the structure and size of the self-assembled aggregates. Initial investigations at lower concentrations yielded poor scattering. Increasing the range of concentrations investigated, we focused our efforts on the 16 mM **TANI-(PTAB)$_2$** sample. The intensity *vs* scattering vector (q) data show the expected q = -2 dependence, which is supportive of vesicle or disk-like structures (see **Figure 4.9**). The SAXS and SANS data are similar with a greater contrast being seen in the 16mM SANS as expected. However, due to the polydispersity of the sample no physically

meaningful fitting of the data was possible. The structure reported here is not clear but is more likely to be a vesicle structure as bolaamphiphiles tend primarily to form vesicles.[28] It also reported that bolaamphiphiles formed so-called monolayer membrane (MLM) vesicles, and showed promising properties in terms of drug and gene delivery[11] and biosensing devices.[29,30]

Furthermore, dynamic and static light scattering were also employed in an attempt to measure the size of the aggregates in solution, but these techniques failed due to the strong absorbance of the **EB TANI-(PTAB)$_2$** species in solution.

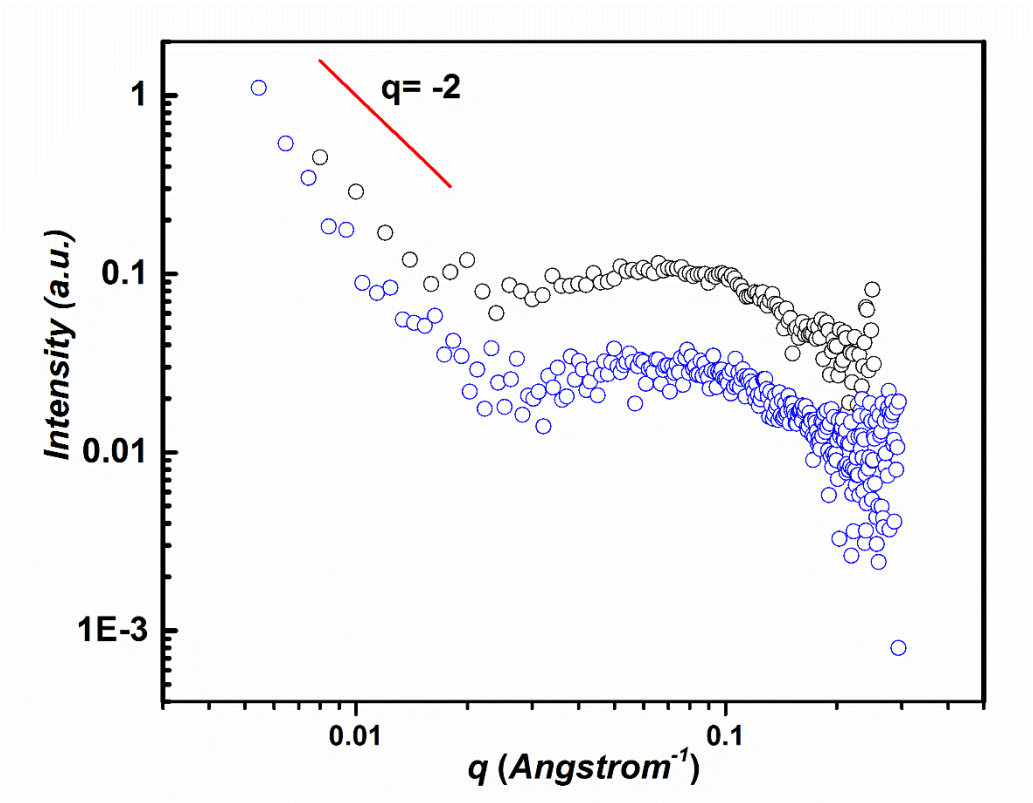

Figure 4.9 Small angle x-ray scattering data (blue circles) and small angle neutron scattering data (black circles) collected for 16mM **EB TANI-(PTAB)$_2$**. A simulated line (red) indicated the q=-2 dependence.

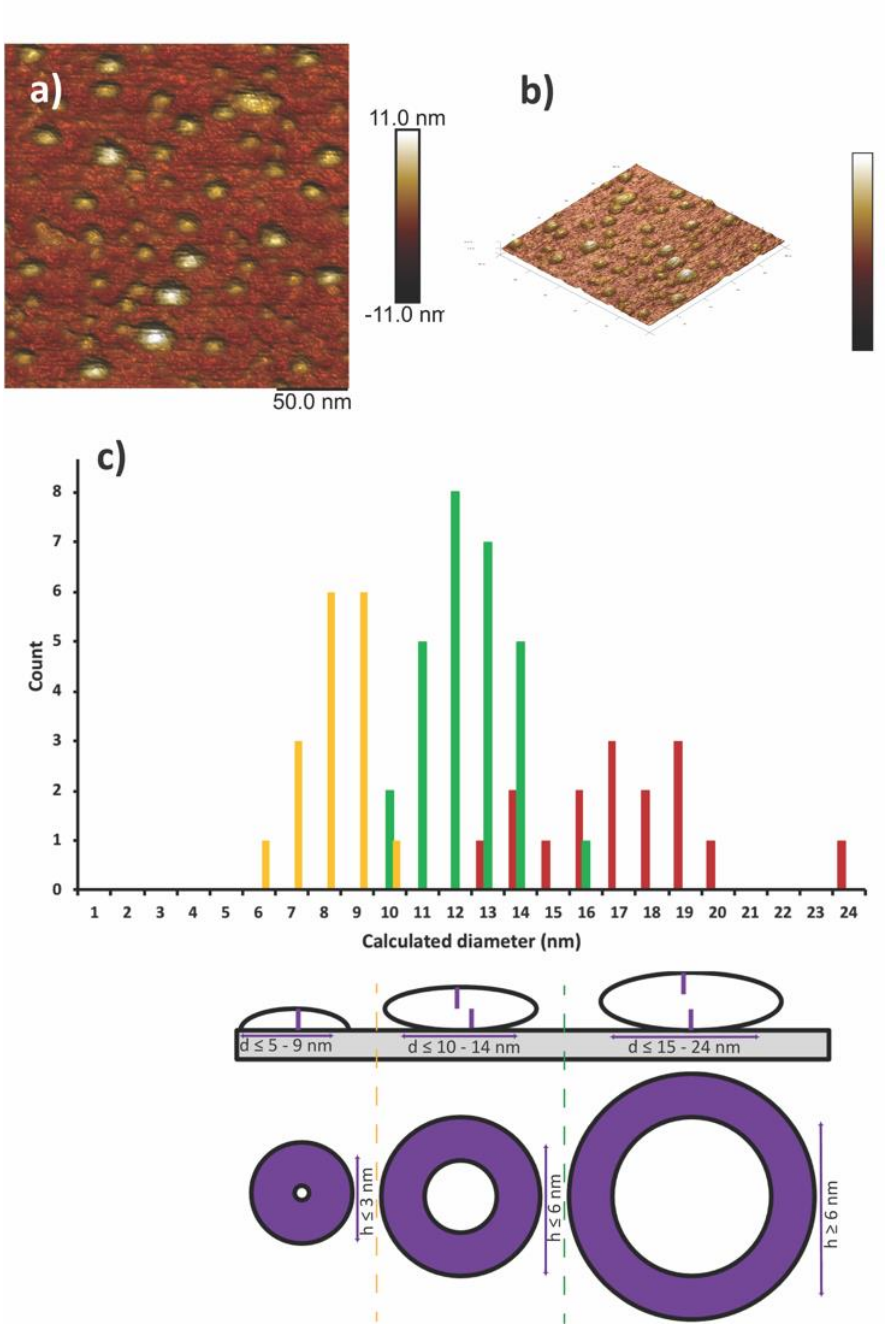

Figure 4.10 a) AFM image of 0.05 mM solution of **EB TANI-(PTAB)$_2$** drop-cast onto silicon wafer, b) 3D AFM image of image (a), c) histogram showed different populations of spheres of the region used in image a), inset: the proposed molecular packing corresponding to each populations.

By far the strongest argument that can be used to provide support for the formation of vesicle-like structures for **EB TANI-$(PTAB)_2$** species in solution is based on in-situ liquid AFM measurements. AFM studies were undertaken by drop casting a 0.5 mM solution of **EB TANI-$(PTAB)_2$** onto a silicon wafer: it is noteworthy that the aggregated structures were more stable on this hydrophobic surface compared with the collapsed structures observed on other surfaces such as mica and HOPG (see **Appendix D Figure D3 a and b**, respectively). Detailed high-resolution AFM imaging was used to count over 400 particles (**Figure 4.10**); these investigations showed the presence of a range of polydisperse spherical structures with different diameters. Careful analysis showed that these structures could be classified into three populations as labelled in **Figure 4.10**.

The first set (yellow) is indicative of circular features with an average height of 3 nm and below. This value, which is slightly lower than the fully extended length of **TANI-$(PTAB)_2$**, 3.96 nm, implies that the spheres found in this population tend to form a collapsed, largely disordered compact structure, with a maximum height of one molecular length only. The resultant calculated diameters are within the 6 - 10 nm range, which indicates the formation of compact spherical structures as shown **Figure 4.10c,** diameters being in the range of two molecules end to end with a very small central separation.

The second population (green) showed structures on the surface with a height between 3 to 6 nm, corresponding to the length of between one and two **TANI-$(PTAB)_2$** molecules (i.e., a collapsed bi-layered structure with varying degrees of intercalation). Keeping these dimensions in mind for the collapsed structure, it would therefore suggest spherical vesicles with a single bolaamphiphilic layered wall, most probably with a water-filled centre. This is supported by the reconstructed diameters of these structures in solution which fall between 10 and 15 nm (**Figure 4.10c**, **Figure D4**, y-axis).

Finally, the most stable and well-defined structures were found in the third population (red). These domed structures showed an height 6 nm or above indicating no intercalation occurring as surface effects induce oblation of the vesicle structure upon sedimentation. This suggests a

greater integrity of structure at larger scales, with calculated diameters in solution being above 15nm (**Figure 4.20c**, **Figure D4**, y-axis).

Further evidence of relevance to consider for the proposed packing model of our electroactive **EB TANI-(PTAB)$_2$**, is the bathochromic shift detected in the characteristic peak at 597 nm by UV/Vis-NIR spectroscopy (after the formation of aggregated structures). Such behavior, indictive of J-aggregate formation, has been proposed previously for **PANI**.[31] Taking into account that J-aggregates imply a slipped-stack arrangement of the electroactive cores, it is plausible that collapsed double-layer structures of >6nm could easily form.

Finally, detailed inspection of selected spheres from the largest population at the highest resolution scan parameters (at better than 1nm/pixel) shows no discernible substructure to the smooth surface (**Figure 4.11a**). As part of this population we also observed domed structures, which over time, partially collapsed to yield structures with a height of 16 nm (**Figure 4.11c**), suggesting the presence of multilayer vesicles consisting of at least four molecular lengths of EB **TANI-(PTAB)$_2$**, as clearly shown in the line profile of the spheres in **Figure 4.11d**. The collapsed structures observed for **EB TANI-(PTAB)$_2$** might well be owing to the enhanced favorable interactions between the hydrophobic spacers and cores with the Si surface, leading to the slow collapse (and potential expulsion of any content in the core of the structure). However, a full picture of how the self-assembled structures of the EB **TANI-(PTAB)$_2$** behave and form a range of different collapsed and domed spheres is still unclear.

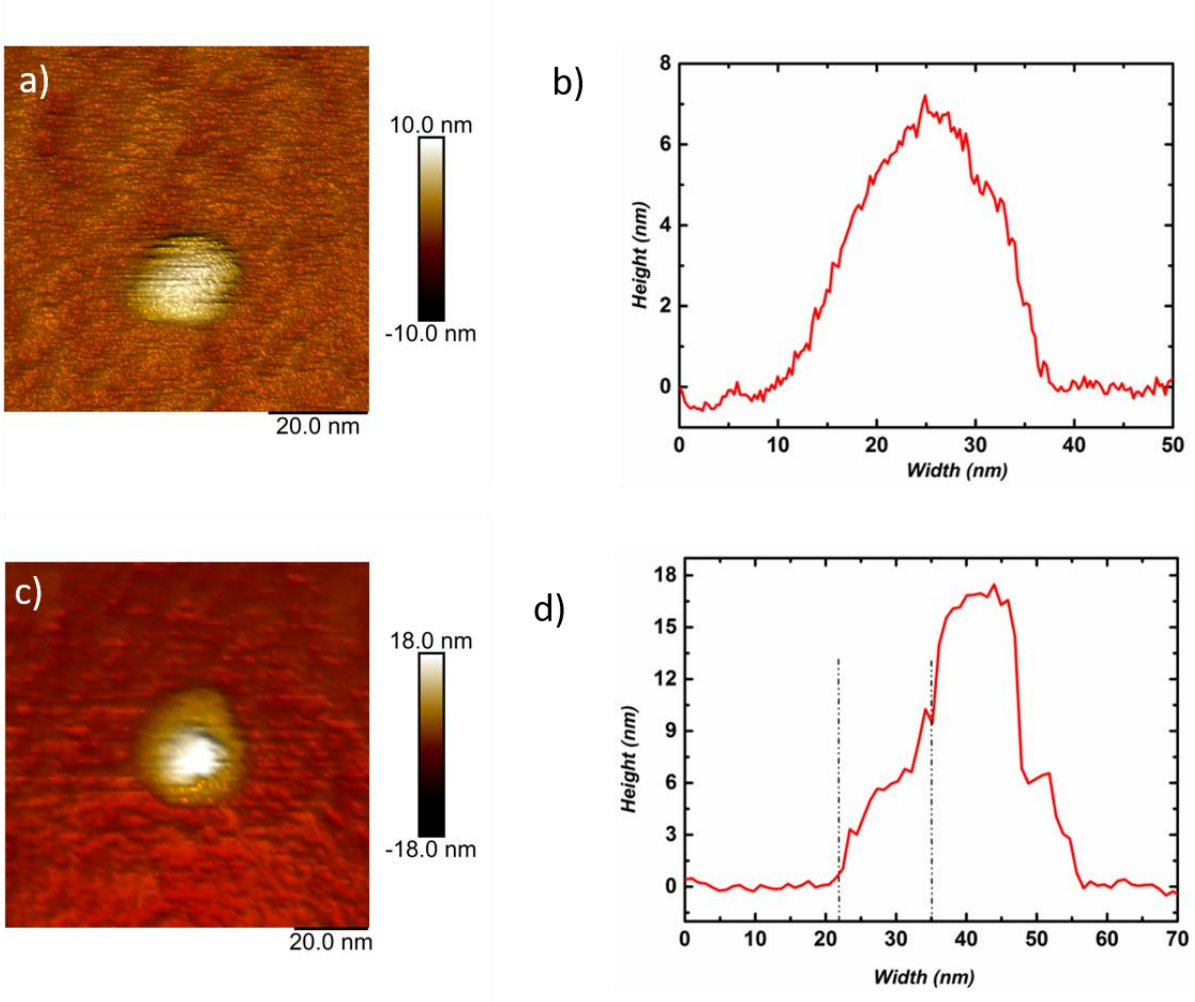

Figure 4.11 a and c) High-resolution AFM images of the spheres representing the third population, b) line profile of the corresponding sphere in image (a) and d) line profile of the corresponding sphere of image (c). The dashed lines show the region of collapse of the domed structure.

4.2.1.5 Temperature-dependent UV/Vis and thermodynamic parameters

To understand the aggregation behaviour and identify the mode of self-assembly of **EB TANI-(PTAB)$_2$**, temperature-dependent UV/Vis spectroscopy was carried out in aqueous solution (**Figure 4.12**). A 1 mM aqueous solution of **TANI-(PTAB)$_2$** was heated from 15 to 75°C and spectra taken at 5°C intervals during heating. The spectra showed that heating caused a gradual hypsochromic shift in the peak at 597 nm by 50 nm to 547 nm. This investigation indicated that the transition from aggregated structures to a molecularly dissolved state occurred in a similar fashion to that observed previously in the conventional **TANI** amphiphile.[14] Cooling a 1 mM aqueous solution of **TANI-(PTAB)$_2$** caused an exact 50 nm bathochromic shift of the absorbance peak (from 547 to 597 nm), confirming that the aggregated morphology of **EB TANI-(PTAB)$_2$** was recovered as the temperature decreased, indicating fully reversible assembly and disassembly with varying temperature.

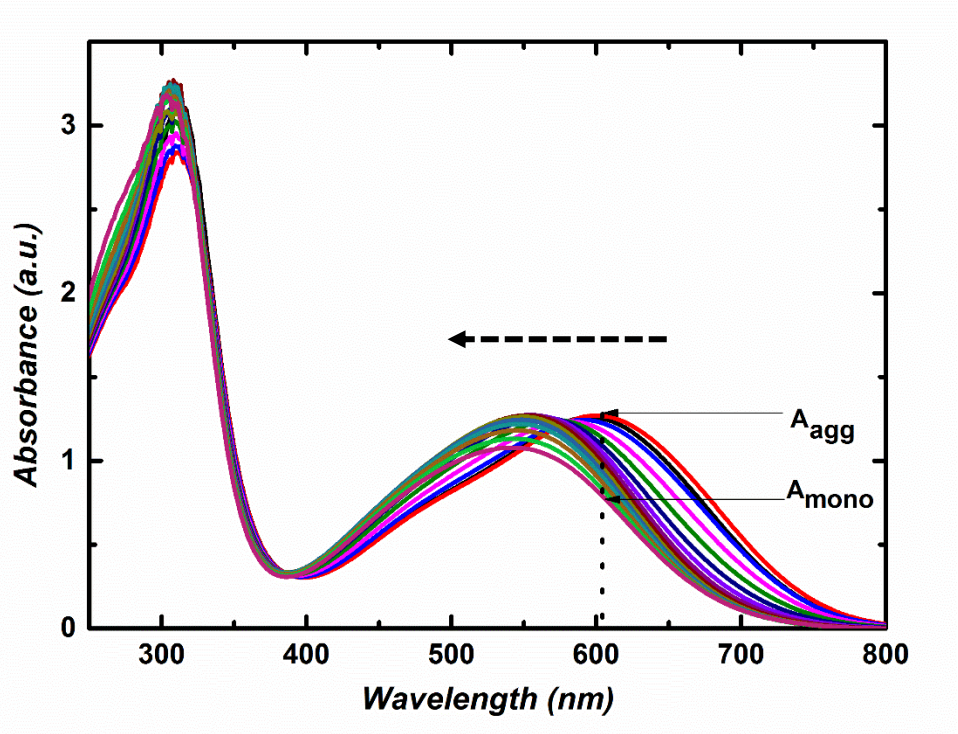

Figure 4.12 Effect of temperature on UV/Vis absorbance of 1mM of **EB TANI-(PTAB)$_2$**, the dashed arrow indicates change on heating solution (T = 15 to 75°C).

Changes in the mole fraction of aggregate, α(*T*), with temperature were calculated using Equation 1. The self-assembly behaviour of **TANI-(PTAB)$_2$** can be fitted well with an isodesmic (or equal-*K*) model.

$$\alpha(\mathrm{T}) = \frac{\mathrm{A(T)} - \mathrm{A_{mon}}}{\mathrm{A_{agg}} - \mathrm{A_{mon}}} \qquad \textbf{(1)}$$

The absorbance values of each temperature were recorded at λ_{max} = 597 nm; A_{mon} and A_{agg} are the absorbance values of the monomer and aggregated species, respectively.

$$\mathrm{DP_N(T)} = \frac{1}{\sqrt{1-\alpha(\mathrm{T})}} \qquad \textbf{(2)}$$

$$\mathrm{DP_N(T)} = \frac{1}{2} + \frac{1}{2}\sqrt{4\mathrm{K_e}\ (\mathrm{T})_{\mathrm{cT}+1}} \qquad \textbf{(3)}$$

The average degree of polymerization (DP_n) was calculated using Equation 2, followed by Equation 3 to calculate equilibrium constant (K_e) for the aggregation process.

$$\Delta G = \Delta H - T\Delta S \qquad \textbf{(4)}$$

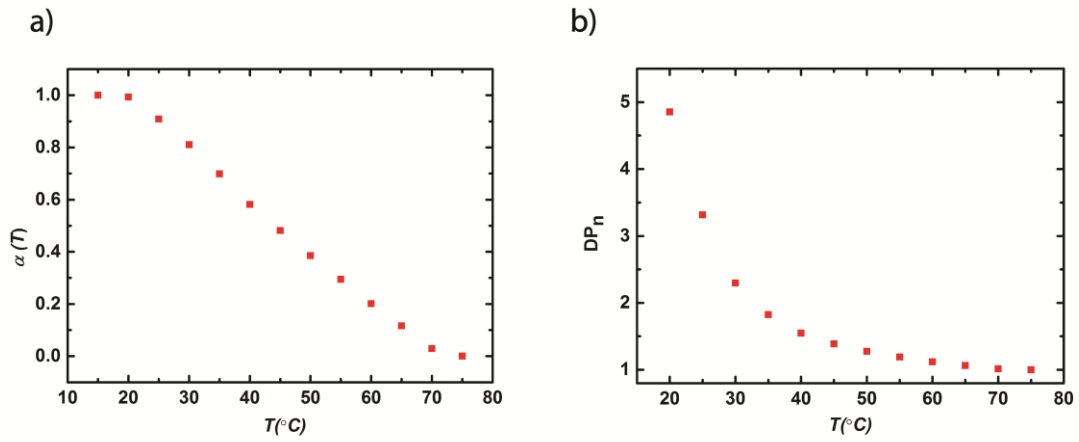

Figure 4.13 a) Change in the mole fraction of aggregation and b) number-averaged aggregation length with change of temperature for **TANI-(PTAB)$_2$**, all data were taken at λ=597 nm.

The changes in thermodynamic parameters (entropy (ΔS), enthalpy (ΔH) and free energy ΔG, Equation 4) during the aggregated stage were calculated from a van't Hoff plot (ln*K* vs T^{-1}) see the **Appendix D** for further details. These values, and the melting temperature, T_m, of the aggregates (the temperature, *T*, at which $\alpha(T)= 0.5$, as calculated from Equation 1) are shown in **Table 4.1**. The values of ΔG, ΔS, and ΔH of the bolaamphiphile are negative, which confirm spontaneous formation of the observed aggregated structures and follow a similar trend as observed previously for the single-tailed **TANI-PTAB**. In this regard, the energetically favorable assembly presumably results from strong stacking between **TANI** moieties upon self-assembly process.

Table 4.1 Thermodynamic parameters of **EB TANI-$(PTAB)_2$**

	EB TANI-$(PTAB)_2$
ΔH/ kJ mol^{-1}	-79
ΔS/ J mol^{-1} K^{-1}	-180
ΔG/ kJ mol^{-1}	-26
DP_n	5

4.2.1.6 Temperature-dependent ^{1}H NMR

The self-assembling and thermal reversible behavior of **EB TANI-(PTAB)$_2$** was also investigated by variable temperature NMR (**Figure 4.14**). **EB TANI-(PTAB)$_2$** in D_2O was heated from 25 to 75°C and spectra taken at 5°C intervals during heating. The spectra showed that heating caused a downfield shift in the chemical shift values of the **TANI** as well as the alkyl chain protons. This investigation indicated that the transition from aggregated structures to molecularly dissolved solution matches the temperature-dependent UV/Vis studies. At low temperature (25°C), the aggerated structures were formed as confirmed in TEM, whereas at higher temperature, the self-assembled structures were disturbed and broken. This suggests the noncovalent interactions that formed the self-assembled structures such as hydrogen bonds and van der Waals interactions were disturbed, resulting in an interruption to the steric environment. Cooling a solution of **TANI-(PTAB)$_2$** caused an upfield shift of the chemical shift, confirming that the aggregated morphology of **EB TANI-(PTAB)$_2$** was recovered as the temperature decreased. This indicates a reversible assembly and disassembly with varying temperature, and has been previously observed in other amphiphile system (urea-linked glycolipids).[32]

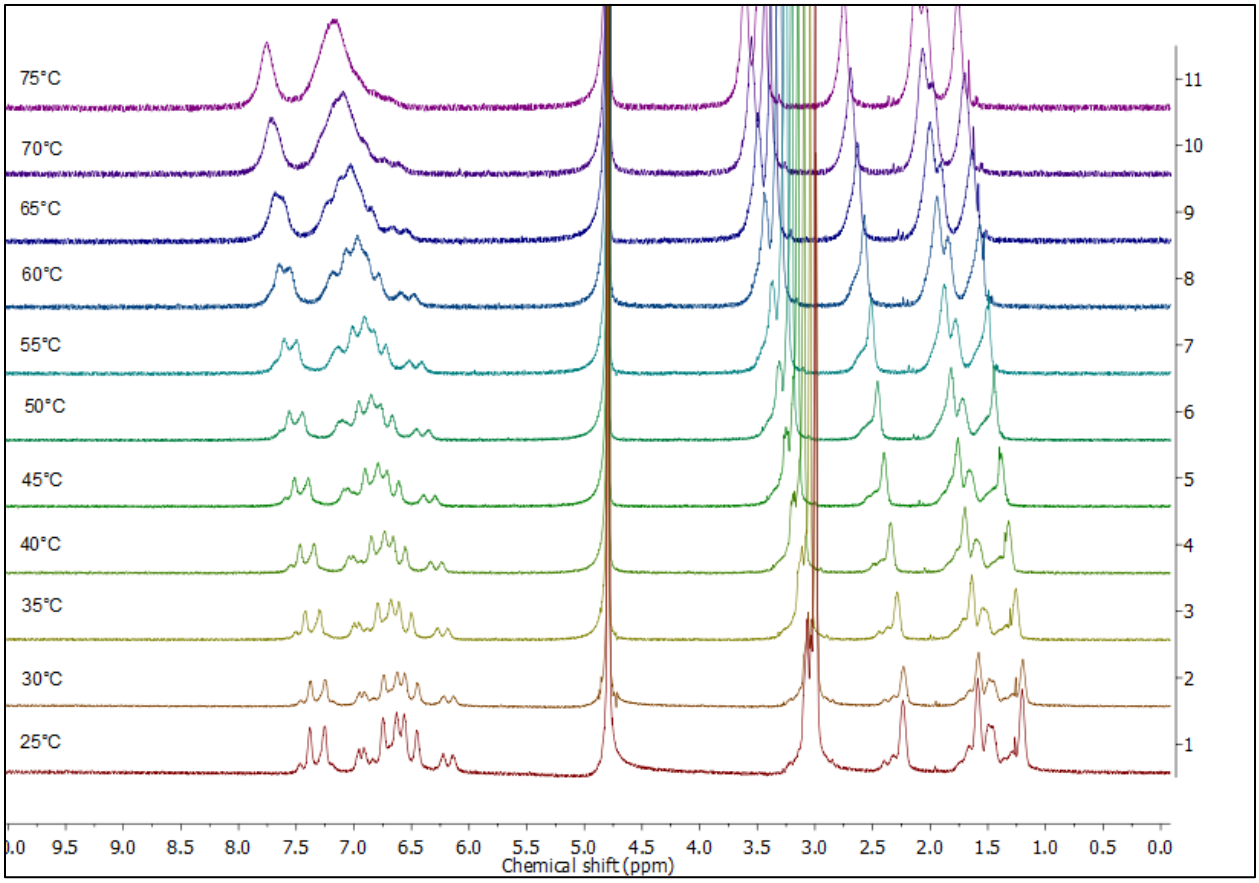

Figure 4.14 Temperature-dependant ^{1}H NMR spectra of **EB TANI(PTAB)$_2$.**

4.2.1.7 Doping of TANI(HX)$_2$-(PTAB)$_2$

A very attractive feature of electroactive **TANI**-amphiphiles is the potential to tune the formation of self-assembled structures by changing the packing parameter through doping, the so-called addressable packing parameter (APP) concept.[19] As mentioned earlier, the packing parameter relies on the length and volume of hydrophobic components and the area of the head group of conventional amphiphiles. In this study we thus used the APP concept to tune the morphology. Doping **EB TANI-(PTAB)$_2$** with different types of acids to form the ES state lead to large changes in the volume of the hydrophobic **TANI**-based "core" structure. A range of suitable organic and inorganic dopants were therefore selected (hydrobromic acid, **HBr**, trifluoracetic acid, **TFA**, p-toluene sulfonic acid, **TsH**, racemic camphorsulfonic acid, ***rac*-CSA**, and 1,5- naphthalendisulfonic

acid, **NDS**) to dope **EB TANI-(PTAB)$_2$** (**Table 4.2**). **HBr** was chosen in this study as an inorganic dopant because it has the same counterion (Br^-) as the trimethylammonium head group of **TANI-(PTAB)$_2$**. However, **TFA**, an organic dopant, was selected because of the interesting morphological changes found when used in conjunction with **TANI-PTAB** in our earlier studies (**Chapter 3**). The interesting 2D sheet-like structures[2] found when using **TsH** in combination with bolaamphiphile systems inspired us to explore their effect on our bolaamphiphiles. The fibrous morphology observed for **TANI(CSA)$_2$-PTAB** inspired us to use it as a dopant and explore the effect of the hydrogen-bonding capability of **CSA** (i.e., the carbonyl oxygen of **CSA** acting as a hydrogen-bonding acceptor). Furthermore, we chose ***rac*-CSA** to exclude any effects of molecular chirality on structure formation. In addition to these aspects, the use of a diacid has not been exploited to date to dope **TANI**-amphiphiles; hence, **NDS** was chosen. In addition, **NDS** also has the largest volume (230.54 $Å^3$) of all the selected dopants.

The color change from blue to intense green was indicative of the formation of the ES state and confirmed that the **TANI** amphiphiles were doped. This change is attributed to the well-known formation of a polaron species containing cation radicals, which was further supported by UV-Vis/NIR absorption spectroscopy. The doping ratio of 2 moles of acid: 1 mole of **TANI-(PTAB)$_2$** allowed protonation iminic nitrogen atoms of the electroactive **TANI** core. The three characteristic absorbance bands around 300, 400 and 800-1000 nm are attributed to the presence of the **ES** state (π-π, polaron-π* and π-polaron transitions, respectively). However, the absence of any defined features at 600 nm (associated with the **EB** state) confirmed that the doping process was successfully completed as shown in **Figure 4.15**.

Table 4.2 Chemical structures of various acids with their pKa values. Volumes were calculated using QSAR calculations based on DFT models.

Name with abbreviation	Structure	pK_a	Volume
Hydrobromic acid (**HBr**)		-9	30.59 Å^3
Trifluoracetic acid (**TFA**)		0.23	75.44 Å^3
p-toluene sulfonic acid (**TsH**)	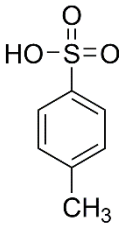	-2.8	157,82 Å^3
rac-campsulfonic acid (***rac*-CSA**)	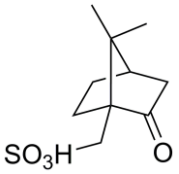	1.2	217.05 Å^3
1,5-Naphthalendisulfonic acid (**NDS**)	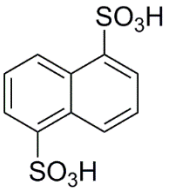	-1.8	230.54 Å^3

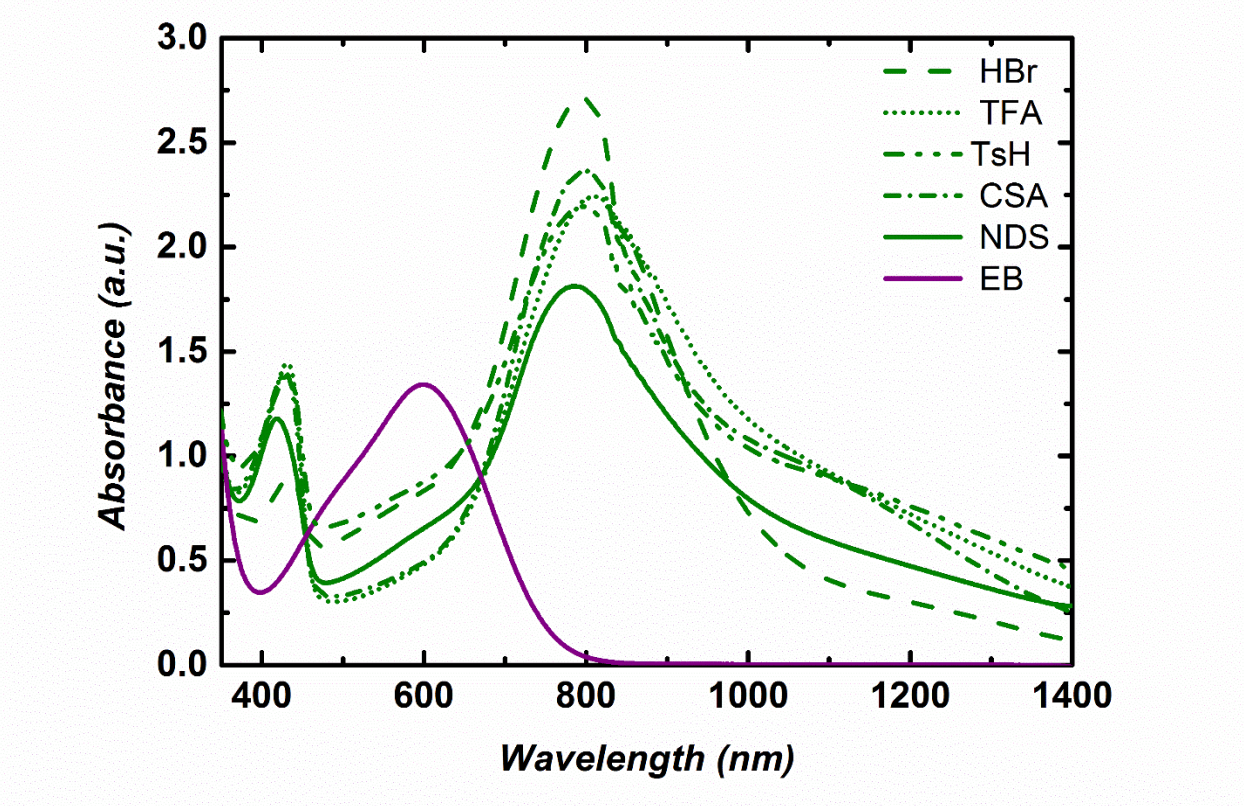

Figure 4.15 UV/Vis-NIR spectra showing **EB TANI-$(PTAB)_2$** and the resultant spectra after doping by various acids in aqueous solutions to form the ES state.

4.2.1.8 DFT-modelling: comparison studies of simulated UV/Vis-NIR of ES TANI$(HX)_2$-$(PTAB)_2$ and experimental spectra

Recent work in our group provided detailed theoretical understanding of UV/Vis-NIR spectra and spin properties of **TANI**.[33] Similar TD-DFT calculations were carried out on **ES TANI-$(PTAB)_2$** using the CAM-B3LYP functional, and showed the presence of both triplet and singlet spin states, with absorption maxima at λ_{max} ~ 897 nm and 1050 nm, respectively. When these systems were investigated experimentally (by UV/Vis-NIR spectroscopy), we found that the electronic structures of **TANI$(CSA)_2$-$(PTAB)_2$** transitioned from the triplet (λ_{max} ~ 797 nm) to the singlet state (λ_{max} ~ 1040 nm) as depicted in Figure **4.16a** and **4.16b**. Although the match with the triplet state was not close (87 nm), the absorbance maxima of the singlet state **TANI-^{1}ES** very closely matched that of the simulation for the **CSA**-doped system (4 nm, also observed for **TFA**-doped system as

depicted in **Figures 4.17b** and **4.17b)**. Time-dependent electron spin isomerism of doped **TANI-(PTAB)$_2$** was studied using electron spin resonance (ESR) spectroscopy. We obtained ESR spectra of 1mM of **TANI(CSA)$_2$-(PTAB)$_2$** over seven days, which showed a decrease of the ESR signal over time (**Figure 4.18**) until it disappeared completely within one week. These observations were also confirmed by UV/Vis-NIR spectroscopy, providing a route to switching spin states in our doped bolaamphiphile from the triplet (**TANI-^{3}ES**) to the singlet (**TANI-^{1}ES**) state.

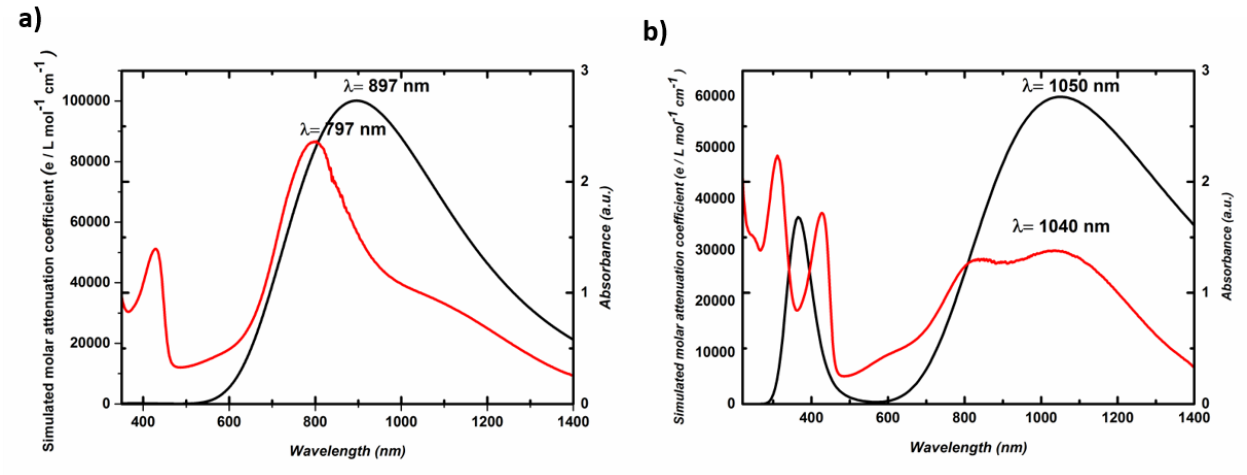

Figure 4.16 Comparison of simulated UV/Vis-NIR (black lines) and experimentally obtained spectra (red lines) of **ES TANI-(PTAB)$_2$**. a) Calculated high spin **(^{3}ES)** spectrum matched with the experimental spectrum obtained 24h after solution preparation; and b) calculated low spin **(^{1}ES)** matched with the experimental spectrum (red line) of **TANI(CSA)$_2$-(PTAB)$_2$** one week after solution preparation.

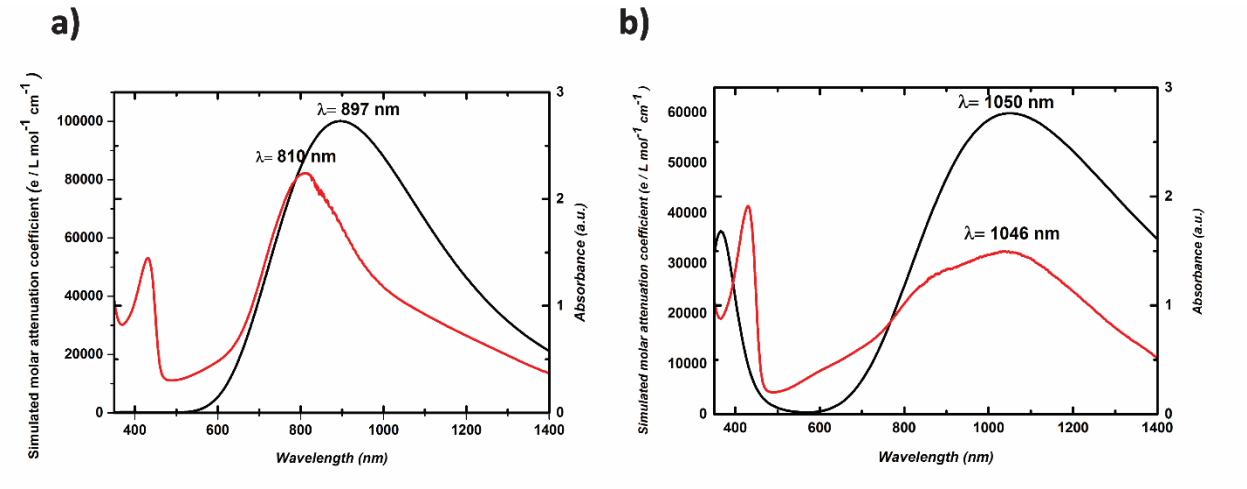

Figure 4.17 Comparison of simulated UV/Vis-NIR (black lines) and experimentally obtained spectra (red lines) of **ES TANI-(PTAB)$_2$**. a) Calculated high spin **(^{3}ES)** spectrum matched with the experimental spectrum obtained 24h after solution preparation; and b) calculated low spin **(^{1}ES)** matched with the experimental spectrum (red line) of **TANI(TFA)$_2$-(PTAB)$_2$** one week after solution preparation.

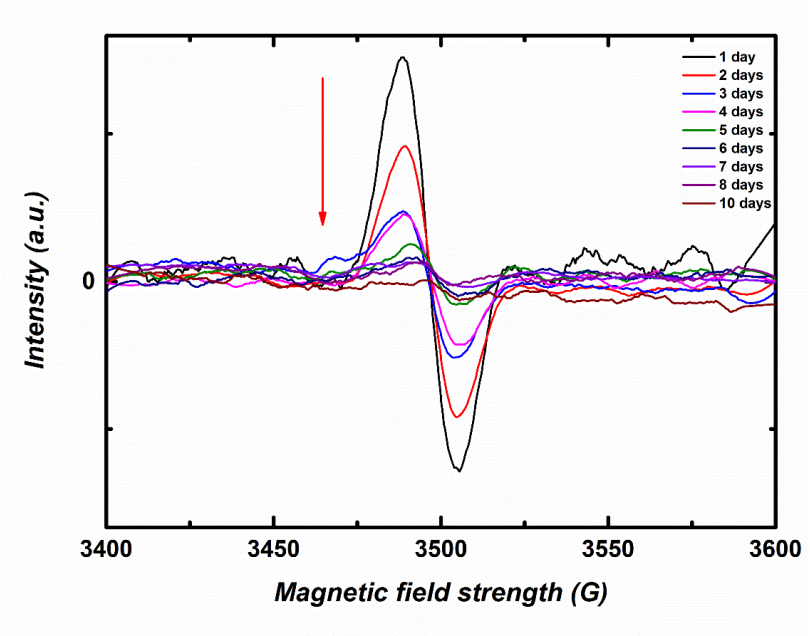

Figure 4.18 Experimental ESR spectra of solution of **TANI(CSA)$_2$-(PTAB)$_2$**. The row indicates the change on leaving the solution over time.

4.2.1.9 Self-assembly studies of ES TANI$(HX)_2$-$(PTAB)_2$

As we showed in our earlier studies, the addition of a dopant will lead to a change in the volume of the alkyl tail portion and thus the packing parameter. Although this parameter, and approach, is not directly applicable for the case of bolaamphiphiles, we did explore tuning the self-assembled morphology by varying the dopant acids (**HBr, TFA, TsH, CSA, NDS**) and their volumes. Starting with the smallest volume dopant, **HBr**, TEM showed the predominant morphology to be spherical structures with a 21 nm diameter, which was also confirmed by AFM (**Figure 4.19**). AFM images showed the presence of spherical structures with an average diameter of 22 nm, over 60 counted structures, in a good agreement with TEM. However, the height of the spheres varied between 1.5 to 6 nm height, implies that the spheres found on the surface tend to form a compact structure.

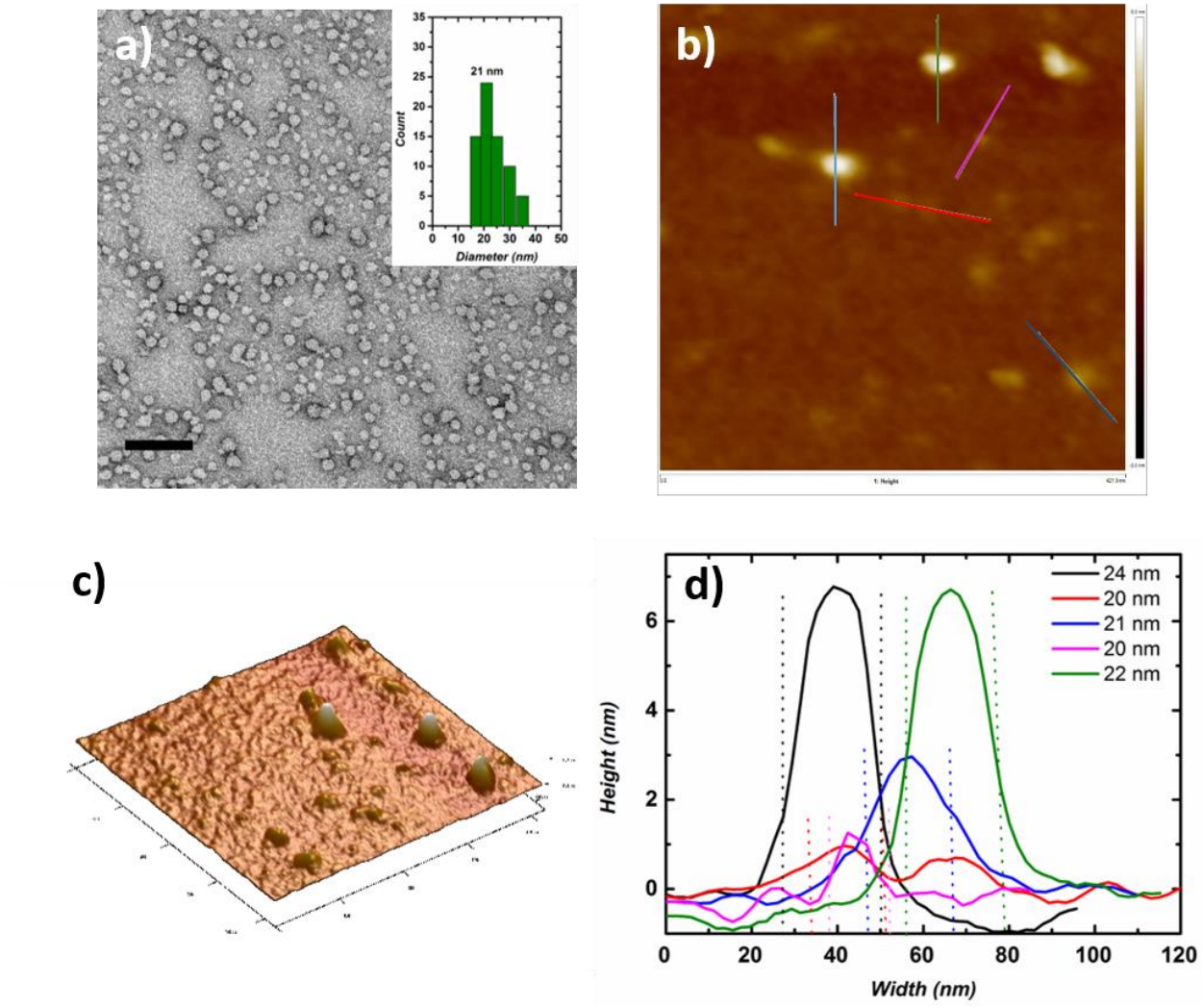

Figure 4.19 a) TEM image of **ES TANI(HBr)$_2$-(PTAB)$_2$**, histogram of particle size distribution by TEM for a 1 mM **TANI(HBr)$_2$-(PTAB)$_2$** solution, scale bar=200 nm. b) AFM image of the selected area of 1mM solution of **ES TANI(HBr)$_2$-(PTAB)$_2$** drop-cast onto coated- carbon grid, c) the corresponding 3D image with Z-ratio increased by a factor of 3 for clarity, and e) their cross-sectional height profile.

TFA, **TsH** and ***rac*-CSA** have different volumes (75.44 Å^3,157.82 Å^3, 217.05 Å^3, respectively), but they all produced well-defined spherical structures with average diameters of 28 nm, 29 nm, and 28nm, respectively, as depicted in **Figure 4.20**. The diameter is larger than for the structures observed for **EB TANI-(PTAB)$_2$**, which were 22 nm in diameter.

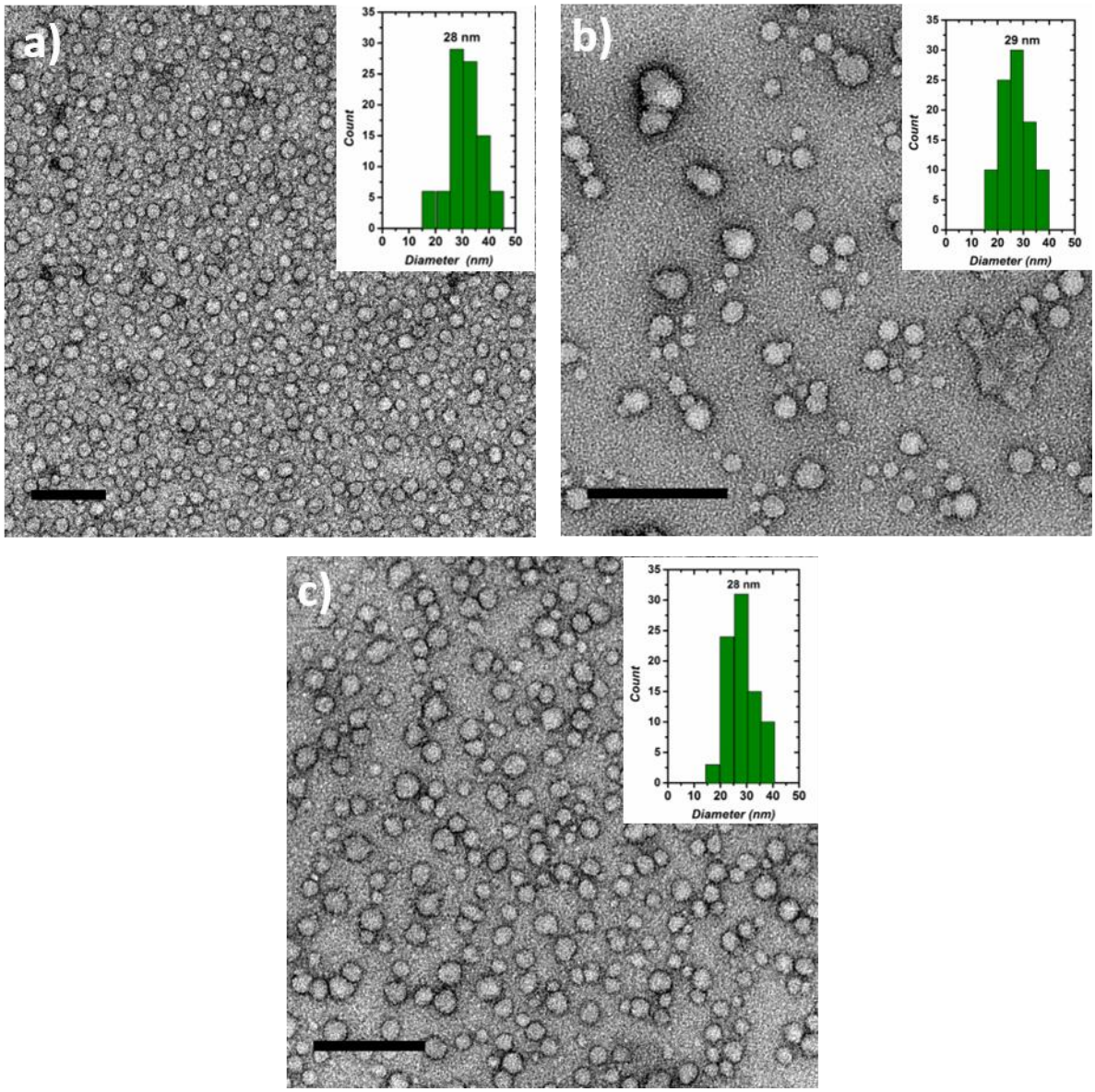

Figure 4.20 TEM image of **ES TANI(TFA)$_2$-(PTAB)$_2$**, **ES TANI(TsH)$_2$-(PTAB)$_2$, ES TANI(CSA)$_2$-(PTAB)$_2$** histogram of particle size distribution by TEM for a 1 mM of each solution, scale bar=200 nm.

The addition of **TFA** to **TANI-(PTAB)$_2$**, leads to the formation of vesicle-like structures with the average diameter 28 nm, as presented in **Figure 4.21** at the selected concentrations (1,2,4 mM). **TFA** increases the volume of **TANI-(PTAB)$_2$**, which in turn increases the packing parameter and causes the morphology changes. The AFM line profile shown for **TANI(TFA)$_2$-(PTAB)$_2$** indicates the collapsed spheres are approximately 6.30 nm high. The average diameter of spherical

structures was determined over 70 counted structures, and calculated to be 28 nm, which agrees well with the measurements from TEM. These dimensions are indicative of collapsed single-layered structure that will form a double layered structure on the surface as presented in **Figure 4.22**.

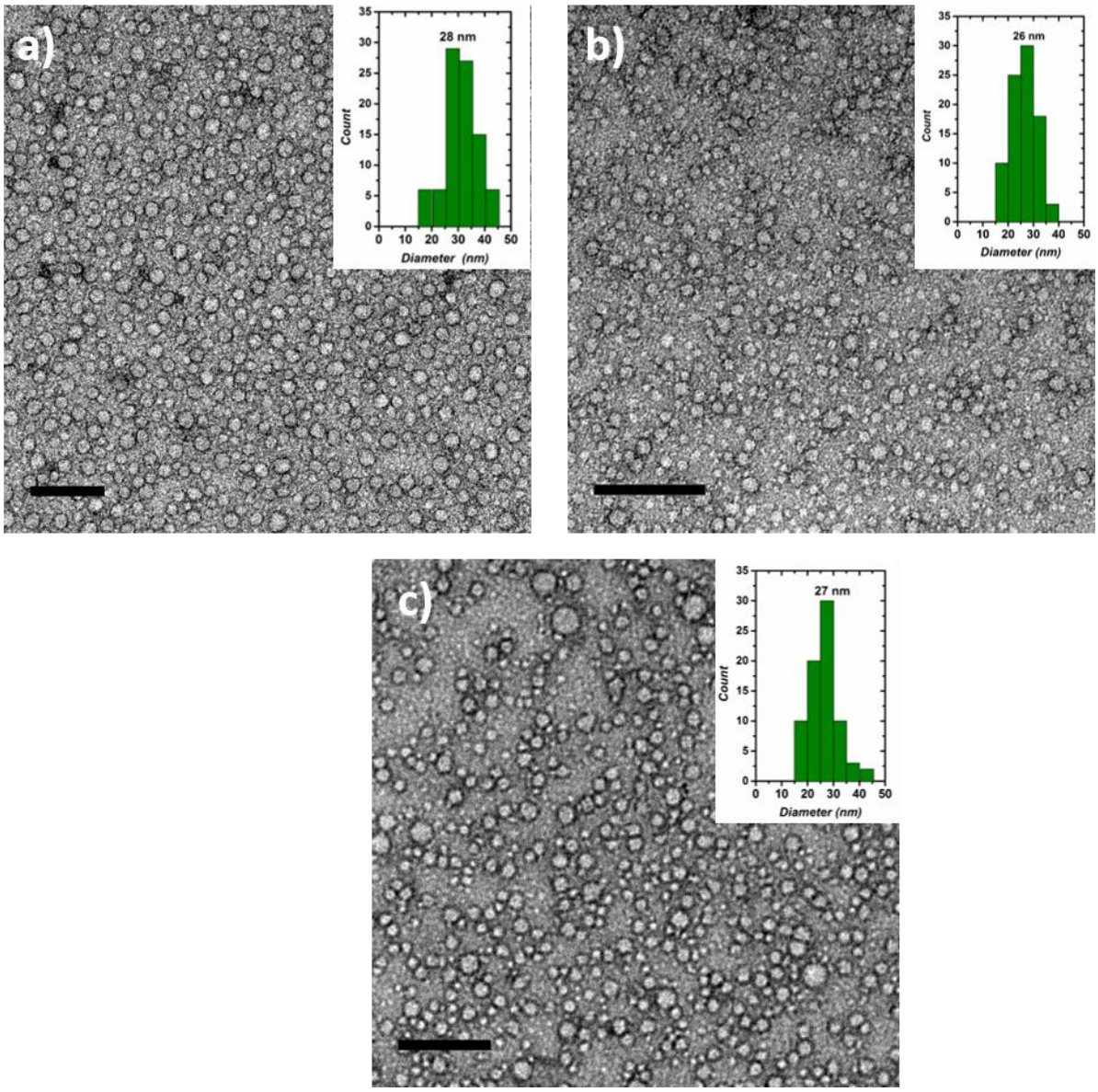

Figure 4.21 TEM images of **TANI(TFA)$_2$-(PTAB)$_2$** solutions at different concentrations (stained with 1% uranyl acetate) a) 1 mM, b) 2 mM, c) 4 mM, respectively. Scale bars: 200 nm.

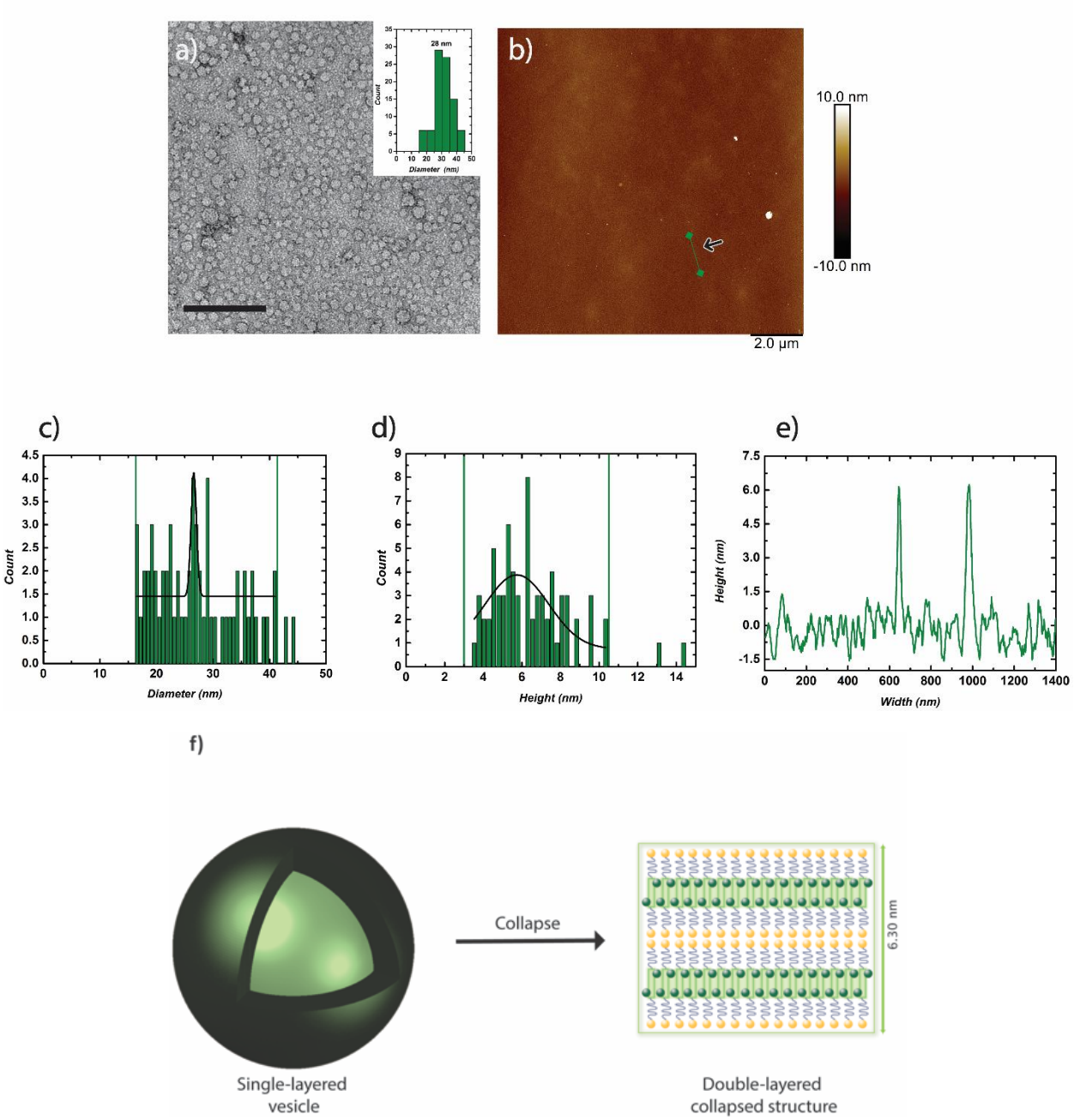

Figure 4.22 a) AFM image of **ES TANI(TFA)$_2$-(PTAB)$_2$** solution (concentration = 1 mM), b), c) the histogram of particle diameter and height distributions counted from 70 particles, respectively, e) height profile of **ES TANI(TFA)$_2$-(PTAB)$_2$** corresponding to the to the green lines shown in (b), f) the proposed molecular packing of **TANI(TFA)$_2$-(PTAB)$_2$**

Even **rac-CSA** has a larger volume than **TFA** and **TsH, TANI(CSA)$_2$-(PTAB)$_2$** is still self-produced spherical-like structures at all the selected concentrations (1,2,4 mM) as shown in **Figure 4.23**. The AFM line profile shown for **TANI(CSA)$_2$-(PTAB)$_2$** indicates the collapsed spheres are approximately 7±2 nm. The average diameter of the spherical structures were determined over 60 counted structures, and calculated to be 28±2 nm, which agrees well with the measurements from TEM. These dimensions are indicative of vesicular structures as presented in **Figure 4.24**.

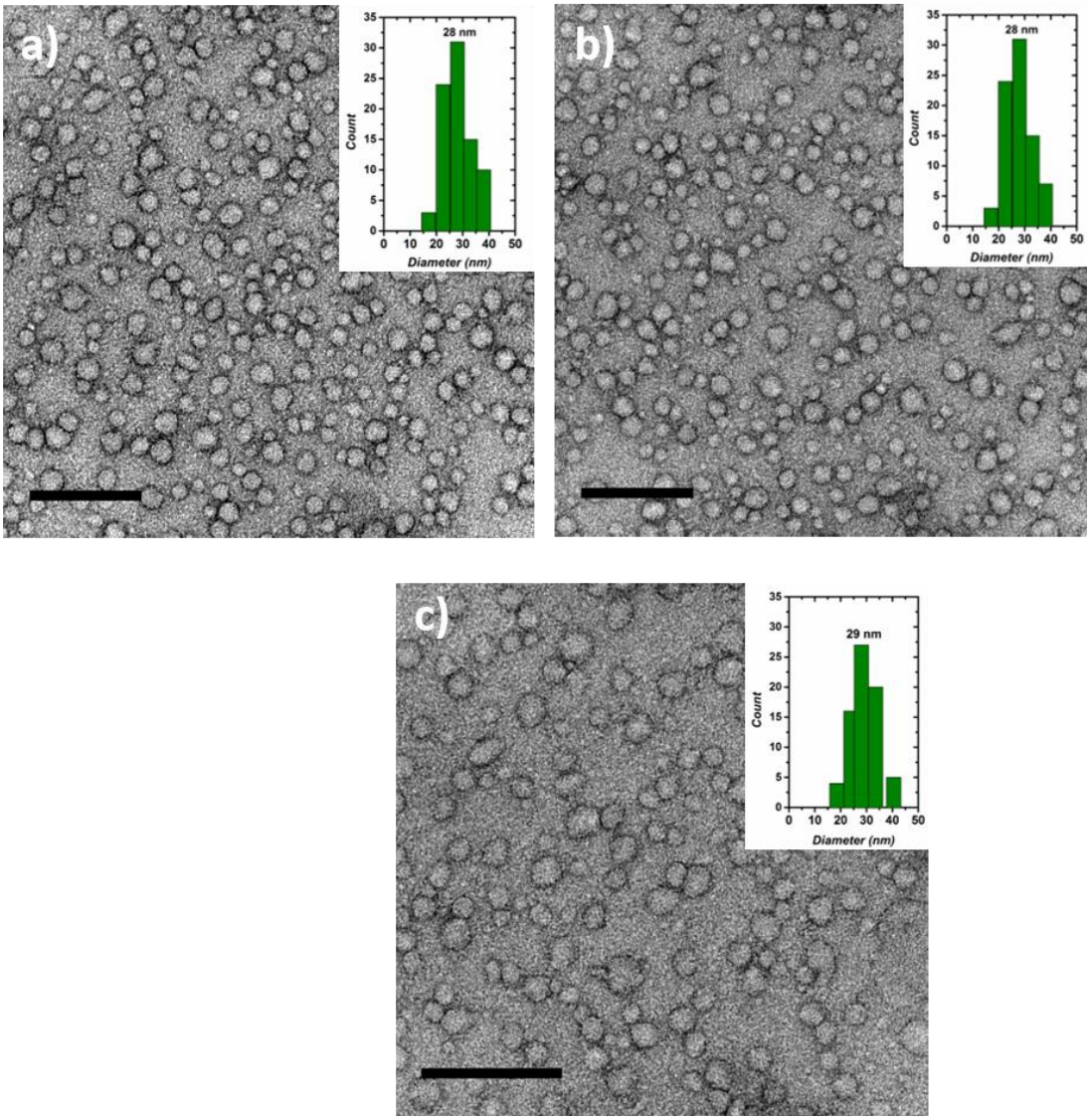

Figure 4.23 TEM images of **ES TANI(CSA)$_2$-(PTAB)$_2$** solutions at different concentrations (stained with 1% uranyl acetate) a) 1 mM, b) 2 mM, c) 4 mM, respectively. Scale bars: 200 nm.

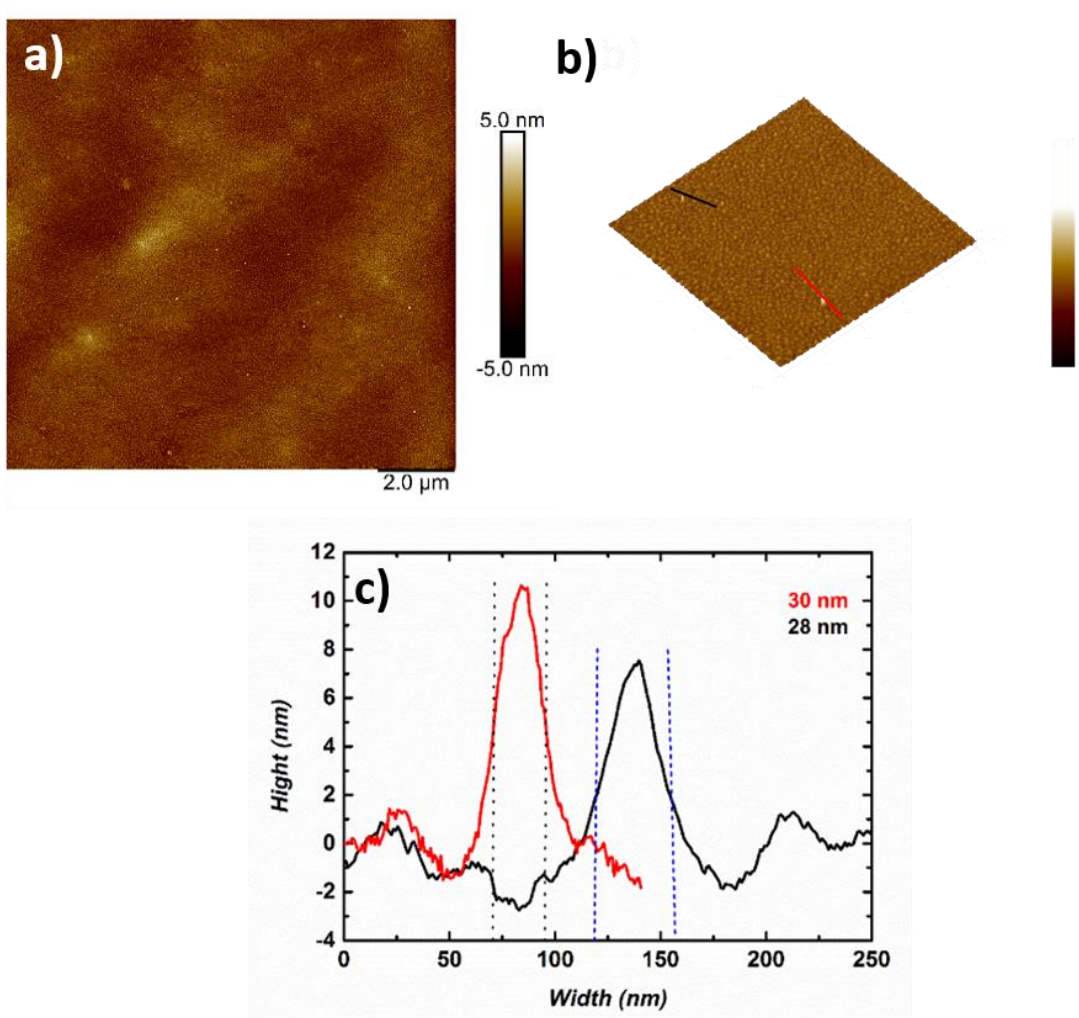

Figure 4.24 a), b) AFM images of 1 mM solution of **ES TANI(CSA)$_2$-(PTAB)$_2$** drop-cast onto carbon-coated grid, c) height profile of **ES TANI(CSA)$_2$-(PTAB)$_2$** corresponding to the red and black line shown in (b).

As mentioned earlier, rac-**CSA** was selected to exclude any effect associated with chirality as we are not interested in investigation the effect of chirality. It is worth mentioning that **CSA** has been explored widely for its ability to induce chirality to self-assembled fibres of **PANI** once doped with a specific **CSA** enantiomer.[34,35] However, there have been no reports regarding studying the effect of chirality on oligo(aniline)-based materials. We reported, for the first time, the effect of chirality of **CSA** on the fibrous structures formed in the case of **TANI-PTAB**.[14] However, **TANI-(PTAB)$_2$** does not show any fibrous morphology either in the EB state or when doped with **CSA**. We would not expect a vast change on the volume of **CSA** as an enantiomer. However, there

might be an effect on the self-assembled structures due to their interactions. Hence, we prepared 1 mM solutions of **TANI-(PTAB)$_2$** doped by either *R*-**CSA** or *S*-**CSA**. TEM images indicated that when **TANI-(PTAB)$_2$** doped by individual enantiomer either *R*-**CSA** or *S*-**CSA** exhibit the interesting self-assembled structures of elongated worm-like micelles as shown in **Figure 4.25**. Further characterisation such as circular dichroism (CD) spectroscopy are required to investigate whether the any chirality was expressed within the self-assembled structures.

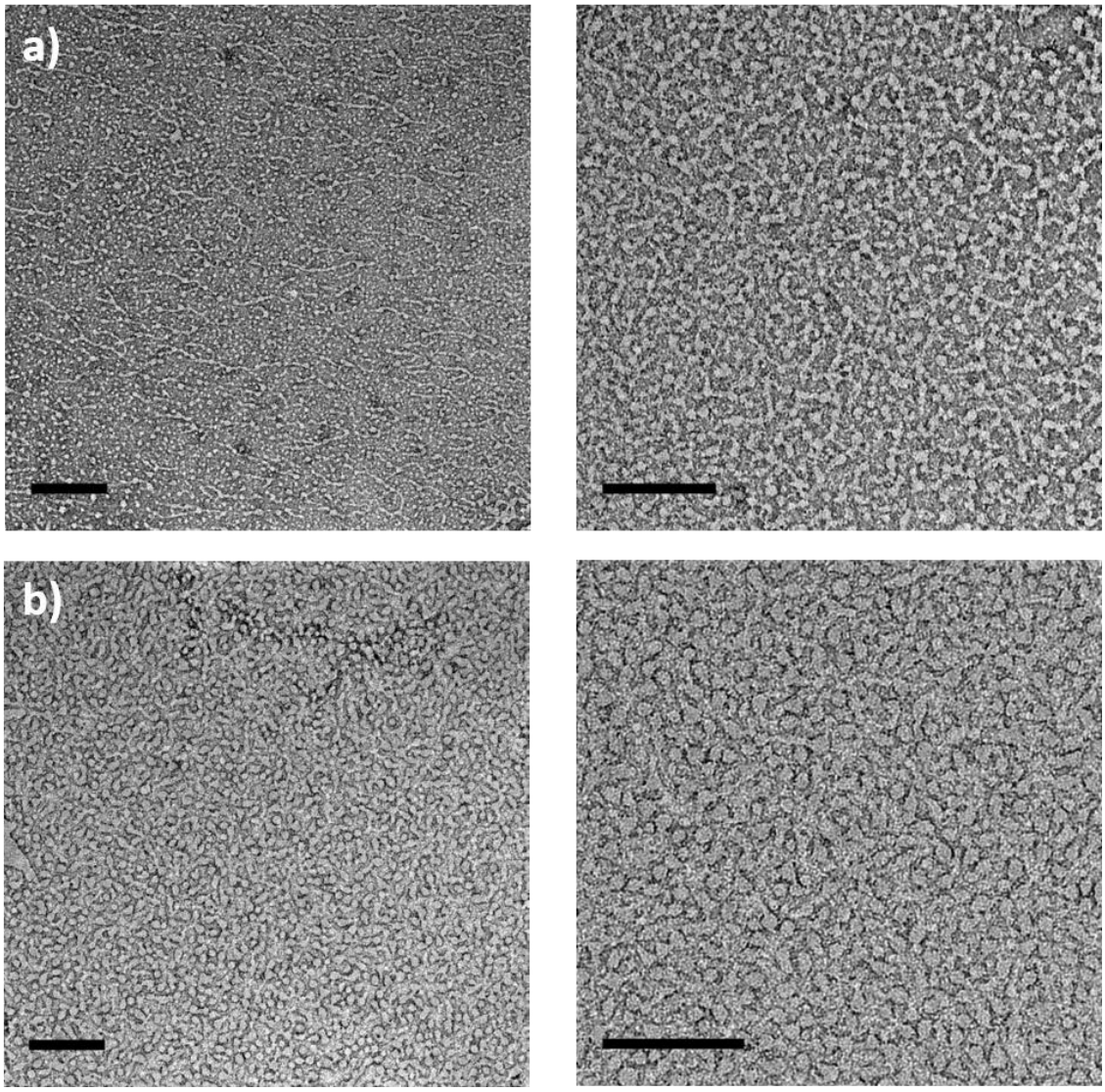

Figure 4.25 TEM images of 1mM solution of **ES TANI(CSA)$_2$-(PTAB)$_2$** solutions (stained with 1% uranyl acetate), a) R-CSA, b) S-CSA. Scale bars: 200 nm. The images on the right and left side represent the same images with different magnifications.

Very interestingly, the strong diacid dopant **NDS** caused the **TANI-$(PTAB)_2$** to form 4nm-wide nanofibers in the ES state as shown in **Figure 4.26** and **4.27**. **TANI(NDS)-$(PTAB)_2$** self-assembled nanofiber structures were present in solution at all the selected concentrations. TEM and high resolution TEM were utilized to probe aggregated structures formed by **TANI(NDS)-$(PTAB)_2$** from aqueous solution for the same range of concentrations to those used for **EB TANI-$(PTAB)_2$**. All samples were negatively stained with 1% aqueous uranyl acetate to increase contrast. At higher concentration 8, 16 mM the width of fibres are slightly larger (4, 5 nm) than the lower concentrations 1, 2 mM.

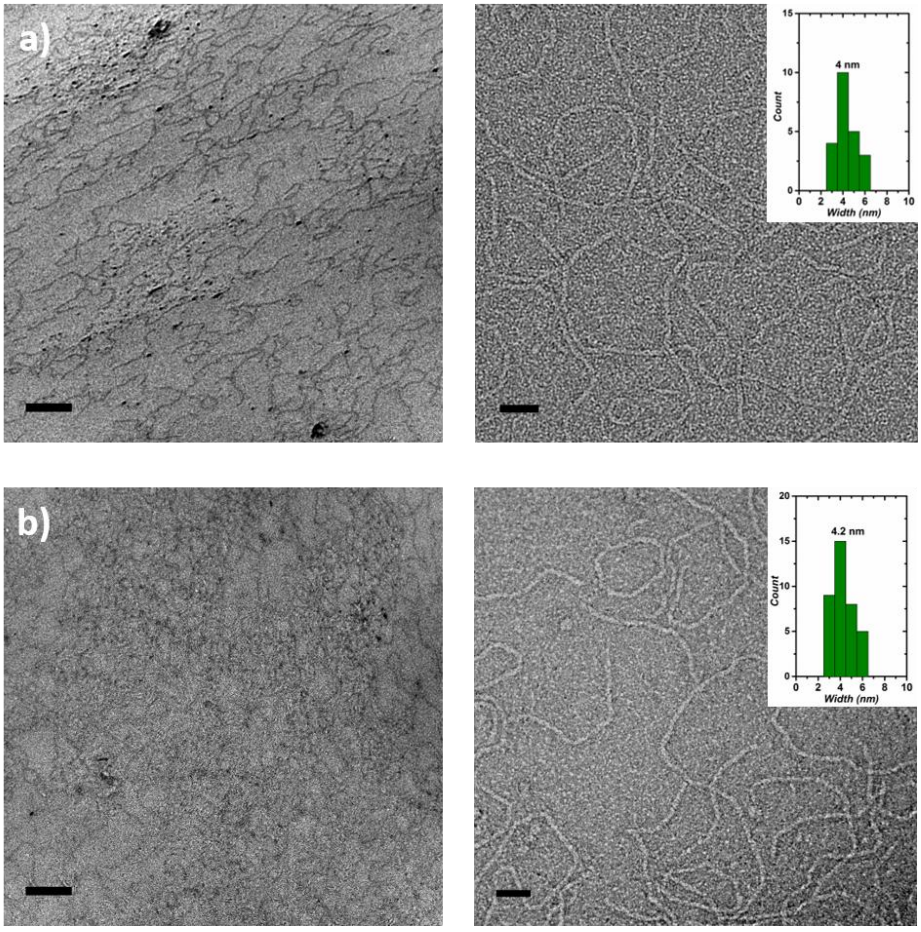

Figure 4.26 TEM and high-resolution TEM images of **ES TANI(NDS)-$(PTAB)_2$** in solution at different concentrations a) 1 mM, b) 2 mM. Scale bar=200 nm, HRTEM images on the right-hand side.

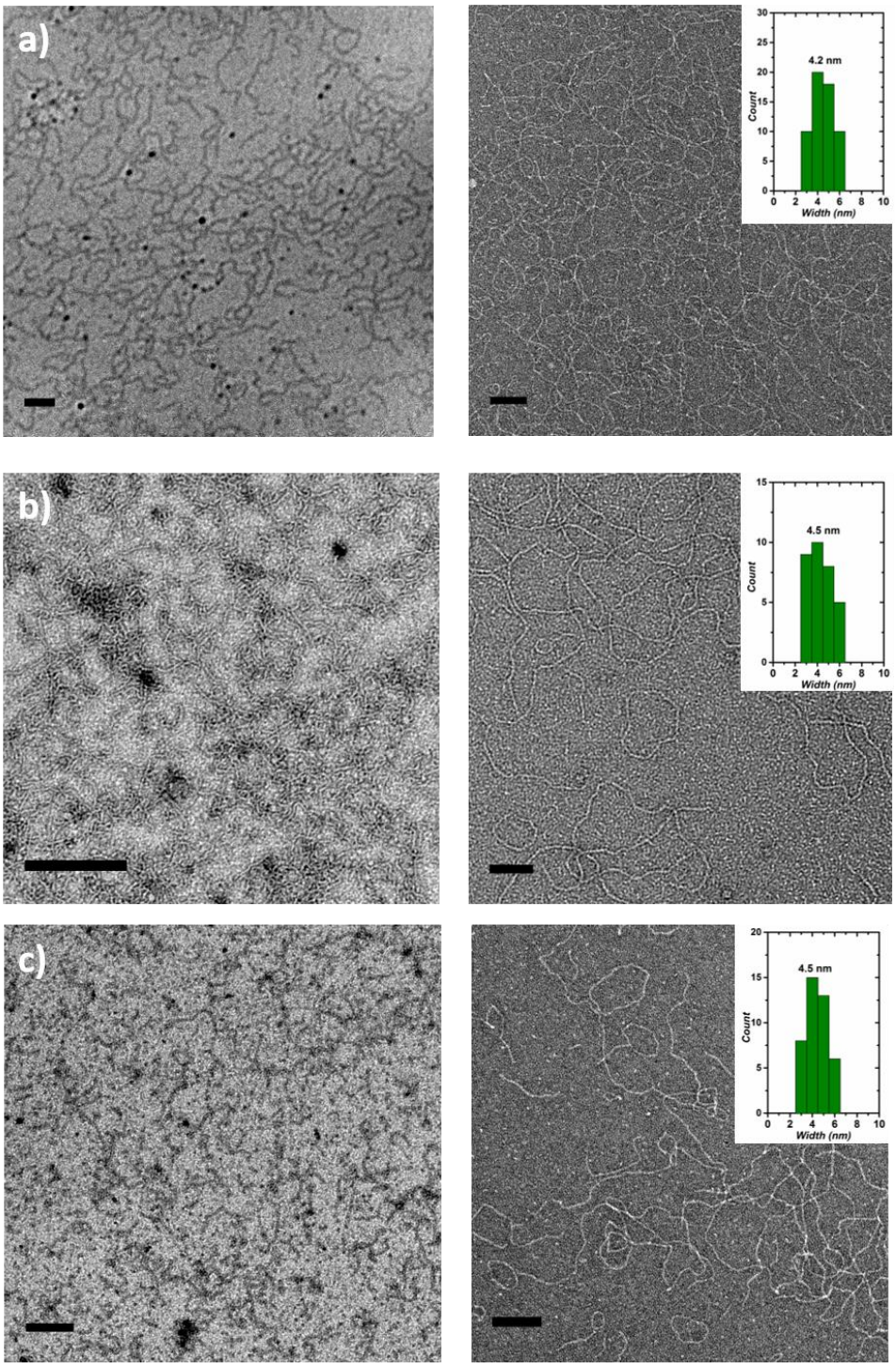

Figure 4.27 TEM and high-resolution TEM images of **ES TANI(NDS)-$(PTAB)_2$** in solution at different concentrations. a) 4 mM, b) 8 mM, c) 16 mM. Scale bar=200 nm, HRTEM images on the right-hand side.

AFM was also used to gain insight regarding the size of the self-assembled fibres. AFM investigations also confirmed the formation of nanofibers (**Figure 4.28** and **4.29**) and initial results were obtained on carbon-coated TEM grids that were used for TEM imaging. As shown in **Figure 4.28**, 1 mM solution of **TANI(NDS)-(PTAB)$_2$** drop-cast on a carbon-coated TEM grid and analysed by AFM showed fibre-like structures similar to those observed by TEM. However, the width of the fibres observed by AFM (10 nm width) was larger than that observed by TEM. Close inspection of the fibres showed that a dense layer of fibrous structures covered the surface, suggesting layers of fibers structures formed during the drying process such as the fibre labelled in **Figure 4.29a**.

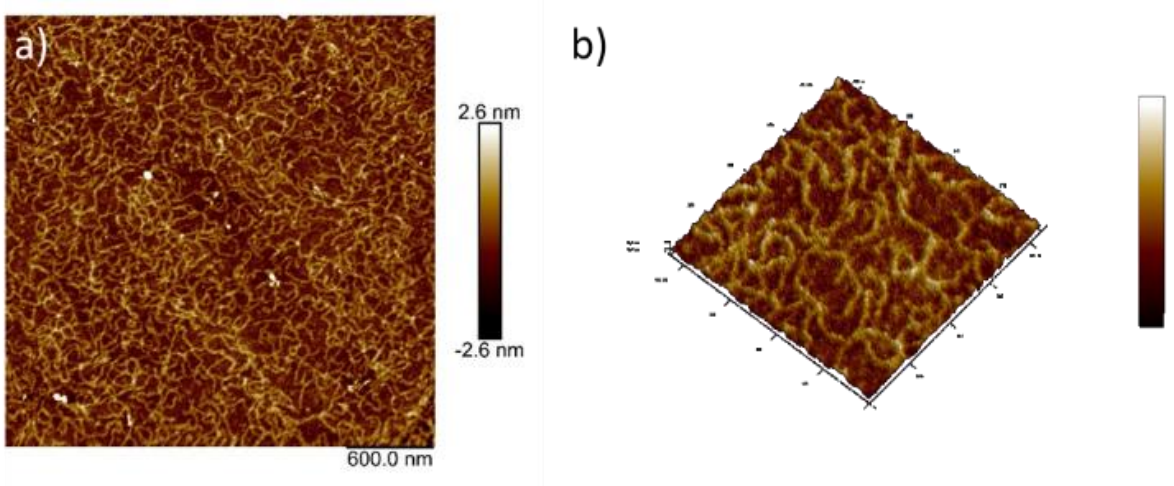

Figure 4.28 a) AFM image and b) 3D AFM images of 1 mM solution of **ES TANI(NDS)-(PTAB)$_2$** drop-cast onto carbon-coated grid.

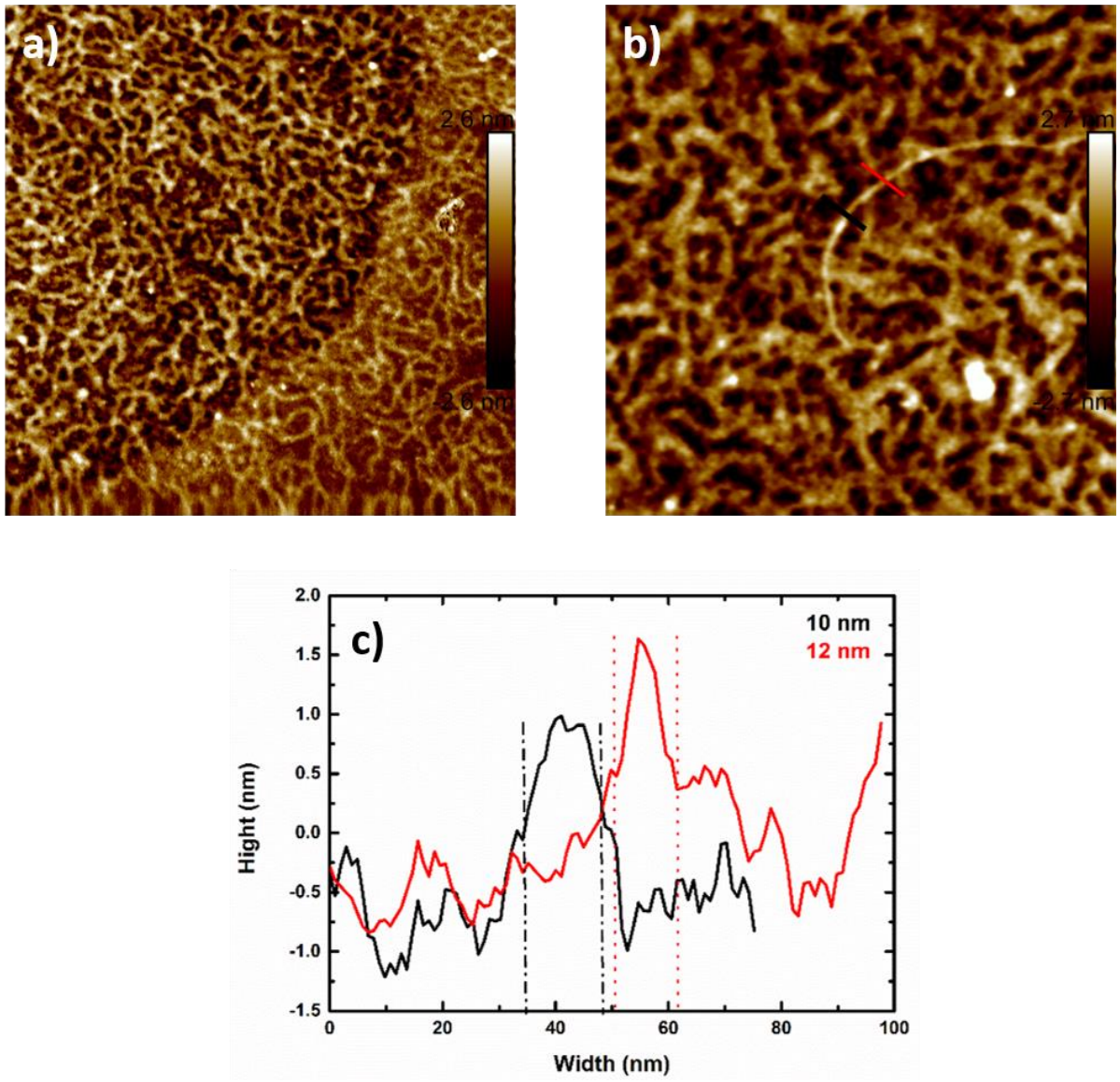

Figure 4.29 a), b) AFM images of 1mM solution of **ES TANI(NDS)-$(PTAB)_2$** drop cast onto carbon-coated grid. c) height profile of **ES TANI(NDS)-$(PTAB)_2$** corresponding to the red and black lines shown in (b).

A further surface type was examined in order to confirm the width of single, 4 nm-wide, fibres as seen by TEM. TEM samples were drop-cast onto mica surface and the surface was purged with nitrogen gas to remove the excess materials formed on surface. A film of fiber structures again

formed, with some single fibers labelled in **Figure 4.30**. The width of fibers formed on mica and seen by AFM (5 nm width) was closely matched to the width of fibers seen by TEM imaging.

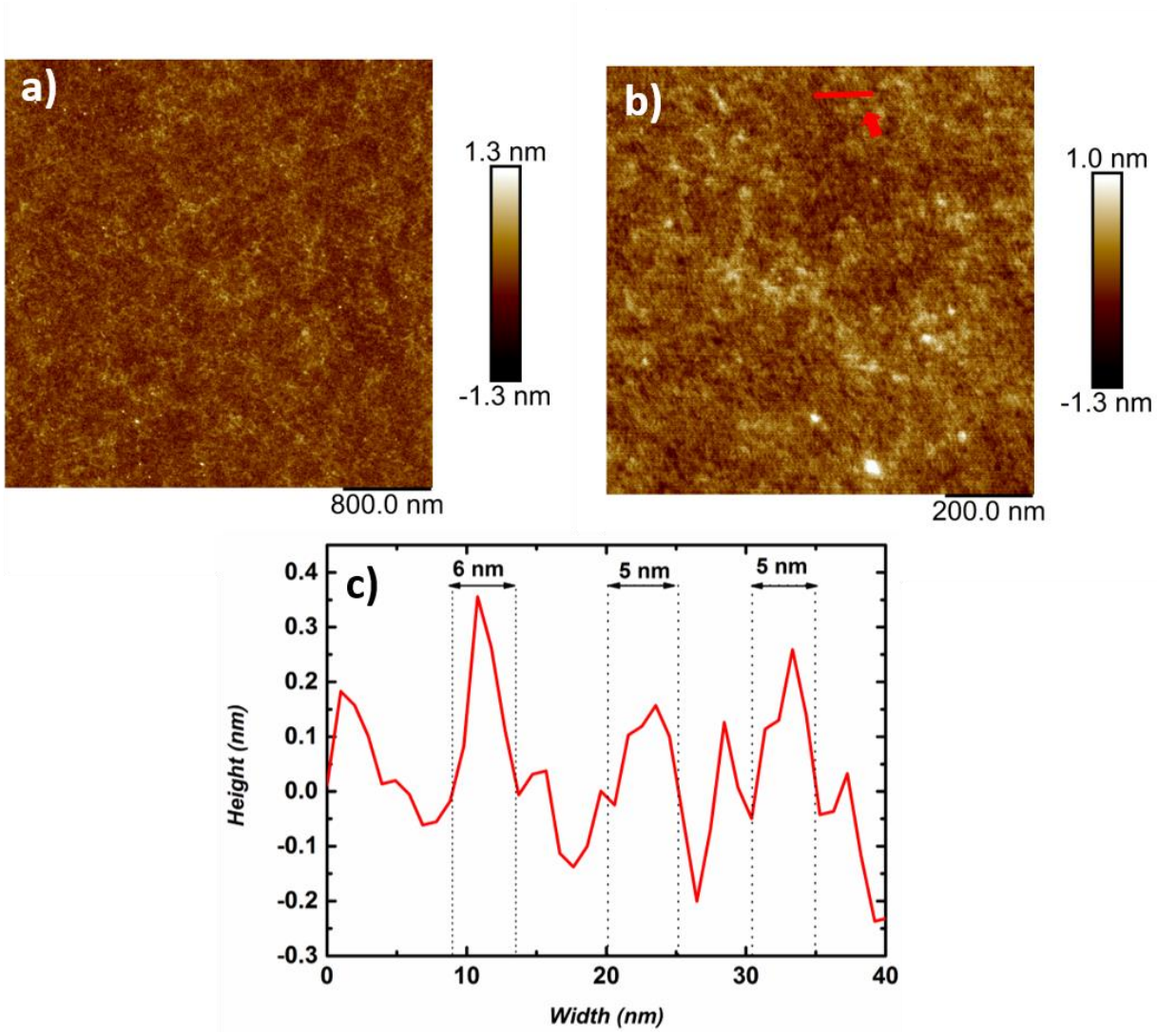

Figure 4.30 a), b) AFM images of 1mM solution of **ES TANI(NDS)-$(PTAB)_2$** drop cast onto mica, c) height profile of **ES TANI(NDS)-$(PTAB)_2$** fibers corresponding to the red line shown in (b).

Analysis of the SAXS and SANS data for these doped systems shows a q = −1 dependence, indicative of rod-like structures in solution. Both SAXS and SANS data fitted to a cylinder model with a cylinder diameter of 4.6nm (**Figure 4.31**, data recorded for 8 mM solutions), which is commensurate with what was observed in TEM. However, the SAXS data (**Figure 4.32**) do not fit as well as the SANS data, particularly at low values of q. This is due to the poor contrast of the

samples in SAXS; however the radius of the cylinder is comparable with that found by SANS and TEM The fitting parameters for both SANS and SAXS are given in the **Appendix D**, Tables D2 and D3, respectively.

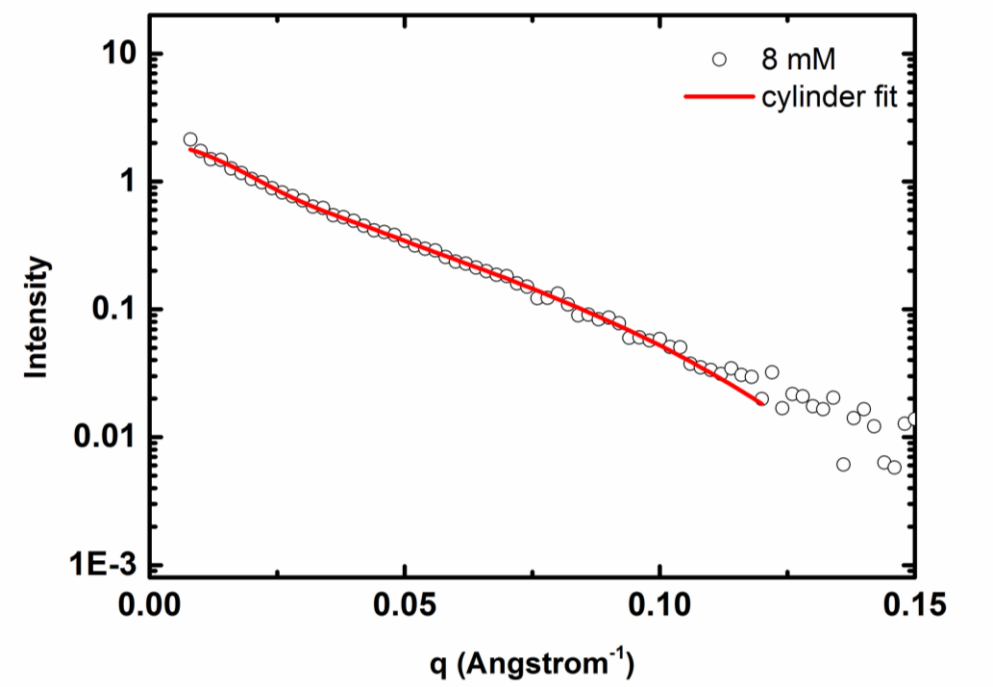

Figure 4.31 SANS data of **ES TANI (NDS)-(PTAB)$_2$** in solution (concentration=8 mM). The parameters used to fit the data, along with their associated errors are given in Appendix Table D2.

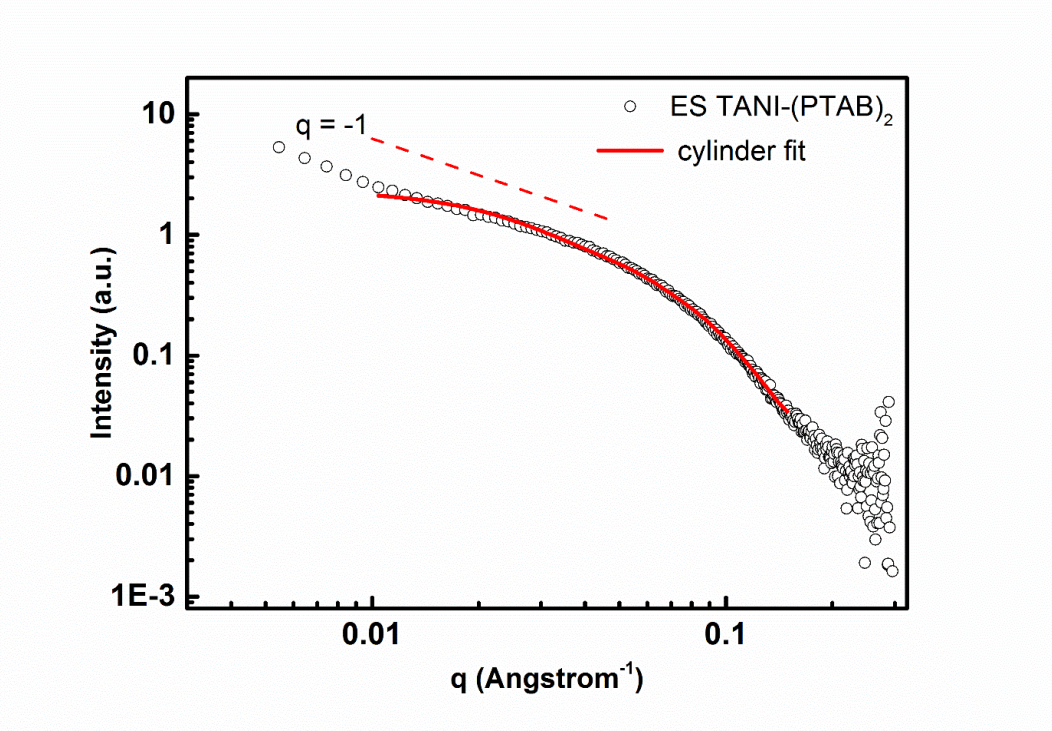

Figure 4.32 Small angle x-ray scattering data collected from **ES TANI(NDS)-(PTAB)$_2$** (concentration=16 mM).

The self-assembling behaviour of the amphiphilic molecules based on π-conjugated systems are attributed to the presence of strong π-stacking.[36] Although this stacking behavior was not immediately evident for lower concentrations, it was clearly identified by X-ray diffraction (XRD) of a freeze-dried sample of 8 mM **ES TANI(NDS)-(PTAB)$_2$**. As shown in **Figure 4.33**, the most pronounced peak in the X-ray diffraction was found at around 2θ = 21.5°, which corresponds to a d-spacing of 0.41 nm. This can be ascribed to **TANI** packing in a parallel fashion, as has been previously observed in **PANI,** this is very similar to the reflections observed for **TANI-PTPB**, in **Chapter3**, **Figure 3.15**.[37,38] The second observed reflection at 2θ= 23.9° corresponds to a d-spacing of 0.37 nm, also typical for π-stacking interactions; the exact nature of the stacking arrangements to produce two regular stacking distances (both well within the acceptable range of spacing for π-stacking) is currently being investigated through drawn fibre diffraction studies (from concentrated solutions).

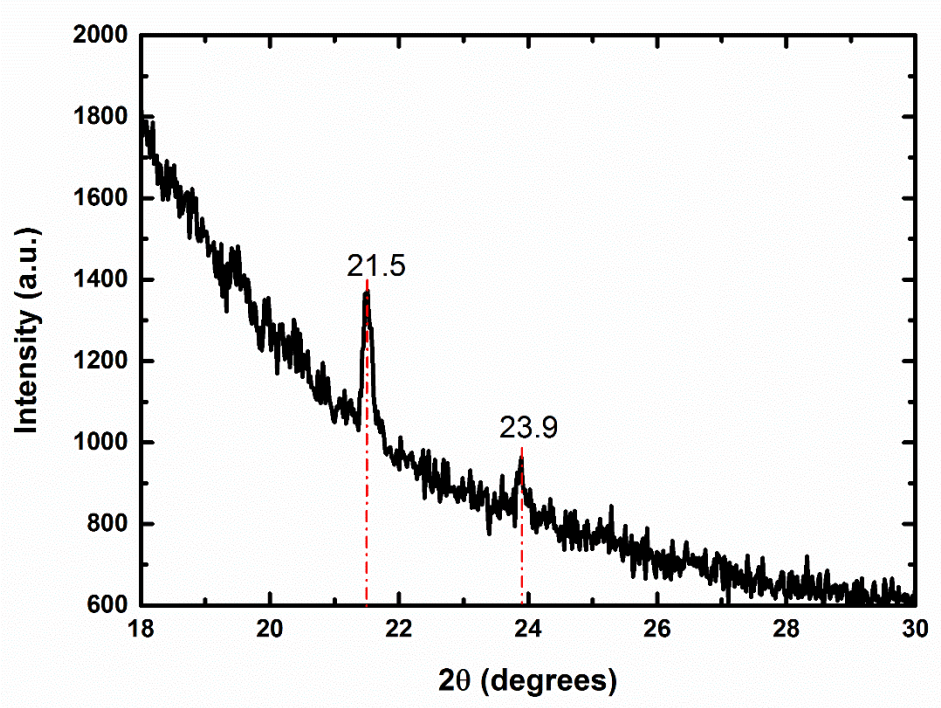

Figure 4.33 PXRD data of freeze-dried **ES TANI(NDS)-(PTAB)$_2$** (concentration=8 mM).

FTIR measurements were further used to identify the oxidation state of **TANI-(PTAB)$_2$** species, starting with the FTIR spectrum of a freeze-dried 8 mM **EB TANI-(PTAB)$_2$** as control. The main three characteristic IR bands of **EB TANI-(PTAB)$_2$** were found to be centered at 1596 cm^{-1}, 1514 cm^{-1}, and 1167 cm^{-1} which correspond to the stretching bands of γC=C for quinoid rings, γC=C γC-H out-of-plane of 1,4-aromatic substituted benzene rings, respectively. Compared with **EB TANI-(PTAB)$_2$**, the FTIR spectrum of **ES TANI(NDS)-(PTAB)$_2$** exhibited three characteristic peaks at 1582 cm^{-1}, 1508 cm^{-1}, 1156 cm^{-1}, which were attributed to γC=C for quinoid rings, γC=C for benzenoid rings, and γ-NH$^+$=, which are typical peaks for **TANI** in **ES** state as shown in **Figure 4.34**. The C=O bands of **EB TANI-(PTAB)$_2$** and **ES TANI(NDS)-(PTAB)$_2$** appeared at 1663 cm^{-1}, 1678 cm^{-1}, respectively. The 15 cm^{-1} shifts of C=O single in **ES TANI(NDS)-(PTAB)$_2$** could be an indication of the formation of hydrogen-bonding interaction occurred in ES sate.

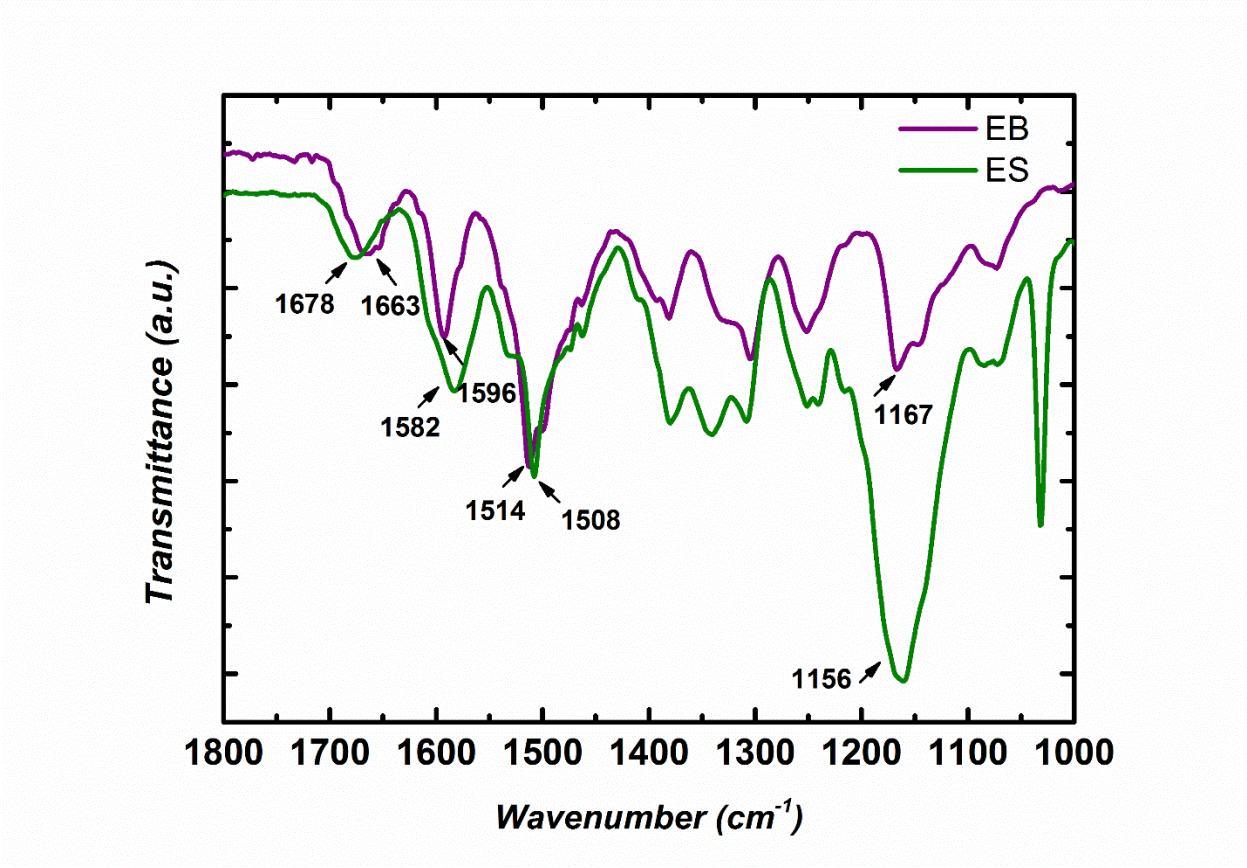

Figure 4.34 FTIR spectra of freeze-dried of **EB TANI-$(PTAB)_2$**, and **ES TANI(NDS)-$(PTAB)_2$**.

Overall, **Figure 4.35** summarized the tunable self-assembled structures of **ES TANI-$(PTAB)_2$** depending on the dopant acids.

Table 4.3 various self-assembled structures of **ES TANI-$(PTAB)_2$** systems.

Molecule	**pK_a**	**observed self-assembled structure**
TANI-$(PTAB)_2$	-	Flexible bilayers, vesicles
TANI$(HBr)_2$-$(PTAB)_2$	-9.00	Flexible bilayers, vesicles
TANI$(TFA)_2$-$(PTAB)_2$	0.23	Flexible bilayers, vesicles
TANI$(TsH)_2$-$(PTAB)_2$	-2.80	Flexible bilayers, vesicles
TANI$(CSA)_2$-$(PTAB)_2$	1.20	Flexible bilayers, vesicles
TANI(NDS)-$(PTAB)_2$	-1.80	Cylindrical micelles

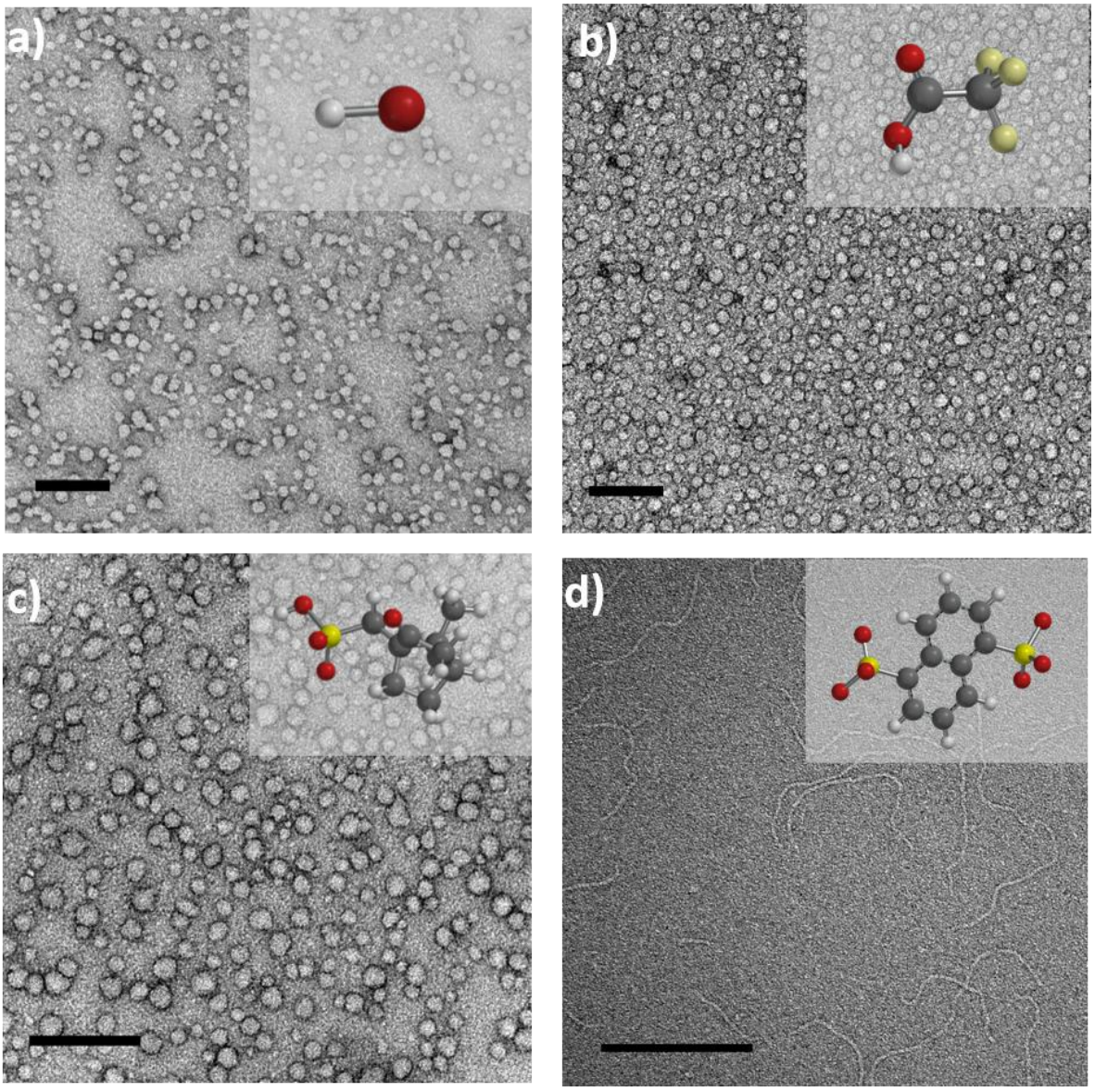

Figure 4.35 TEM images of ES state solutions (1 mM solutions, stained with 1% uranyl acetate) a) High-resolution TEM **TANI(HBr)$_2$-(PTAB)$_2$** b)) **TANI(TFA)$_2$-(PTAB)$_2$**, c) **TANI(CSA)$_2$-(PTAB)$_2$** and d) High-resolution TEM **TANI(NDS)-(PTAB)$_2$**. Scale bars: 200 nm.

4.2.1.10 Conductive AFM

Conductive AFM was used to measure the conductivity of **ES TANI(NDS)-(PTAB)$_2$** by measuring the electric current flowing between the sample and conductive probe when a voltage introduced. Tunneling AFM (TUNA) and conductive AFM (CAFM) are generally used a conductive

probe. However, TUNA showed greater current sensitivity (up to 50 femtoampere, fA) compared to regular CAFM (microampere, µA). A 1 mM solution of **ES TANI(NDS)-(PTAB)$_2$** was drop-cast onto a glass surface and spin-coated, resulting in a very thin film formed on the surface. The glass edge then was coated with silver to make a conducting link. **Figure 4.36** showed the AFM image of **ES TANI(NDS)-(PTAB)$_2$** fibres and its current histogram. Two distinct peaks are clearly seen in the histogram, one peak at 1 pA corresponding to the current measured without applied voltage and another peak at 7 pA corresponding to the current measured with an applied voltage of 9.4 Volt. The resulting current would be an indication of the formation of poorly conductive materials due to high value of resistivity calculated using Ohm's law (Equation 5). The value of 1.34 TOhm found was much higher than the single-tailed amphiphiles **ES TANI(CSA)$_2$-PTAB** where resistance was 17.5 MOhm.[14]

$$R = \frac{V}{I} \qquad \textbf{(5)}$$

Where **R** refers to resistvity, **I** refers to current flowing through the resistance and **V** is the voltage.

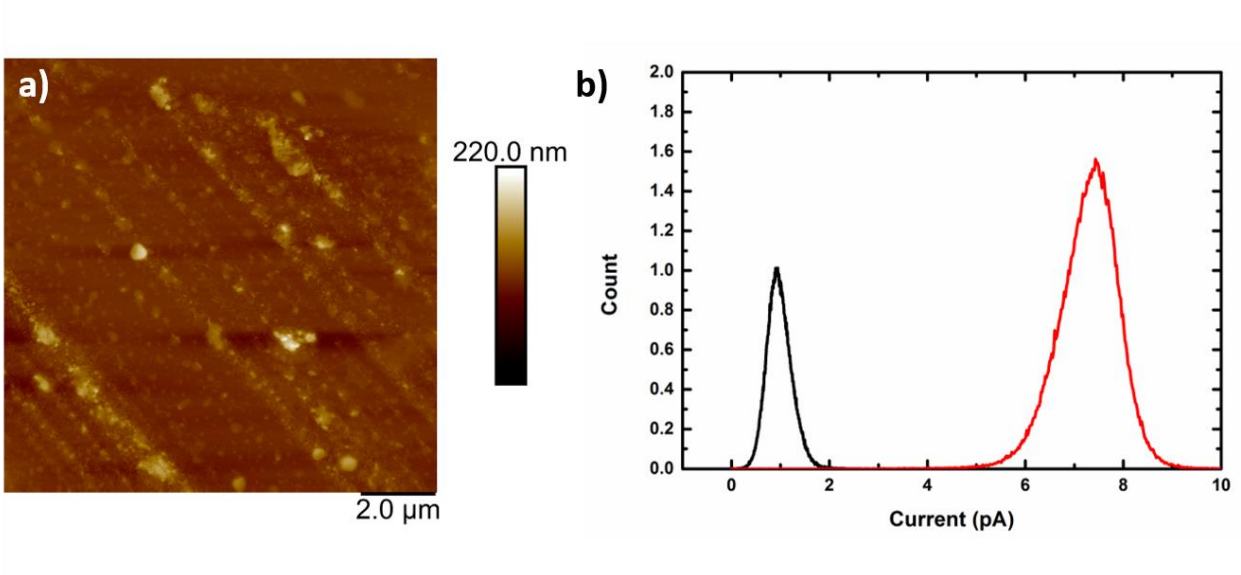

Figure 4.36 a) AFM image of **TANI(NDS)-(PTAB)$_2$** fibre film, b) current histogram for a **TANI(NDS)-(PTAB)$_2$** film.

4.2.1.11 Reversibly controlled assembly through acid/base interactions

The (optoelectronic) transition from the **EB** to the **ES** state of **TANI**-based takes place through the well-known doping/de-doping process, as followed by UV/Vis-NIR spectroscopy (**Figure 4.37**) To investigate the ability to switch between two different self-assembled structures in our **TANI**-based bolaamphiphile, we selected the example with the most significant change of morphology: vesicles with 22 nm diameter (**Figure 4.37a**) were first formed in the **EB** state and then turned into 4 nm-wide nanofibers when doped by **NDS** (**Figure 4.37b**). Once base (NaOH) was added to de-dope the **TANI** core and stirred for 5 minutes, the structure returned to a vesicle-only morphology (**Figure 4.37c**). Furthermore, two cycles of doping/de-doping were performed to confirm the structural changes as well as the full reversibility of the transition. We observed the full conversion of **ES** to **EB** state and *vice versa*, as confirmed by UV/Vis-NIR and TEM investigations, with data shown in **Figure 4.37 (dashed line)** and **4.38c and d**. Tuning the morphology of **TANI-(PTAB)$_2$** through doping/de-doping provide a feasible way to control the aggregation and stacking of **TANI-(PTAB)$_2$** in a simple fashion.

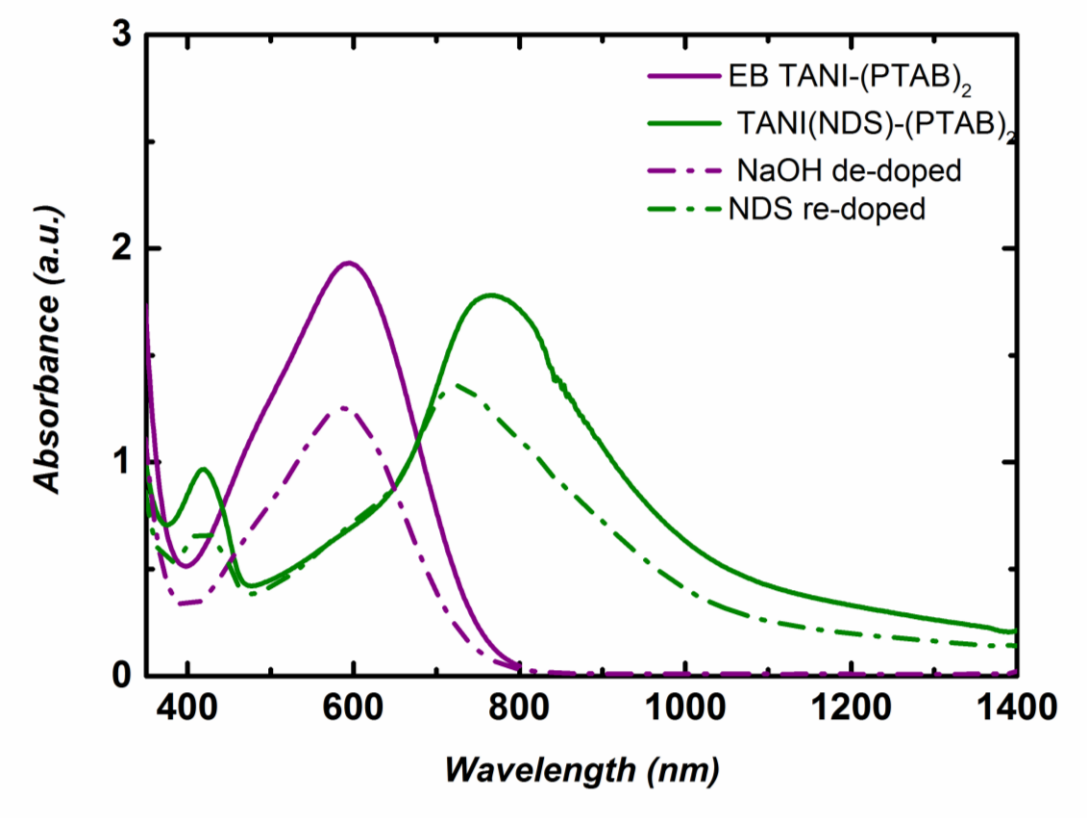

Figure 4.37 UV/Vis-NIR spectra of **EB TANI-$(PTAB)_2$**, **ES TANI(NDS)-$(PTAB)_2$** in solution (concentration = 1 mM), NaOH de-doped sample and NDS re-doped sample.

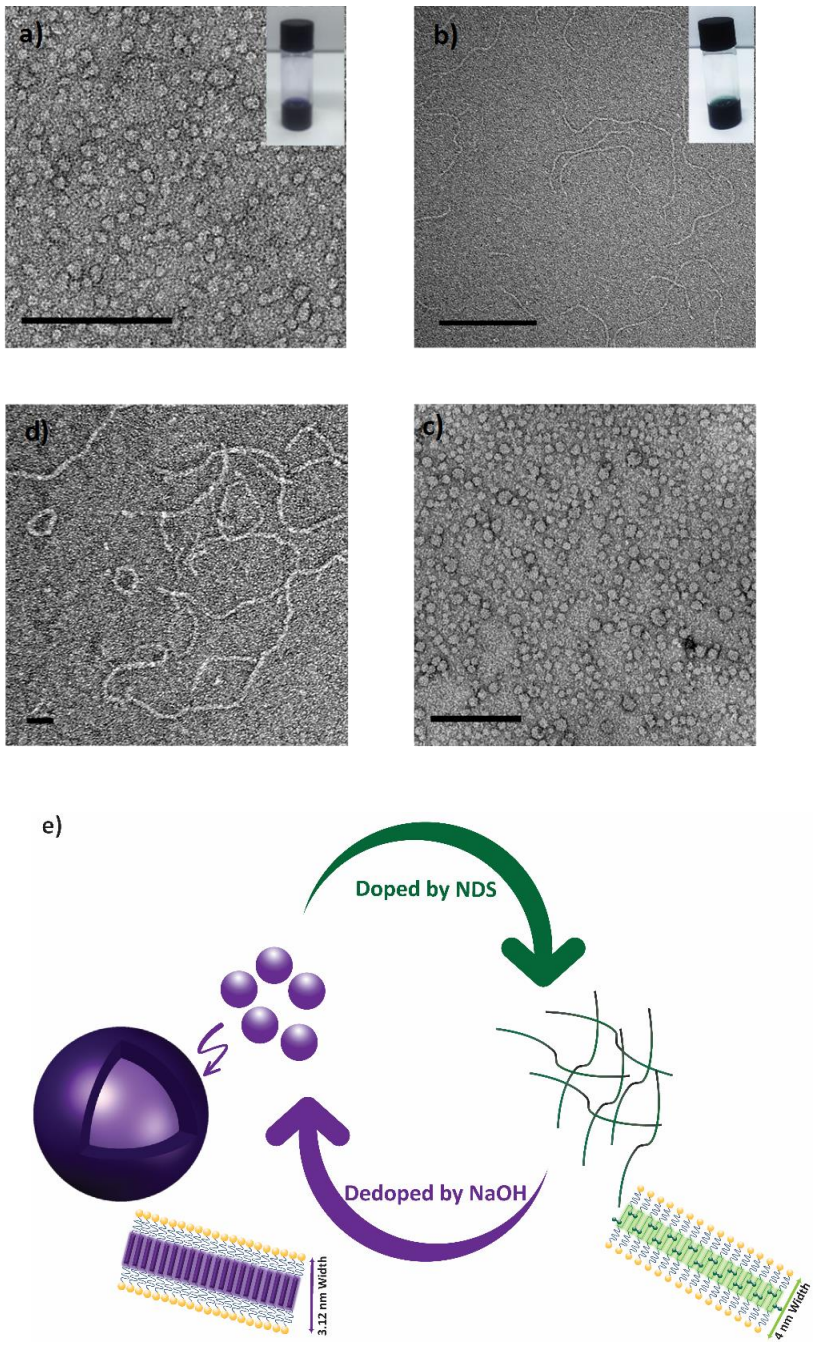

Figure 4.38 a) TEM images of **EB TANI-$(PTAB)_2$**, b) High resolution-TEM **ES TANI(NDS)-$(PTAB)_2$**, c) NaOH de-doped sample, d) High resolution-TEM of re-doped **ES TANI(NDS)-$(PTAB)_2$** (concentration=1mM), e) cartoon showing the reversible process of spheres and fibers through doping and de-doping, scale bar in all images=200 nm.

4.2.1.12 Tuning the self-assembled structure by diacid dopants

To investigate the effect of the presence of two acidic groups, a selection of diacids were chosen in order to trigger morphological changes. Oxalic acid (**OA**) and malonic acid (**MA**) are relatively weak acids due to the high pK_a values (1.46, 2.85, respectively), and are thus unable to fully dope **TANI-(PTAB)$_2$** as shown in **Figure 4.39** by presence of the absorption feature at 600 nm, typical for the **EB** state. TEM investigations showed that a mixture of sphere-like structures with some fibers are present in **ES TANI-(PTAB)$_2$** solutions doped by **OA** and **MA**. However, unlike **OA** and **MA**, ethanedisulfonic acid (**EDS**) is a strong diacid, but without the conjugated structure that **NDS** possesses. **TANI(EDS)-(PTAB)$_2$**, as shown in **Figure 4.40**, formed a fused-vesicle chain-like structure (**Figure 4.40b).** We also chose naphthalenesulfonic acid **(NS)** as a single-acid control, with TEM showing a sphere-like structure without any fibers present (**Figure 4.40d**). This important control suggests that fibrous structures were forming in solution due to two factors: a cross-linking effect of using an aromatic diacid molecule and π interaction occurring between TANI molecules and dopants. These subtle influences of the dopant over structure formation thus provides further opportunities to exert control over these electroactive amphiphilic structures.

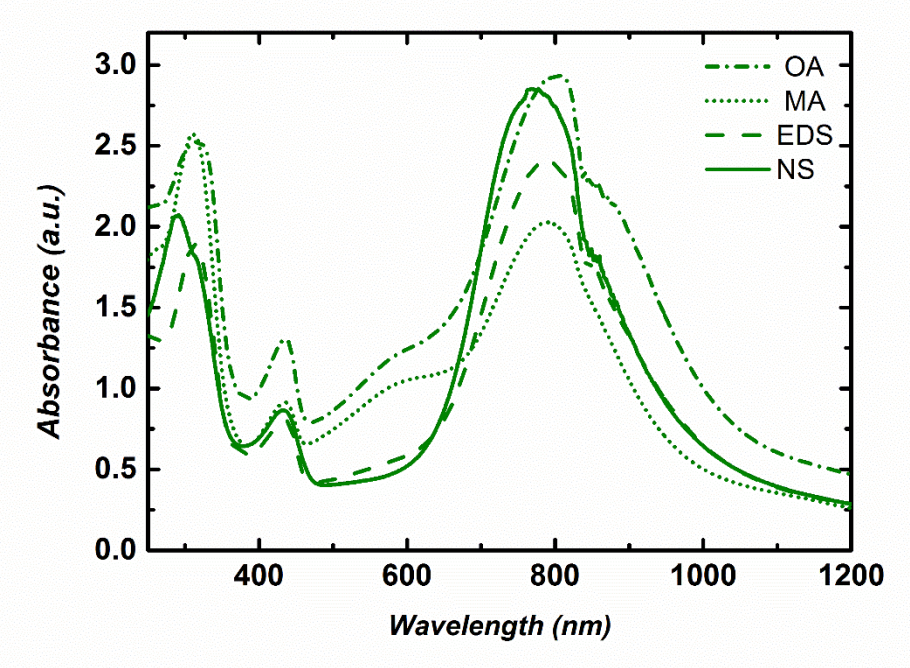

Figure 4.39 UV/Vis spectra showing **EB TANI-$(PTAB)_2$** and doping of **TANI-$(PTAB)_2$** by various acids in aqueous solutions to form ES state.

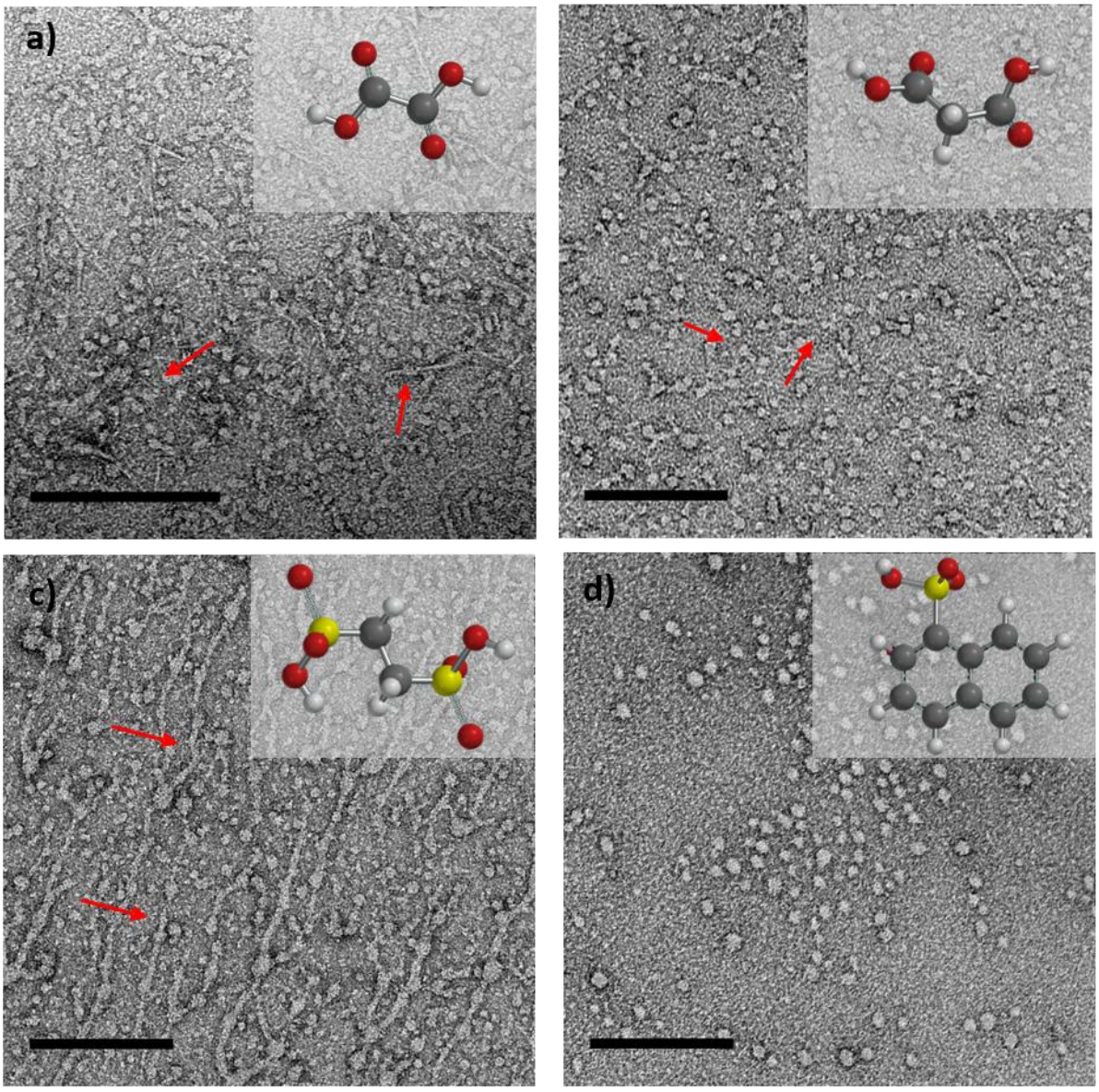

Figure 4.40 TEM images (1 mM solutions, stained with 1% uranyl acetate) of ES state (a) **ES TANI(OA)-$(PTAB)_2$**, (b) **ES TANI(MA)-$(PTAB)_2$**, (c) **ES TANI(EDS)-$(PTAB)_2$** and (d) **ES TANI$(NS)_2$-$(PTAB)_2$** as a control experiment, with corresponding dopant molecular structures inset. Scale bars:200 nm.

4.2.2 Synthesis and self-assembly of electroactive phosphonium bolaamphiphiles

4.2.2.1 Synthesis of tetra(aniline) bolaamphiphile TANI-$(PTPB)_2$

We reported in the previous chapter the preparation of a conventional amphiphile EB Ph/NH_2–**TANI**–($C_6PMe_3^+Br^-$) **TANI-PTPB**. The synthesis of bolaamphiphiles comprising **TANI** functionalised with two alkyltrimethylphosphonium head groups built on the successful synthesis of NH_2/NH_2 **TANI** reported previously.[24] Boc-protected NH_2/NH_2 **TANI** was first synthesised via a nucleophilic substitution reaction as discussed in the **Experimental Chapter.** Subsequently, NH_2/NH_2 **TANI** was used to prepare the electroactive bolaamphiphile **TANI-$(PTPB)_2$** (**Scheme 2.6**). The formation of the desired symmetrical water-soluble bolaamphiphile was confirmed using different characterization techniques, including ^1H NMR spectroscopy and high-resolution mass spectrometry. All the synthetic details are presented in the Experimental Chapter.

4.2.2.2 Self-assembly studies of EB TANI-$(PTPB)_2$

The self-assembling behavior of the phosphonium bolaamphiphile was investigated in a similar way to that used for the ammonium bolaamphiphiles. First, the critical aggregation concentration (CAC) was measured using pyrene as a fluorescent probe and determined to be 0.070 mM. This value was assigned by the sharp change in I_1/I_3 ratio as presented in (**Figure 4.41a**). The CAC of the phosphonium bolaamphiphile is slightly less than that of the ammonium bolaamphiphile (0.072 mM), which suggests that the phosphonium bolaamphiphile has a stronger tendency to aggregate in solution as a result of the increase of the size of the headgroups.

Aqueous solutions of **EB TANI-$(PTPB)_2$** with different concentrations were prepared and analysed by UV/Vis spectroscopy to further elucidate the aggregation phenomena. A clear 44 nm bathochromic shift in the characteristic absorbance peak was observed as the concentration increased, with λ_{max} = 553 nm for 0.001 mM vs.600 nm for 1 mM solutions, as shown in (**Figure 4.40b**). Bathochromic shifts have been reported previously as a result of the changes in the environment, molecular packing and aggregation mode (i.e., J-aggregate).[26]

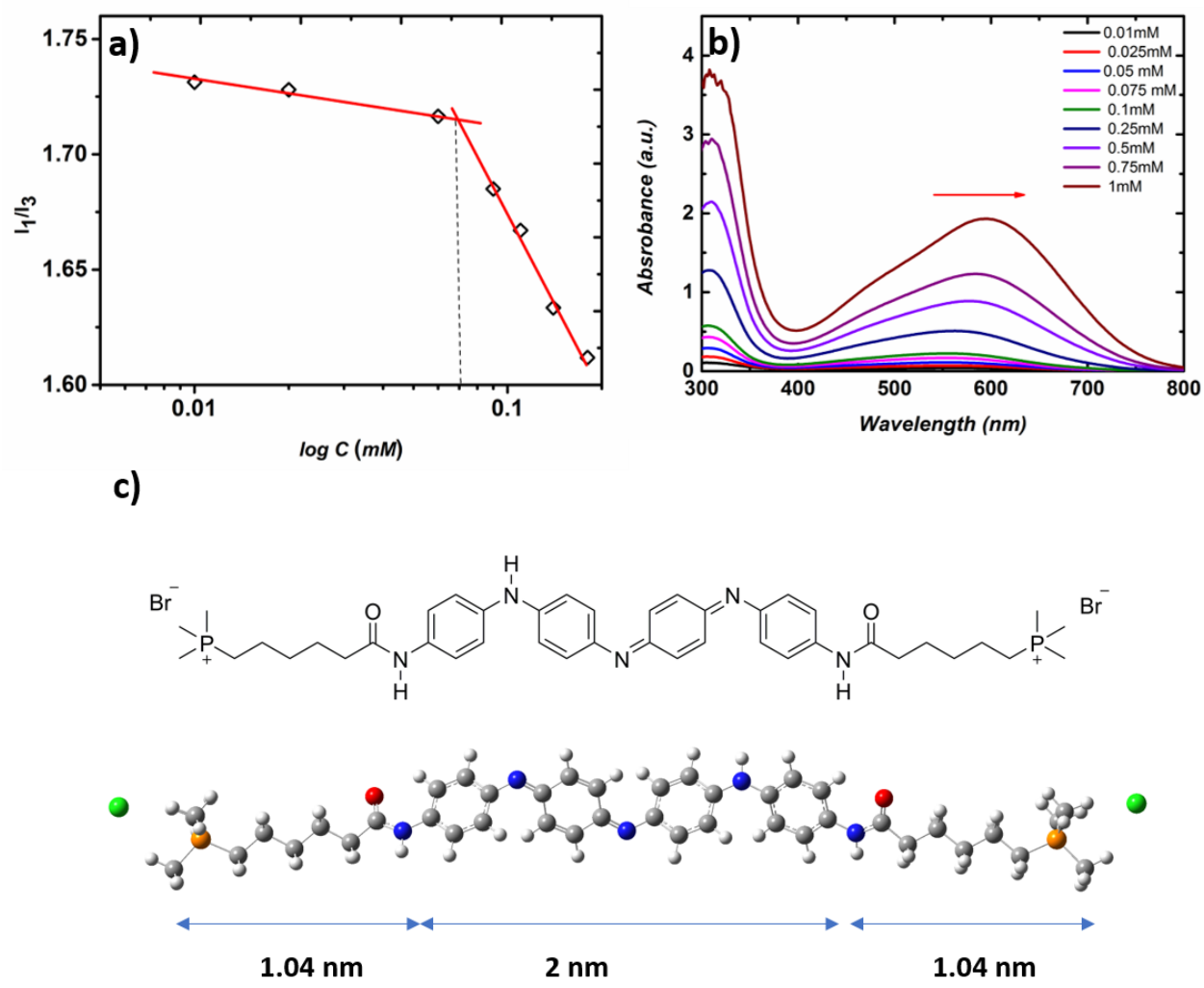

Figure 4.41 a) Fluorescence of a pyrene probe to determine the CAC of **EB TANI-(PTPB)$_2$**. CAC = 0.076 mM. b) Change of λ_{max} of **EB TANI-(PTPB)$_2$** with concentration. The arrow indicates change on increasing concentration. c) Chemical structure and DFT-optimised structure of **EB TANI-(PTPB)$_2$**.

4.2.2.3 DFT-modelling: comparison of simulated UV/Vis of EB TANI-$(PTPB)_2$ and experimental spectra

The structure of **EB TANI-$(PTPB)_2$** was also modelled and optimised in Gaussian as the same condition that used for the ammonium bolaamphiphiles: the B3LYP functional, the 6-31G* basis set, and a polarisable continuum model (PCM) solvent environment. In the case of simulated UV-Vis data, CAM-B3LYP was used as suggested for charge-transfer and π conjugated systems.[27] TD-DFT simulations of **TANI-$(PTPB)_2$** yielded spectra similar to experimental spectra in acetonitrile (**Figure 4.41**), which was chosen to avoid the red shift corresponding to aggerated structures in water. The absorbance maximum at 521.28 nm was attributed to the HOMO−LUMO transition of aqueous **TANI-$(PTPB)_2$** (**Figure 4.42**), where π-π* transitions dominate. The absorbance peak of the first singlet excited state of **EB** state (2.37 eV, 521 nm) matched the transition observed experimentally in the UV/Vis spectrum (552 nm, see the **Appendix D** for further details).[14,27]

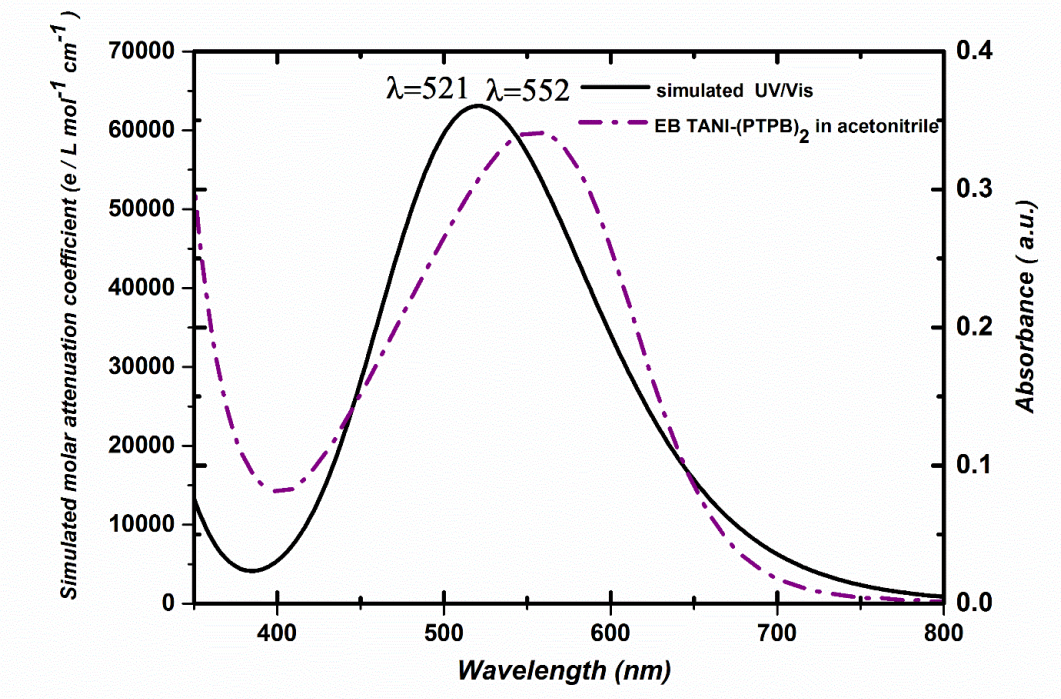

Figure 4.42 Comparison of the simulated UV/Vis of **EB TANI-$(PTPB)_2$** and experimental spectra in acetonitrile.

LUMO

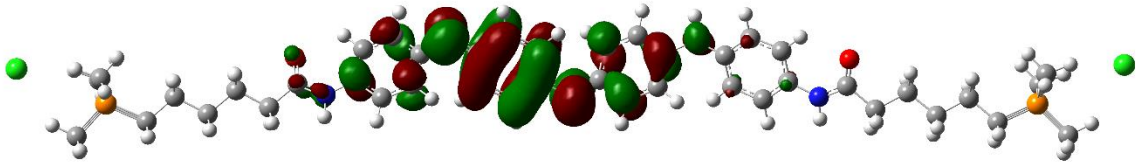

HOMO

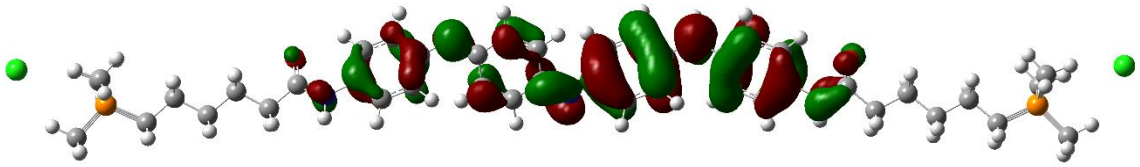

Figure 4.43 MOs of **EB TANI-(PTPB)$_2$** transition.

The self-assembled structure of **EB TANI-(PTPB)$_2$** was revealed using transmission electron microscopy (TEM) and atomic force microscopy (AFM). TEM showed that **EB TANI-(PTPB)$_2$** self-assembled into sphere-like structures at all selected concentrations (**Figure 4.45** for 1, 2, 4 mM). The diameter of structures formed at 1 mM of **EB TANI-(PTPB)$_2$** was approximately 20 nm (**Figure 4.45a**). Furthermore, 2 and 4 mM showed spheres structures with average diameter 22 nm as shown in **Figure 4.44b** and **c.**

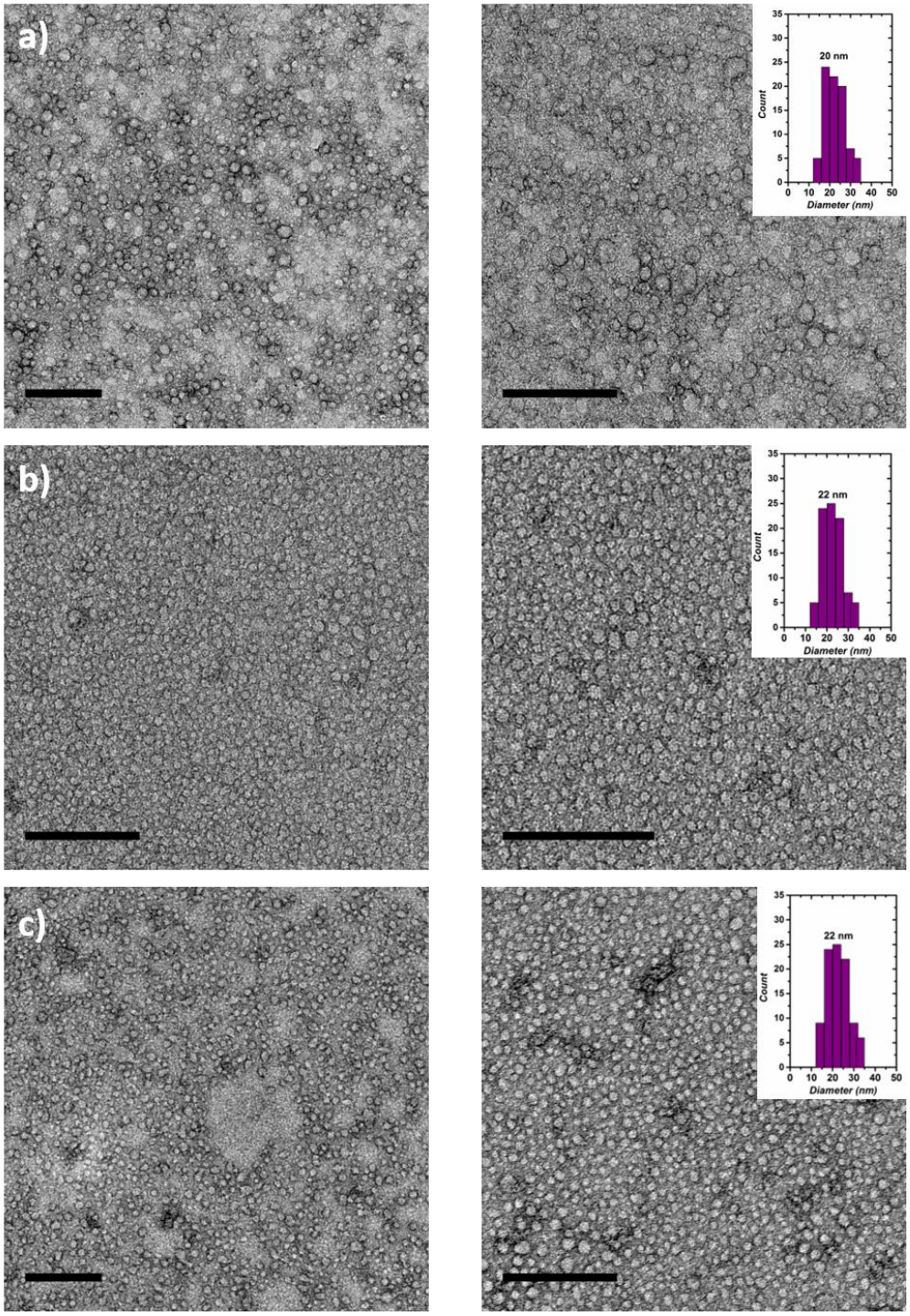

Figure 4.44 TEM images (stained with 1% uranyl acetate) of **EB TANI-(PTPB)$_2$** in solution at different concentrations a) 1mM, b) 2mM, c) 4 mM. Scale bar=200 nm. The images on the right and left side represent the same images with different magnifications.

Detailed AFM measurements were carried out to gain insight into the topology of these aggregates. AFM images of a **TANI-(PTPB)$_2$** solution (1 mM), drop-cast onto carbon-coated copper grids are shown in (**Figure 4.45a** and **b**). The average diameter and height of these structures were determined over 183 samples, and calculated to be 22 nm and 6 nm, respectively (**Figure 4.45a** and **c**). The value obtained for the average diameter agreed very well with the sizes obtained from TEM measurements. The theoretical length of the optimised **TANI-(PTPB)$_2$** is 4.08 nm (2 nm of TANI, 1.04 nm of each alkyl chains, see **Figure 4.41c**). The measured heights of these two objects were 6 nm and 5.5 nm, respectively (**Figure 4.45c**). Given the theoretical stretched length of a **TANI(TFA)$_2$-PTAB** molecule, (we assume that the height is determined by the thickness of an interdigitated double layer of **TANI-(PTPB)$_2$**. This layer is calculated to have an average height of ~6 nm (with fully interdigitated and overlapping π-conjugated surfaces and tilt with respect to the J-aggregates), with the proposed molecular packing models shown in **Figure 4.45d**. Taking into account the measured average diameter with the proposed interdigitated double layer packing model, we propose that these objects are hollow double-layer vesicles.

Small-angle X-ray and neutron scattering (SAXS and SANS, respectively) are usually used to probe the structure and size of the self-assembled aggregates and would be considered as a future work. Considering all the measurements and dimensions we therefore propose a bilayer vesicle-like structure for **EB TANI-(PTPB)$_2$** aggregates, as shown in **Figure 4.45d**.

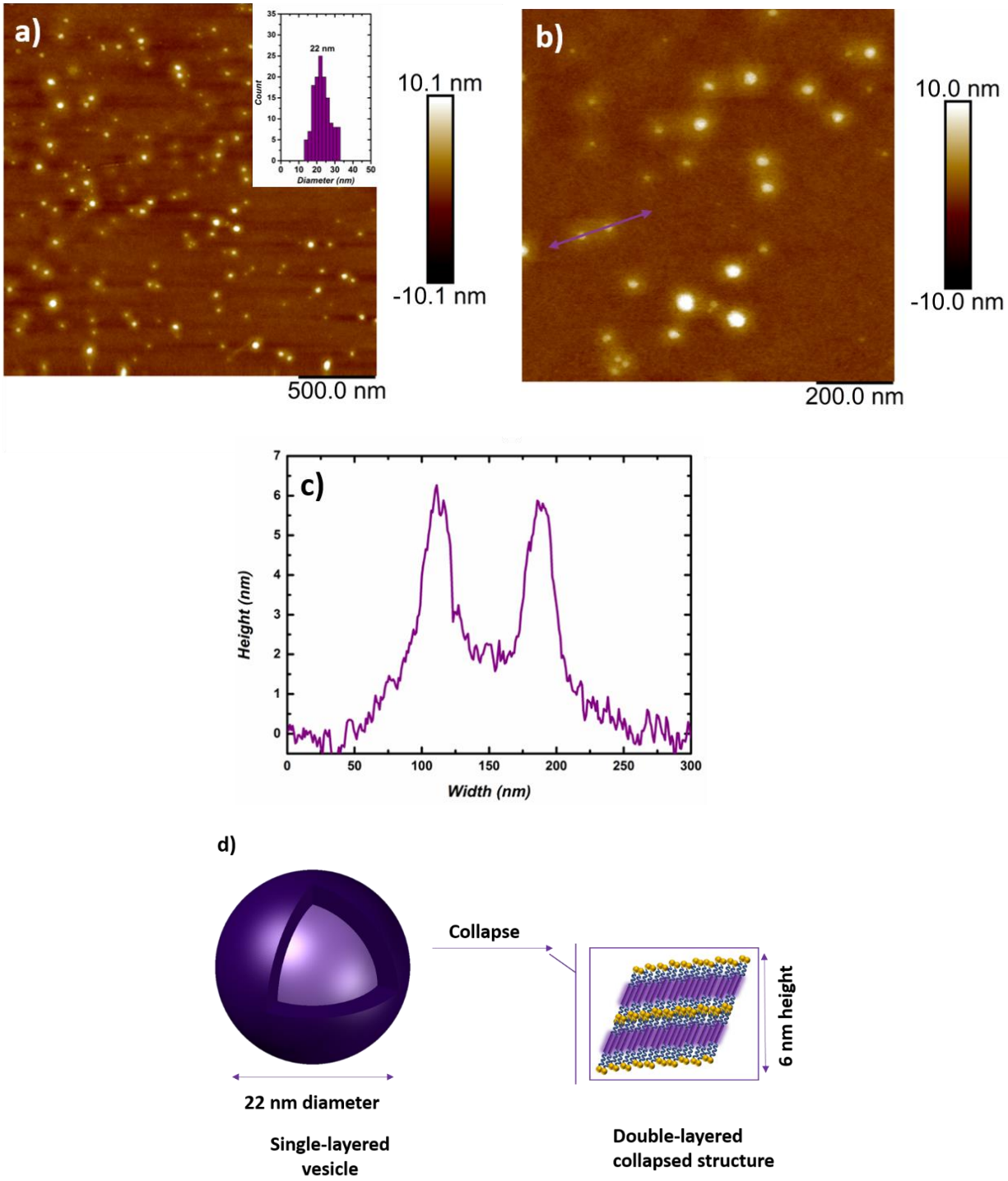

Figure 4.45 a), b) AFM image of **EB TANI-(PTPB)$_2$** solution (concentration = 1 mM), the histogram of particle diameter distributions counted from 183 particles, respectively, c) height profile of **EB TANI-(PTPB)$_2$** corresponding to the line shown in (b). d) The proposed self-assembled structure of **EB TANI-(PTPB)$_2$**.

4.2.2.4 Doping of TANI(HX)$_2$-(PTPB)$_2$

As mentioned previously, the interesting aspect of electroactive **TANI**-amphiphiles is the ability to form various self-assembled structures by changing the packing parameter through dopant addition and this process is called the addressable packing parameter (APP)[19] **EB TANI-(PTPB)$_2$** and **EB TANI-(PTAB)$_2$** have the same chemical structure with different head group, which would show different morphology the packing parameter is different . Doping **EB TANI-(PTPB)$_2$** with different types of acids lead to large changes in the volume of the hydrophobic **TANI**-based "tail" structure. As mentioned before in case of the ammonium amphiphile, a range of suitable organic and inorganic dopants were therefore selected (hydrobromic acid, **HBr**, trifluoracetic acid, **TFA**, racemic camphorsulfonic acid, ***rac*-CSA**) to dope **EB TANI-(PTPB)$_2$**. All those acids showed interesting self-assembled structures when used to dope **TANI-PTPB** as mentioned in the previous chapter. In addition to these acids, dopants with multiple acidic groups such phytic acid, **PA**, have been used to form multifunctional polyaniline (PANI) hydrogel. The use of **PA** result in a mesh-like hydrogel network due to the crosslinking effect as **PA** molecule tends to interact with more than one **PANI** chain.[39] It is worth mentioning that **PA** has not been used to date to dope **TANI**-amphiphiles; hence, **PA** was chosen. In addition, **PA** also has the largest volume (230.54 Å^3) of all the selected dopants.

The color change from blue to green was a strong indication of the formation of the ES state and confirmed that the **TANI** amphiphiles were doped. This change is caused due to the formation of a polaron species containing cation radicals, which was further confirmed by UV-Vis/NIR absorption spectroscopy. The doping concentration ratio of 2 moles of acid: 1 mole of **TANI-(PTPB)$_2$** allowed protonation of both imine nitrogens of **TANI**. The three characteristic absorbance bands around 300, 400 and 800-1000 nm are attributed to the presence of the **ES** state (π-π, polaron-π* and π-polaron transitions, respectively). However, the absence of any features at 600 nm (associated with the **EB** state) confirmed that the doping process was successfully performed as shown in **Figure 4.46**.

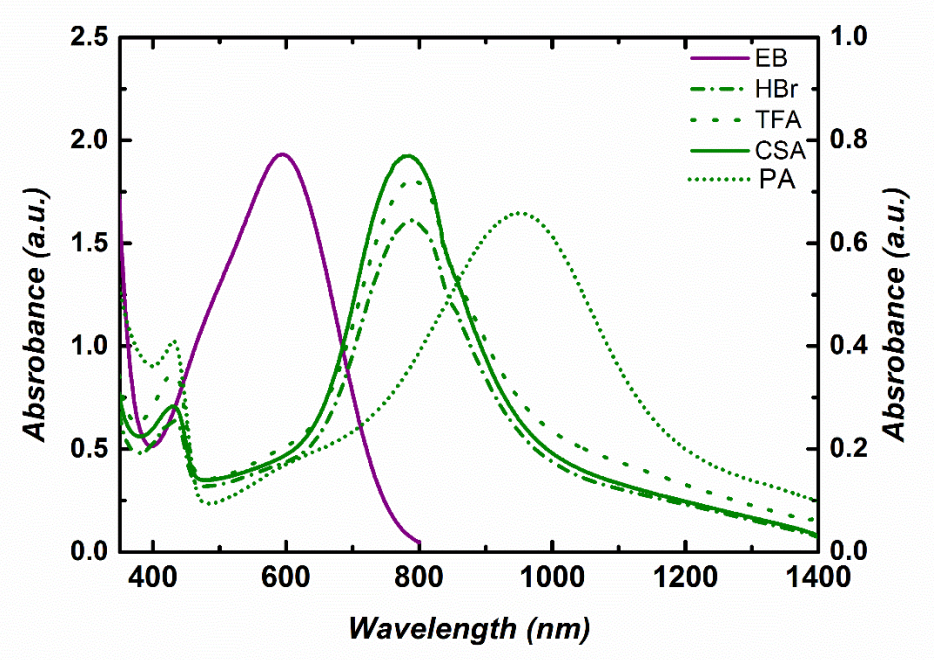

Figure 4.46 UV/Vis-NIR spectra showing **EB TANI-(PTPB)$_2$** and the resultant spectra after doping by various acids in aqueous solutions to form the ES state.

4.2.2.5 Self-assembly studies of ES TANI(HX)$_2$-(PTPB)$_2$

As we showed in our earlier studies of **EB TANI-(PTAB)$_2$**, the addition of a dopant will lead to a change in the self-assembled structures through our APP approach. We also explored the effects of addition of dopant acids of various volumes on the self-assembled morphology. The dopant acid (**HBr, CSA, TFA, PA**) and their volumes are presented in Table 4.2 (**PA** volume was calculated to be 414.56 Å^3). In general, the addition of **acid** to **TANI-(PTPB)$_2$**, leads to increases the volume of **TANI-(PTPB)$_2$**, which in turn increases the packing parameter and causes the morphology changes as seen in case of the single tailed amphiphiles **TANI-PTPB.**

Starting with the smallest volume dopant, **HBr**, TEM showed the predominant morphology to be spherical structures with a 21 nm diameter (**Figure 4.46a**). **TFA** and ***rac*-CSA** have different volumes (75.44 Å^3 and 217.05 Å^3, respectively), but they both produced well-defined spherical

structures with average diameters of 28 nm, as depicted in **Figure 4.47b** and **c**. The diameter is larger than for the structures observed for **EB TANI-(PTPB)$_2$**, which were 20 nm in diameter. However, the bulky acid **PA** doped **TANI-(PTPB)$_2$** formed elongated worm-like micelles, as shown in **Figure 4.47d**. The worm-like micelles are an interesting morphology and inspires us to explore various kinds of acid with either increased size or with multi acidic groups, see future work. Furthermore, due to time limitations we could not explore the tuning behavior in detail for **TANI-(PTPB)$_2$**.

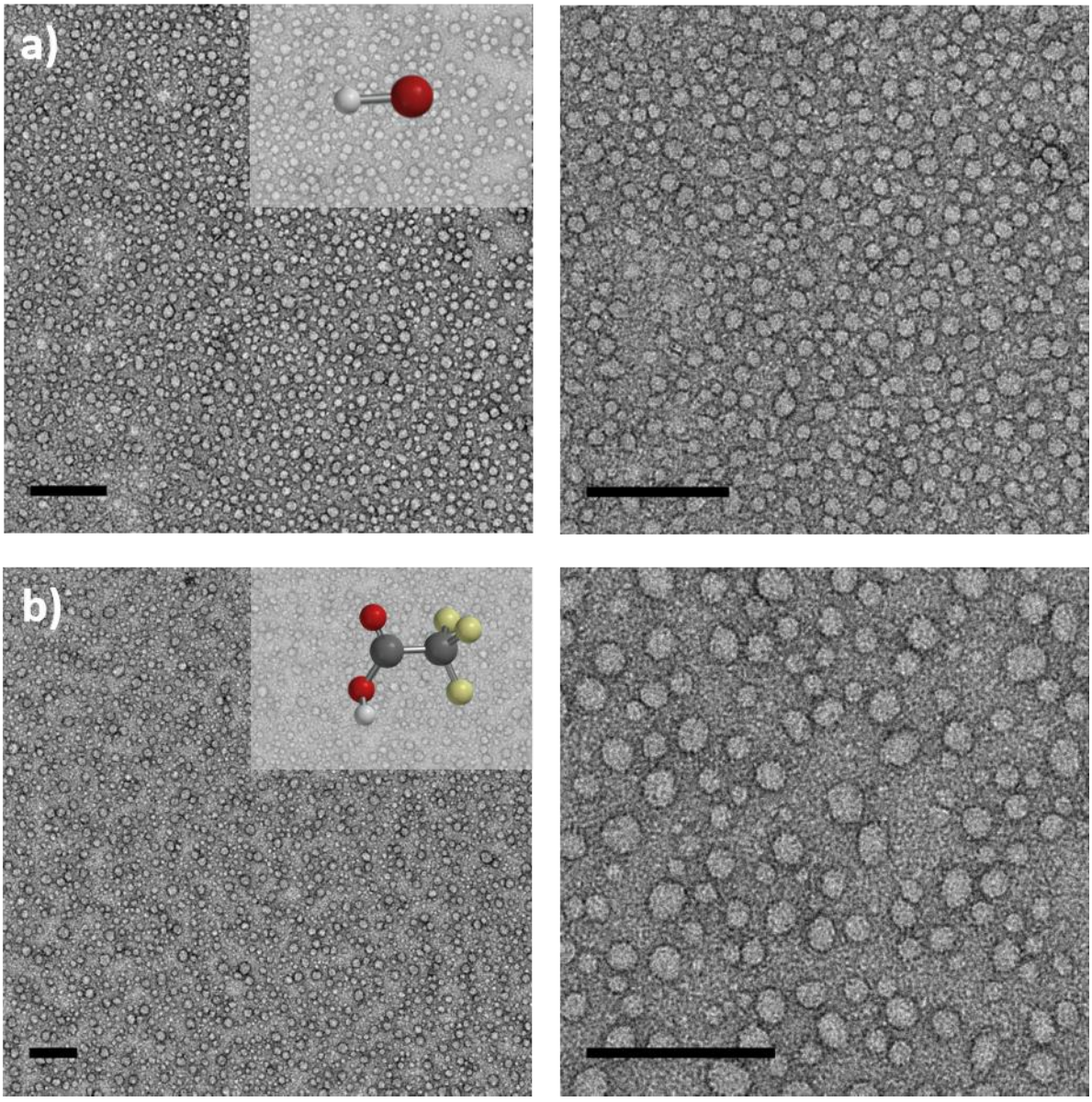

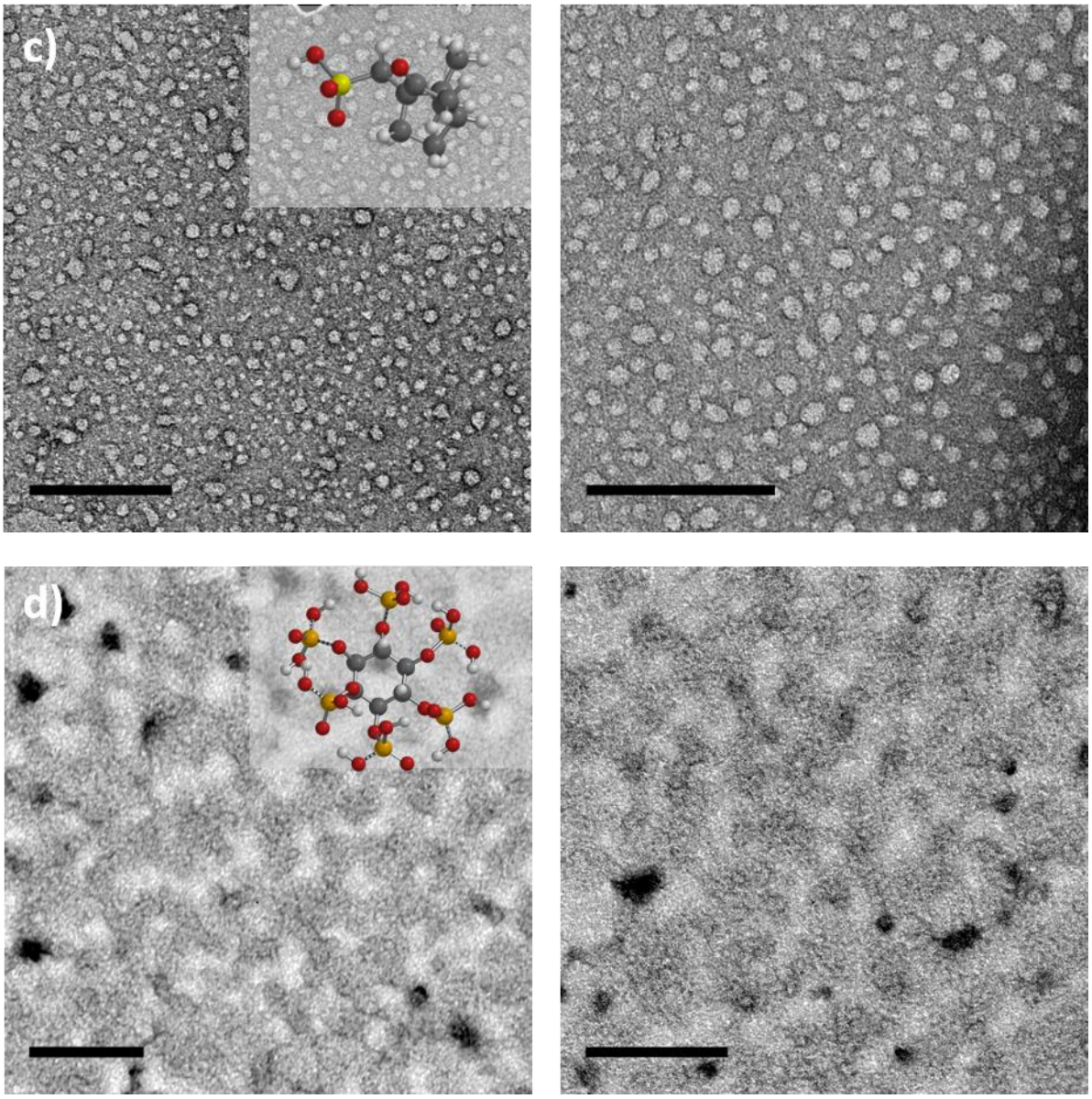

Figure 4.47 TEM images of ES state solutions (1 mM solutions, stained with 1% uranyl acetate) a) **TANI(HBr)$_2$-(PTPB)$_2$** b) **TANI(TFA)$_2$-(PTPB)$_2$**, c) **TANI(CSA)$_2$-(PTPB)$_2$** and d) **TANI(PA)-(PTPB)$_2$**. Scale bars: 200 nm. The images on the right and left side represent the same images at different magnifications.

4.3 Applications

Oligo(aniline)s based amphiphiles are tunable materials that have been used for many applications such as drug release, biosensors and smart coatings owing to their pH-responsive properties and more frequently used for loading and release of drugs or bioactive molecules.[12,40,41,42,43] Specifically, ammonium bolaamphiphiles **EB TANI-(PTAB)$_2$** have been used for drug delivery systems (related to eye infections) and showed significantly improved results when compared to single-tailed amphiphiles (**TANI-PTAB, TANI-PTPB)**. These experiments were carried out by a visiting PhD student from the Shah Schulman Center for Surface Science and Nanotechnology at Dharmsinh Desai University in India. These results from these investigations are currently being prepared for publication.

4.4 Conclusion

New electroactive cationic bolaamphiphiles bearing either two ammonium head groups or two phosphonium head groups were successfully synthesized and the structures confirmed using different characterization techniques. Detailed and comprehensive self-assembly studies of the half-oxidized **EB TANI-(PTAB)$_2$** using TEM, AFM, SAXS, SANS and temperature-dependent UV/Vis and ^{1}H NMR spectroscopy were performed, showing the formation of vesicle-like assembled structures. Using our addressable packing parameter approach APP, develop for single-tailed electroactive amphiphiles, we explored how this concept can be applied to our TANI-based bolaamphiphiles. We introduced a range of dopants with different volumes, structures, and number of acid groups to explore their effect on the formation of varied self-assembled structures. In addition to inducing such structural changes, we also showed the facile and reversible switching of structures, exemplified by reversibly switching structures from well-defined vesicles of 20 nm diameter, to infinitely long 4nm fibre-like structures. We envisage these drastic, but reversible alterations of the morphologies of this electroactive bolaamphiphiles system will open a venue for new applications in a range of related fields, especially in the field of controlled delivery of loaded drug cargoes. We also studied self-assembling behaviors of the half-oxidized **EB TANI-(PTPB)$_2$** using TEM and AFM, showing the formation of vesicle-like assembled structures with average diameter of 20 nm. We also aimed to tune the self-assembled

structures of **EB TANI-(PTPB)$_2$** by introducing a range of dopants with different volumes. The work reported here about **EB TANI-(PTPB)$_2$** represents a very promising start, however more investigations are required.

4.5 Materials and instruments

High-resolution mass spectrometry measurements were carried out on a MicrOTOF II (ESITOF) mass spectrometer. ^{1}H NMR experiments were carried out on either a 400 MHz Varian VNMR 400 or a 500 MHz Bruker NMR spectrometer with CryoProbe, and deuterated solvents were used.

UV/Vis-NIR spectra were measured using a Shimadzu UV2600 spectrophotometer. Due to strong absorbance of the samples the spectra were analysed in a 1mm path length quartz cuvette. Temperature-dependent UV/Vis measurements were measured using a Perkin-Elmer Lambda 35 spectrophotometer with a Peltier temperature controller, preparing 1 mM aqueous solutions in a 1 mm quartz cuvette. Subtracting the baselines from the sample spectra to produce the final spectra. Fluorescence spectra were measured on a Hitachi F-7000 spectrofluorometer, using a cuvette with 10.0 mm path length, with the temperature controlled at 25 °C for all experiments. 10.0 µL of a 0.50 mg/ml pyrene solution in acetone was added to 1000 µL EB TANI-(PTAB)$_2$ aqueous solutions with different concentrations. After sonicating for 10 min, the pyrene emission band (between 360 and 450 nm excited at 337 nm) was recorded for each solution. The CAC was chosen as the concentration where the pyrene showed an apparent decrease in the I_{373nm}/I_{383nm} ratio (denoted as I_1/I_3) with increasing concentration.

FTIR spectra were recorded using a Perkin Elmer Spectrum 100 FTIR spectrometer.

Transmission electron microscopy (TEM) measurements were carried out using a JEOL 1400 TEM with a tungsten filament, performed at 120 kV and equipped with a Orius SC 200 (Gatan) camera using Digital Micrograph GMS 3 image software. High-resolution transmission electron microscopy (HTEM) images were performed on a Field Emission JEOL 2100F TEM, operated at 200 kV and equipped with a Orius SC 1000 (Gatan) camera using Digital Micrograph GMS 3 image software. All TEM samples were prepared by drop-casting of 5 µL of the samples onto carbon-coated copper grids, standing for few seconds (30-90s) then remove the excess using filter paper.

The TEM samples were stained with an aqueous uranyl acetate solution (1 wt. %) and the excess wicked away by filter paper after few second (20s), allowing all the samples to dry at room temperature. Cryo-transmission electron microscopy (cryo-TEM) imaging was carried out using a FEI Tecnai 20 TEM fitted with a LaB6 filament. Samples were prepared by plunge freezing into liquid ethane using a Leica GP freezing apparatus, then transferred under liquid nitrogen into a Gatan 626 cryotransfer holder. Images were recorded on a 4k by 4k FEI Eagle CCD camera.

Atomic force microscopy (AFM) measurements were carried out under ambient conditions using a Bruker Multimode VIII atomic force microscope equipped with a ScanAsyst-HR fast scanning module and a ScanAsyst-Air-HR probe (tip radius, 2 nm), utilizing peak force feedback control. Samples were drop-cast onto either carbon-coated copper grids or freshly cleaved mica.

Small-angle X-ray scattering (SAXS) data were carried out on a Ganesha SAXS/WAXS instrument (SAXSLAB) at room temperature over a Q-range of $0.01 < Q < 0.15$ Å^{-1}. Samples were loaded into borosilicate glass capillaries (Capillary Tube Supplies) and sealed with UV-curable adhesive (Norland Optical Adhesive). Data were collected over an exposure time of 3 hours and blank (water) was subtracted. Data analysis was analysed using SasView.[44]

Small-angle neutron scattering (SANS) data were measured at the ISIS Pulsed Neutron Source using the LOQ small-angle diffractometer. This is a fixed-geometry "white beam" time-of-flight instrument which uses neutrons with wavelengths between 2.2 and 10 Å. Data are simultaneously recorded on two, two-dimensional, position-sensitive, neutron detectors, to provide a simultaneous Q range of 0.008−1.2 Å^{-1}. The sample and background placed in 2 mm path length quartz cells and was measured for a total of 2 hours. The beam diameter was 8 mm. Each raw scattering data set was then corrected for the detector efficiencies, sample transmission and background scattering and converted to scattering cross-section data ($\partial\Sigma/\partial\Omega$ vs Q) using the instrument-specific software.[45] These data were placed on an absolute scale (cm^{-1}) using the scattering from a standard sample (a solid blend of hydrogenous and perdeuterated polystyrene) in accordance with established procedures. The SANS data were fitted to models using SasView.[44]

X-ray diffraction (XRD) data was collected with Cu-Kα radiation (λ = 1.5418 Å) on a Bruker D8 advance powder diffractometer fitted with a 0.6 mm fixed divergence slit, a LynxEye detector was used. Freeze-dried samples were placed onto a silicon wafer

For self-assembly experiments, solutions were prepared by dissolving the required mass of solid either **EB TANI-(PTAB)$_2$** or **EB TANI-(PTPB)$_2$** in ultrapure deionised water and sonicated for 10 min in a bath sonicator to ensure homogeneity. The solutions should be allowed to sit, undisturbed, for 24 hours before analysis.

For doping experiments, acid-doped solutions were prepared by measuring the required mass of solid either **EB TANI-(PTAB)$_2$** or **EB TANI-(PTPB)$_2$**, followed by addition of the appropriate volume of an aqueous solution of the selected dopants to the solid. The appropriate volume of deionised water was added to reach the final concentrations where a doping ratio 2 acid: 1 **TANI**-bolaamphiphiles. The prepared solutions were sonicated for 10 min to ensure homogeneity, and then allowed undisturbed for 24 hours before analysis. All the doped samples were kept in a fridge during the measurement.

4.6 References

1 E. W. Kaler, A. K. Murthy, B. E. Rodriguez and J. A. N. Zasadzinski, *Science*, 1989, **245**, 1371–1374.

2 G. Wu, P. Verwilst, K. Liu, M. Smet, C. F. J. Faul and X. Zhang, *Chem. Sci.*, 2013, **4**, 4486–4493.

3 G. Wu, P. Verwilst, J. Xu, H. Xu, R. Wang, M. Smet, W. Dehaen, C. F. J. Faul, Z. Wang and X. Zhang, *Langmuir*, 2012, **28**, 5023–5030.

4 N. Mizoshita and T. Seki, *Soft Matter*, 2006, **2**, 157–165.

5 E. R. Da Silva, M. N. M. Walter, M. Reza, V. Castelletto, J. Ruokolainen, C. J. Connon, W. A. Alves and I. W. Hamley, *Biomacromolecules*, 2015, **16**, 3180–3190.

6 G. Wang, C. Wang, Z. Wang and X. Zhang, *Langmuir*, 2011, **27**, 12375–12380.

7 B. Song, B. Liu, Y. Jin, X. He, D. Tang, G. Wu and S. Yin, *Nanoscale*, 2015, **7**, 930–935.

8 J. Song, Q. Cheng, S. Kopta and R. C. Stevens, *J. Am. Chem. Soc.,* 2001, **123**, 3205–3213.

9 Z. Zhao, I. A. Banerjee and H. Matsui, *J. Am. Chem. Soc.,* 2005, **127**, 8930–8931.

10 E. Quesada, A. U. Acun and F. Amat-guerri, *Angew. Chem. Int. Ed.*, 2001, **40**, 2095–2097.

11 Y. Jin, N. Qi, L. Tong and D. Chen, *Int. J. Pharm.*, 2010, **386**, 268–274.

12 H. Kim, S.-M. Jeong and J.-W. Park, *J. Am. Chem. Soc.*, 2011, **133**, 5206–5209.

13 Z. Yang, X. Wang, Y. Yang, Y. Liao, Y. Wei and X. Xie, *Langmuir*, 2010, **26**, 9386–9392.

14 O. A. Bell, G. Wu, J. S. Haataja, F. Brömmel, N. Fey, A. M. Seddon, R. L. Harniman, R. M. Richardson, O. Ikkala, X. Zhang and C. F. J. Faul, *J. Am. Chem. Soc.*, 2015, **137**, 14288–14294.

15 R. Yang, D. Chao, H. Liu, E. B. Berda, S. Wang, X. Jia and C. Wang, *Electrochim. Acta*, 2013, **93**, 107–113.

16 C.-W. Lin, S. Aguilar, E. Rao, W. H. Mak, X. Huang, N. He, D. Chen, D. Jun, P. A. Curson, B. T. McVerry, E. Hoek, S.-C. Huang and R. B. Kaner, *Chem. Sci.*, 2019, **10**, 4445–4457.

17 J. Hu, X. Zhuang, L. Huang, L. Lang, X. Chen, Y. Wei and X. Jing, *Langmuir*, 2008, **24**, 13376–13382.

18 C. Wang, Z. Wang and X. Zhang, *Small*, 2011, **7**, 1379–1383.

19 W. Lyu, M. Alotaibi, O. A. Bell, K. Watanabe, R. Harniman, B. M. Mills, A. M. Seddon, S. E.

Rogers, S. M. King, W. Yan and C. F. J. Faul, *Chem. Sci.*, 2018, **9**, 4392–4401.

20 Z. Shao, P. Rannou, S. Sadki, N. Fey, D. M. Lindsay and C. F. J. Faul, *Chem. - A Eur. J.*, 2011, **17**, 12512–12521.

21 E. J. Townsend, M. Alotaibi, B. M. Mills, K. Watanabe, A. M. Seddon and C. F. J. Faul, *ChemNanoMat*, 2018, **4**, 741–752.

22 Y. Yan, W. Xiong, X. Li, T. Lu, J. Huang, Z. Li and H. Fu, *J. Phys. Chem. B*, 2007, **111**, 2225–2230.

23 R. Nagarajan, *Chem Eng Commun*, 1987, **55**, 251–273.

24 Y. Hu, B. T. Miles, Y.-L. D. Ho, M. P. C. Taverne, L. Chen, H. Gersen, J. G. Rarity and C. F. J. Faul, *Adv. Opt. Mater.*, 2017, **5**, 1600458–1600463.

25 I. Kulszewicz-Bajer, I. Rozalska and M. Kurylek, *New J. Chem.*, 2004, **28**, 669–675.

26 F. Würthner, T. E. Kaiser and C. R. Saha-möller, *Angew. Chem. Int. Ed.*, 2011, **50**, 3376–3410.

27 B. M. Mills, N. Fey, T. Marszalek, W. Pisula, P. Rannou and C. F. J. Faul, *Chem. - A Eur. J.*, 2016, **22**, 16950–16956.

28 A. Meister and A. Blume, *Curr. Opin. Colloid Interface Sci.*, 2007, **12**, 138–147.

29 S. Landsmann, M. Luka and S. Polarz, *Nat. Commun.*, 2012, **3**, 1296–1299.

30 N. Nuraje, H. Bai and K. Su, *Prog. Polym. Sci.*, 2013, **38**, 302–343.

31 N. G. Olga Omelchenko , Elena Tomsˇík , Alexander Zhigunov , Olga Guskova , Oxana Gribkova, *Macromol. Chem. Phys.*, 2013, **214**, 2739−2743.

32 M. Mathiselvam, D. Loganathan and B. Varghese, *RSC Adv.*, 2013, **3**, 14528–14542.

33 B. M. Mills, Z. Shao, S. R. Flynn, P. Rannou, D. M. Lindsay, F. Charl, J. Faul and N. Fey, *Mol. Syst. Des. Eng.*, 2019, **4**, 103 – 109.

34 W. Li and H. Wang, *J. Am. Chem. Soc.*, 2004, **126**, 2278–2279.

35 Y. Yan, Y. Zhang, W. Hu and Z. Wei, *Chem. - A Eur. J.*, 2010, **16**, 8626–8630.

36 F. Biedermann, W. M. Nau and H.-J. Schneider, *Angew. Chem. Int. Ed. Engl.*, 2014, **53**, 11158–11171.

37 Q. Tang, J. Wu, X. Sun, Q. Li and J. Lin, *Langmuir*, 2009, **25**, 5253–5257.

38 M. J. Winokur and B. R. Mattes, *Macromolecules*, 1998, **31**, 8183–8191.

39 L. Pana, G. Yub, D. Zhaia, H. R. Lee, W. Zhaod, N. Liue, H. Wangd, B. C.-K. Teec, Y. Shia, Y. Cuid and Z. Bao, *Proc. Natl. Acad. Sci.*, 2012, **109**, 9287–9292.

40 H. Kim, T.-G. Kim and J.-W. Park, *Macromol. Res.*, 2013, **21**, 815–820.

41 T. Kim, C. Kim and J. Park, *Macromolecules*, 2017, **50**, 8185–8191.

42 Y. Wu, S. Liu, Y. Tao, Y. Zhang, J. Xu and Y. Wei, *ACS Appl. Mater. Interfaces*, 2014, **6**, 1470–1480.

43 I. Arioz, O. Erol, G. Bakan, F. B. Dikecoglu, A. E. Topal, M. Urel, A. Dana, A. B. Tekinay and M. O. Guler, *ACS Appl. Mater. Interfaces*, 2018, **10**, 308–317.

44 Www.sasview.org.

45 Http://www.mantidproject.org.

CHAPTER 5 EXPLORING NON-IONIC AMPHIPHILES BASED ON TANI

5.1 Introduction

There has been a growing interest in the synthesis and investigation of block-like structures based on **TANI,** owing to their potential biomedical applications in biosensing and drug release.[1,2,3] The interesting aspect of using **TANI**-based materials in biomedical applications relies on its biocompatibility and biodegradability properties, while the **TANI** block preserves its electroactive properties.[1,4,5,6,7] Moreover, the chemical structure of **TANI** block-like structures can be covalently modified to enhance its physical and optoelectronic properties, including electronic spin states, and solubility, for example. As discussed in the previous chapters, **TANI** precursors have been functionalised with flexible alkyl substituents (which have high solubility) to prepare amphiphilic molecules and, in turn, to provide water solubility to its highly hydrophobic moieties.[6,8]

Structures like block copolymers containing aniline oligomers and PEG chains have been investigated over the past few years.[4,5,6,9] PEG can be directly attached to **TANI**, as shown in **Figure 5.1**, or through various terminal functional groups using different coupling strategies. Furthermore, PEG can be modified to have different terminal functional groups such as –COOH, —SH, $–NH_2$ and OH.[10]

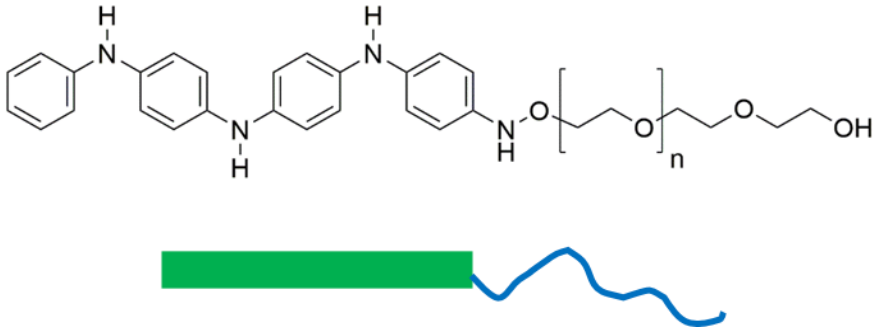

Figure 5.1 Chemical structures of **TANI-PEG.**

Triblock copolymer PEG1500-aniline pentamer-PEG1500 was synthesized by Huang *et al*. These copolymers self-assembled into micelles in alkali aqueous solution, with the size of the

aggregates relying on the oxidation states of the copolymer.[11] Hu et al synthesised mPEG750-aniline pentamer-mPEG750 triblock copolymer, which was able to self-assemble into large aggregates (either large spheres or microspheres) by changing pH or oxidation states.[12] Furthermore, Zhang and Yang prepared a diblock structure, **TANI**-PEG (molecular weight 570), and found that the electroactivity of their diblock structure was similar to that of **TANI**.[13] Yang and co-workers successfully synthesised a triblock copolymer **TANI**–PEO–**TANI** by a condensation reaction. This rod–coil–rod triblock copolymer self-assembled into vesicles, spheres and bowl-like structures at different conditions including pH, various solvents, and copolymer concentration.[14] A **TANI**-containing diblock, **TANI**–PEG, molecular architecture was also prepared by Park *et al*. The self-assembled structure can be switched between vesicles and micelles by applying varying electric potential. The vesicles could be split by applying an oxidising voltage to form puck-like micelles that can regenerate to form vesicles once again by exposure to a reducing agent.[6] The same group also prepared amphiphilic rod-coil polymers containing **TANI** and PEG blocks, **TANI**-PEG-**TANI**. They investigated the effect of solvents on the electrochemical activities of the block oligomer.[5] We expect that a diblock structure comprising biocompatible and biodegradable moieties (PEG) and biocompatible moieties (**TANI**) might open doors to explore innovative aspects of several applications, especially in drug delivery.[15,16]

Here we provide the synthetic pathway to design non-ionic **TANI**-based amphiphiles with slightly different architectures: Boc **TANI(CO)-TEG** and Boc **TANI-TEG**. Furthermore, we investigated the effect of these variations in structure on the self-assembling behaviour of **TANI**-based materials. It is noteworthy that the published papers in which diblocks of **TANI**-PEG were prepared have not explored the effect of doping. Hence, we will attempt to remove the Boc protecting groups and investigate the effect of dopants on the electroactivity and self-assembly of the prepared materials.

5.2 Results and Discussion

5.2.1 Synthesis of Boc Ph/NH_2 TANI

As a PEG chain is used to functionalise Ph/NH_2-capped **TANI**, this reactive **TANI** precursor was initially synthesised. Ph/NH_2 **TANI** is generally made *via* an oxidative route, but this method still presents issues in terms of the purity and stability. Hence a Boc-protected Buchwald-Hartwig amination route was used, based on that reported by Chen *et al*.[17] This method allows for a controlled, step-by-step preparation of fully Boc-protected Ph/NH_2 **TANI** in the LEB state in high purity and stability. Boc Ph/NH_2 **TANI** was prepared by a reported method[8] and confirmed by ^{1}H NMR spectroscopy, mass spectrometry and elemental analysis, the details of which are available in **Chapter 2**.

5.2.2 Synthesis of TANI-PEG

Several coupling strategies and methods were trialed to prepare block-like structures comprising **TANI** as the rigid block and PEG chains as the flexible tail. Due to the lack of reactivity between alcohol and amine groups, catalysts have been employed to facilitate this reaction. As mentioned earlier, there are reports on the synthesis of **TANI** terminated with several lengths of PEG chains using different coupling agents. Particularly, toluene diisocyanate (TDI) was used in different publications with different conditions.[13,14] Following the reported procedure,[13] TDI was coupled to the PEG (MW= 350) chain and then subsequently to LEB Ph/NH_2 **TANI**, as shown in **Scheme 5.1**. TDI is a good coupling agent owing to the presence of a methyl group, which increases the reactivity of the *para*-position in -NCO group. The increased activity of the 4-NCO group allows initial nucleophilic addition of PEG-350 to this position, followed by a subsequent reaction with **TANI** in the 2-NCO position to give the final diblock product.[13]

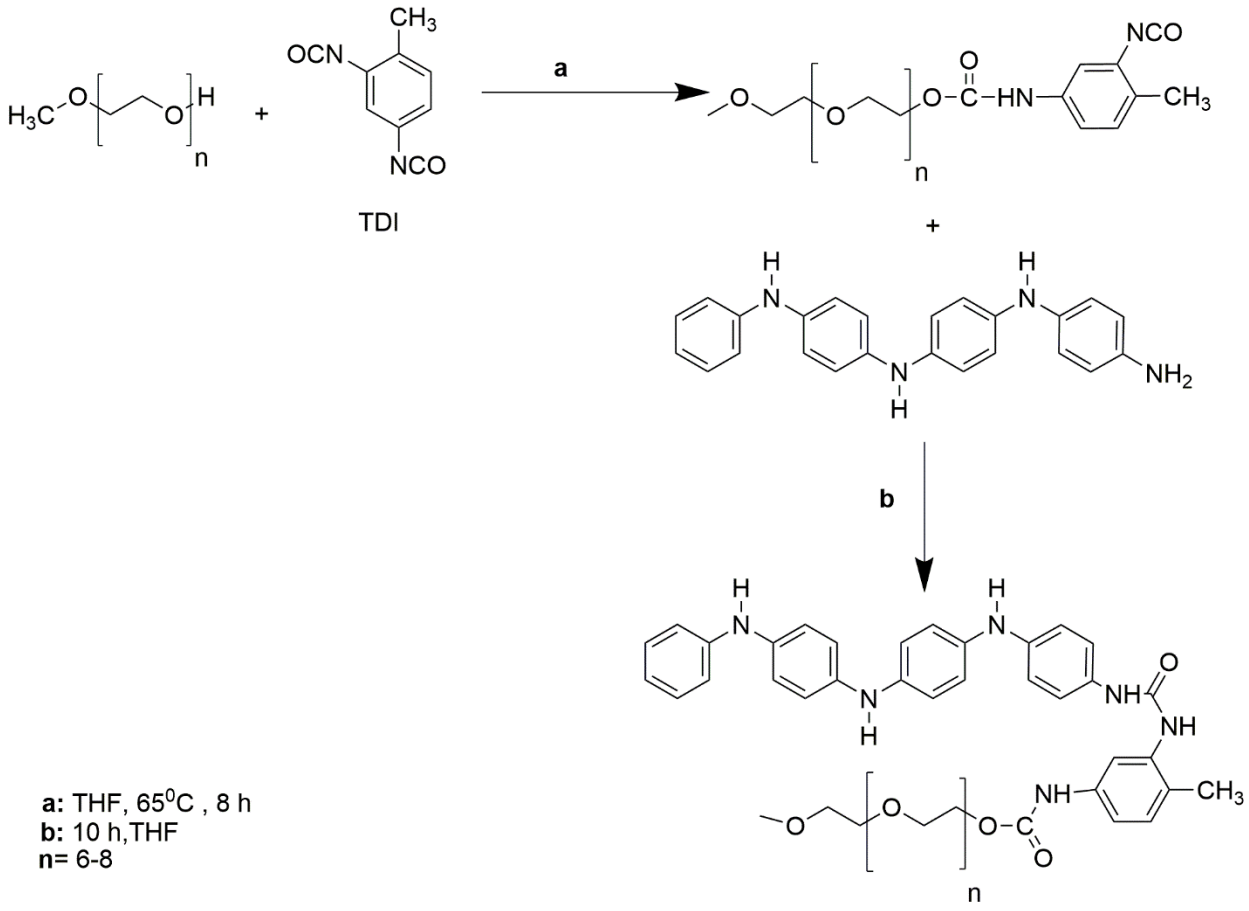

Scheme 5.1 Coupling reaction of LEB **TANI** and PEG350 using TDI.

This reaction was successful, with MALDI mass spectrometry showing the product is formed as shown in **Figure 5.2**. According to the MALDI spectrum, a wide molecular weight distribution for the LEB **TANI-mPEG** 350 couple is observed, as shown in **Figure 5.2**. These distributions are due to the polydispersity of the starting material (mPEG350). However, mass spectroscopic characterisation indicates unreacted LEB **TANI** is present at m/z = 366.2. Several unreacted materials (**TANI**) were also observed, and ^{1}H NMR also showed the presence of impurities potentially from the previous reaction. It was not immediately obvious how many units of PEG chains coupled to **TANI**, because of the interference between the signal of water in the solvent (dimethyl sulfoxide, DMSO) and ethylene group in PEG chain (**Figure 5.3**). From the ^{1}H NMR spectrum (**Figure 5.3**), the interpretation of the data can be challenging due to the instability of the diblock **TANI** in the LEB state, resulting in a mixture of oxidation states. It is clear that some

unreacted TANI is also present, confirmed by the presence of the signal at 4.64ppm. This signal is ascribed to the terminal amine protons of Boc Ph/NH_2 **TANI.** Furthermore, the integration does not match to what we expected to observe, as there is residual unreacted mPEG350 and **TANI** present, accounting for the presence of the peak at δ = 3.42 as well as the slightly higher than expected integrations of the peaks at δ = 3.23 and δ = 3.50. The NMR solvent and water peaks were present, as shown in **Figure 5.3**. Furthermore, column chromatography (silica gel, 10:1 chloroform: methanol) was attempted to purify the product. As the stability of the LEB state was poor, it rapidly oxidises to attain a mixture of LEB and EB states, resulted a mixture of LEB and EB states. Purification of the EB state material by column chromatography caused a degradation of the product, as a result of the lability of quinoid C=N-C groups to hydrolysis by silica gel.

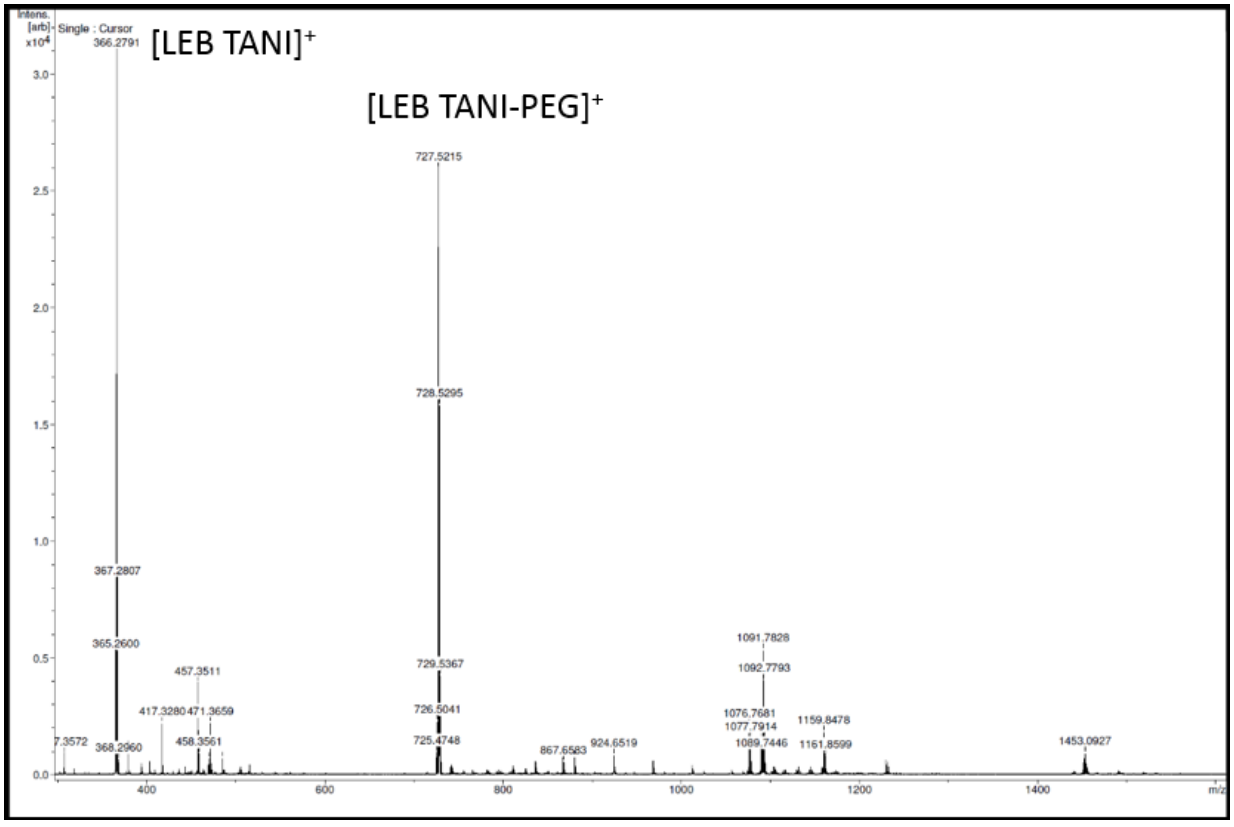

Figure 5.2 MALDI-TOF mass spectrum analysis of LEB **TANI-mPEG350**.

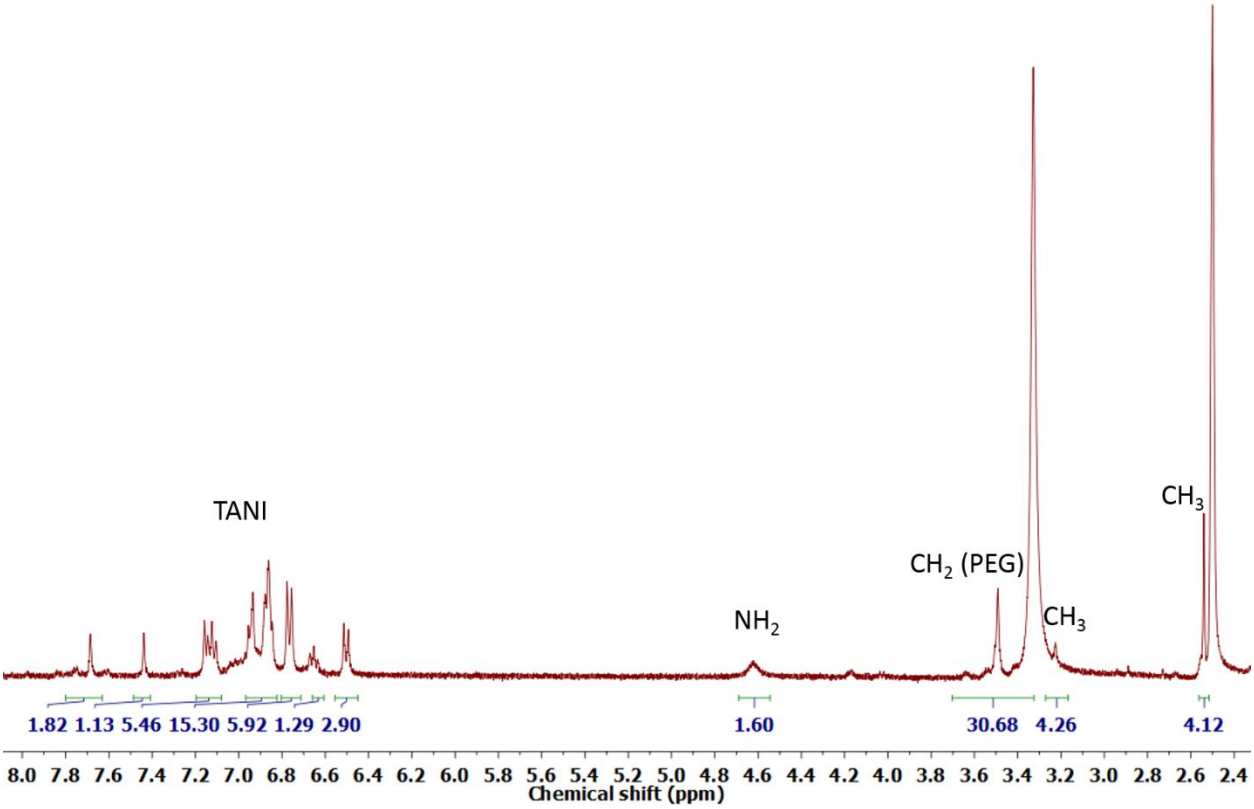

Figure 5.3 ^{1}H NMR spectrum of LEB **TANI-mPEG350**.

The coupling reaction was previously attempted with the LEB Ph/NH_2 **TANI**; however, it was difficult to purify the product, as it is well known that **TANI** in the LEB state rapidly oxidises to attain a mixture of LEB and EB states. Therefore, the use of Boc **TANI** was explored to functionalise **TANI** with PEG, as Boc **TANI** is easier to handle and, once the desired pure product is obtained, the Boc groups can be easily removed.

Interestingly, the same conditions of the previous coupling reaction were used, but it was found that the product does not form without a catalyst (DMAP), as shown in **Scheme 5.2**. TEA and DMAP were added and the reaction time was extended (from 8 to 24 hours), due to the low basicity of Boc **TANI**. The formation of the desired product was confirmed by TLC (ethyl acetate: hexane 1:1). On workup, hexane was added to the reaction mixture, allowing precipitation of Boc **TANI-mPEG**. Mass spectrometry and ^{1}H NMR revealed complicated spectra with the presence of some unreacted materials and impurities. Column chromatography (silica gel, 1:1 ethyl acetate:

n-hexane) was used to purify the desired product resulting in impure product with poor yields (20%).

As TDI is considered as a toxic and carcinogenic reagent, the use of another isocyanate, 4,4'-diphenylmethane diisocyanate (MDI), was explored (which worked in a similar way to TDI as well as being a non-carcinogenic material). MDI is an aromatic isocyanate and more reactive than aliphatic or cycloaliphatic isocyanates. It is *para*-substituted, so is more reactive than *ortho* or *meta* substitution. MDI was used as the coupling agent and the same reaction conditions applied as used in the MDI reaction.

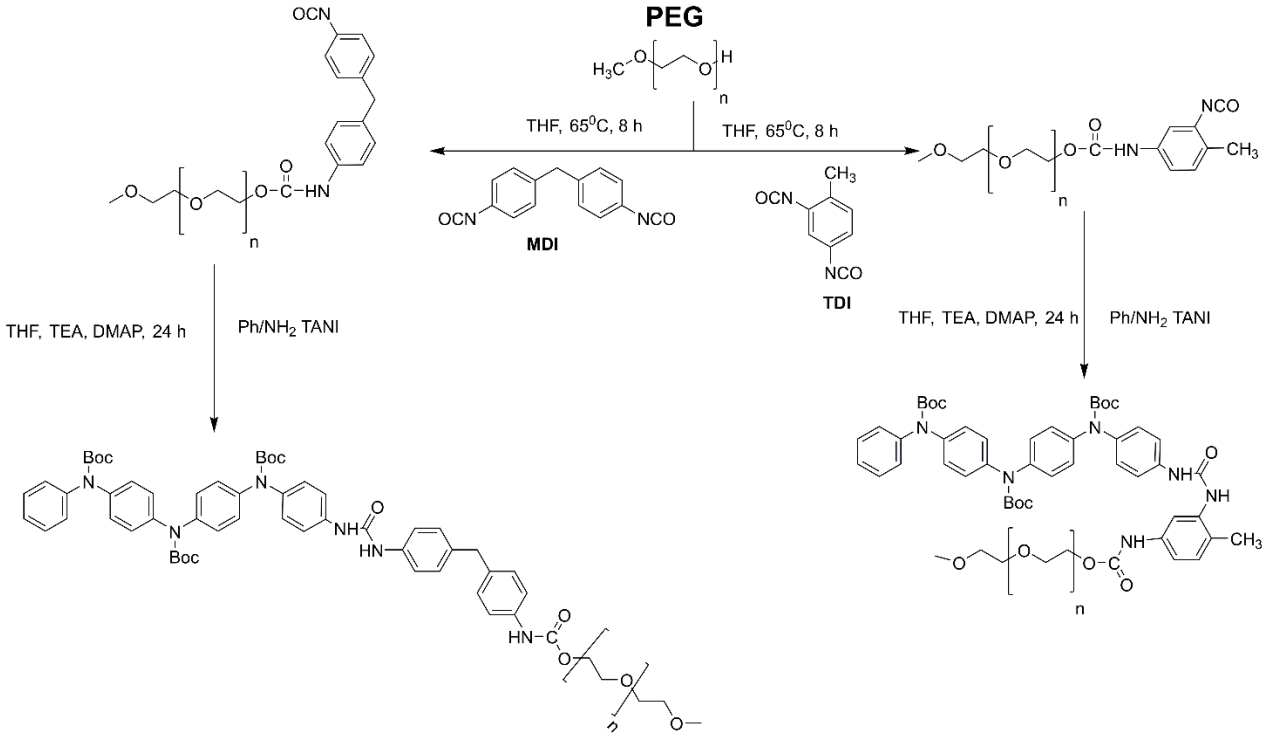

Scheme 5.2 Coupling reaction of Boc **TANI** and PEG-350 using TDI and MDI.

MDI has a linear structure, but there are many possible side reactions that might take place, due to the presence of two reactive *para*-substitutions as demonstrated by the NMR data. In case of this experiment, the workup was performed by taking up the reaction mixture into deionised water and the resulting precipitate was filtrated then washed by diethyl ether and dried over anhydrous $MgSO_4$. ^1H NMR investigations (**Figure 5.4**) confirmed the formation of the desired

product (Boc **TANI-mPEG**) with the presence of some side reactions (MDI bearing two PEG groups) and unreacted **TANI**. Furthermore, the integrations of each signal (Boc groups, PEG and **TANI**) did not match to what we expected to observe, as there is unreacted starting materials mPEG350 and **TANI** present. Purification to remove these undesired materials of the MDI coupling reaction was required. Column chromatography (silica gel, 1:1 ethyl acetate: n-hexane) was used to purify the desired product resulting in a compound with poor yields (25%). However, ^{1}H NMR spectrum still showed some side reactions (MDI bearing two PEG groups) and starting materials present (**TANI**).

PEG with a hydroxyl end is not reactive enough to couple with **TANI**, hence, the modification of the PEG hydroxyl group to other more reactive or suitable functional groups, such as carboxylic acid, for coupling with **TANI** would be suggested. Furthermore, in order to obtain well-defined and controlled structures, we attempted to use a short unit of PEG, hence, triethylene glycol (TEG) was selected. In the next section, routes to modify TEG are described, which should enable coupling of TEG with **TANI**.

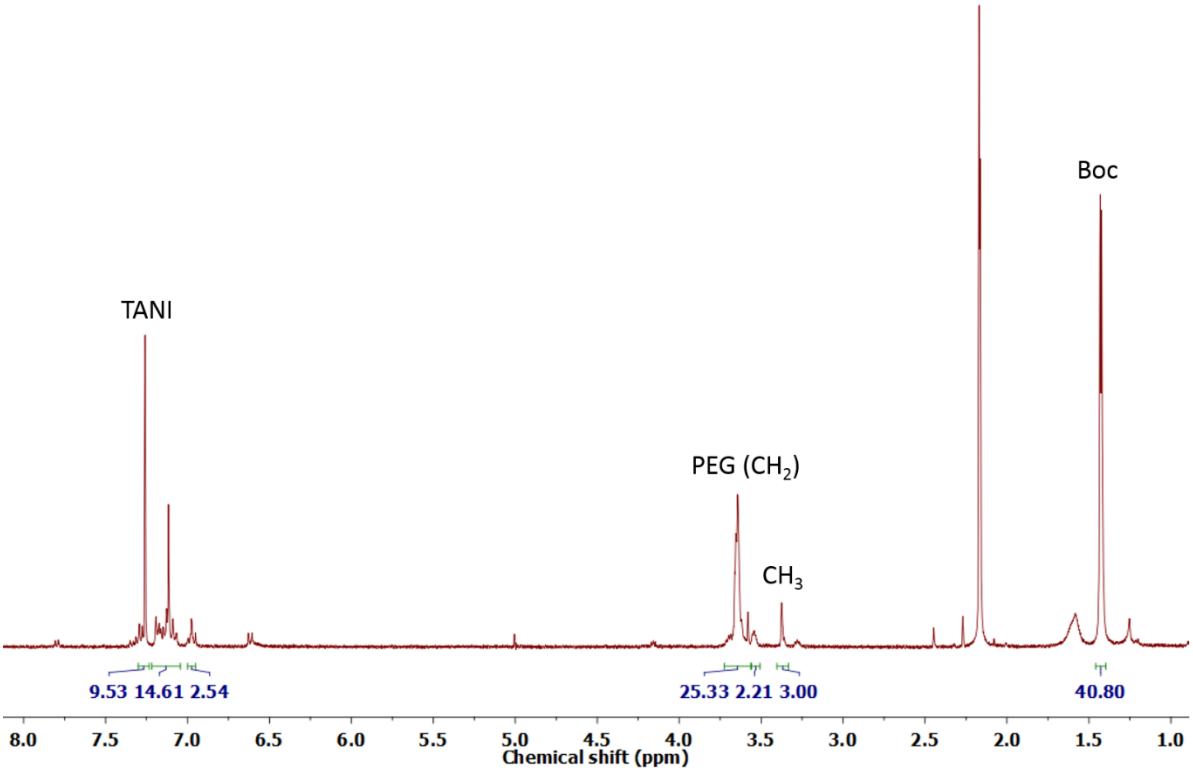

Figure 5.4 ^{1}H NMR spectrum of Boc **TANI**-mPEG350 using MDI.

Triethylene glycol (TEG, Mw = 164) is a short unit of PEG and possesses one hydroxyl end group, and was selected to be modified with different terminal groups. There are routes available to convert the hydroxyl group to good leaving groups, such as tosylated TEG and succinylated TEG. These groups simplify the reaction between **TANI** and TEG, as shown in **Scheme 5.3.** Two different architectures were designed and synthesised depending on the coupling agents, as depicted in **Scheme 5.3**.

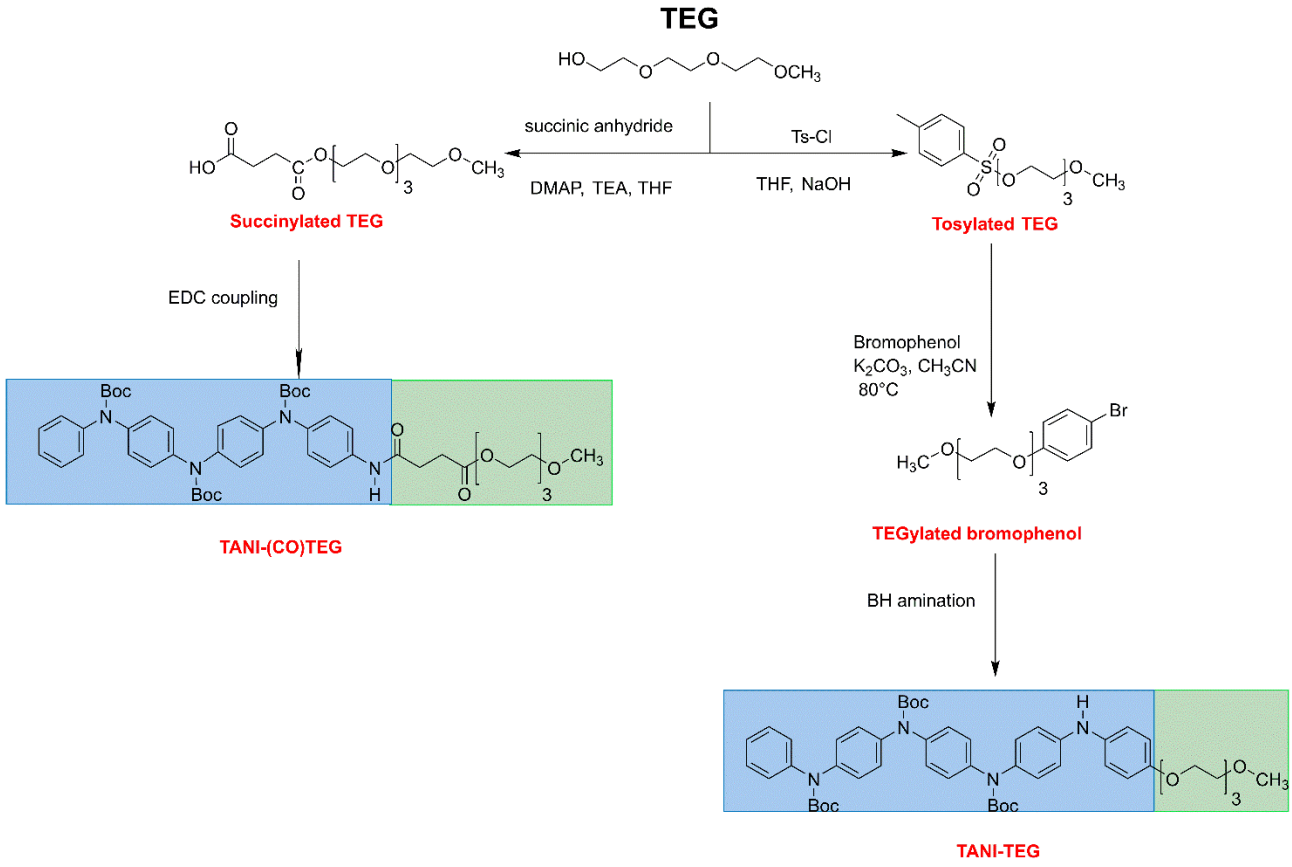

Scheme 5.3 The synthetic routes to modify TEG and then coupled with Boc **TANI**.

5.2.2.1 Coupling of succinylated TEG with Boc Ph/NH_2 TANI

Succinylation of TEG was carried out by a reported method[18] as shown in **Scheme 5.3**; the hydroxyl end group of the TEG was first transformed into carboxylic groups before coupling with **TANI**. This reaction was conducted under nitrogen at room temperature with DMAP present as a catalyst. Furthermore, the most common activating agents for PEG were 1-ethyl-3-(3-dimethylaminopropyl) carbodiimide (EDC), dicyclohexylcarbodiimide (DCC) and N-hydroxysuccinimide (NHS). Succinylated TEG acid, (4-(2-(2-(2-hydroxyethoxy)ethoxy)ethoxy)-4-oxobutanoic acid), can easily couple with **TANI** through EDC coupling, as depicted in **Scheme 5.4**. Synthesis of functionalised Boc **TANI** with the TEG head group was prepared successfully and the reaction was monitored by TLC (1: 1 ethyl acetate: n-hexane) and using bromocresol green as a

staining agent (which is used to detect any excess acidic compound, to ensure the consumption of starting materials). However, TLC showed the formation of the final product as well as the presence of the starting materials (**TANI**). Column chromatography (silica gel, 5:1 ethyl acetate: n-hexane) was used to purify the desired product resulting in pure compound with moderate yields (45%). The formation of the desired product was confirmed by mass spectrometry (**Appendix E**, **Figure E2**) and ^{1}H NMR (**Figure 5.4**). The signals at 7.10-7.54 ppm are ascribed to aromatic protons, while the signal at 1.41 ppm is attributed to methyl protons of the Boc groups. The signal of the terminal amine protons of Boc Ph/NH_2 **TANI** disappeared when the attachment of the TEG chain occurred successfully, to now produce a signal at 8.44ppm. This signal is attributed to the proton in the amide group as well as the presence of the protons of the ethylene groups of TEG at 3.42-4.20ppm.

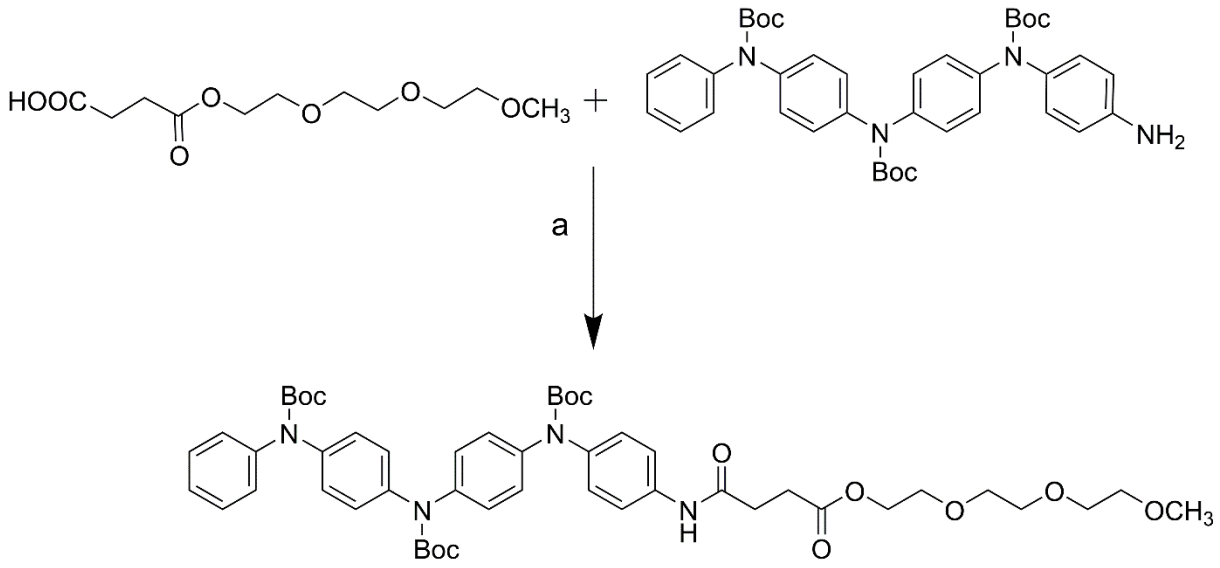

a: 0^{o}C-room temperature

EDC, CH_2Cl_2

Scheme 5.4 Synthesis of coupled succinylated TEG with Boc Ph/NH_2 **TANI**.

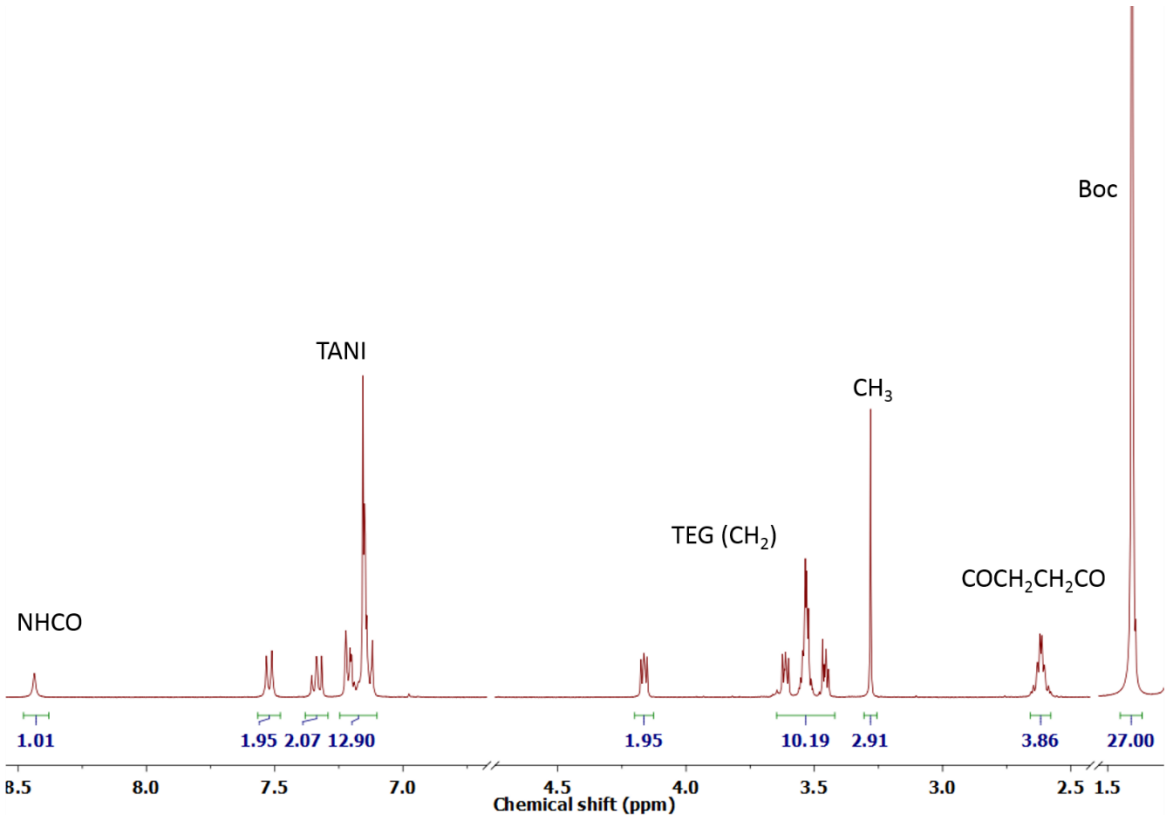

Figure 5.5 ^{1}H NMR spectrum of **TANI(CO)-TEG**.

5.2.2.2 Coupling of TEGylated bromophenol with Boc Ph/NH$_2$ TANI

A further interesting architecture based on a diblock structure was **TANI** bearing TEG without the presence of an amide linker (and thus less opportunities for intermolecular hydrogen bonding). Since tosylate is a good leaving group, tosyl chloride would be used to convert an alcohol to a tosyl ester, which would then be the desired product exploited for nucleophilic substitution reactions. Tosylation of TEG was carried out using a reported method[19] via nucleophilic substitution (S_N2), as shown in **Scheme 5.5**. In order to exploit the success of the Buchwald-Hartwig (BH) reaction, an S_N2 reaction of tosylated TEG and bromophenol were carried out using a reported method.[20] These TEG-functionalised aryl halides, as shown **Scheme 5.3**, were subsequently reacted with **TANI** using Pd-catalysed amination, as shown in **Scheme 5.5**. Boc **TANI** was coupled with TEGylated bromophenol in the presence of toluene as the solvent and XPhos

as the catalyst. The functionalisation of Boc **TANI** with the TEG head group using a BH reaction was monitored by TLC (silica gel, ethyl acetate: n-hexane 1:1). TLC showed the formation of the final product as well as the presence of the starting materials. Column chromatography (silica gel, 5:1 ethyl acetate: n-hexane) was performed to purify the mixture and yield the desired product. The desired product was obtained in moderate yield (60%). Details of this reaction are provided in the experimental section. The purity of the final product was confirmed by ^{1}H NMR (**Figure 5.5**). The signals at 6.81 -7.31 ppm are ascribed to aromatic protons, whilst the signal at 1.42-1.57 ppm is attributed to Boc groups. The signal of the terminal amine protons of Boc Ph/NH_2 **TANI** disappeared when the attachment of the TEG chain occurred successfully to yield a signal at 5.48ppm, which is attributed to the proton in the primary amine group as well as the presence of the protons of the ethylene groups of TEG at 3.54-4.11 ppm.

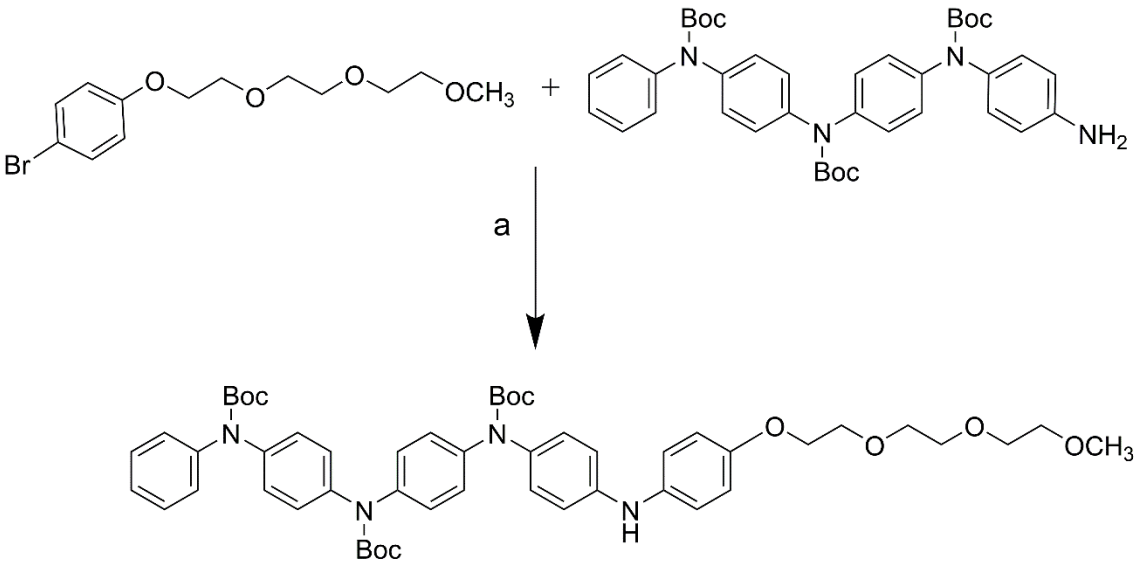

a: XPhos, $Pd(dba)_2$
NaOBt, toluen, 110^{o}C

Scheme 5.5 Synthesis of TEGylated bromophenol with Boc Ph/NH_2 **TANI**.

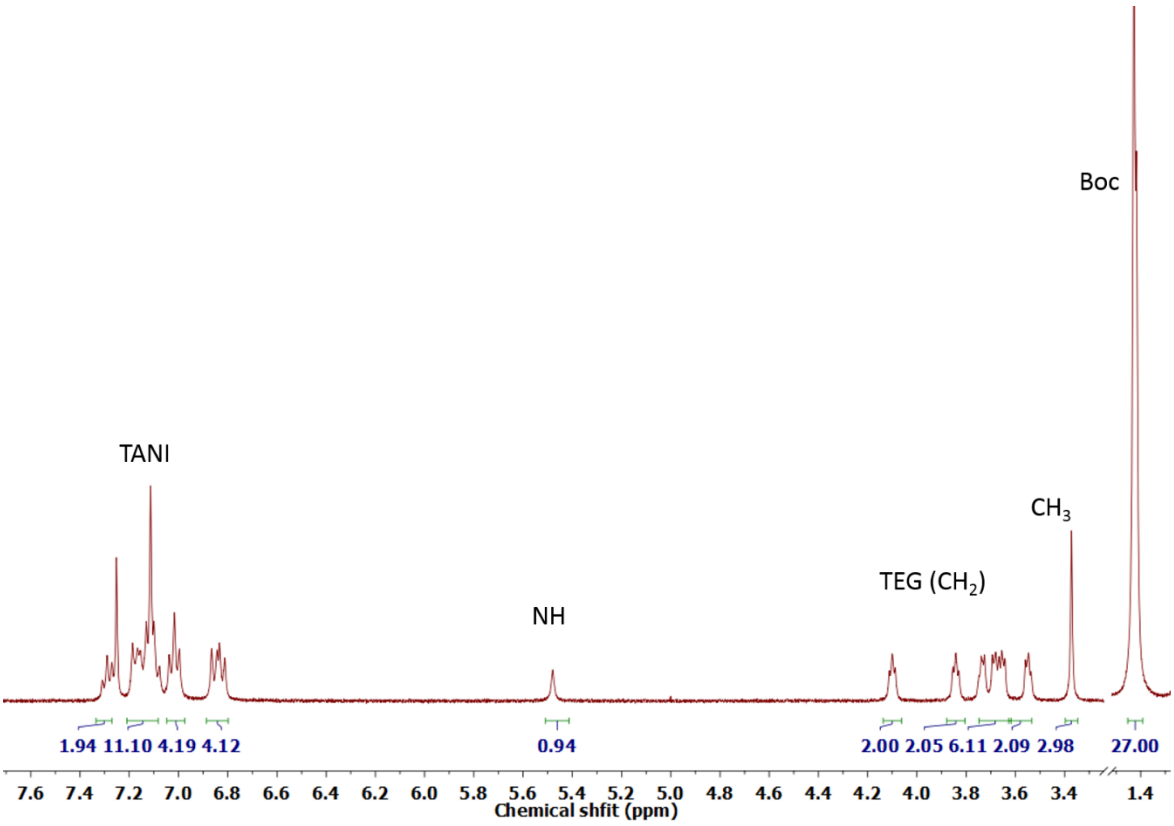

Figure 5.6 ^{1}H NMR spectrum of Boc **TANI-TEG**.

5.2.3 Self-assembly studies

Initially, we examined the self-assembled structures of the two architectures (**TANI-(CO)TEG**, and **TANI-TEG**) of the **TANI**-based amphiphile in the presence of Boc groups. **TANI** bearing 10 units or less of ethylene glycol could be dissolved in aqueous solution at concentrations below 0.05wt%.[6] Hence, **TANI-(CO)TEG** and **TANI-TEG** were dissolved into 0.05 wt%, 1: 5 water: THF. As expected, the presence of the groups capable of hydrogen bonds in **TANI-(CO)TEG** might have had an impact of inducing π-π stacking interactions and forming rod-like structures of 380 nm width (**Figure 5.7a**); however, **TANI-TEG** showed a spherical-like structure with an average diameter of 250 nm, as depicted in **Figure 5.7b**.

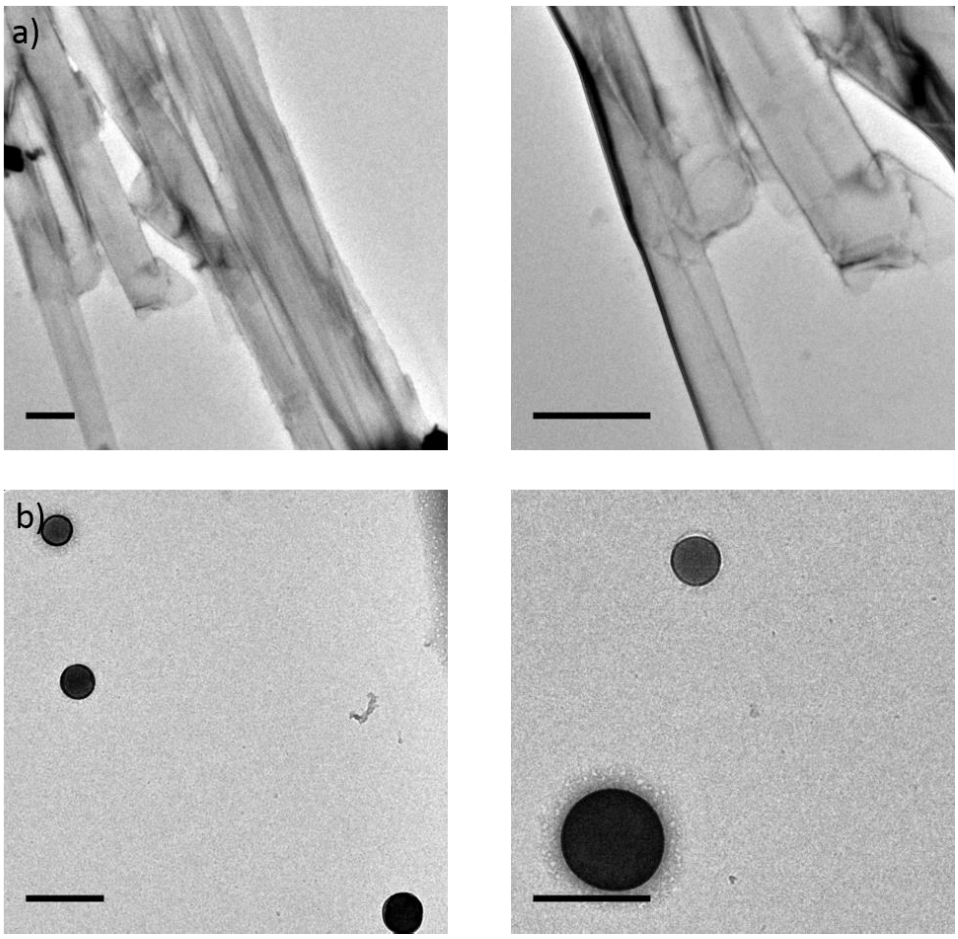

Figure 5.7 TEM images of 1:5 water: THF solutions, a) Boc **TANI-(CO)TEG** and b) Boc **TANI-TEG**. Scale bar=500nm. The images on the left and right side represent the same images with different magnifications.

5.2.4 Some obstacles to deprotect TANI functionalised with TEG

5.2.4.1 Deprotection of Boc groups in TANI-(CO)TEG

Cleavage of the Boc group can be achieved with a strong acid, Lewis acid or by exposing the protected molecule to high temperatures. The most effective method uses a strong acid, such as trifluoroacetic acid (TFA); however, **TANI** is likely to interact with acid, possibly generating a mixture of different oxidation states. Hence, trimethylsilyl iodide (TMSI) was selected for deprotection and the reaction was carried out under nitrogen in order to prevent any oxidation.

5.2.4.2 Using TMSI

TMSI was found as an effective reagent to remove Boc groups. Deprotection of Boc **TANI-(CO)TEG** was carried out by a reported method,[8] as shown in **Scheme 5.7**.

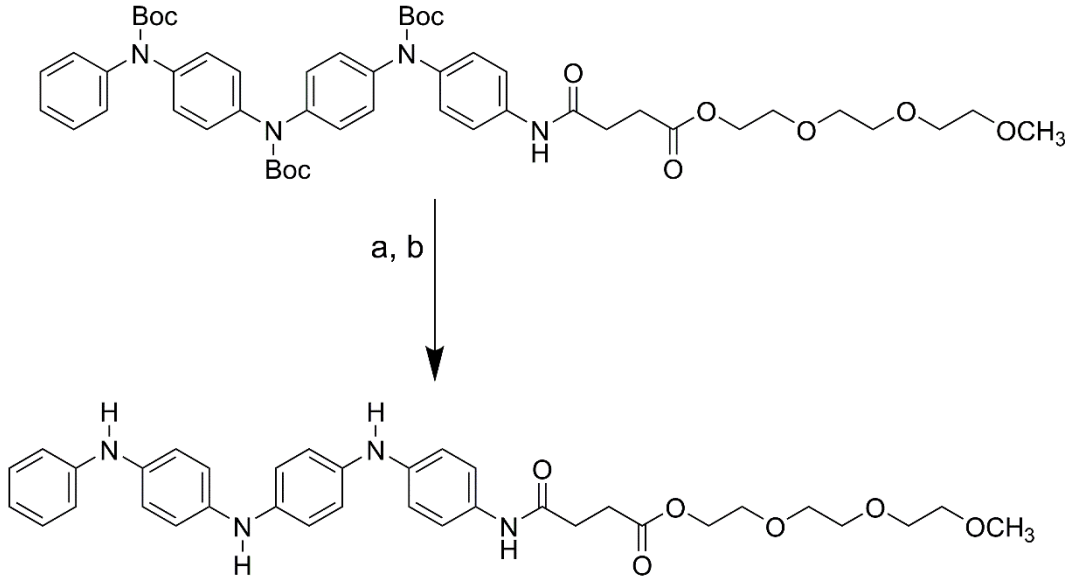

a: TMSI, CH_2Cl_2, 2h

b: MeOH, TEA

Scheme 5.6 Deprotection reaction of Boc **TANI-(CO)TEG.**

Due to the low solubility of the final product in DCM, toluene was used instead. However, LEB **TANI**-TEG was found to be partially soluble in toluene, hence, hexane was added to precipitate all the crude product. The proposed mechanism of this reaction is shown in **Scheme 5.7** below. The mechanism proposed for this cleavage is the reaction of alkyl esters with trimethylsilyl iodide. This mechanism involves two main steps; the first is the fast reversible formation of intermediate (**1**) from the complexation of the trimethylsilyl group with the carbamate. The intermediate can then continue ***via*** an S_N1 or S_N2 process to form the trimethylsilyl carbamate (**2**) and alkyl iodide (**3**). The second step is addition of methanol to cleave the oxygen-silicon bond of the trimethylsilyl carbamate to yield the carbamic acid (**4**) and methyl trimethylsilyl ether (**5**)**.** Carbamic acid will spontaneously decarboxylate to leave the desired product (**6**) and other byproducts removed

during workup. However, after the workup procedure, mass spectrometry and ^{1}H NMR were carried out to confirm the presence of the desired compound. According to mass spectrometry, there was a mixture of starting material and impurities present as well as the final product, as shown in Figure **TANI-(CO)TEG or TANI-TEG** (**Figure 5.8** and **5.9**), respectively. A proposed mechanism of the formation of these unexpected compounds is presented in **Scheme 5.7**. It was found that alkyl methyl ethers (TEG) also react with trimethylsilyl iodide to afford the silylated oxonium iodide (**7**) in a fast and reversible process. The silylated oxonium iodide can then proceed to **8** and **9** ***via*** an S_N1 or S_N2 process. From this perspective, this method is not suitable for TANI functionalised with PEG groups.

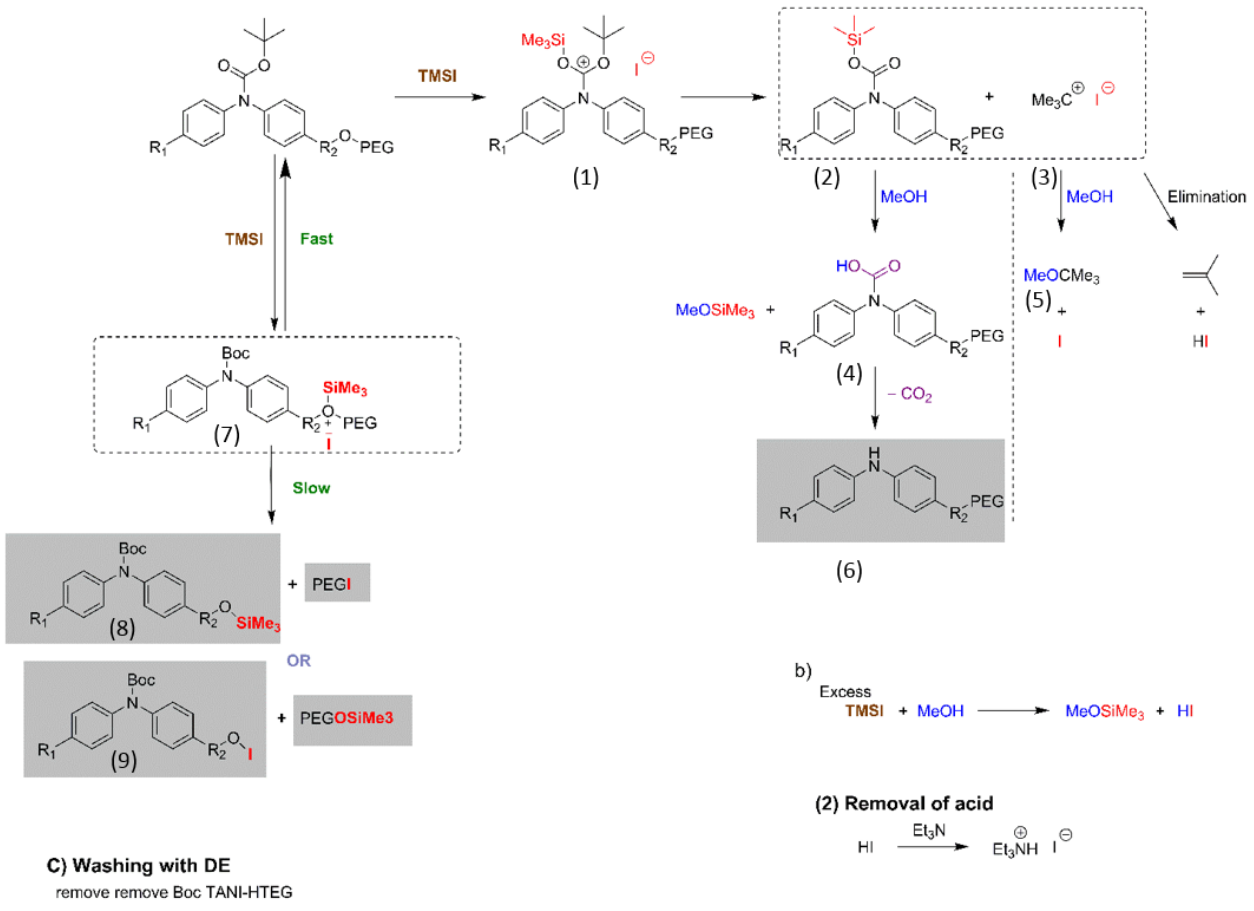

Scheme 5.7 Proposed mechanism of deprotection of Boc **TANI-TEG** using TMSI.

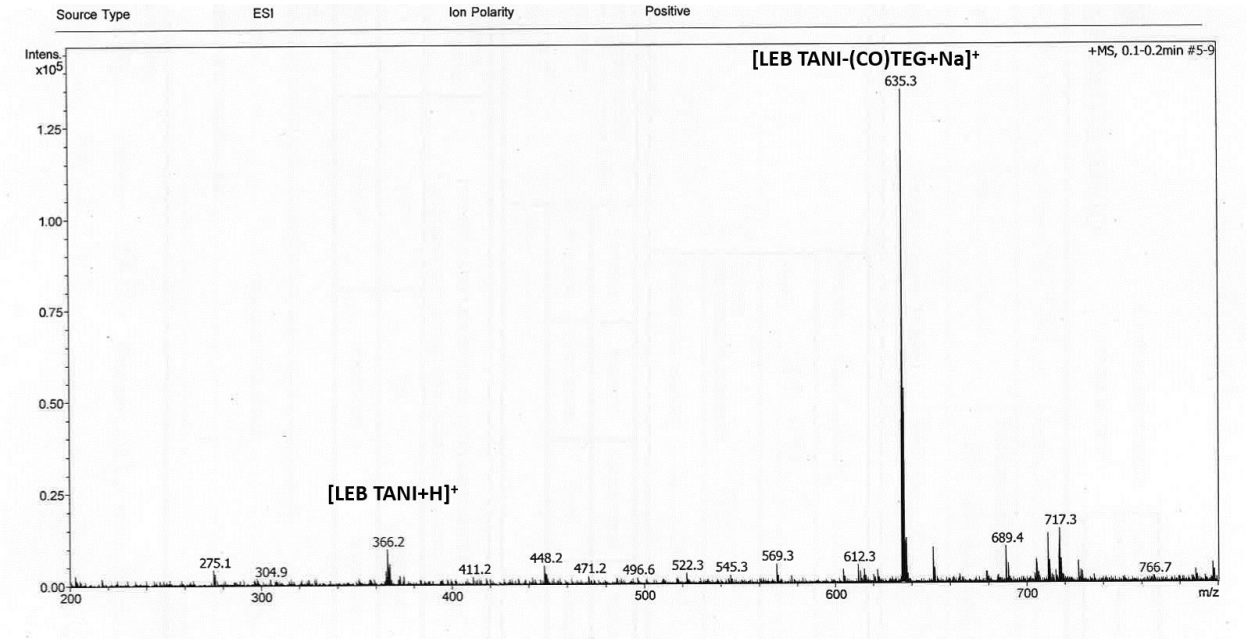

Figure 5.8 ESI mass spectrum analysis of **LEB TANI-(CO)TEG**.

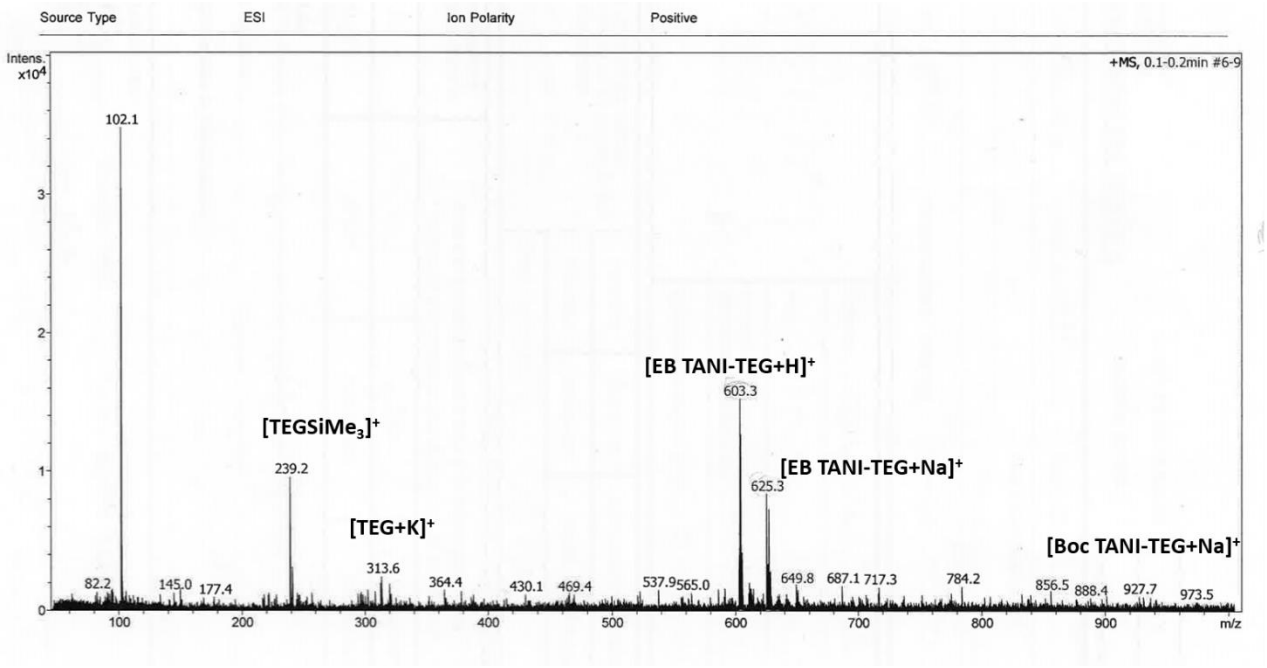

Figure 5.9 ESI mass spectrum analysis of **LEB TANI-TEG**.

Using TFA

TMSI was not suitable for materials containing TEG chains, hence, the option of using TFA for deprotection was explored. As mentioned earlier, TFA is a more successful reagent to remove Boc groups; however, it presents a challenge with **TANI** due to the potential to form a mixture of oxidation states. As the resultant LEB product is highly unstable, it rapidly oxidises to attain a mixture of LEB and EB states. EB product is immediately protonated to form the ES state product. This issue can be overcome by de-doping using a base. However, this procedure was not suitable for **TANI**-PEG materials as is explained in the proposed mechanism shown in **Scheme 5.8** below. The mechanism proposed for this cleavage involves the protonation of tert-butyl carbamate by TFA (**1**), followed by loss of the tert-butyl cation, yielding a carbamic acid (**3**). Decarboxylation then results in the free amine (**4**). However, it was found that TEG can be cleaved completely by acid (**6**,**8**), as shown in the **Scheme 5.8**. Overall, the mentioned methods to cleave Boc groups are not suitable for **TANI-(CO)TEG** and **TANI-TEG.** Due to limitation of time and materials, we were not able to perform more trial experiments in order to remove Boc groups. However, some suggestions to cleave the Boc groups will be considered in the future work.

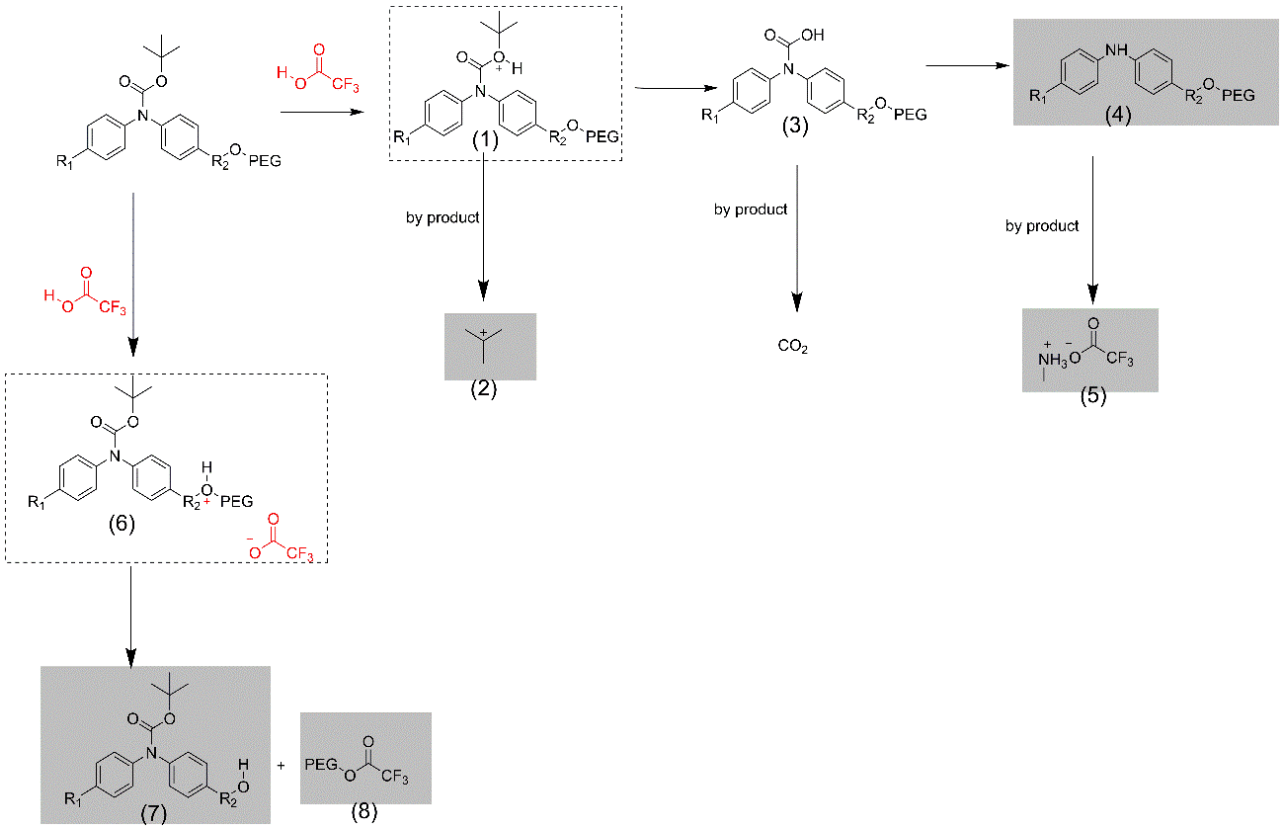

Scheme 5.8 Proposed mechanism of deprotection of Boc **TANI-TEG** using TFA.

5.3 Conclusion

This chapter shows some suggested methods that have been used to synthesize tetra(aniline) non-ionic amphiphiles following some reported papers. Furthermore, none of these methods provide pure **TANI-PEG** materials with moderate yield. We describe in detail the stepwise synthesis of a pure TANI-TEG material using two strategies: EDC coupling and B-H amination. We successfully synthesised Boc **TANI** functionalised with TEG and forming two architectures, Boc **TANI-(CO)TEG** (with an amide to enhance potential intermolecular hydrogen bonding) and Boc **TANI-TEG** (no hydrogen bonding capability). We confirmed the structures using different characterisation techniques: ^{1}H NMR, mass spectrometry and elemental analysis. Initial self-assembling studies showed the formation of different morphologies depending on the structure. In order to remove Boc groups, Boc deprotection of the prepared amphiphiles was trialed using

different methods. The challenges of removing Boc groups were addressed and discussed in detail. Much of the work reported here represents a very promising start; however, finding appropriate methodologies to remove Boc groups for these, and related, materials continues to be a challenge to be explored in the future. Once achieved, such non-ionic systems can be explored using the developed APP approach to tune the packing parameter, and, ultimately, the self-assembled structures.

5.4 Experimental

5.4.1 Materials and instruments

Materials

All chemicals were purchased from Sigma-Aldrich UK and used as received without further purification. Molecular sieves were heated to 200°C overnight under vacuum to yield dried and activated molecular sieves. Unless specified, all solvents used were anhydrous. The dry solvents were obtained using a column of anhydrous alumina from Anhydrous Engineering (University of Bristol) and a drying system based on the Grubbs' design.

NMR spectrometry

^{1}H and ^{13}C NMR experiments were conducted using either a 400 MHz Varian VNMR 400 or a 500 MHz Bruker 500 NMR spectrometer and carried out in deuterated solvents.

Mass spectrometry

Mass spectrometry was conducted using either a Bruker Daltronics UltrafleXtreme or an Applied Biosystems 4700 Proteomic Analyser with *A*-Cyano-4-hydroxycinnamic acid matrix for matrix-assisted laser desorption/ionisation time-of-flight (MALDI-TOF), and either a Bruker Daltonics 7 Tesla Apex 4 or a MicrOTOF II for ESI-TOF. All mass spectra of the synthesised materials of this chapter are available in the **Appendix E.**

Elemental analysis

Elemental analysis was carried out on a Euro Vector Euro EA 3000 in the Microanalytical Laboratory of the University of Bristol.

5.4.2 Coupling of modified TEG with Boc Ph/NH_2 TANI

5.4.2.1 Modification of hydroxyl end group of triethylene glycol

5.4.2.1.1 Tosylated TEG 164

A dried round-bottom flask containing TEG (10 g, 28 mmol) in 40 mL THF was cooled in an ice bath, and sodium hydroxide (3.42 g, 85 mmol, 50 % aq. solution) added. p-Toluene sulfonylchloride (6.5 g, 34 mmol) in 20 mL was slowly added using a dropping funnel over a period of 1 h. The reaction mixture was stirred overnight at room temperature. 20 mL of water was added and the mixture stirred until two distinct layers were seen. The organic layer was separated and the solvent evaporated. After that, 50 mL of deionized water was added and the mixture extracted with ethyl acetate. The ethyl acetate layer was washed with brine, separated and dried using dried sodium sulphate. Solvent was removed, 50 mL of diethyl ether was added and the solution kept in a fridge overnight, during which residual unreacted tosyl chloride precipitated. The precipitate was filtered and the solvent was removed to give the desired product as colourless liquid. Yield: 70 %. ^{1}H NMR (400 MHz, Chloroform-*d*) δ 7.81 – 7.74 (m, 2H), 7.32 (d, *J* = 8.0 Hz, 2H), 4.13 (dd, *J* = 5.6, 4.1 Hz, 2H), 3.68 – 3.49 (m, 10H), 3.34 (s, 3H), 2.42 (s, 3H). Anal. Calcd. for $C_{14}H_{22}O_6S$: C 52.81, H 6.97, S 10.07 %; found C 52.569, H 7.02, S 0.877 %. MS (ESI) m/z =341.1 $[M+Na]^+$.

5.4.2.1.2 TEGylated 164 bromophenol

A mixture of bromophenol (1 g, 5.78 mmol, 1 eq.) and tosylated TEG 164 (1,761 ml, 5.70 mmol,1 eq.) and potassium carbonate (K_2CO_3, .99 g,14.45 mmol, 2.4 eq.) in acetonitrile (0.1 M) was refluxed for 24 h and some crown-16 was added to accelerate the solubility of K_2CO_3 in CH_3CN. The mixture was cooled to room temperature, insoluble materials were precipitated out, and the filtrate was evaporated to yield a colourless oil. The product was taken in diethyl ether then n-hexane to remove unreacted materials. Yield: 71 %. ^{1}H NMR (400 MHz, Acetonitrile-d_3) δ 7.47 –

7.36 (m, 2H), 6.91 – 6.81 (m, 2H), 4.12 – 4.03 (m, 2H), 3.79 – 3.72 (m, 2H), 3.62 – 3.52 (m, 6H), 3.47 – 3.41 (m, 2H), 3.28 (s, 3H). Anal. Calcd. for $C_{13}H_{19}BrO_4$: C 48.92, H 6.00, Br 25.03 %; found C 48.527, H 6.037, Br 24.82 %. Anal. Calcd for $C_{13}H_{19}BrO_4C$: C 48.92, H 6.00, Br 25.03 %; found C 48.627, H 6.03, Br 24.82 %. MS (ESI) m/z = 341.0 $[M+Na]^+$.

5.4.2.1.3 Succiniylated TEG 164

A round bottom containing succinic anhydride (4.20 g, 42 mmol) and DMAP (209 mg, 1.71 mmol) were dissolved in 20 ml of dry THF and kept at 0^{o}C under nitrogen for 30 min. PEG (5 g, 33 mmol) and TEA (1.8 mL, 12.8 mmol) were mixed in 15 mL of dry THF and transferred slowly into the succinic anhydride solution using a syringe under nitrogen atmosphere. The mixture was stirred at 0^{o}C for 2 h, and the reaction was kept stirring under nitrogen atmosphere at room temperature overnight. The reaction solution was then concentrated by evaporating the solvent. The succinylated TEG was precipitated in cold diethyl ether. The precipitates were dissolved in dichloromethane a second time and then reprecipitated in cold diethyl ether. The precipitates were dried under vacuum at room temperature and purified by flash column chromatography (silica gel, 1:1 chloroform: methanol) to yield the product as a colorless oil. Yield: 71 %. ^{1}H NMR (400 MHz, DMSO-d_6) δ 4.16 – 4.08 (m, 2H), 3.63 – 3.55 (m, 2H), 3.55 – 3.47 (m, 6H), 3.47 – 3.39 (m, 2H), 3.24 (s, 3H), 2.51 – 2.42 (m, 4H). Anal. Calcd. for $C_{10}H_{18}O_7$: C 48.00, H 7.25 %; found C 47.63, H 7.35 %. MS (ESI) m/z = 287.1 $[M+Na]^+$.

5.4.2.2 Succinylated TEG 164 coupled with Boc TANI

A mixture of succinylated TEG 164 (29.25 mg, 0.114 mmol), Boc Ph/NH_2 TANI (100 mg, 0.149 mmol), and 4-(dimethylamino)pyridine (DMAP, 13.92 g, 0.114 mmol) was dissolved in anhydrous CH_2Cl_2 (10 mL) and stirred at 0^{o}C for 10 min. N-ethyl-N -(3-dimethylaminopropyl)carbodiimide hydrochloride (EDCI) (21.85 g, 0.114 mmol) was added to the mixture with stirring at 0^{o}C. The reaction mixture was stirred at room temperature for 65 h, and the mixture taken into water, followed by extraction with CH_2Cl_2. The organic layer was washed with 1 M HCl and saturated aqueous $NaHCO_3$, and dried over anhydrous $MgSO_4$. The solvent was removed under reduced pressure, and the residue was purified by column chromatography (silica gel, 5:1 ethyl acetate: n-hexane) to give the desired product. Yield: 45 %. ^{1}H NMR (400 MHz, Acetonitrile-d_3) δ 8.45 (s,

1H), 7.58 – 7.49 (m, 2H), 7.39 – 7.30 (m, 2H), 7.26 – 7.11 (m, 13H), 4.21 – 4.14 (m, 2H), 3.66 – 3.43 (m, 10H), 3.29 (s, 3H), 2.63 (q, *J* = 3.9 Hz, 4H), 1.42 (d, *J* = 1.4 Hz, 27H). Anal. Calcd. for $C_{45}H_{56}N_4O_{10}$: C 66.48, H 6.94, N 6.89 %; found C 67.423, H 7.01, N 6.77 %. MS (ESI) m/z = 935.4 $[M+Na]^+$

5.4.2.3 TEGylated 164 bromophenol coupled with Boc TANI

To a conical flask were added TEGylated 164 bromophenol (350 mg, 1.09 mmol, 1eq), Boc Ph/NH_2 TANI (872.19 mg, 1.31 mmol, 1.2 eq), $Pd(dba)_2$ (12.54 mg, 2 mol%), XPhos (10.39 mg, 2 mol%) and sodium tert-butoxide (209.63 mg, 2 eq). The reagents were protected under nitrogen and toluene (anhydrous, 20 mL) was added. The flask was sealed and heated at 110°C for 2 days. The reaction was cooled to room temperature and filtered through celite, then all solvent removed under vacuum. The residue was taken up in dichloromethane and washed with deionised water, followed by drying of the organic phase over $MgSO_4$ and evaporation of the solvent. The residue was purified by column chromatography (silica gel, 5:1 ethyl acetate: n-hexane) to give the product. Yield: 60 %. ^{1}H NMR (400 MHz, Acetonitrile-d_3) δ 7.16 (dd, *J* = 8.5, 7.0 Hz, 2H), 7.07 – 6.96 (m, 11H), 6.88 – 6.83 (m, 4H), 6.71 – 6.67 (m, 4H), 6.38 (s, 1H), 3.91 – 3.86 (m, 2H), 3.60 – 3.57 (m, 2H), 3.48 – 3.44 (m, 2H), 3.41 (ddd, *J* = 9.2, 3.9, 1.8 Hz, 4H), 3.33 – 3.29 (m, 2H), 3.13 (s, 3H), 1.26 (s, 27H). Anal. Calcd. for $C_{52}H_{64}N_4O_{10}$: C 69.01, H 7.13, N 6.19 %; found C 69.045, H 7.32, N 6.115%. MS (ESI) m/z = 927.5 $[M+Na]^+$.

5.5 References

1 Y. Wu, S. Liu, Y. Tao, Y. Zhang, J. Xu and Y. Wei, *ACS Appl. Mater. Interfaces*, 2014, **6**, 1470–1480.

2 B. Guo, A. Finne-Wistrand and A. C. Albertsson, *Chem. Mater.*, 2011, **23**, 4045–4055.

3 Y. Guo, M. Li, A. Mylonakis, J. Han, A. G. MacDiarmid, X. Chen, P. I. Lelkes and Y. Wei, *Biomacromolecules*, 2007, **8**, 3025–3034.

4 H. Kim, T.-G. Kim and J.-W. Park, *Macromol. Res.*, 2013, **21**, 815–820.

5 T. Kim, C. Kim and J. Park, *Macromolecules*, 2017, **50**, 8185–8191.

6 H. Kim, S. Jeong and J. Park, *J. Am. Chem. Soc.*, 2011, **133**, 5206–5209.

7 I. Arioz, O. Erol, G. Bakan, F. B. Dikecoglu, A. E. Topal, M. Urel, A. Dana, A. B. Tekinay and M. O. Guler, *ACS Appl. Mater. Interfaces*, 2018, **10**, 308–317.

8 O. A. Bell, G. Wu, J. S. Haataja, F. Brömmel, N. Fey, A. M. Seddon, R. L. Harniman, R. M. Richardson, O. Ikkala, X. Zhang and C. F. J. Faul, *J. Am. Chem. Soc.*, 2015, **137**, 14288–14294.

9 S. S. Banerjee, N. Aher, R. Patil and J. Khandare, *J. Drug Deliv.*, 2012, **2012**, 1–17.

10 J. Li and W. J. Kao, *Biomacromolecules*, 2003, **4**, 1055–1067.

11 L. Huang, J. Hu, L. Lang, X. Wang, P. Zhang, X. Jing, X. Wang, X. Chen, P. I. Lelkes, A. G. MacDiarmid and Y. Wei, *Biomaterials*, 2007, **28**, 1741–1751.

12 J. Hu, X. Zhuang, L. Huang, L. Lang, X. Chen, Y. Wei and X. Jing, *Langmuir*, 2008, **24**, 13376–13382.

13 Z. Zhang and J. Yang, *Rare Met.*, 2011, **30**, 563–566.

14 Z. Yang, X. Wang, Y. Yang, Y. Liao, Y. Wei and X. Xie, *Langmuir*, 2010, **26**, 9386–9392.

15 J. Zhang, Y. Zhao, S. Han, C. Chen and H. Xu, *Sci. China Chem.*, 2014, **57**, 1634–1645.

16 R. Chen and B. C. Benicewicz, *Macromolecules*, 2003, **36**, 6333–6339.

17 S. Hou, L. K. McCauley and P. X. Ma, *Macromol. Biosci.*, 2007, **7**, 620–628.

18 S. Chatterjee and S. Ramakrishnan, *ACS Macro Lett.*, 2014, **3**, 953–957.

19 M. R. J. Vallée, P. Majkut, I. Wilkening, C. Weise, G. Müller and C. P. R. Hackenberger, *Org. Lett.*, 2011, **13**, 5440–5443.

CHAPTER 6 CONCLUSIONS AND FUTURE WORK

Conclusions

The overall aim of this project was to design water-soluble amphiphiles based on oligo(anilines), and explore and control their tunable self-assembled structures using our innovative approach, the addressable packing parameter (APP) approach.

The preparation of oligo(aniline) amphiphiles was achieved using cationic or non-ionic head groups; these head groups provide water-solubility and the ability to assemble into intricate structures in aqueous environments. Various **AB** diblock and **ABA** triblock architecture structures of **TANI**-based amphiphiles were synthesised. For the case of **AB**-type structures, **TANI** was functionalised with either cationic or non-ionic head groups, resulting in single-tailed amphiphiles. The **ABA** structures involved difunctional **TANI** modified with two head groups to yield bolaamphiphilic structures. We have chosen the well-known ammonium amphiphiles (trimethyl ammonium head group, 83.16 $Å^3$) to compare with phosphonium amphiphiles (trimethyl phosphonium head group, 95.58 $Å^3$. These bolaamphiphiles, **TANI-(PTAB)$_2$** and **TANI-(PTPB)$_2$**, were designed for comparison with the corresponding single-tailed amphiphiles (**TANI-PTAB**, **TANI-PTPB**).

With these materials prepared, we developed a reversibly switchable self-assembling system using an electroactive oligo(aniline)-based **eSA**, **TANI(TFA)$_2$-PTAB**. This system exhibited dopant-dependent morphology transitions between vesicles and nanowires. This behaviour was attributed to changes in the packing parameter of the protonated ES form vs. the unprotonated EB form. The transition from the EB to the ES state, and vice versa, and the consequent changes in morphologies, could be controlled, as was set out as the aim of this thesis. We verified the switchable behaviour of **TAN**-based amphiphiles from EB to ES state, and vice versa, with our further AB-type amphiphile, **TANI-PTPB**. Moreover, a range of dopants with different volumes and structures was also introduced to **TANI-PTPB** to explore their effect on the formation of varied self-assembled structures. A polymerisable dopant was polymerised using different photoinitiators (DMAP, PBTBO) and introduced to **TANI-PTPB**, resulting in new and interesting

morphologies not observed before. The morphology was tuned from chain-like structures to form spherical and worm structures, respectively. These are interesting structures and inspired us to investigate the effect of an acid polyelectrolyte such as poly(acrylic acid), PAA, on the self-assembling behaviour of our **TAN**-based amphiphiles; we consider this study for future work.

This study showed the variations of the self-assembled structures of **TANI-PTAB** and **TANI-PTPB** depending on the headgroups. Furthermore, acid-doping studies of **TANI**-based amphiphiles showed different self-assembled structures as a result of changes in the volume of hydrophobic tail. In other words, increasing the packing parameter through changes in volume v or changes in the size of headgroup. This thesis showed novel ways to tune the self-assembly of **TANI**-based amphiphiles in an unprecedented way, simply by changing the packing parameter.

To investigate the ability to tune the self-assembled structures of our **TANI**-based bolaamphiphiles, **TANI-(PTAB)$_2$** and **TANI-(PTPB)$_2$**, the bolaamphiphiles were doped with different volumes, structures and numbers of acid moieties. Theses variations provided changes in the packing parameter leading to the formation of various self-assembled structures (spheres, vesicles and fibres). Furthermore, tuning the morphology of **TANI-(PTAB)$_2$** from 22nm diameter spheres to fibres with 4nm width was achieved in a reversible fashion through a doping and de-doping process. This result confirmed that our addressable packing parameter approach can also be applied successfully to our bolaamphiphiles. Keeping in mind that the concept of a packing parameter for bolas does not exist in the same form as for simple amphiphiles.

This study showed the tunable structures of bolaamphiphiles by addressing the role of packing parameters. These variations are attributed to the presence of two headgroups; an increase in the area of the headgroup thus led to a decrease in the packing parameter. Furthermore, the changes in volume of dopants led to an increase in the packing parameter, resulting in different self-assembled structures. All these variations imply the role of the packing parameter on our bolaamphiphiles.

We also showed, for the first time, that doping the **TANI** core of our amphiphiles yielded a mixture of spin isomers (polaronic and bipolaronic forms) in solution, providing a novel strategy to tune **TANI**'s spin isomers.

Preliminary results indicate that non-ionic amphiphile based on Boc **TANI-TEG** could also self-assemble into various structures depending on their molecular architecture; **TANI-(CO)TEG** formed rod-like structures while **TANI-TEG** formed spherical structures. However, no or little control over the formed self-assembled structures was evident.

This thesis was dedicated to providing a simple and feasible strategy to produce tunable assembled structures of various **TANI**-based amphiphiles. We believe this strategy will open paths for applications in a range of related fields, especially in the field of controlled delivery of loaded drug cargoes and stimuli-responsive viscosity modifiers.

Future work

In order to gain a comprehensive understanding of further aspects of the prepared materials during this thesis, the following ideas and techniques for future work are suggested.

- The packing parameter, expressed in the equation, $p = v / a_0 l_c$, is discussed in detail in the previous chapters. p relies on the volume of the hydrophobic chain, l_c is the critical chain length, and a_0 is the surface area of the hydrophilic head group. Hence, a range of cationic head groups with different size could be used to prepare amphiphiles such as pyridinium and isoquinolinium. The increase of the head group size would normally cause a decrease in the packing parameter, resulting in a change in the self-assembled structure from (for example) cylindrical micelles to spherical structures. Furthermore, the calculation of the surface area of various headgroups (by measuring the surface tension) could be useful for comparison between the observed structures and the proposed structures, based on the calculated packing parameter. Moreover, the variations of hydrophobic tail have a strong impact on changing the packing parameter. Increase of the tail length could be achieved by increasing the alkyl spacer length ($C_{8\text{-}14}$) or conjugation length such as octa(aniline)s. Furthermore, the increase of the conjugated oligo(aniline)

core lengths would lead to a decrease in solubility and yield. From our recent group paper, we found that the addition of salt to the reaction mixture during synthesis of highly cross-linked aniline-based polymers would increase the solubility of the oligomers, and thus yields. Hence, we can synthesize a range of amphiphiles with highly conjugated core lengths. In general, the increase of tail lengths leads to a decrease in the packing parameter and the morphology could be altered. The morphology of the oligo(aniline)-based amphiphiles can also be changed by adding various volume of dopants to the hydrophobic core. The volume of hydrophobic parts would normally increase as a result of the dopants volume added. The packing parameter will be decreased as a consequence, and result in an alteration to the morphology. The proposed variations of an amphiphilic structure shown in **Figure 6.1**.

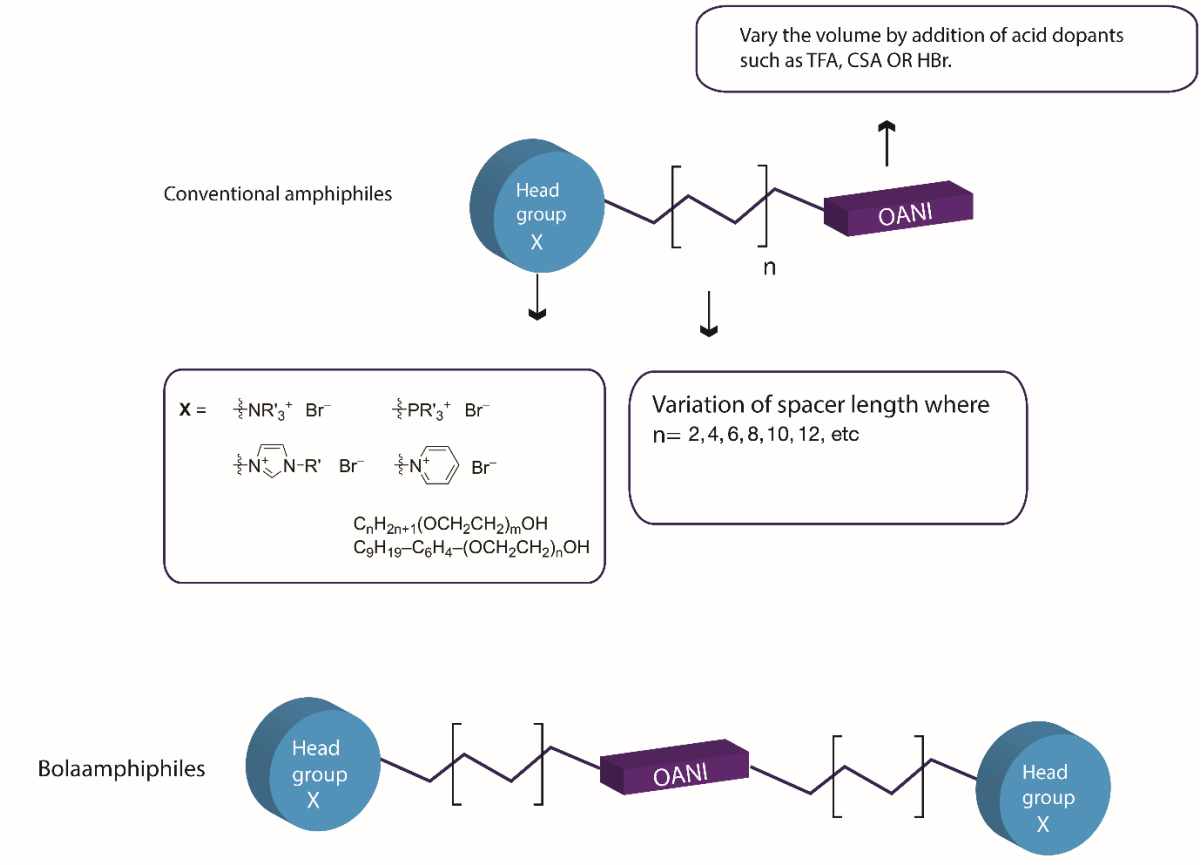

Figure 6.1 Scheme showing the possible variations of an **OANI**-based amphiphile.

- In Chapter 3, the polymerised **TANI(AMPS)$_2$-PTPB** showed an interesting morphology (chain-like structures). The dilution of the polymerised **TANI(AMPS)$_2$-PTPB** solutions below the CAC showed the same morphology of the concentrated solutions. These observations inspire us to explore more examples of polymerisable dopants and verify that polymerisation has taken place completely, using either ^{1}H NMR or mass spectrometry.

- In Chapter 5, we showed the challenges and difficulties to remove Boc protecting groups and retain the chemical structure of the non-ionic amphiphile **TANI-TEG**. We will follow another procedure used in our group to remove Boc groups: Boc **TANI-(CO) TEG** dispersed in a mixture of water, TFA and triisopropylsilane (TIPS, a mild reducing agent) and stirred at room temperature for 1 hour as shown in **Scheme 6.2**. The volatile compounds can be removed under vacuum and the obtained product recovered by precipitation and purification from organic solvents (e.g. diethyl ether).

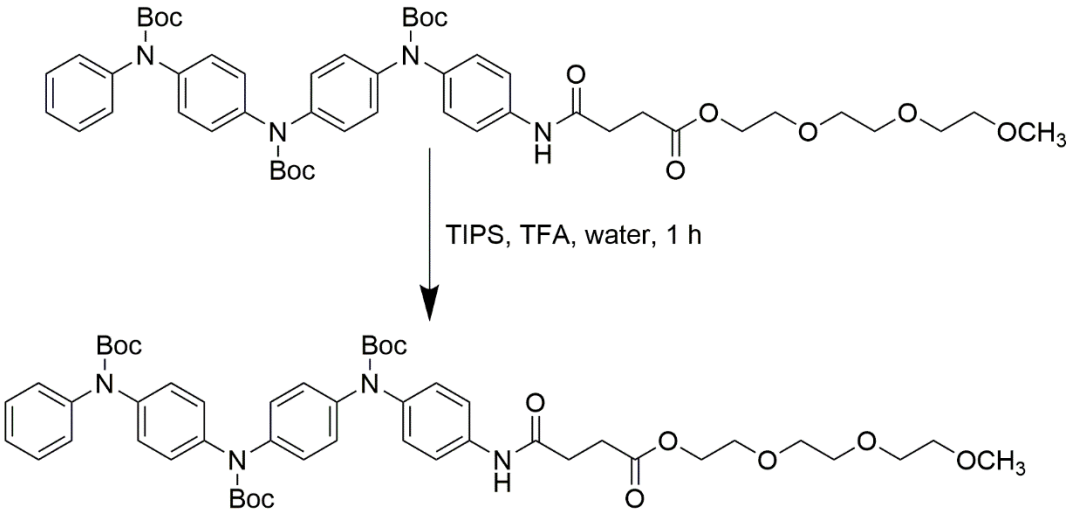

Scheme 6.1 Boc deprotection of **TANI-(CO)TEG.**

- In terms of application, the ammonium bolaamphiphiles **TANI-(PTAB)$_2$** showed significant results with the encapsulation and release formulation of dexamethasone compared to a conventional amphiphile based on **TANI**. This result inspires us to design various biocompatible bolaamphiphiles based on **TANI** and explore their efficiency for drug delivery. **TANI-PEG** has also been used previously in drug delivery and biomedical applications. Hence, once we prepare the materials, it is worth exploring their potential biomedical applications.

Appendix A

Buchwald-Hartwig amination mechanism

The key step of this reaction was the palladium-catalysed coupling of an aryl halide with an amine, leading to the formation of a new carbon-nitrogen bond, also known as Buchwald-Hartwig amination.[1,2] The reaction was conducted with a palladium dibenzylideneacetone (dba) precatalyst in the presence of a 2-dicyclohexylphosphino-2',4',6'-triisopropylbiphenyl (XPhos) ligand.[3]

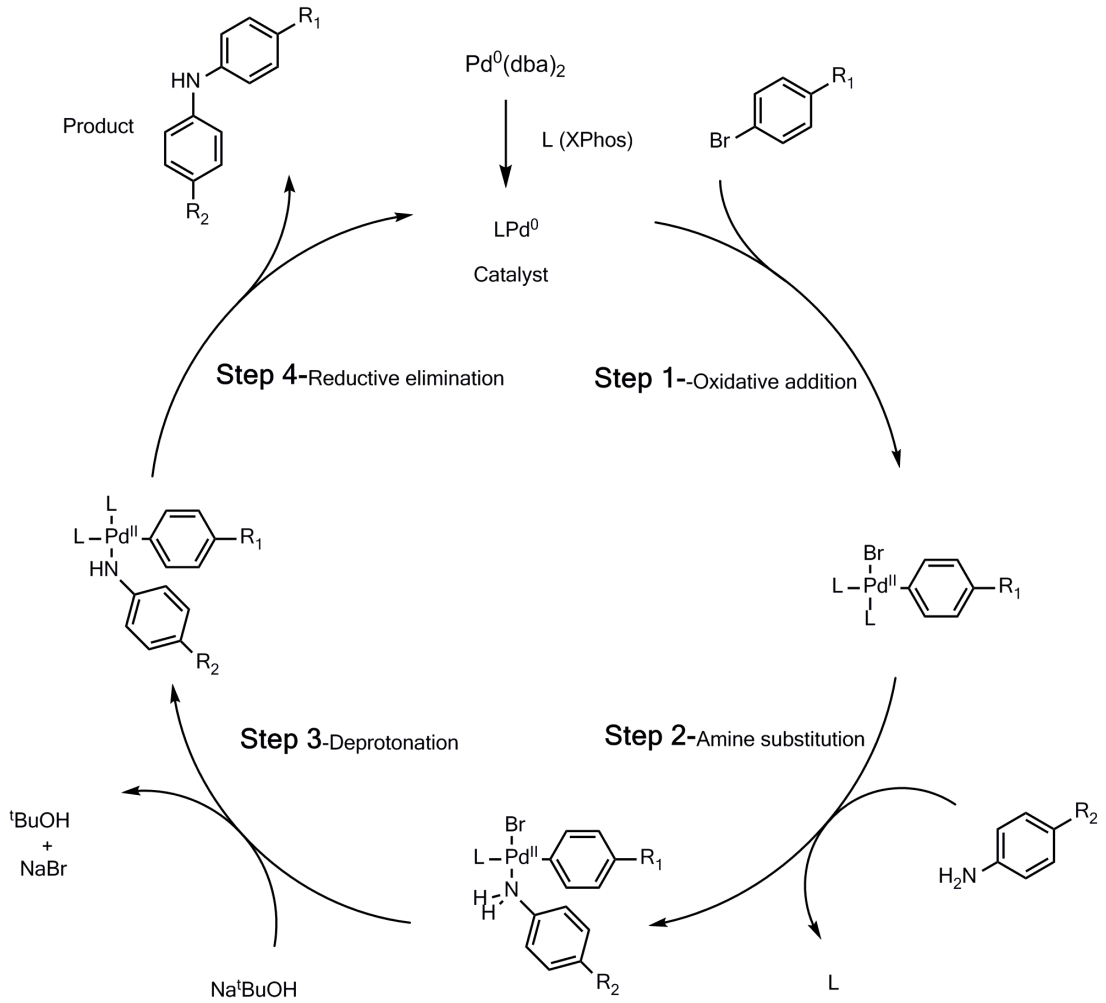

Scheme A.1 Catalytic cycle of Buchwald-Hartwig amination.

Boc protection mechanism

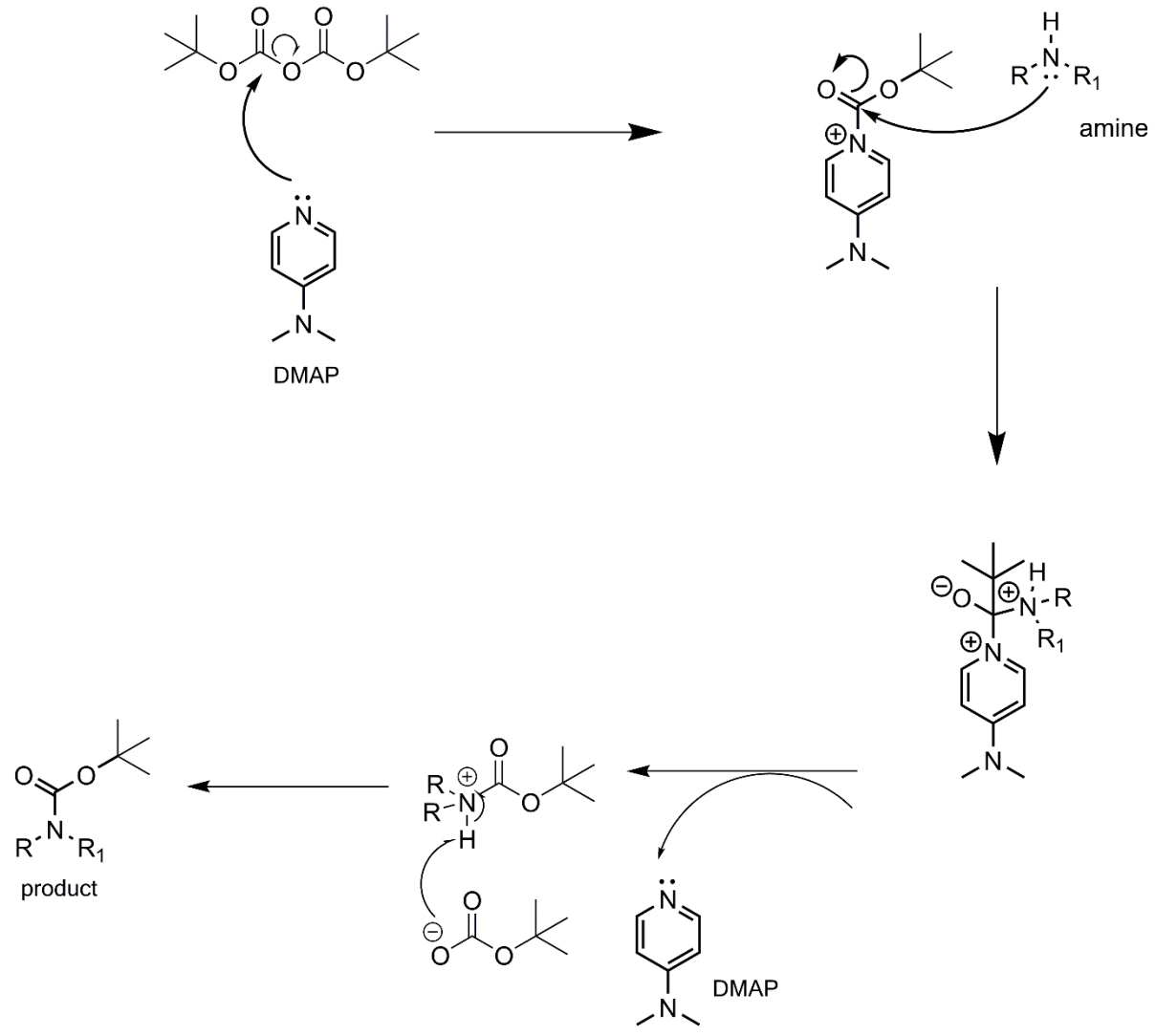

Scheme A.2 Boc protection mechanism.

Appendix B

Ph/NH$_2$ TANI synthesis

Benzophenone-protected N-phenyl-p-phenylene diamine (**1**)

^{1}H NMR (400 MHz, Chloroform-*d*) δ 7.74 – 7.66 (m, *J* = 7.0 Hz, 2H), 7.44 – 7.31 (m, 3H), 7.28 – 7.14 (m, 5H), 7.13 – 7.09 (m, 2H), 6.90 (d, 2H), 6.86 – 6.78 (m, 3H), 6.63 (dd, *J* = 73.3, 8.7 Hz, 2H), 5.50 (s, 1H).

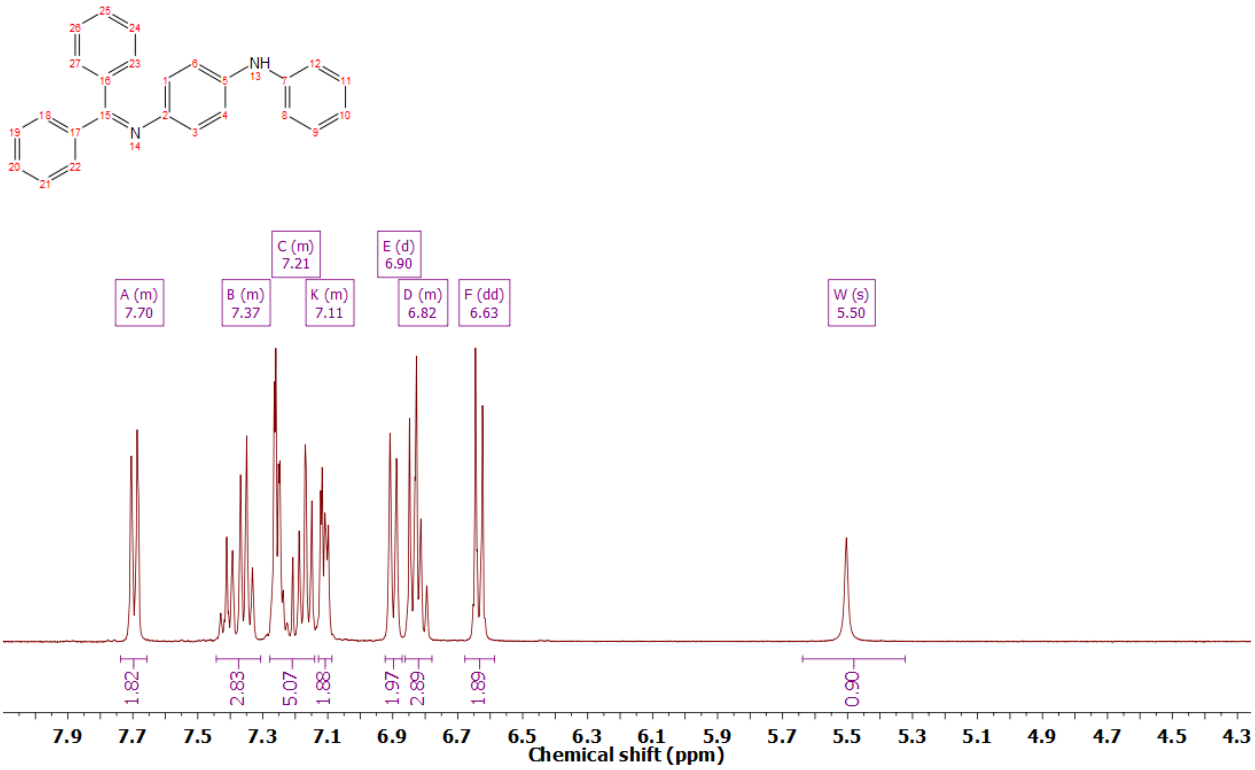

Figure B.1 ^{1}H NMR spectrum of benzophenone-protected N-phenyl-p-phenylene diamine (**1**).

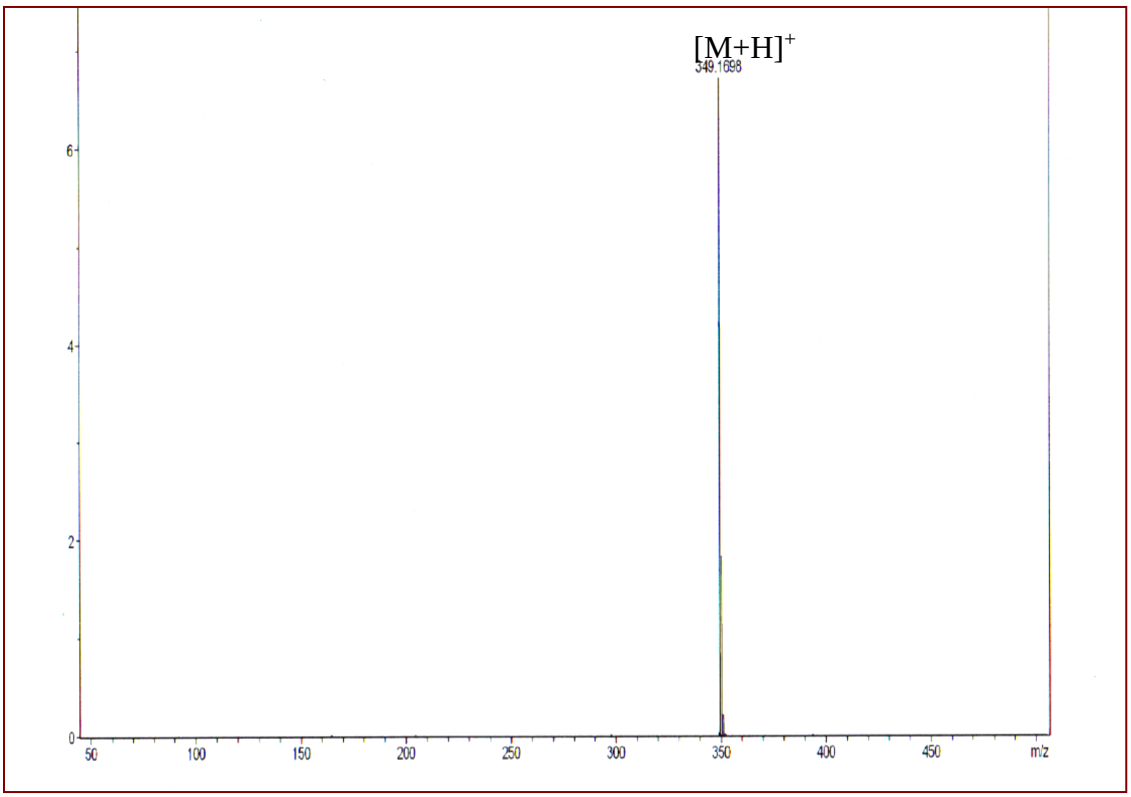

Figure B.2 ESI mass spectrum of benzophenone-protected N-phenyl-p-phenylene diamine (**1**).

Boc/benzophenone-protected N-phenyl-p-phenylene diamine (**2**)

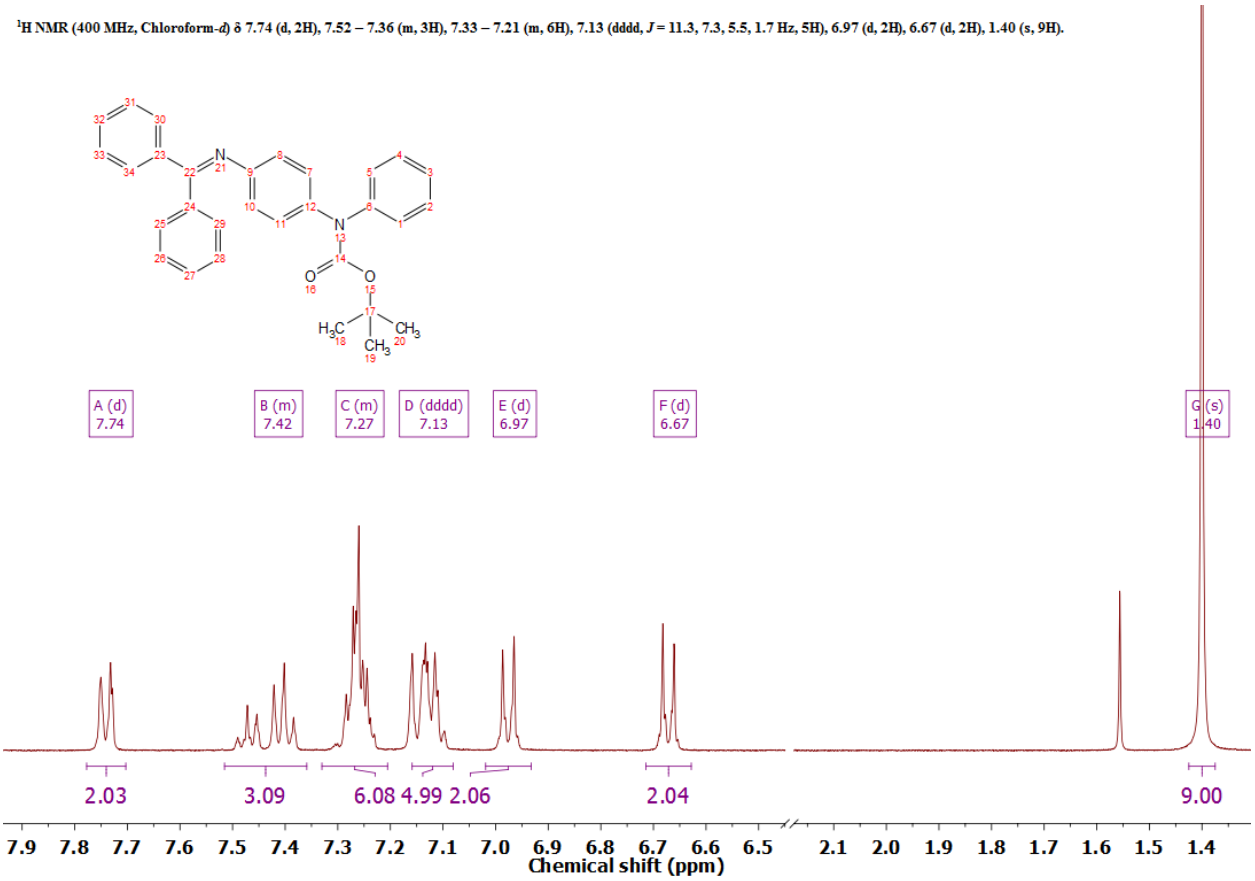

Figure B.3 ^{1}H NMR spectrum of Boc/benzophenone-protected N-phenyl-p-phenylene diamine (**2**).

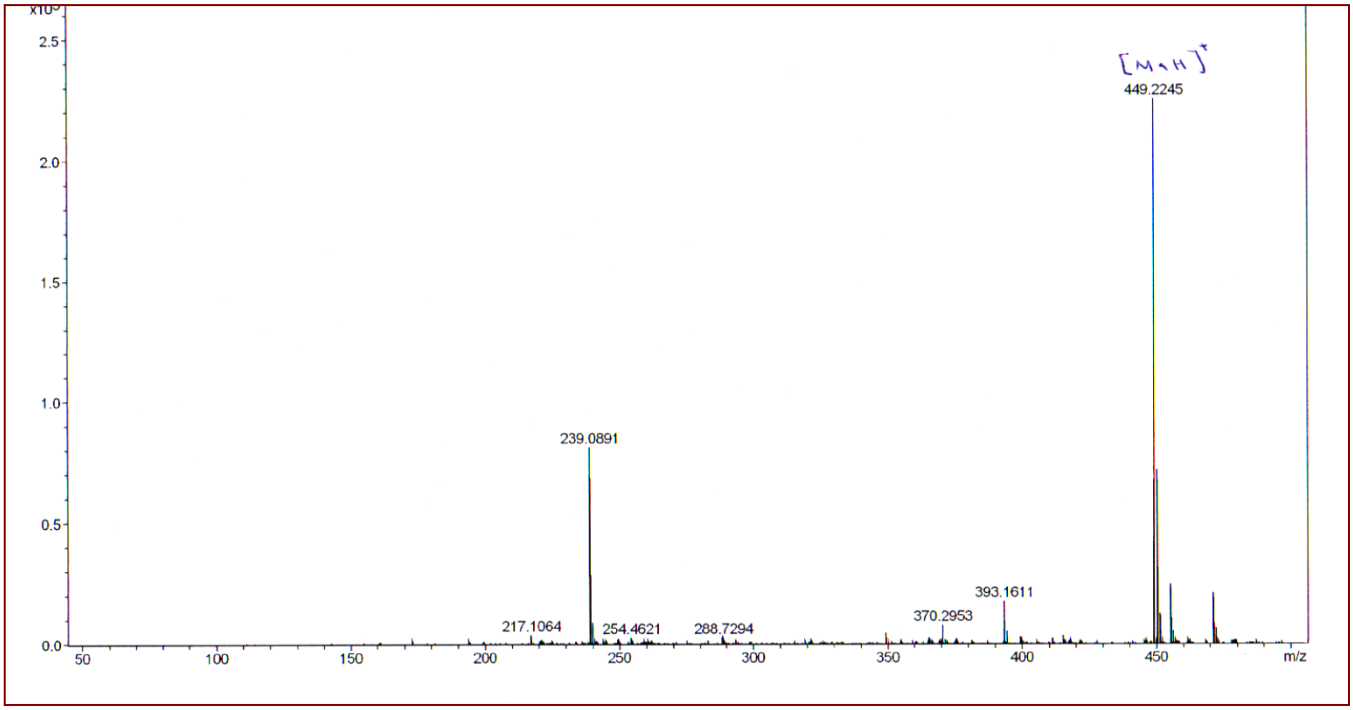

Figure B.4 ESI mass spectrum of Boc/benzophenone-protected N-phenyl-p-phenylene diamine (**2**).

Brominated boc/benzophenone-protected N-phenyl-p-phenylene diamine (**3**)

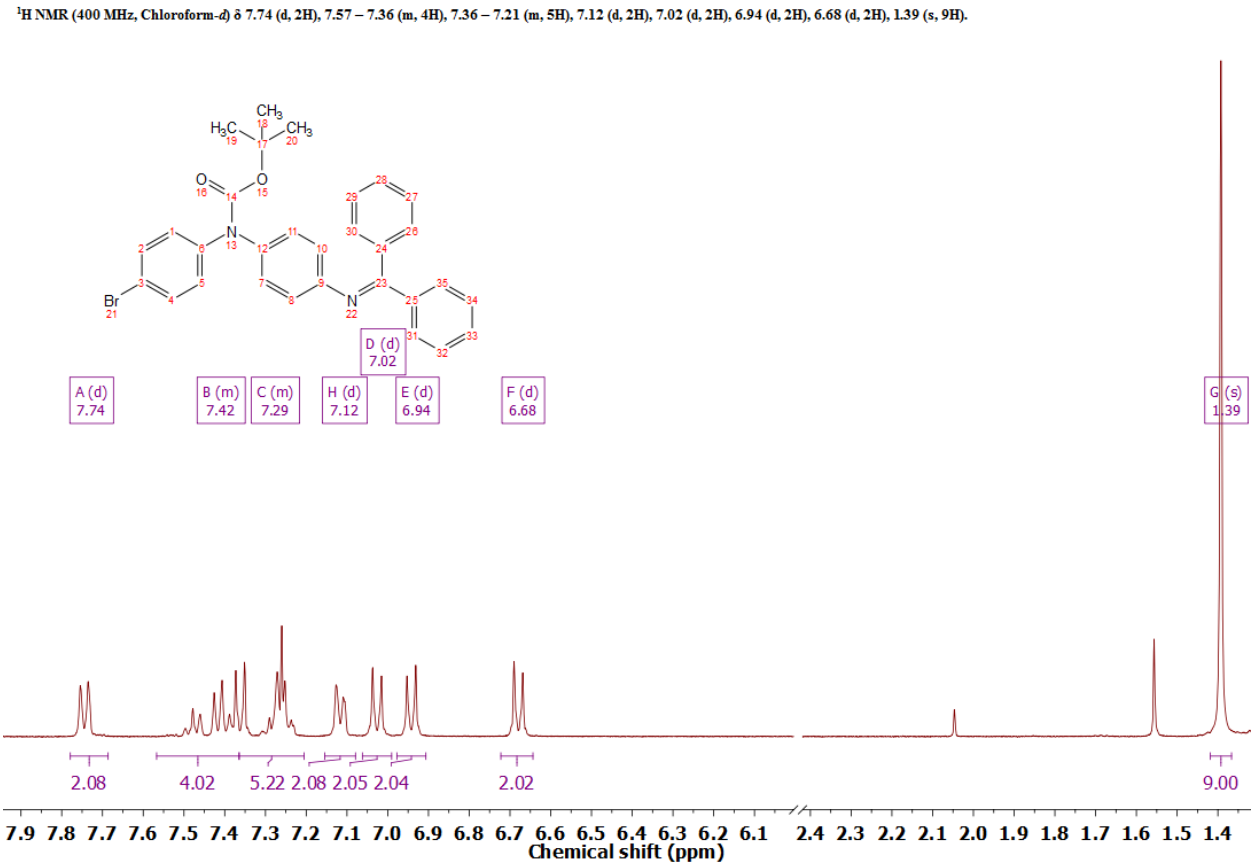

Figure B.5 ^{1}H NMR spectrum of brominated boc/benzophenone-protected N-phenyl-p-phenylene diamine (**3**)

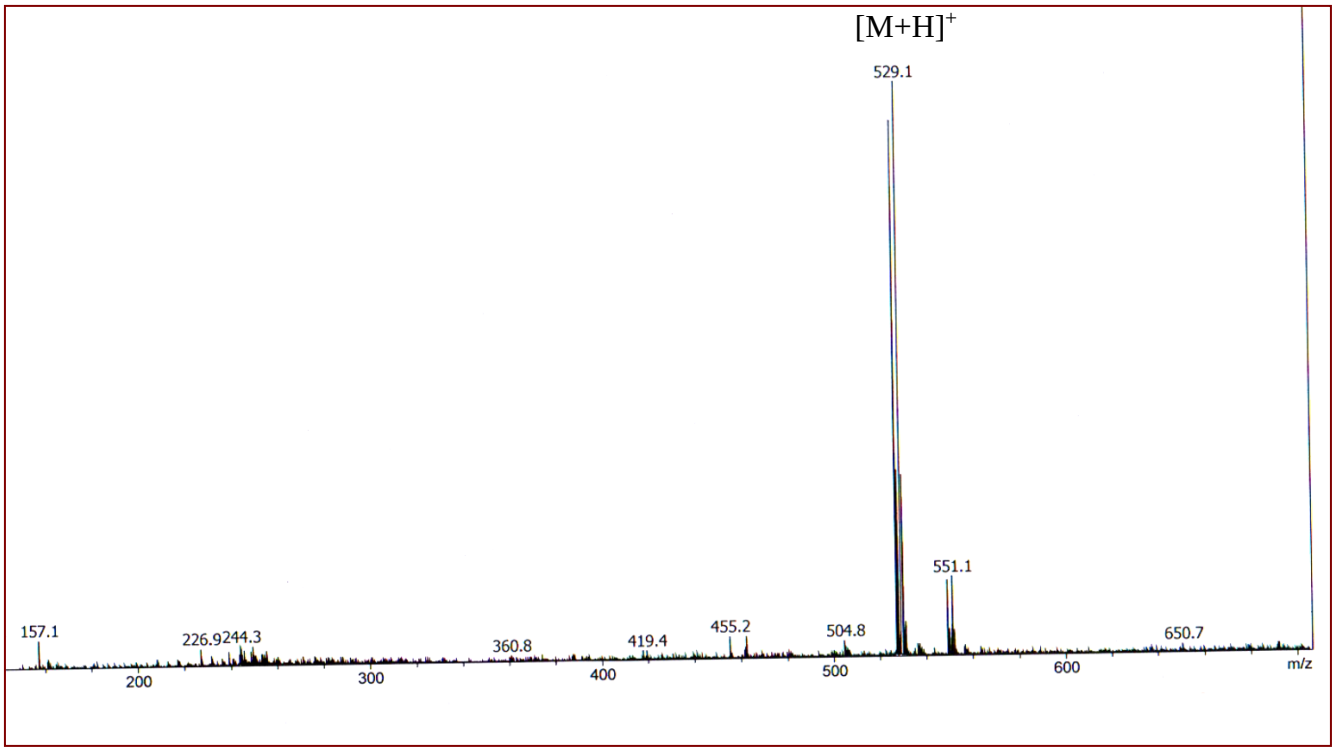

Figure B.6 ESI mass spectrum of brominated boc/benzophenone-protected N-phenyl-p-phenylene diamine (**3**)

Boc-protected N-phenyl-p-phenylene diamine (**4**)

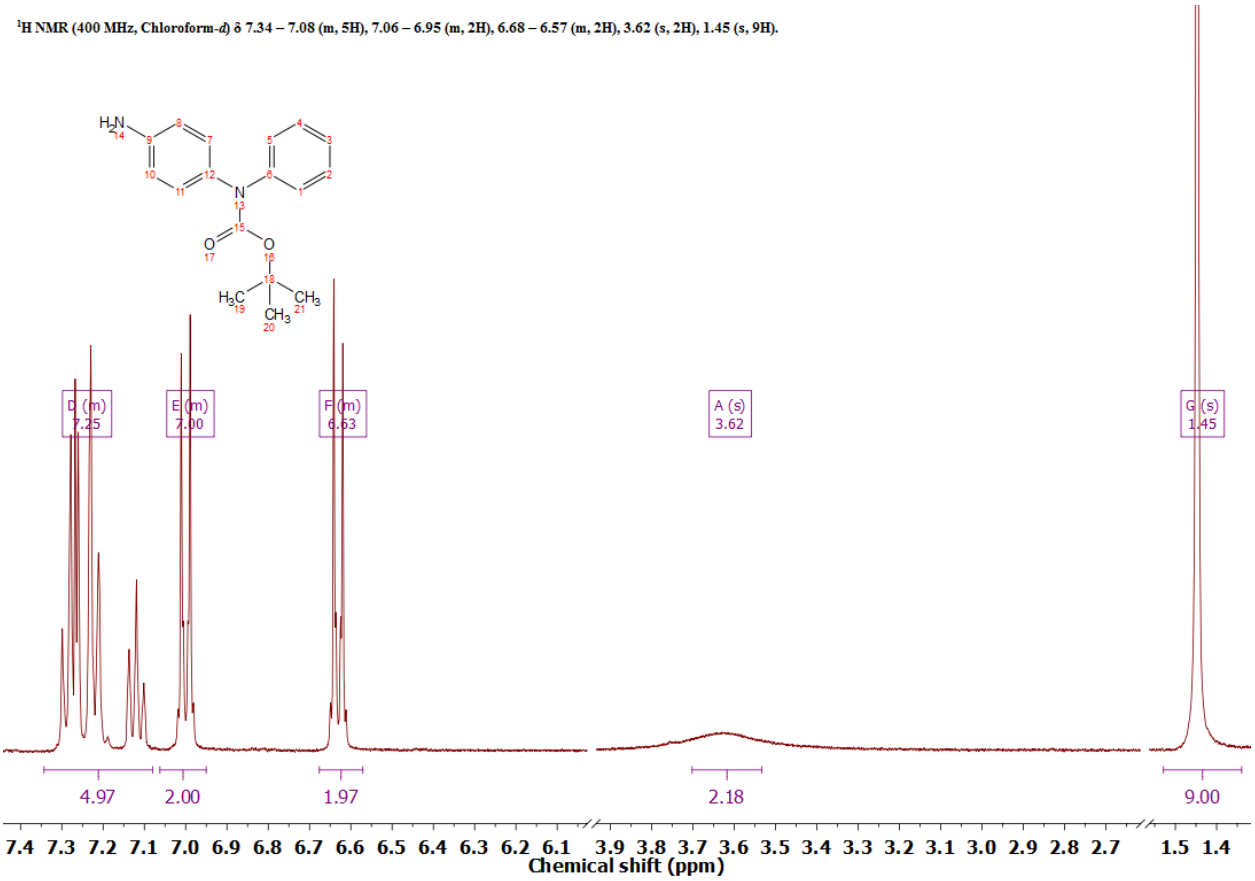

Figure B.7 ^{1}H NMR spectrum of Boc-protected N-phenyl-p-phenylene diamine (**4**)

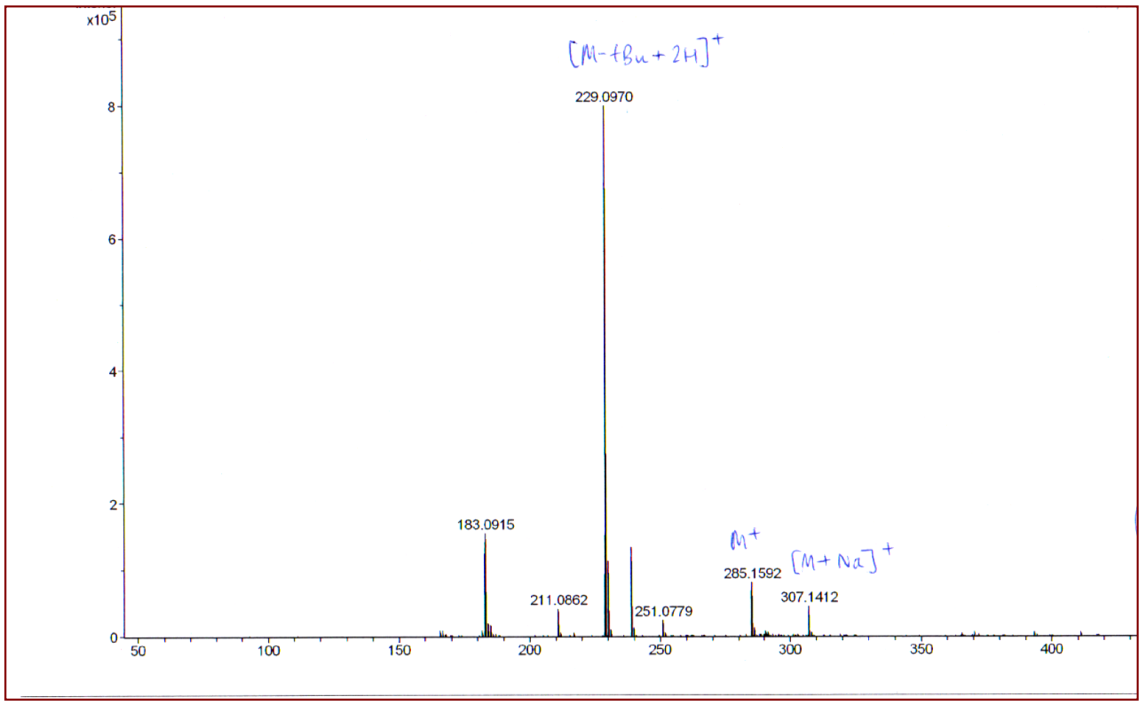

Figure B.8 ESI mass spectrum of Boc-protected N-phenyl-p-phenylene diamine (**4**)

Boc/benzophenone protected Ph/NH_2 TANI (**5**)

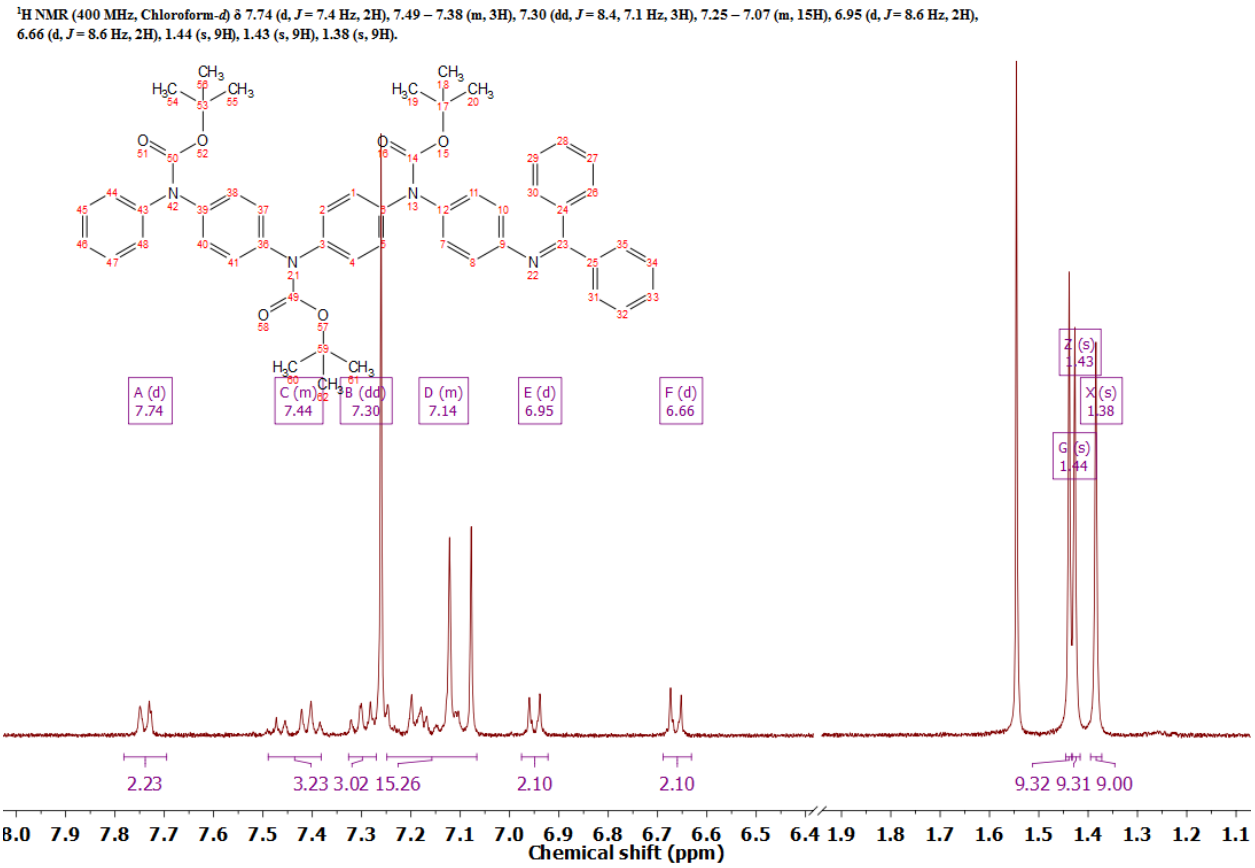

Figure B.9 ^{1}H NMR spectrum of Boc/benzophenone protected Ph/NH_2 TANI (**5**)

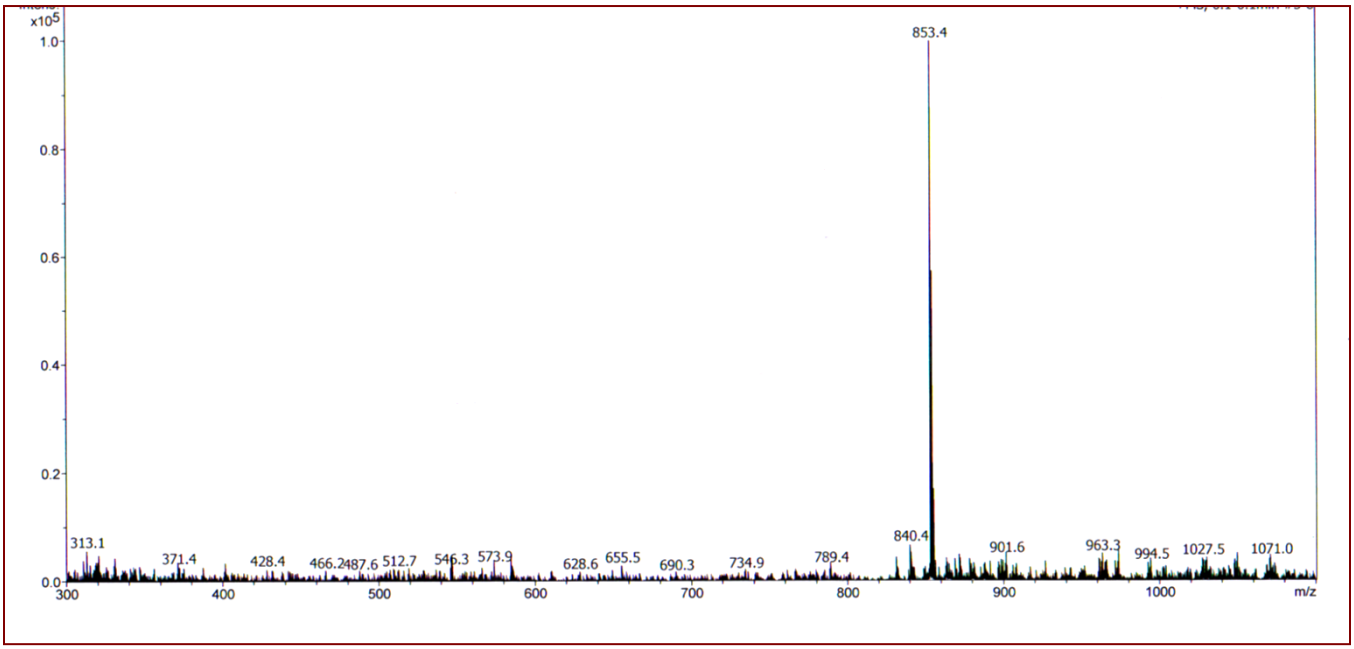

Figure B.10 ESI mass spectrum of Boc/benzophenone protected Ph/NH_2 TANI (**5**)

Boc-protected Ph/NH_2 TANI (**6**)

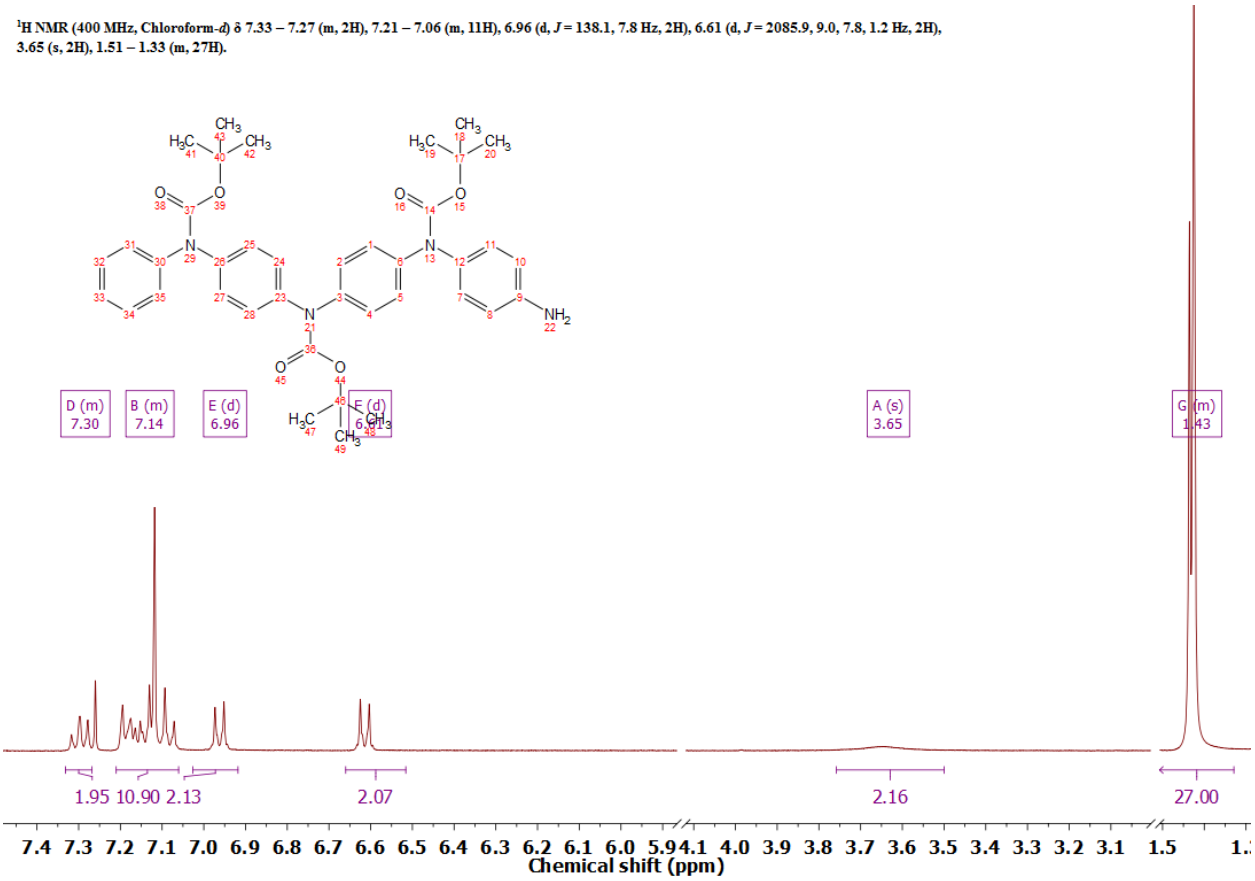

Figure B.11 ^{1}H NMR spectrum of Boc-protected Ph/NH_2 TANI (**6**)

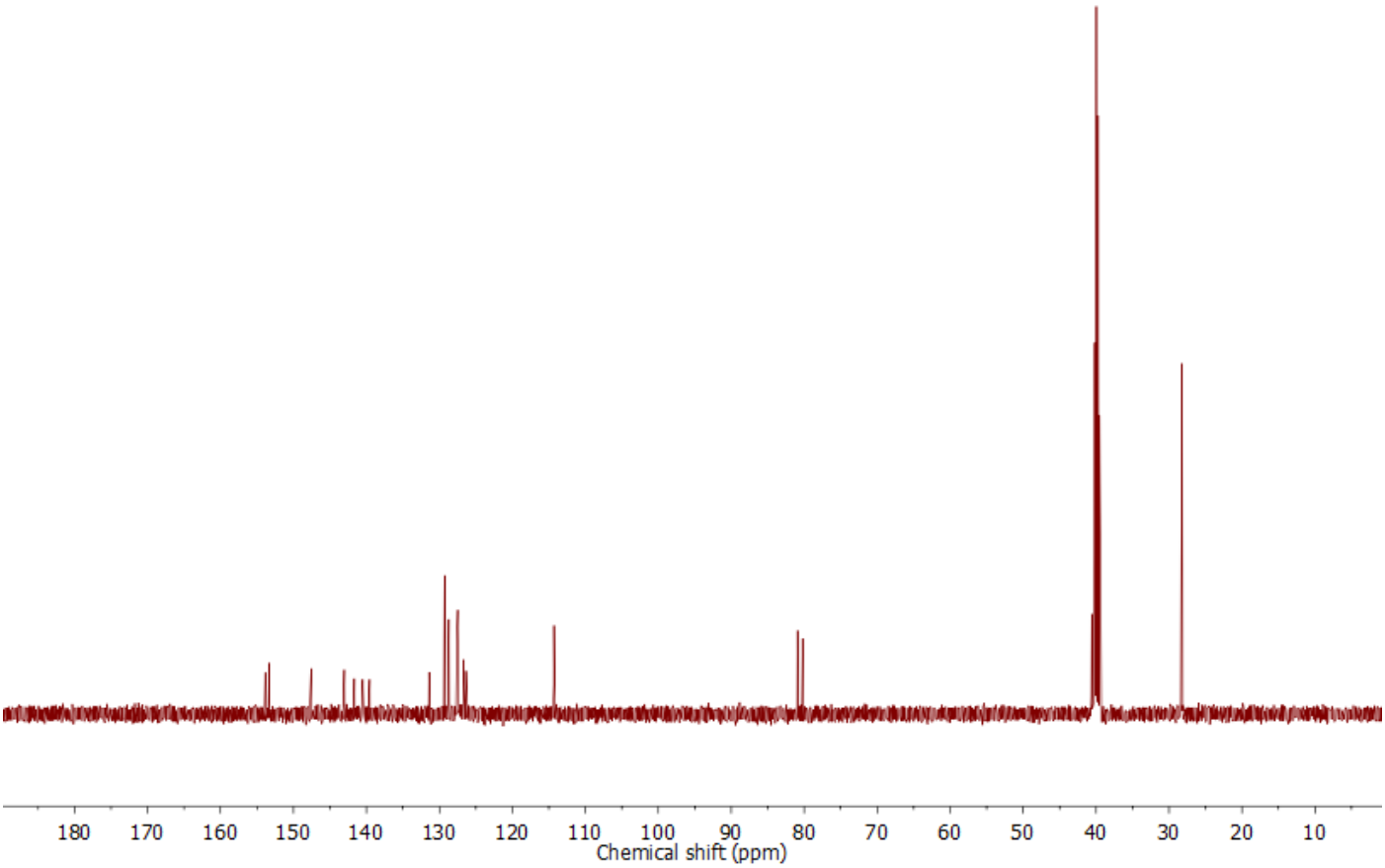

Figure B.12 ^{13}C NMR spectrum of Boc-protected Ph/NH_2 TANI (**6**)

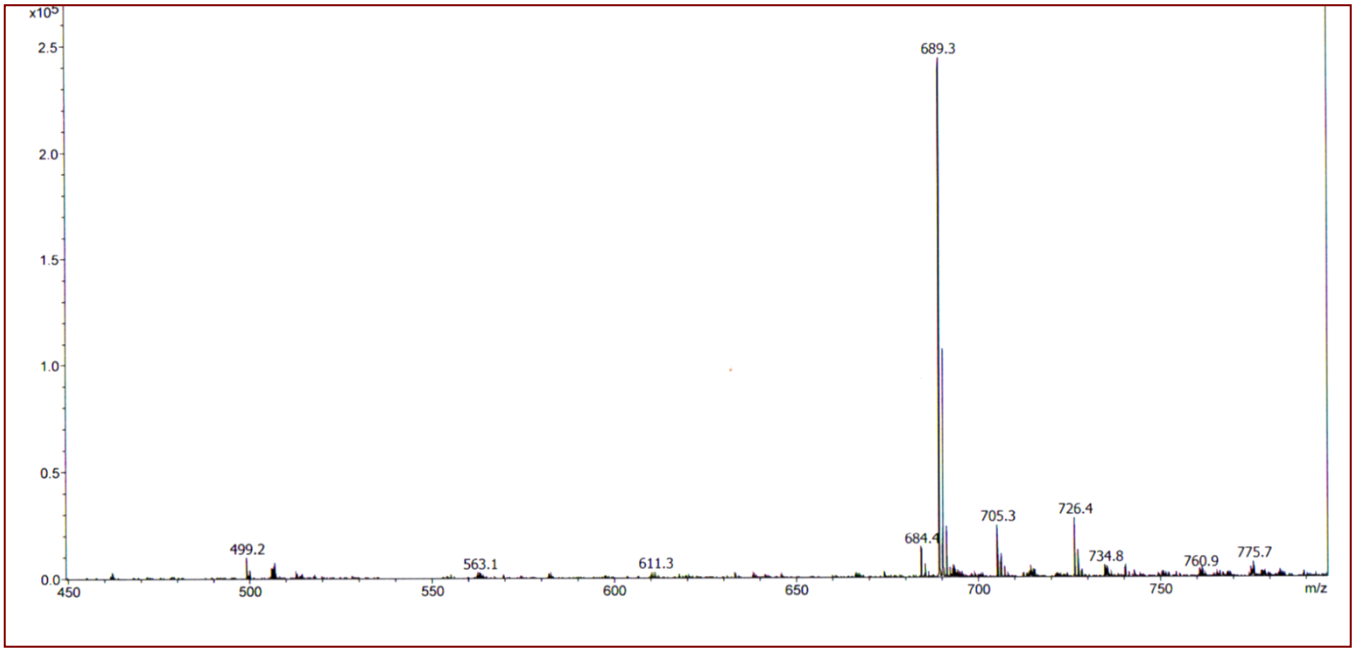

Figure B.13 ESI mass spectrum of Boc-protected Ph/NH_2 TANI (**6**).

NH_2/NH_2 TANI synthesis

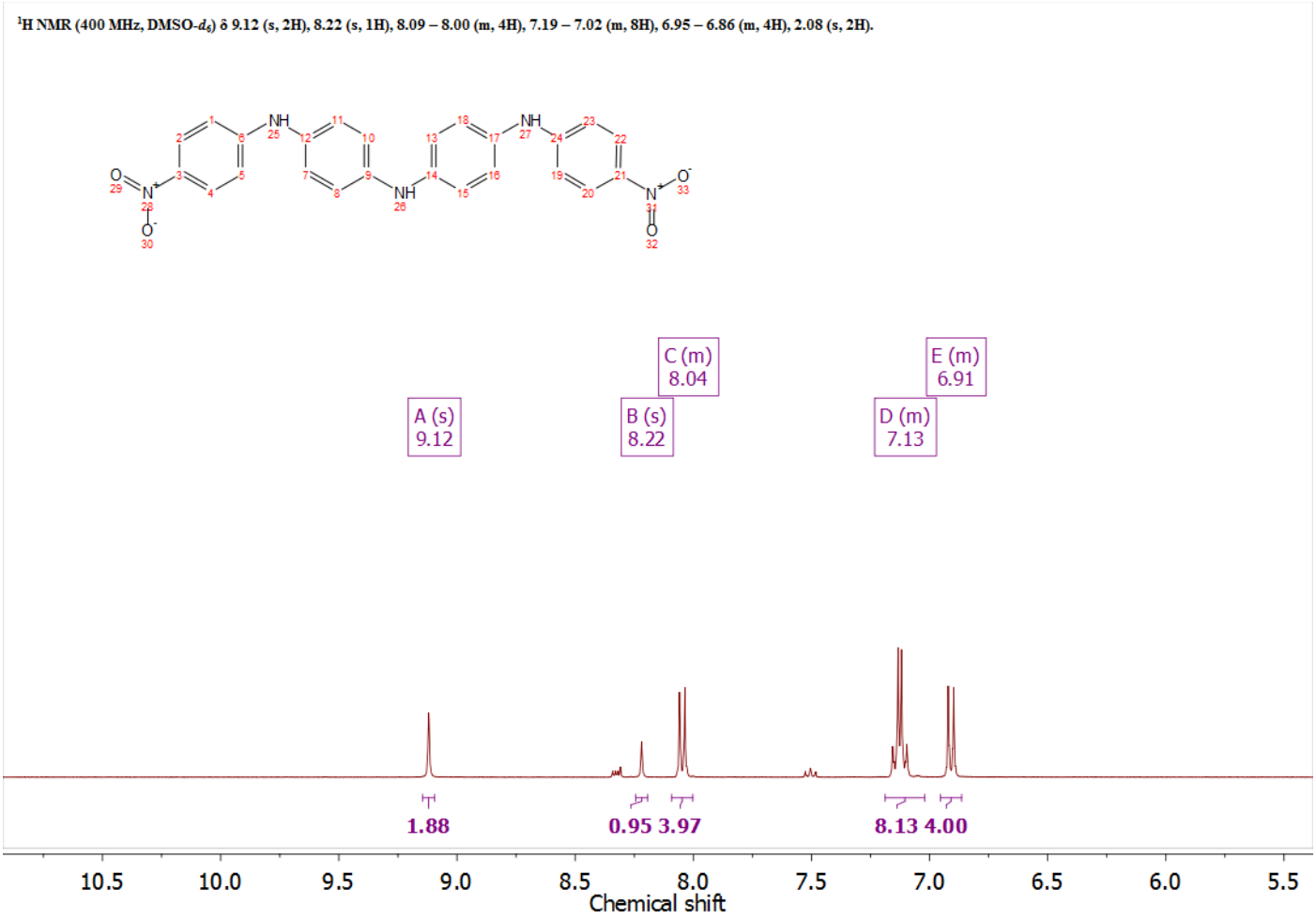

Figure B.14 ^{1}H NMR of LEB NO_2/NO_2 TANI.

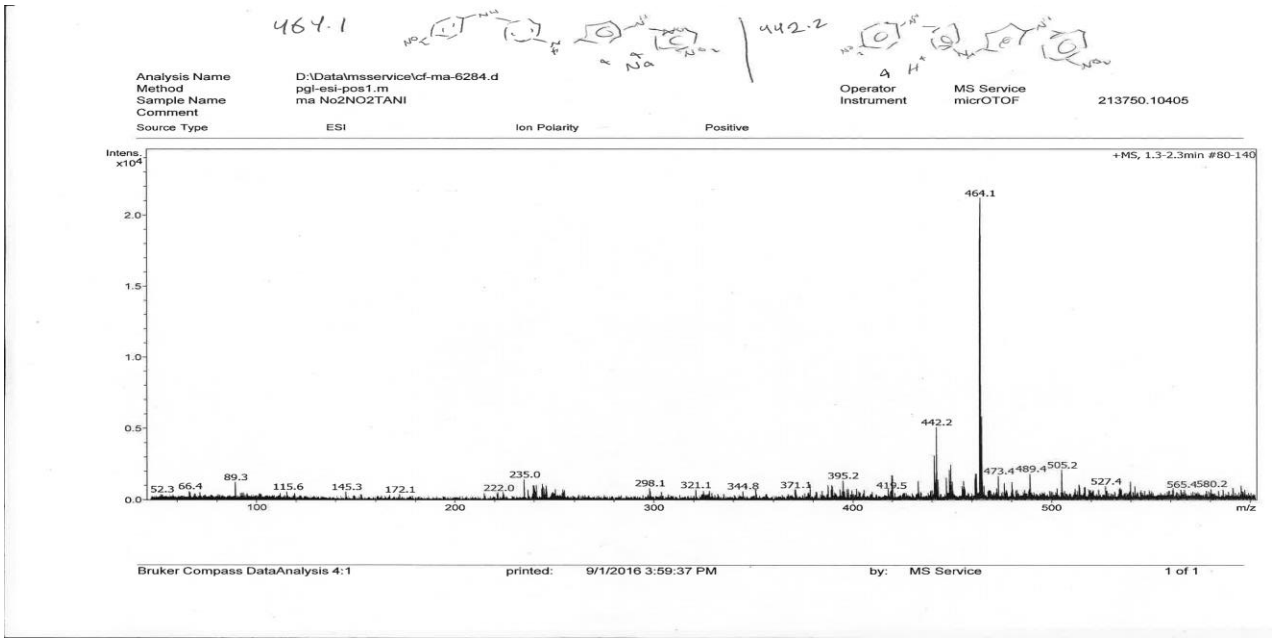

Figure B.15 ESI spectrum of LEB NO_2 /NO_2 TANI.

^{1}H NMR (400 MHz, DMSO-d_6) δ 7.21 – 7.04 (m, 8H), 6.87 – 6.78 (m, 4H), 6.53 – 6.45 (m, 4H), 5.08 (s, 4H), 1.37 – 1.33 (m, 27H).

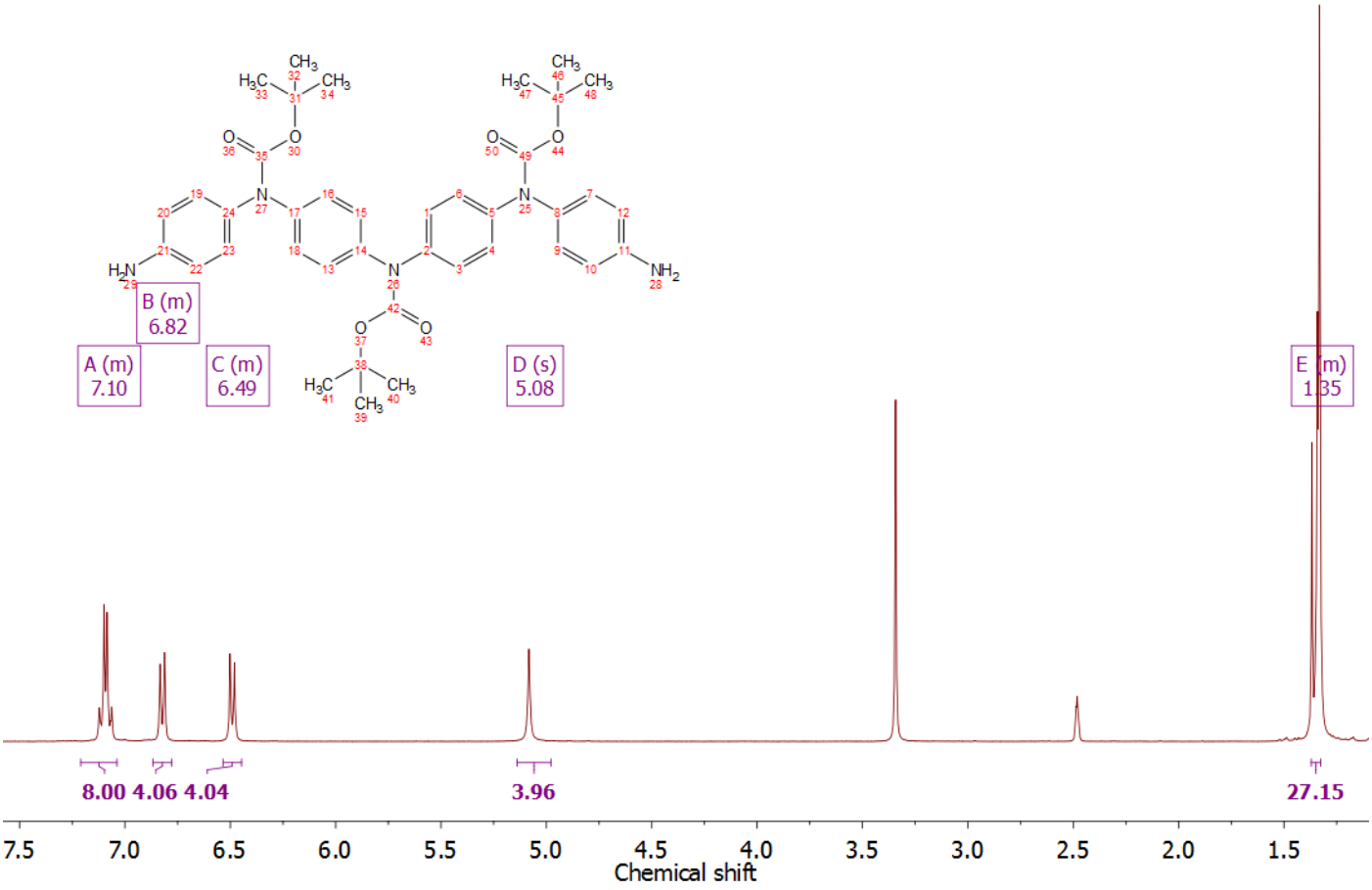

Figure B.16 ^{1}H NMR of Boc NH_2 /NH_2 TANI.

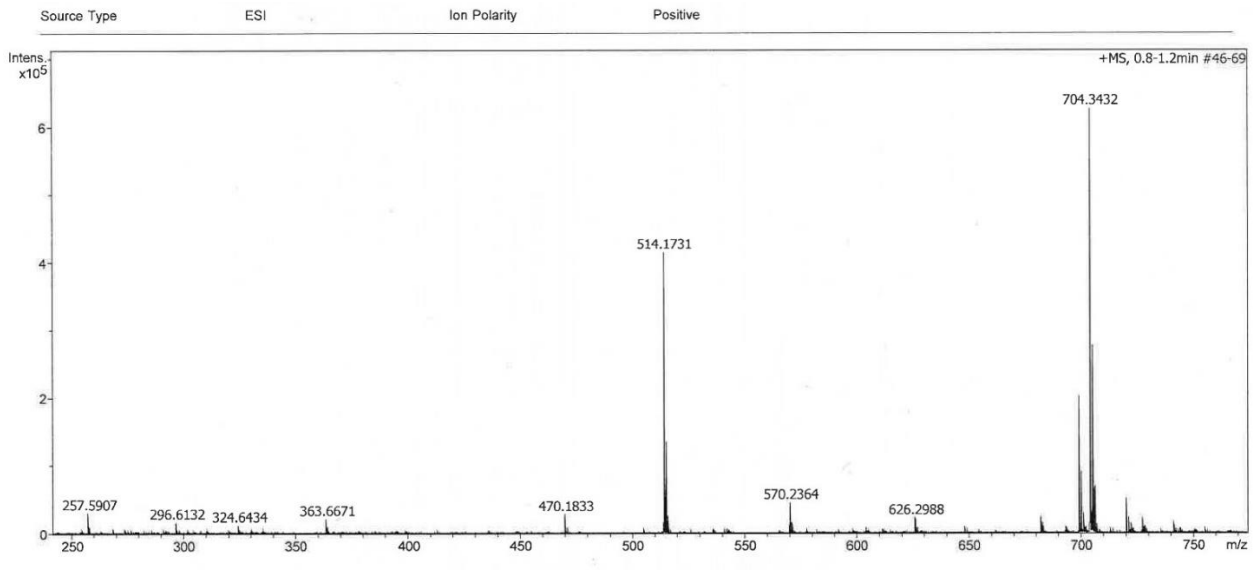

Figure B.17 ESI spectrum of Boc NH_2 /NH_2 TANI.

TANI single-tailed amphiphile synthesis

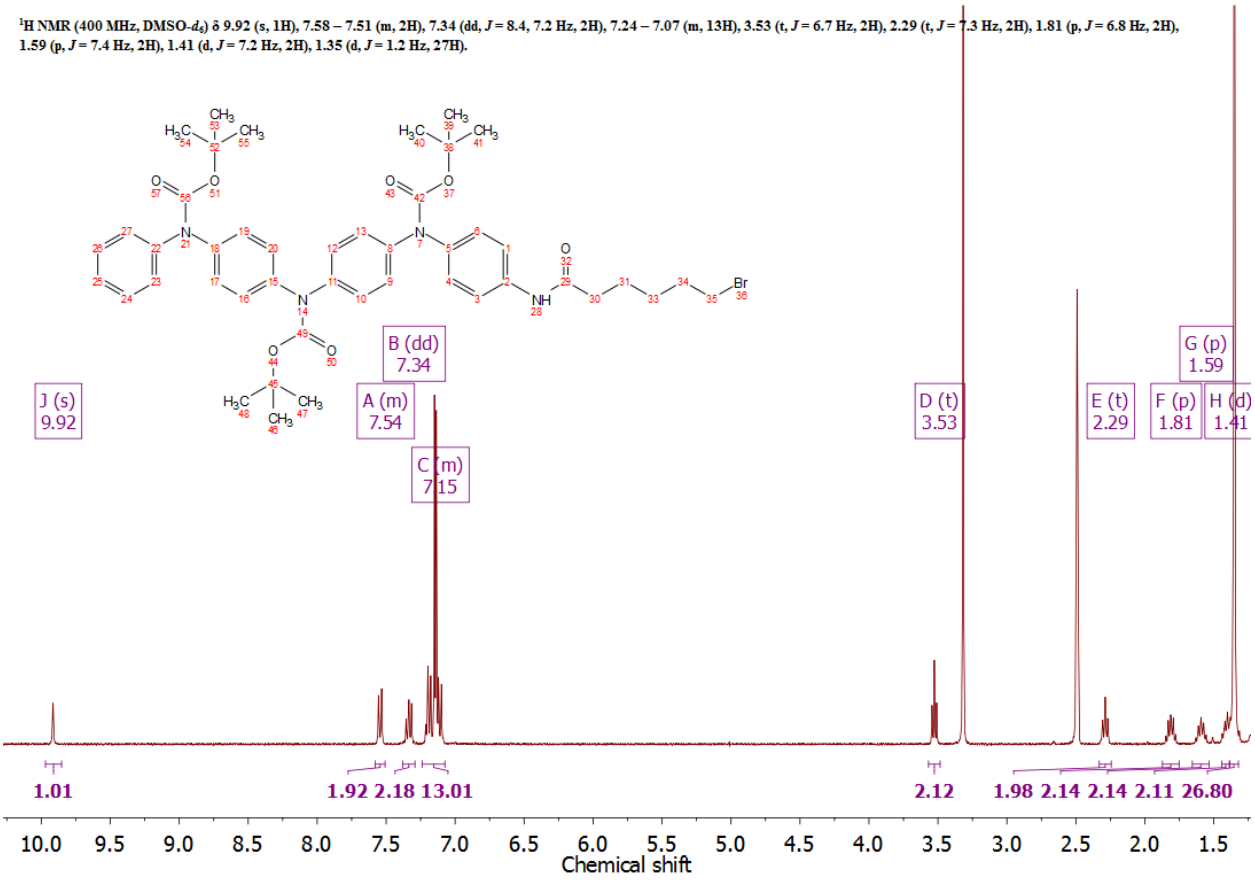

Figure B.18 ^{1}H NMR of Boc Ph/NH2 (C6Br).

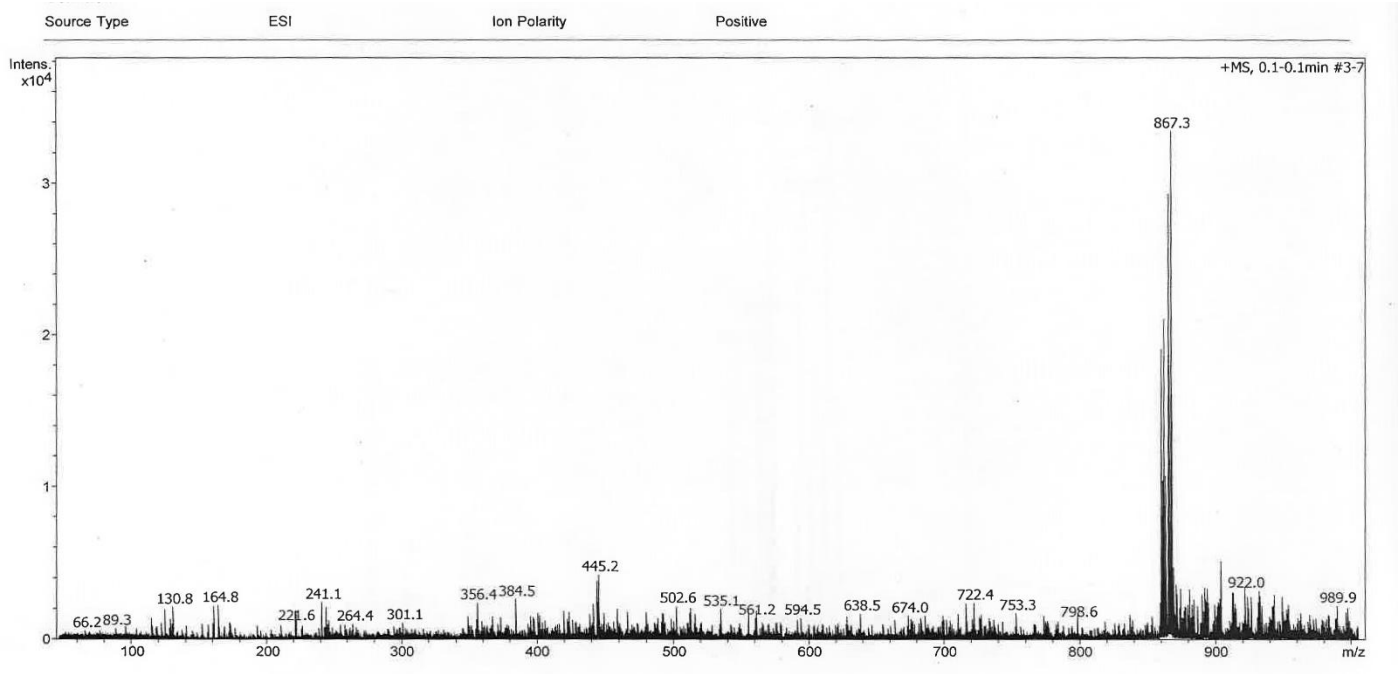

Figure B.19 ESI sepctrum of Boc Ph/NH2 (C6Br).

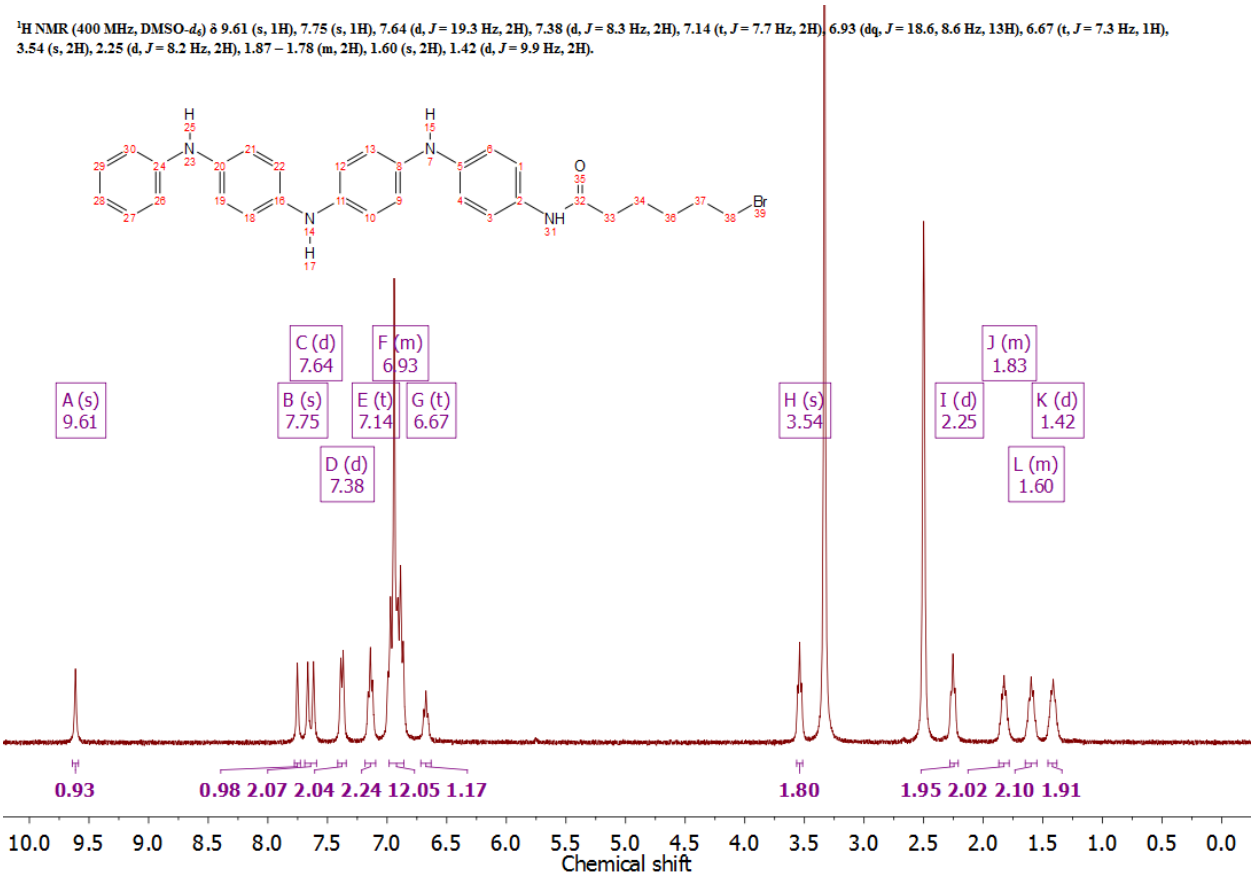

Figure B.20 ^{1}H NMR of LEB Ph/NH_2 (C6Br).

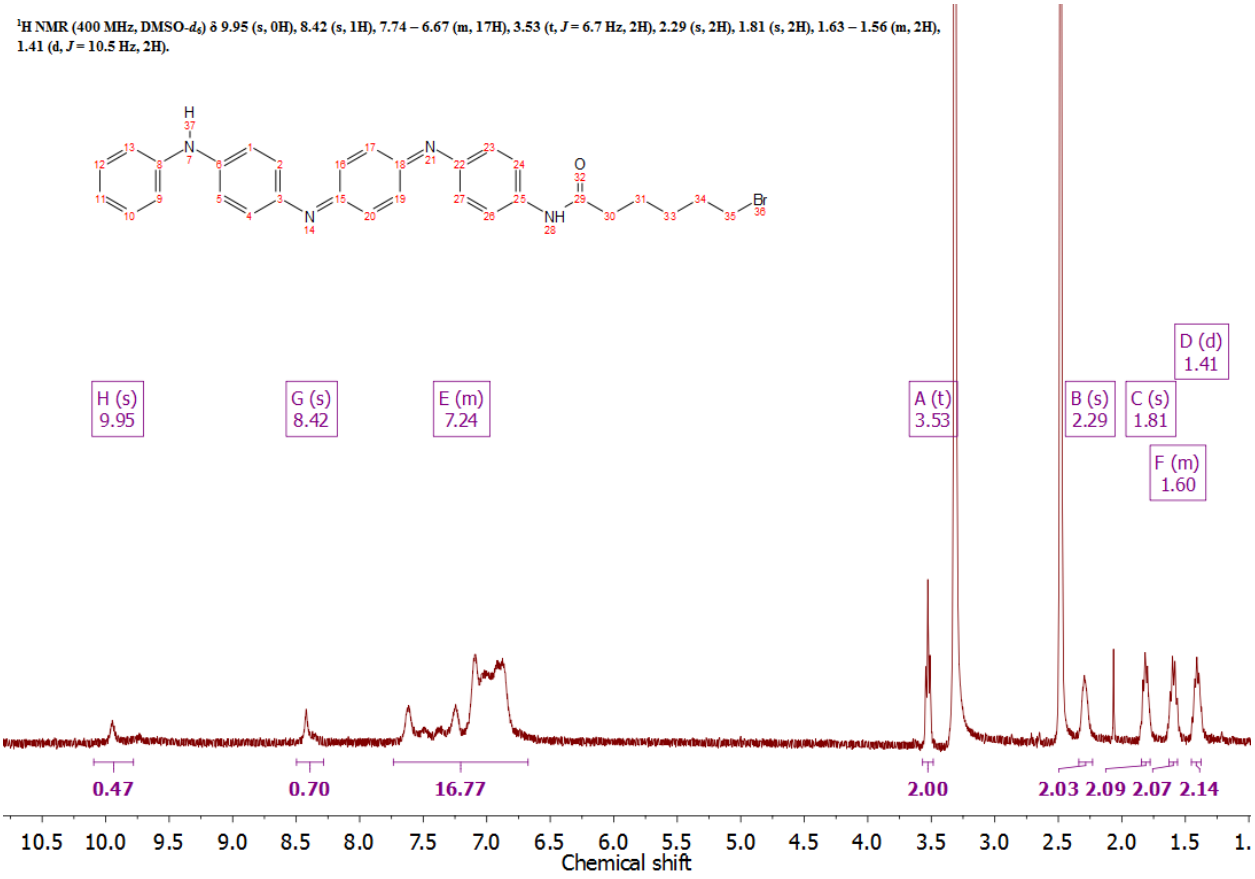

Figure B.21 ^{1}H NMR of EB Ph/NH_2 (C6Br).

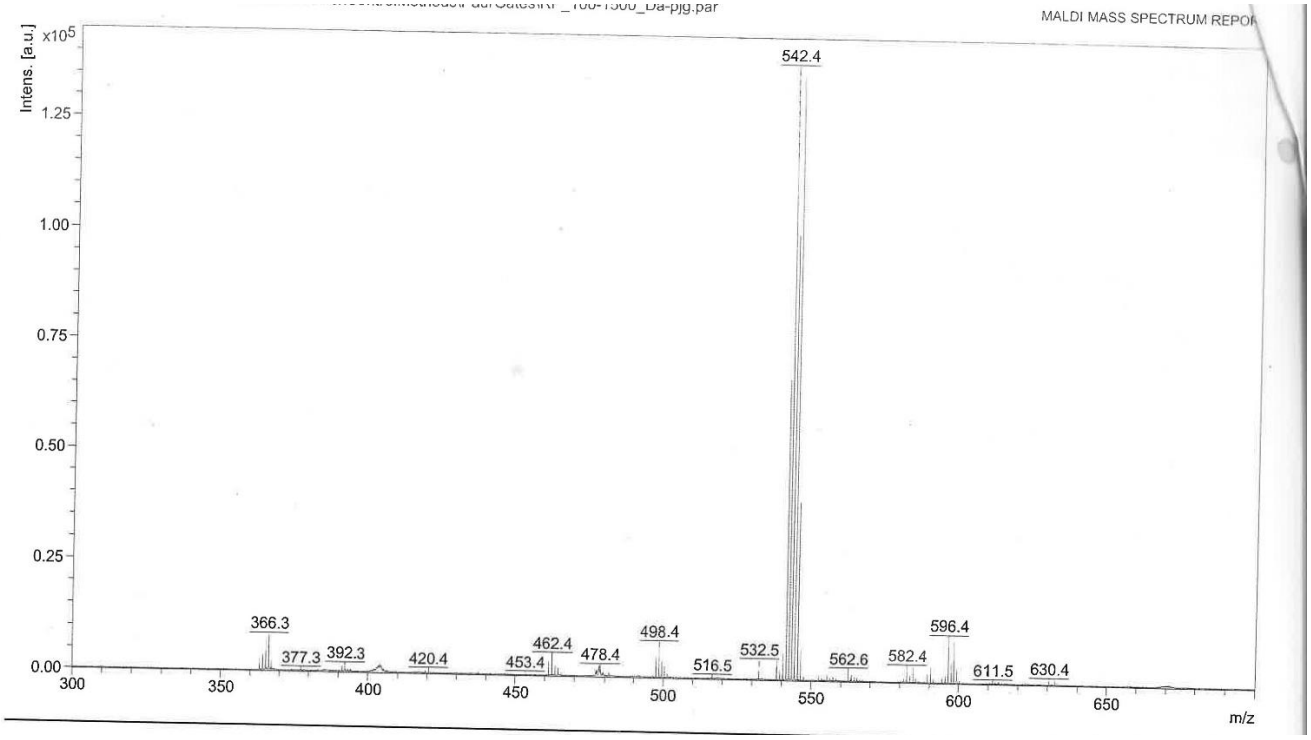

Figure B.22 ESI spectrum of EB Ph/NH_2 (C6Br).

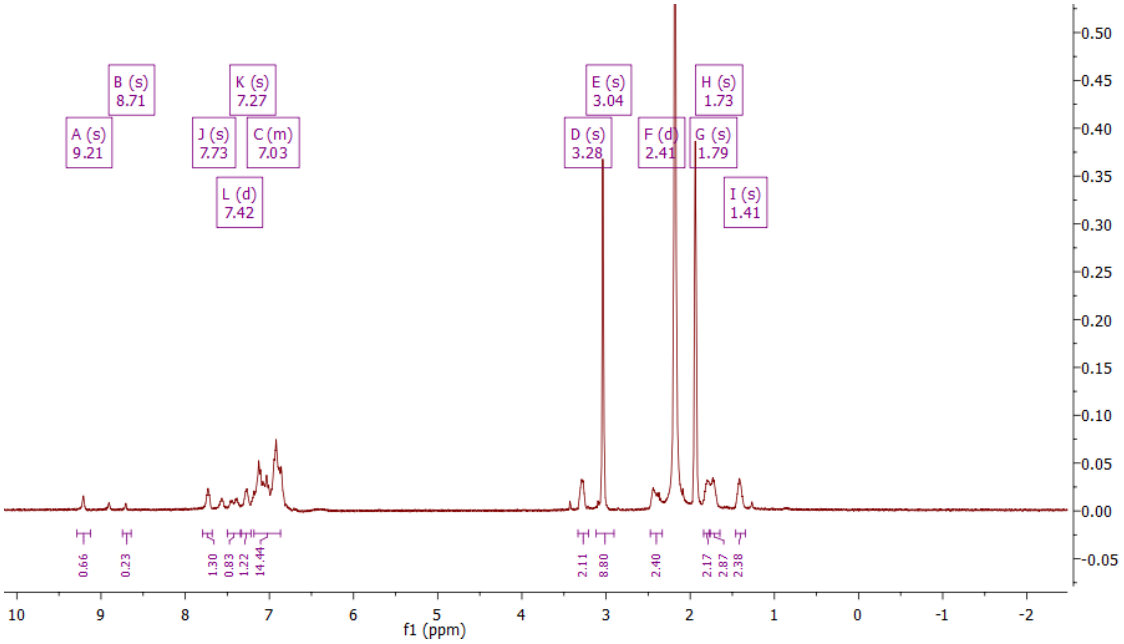

Figure B.23 ^{1}H NMR spectrum of TANI-PTAB.

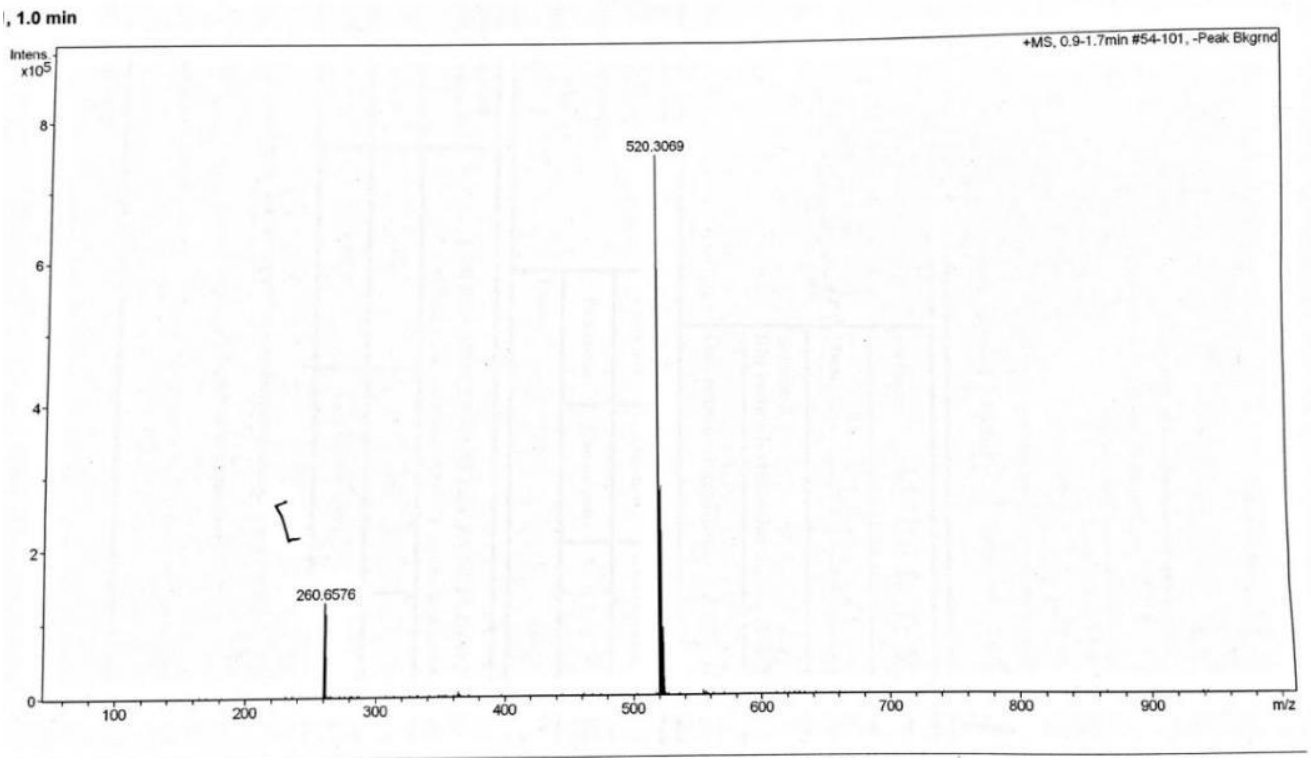

Figure B.24 ESI spectrum of TANI-PTAB.

^{1}H NMR (500 MHz, DMSO-d_6) δ 9.70 (s, 1H), 7.71 (s, 1H), 7.65 (s, 1H), 7.58 (s, 1H), 7.37 – 7.31 (m, 2H), 7.16 – 7.09 (m, 2H), 6.97 – 6.84 (m, 12H), 6.67 (t, J = 7.3 Hz, 1H), 2.26 (t, J = 7.3 Hz, 2H), 2.18 – 2.08 (m, 2H), 1.77 (d, J = 14.7 Hz, 9H), 1.59 (p, J = 7.4 Hz, 2H), 1.49 (dq, J = 11.2, 8.2, 7.4 Hz, 2H), 1.39 (td, J = 8.1, 4.9 Hz, 2H).

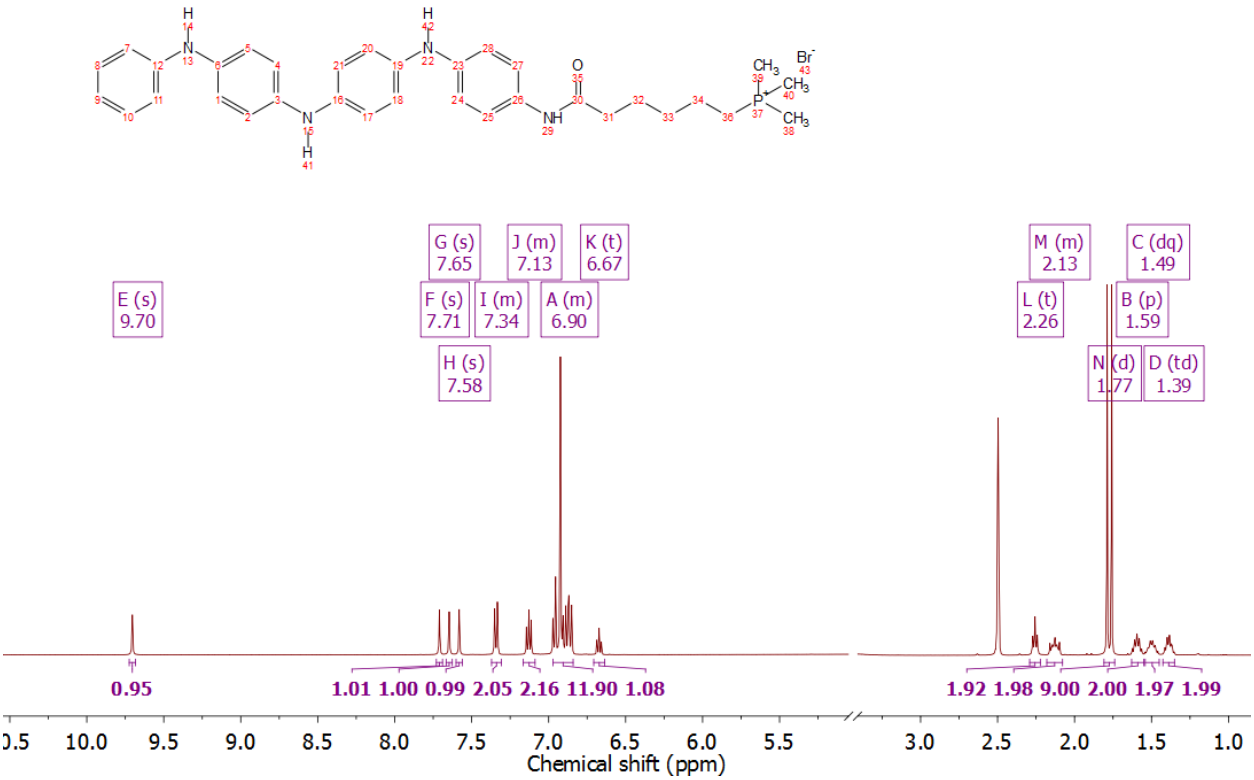

Figure B.25 ^{1}H NMR spectrum of LEB TANI-PTPB.

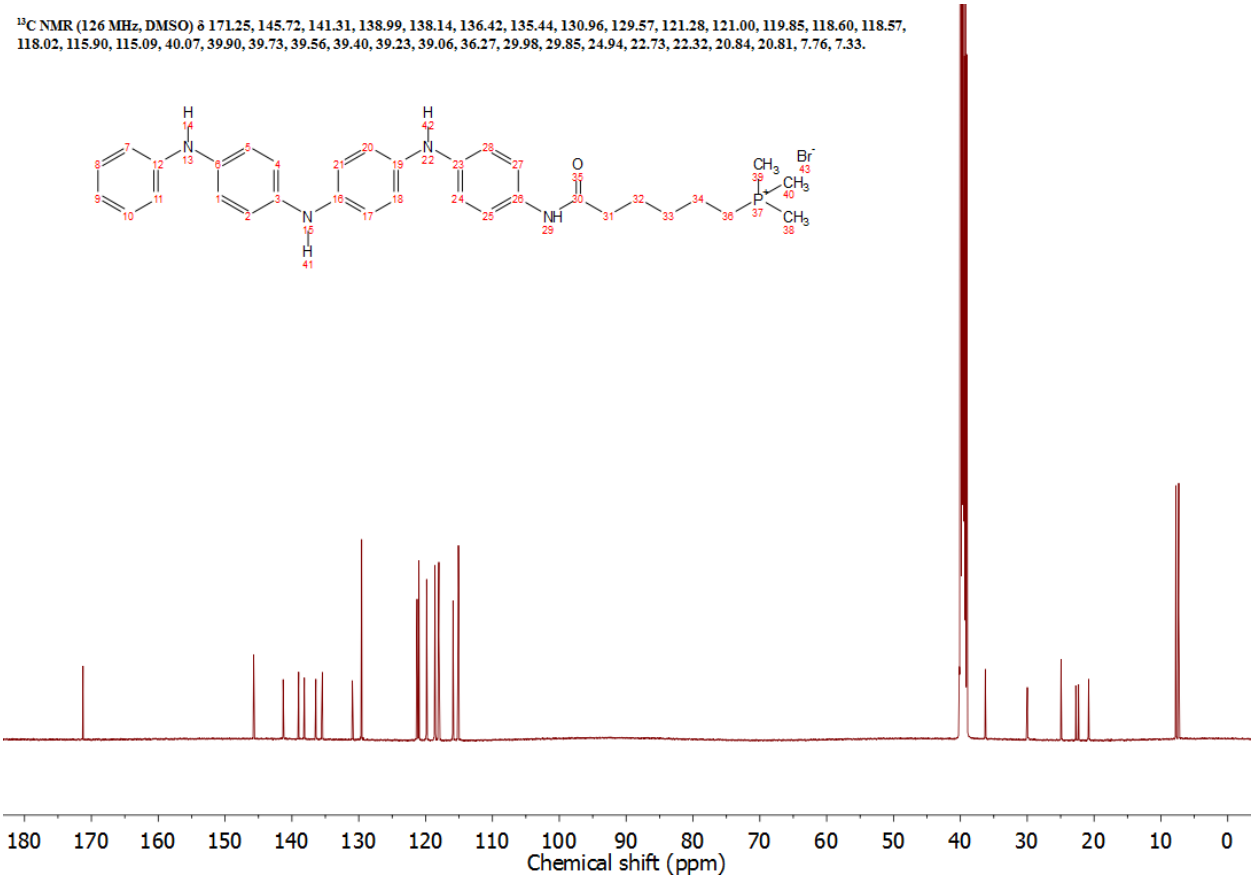

Figure B.26 ^{13}C NMR spectrum of LEB TANI-PTPB.

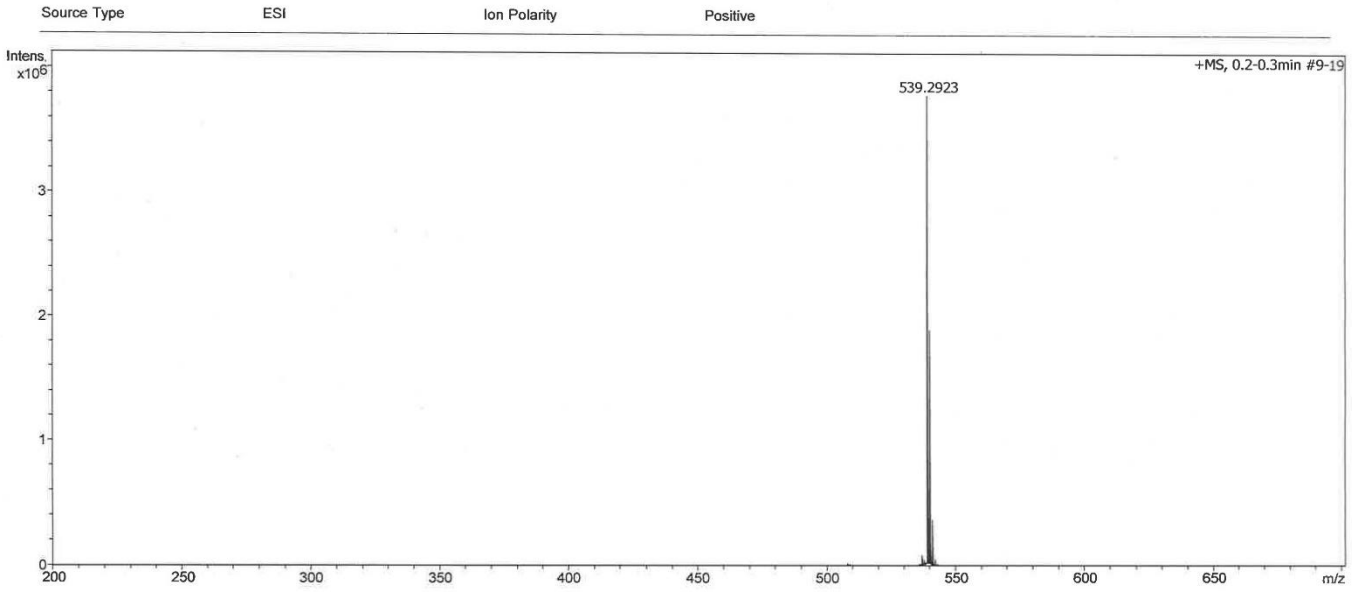

Figure B.27 ESI spectrum of LEB TANI-PTPB.

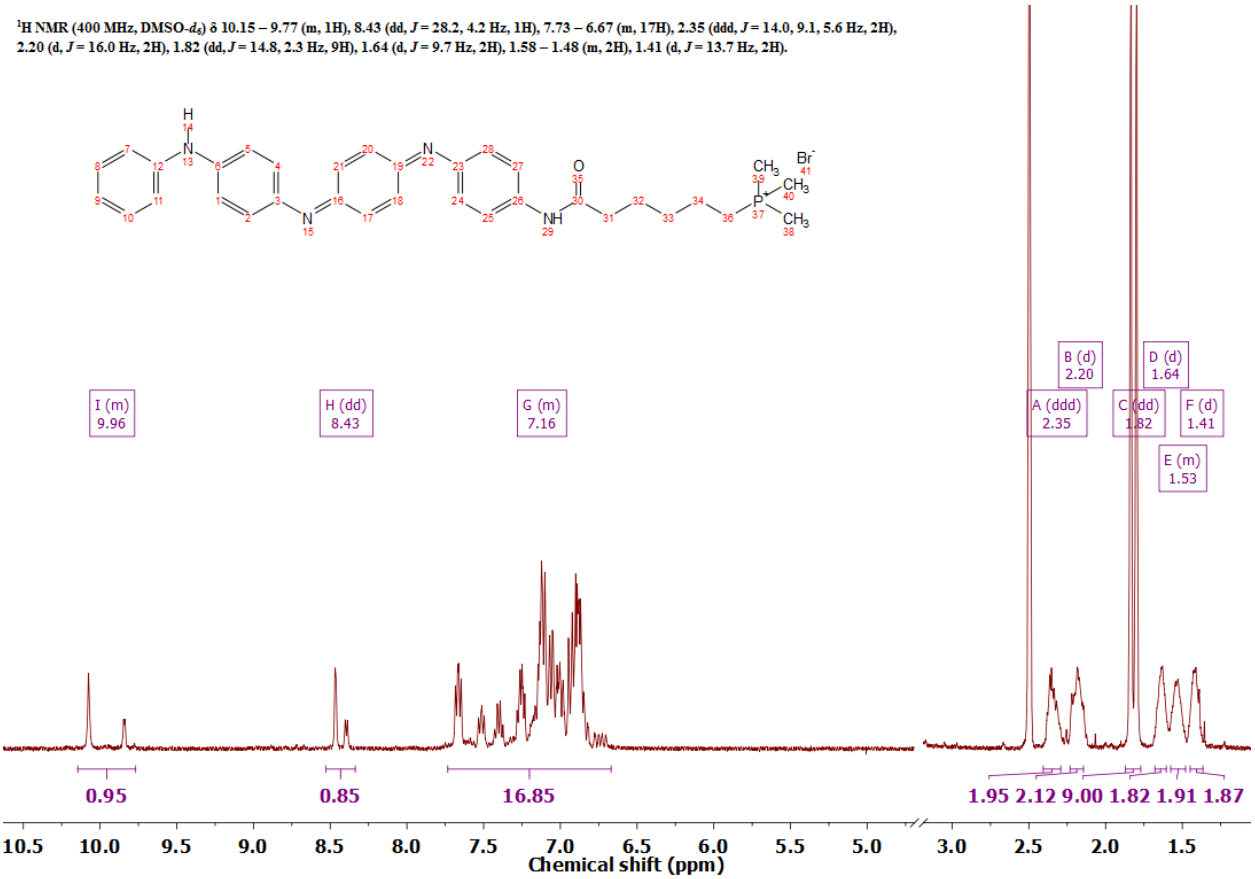

Figure B.28 ^{1}H NMR spectrum of EB TANI-PTPB.

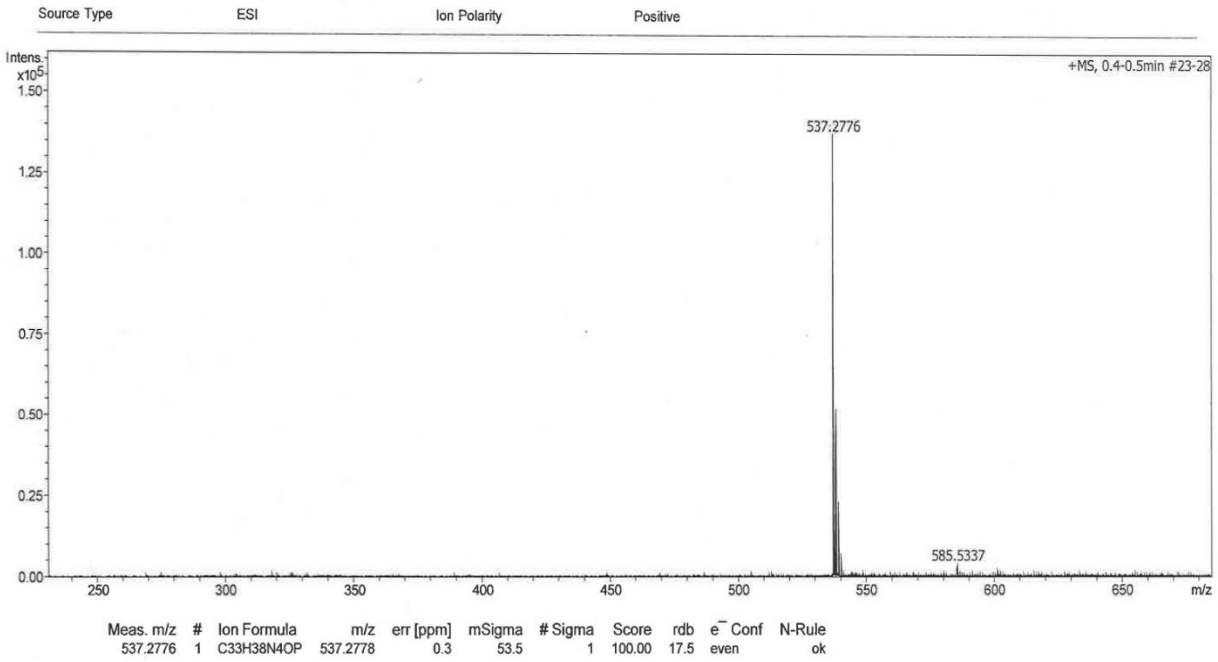

Figure B.29 ESI spectrum of EB TANI-PTPB.

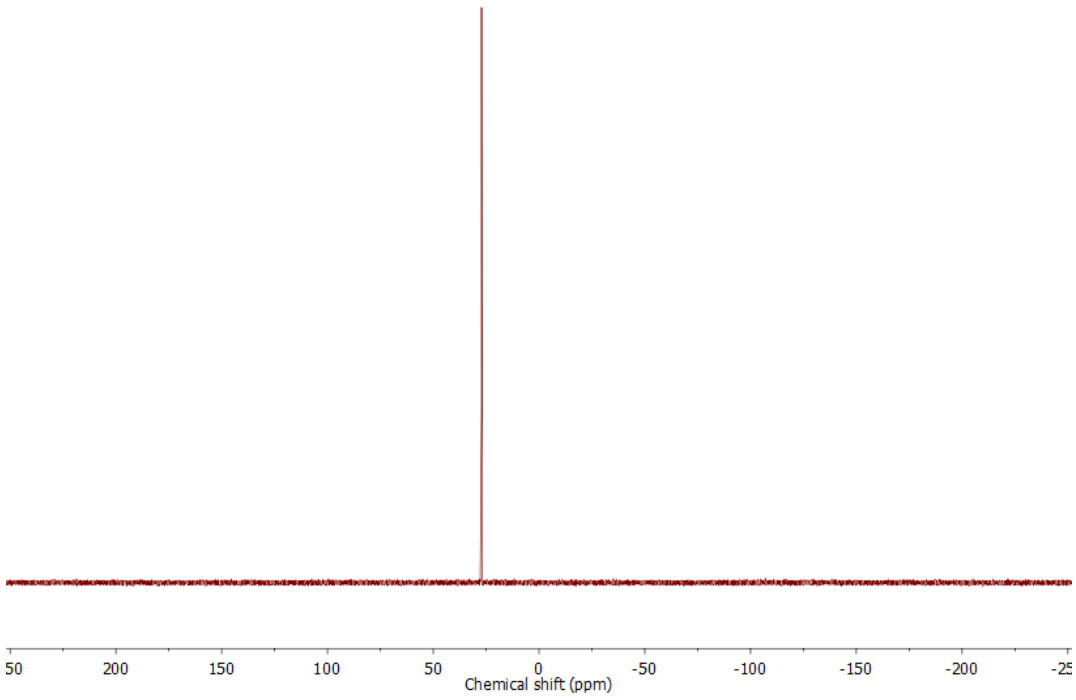

Figure B.30 ^{31}P NMR spectrum of EB TANI-PTPB.

TANI bolaamphiphile synthesis

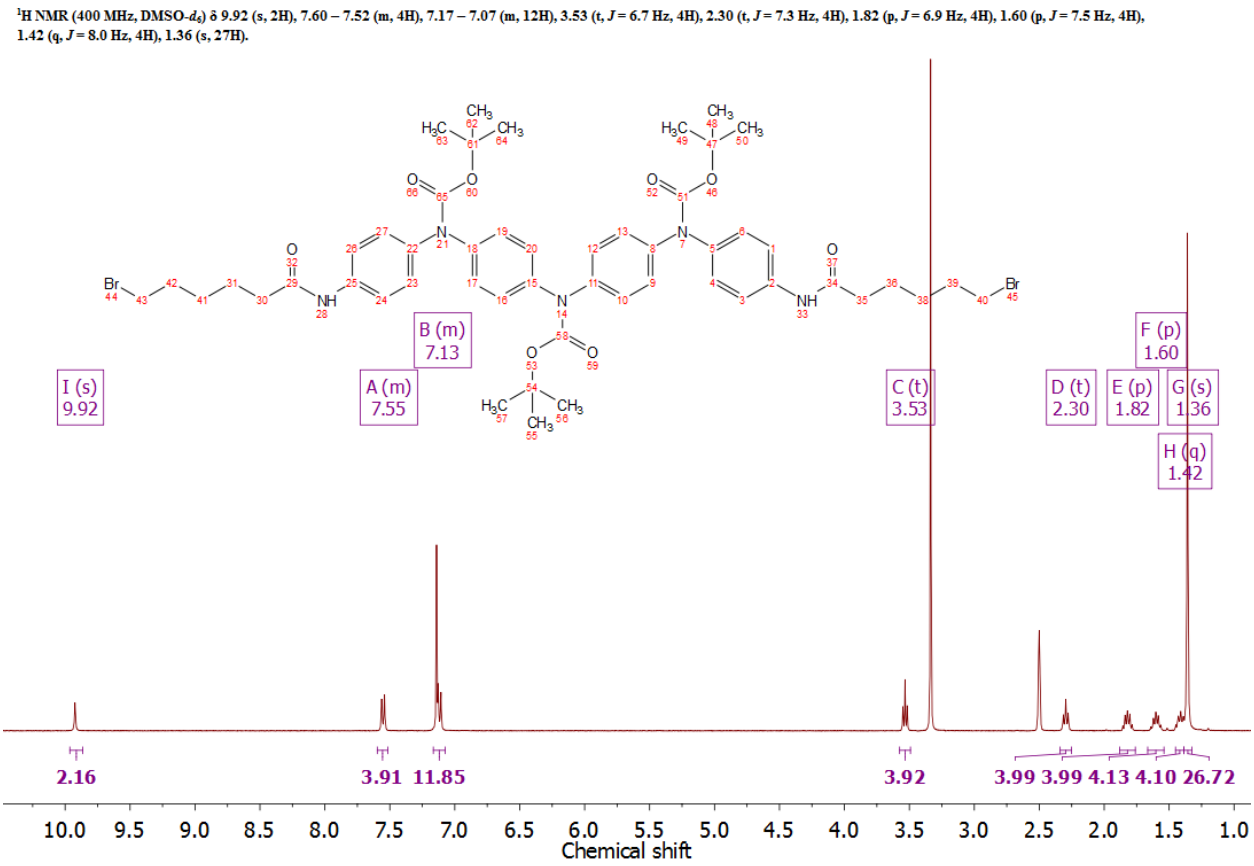

Figure B.31 ^{1}H NMR of Boc NH_2/NH_2 $(C6Br)_2$.

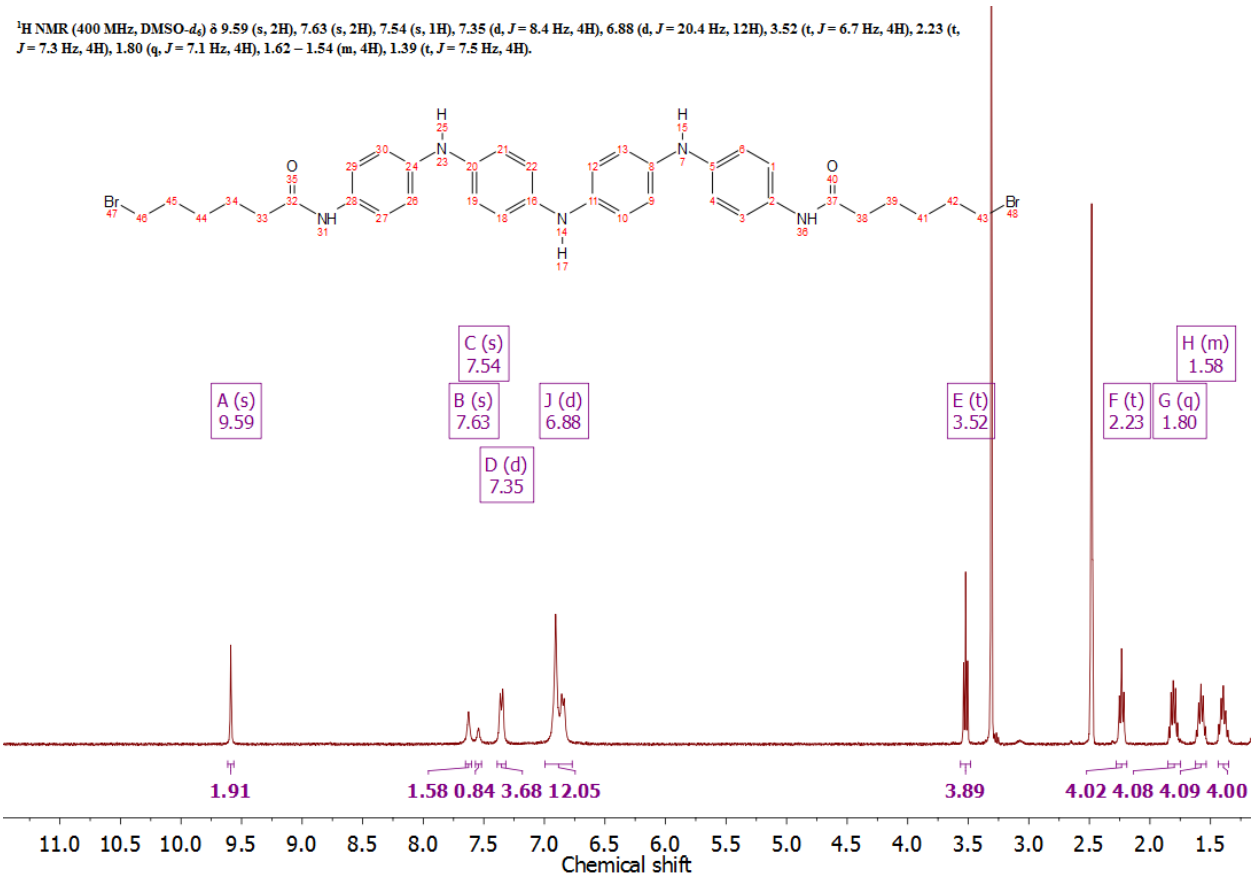

Figure B.32 ^{1}H NMR of LEB $NH_2/NH_2(C6Br)_2$.

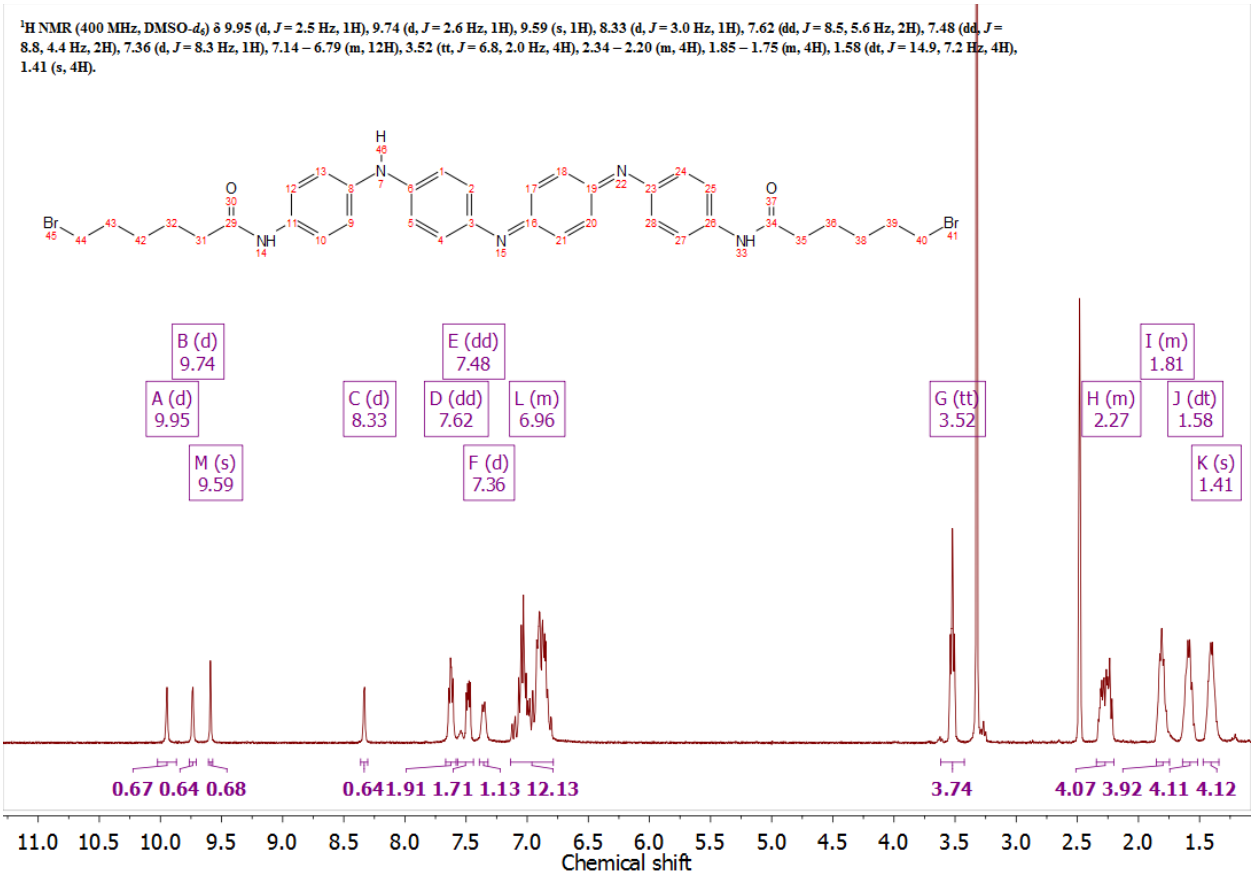

Figure B.33 ^{1}H NMR of EB NH_2/NH_2 $(C6Br)_2$.

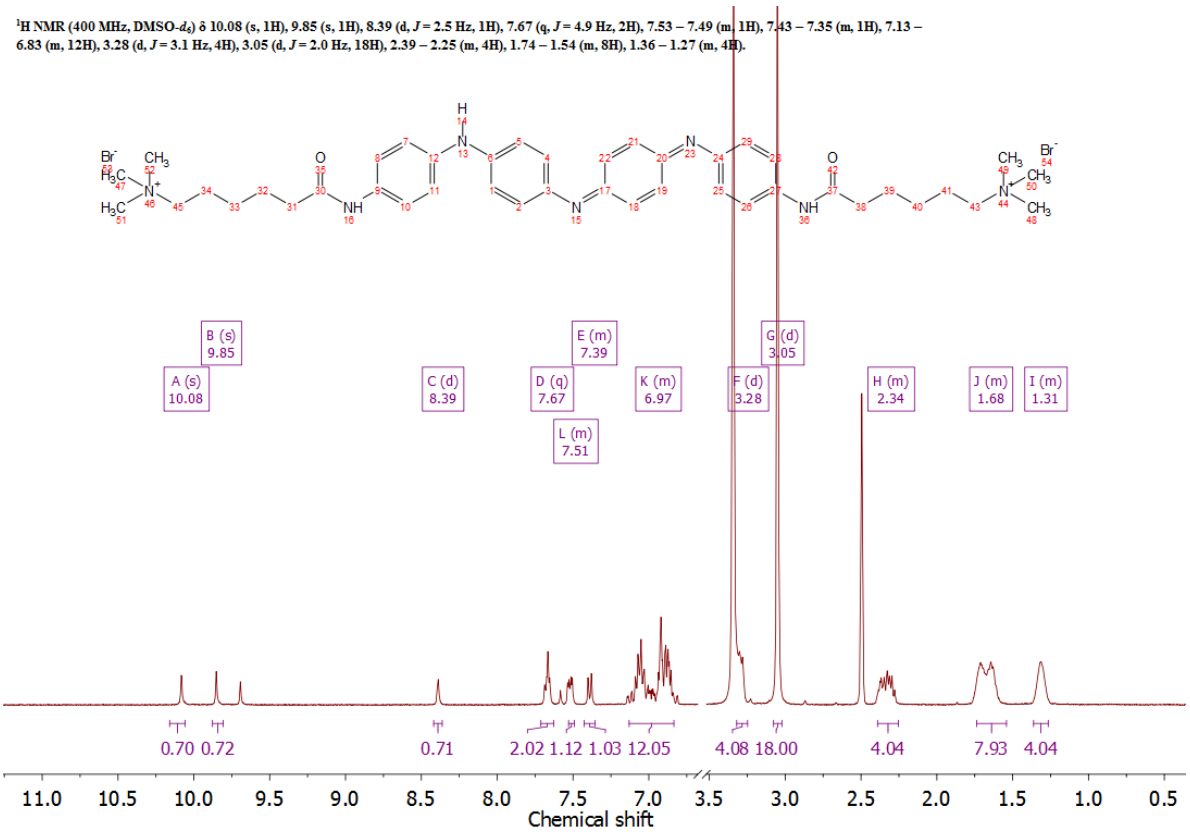

Figure B.34 ^{1}H NMR of EB TANI-(PTAB)$_2$.

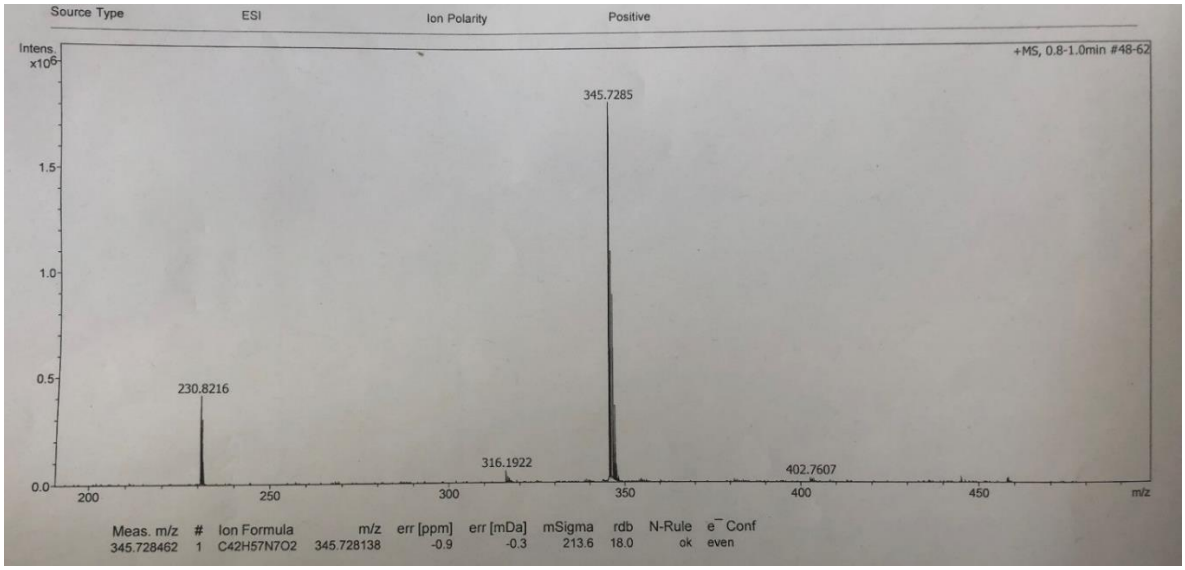

Figure B.35 High-resolution mass spectrum of EB TANI-(PTAB)$_2$

^{1}H NMR (400 MHz, DMSO-d_6) δ 9.91 (s, 2H), 7.59 – 7.52 (m, 4H), 7.17 – 7.08 (m, 12H), 3.52 (t, J = 6.7 Hz, 4H), 2.28 (t, J = 7.4 Hz, 4H), 1.84 – 1.69 (m, 4H), 1.58 (s, 4H), 1.36 (s, 27H), 1.30 (q, J = 3.9 Hz, 8H).

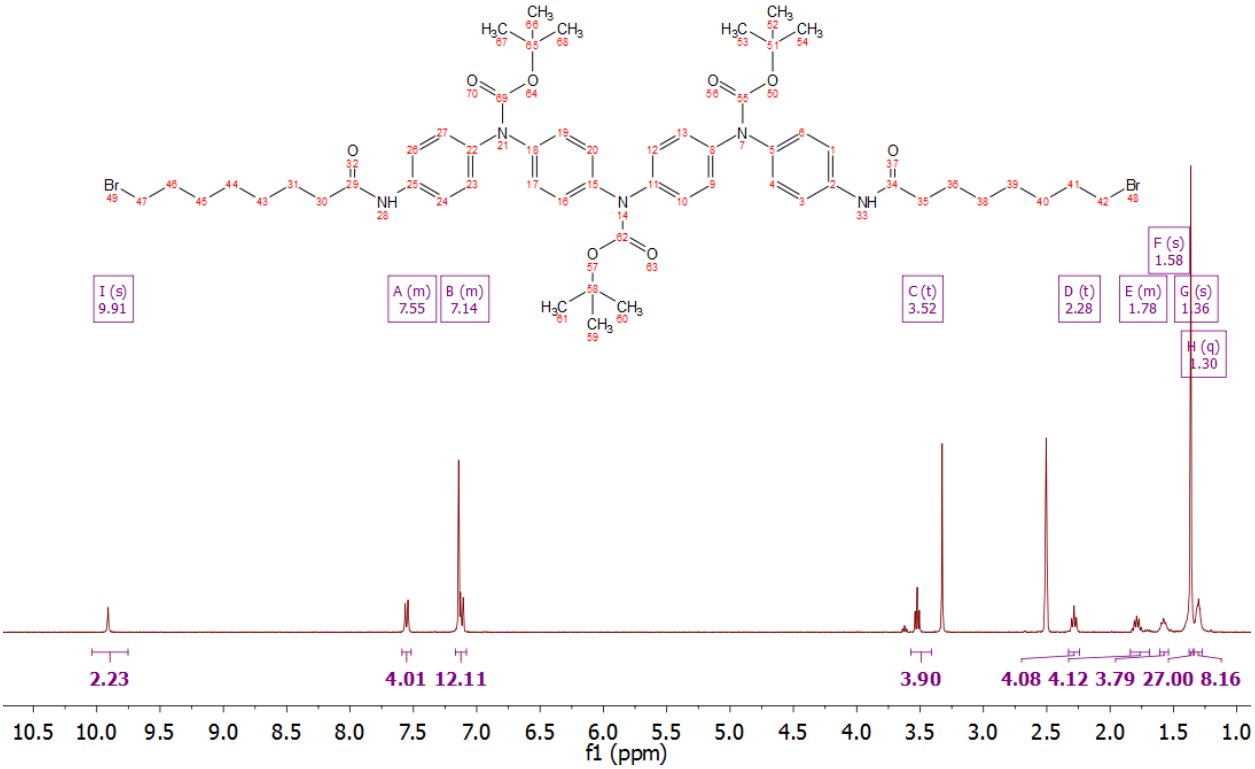

Figure B.36 ^{1}H NMR of Boc NH_2/NH_2 $(C8Br)_2$.

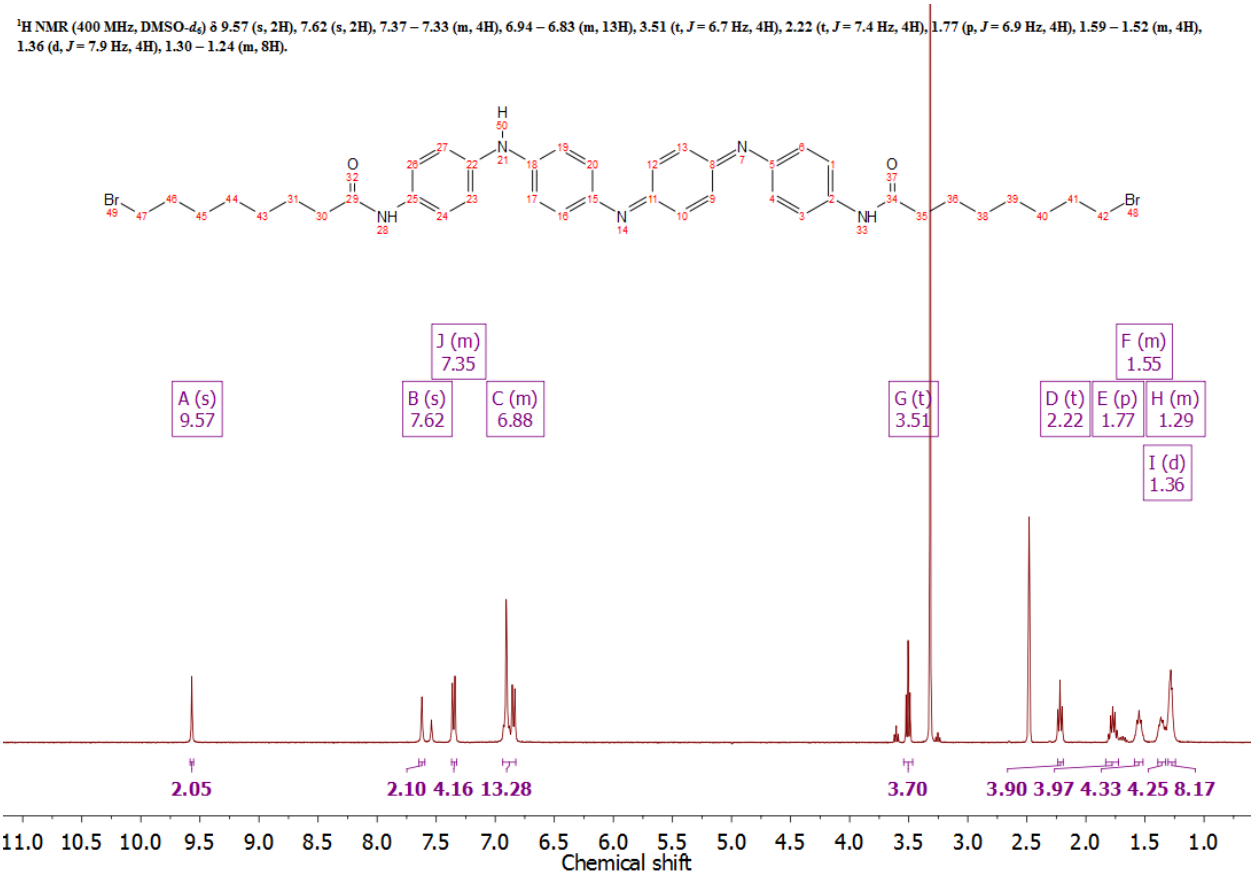

Figure B.37 ^{1}H NMR of LEB NH_2/NH_2 $(C8Br)_2$.

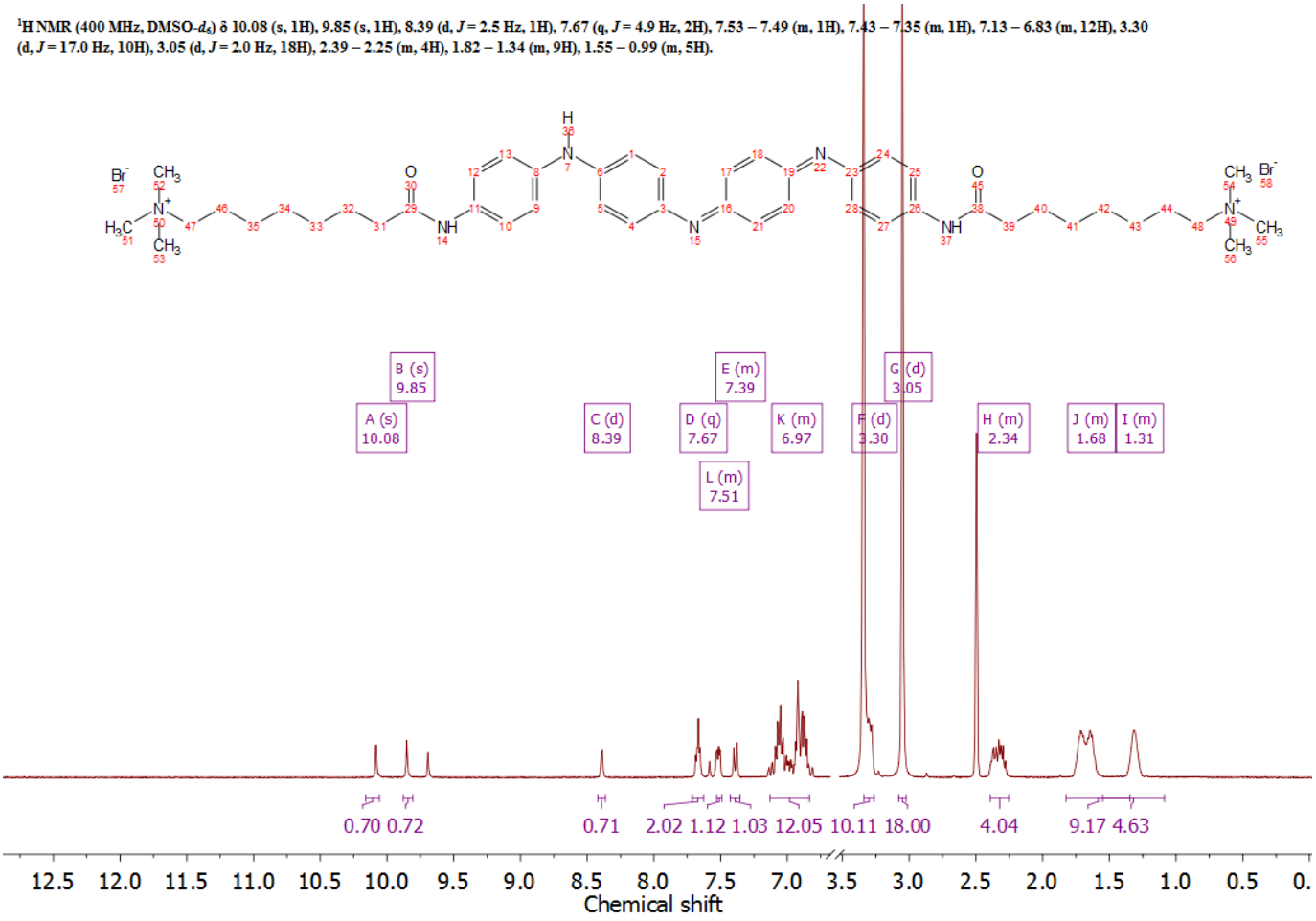

Figure B.38 ^{1}H NMR of EB TANI-$(HTAB)_2$

Appendix C

Coordinates of optimized geometry: TANI PTAB

	X	Y	Z
C	-3.61962868	0.50060859	1.99647805
H	-3.44091429	0.33957231	3.05688537
C	-4.86689194	0.95391971	1.57851734
H	-5.63667054	1.14886486	2.31591064
C	-5.11828586	1.20192630	0.21778669
C	-4.07434936	0.97107534	-0.69537338
H	-4.25108715	1.13499049	-1.75582941
C	-2.83099254	0.51063052	-0.27607363
H	-2.06042000	0.31044416	-1.01239652
C	-2.57911657	0.26877338	1.08425227
N	-6.33559377	1.70051415	-0.25969449
N	-1.35519905	-0.24096474	1.55492647
C	-7.59336914	1.69117710	0.35965237
C	-10.20447156	1.70172585	1.48089152
C	-8.50429216	2.72259363	0.07924450
C	-8.01586330	0.65728643	1.21258549
C	-9.29484015	0.66806538	1.75887291
C	-9.78401155	2.73324129	0.62544204
H	-8.19617415	3.54351798	-0.56420840
H	-7.35416520	-0.17519599	1.42379240
H	-9.60535792	-0.15370288	2.39973088
H	-10.44661158	3.56355633	0.41033802
C	-0.07121048	-0.02517487	1.05898722
C	2.59317023	0.36455531	0.17662157
C	0.25919559	1.05913193	0.22607605
C	0.96460220	-0.89876871	1.43802490
C	2.27708052	-0.71204639	1.01884854
C	1.56756412	1.23784652	-0.20907654
H	-0.50154667	1.77314892	-0.06640476
H	0.73400094	-1.74731911	2.07807193
H	3.05598820	-1.39536140	1.32590866
H	1.79469688	2.08664307	-0.85156963
N	3.89815416	0.62584089	-0.31016802
N	-11.46333878	1.67805220	2.10310259
H	3.97410027	1.44766522	-0.89329917
H	-11.48181458	1.25203979	3.01741586
C	-12.64834857	2.30802602	1.71631480
C	-15.11388263	3.49430113	1.02347944
C	-13.60685203	2.61039002	2.70170014
C	-12.95051894	2.59993942	0.37334432
C	-14.16727428	3.19370818	0.04215396
C	-14.82491815	3.18831796	2.35531681
H	-13.38461801	2.39224366	3.74391449
H	-12.24463924	2.33978850	-0.40705010
H	-14.38044619	3.40906980	-1.00147541
H	-15.54803939	3.41004507	3.13541409
H	-16.05985698	3.95416033	0.75559669
C	5.06539822	-0.04881465	-0.06600502
O	5.14892324	-1.05735627	0.62778784
C	6.29730245	0.59231350	-0.72143013
H	6.49506271	1.54171035	-0.20568497
H	6.07061710	0.85244171	-1.76442328
C	7.53762481	-0.30472087	-0.64219733
H	8.41417491	0.29955589	-0.90548915
H	7.66044463	-0.62401535	0.39857014
C	7.44556591	-1.54827127	-1.54079827
H	7.40556392	-1.24410053	-2.59659911
H	6.50436840	-2.06096723	-1.32255675
C	8.58268442	-2.56897684	-1.33977584
H	8.34996491	-3.46564515	-1.92302621
H	8.60353141	-2.86675911	-0.28599351
C	9.93950579	-2.00667047	-1.76379161
N	11.12359164	-2.95146665	-1.66489269
H	9.90452357	-1.68323859	-2.80926045
H	10.20694440	-1.13932762	-1.15457160
C	12.36646299	-2.21246338	-2.11226777
H	13.20927433	-2.91780486	-2.03160681
H	12.50386540	-1.34894315	-1.45910074
H	12.21687390	-1.88484487	-3.14265356
C	11.34832834	-3.42338717	-0.24652558
H	12.26261296	-4.03796852	-0.25908807
H	10.48855227	-4.01220654	0.07069351
H	11.46219358	-2.54519364	0.39212884
C	10.95717836	-4.16007606	-2.55795093
H	10.78011268	-3.81067528	-3.57711371
H	10.10964993	-4.74770292	-2.20699437
Br	14.13392416	-5.15059466	-1.48340308
H	11.89103782	-4.74037372	-2.48296419
H	-6.28020061	2.22674969	-1.11824371
H	-1.41420466	-0.84729460	2.35868319

Scattering analysis of 4 mM TANI(TFA)$_2$-PTAB

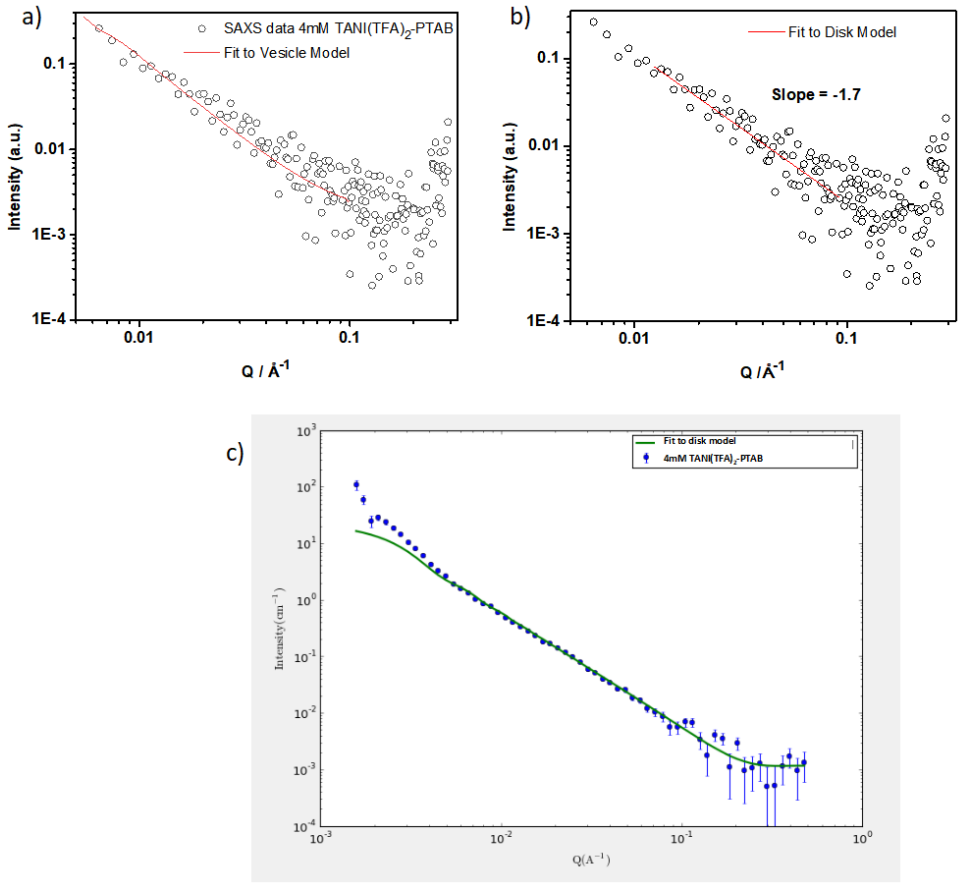

Figure C.1 (a) Solution SAXS data for 4 mM ES TANI(TFA)$_2$-PTAB (open circles) with fit to the vesicle model overlaid (solid red line);(b) Solution SAXS data for 4 mM ES TANI(TFA)$_2$-PTAB (open circles) with fit to the disk model overlaid (solid red line);(c) Solution SANS data for 4 mM ES TANI(TFA)$_2$-PTAB with fit to the disk model overlaid.

SAXS and SANS data on 4mM TANI doped with TFA show a ~q = -2 dependence, suggesting that the sample is present as a spherical or disk-like aggregate. However a fitting the data to a vesicle model gives a radius of 400.79 +/-50.79 Å corresponding to a diameter of ~800 Å which far exceeds that seen by AFM, TEM or DLS. A thickness of 29A +/- 1.30 Å is also observed in this model, which is commensurate with the thickness of one interdigitated layer of **TANI(TFA)$_2$-PTAB**. This is likely caused by polydispersity in the sample and the poor fit to data at low q values. A fit to a disk model gives a radius of 877 Å, and a thickness of 18 Å.

Table C.1 The relative fitting data

Fit parameter	Value	Error
Background	0.0023662	0.004136
Radius	400.79	50.971
Scale	2.7215×10^{-5}	1.267×10^{-6}
Thickness	29.67	1.2991
PD (ratio)	0.4	0.009
Chi2	1.37	

Coordinates of optimized geometry: TANI-PTPB

C	4.14675900	1.61437100	0.59236500
H	4.05942400	2.62689300	0.97562500
C	5.35651600	1.02639100	0.44373400
H	6.25595800	1.56148700	0.72587900
C	5.47318800	-0.34812300	-0.03794200
C	4.21940500	-1.04913600	-0.29488400
H	4.30690300	-2.06742300	-0.66274200
C	3.00890500	-0.46101500	-0.15239400
H	2.10715700	-1.00188300	-0.41608000
C	2.89226200	0.91929600	0.31479200
N	6.57242900	-1.03141300	-0.24061800
N	1.79104800	1.60131600	0.49428900
C	7.85139700	-0.49277100	-0.23536600

C	10.56746900	0.36840800	-0.27267000
C	8.89965300	-1.32698900	0.21302500
C	8.21037800	0.77886400	-0.74370000
C	9.53320100	1.18993000	-0.77172300
C	10.21942100	-0.90351900	0.23047200
H	8.64430000	-2.31291900	0.59003300
H	7.45122000	1.42093600	-1.17814900
H	9.78491900	2.15693400	-1.20023400
H	10.98137600	-1.55425300	0.64257900
C	0.51597200	1.03768000	0.44215100
C	-2.16047700	0.10396900	0.38011700
C	0.15479400	-0.17361800	1.07072500
C	-0.50910800	1.78309000	-0.17357500
C	-1.81961100	1.32386400	-0.23169200
C	-1.15860000	-0.62399300	1.04439000
H	0.90043600	-0.74113000	1.61827800
H	-0.25142200	2.73355900	-0.63167900
H	-2.58415700	1.90158600	-0.73075600
H	-1.41375300	-1.55259000	1.54983100
N	-3.46230600	-0.43434600	0.38450600
N	11.86427100	0.86470300	-0.28026800
H	-3.55022100	-1.32569300	0.85636400
H	11.93779100	1.87067100	-0.35927600
C	13.08649300	0.18939200	-0.14408900
C	15.61177300	-1.03849100	0.09614400
C	14.18247700	0.89733000	0.38289300
C	13.27690200	-1.13814500	-0.56676900
C	14.52796900	-1.74136400	-0.43443100

C	15.43045800	0.28926600	0.49405700
H	14.04512200	1.92568900	0.70821800
H	12.46061700	-1.68707900	-1.02222900
H	14.65523100	-2.76825900	-0.76679700
H	16.26283300	0.85562400	0.90313300
H	16.58306800	-1.51456100	0.19232000
O	-4.67272800	1.12505400	-0.78957900
C	-4.61152500	0.05319000	-0.19080200
C	-5.81536100	-0.87622700	-0.05271000
H	-5.78149400	-1.57743900	-0.89953700
H	-5.72493500	-1.48669900	0.85425900
C	-7.14971000	-0.12312900	-0.06117500
H	-7.19062400	0.51371900	-0.95194800
H	-7.19284000	0.55053400	0.80501000
C	-8.35376400	-1.07176000	-0.03858900
H	-8.30540100	-1.74543800	-0.90568400
H	-8.30592400	-1.71130200	0.85386800
C	-9.69574000	-0.32503300	-0.05355400
H	-9.74259800	0.31684700	-0.94191600
H	-9.75305600	0.33598600	0.82017600
C	-10.88182500	-1.30520900	-0.05131500
H	-10.83952800	-1.96513500	-0.92666400
H	-10.85014300	-1.95066700	0.83533800
Cl	-16.21021100	0.95949000	-0.09740500
C	-13.78898700	-1.85916200	-0.11431100
H	-14.77558300	-1.38288800	-0.11783100
H	-13.65763100	-2.46044000	-1.01820400
H	-13.68270500	-2.49865600	0.76608100

C	-12.75484800	0.51370900	-1.53161900
H	-13.77921500	0.90150300	-1.50911400
H	-12.59737200	-0.07493400	-2.43971900
H	-12.04368300	1.34331100	-1.50734000
C	-12.80736600	0.46308100	1.42184200
H	-12.69681400	-0.16075500	2.31327800
H	-12.08583900	1.28315600	1.45961000
H	-13.82514000	0.86511100	1.36942500
P	-12.54398500	-0.54012300	-0.06844300

Excitation energies and oscillator strengths:

Excited State 1: Singlet-A 2.4149 eV 513.41 nm f=1.4526 <S**2>=0.000
147 ->153 -0.10637
152 ->153 0.66448
This state for optimization and/or second-order correction.
Total Energy, E(TD-HF/TD-KS) = -2375.25728661
Copying the excited state density for this state as the 1-particle RhoCI density.

Excited State 2: Singlet-A 2.9397 eV 421.76 nm f=0.0600 <S**2>=0.000
140 ->153 -0.12219
141 ->153 -0.19514
147 ->153 0.22186
151 ->153 0.60710

Excited State 3: Singlet-A 3.9054 eV 317.47 nm f=0.5513 <S**2>=0.000
139 ->153 0.37259
143 ->153 0.42090
145 ->153 0.23385
147 ->153 0.14492
151 ->153 -0.10115
152 ->153 0.17674

Excited State 4: Singlet-A 4.1517 eV 298.64 nm f=0.3334 <S**2>=0.000
141 ->153 -0.39548

143 ->153 -0.16074
144 ->153 0.12412
147 ->153 0.40329
151 ->153 -0.28908

Excited State 5: Singlet-A 4.2917 eV 288.89 nm f=0.0075 <S**2>=0.000
140 ->153 0.56351
141 ->153 -0.32034
144 ->153 0.14916
147 ->153 -0.14281

Excited State 6: Singlet-A 4.3922 eV 282.29 nm f=0.0053 <S**2>=0.000
140 ->153 -0.12386
141 ->153 0.10410
143 ->153 0.14305
144 ->153 0.41169
144 ->154 0.11245
145 ->153 -0.11496
152 ->154 0.13742
152 ->155 -0.35374
152 ->156 0.14512
152 ->157 0.19221

Excited State 7: Singlet-A 4.5448 eV 272.80 nm f=0.0008 <S**2>=0.000
140 ->153 -0.11847
143 ->153 -0.20719
144 ->153 0.16848
145 ->153 0.51338
145 ->154 -0.13309
151 ->156 -0.22252
151 ->159 0.10628
152 ->156 -0.13900

Excited State 8: Singlet-A 4.6866 eV 264.55 nm f=0.0958 <S**2>=0.000
144 ->153 -0.20257
151 ->156 -0.11353
151 ->157 0.12453
152 ->154 0.51127
152 ->155 -0.14295
152 ->156 0.17036
152 ->157 -0.22387

Excited State 9: Singlet-A 4.7310 eV 262.07 nm f=0.0238 <S**2>=0.000

138 ->153 0.17952
140 ->153 0.29855
141 ->153 0.35631
143 ->153 -0.14480
147 ->153 0.40993

Excited State 10: Singlet-A 4.8472 eV 255.79 nm f=0.1069 <S**2>=0.000
143 ->153 0.10475
144 ->153 0.31554
147 ->158 0.15410
151 ->157 0.11613
151 ->158 -0.13819
152 ->154 0.13669
152 ->155 0.27964
152 ->157 -0.31480
152 ->158 0.28252

Excited State 11: Singlet-A 4.8818 eV 253.97 nm f=0.0643 <S**2>=0.000
144 ->153 -0.26217
146 ->153 0.14099
147 ->158 0.17216
151 ->158 -0.19547
152 ->155 -0.17625
152 ->157 0.15960
152 ->158 0.45768
152 ->159 0.10925

Excited State 12: Singlet-A 5.0644 eV 244.82 nm f=0.0747 <S**2>=0.000
143 ->153 -0.11891
145 ->153 0.23178
147 ->159 -0.10806
151 ->154 -0.21832
151 ->155 0.12261
151 ->156 0.26051
152 ->155 0.12326
152 ->156 0.39198
152 ->159 0.22748

Excited State 13: Singlet-A 5.1636 eV 240.11 nm f=0.0713 <S**2>=0.000
145 ->153 -0.22312
151 ->156 -0.23817
151 ->157 -0.10653
151 ->159 0.25133

152 ->157 -0.13081
152 ->159 0.44942

Excited State 14: Singlet-A 5.1921 eV 238.80 nm f=0.3775 <S**2>=0.000
139 ->153 0.12654
151 ->154 0.37879
151 ->155 0.17777
151 ->157 0.15410
152 ->154 0.18049
152 ->155 0.25965
152 ->157 0.25064
152 ->159 0.22116

Excited State 15: Singlet-A 5.2959 eV 234.11 nm f=0.0014 <S**2>=0.000
142 ->153 0.41830
142 ->154 -0.31935
142 ->155 -0.16667
142 ->156 0.12023
142 ->157 -0.20609
142 ->160 0.17652
142 ->161 0.20067
143 ->153 0.12937

Excited State 16: Singlet-A 5.4006 eV 229.58 nm f=0.0225 <S**2>=0.000
136 ->153 -0.14299
139 ->153 0.45984
142 ->153 0.10684
143 ->153 -0.31761
146 ->153 -0.12625
147 ->153 -0.16507

Excited State 17: Singlet-A 5.4848 eV 226.05 nm f=0.0103 <S**2>=0.000
144 ->153 0.11571
146 ->153 0.65852
152 ->158 -0.14338

Excited State 18: Singlet-A 5.5371 eV 223.92 nm f=0.0000 <S**2>=0.000
150 ->153 0.70674

Excited State 19: Singlet-A 5.5683 eV 222.66 nm f=0.0000 <S**2>=0.000
149 ->153 0.70677

Excited State 20: Singlet-A 5.5698 eV 222.60 nm f=0.0000 <S**2>=0.000
148 ->153 0.70694

Table C.2 fit parameters from fitting a cylinder model of SAXS data.

6mM		error
SLD	3.28E-05	
scale	0.000141	1.54E-05
background	1.00E-04	
length	1000	
kuhn	249.98	0.0178
radius	12.961	0.76891
PD	0	
chi2	1.3294	
q range	0.006-0.1	

Appendix D

EB TANI-$(PTAB)_2$

Coordinates of optimised geometry for EB TANI-$(PTAB)_2$

C	3.657163	1.85038	0.490531
H	3.514109	2.871048	0.833293
C	4.896123	1.315278	0.38977
H	5.762561	1.902508	0.671223
C	5.087759	-0.06898	-0.03601
C	3.874281	-0.83885	-0.28786
H	4.017208	-1.86567	-0.61211
C	2.634496	-0.30358	-0.19452
H	1.76498	-0.89646	-0.45444
C	2.443223	1.087216	0.212516
N	6.222983	-0.70529	-0.19164
N	1.308107	1.724421	0.337591
C	7.472824	-0.10353	-0.18924
C	10.14227	0.894703	-0.21634
C	8.555034	-0.86665	0.303999
C	7.775999	1.165829	-0.73927
C	9.075945	1.64319	-0.76216
C	9.851142	-0.37614	0.3255
H	8.343432	-1.85032	0.712679
H	6.993203	1.751483	-1.20973
H	9.285772	2.605755	-1.22205
H	10.63862	-0.97226	0.771115
C	0.060092	1.104006	0.278831
C	-2.57688	0.063983	0.205682
C	-0.2667	-0.09434	0.949659
C	-0.9793	1.77995	-0.3907
C	-2.26947	1.267429	-0.45443
C	-1.56141	-0.59643	0.918065
H	0.488927	-0.60943	1.534232
H	-0.74904	2.719754	-0.88409
H	-3.04453	1.792402	-0.99381
H	-1.79102	-1.51222	1.458077
N	-3.86054	-0.51715	0.217559
N	11.41092	1.454581	-0.22326
H	-3.93165	-1.37718	0.746605
H	11.43846	2.456904	-0.35777

C	12.65984	0.845163	-0.02194
C	15.24504	-0.24835	0.338892
C	13.70281	1.607762	0.528376
C	12.9384	-0.47717	-0.40734
C	14.20747	-1.01263	-0.2174
C	14.97959	1.08179	0.702102
H	13.50951	2.634808	0.8281
H	12.174	-1.08348	-0.87969
H	14.3983	-2.03841	-0.52411
H	15.76742	1.687517	1.126004
O	-5.08975	0.92373	-1.08114
C	-5.01225	-0.10031	-0.4052
C	-6.20134	-1.03906	-0.21116
H	-6.17501	-1.77209	-1.03064
H	-6.09208	-1.61136	0.718138
C	-7.54041	-0.29362	-0.22871
H	-7.6041	0.295027	-1.15063
H	-7.5672	0.42449	0.601538
C	-8.74124	-1.24114	-0.1268
H	-8.71155	-1.96213	-0.95537
H	-8.67212	-1.8275	0.799756
C	-10.08	-0.48348	-0.15437
H	-10.1455	0.086343	-1.08772
H	-10.0983	0.23664	0.671045
C	-11.2416	-1.4671	-0.03645
H	-11.2183	-2.19065	-0.85576
H	-11.1808	-2.01947	0.905189
N	-12.6426	-0.86355	-0.06543
Cl	-16.3564	0.554663	-0.07583
C	-13.6399	-1.98644	0.084305
H	-14.6411	-1.551	0.060729
H	-13.4999	-2.68634	-0.74027
H	-13.4576	-2.48762	1.035583
C	-12.9161	-0.16025	-1.37068
H	-13.9526	0.183082	-1.34765
H	-12.7592	-0.86685	-2.18686
H	-12.2397	0.687218	-1.47101
C	-12.8503	0.108435	1.067971
H	-12.6301	-0.40023	2.00747
H	-12.1851	0.960597	0.936245
H	-13.893	0.432477	1.034606
N	16.50519	-0.86859	0.487533

C	17.66237	-0.36569	1.024318
O	17.77248	0.779855	1.461018
C	18.82339	-1.35649	1.062337
H	18.85978	-1.77339	2.078953
H	18.64301	-2.20019	0.385524
C	20.16434	-0.68618	0.736261
H	20.30079	0.170398	1.405669
H	20.13035	-0.2836	-0.28498
C	21.34864	-1.65064	0.867468
H	21.37897	-2.05837	1.887219
H	21.20372	-2.50602	0.193405
C	22.69058	-0.96898	0.548157
H	22.83907	-0.13452	1.242378
H	22.64471	-0.55015	-0.46305
C	23.82869	-1.98055	0.66017
H	23.86187	-2.41376	1.663284
H	23.68679	-2.79464	-0.0555
N	25.23415	-1.44791	0.399541
C	26.20242	-2.60023	0.51297
C	25.62428	-0.40223	1.412839
C	25.35615	-0.86215	-0.98394
H	27.20775	-2.21192	0.335313
H	26.12017	-3.025	1.514159
H	25.93881	-3.34928	-0.2347
H	26.65904	-0.11778	1.209978
H	25.52869	-0.83232	2.410887
H	24.96717	0.460015	1.310428
H	25.04788	-1.61685	-1.70893
H	24.71662	0.016	-1.0596
H	26.40201	-0.5835	-1.13139
Cl	28.96082	-0.26055	-0.2945
H	16.54698	-1.82598	0.162678
H	26.40201	-0.5835	-1.13139
Cl	28.96082	-0.26055	-0.2945
H	16.54698	-1.82598	0.162678

Excitation energies and oscillator strengths:

Excited State 1: Singlet-A 2.3762 eV 521.76 nm f=1.5566
198 ->205 0.12469
203 ->205 0.14691
204 ->205 0.65324

This state for optimization and/or second-order correction.
Total Energy, E(TD-HF/TD-KS) = -3087.68441932
Copying the excited state density for this state as the 1-particle RhoCI density.

Excited State 2: Singlet-A 2.9298 eV 423.19 nm f=0.0661
187 ->205 -0.11670
189 ->205 0.20163
198 ->205 -0.29544
203 ->205 0.57114

Excited State 3: Singlet-A 3.8367 eV 323.15 nm f=0.4380
186 ->205 0.11677
188 ->205 0.27133
189 ->205 0.33374
192 ->205 0.12994
193 ->205 0.12038
195 ->205 0.26229
198 ->205 -0.25989
203 ->205 -0.18391
204 ->205 0.20540

Excited State 4: Singlet-A 4.0742 eV 304.31 nm f=0.5354
187 ->205 0.14604
188 ->205 0.23835
189 ->205 -0.17196
192 ->205 0.14536
193 ->205 0.19868
195 ->205 0.29553
198 ->205 0.33204
203 ->205 0.30282

Excited State 5: Singlet-A 4.2953 eV 288.65 nm f=0.0010
187 ->205 0.50414
188 ->205 -0.35866
189 ->205 0.20647
194 ->205 0.15148

Excited State 6: Singlet-A 4.3710 eV 283.65 nm f=0.0237
187 ->205 -0.14173
188 ->205 0.10919
192 ->205 0.27205
193 ->205 -0.11651

194 ->205 0.21101
195 ->205 -0.13821
198 ->210 0.10639
204 ->206 -0.24300
204 ->208 -0.27652
204 ->210 0.30866

Excited State 7: Singlet-A 4.5185 eV 274.39 nm f=0.3027
192 ->205 0.20099
203 ->207 -0.15881
204 ->206 0.51656
204 ->207 0.18518
204 ->210 0.18584

Excited State 8: Singlet-A 4.5527 eV 272.33 nm f=0.0123
187 ->205 -0.12046
192 ->205 -0.21184
193 ->205 -0.29520
194 ->205 0.28972
195 ->205 0.33458
203 ->209 0.21089
203 ->210 -0.12803
203 ->211 0.10326
204 ->209 0.13559

Excited State 9: Singlet-A 4.6104 eV 268.92 nm f=0.0809
198 ->208 -0.17792
203 ->208 -0.21827
204 ->206 -0.13194
204 ->208 0.49220
204 ->209 0.19185
204 ->210 0.19195

Excited State 10: Singlet-A 4.6572 eV 266.22 nm f=0.0076
185 ->205 -0.13413
186 ->205 0.16668
187 ->205 -0.31447
188 ->205 -0.12791
189 ->205 0.36496
198 ->205 0.39261

Excited State 11: Singlet-A 4.8368 eV 256.34 nm f=0.1310
192 ->205 -0.33647

193 ->205 0.15691
194 ->205 -0.29621
195 ->205 0.14518
204 ->208 -0.17315
204 ->209 0.15712
204 ->210 0.39134

Excited State 12: Singlet-A 5.0170 eV 247.13 nm f=0.1229
195 ->205 -0.13599
198 ->211 -0.10645
203 ->206 -0.25279
203 ->207 0.17874
203 ->209 0.18389
204 ->206 -0.11750
204 ->207 0.33935
204 ->209 0.22434
204 ->211 -0.26022

Excited State 13: Singlet-A 5.1291 eV 241.73 nm f=0.0477
186 ->205 0.13360
187 ->205 0.11961
188 ->205 0.20717
189 ->205 0.11587
195 ->205 -0.26276
198 ->205 0.10244
198 ->209 -0.10221
203 ->207 0.13371
203 ->211 0.20099
204 ->209 -0.10555
204 ->211 0.38132

Excited State 14: Singlet-A 5.1404 eV 241.20 nm f=0.2925
192 ->205 0.12351
193 ->205 0.14302
194 ->205 -0.11849
195 ->205 -0.12674
203 ->206 0.22150
203 ->207 -0.12732
203 ->209 0.32533
203 ->210 -0.16732
203 ->211 0.10724
204 ->206 0.11434
204 ->207 -0.21575

204 ->209 0.25839
204 ->210 -0.11867

Excited State 15: Singlet-A 5.2033 eV 238.28 nm f=0.0552
186 ->205 -0.14163
187 ->205 -0.11329
188 ->205 -0.22260
189 ->205 -0.10168
192 ->205 0.24323
193 ->205 0.22050
195 ->205 0.16675
198 ->205 -0.12647
203 ->206 -0.13604
203 ->211 0.18489
204 ->207 0.13463
204 ->211 0.27398
204 ->212 0.12829

Excited State 16: Singlet-A 5.2708 eV 235.23 nm f=0.0000 <S**2>=0.000
202 ->205 0.70580

Excited State 17: Singlet-A 5.2852 eV 234.59 nm f=0.0000 <S**2>=0.000
200 ->205 0.70394

Excited State 18: Singlet-A 5.2859 eV 234.56 nm f=0.0000 <S**2>=0.000
199 ->205 0.70619

Excited State 19: Singlet-A 5.3025 eV 233.82 nm f=0.0004 <S**2>=0.000
190 ->205 0.40789
190 ->206 0.24730
190 ->207 -0.33974
190 ->212 0.20336
190 ->213 0.19877
190 ->216 0.12294

Excited State 20: Singlet-A 5.3684 eV 230.95 nm f=0.0000 <S**2>=0.000
201 ->205 0.70496

Scattering analysis of EB TANI-(PTAB)$_2$

EB state SAXS and SANS

The SAXS and SANS data are similar with a greater contrast being seen in the 16mM SANS as expected. The data show a q = -2 dependence indicative of a disk or a vesicle in solution.

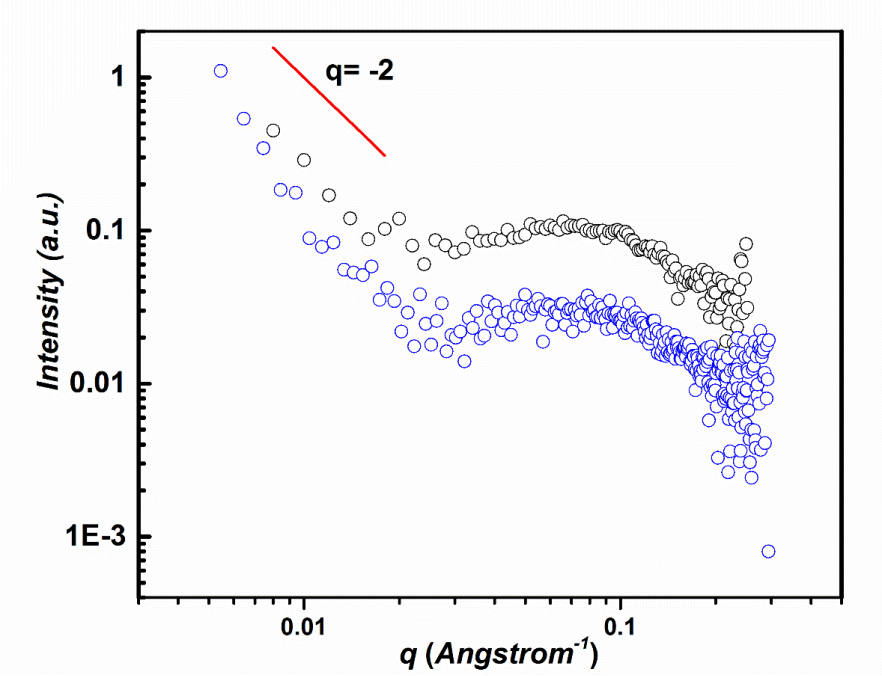

Figure D.1 Small angle x-ray scattering data (blue circles) and small angle neutron scattering data (black circles) collected for 16mM EB TANI-(PTAB)$_2$. A simulated line (red) indicated the q=-2 dependence.

Liquid AFM studies of EB TANI-(PTAB)$_2$

High resolution imaging on mica clearly shows a film of collapsed material on the surface. There are some discrete objects. These only exist on top of the film as here the surface cannot influence them. Furthermore, on HOPG surface the particles are also collapsed and also diffuse. The background structure of the HOPG is clearly visible which suggests that there is not a film formed. However, the stepped structure of the HOPG and low number of particles sedimenting to the surface makes statistical analysis of a significant number of particles very difficult.

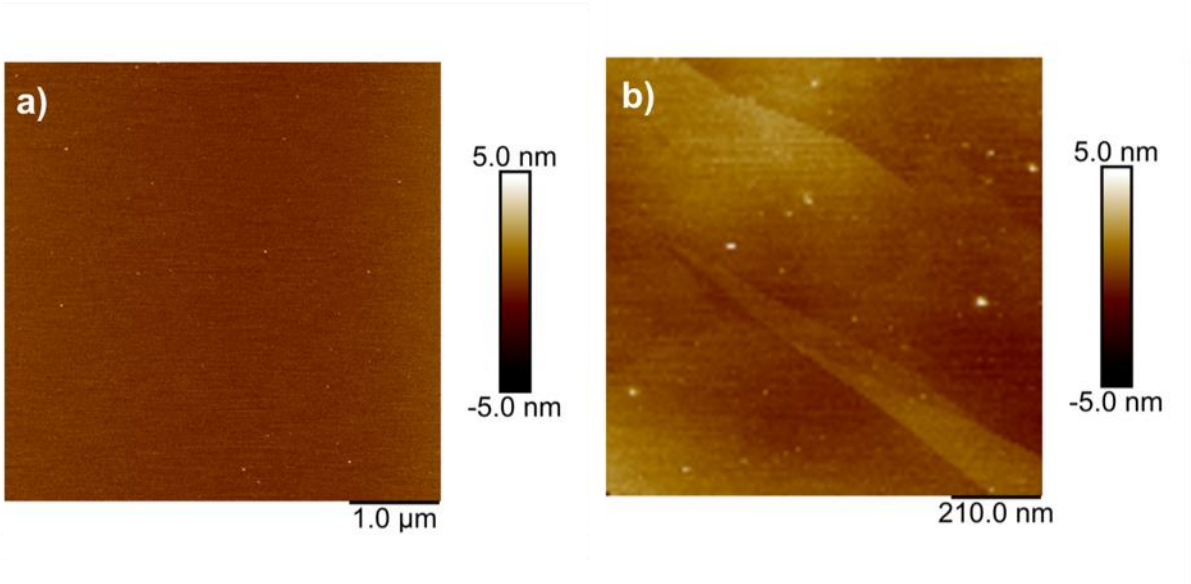

Figure D.2 AFM images of 0.5 mM solution of EB TANI-$(PTAB)_2$ drop-cast onto a) mica surface and b) on HOPG.

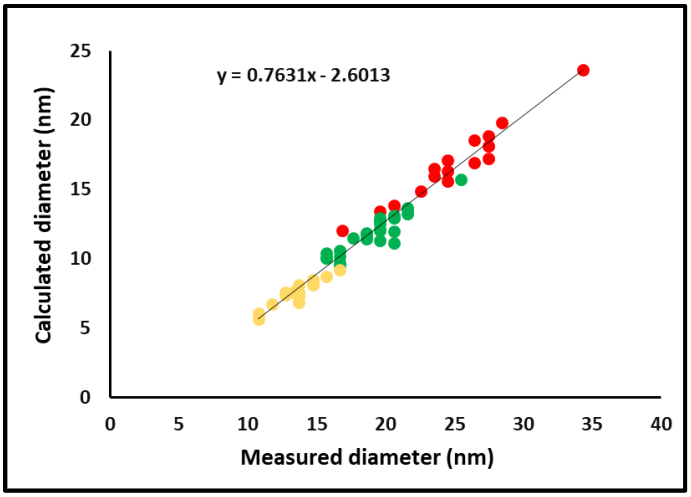

Figure D.3 graph showed a comparison between the measured (oblate) diameter and the diameter calculated based upon the oblate diameter and height of the structure, the colour scheme corresponds to the 3 populations shown in the histogram (Figure 4.10c).

$$V_{srf} = V_{sol}$$

Where V_{srf} is the volume of the measured oblate sphere at the surface and V_{sol} is the volume of the same sphere in solution unaffected by surface influences.

$$V_{srf} = \frac{4}{3}\pi\left(\frac{D_m}{2}\right)^2\frac{h_m}{2}$$

Where D_m is the measured lateral diameter and h_m is the measured height

$$V_{sol} = \frac{4}{3}\pi\left(\frac{D_C}{2}\right)^3$$

Where D_C is the calculated diameter of the sphere free of surface influences in solution

Using the initial assumption D_C is calculated from the measured V_{srf}

$$\frac{4}{3}\pi\left(\frac{D_C}{2}\right)^3 = V_{srf}$$

$$D_C = 2\sqrt[3]{\frac{3}{4}\pi V_{srf}}$$

Supplementary analysis

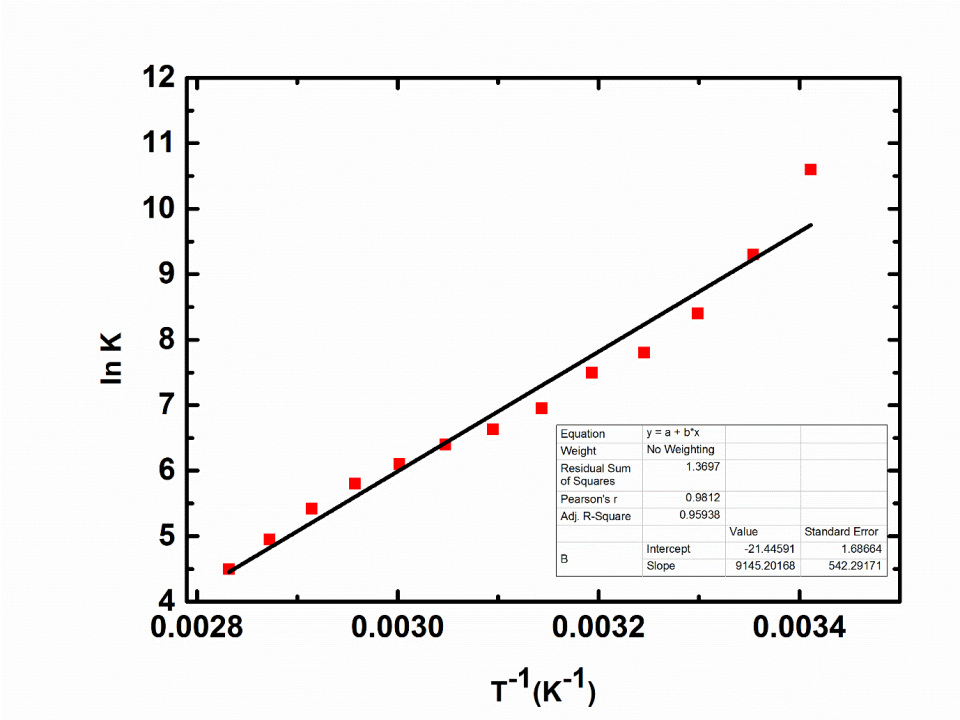

Figure D.4 van't Hoff plot for EB TANI-$(PTAB)_2$

ES TANI-$(PTAB)_2$

Scattering analysis of ES TANI-$(PTAB)_2$

SANS: The 8mM sample of **ES TANI-$(PTAB)_2$** was fitted to a cylinder model. The scattering length densities of the molecule and D_2O were calculated using the SLD tool within SasView. The actual length of the fibres is outside of the q range that can be accessed by SANS2D and therefore we only report the value of the radius in the text. Full fitting parameters for the data are given in Table D2.

Table D.1 fit parameters from fitting a cylinder model of SANS data.

Fit Parameter	Value	Error
Scale	0.51	0.01
Background	1 x 10-4	
SLD sample	4.7 x 10^{-6} $Å^{-2}$	
SLD solvent	6.3 x 10^{-6} $Å^{-2}$	
Radius (nm)	2.37	0.2
Length (nm)	246.6	7.7
Reduced Chi^2	1.3	
Q min ($Å^{-1}$)	0.008	
Q max ($Å^{-1}$)	0.12	

SAXS: ES state 16mM

Analysis of the SAXS data shows a q = -1 dependence indicative of a rod like structure. The data were fit to a cylinder model with the parameters given in Table D.2. The fit to the data is given in figure 4.32, with a line indicating the q = -1 dependence. The SAXS data do not fit as well as the SANS data, particularly at low values of q. This is due to the poor contrast of the samples in SAXS; however the radius of the cylinder is comparable with that found by SANS and TEM.

Table D.2 fit parameters from fitting a cylinder model of SAXS data.

Fit parameter	Value	Error
scale	7.8 x 10^{-6}	7.1 x 10^{-8}
background	0.025	0.001
SLD sample	0.000115 $Å^{-2}$	
SLD solvent	9.7 x 10^{-6} $Å^{-2}$	
Radius (nm)	2.1	0.1
Length (nm)	19.2	
Reduced Chi^2	4.1	
Q min ($Å^{-1}$)	0.01	
Q max ($Å^{-1}$)	0.15	

Appendix E

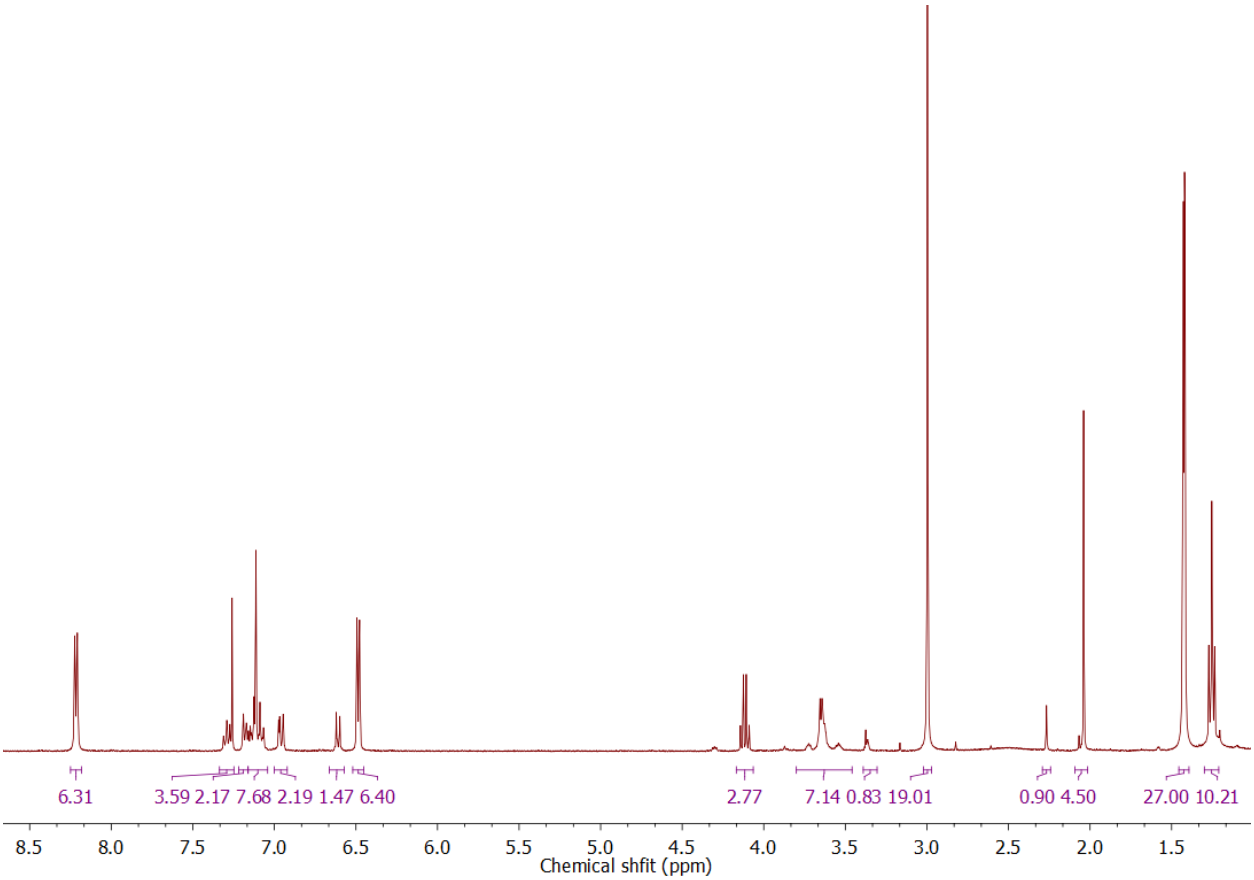

Figure E.1 ^{1}H NMR spectrum of Boc TANI-mPEG350 (using MDI as coupling agent).

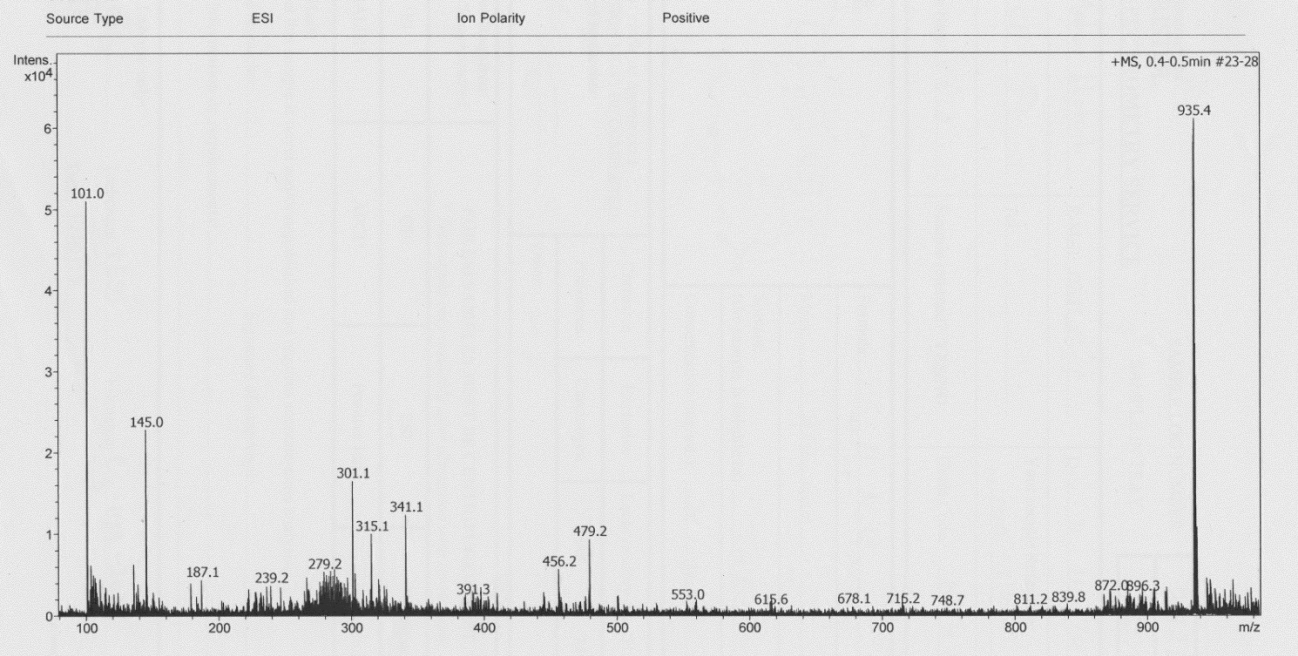

Figure E.2 ESI spectrum of Boc TANI-(CO)TEG.

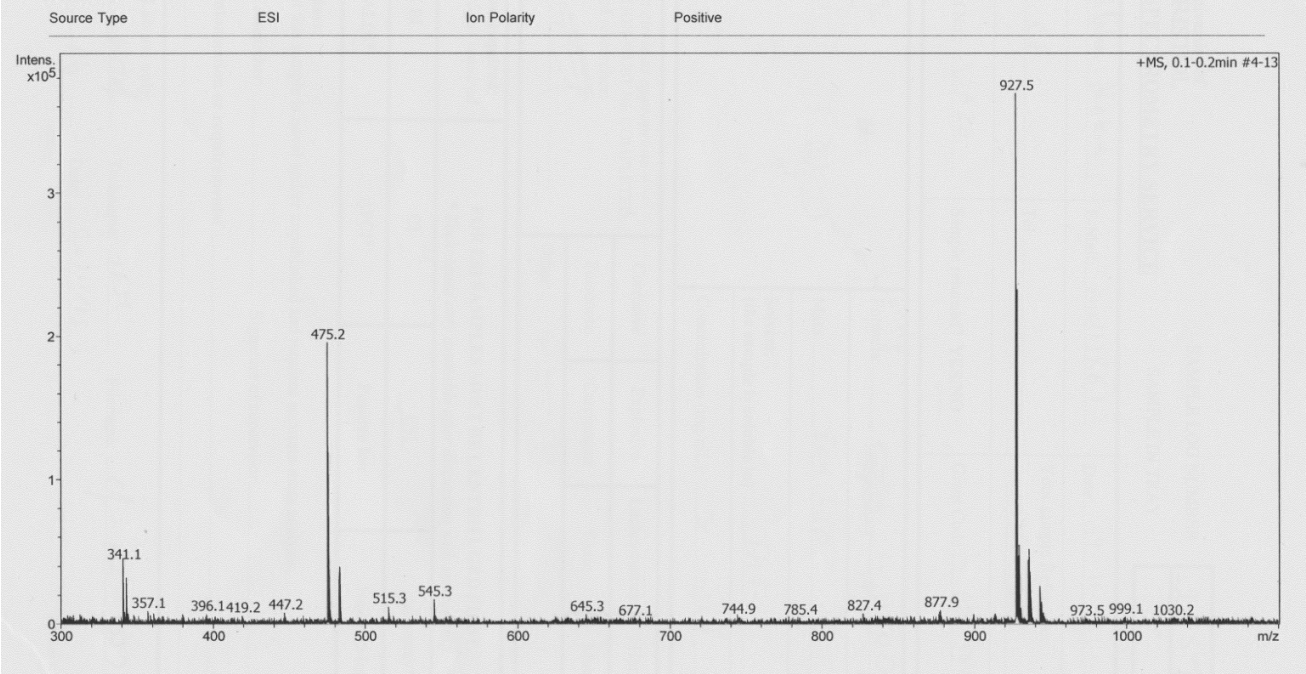

Figure E.1 ESI spectrum of Boc TANI-TEG.